

Project AMIGA: The Circumgalactic Medium of Andromeda*

NICOLAS LEHNER,¹ SAMANTHA C. BEREK,^{1,2,†} J. CHRISTOPHER HOWK,¹ BART P. WAKKER,³ JASON TUMLINSON,^{4,5}
EDWARD B. JENKINS,⁶ J. XAVIER PROCHASKA,⁷ RAMONA AUGUSTIN,⁴ SUOQING JI,⁸ CLAUDE-ANDRÉ FAUCHER-GIGUÈRE,⁹
ZACHARY HAFEN,⁹ MOLLY S. PEEPLES,^{4,5} KAT A. BARGER,¹⁰ MICHELLE A. BERG,¹ RONGMON BORDOLOI,¹¹
THOMAS M. BROWN,⁴ ANDREW J. FOX,¹² KAROLINE M. GILBERT,^{4,5} PURAGRA GUHATHAKURTA,⁷ JASON S. KALIRAI,¹³
FELIX J. LOCKMAN,¹⁴ JOHN M. O'MEARA,¹⁵ D.J. PISANO,^{16,17,‡} JOSEPH RIBAUDO,¹⁸ AND JESSICA K. WERK¹⁹

¹Department of Physics, University of Notre Dame, Notre Dame, IN 46556

²Department of Astronomy, Yale University, New Haven, CT 06511 USA

³Department of Astronomy, University of Wisconsin Madison, WI 53706

⁴Space Telescope Science Institute, 3700 San Martin Drive, Baltimore, MD, 21218

⁵Department of Physics & Astronomy, Johns Hopkins University, 3400 N. Charles Street, Baltimore, MD 21218

⁶Department of Astrophysical Sciences, Princeton University, Princeton, NJ 08544

⁷UCO/Lick Observatory, Department of Astronomy & Astrophysics, University of California Santa Cruz, 1156 High Street, Santa Cruz, CA 95064

⁸TAPIR, Walter Burke Institute for Theoretical Physics, California Institute of Technology, Pasadena, CA, 91125

⁹CIERA and Department of Physics and Astronomy, Northwestern University, 2145 Sheridan Road, Evanston, IL 60208

¹⁰Department of Physics & Astronomy, Texas Christian University, Fort Worth, TX 76129

¹¹North Carolina State University, Department of Physics, Raleigh, NC 27695-8202

¹²AURA for ESA, Space Telescope Science Institute, 3700 San Martin Drive, Baltimore, MD 21218

¹³Johns Hopkins Applied Physics Laboratory, 11100 Johns Hopkins Road, Laurel, MD 20723

¹⁴Green Bank Observatory, Green Bank, WV 24944

¹⁵W.M. Keck Observatory 65-1120 Mamalahoa Highway Kamuela, HI 96743

¹⁶Department of Physics & Astronomy, West Virginia University, P.O. Box 6315, Morgantown, WV 26506

¹⁷Center for Gravitational Waves and Cosmology, West Virginia University, Chestnut Ridge Research Building, Morgantown, WV 26505

¹⁸Department of Engineering and Physics, Providence College, Providence, RI, 02918

¹⁹Department of Astronomy, University of Washington, Seattle, WA 98195

ABSTRACT

Project AMIGA (Absorption Maps In the Gas of Andromeda) is a large ultraviolet *Hubble Space Telescope* program, which has assembled a sample of 43 QSOs that pierce the circumgalactic medium (CGM) of Andromeda (M31) from $R = 25$ to 569 kpc (25 of them probing gas from 25 kpc to about the virial radius— $R_{\text{vir}} = 300$ kpc—of M31). Our large sample provides an unparalleled look at the physical conditions and distribution of metals in the CGM of a single galaxy using ions that probe a wide range of gas phases (Si II, Si III, Si IV, C II, C IV, and O VI, the latter being from the *Far Ultraviolet Spectroscopic Explorer*). We find that Si III and O VI have near unity covering factor maintained all the way out to $1.2R_{\text{vir}}$ and $1.9R_{\text{vir}}$, respectively. We show that Si III is the dominant ion over Si II and Si IV at any R . While we do not find that the properties of the CGM of M31 depend strongly on the azimuth, we show that they change remarkably around $0.3\text{--}0.5R_{\text{vir}}$, conveying that the inner regions of the CGM of M31 are more dynamic and have more complicated multi-phase gas-structures than at $R \gtrsim 0.5R_{\text{vir}}$. We estimate the metal mass of the CGM within R_{vir} as probed by Si II, Si III, and Si IV is $2 \times 10^7 M_{\odot}$ and by O VI is $> 8 \times 10^7 M_{\odot}$, while the baryon mass of the $\sim 10^4\text{--}10^{5.5}$ K gas is $\gtrsim 4 \times 10^{10} (Z/0.3 Z_{\odot})^{-1} M_{\odot}$ within R_{vir} . We show that different zoom-in cosmological simulations of L^* galaxies better reproduce the column density profile of O VI with R than Si III or the other studied ions. We find that observations of the M31 CGM and zoom-in simulations of L^* galaxies have both lower ions showing higher column density dispersion and dependence on R than higher ions, indicating that the higher ionization structures are larger and/or more broadly distributed.

* Based on observations made with the NASA/ESA Hubble Space Telescope, obtained from the data archive at the Space Telescope Science Institute. STScI is operated by the Association of Universities for Research in Astronomy, Inc. under NASA contract NAS 5-26555.

Keywords: galaxies: halos — galaxies: individual (M31) — Local Group — quasars: absorption lines

1. INTRODUCTION

Over the last 10 years, in particular since the installation of the Cosmic Origins Spectrograph (COS) on the *Hubble Space Telescope* (*HST*), we have made significant leaps in empirically characterizing the circumgalactic medium (CGM) of galaxies at low redshift where a wide range of galaxy masses can be studied (see recent review by Tumlinson et al. 2017). We appreciate now that the CGM of typical star-forming or quiescent galaxies have a large share of galactic baryons and metals in relatively cool gas-phases (10^4 – $10^{5.5}$ K) (e.g., Stocke et al. 2013; Bordoloi et al. 2014; Liang & Chen 2014; Peebles et al. 2014; Werk et al. 2014; Johnson et al. 2015; Burchett et al. 2016; Prochaska et al. 2017b; Chen et al. 2019; Poisson et al. 2019). We have come to understand that the CGM of galaxies at $z \lesssim 1$ is not just filled with metal-enriched gas ejected by successive galaxy outflows, but has also a large amount of metal poor gas (< 1 –2% solar) in which little net chemical enrichment has occurred over several billions of years (e.g., Ribaldo et al. 2011; Thom et al. 2011; Lehner et al. 2013, 2018, 2019; Wotta et al. 2016, 2019; Prochaska et al. 2017b; Kacprzak et al. 2019; Poisson et al. 2019; Zahedy et al. 2019). The photoionized gas around $z \lesssim 1$ galaxies is very chemically inhomogeneous, as shown by large metallicity ranges and the large metallicity variations among kinematically distinct components in a single halo (Wotta et al. 2019; Lehner et al. 2019, and see also Crighton et al. 2013; Muzahid et al. 2015, 2016; Rosenwasser et al. 2018). Such a large metallicity variation is not only observed in the CGM of star-forming galaxies, but also in the CGM of passive and massive galaxies where there appears to be as much cold, bound H I gas as in their star-forming counterparts (e.g., Thom et al. 2012; Tumlinson et al. 2013; Berg et al. 2019; Zahedy et al. 2019).

These empirical results have revealed both expected and unexpected properties of the CGM of galaxies and they all provide new means to understand the complex relationship between galaxies and their CGM. Prior to these empirical results, the theory of galaxy formation and evolution was mostly left constraining the CGM properties indirectly by their outcomes, such as galaxy stellar mass and ISM properties. Thus the balance between outflows, inflows, recycling, and ambi-

ent gas—and the free parameters controlling them—were tuned to match the optical properties of galaxies rather than implemented directly as physically-rigorous and self-consistent models. These indirect constraints suffer from problems of model uniqueness: it is possible to match stellar masses and metallicities with very different treatments of feedback physics (e.g., Hummels et al. 2013; Liang et al. 2016). Recent empirical and theoretical advances offer a way out of this model degeneracy. New high-resolution, zoom-in simulations employ explicit treatments of the multiple gas-phase nature and feedback from stellar population models (e.g., Hopkins et al. 2014, 2018). It is also becoming clear that not only high resolution inside the galaxies but also in their CGM is required to capture more accurately the complex processes in the cool CGM, such as metal mixing (Hummels et al. 2019; Peebles et al. 2019; Suresh et al. 2019; van de Voort et al. 2019; Corlies et al. 2020).

A significant limitation in interpreting the new empirical results in the context of new high-resolution zoom simulations is that only average properties of the CGM are robustly derived from traditional QSO absorption-line techniques for examining halo gas. In the rare cases where there is a UV-bright QSO behind a given galaxy, the CGM is typically probed along a single “core sample” through the halo of each galaxy. These measurements are then aggregated into a statistical map, where galaxies with different inclinations, sizes, and environments are blended together and the radial-azimuthal dependence of the CGM is essentially lost. All sorts of biases can result: phenomena that occur strongly in only a subset of galaxies can be misinterpreted as being weaker but more common, and genuine trends with mass or star formation rate can be misinterpreted as simply scatter with no real physical meaning (see also Bowen et al. 2016). Simulations also suggest that time-variable winds, accretion flows, and satellite halos can induce strong halo-to-halo variability, further complicating interpretation (e.g. Hafen et al. 2017; Oppenheimer et al. 2018a). Observational studies of single galaxy CGM with multiple sightlines are therefore required to gain spatial information on the properties of the CGM.

Multi-sightline information on the CGM of single galaxies has been obtained in a few cases from binary or multiple (2–4) grouped QSOs behind foreground galaxies (e.g., Bechtold et al. 1994; Martin et al. 2010; Keeney et al. 2013; Bowen et al. 2016), gravitationally-lensed quasars (e.g., Smette et al. 1992; Rauch et al. 2001; Ellison et al. 2004; Lopez et al. 2005; Zahedy et al. 2016; Ru-

[†] NSF REU student.

[‡] Adjunct Astronomer, Green Bank Observatory.

bin et al. 2018; Kulkarni et al. 2019), giant gravitational arcs (e.g., Lopez et al. 2020), or extended bright background objects observed with integral field units (e.g., Péroux et al. 2018). These observations provide better constraints on the kinematic relationship between the CGM gas and the galaxy and on the size of CGM structures. However, they yield limited information on the gas-phase structure owing to a narrow range of ionization diagnostics or poor quality spectral data. Thus, it remains unclear how tracers of different gas phases vary with projected distance R or azimuth Φ around the galaxy.

The CGM that has been pierced the most is that of the Milky Way (MW), with several hundred QSO sightlines (Wakker et al. 2003; Shull et al. 2009; Lehner et al. 2012; Putman et al. 2012; Richter et al. 2017) through the Galactic halo. However, our position as observers within the MW disk severely limits the interpretation of these data (especially for the extended CGM, see Zheng et al. 2015, 2020) and makes it difficult to compare with observations of other galaxies.

With a virial radius that spans over 30° on the sky, M31 is the only L^* galaxy where we can access more than 5 sightlines without awaiting the next generation of UV space-based telescope (e.g., The LUVUOIR Team 2019). With current UV capabilities, it is the only single galaxy where we can study the global distribution and properties of metals and baryons in some detail.

In our pilot study (Lehner et al. 2015, hereafter LHW15), we mined the *HST*/COS G130M/G160M archive available at the *Barbara A. Mikulski Archive for Space Telescopes* (MAST) for sightlines piercing the M31 halo within a projected distance of $\sim 2R_{\text{vir}}$ (where $R_{\text{vir}} = 300$ kpc for M31, see below). There were 18 sightlines, but only 7 at projected distance $R \lesssim R_{\text{vir}}$. Despite the small sample, the results of this study were quite revealing, demonstrating a high covering factor (6/7) of M31 CGM absorption by Si III (and other ions including, e.g., C IV, Si II) within $1.1R_{\text{vir}}$ and a covering factor near zero (1/11) between $1.1R_{\text{vir}}$ and $2R_{\text{vir}}$. We found also a drastic change in the ionization properties, as the gas is more highly ionized at $R \sim R_{\text{vir}}$ than at $R < 0.2R_{\text{vir}}$. The LHW15 results strongly suggest that the CGM of M31 as seen in absorption of low ions (C II, Si II) through intermediate (Si III, Si IV) and high ions (C IV, O VI) is very extended out to at least the virial radius. However, owing to the small sample within R_{vir} , the variation of the column densities (N) and covering factors (f_c) with projected distances and azimuthal angle remain poorly constrained.

Our Project AMIGA (Absorption Maps In the Gas of Andromeda) is a large *HST* program (PID: 14268,

PI: Lehner) that aims to fill the CGM with 18 additional sightlines at various R and Φ within $1.1R_{\text{vir}}$ of M31 using high-quality COS G130M and G160M observations, yielding a sample of 25 background QSOs probing the CGM of M31. We have also searched MAST for additional QSOs beyond $1.1R_{\text{vir}}$ up to $R = 569$ kpc from M31 ($\sim 1.9R_{\text{vir}}$) to characterize the extended gas around M31 beyond its virial radius. This archival search yielded 18 suitable QSOs. Our total sample of 43 QSOs probing the CGM of a single galaxy from 25 to 569 kpc is the first to explore simultaneously the azimuthal and radial dependence of the kinematics, ionization level, surface-densities, and mass of the CGM of a galaxy over its entire virial radius and beyond. With these observations, we can also test how the CGM properties derived from one galaxy using multiple sightlines compares with a sample of galaxies with single sightline information and we can directly compare the results with cosmological zoom-in simulations.

With the COS G130M and G160M wavelength coverage, the key ions in our study are C II, C IV, Si II, Si III, Si IV (other ions and atoms include Fe II, S II, O I, N I, N V, but are typically not detected, although the limit on O I constrains the level of ionization). These species span ionization potentials from < 1 to ~ 4 Rydberg and thus trace neutral to highly ionized gas at a wide range of temperatures and densities. We have also searched the *Far Ultraviolet Spectroscopic Explorer* (*FUSE*) to have coverage of O VI, which resulted in 11 QSOs in our sample having both COS and *FUSE* observations. The H I Ly α absorption can unfortunately not be used because the MW dominates the entire Ly α absorption. Instead we have obtained deep H I 21-cm observations with the Robert C. Byrd Green Bank Telescope (GBT) toward all the targets in our sample and several additional ones (Howk et al. 2017, hereafter Paper I), showing no detection of any H I down to a level $N_{\text{HI}} \simeq 4 \times 10^{17} \text{ cm}^{-2}$ (5σ ; averaged over an area that is 2 kpc at the distance of M31). Our non-detections place a limit on the covering factor of such optically thick H I gas around M31 to $f_c < 0.051$ (at 90% confidence level) for $R \lesssim R_{\text{vir}}$.

This paper is organized as follows. In §2, we provide more information about the criteria used to assemble our sample of QSOs and explain the various steps to derive the properties (velocities and column densities) of the absorption. In that section, we also present the line identification for each QSO spectrum, which resulted in the identification of 5,642 lines. In §2.5, we explain in detail how we remove the foreground contamination from the Magellanic Stream (MS, e.g., Putman et al. 2003; Nidever et al. 2008; Fox et al. 2014), which extends to the

M31 CGM region of the sky with radial velocities that overlap with those expected from the CGM of M31. For this work, we have developed a more systematic and automated methodology than in LHW15 to deal with this contamination. In §3, we present the sample of the M31 dwarf satellite galaxies to which we compare the halo gas measurements. In §4, we derive the empirical properties of the CGM of M31 including how the column densities and velocities vary with R and Φ , the covering factors of the ions and how they change with R , and the metal and baryon masses of the CGM of M31. In §5, we discuss the results derived in §4 and compare them to observations from the COS-Halos survey (Tumlinson et al. 2013; Werk et al. 2014) and to state-of-the-art cosmological zoom-ins from in particular the Feedback in Realistic Environments (FIRE, Hopkins et al. 2019) and Figuring Out Gas & Galaxies In Enzo (FOG-GIE, Peebles et al. 2019) simulations projects. In §6, we summarize our main conclusions.

To properly compare to other work, and to simulations, we must estimate a characteristic radius for M31. We use the radius R_{200} enclosing a mean overdensity of 200 times the critical density: $R_{200} = (3M_{200}/4\pi\Delta\rho_{\text{crit}})^{1/3}$, where $\Delta = 200$ and ρ_{crit} is the critical density. For M31, we adopt $M_{200} = 1.26 \times 10^{12} M_{\odot}$ (e.g., Watkins et al. 2010; van der Marel et al. 2012), implying $R_{200} \simeq 230$ kpc. For the virial mass and radius (M_{vir} and R_{vir}), we use the definition that follows from the top-hat model in an expanding universe with a cosmological constant where $M_{\text{vir}} = 4\pi/3 \rho_{\text{vir}} R_{\text{vir}}^3$ where the virial density $\rho_{\text{vir}} = \Delta_{\text{vir}} \Omega_{\text{m}} \rho_{\text{crit}}$ (Klypin et al. 2011; van der Marel et al. 2012). The average virial overdensity is $\Delta_{\text{vir}} = 360$ assuming a cosmology with $h = 0.7$ and $\Omega_{\text{m}} = 0.27$ (Klypin et al. 2011). Following, e.g., van der Marel et al. (2012), $M_{\text{vir}} \simeq 1.2M_{200} \simeq 1.5 \times 10^{12} M_{\odot}$ and $R_{\text{vir}} \simeq 1.3R_{200} \simeq 300$ kpc. The escape velocity at R_{200} for M31 is then $v_{200} \simeq 212 \text{ km s}^{-1}$. A distance of M31 of $d_{\text{M31}} = 752 \pm 27$ kpc based on the measurements of Cepheid variables (Riess et al. 2012) is assumed throughout. We note that this distance is somewhat smaller than the other often adopted distance of M31 of 783 kpc (e.g., Brown et al. 2004; McConnachie et al. 2005), but for consistency with our previous survey as well as the original design of Project AMIGA, we have adopted $d_{\text{M31}} = 752$ kpc. All the projected distances were computed using the three dimensional separation (coordinates of the target and distance of M31).

2. DATA AND ANALYSIS

2.1. The Sample

The science goals of our *HST* large program require estimating the spatial distributions of the kinematics and metal column densities of the M31 CGM gas within about $1.1R_{\text{vir}}$ as a function of azimuthal angle and impact parameter. The search radius was selected based on our pilot study where we detected M31 CGM gas up to $\sim 1.1R_{\text{vir}}$, but essentially not beyond (LHW15) (a finding that we revisit in this paper with a larger archival sample, see below). With our *HST* program, we observed 18 QSOs at $R \lesssim 1.1R_{\text{vir}}$ that were selected to span the M31 projected major axis, minor axis, and intermediate orientations. The sightlines do not sample the impact parameter space or azimuthal distribution at random. Instead, the sightlines were selected to probe the azimuthal variations systematically. The sample was also limited by a general lack of identified UV-bright AGNs behind the northern half of M31s CGM owing to higher foreground MW dust extinction near the plane of the Milky Way disk. Combined with 7 archival QSOs, these sightlines probe the CGM of M31 in azimuthal sectors spanning the major and minor axes with a radial sample of 7–10 QSOs in each ~ 100 kpc bin in R .

In addition to target locations, the 18 QSOs were optimized to be the brightest available QSOs (to minimize exposure time) and to have the lowest available redshifts (in order to minimize the contamination from unrelated absorption from high redshift absorbers). For targets with no existing UV spectra prior to our observations, we also required that the GALEX NUV and FUV flux magnitudes are about the same to minimize the likelihood of an intervening Lyman limit system (LLS) with optical depth at the Lyman limit $\tau_{\text{LL}} > 2$. An intervening LLS could absorb more or all of the QSO flux we would need to measure foreground absorption in M31. This strategy successfully kept QSOs with intervening LLS out of the sample.

As we discuss below and as detailed by LHW15, the MS crosses through the M31 region of the sky at radial velocities that can overlap with those of M31 (see also Nidever et al. 2008; Fox et al. 2014). To understand the extent of MS contamination and the extended gas around M31 beyond the virial radius, we also searched for targets beyond $1.1R_{\text{vir}}$ with COS G130M and/or G160M data. This search identified another 18 QSOs at $1.1 \lesssim R/R_{\text{vir}} < 1.9$ that met the data quality criteria for inclusion in the sample¹. Our final sample consists

¹ This search found eight additional targets at $R > 1.6R_{\text{vir}}$ that are not included in our sample. SDSSJ021348.53+125951.4, 4C10.08, LBQS0052-0038 were excluded because of low S/N in the COS data. NGC7714 has smeared absorption lines. LBQS0107-0232/3/5 lie at $z_{\text{em}} \simeq 0.7$ –1 and have extremely complex spectra.

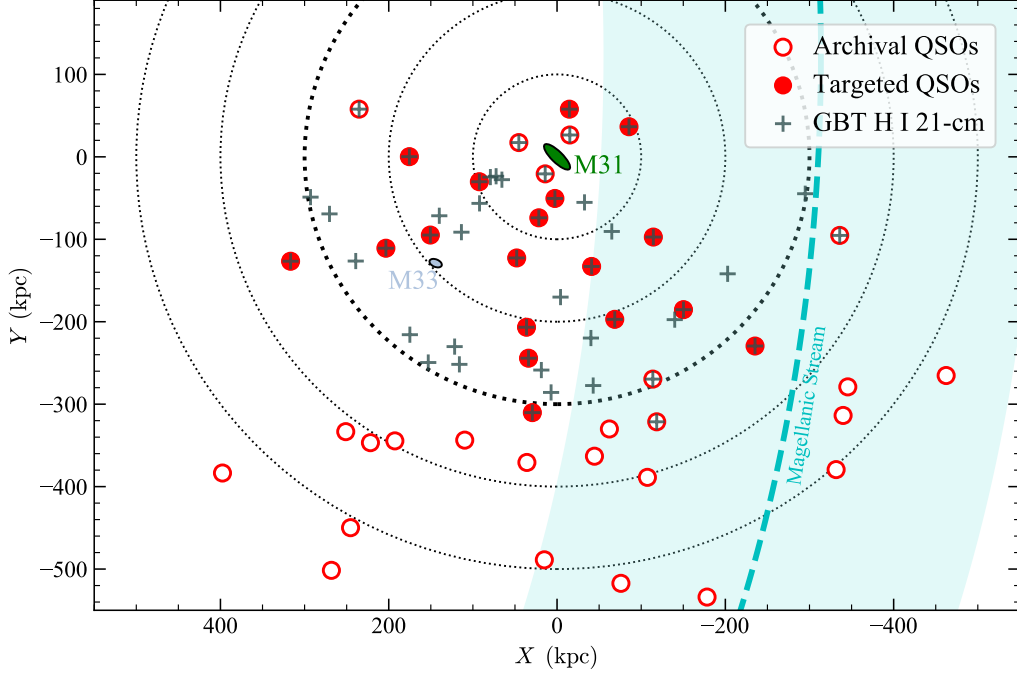


Figure 1. Locations of the Project AMIGA pointings relative to the M31–M33 system. The axes show the angular separations converted into physical coordinates relative to the center of M31. North is up and east to the left. The 18 sightlines from our large *HST* program are in red filled circles; the 25 archival COS targets are in open red circles. Crosses show the GBT H I 21-cm observations described in Paper I. Dotted circles show impact parameters $R = 100, 200, 300, 400, 500$ kpc. $R_{\text{vir}} = 300$ kpc is marked with a heavy dashed line. The sizes and orientations of the two galaxies are taken from RC3 (de Vaucouleurs et al. 1991) and correspond to the optical R_{25} values. The light blue dashed line shows the plane of the Magellanic Stream ($b_{\text{MS}} = 0^\circ$) as defined by Nidever et al. (2008). The shaded region within $b_{\text{MS}} \pm 20^\circ$ of the MS midplane is the approximate region where we identify most of the MS absorption components contaminating the M31 CGM absorption (see §2.5).

of 43 sightlines probing the CGM of M31 from 25 to 569 kpc; 25 of these probe the M31 CGM from 25 to 342 kpc, corresponding to $0.08 - 1.1R_{\text{vir}}$. Fig. 1 shows the locations of each QSO in the M31–M33 system (the filled circles being targets obtained as part of our *HST* program PID: 14268 and the open circles being QSOs with archival *HST* COS G130M/G160M data), and Table 1 lists the properties of our sample QSOs ordered by increasing projected distances from M31. In this table, we list the redshift of the QSOs (z_{em}), the J2000 right ascension (RA) and declination (Dec.), the MS coordinate ($l_{\text{MS}}, b_{\text{MS}}$, see Nidever et al. 2008 for the definition of this coordinate system), the radially (R) and cartesian (X, Y) projected distances, the program identification of the *HST* program (PID), the COS grating used for the observations of the targets, and the signal-to-noise ratio (SNR) per COS resolution element of the COS spectra near the Si III transition (except otherwise stated in the footnote of this table).

HS2154+2228 at $z_{\text{em}} = 1.29$ has no G130M wavelength coverage making the line identification highly uncertain.

2.2. UV Spectroscopic Calibration

To search for M31 CGM absorption and to determine the properties of the CGM gas, we use ions and atoms that have their wavelengths in the UV (see §2.4). Any transitions with $\lambda > 1144 \text{ \AA}$ are in the *HST* COS bandpass. All the targets in our sample were observed with *HST* using the COS G130M grating ($R_\lambda \approx 17,000$). All the targets observed as part of our new *HST* program were also observed with COS G160M, and all the targets but one within $R < 1.1R_{\text{vir}}$ have both G130M and G160M wavelength coverage.

We also searched for additional archival UV spectra in MAST, including the *FUSE* ($R_\lambda \approx 15,000$) archive to complement the gas-phase diagnostics from the COS spectra with information from the O VI absorption. We use the *FUSE* observations for 11 targets with adequate SNR near O VI (i.e., $\gtrsim 5$): RX J0048.3+3941, IRAS F00040+4325, MRK352, PG0052+251, MRK335, UGC12163, PG0026+129, MRK1502, NGC7469, MRK304, PG2349-014 (only the first 6 targets in this list are at $R \lesssim 1.1R_{\text{vir}}$). We did not consider *FUSE* data for quasars without COS observations because the available UV transitions in the

far-UV spectrum (O VI, C II, C III, Si II, Fe II) are either too weak or too contaminated to allow for a reliable identification of the individual velocity components in their absorption profiles.

There are also 3 targets (MRK335, UGC12163, and NGC7469) with *HST* STIS E140M ($R_\lambda \simeq 46,500$) observations that provide higher resolution information.²

Information on the design and performance of COS, STIS, *FUSE* can be found in Green et al. (2012), Woodgate et al. (1998), and Moos et al. (2000), respectively. For the *HST* data, we use the pipeline-calibrated final data products available in MAST. The *HST* STIS E140M data have an accurate wavelength calibration and the various exposure and echelle orders are combined into a single spectrum by interpolating the photon counts and errors onto a common grid, adding the photon counts and converting back to a flux.

The processing of the *FUSE* data is described in detail by Wakker et al. (2003) and Wakker (2006). In short, the spectra are calibrated using version 2.1 or version 2.4 of the *FUSE* calibration pipeline. The wavelength calibration of *FUSE* can suffer from stretches and misalignments. To correct for residual wavelength shifts, the central velocities of the MW interstellar lines are determined for each detector segment of each individual observation. The *FUSE* segments are then aligned with the interstellar velocities implied by the STIS E140M spectra or with the velocity of the strongest component seen in the 21-cm H I spectrum. Since the O VI absorption can be contaminated by H₂ absorption, we remove this contamination following the method described in Wakker (2006). This contamination can be removed fairly accurately with an uncertainty of about ± 0.1 dex on the O VI column density (Wakker et al. 2003).

For the COS G130M and G160M spectra, the spectral lines in separate observations of the same target are not always aligned, with misalignments of up to ± 40 km s⁻¹ that varying as function of wavelength. This is a known issue that has been reported previously (e.g., Savage et al. 2014; Wakker et al. 2015). While the COS team has improved the wavelength solution, we find that this problem can still be present sometimes. Since accurate alignment is critical for studying multiple gas-phases probed by different ions and since there is no way to determine *a priori* which targets are affected, we uniformly apply the Wakker et al. (2015) methodology to coadd the different exposures of the COS data

to ensure proper alignment of the absorption lines. In short, we identify the various strong ISM and IGM weak lines and record the component structures and identify possible contamination of the ISM lines by IGM lines. We cross-correlate each line in each exposure, using a ~ 3 Å wide region, and apply a shift as a function of wavelength to each spectrum. To determine the absolute wavelength calibration, we compare the velocity centroids of the Gaussian fits to the interstellar UV absorption lines (higher velocity absorption features being Gaussian fitted separately) and the H I emission observed from our 9' GBT H I survey (Paper I) or otherwise from 21-cm data from the Leiden/Argentine/Bonn (LAB) survey (Kalberla et al. 2005) or the Parkes Galactic All Sky Survey (GASS) (Kalberla et al. 2010). The alignment is coupled with the line identification into an iterative process to simultaneously determine the most accurate alignment and line identification (see §2.3). To combine the aligned spectra, we add the total counts in each pixel and then convert back to flux, using the average flux/count ratio at each wavelength (see also Tumlinson et al. 2011; Tripp et al. 2011); the flux error is estimated from the Poisson noise implied by the total count rate.

2.3. Line Identification

We are interested in the velocity range $-700 \leq v_{\text{LSR}} \leq -150$ km s⁻¹ where absorption from the M31 CGM may occur (see §2.4 for the motivation of this velocity range). It is straightforward to identify M31 absorption or its absence in this pre-defined velocity range, but we must ensure that there is either no contamination from higher redshift absorbers, or if there is, that we can correct for it.

For ions with multiple transitions, it is relatively simple to determine whether contamination is at play by comparing the column densities and the shapes of the velocity profiles of the available transitions. The profiles of atoms or ions with a single transition can be compared to other detected ions to check if there is some obvious contamination in the single transition absorption. However, some contamination may still remain undetected if it directly coincides with the absorption under consideration. Furthermore, when only a single ion with a single transition is detected (Si III $\lambda 1206$ being the prime example), the only method that determines if it is contaminated or not is to undertake a complete line identification of all absorption features in each QSO spectrum.

For the 18 targets in our large *HST* program, our instrument setup ensures that we have the complete wavelength coverage with no gap between 1140 and 1800 Å. As part of our target selection, we also favor QSOs at low

² For 2 targets, we also use COS G225M (3C454.3) and FOS NUV (3C454.3, PG0044+030) observations to help with the line identification (see §2.3). The data processing follows the same procedure as the other data.

redshift (44% are at $z_{\text{em}} \leq 0.1$, 89% at $z_{\text{em}} \leq 0.3$). This assures that Ly α remains in the observed wavelength range out to the redshift of the QSO (Ly α redshifts out the long end of the COS band at $z = 0.48$) and greatly reduces the contamination from EUV transitions in the COS bandpass. The combination of wavelength coverage and low QSO redshift ensures the most accurate line identification. At $R < 351$ kpc (i.e., $\lesssim 1.2R_{\text{vir}}$), 93% have Ly α coverage down to $z = z_{\text{em}}$ that remains in the observed wavelength range (one target has only observation of G130M and another QSO is at $z = 0.5$, see Table 1). On the other hand, for the targets at $R > 351$ kpc, the wavelength coverage is not as complete over 1140–1800 Å (55% of the QSOs have only 1 COS grating—all but one have G130M, and 4 QSOs have $z_{\text{em}} \gtrsim 0.48$). We note that the QSOs of 6/10 G130M observations have $z_{\text{em}} < 0.17$, setting all the Ly α transitions within the COS G130M bandpass.

The overall line identification process is as follows. First, we mark all the ISM absorption features (i.e., any absorption that could arise from the MW or M31) and the velocity components (which is done as part of the overall alignment of the spectra, see §2.2). Local (approximate) continua are fitted near the absorption lines to estimate the equivalent widths (W_λ) and their ratios for ions with several transitions are checked to determine if any are potentially contaminated. We then search for any absorption features at $z = z_{\text{em}}$, again identifying any velocity component structures in the absorption. We then identify possible Ly α absorption and any other associated lines (other H I transitions and metal transitions) from the redshift of QSO down to $z = 0$. In each case, if there are simultaneous detections of Ly α , Ly β , and/or Ly γ (and weaker transitions), we check that the equivalent width ratios are consistent. If there are any transitions left unidentified, we check whether it could be O VI $\lambda\lambda 1031, 1037$ as this doublet can be sometimes detected without any accompanying H I (Tripp et al. 2008). Finally we check that the alignment in each absorber with multiple detected absorption lines is correct or whether it needs some additional adjustment.

In the region $R \lesssim 1.1R_{\text{vir}}$ and for 84% of the sample at any R , we believe the line identifications are reliable and accurate at the 98% confidence level. In the Appendix, we provide some additional information regarding the line identification, in particular for the troublesome cases. We also make available in a machine-readable format the full line identification for all the targets listed in Table 1 (see Appendix A).

2.4. Determination of the Properties of the Absorption at $-700 \leq v_{\text{LSR}} \leq -150 \text{ km s}^{-1}$

Our systematic search window for absorption that may be associated with the CGM of M31 is $-700 \leq v_{\text{LSR}} \leq -150 \text{ km s}^{-1}$ (LHW15). The -700 km s^{-1} cutoff corresponds to about -100 km s^{-1} less than the most negative velocities from the rotation curve of M31 ($\sim -600 \text{ km s}^{-1}$, see Chemin et al. 2009). The -150 km s^{-1} cutoff is set by the MW lines that dominate the absorption in the velocity range $-150 \lesssim v_{\text{LSR}} \lesssim +50 \text{ km s}^{-1}$. The $-100 \lesssim v_{\text{LSR}} \lesssim -50 \text{ km s}^{-1}$ range is dominated by low and intermediate-velocity clouds that are observed in and near the Milky Way disk. Galactic high-velocity clouds (HVCs) down to velocities $v_{\text{LSR}} \sim -150 \text{ km s}^{-1}$ further above the MW disk have also been observed toward distant Galactic halo stars in the general direction of M31 (Lehner et al. 2015, 2012; Lehner & Howk 2011). Since the M31 disk rotation velocities extend to about -150 km s^{-1} in the northern tip of M31, there is a small window that is inaccessible for studying the CGM of M31 (see also Lehner et al. 2015 and §3.2).

To search for M31 CGM gas and determine its properties, we use the following atomic and ionic transitions: O I $\lambda 1302$, C II $\lambda\lambda 1036, 1334$, C IV $\lambda\lambda 1548, 1550$, Si II $\lambda\lambda 1190, 1193, 1260, 1304, 1526$ Si III $\lambda 1206$, Si IV $\lambda\lambda 1393, 1402$, O VI $\lambda 1031$, Fe II $\lambda\lambda 1144, 1608$, Al II $\lambda 1670$. We also report results (mostly upper limits on column densities) for N V $\lambda\lambda 1238, 1242$, N I $\lambda 1199$ (N I $\lambda\lambda 1200, 1201$ being typically blended in the velocity range of interest $-700 \leq v_{\text{LSR}} \leq -150 \text{ km s}^{-1}$), P II $\lambda 1301$, S III $\lambda 1190$, and S II $\lambda\lambda 1250, 1253, 1259$.

To determine the column densities and velocities of the absorption, we use the apparent optical depth (AOD) method (see §2.4.2), but in the Appendix D we confront the AOD results with measurements from Voigt profile fitting (see also §2.4.3). As much as possible at COS resolution, we derive the properties of the absorption in individual components. Especially toward M31, this is important since along the same line of sight in the velocity window $-700 \leq v_{\text{LSR}} \leq -150 \text{ km s}^{-1}$, there can be multiple origins of the gas (including the CGM of M31 or MS, see Fig. 1 and LHW15) as we detail in §2.5. However, the first step to any analysis of the absorption imprinted on the QSO spectra is to model the QSO’s continuum.

2.4.1. Continuum Placement

To fit the continuum near the ions of interest, we generally use the automated continuum fitting method developed for the COS CGM Compendium (CCC, Lehner et al. 2018). Fig. 3 in Lehner et al. (2018) shows an example of an automatic continuum fit. In short, the continuum is fitted near the absorption features using Legendre polynomials. A velocity region of about ± 1000 –

2000 km s⁻¹ around the relevant absorption transition is initially considered for the continuum fit, but could be changed depending on the complexity of the continuum placement in this region. In all cases the interval for continuum fitting is never larger than ± 2000 km s⁻¹ or smaller than ± 250 km s⁻¹. Within this pre-defined region, the spectrum is broken into smaller sub-sections and then rebinned. The continuum is fitted to all pixels that did not deviate by more than 2σ from the median flux, masking pixels from the fitting process that may be associated with small-scale absorption or emission lines. Legendre polynomials of orders between 1 and 5 are fitted to the unmasked pixels, with the goodness of the fit determining the adopted polynomial order. Typically the adopted polynomials are of orders between 1 and 3 owing to the relative simplicity of the QSO continua when examined over velocity regions of 500–4000 km s⁻¹. The only systematic exception is Si III where the polynomial order is always between 2–3 and 5 owing to this line being in the wing of the broad local Ly α absorption profile.

This procedure is applied to our pre-defined set of transitions, with the continuum defined locally for each. Each continuum model is visually inspected for quality control. In a few cases, the automatic continuum fitting fails owing to a complex continuum (e.g., near the peak of an emission line or where many absorption lines were present within the pre-defined continuum window). In these cases, we first try to adjust the velocity interval of the spectrum to provide better-constrained fits; if that still fails, we manually select the continuum region to be fitted.

2.4.2. Velocity Components and AOD Analysis

The next step of the analysis is to determine the velocity components and integrate them to determine the average central velocities and column densities for each absorption feature. In Fig. 2, we show an example of the normalized velocity profiles. In the supplemental material, we provide a similar figure for each QSO in our sample. Although we systematically search for absorption in the full velocity range $-700 \leq v_{\text{LSR}} \leq -150$ km s⁻¹, the most negative velocity of detected absorption in our sample is $v_{\text{LSR}} = -508$ km s⁻¹; that is, we do not detect any M31 absorption in the range $-700 \lesssim v_{\text{LSR}} \lesssim -510$ km s⁻¹. In Fig. 2, MW absorption at $-100 \lesssim v_{\text{LSR}} \lesssim 100$ km s⁻¹ is clearly seen in all species but N V. Absorption observed in the $-510 \leq v_{\text{LSR}} \leq -150$ km s⁻¹ that is not color-coded is produced by higher-redshift absorbers or other MW lines.

To estimate the column density in each observed component, we use the AOD method (Savage & Sembach

1991). In this method, the absorption profiles are converted into apparent optical depth per unit velocity, $\tau_a(v) = \ln[F_c(v)/F_{\text{obs}}(v)]$, where $F_c(v)$ and $F_{\text{obs}}(v)$ are the modeled continuum and observed fluxes as a function of velocity. The AOD, $\tau_a(v)$, is related to the apparent column density per unit velocity, $N_a(v)$, through the relation $N_a(v) = 3.768 \times 10^{14} \tau_a(v) / (f \lambda (\text{\AA}))$ cm⁻² (km s⁻¹)⁻¹, where f is the oscillator strength of the transition and λ is the wavelength in \AA . The total column density is obtained by integrating the profile over the pre-defined velocity interval, $N = \int_{v_1}^{v_2} N_a(v) dv$, where $[v_1, v_2]$ are the boundaries of the absorption. We estimate the line centroids with the first moment of the AOD $v_a = \int v \tau_a(v) dv / \int \tau_a(v) dv$ km s⁻¹. As part of this process, we also estimate the equivalent widths, which we use mainly to determine if the absorption is detected at the $\geq 2\sigma$ level. In cases where the line is not detected at $\geq 2\sigma$ significance, we quote a 2σ upper limit on the column density, which is defined as twice the 1σ error derived for the column density assuming the absorption line lies on the linear part of the curve of growth.

For features that are detected above the 2σ level, the estimated column densities are stored for further analysis. Since we have undertaken a full identification of the absorption features in each spectrum (see §2.3, Appendix A), we can reliably assess if a given transition is contaminated using in particular the conflict plots described in the Appendix (see Appendix B). If there is evidence of some line contamination and several transitions are available for this ion (e.g., Si II, Si IV, C IV), we exclude it from our list.

We find contamination affects the Si III and C II in the velocity range $-700 \leq v_{\text{LSR}} \leq -150$ km s⁻¹ in a few rare cases (6 components of Si III and 3 components of C II $\lambda 1334$).³ For all but one of these contaminated Si III components, we can correct the contamination because the interfering line is a Lyman series line from a higher redshift and the other H I transitions constrain the equivalent width of the contamination. The one case we cannot correct this way is the -340 km s⁻¹ component toward PHL1226 (see also Appendix A), which is associated with the MS. In the footnote of Table 2, we list the ions that are found to be contaminated at some level. For any column density that is corrected for contamination, the typical correction error is about 0.05–0.10 dex depending on the level of contamination as well as the SNRs of the spectrum in that region.

³ Toward RXJ0048.3+3941, C II $\lambda 1334$ is contaminated in the third component, but C II $\lambda 1036$ is available to correct for it in this case.

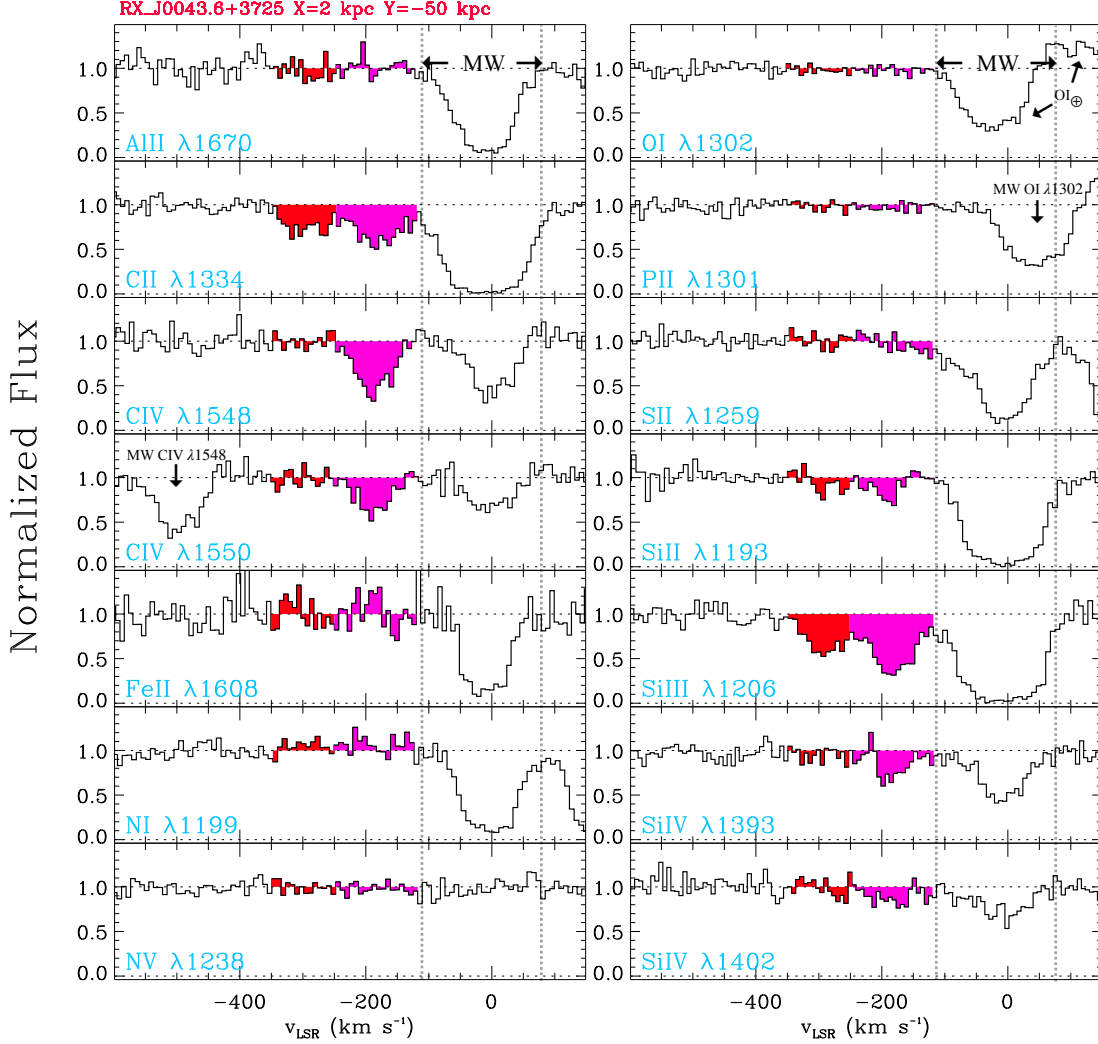


Figure 2. Example of normalized absorption lines as a function of the LSR velocity toward RX_J0043.6+3725 showing the typical atoms and ions probed in our survey. High negative velocity components likely associated with M31 are shown in colors, and each color represents a different component identified at the COS G130M-G160M resolution. In this case, significant absorption is observed in the two identified components in C II, Si II, and Si III. Higher ions (Si IV, C IV) are observed in only one of the components, showing a change in the ionization properties with velocity. Some species are not detected, but their limits can still be useful in assessing the physical properties of the gas. The MW absorption is indicated between the two vertical dotted lines and is observed in all the species but N V. At $v_{\text{LSR}} \gtrsim -100 \text{ km s}^{-1}$, airglow emission lines can contaminate O I, and hence the MW absorption is contaminated, but typically that is not an issue for the surveyed velocity range $-700 \leq v_{\text{LSR}} \leq -150 \text{ km s}^{-1}$.

The last step is to check for any unresolved saturation. When the absorption is clearly saturated (i.e., the flux level reaches zero-flux in the core of the absorption), the line is automatically marked as saturated and a lower limit is assigned to the column density. In §2.5, we will show how we separate the MS from the M31 CGM absorption, but we note that only the Si III components associated with the MS and the MW have their absorption reaching zero-flux level, not the components associated with the CGM of M31.

When the flux does not reach a zero-flux level, the procedure for checking saturation depends on the number of

transitions for a given ion or atom. We first consider ions with several transitions (Si II, C IV, Si IV, sometimes C II) since they can provide information about the level of saturation for a given peak optical depth. For ions with several transitions, we compare the column densities with different $f\lambda$ -values to determine whether there is a systematic decrease in the column density as $f\lambda$ increases. If there is not, we estimate the average column density using all the available measurements and propagate the errors using a weighted mean. For the Si II transitions, Si II $\lambda 1526$ shows no evidence for saturation when detected based on the comparison with stronger

transitions while Si II $\lambda 1260$ or $\lambda 1193$ can be saturated if the peak optical $\tau_a \gtrsim 0.9$. For doublets (e.g., C IV, Si IV), we systematically check if the column densities of each transition agree within 1σ error; if they do not and the weak transition gives a higher value (and there is no contamination in the weaker transition), we correct for saturation following the procedure discussed in [Lehner et al. \(2018\)](#) (and see also [Savage & Sembach 1991](#)). For C IV and Si IV, there is rarely any evidence for saturation (we only correct once for saturation of C IV in the third component observed in the MRK352 spectrum; in that component the peak optical $\tau_a \sim 0.9$). For single strong transitions (in particular Si III and often C II), if the peak optical depth is $\tau_a > 0.9$, we conservatively flag the component as saturated and adopt a lower limit for that component. We adopt $\tau_a > 0.9$ as the threshold for saturation based on other ions with multiple transitions (in particular Si II) where the absorption starts to show some saturation at this peak optical depth.

To estimate how the column density of silicon varies with R (which has a direct consequence for the CGM mass estimates derived from silicon in §§4.5 and 4.8), it is useful to assess the level of saturation of Si III, which is the only silicon ion that cannot be directly corrected for saturation⁴. The lower limits of the Si III components associated with the CGM of M31 are mostly observed at $R \lesssim 140$ kpc (only 2 are observed at $R > 140$ kpc), but they do not reach zero-flux level; these components are conservatively marked as saturated because their peak apparent optical depth is $\tau_a > 0.9$ (not because $\tau_a \gg 2$) and because the comparison between the different Si II transitions show in some cases evidence for saturation (see above). Hence the true values of the column densities of these saturated components is most likely higher than the adopted lower-limit values but are very unlikely to be overestimated by a factor $\gg 3$ –4. We can estimate how large the saturation correction for Si III might be using the strong Si II lines (e.g., Si II $\lambda 1193$ or Si II $\lambda 1260$) compared to the weaker ones (e.g., Si II $\lambda 1526$). Going through the 8 sightlines showing some saturation in the components of Si III associated with the CGM of M31 (see Table 2), for all the targets beyond 50 kpc, the saturation correction is likely to be small < 0.10 – 0.15 dex based on the fact that many show no evidence of saturation in Si II $\lambda 1260$ (when there is no contamination for this transition) or Si II $\lambda 1193$. On the other hand, for the two most inner targets, the saturation cor-

rection is at least 0.3 dex and possibly as large as 0.6 dex based on the column density comparison between saturated Si II and weaker, unsaturated transitions. The latter would put $N_{\text{Si}} \simeq 14.5$ close to the maximum values derived with photoionization modeling in the COS-Halos sample (see §5.2). Therefore for the components associated with the CGM of M31 at $R > 50$ kpc when we estimate the functional form of N_{Si} with R , we adopt an increase of 0.1 dex of the lower limits. For the two inner targets at $R < 50$ kpc, we explore how an increase of 0.3 and 0.6 dex affects the estimation of $N_{\text{Si}}(R)$.

2.4.3. High Resolution Spectra and Profile Fitting Analysis

In the Appendices C and D we explore the robustness of the AOD results by comparing high- and low-resolution spectra and by comparing to a Voigt profile fitting analysis. There is good overall agreement in the column densities derived from the STIS and COS data and our conservative choice of $\tau_a \sim 0.9$ as the threshold for saturation in the COS data is adequate (see Appendix C). For the profile fitting analysis, we consider the most complicated blending of components in our sample and demonstrate there are some small systematic differences between the AOD and PF derived column densities (see Appendix D). However these difference are small and a majority of our sample is not affected by heavy blending. Hence the AOD results are robust and are adopted for the remaining of the paper.

2.5. Correcting for Magellanic Stream Contamination

Prior to determining the properties of the gas associated with the CGM of M31, we need to identify that gas and distinguish it from the MW and the MS. We have already removed from our analysis any contamination from higher redshift intervening absorbers and any contamination from the MW (defined as $-150 \lesssim v_{\text{LSR}} \lesssim 100 \text{ km s}^{-1}$). However, as shown in Fig. 1 and discussed in [LHW15](#), the MS is another potentially large source of contamination: in the direction of M31, the velocities of the MS can overlap with those expected from the CGM of M31. The targets in our sample have MS longitudes and latitudes in the range $-132^\circ \leq l_{\text{MS}} \leq -86^\circ$ and $-14^\circ \leq b_{\text{MS}} \leq +41^\circ$. The H I 21-cm emission GBT survey by [Nidever et al. \(2010\)](#) finds that the MS extends to about $l_{\text{MS}} \simeq -140^\circ$. Based on this and previous H I emission surveys, [Nidever et al. \(2008, 2010\)](#) found a relation between the observed LSR velocities of the MS and l_{MS} that can be used to assess contamination in our targeted sightlines based on their MS coordinates. Using Fig. 7 of [Nidever et al. \(2010\)](#), we estimate the upper and lower boundaries of the H I velocity range as a function of l_{MS} , which we show in Fig. 3 by the curve

⁴ Some of the Si II transitions (especially, Si II $\lambda\lambda 1193, 1260$) have evidence for saturation, but weaker transitions are always available (e.g., Si II $\lambda 1526$), and therefore we can determine a robust value of the column density of Si II.

colored area. The MS velocity decreases with decreasing l_{MS} up to $l_{\text{MS}} \simeq -120^\circ$ where there is an inflection point where the MS LSR velocity increases. We note that the region beyond $l_{\text{MS}} \lesssim -135^\circ$ is uncertain but cannot be larger than shown in Fig. 3 (see also Nidever et al. 2010)—however, this does not affect our survey since all our data are at $l_{\text{MS}} \gtrsim -132^\circ$.

We take a systematic approach to removing the MS contamination that does not reject entire sightlines based on their MS coordinates. Not all velocity components may be contaminated even on sightlines close to the MS. In Fig. 3, we show LSR velocity of the Si III components as a function of the MS longitude. We choose Si III as this ion is the most sensitive to detect both weak and strong absorption and is readily observed the physical conditions of the MS and M31 CGM (Fox et al. 2014; Lehner et al. 2015). We consider the individual components as for a given sightline, several components can be observed falling in or outside the boundary region associated with the MS as illustrated in Fig. 3. We find that $28/74 \simeq 38\%$ of the detected Si III components are within MS boundary region shown in Fig. 3. We note that changing the upper boundary by $\pm 5 \text{ km s}^{-1}$ would change this number by about $\pm 3\%$.

To our own sample, we also add data from two different surveys: the *HST*/COS MS survey by Fox et al. (2014) and the M31 dwarfs (McConnachie 2012 and see §3). For the MS survey, we restrict the sample $-150^\circ \leq l_{\text{MS}} \leq -20^\circ$, i.e., overlapping with our sample but also including higher l_{MS} value while still avoiding the Magellanic Clouds region where conditions may be different. The origin of the sample for the M31 dwarf galaxies is fully discussed in §3. The larger galaxies M33, M32, and NGC 205 are excluded here from that sample as their large masses are not characteristic. The LSR velocities of the M31 dwarfs as a function of l_{MS} are plotted with a star symbol in Fig. 3. For the MS survey, we select the LSR velocities of Si III for the MS survey (note these are average velocities that can include multiple components), which are shown with squares in Fig. 3. Most ($\sim 90\%$) of the squares fall between the two curves in Fig. 3, confirming the likelihood that these sightlines probe the MS (although we emphasize that this test was not initially used by Fox et al. 2014 to determine the association with the MS).

The M31 dwarf galaxies are of course not affected by the MS, but can help us to determine how frequently they fall within the velocity range where MS contamination is likely. For $l_{\text{MS}} \gtrsim -132^\circ$ (where all the QSOs are and to avoid the uncertain region), only 9% (2/22) of the dwarfs are within the velocity region where MS contamination occurs. If the velocity distributions of the

M31 dwarfs and M31 CGM gas are similar, this would strongly suggest that velocity components with the expected MS velocities are indeed more likely associated with the MS. We, however, note two additional dwarfs are close to the upper boundary, which would change the frequency of the dwarfs in the MS velocity-boundary region to 18%.

Observations of H I 21-cm emission toward the QSOs observed with COS in MS survey (Fox et al. 2014) and Project AMIGA (Howk et al. 2017) show only H I detections within $|b_{\text{MS}}| \lesssim 11^\circ$. In the region defined by $-150^\circ \leq l_{\text{MS}} \leq -20^\circ$, the bulk of the H I 21-cm emission is observed within $|b_{\text{MS}}| \lesssim 5^\circ$ (Nidever et al. 2010). We therefore expect the metal ionic column densities to have a strong absorption when $|b_{\text{MS}}| \lesssim 10^\circ$ and a weaker absorption as $|b_{\text{MS}}|$ increases. In Fig. 4, we show the total column densities of Si III for the velocity components from the Project AMIGA sample found within the MS boundary region shown in Fig. 3, i.e., we added the column densities of the components that are likely associated with the MS. We also show in the same figure the results from the Fox et al. (2014) survey. Both datasets show the same behavior of the total Si III column densities with $|b_{\text{MS}}|$, an overall decrease in $N_{\text{Si III}}$ as $|b_{\text{MS}}|$ increases. Treating the limits as values, combining the two samples, and using the Spearman rank order, the test confirms the visual impression that there is a strong monotonic anti-correlation between $N_{\text{Si III}}$ and $|b_{\text{MS}}|$ with a correlation coefficient $r_s = -0.72$ and a p-value $\ll 0.1\%$.⁵ There is a large scatter (about ± 0.4 dex around the dotted line) at any b_{MS} , making it difficult to determine if any data points may not be associated with the MS (as, e.g., the three very low $N_{\text{Si III}}$ at $12^\circ < |b_{\text{MS}}| < 18^\circ$ from our sample or the very high value at $|b_{\text{MS}}| \sim 27^\circ$ from the Fox et al. 2014 sample).

In Fig. 5, we show the individual column densities of Si III as a function of the impact parameter from M31 for the Project AMIGA sightlines where we separate components associated with the MS from those that are not. Looking at Figs. 1 and 4, we expect the strongest column densities associated with the MS to be at $|b_{\text{MS}}| \lesssim 10^\circ$ and $R \gtrsim 300$ kpc, which is where they are located on Fig. 5. We also expect a positive correlation between $N_{\text{Si III}}$ and R for the MS contaminated components while for uncontaminated components, we expect the opposite (see LHW15). Treating again limits as values, the Spearman rank order test demonstrates a strong monotonic correlation between $N_{\text{Si III}}$ and R

⁵ We note that if we increase the lower limits by 0.15 dex or more and similarly decrease the upper limits, the significance of the anti-correlation would be similar.

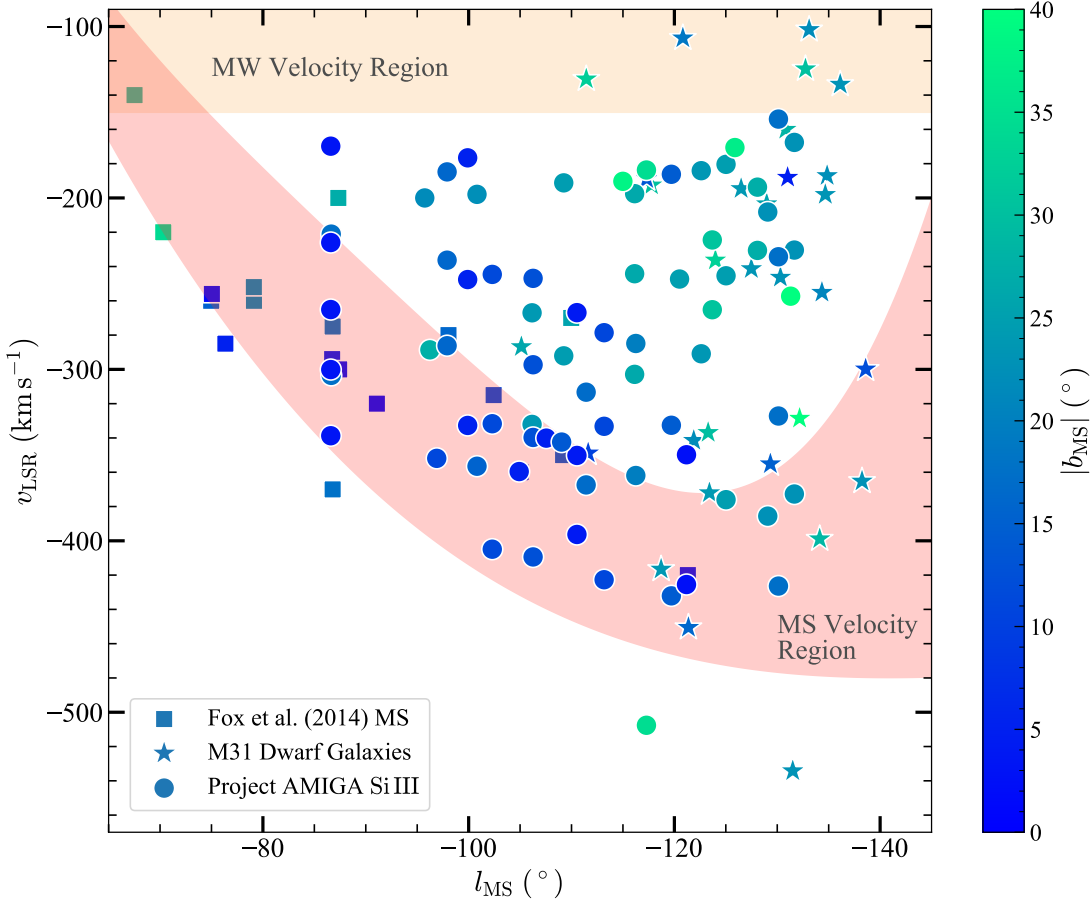


Figure 3. The LSR velocity of the Si III components (circles) observed in our sample as a function of the MS longitude l_{MS} , color-coded according to the absolute MS latitude. Shaded regions show the velocities that can be contaminated by the MS and MW (by definition of our search velocity window, any absorption at $v_{\text{LSR}} > -150 \text{ km s}^{-1}$ was excluded from our sample). We also show the data (squares) from the MS survey from Fox et al. (2014) and the radial velocities of the M31 dwarf galaxies (stars).

($r_s = 0.68$ with $p \ll 0.1\%$) while for uncontaminated components there is a strong monotonic anti-correlation ($r_s = -0.57$ with $p \ll 0.1\%$), in agreement with the expectations. Based on these results, it is therefore reasonable to consider any absorption components observed in the COS spectra within the MS boundary region defined in Fig. 3 as most likely associated with the MS. We therefore flag any of these components (28 out of 74 components for Si III) as contaminated by the MS and those are not included further in our sample.

Finally, we noted above that only a small fraction of the dwarfs are found in the MS contaminated region. While that fraction is small (9%), this could still suggest that in the MS contaminated region, some of the absorption could be a blend between of both MS and M31 CGM components. However, considering the uncontaminated velocities along sightlines in (29 components) and outside (17 components) the contaminated regions, with p -value of 0.74 the Kolmogorov-Smirnov

(KS) comparison of the two samples cannot reject the null-hypothesis that the distributions are the same. This strongly suggests that the correction from the MS contamination does not bias much the velocity distribution associated with the CGM of M31 (assuming that there is no strong change of the velocity with the azimuth Φ ; as we explore this further in §§3.2 and 4.10, there is, however, no strong evidence a velocity dependence with Φ).

3. M31 DWARF GALAXY SATELLITES

While Project AMIGA is dedicated to understanding the CGM of M31, our survey also provides a unique probe of the dwarf galaxies found in the halo of M31. In particular, we have the opportunity to assess if the CGM of dwarf satellites plays an important role in the CGM of the host galaxy, as studied by cosmological and idealized simulations (e.g. Anglés-Alcázar et al. 2017; Hafen et al. 2019a,b; Bustard et al. 2018). When con-

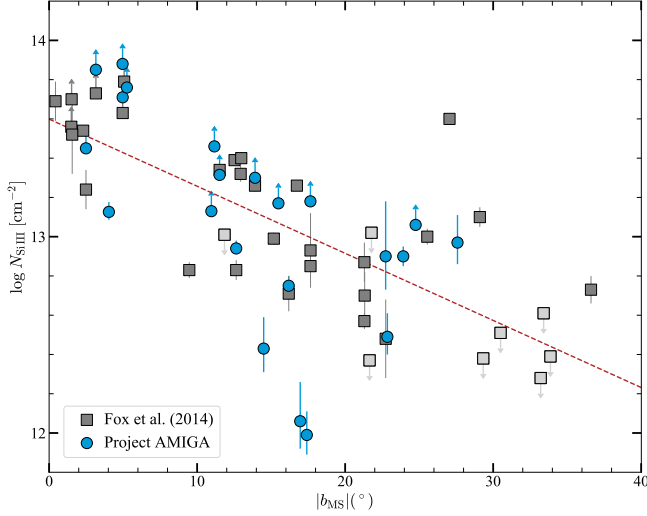


Figure 4. The total column density of Si III that are associated with the MS as a function of the absolute MS latitude. We also show the MS survey by Fox et al. (2014) restricted to data with $-150^\circ \leq l_{\text{MS}} \leq -20^\circ$. The lighter gray squares with downward arrows are non-detections in the Fox et al. sample. The dashed line is a linear fit to the data treating the limits as values. A Spearman ranking correlation test implies a strong anti-correlation with a correlation coefficient $r_s = -0.72$ and $p \ll 0.1\%$.

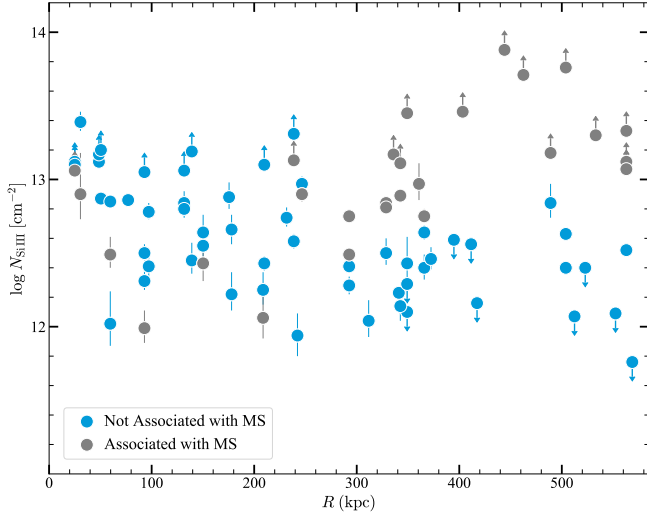


Figure 5. Logarithm of the column densities of the individual components for Si III as a function of the projected distances from M31 of the background QSOs where the separation is made for the components associated or not with the MS.

sidering the dwarf galaxies in our analysis we have two main goals: 1) to determine if the velocity distribution of the dwarfs and the absorbers are similar, and 2) assess if some of absorption observed toward the QSOs could

be associated directly with the dwarfs, either as gas that is gravitationally bound or recently stripped.

The sample for the M31 dwarf galaxies is mostly drawn from the McConnachie (2012) study of Local Group dwarfs, in which the properties of 29 M31 dwarf satellites were summarized. Four additional dwarfs (Cas II, Cas III, Lac I, Per I) are added from recent discoveries (Collins et al. 2013; Martin et al. 2014, 2016, 2017). M33 is excluded from that sample as its large mass is not characteristic of satellites.⁶ Table 3 summarizes our adopted sample of M31 dwarf galaxies (sorted by increasing projected distance from M31), listing some of their key properties. As listed in this table, most of the M31 satellite galaxies are dwarf spheroidal (dSph) galaxies, which have been shown to have been stripped of most of their gas most likely via ram-pressure stripping (Grebel et al. 2003), a caveat that we keep in mind as we associate these galaxies with absorbers.

3.1. Velocity Transformation

So far we have used LSR velocity to characterize MW and MS contamination of gas in the M31 halo. However, as we now consider relative motions over 30° on the sky, we cannot simply subtract M31’s systemic radius velocity to place these relative motions in the correct reference frame. Over such large sky areas, tangential motion must be accounted for because the “systemic” sightline velocity of the M31 system changes with sightline. To eliminate the effects of “perspective motion”, we follow Gilbert et al. (2018) (and see also Veljanoski et al. 2014) by first transforming the heliocentric velocity (v_\odot) into the Galactocentric frame, v_{Gal} , which removes any effects the solar motion could have on the kinematic analysis. We converted our measured radial velocities from the heliocentric to the Galactocentric frame using the relation from Courteau & van den Bergh (1999) with updated solar motions from McMillan (2011) and Schönrich et al. (2010):

$$v_{\text{Gal}} = v_\odot + 251.24 \sin(l) \cos(b) + 11.1 \cos(l) \cos(b) + 7.25 \sin(b), \quad (1)$$

where (l, b) are the Galactic longitude and latitude of the object. To remove the bulk motion of M31 along the sightline to each object, we use the heliocentric systemic radial velocity for M31 of -301 km s^{-1} (van der Marel & Guhathakurta 2008; Chemin et al. 2009), which is $v_{\text{M31,r}} = -109 \text{ km s}^{-1}$ in the Galactocentric velocity frame. The systemic transverse velocity of M31 is

⁶ In Appendix E, we further discuss and present some evidence that the CGM of M33 is unlikely to contribute much to the observed absorption in our sample.

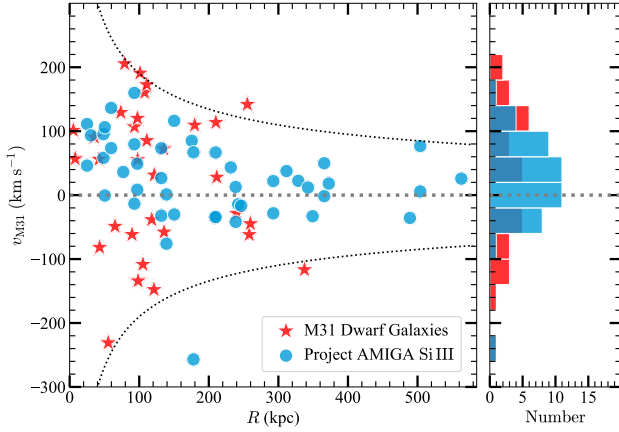


Figure 6. *Left:* The M31 peculiar velocity (as defined by Eqn. 2) against the projected distances for the observed absorption components associated with M31 (using Si III) and M31 dwarf galaxies. The dotted curves show the escape velocity divided by $\sqrt{3}$ to account for the unknown tangential motions of the absorbers and galaxies. *Right:* The M31 velocity distributions with the same color-coding definition.

$v_{\text{M31,t}} = -17 \text{ km s}^{-1}$ in the direction on the sky given by the position angle $\theta_t = 287^\circ$ (van der Marel et al. 2012). The removal of M31’s motion from the sightline velocities resulting in peculiar line-of-sight velocities for each absorber or dwarf, v_{M31} , is then given by (van der Marel & Guhathakurta 2008):

$$v_{\text{M31}} = v_{\text{Gal}} - v_{\text{M31,r}} \cos(\rho) + v_{\text{M31,t}} \sin(\rho) \cos(\phi - \theta_t), \quad (2)$$

where ρ is the angular separation between the center of M31 to the QSO or dwarf position, ϕ the position angle of the QSO or dwarf with respect to M31’s center. We note that the transverse term in Eqn. 2 is more uncertain (van der Marel & Guhathakurta 2008; Veljanoski et al. 2014), but its effect is also much smaller, and indeed including it or not would not quantitatively change the results; we opted to include that term in the velocity transformation. We apply these transformations to change the LSR velocities to heliocentric velocities to Galactocentric velocities to peculiar velocities for each component observed in absorption toward the QSOs and for each dwarf. With this transformation, an absorber or dwarf with no peculiar velocity relative to M31’s bulk motion has $v_{\text{M31}} = 0 \text{ km s}^{-1}$, regardless of its position on the sky (Gilbert et al. 2018).

3.2. Velocity Distribution

In Fig. 6, we compare the M31 peculiar velocities of the absorbers using Si III and dwarfs against the projected distance (see §3.1). In Fig. 6, we also show the

expected escape velocity, v_{esc} , as a function of R for a $1.3 \times 10^{12} M_\odot$ point mass. We conservatively divide v_{esc} by $\sqrt{3}$ in that figure to account for remaining unconstrained projection effects. Nearly all the CGM gas traced by Si III within R_{vir} is found at velocities consistent with being gravitationally bound, and this is true even at larger R for most of the absorbers. This finding also holds for most of the dwarf galaxies, and, as demonstrated by McConnell (2012), it holds when the galaxies’ 3D distances are used (i.e., using the actual distance of the dwarf galaxies, instead of the projected distances used in this work). Therefore, both the CGM gas and galaxies probed in our sample at both small and large R are consistent with being gravitationally bound to M31.

Fig. 6 also informs us that the dwarf satellite and CGM gas velocities overlap to a high degree but do not follow identical distributions. The mean and standard deviation of the M31 velocities for the dwarfs are $+34.2 \pm 110.0 \text{ km s}^{-1}$ and $+36.6 \pm 68.0 \text{ km s}^{-1}$ for the CGM gas. There is therefore a slight asymmetry favoring more positive peculiar motions. A simple two-sided KS test of the two samples rejects the null hypothesis that the distributions are the same at 95% level confidence ($p = 0.04$). And indeed while the two distributions overlap and the means are similar, the velocity dispersion of the dwarfs is larger than that of the QSO absorbers. For the QSO absorbers, all the components but one have their M31 velocities in the interval $-80 \leq v_{\text{M31}} \leq +160 \text{ km s}^{-1}$, but 9/32 (28%) of the dwarfs are outside that range. Four of the dwarfs are in the range $+160 < v_{\text{M31}} \leq +210 \text{ km s}^{-1}$, a velocity interval that cannot be probed in absorption owing to foreground MW contamination. The other five dwarfs have $v_{\text{M31}} < -80 \text{ km s}^{-1}$, while only one out of 46 Si III components (2%) have $v_{\text{M31}} < -80 \text{ km s}^{-1}$. Both the small fraction of dwarfs at $v_{\text{M31}} > +160 \text{ km s}^{-1}$ and $v_{\text{M31}} < -80 \text{ km s}^{-1}$ and the even smaller fraction of absorbers at $v_{\text{M31}} < -80 \text{ km s}^{-1}$ suggest that there is no important population of absorbers at the inaccessible velocities $v_{\text{M31}} > +160 \text{ km s}^{-1}$ (see also §2.5).

3.3. The Associations of Absorbers with Dwarf Satellites

Using the information from Table 3, we cross-match the sample of dwarf galaxies and QSOs to determine the QSO sightlines that are passing within a dwarf’s R_{200} radius. There are 11 QSOs (with 58 Si III components) within R_{200} of 16 dwarfs. In Table 4, we summarize the results of this cross-match. Fig. 7, we show the map of the QSOs and dwarf locations in our survey where the M31 velocities of the Si III components and dwarfs are

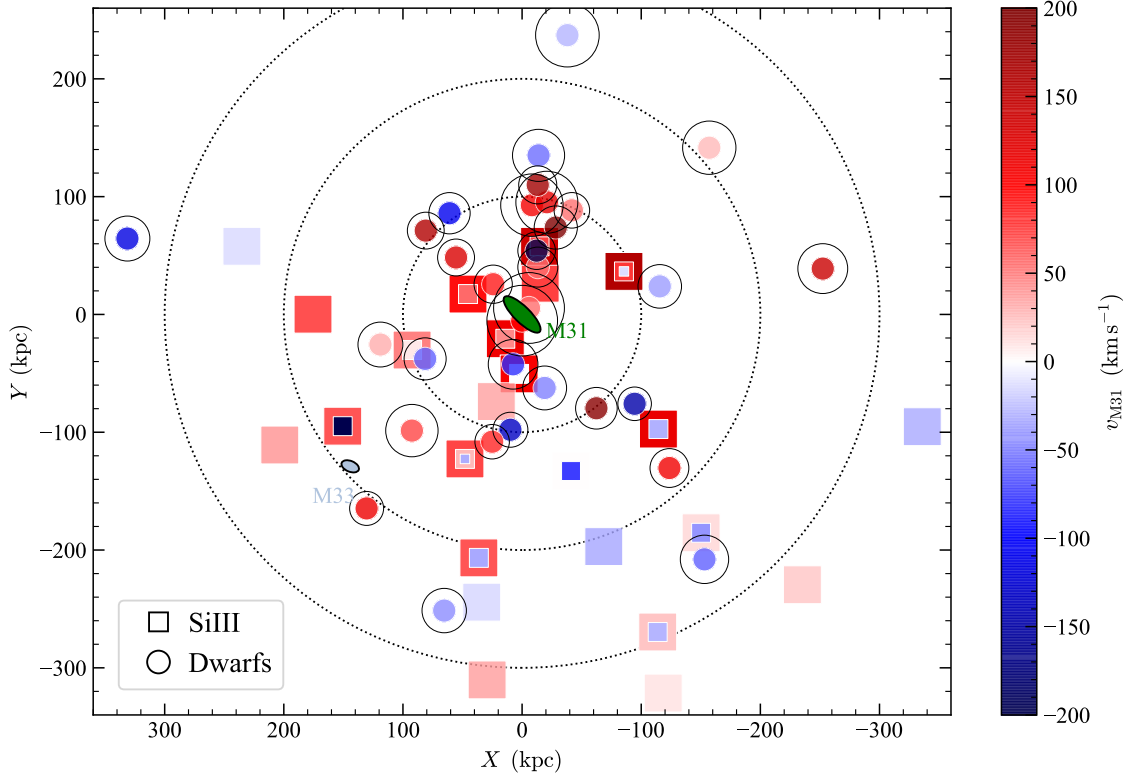


Figure 7. Locations of the QSOs (*squares*) and dwarfs (*circles*) relative to M31 (see Fig. 1). The data are color-coded according to the relative velocities of the detected Si III (multiple colors in a symbol indicate multiple detected components) or the dwarfs. The black circles centered on the dwarfs indicate their individual R_{200} .

color coded on the same scale and the circles around each dwarf represent their R_{200} radius.

Table 4 and Fig. 7 show that several absorbers can be found within R_{200} of several dwarfs when Si III is used as the gas tracer. For example, the two components observed in Si III toward Zw535.012 are found within R_{200} of 6 dwarf galaxies. In Table 4, we also list the escape velocity (v_{esc}) at the observed projected distance of the QSO relative to the dwarf as well as the velocity separation between the QSO absorber and the dwarf ($\delta v \equiv |v_{\text{M31, Si III}} - v_{\text{M31, dwarf}}|$). So far we have not considered the velocity separation δv between the dwarf and the absorber, but it is likely that if $\delta v \gg v_{\text{esc}}$ then the observed gas traced by the absorber is unlikely to be bound to the dwarf galaxy even if $\Delta_{\text{sep}} = R/R_{200} < 1$.

If we set $\delta v < v_{\text{esc}}/\sqrt{3}$, then the sample of components would be reduced to 31 instead of 58. The sample is reduced still further down to 12 if the two most massive dwarfs (M32 and NGC 205) are removed from the sample and down to 6 if the most massive dwarfs with $M_h > 3.9 \times 10^{10} M_\odot$ are removed from the sample. Applying a cross-match where $\delta v < v_{\text{esc}}$ and $\Delta_{\text{sep}} < 1$ can reduce the degeneracy between different galaxies, especially if one excludes the four most massive galaxies. For

example, RXS_J0118.8+3836 is located at $0.40R_{200}$ and $0.72R_{200}$ from Andromeda XV and Andromeda XXIII, but only in the latter case $\delta v \ll v_{\text{esc}}$ (and in the former case $\delta v > v_{\text{esc}}$), making the two components observed toward RXS_J0118.8+3836 more likely associated with Andromeda XXIII.

Several sightlines therefore pass within $\Delta_{\text{sep}} < 1$ of a dwarf galaxy and show a velocity absorption within the escape velocity. This gas could be gravitationally bound to the dwarf. However, there are also 5 absorbers where $\delta v < v_{\text{esc}}/\sqrt{3}$, but the QSO is at $1 < \Delta_{\text{sep}} \leq 2$ from the dwarf, i.e., the velocity separation is small, but the spatial projected separation makes unlikely to be bound to the dwarf. Here the velocity match may be a coincidence or a result of the relative proximity of the dwarfs and QSOs in the CGM of M31 assuming that the gas and dwarfs both follow the same global velocity motion of the M31 CGM. As illustrated in Fig. 7, there are, however, some dwarfs with $\Delta_{\text{sep}} \lesssim 2$ with a radial velocity very different from that observed in absorption toward the QSO or vice-versa, implying not all the dwarfs and gas velocities are tightly connected.

In summary, it is plausible that absorbers with $\Delta_{\text{sep}} < 1$ and $\delta v \ll v_{\text{esc}}$ trace gas associated with the CGM of a

dwarf, but we cannot confirm unambiguously this association. We inspected a number of gas properties (e.g., column densities, ionization levels, kinematics), but did not find any that can differentiate clearly between a dwarf CGM origin from a M31 CGM origin. Nothing in the properties of the components found within $\Delta_{\text{sep}} < 1$ of a dwarf and having $\delta v \ll v_{\text{esc}}$ make them outliers. This is certainly not surprising since any association assumes that the dwarf galaxies have a rich gas CGM. Yet all the satellites listed in the cross-matched Table 4 are dSph galaxies, which are known to be neutral gas poor (Grebel et al. 2003). The dSph galaxies are also likely ionized gas deficient since the favor mechanism to strip their gas is ram-pressure, a stripping mechanism efficient on both the neutral and ionized gas (Grebel et al. 2003; Mayer et al. 2006). Therefore these galaxies are unlikely to have gas rich CGM and based our observations we do not find any persuasive evidence that gas associated with M31 satellites causes the absorption we see in the M31 CGM.

4. PROPERTIES OF THE M31 CGM

We now focus on determining the properties of the CGM of M31 using only the velocity components that are not contaminated by the MS (see 2.5). We use the following atoms and ions to characterize the M31 CGM: O I, Si II, Si III, Si IV, C II, C IV, O VI, Fe II. O I and Fe II are not commonly detected, but even so they are useful in assessing the ionization and depletion levels of the CGM gas. We use the terminology “low ions” for singly ionized species, “intermediate ions” for Si III and Si IV, and “high ions” for C IV and O VI. Also note that we adopt here the solar relative abundances from Asplund et al. (2009).

4.1. Metallicity of the CGM

Radio observations have not detected any H I 21-cm emission toward any of the QSO targets in Project AMIGA down to a 5σ level of $\log N_{\text{HI}} \gtrsim 17.6$ (Paper I); many sightlines could therefore have $\log N_{\text{HI}} \ll 17.6$. As a consequence of this, we cannot directly estimate the metallicities of the CGM in our sample. However, we have some weak detections of O I in 4 components at better than the 3σ level. Since O I and H I have nearly identical ionization potentials and are strongly coupled through charge exchange reactions (Field 1971), O I is an excellent proxy for H I, requiring no or very small ionization correction as long as the photoionization spectrum is not too hard (e.g., Lehner et al. 2003). Therefore O I can be compared to the limit of H I to put a lower limit on the metallicity. The O I logarithmic column densities are in the range 13.3 to 13.7 dex

(see Table 2), with a mean of 13.5 dex. This implies $[\text{O I}/\text{H I}] = \log(N_{\text{OI}}/N_{\text{HI}}) - \log(\text{O}/\text{H})_{\odot} \gtrsim -0.7$ or a metallicity $Z \gtrsim 0.2Z_{\odot}$. This lower limit, however, assumes that there is no beam dilution effect, i.e., we assume the limit on the H I column density in the 2 kpc beam (at the distance of M31) would be the same than in a pencil-beam observed in absorption. Any beam dilution would increase the limit on H I, and therefore the metallicity limit could be less stringent. We therefore caution the reader not to take this limit as a hard lower limit.

4.2. Relative Abundances

While the metallicity remains quite uncertain, from the relative abundances of detected ions, we can assess the level of ionization, dust depletion, nucleosynthetic history. For assessing depletions, we can compare refractory elements like Fe to less refractory elements like Si (e.g., Savage & Sembach 1996; Jenkins 2009). Fe II and Si II have similar ionization energies (8–16 eV) and their observed ratio should be minimally affected by differential ionization. Hence the ratio $[\text{Fe II}/\text{Si II}] = \log(N_{\text{Fe II}}/N_{\text{Si II}}) - \log(\text{Fe}/\text{Si})_{\odot}$ traces dust depletion levels. Unfortunately (but perhaps not surprisingly), Fe II is only detected in the sightline closest to M31, and in that sightline, we derive $[\text{Fe II}/\text{Si II}] = -0.13 \pm 0.16$. In ten other sightlines, we place upper limits on that ratio where the two smallest upper limits imply $[\text{Fe II}/\text{Si II}] \lesssim 0$, while all the others are above 0 dex. While the information is minimal, this still demonstrates that there is no evidence for significant dust depletion in the CGM of M31. As depletions get stronger in denser gas, it is perhaps not surprising that we find little evidence for it in a sample where the sightlines all have $\log N_{\text{HI}} \lesssim 17.6$ and low ions are not commonly detected. While we assume that dust would be the major factor to deplete Fe relative to Si, the lack of evidence for depletion of Fe also points to a negligible nucleosynthesis effect on that ratio that would produce a non-solar α -particle (e.g. Si) enhancement relative to Fe (e.g., Welty et al. 1997).

Using ratios of elements with different nucleosynthetic origins, we can assess the chemical enrichment history of the M31 halo gas by measuring departures from a solar relative abundance ratio in elements of different nucleosynthetic origin. For instance, the $[\text{C}/\alpha]$ ratio should be sensitive to nucleosynthesis effects since there is a time-lag between the production of α -elements and carbon (see, e.g., Cescutti et al. 2009; Mattsson 2010). This analysis would be complicated by large depletions, but as we have shown above the Fe/Si ratios show little if any evidence of large depletions. As Fe is typically the most

depleted element in these conditions (Savage & Sembach 1996; Welty et al. 1999; Jenkins 2009), we can reliably assume that $[C/\alpha]$ does not suffer large depletions and can therefore be used as a nucleosynthetic indicator.

However, we must consider ionization effects in addition to depletions. Differential ionization can affect the C II/Si II (i.e., $[C/\alpha]$) ratio because C II has a higher ionization energy range (12–25 eV) than Si II (8–16 eV). To assess this, we use the nine absorbers with detections of both Si II and C II to estimate $[C \text{ II}/Si \text{ II}] = \log(N_{C \text{ II}}/N_{Si \text{ II}}) - \log(C/Si)_{\odot}$. Since this subsample includes both detections and lower limits owing to saturation of C II, we use a survival analysis where the four censored lower limits are included (Feigelson & Nelson 1985; Isobe et al. 1986). We find that the mean $[C \text{ II}/Si \text{ II}] = 0.07 \pm 0.09$ (where the error is the error on the mean from the Kaplan-Meier estimator) and the 1σ dispersion is 0.19 dex. This ratio is consistent with a solar value. If non-detections of Si II are included the mean rises to $[C \text{ II}/Si \text{ II}] = 0.52 \pm 0.11$, strongly indicating ionization affects this ratio owing to photons ionizing Si II into Si III.

Therefore based on the relative abundances of Fe and C to Si, there is no evidence for strong dust depletion or non-solar nucleosynthesis effects in the CGM of M31. We emphasize that this does not mean there is no dust in the CGM of M31, and indeed several studies have shown that the CGM of galaxies can have a substantial mass of dust (e.g., Ménard et al. 2010; Peek et al. 2015). However, its effect on elemental abundances must be smaller than in the dense regions of galaxies. The lack of nucleosynthesis effects on the abundance of Fe or C relative to Si strongly suggests that the overall metallicity of the gas is not extremely low, as enhancements of α elements are seen in low-metallicity MW halo stars and in low-metallicity gas in CGM absorbers over a range of redshift. For a sample of H I-selected absorbers with $15 \lesssim \log N_{H \text{ I}} \lesssim 18$ at $0.2 \lesssim z \lesssim 1$, Lehner et al. (2019) found little correlation between the $[C/\alpha]$ and the metallicity. However in stars and H II regions in the local universe, there is evidence of a trend between $[C/\alpha]$ and the metallicity where $[C/\alpha] \simeq -0.6$ at $-2 \lesssim \log Z/Z_{\odot} \lesssim -0.5$ and $[C/\alpha] \simeq 0$ near solar metallicities (e.g., Akerman et al. 2004; Fabbian et al. 2010). Therefore the metallicity of the M31 CGM could still be sub-solar, but is unlikely to be much below $1/3 Z_{\odot}$. This is consistent with the rough metallicity estimate set in §4.1.

4.3. Ionization Fractions

The ionization fraction of the CGM gas can be estimated directly by comparing the column densities of O I

to those of Si II, Si III, and Si IV (e.g., Lehner et al. 2001; Zech et al. 2008). O I is an excellent proxy for neutral gas (see §4.1). Si II is found in both neutral and ionized gas, and Si III and Si IV arise only in ionized gas. O and Si are both α -elements with similar nucleosynthetic origins and have similar levels of dust depletion in the diffuse gas (Savage & Sembach 1996; Jenkins 2009). Therefore if the ratio $[O \text{ I}/Si] = \log(N_{O \text{ I}}/N_{Si}) - \log(O/Si)_{\odot}$ is sub-solar, ionization is important in the M31 CGM.

To obtain the total Si column density we use the individual ion columns listed in Table 2. In the case of non-detections of the Si ions or O I, we conservatively add the upper limits to the column densities. When there are lower limits present, we add the column densities using the lower limit values. When both detections and non-detections are present, we consider the two extreme possibilities where we set the column density of the non-detection either to the upper limit value (i.e., the absorption is nearly detected—case 1) or we neglect the upper limit (i.e., it is a true non-detection—case 2). For 28 targets, we can estimate the $[O \text{ I}/Si]$ ratio. Considering case 1, we find that the mean and dispersion is $[O \text{ I}/Si] < -0.95 \pm 0.38$ and the full range is $[< -1.78, < -0.34]$, i.e., on average the gas is ionized at the $> 89\%$ level. In case 2, the mean and dispersion is $[O \text{ I}/Si] < -0.74 \pm 0.51$, so that the ionization fraction is still $> 81\%$ on average. These are upper limits because typically O I is not detected. However, even in the 5 cases where O I is detected, 4/5 are upper limits too because Si III is saturated and hence only a lower limit on the column density of Si can be derived. In that case, $[O \text{ I}/Si]$ ranges from < -1.78 to -0.43 (or to < -0.85 if we remove the absorber where the O I absorption is just detected at the 2σ level), i.e., even when O I is detected to more than 3σ , the gas is still ionized at levels $> 86\%$ – 98% .

The combination of Si II, Si III, and Si IV allows us to probe gas within the ionization energies 8–45 eV, i.e., the bulk of the photoionized CGM of M31. The high ions, C IV and O VI, have ionization energies 48–85 eV and 114–138 eV, respectively, and are not included in the above calculation. The column density of H can be directly estimated in the ionization energy 8–45 eV range from the observations via $\log N_{H} = \log N_{Si} - \log Z/Z_{\odot}$. As we show below, Si varies strongly with R with values $\log N_{Si} \gtrsim 13.7$ at $R \lesssim 100$ kpc and $\log N_{Si} \lesssim 13.3$ at $R \gtrsim 100$ kpc, which implies $N_{H} \gtrsim 1.5 \times 10^{18} (Z/Z_{\odot})^{-1} \text{ cm}^{-2}$ and $\lesssim 0.6 \times 10^{18} (Z/Z_{\odot})^{-1} \text{ cm}^{-2}$, respectively. For the high ions, a ionization correction needs to be added, and, e.g., for O VI, $\log N_{H} = \log N_{O \text{ VI}} - \log Z/Z_{\odot} - \log f_{O \text{ VI}}^i$ where $f_{O \text{ VI}}^i \lesssim 0.2$ is the ionization fraction of O VI that peaks around 20% for any ionizing models (e.g.

Oppenheimer & Schaye 2013b; Gnat & Sternberg 2007; Lehner et al. 2014). As discussed below, there is little variation of $N_{\text{O VI}}$ with R and is always such that $\log N_{\text{O VI}} \gtrsim 14.4\text{--}14.9$ within 300 kpc from M31, which implies $N_{\text{H}} \gtrsim (2.5\text{--}8.1) \times 10^{18} (Z/Z_{\odot})^{-1} \text{ cm}^{-2}$. Therefore the CGM of M31 is not only mostly ionized (often at levels close to 100%), but it also contains a substantial fraction of highly ionized gas with higher column densities than the weakly photoionized gas.

4.4. Ion Column Densities versus R

In Fig. 8, we show the logarithmic (left) and linear (right) values of the total column densities of the components associated with M31 for C II, Si II, Si III, Si IV, C IV, and O VI as a function of the projected distances from M31. Gray data points are upper limits, while blue data with upward arrows are lower limits owing to saturated absorption. Overall, the column densities decrease at higher impact parameter. As the ionization potentials of the ions increase, the decrease in the column densities becomes shallower; O VI is almost flat. These conclusions were already noted in LHW15, but now that the region from 50 to 350 kpc is filled with data, these trends are even more striking. However, our new sample shows also an additional feature with a remarkable change around $R_{200} \simeq 230$ kpc of M31 notable especially for the low and intermediate ions whereby high C II, Si II, Si III, and Si IV column densities are observed solely at $R \lesssim R_{200}$. Low column densities C II, Si II, Si III, and Si IV are observed at all R , but strong absorption is observed only at $R \lesssim R_{200}$. The frequency of strong absorption is also larger at $R \lesssim 0.6R_{200}$ than at larger R for all ions. A similar pattern is observed for C IV and O VI, but the difference between the low and high column densities is smaller: for C II, Si II, Si III, and Si IV, the difference between low and high column densities is a factor $\gtrsim 5\text{--}10$, while it drops to a factor 2–4 for C IV, and possibly even less for O VI.

In Fig. 9, we show the logarithmic values of the column densities derived from the individual components for C II, Si II, Si III, Si IV, C IV, and O VI as a function of the projected distances from M31. Similar trends are observed in Fig. 8, but Fig. 9 additionally shows that 1) more complex velocity structures (i.e., multiple velocity components) are predominantly observed at $R \lesssim R_{200}$, and 2) factor $\gtrsim 2\text{--}10$ changes in the column densities are observed across multiple velocity components along a given sightline.

4.5. Silicon Column Densities versus R

With Si II, Si III, and Si IV, we can estimate the total column density of Si within the ionization energy range

8–45 eV without any ionization modeling. Gas in this range should constitute the bulk of the cool photoionized CGM of M31 (see §4.3). In Fig. 10, we show the total column density of Si (estimated following §4.3) against the projected distance R from M31. The vertical-ticked bar in Fig. 10 indicate data with some upper limits, and the length of the vertical bar represents the range of N_{Si} values allowed between cases 1 and 2 (see §4.3).

Fig. 10 reinforces the conclusions observed from the individual low ions in Figs. 8 and 9. Overall there is a decrease of the column density of Si at larger R . This decrease has a much stronger gradient in the inner region of the M31 CGM between ($R \lesssim 25$ kpc) and about $R \sim 100\text{--}150$ kpc than at $R \gtrsim 150$ kpc. N_{Si} changes by a factor $> 5\text{--}10$ between about 25 kpc and 150 kpc while it changes by a factor $\lesssim 2$ between 150 kpc and 300 kpc. The scatter in N_{Si} is also larger in the inner regions of the CGM than beyond $\gtrsim 120\text{--}150$ kpc.

To model this overall trend (which is also useful to determine the baryon and metal content of the CGM, see §4.8), we consider three models, a hyperbolic (H) model, single-power law (SPL) model, and a Gaussian Process (GP) model. We refer the reader to Appendix F where we fully explain the modeling process and how lower and upper limits are accounted for in the modeling. Fig. 10 shows these 3 models greatly overlap. The non-parametric GP model overlaps more with the SPL model than with the H fit in the range $250 \lesssim R \lesssim 400$ kpc and at $R < 90$ kpc (especially for the high H fit, see Fig. 10). While there are some differences between these models (and we will explore in §4.8 how these affect the mass estimates of the CGM), they all further confirm the strong evolution of the column density of Si with R between $\lesssim 25$ and $90\text{--}150$ kpc and a much shallower evolution with R beyond 200 kpc. In §4.8, we use these models to constrain the metal and baryon masses of the cool CGM gas probed by Si II, Si III, Si IV.

4.6. Covering Factors

As noted in §4.4, the diagnostic ions behave differently with R in a way that probably reflects the underlying physical conditions. For example, Si II has a high detection rate within $R < 100$ kpc, a sharp drop beyond $R > 100$ kpc, and a total absence at $R \gtrsim 240$ kpc (see Figs. 8 and 9). On the other hand, Si III and O VI are mostly detected at all R , but the column densities of Si III fall significantly with R while O VI remains relatively flat. In this section, we quantify further the detection rates, or the covering factors, for each ion.

To calculate the covering factors of the low and high ions, we follow the methodology described in Paper I for H I by assuming a binomial distribution. We assess

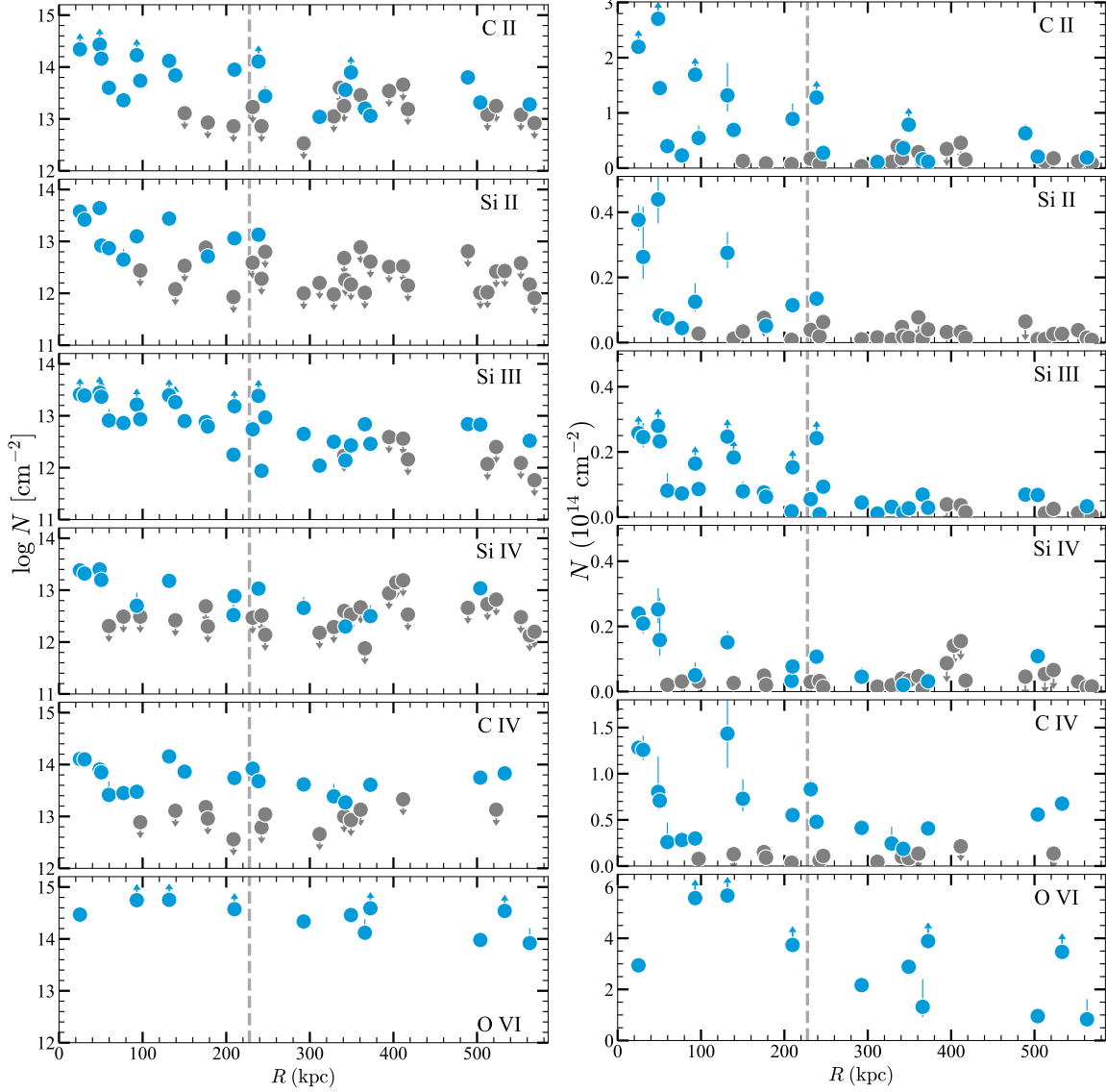


Figure 8. Total column densities of the ions as a function of R with ionization potential increasing from top to bottom panels. The column densities are shown in logarithm values (with the same relative vertical scale of about 3 dex in each panel) on the left and in linear units on the right. Blue circles are detections, while gray circles with downward arrows are non-detections. A blue circle with an upward arrow denotes that the absorption is saturated, resulting into a lower limit. The components associated with the MS have been removed. The dashed vertical line marks R_{200} . Note how Si III and O VI are detected at high frequency well beyond R_{200} .

the likelihood function for values of the covering factor given the number of detections against the total sample, i.e., the number of targets within a given impact parameter range (see Cameron 2011). As demonstrated by Cameron (2011), the normalized likelihood function for calculating the Bayesian confidence intervals on a binomial distribution with a non-informative (uniform) prior follows a β -distribution.

In Fig. 11, we show the *cumulative* covering factors (f_c) for the various ions, where each point represents the covering factor for all impact parameters less than the

given value of R . The vertical bars are 68% confidence intervals. As discussed in §§4.4, 4.5, for all the ions but O VI, the highest column densities are only observed at $R \lesssim 100$ –150 kpc, with a sharp decrease beyond that. For the covering factors, we therefore consider 1) the entire sample (most of the upper limits—non-detections—are at the level of lowest column densities of a detected absorption, so it is adequate to do that), and 2) the sample where we set a threshold column density (N_{th}) to be included in the sample. In the left panel of Fig. 11, we show the first case, while in the right panel, we focus

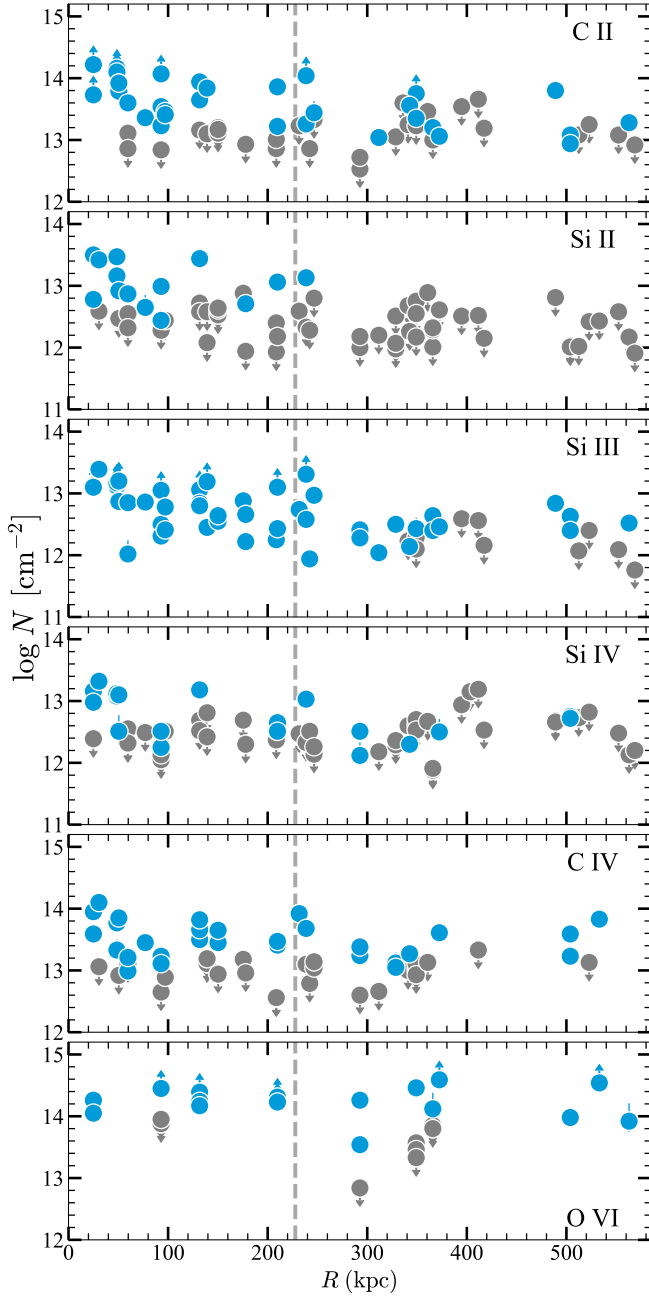


Figure 9. Logarithm of the column densities for the individual components of various ions (low to high ions from top to bottom) as a function of the projected distances from M31 of the background QSOs. Blue circles are detections, while gray circles with downward arrows are non-detections. A blue circle with an upward arrow denotes that the absorption is saturated, resulting into a lower limit. The components associated with the MS have been removed. The dashed vertical lines shows the R_{200} location. The same relative vertical scale of about 3 dex is used in each panel for comparison between the different ions.

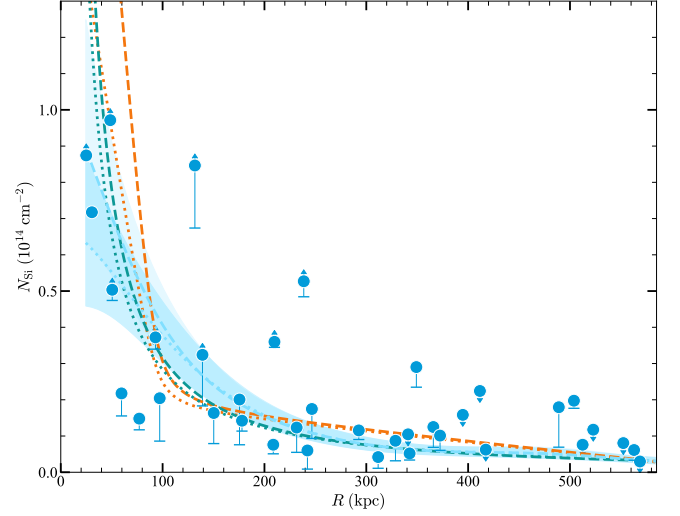


Figure 10. Total column densities of Si (i.e., $N_{\text{Si}} = N_{\text{Si II}} + N_{\text{Si III}} + N_{\text{Si IV}}$) as a function of the projected distances from M31 of the background QSOs. The vertical-ticked bars show the range of values allowed if the upper limit of a given Si ion is negligible or not. The lower limits have upward arrows, and the upper limits are flagged using downward arrows. The orange, green, and blue curves are the H, SPL, GP-derived models to the data, respectively (see text for details regarding how censoring is treated in each model). The dotted and dashed curves correspond to model where the lower limits at $R < 50$ kpc are increased by 0.3 or 0.6 dex. The blue areas correspond to the dispersion derived from the GP models (see Appendix F for more detail).

on the strong absorbers only. For the Si ions, we use $\log N_{\text{th}} = 13$; for the C ions, $\log N_{\text{th}} = 13.8$; for O VI, $\log N_{\text{th}} = 14.5$. These threshold column densities are chosen based on Fig. 8. We also show in the right panel of Fig. 11, the results for the H I emission from Paper I.

These results must be interpreted in light of the fact that the intrinsic strength of the diagnostic lines varies by ion. The oscillator strength, $f\lambda$, of these different ions are listed in Table 5 along with the solar abundances of these elements. The optical depth is such that $\tau \propto f\lambda N$ (see §2.4.2) and $f\lambda$ is a good representation of the strength of a given transition. For the Si ions, Si III has the strongest transition, a factor 2.7–5.5 stronger than Si IV and a factor 1.3–5.7 stronger than Si II (the weaker Si II $\lambda 1526$ is sometimes used but mostly to better constrain the column density of Si II if the absorption is strong). Si II and Si IV have more comparable strength, which is also the case between C II and C IV. Comparing between different species, while $(f\lambda)_{\text{Si III}} \simeq 14.4(f\lambda)_{\text{O VI}}$, but this is counter-balanced by oxygen being 15 times more abundant than silicon (and a similar conclusion applies comparing Si III with C II or C IV).

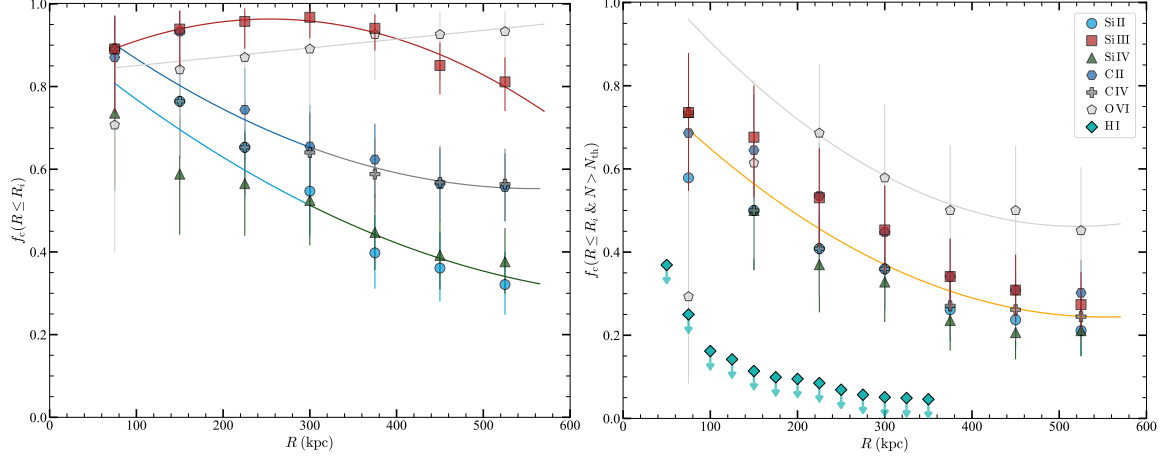


Figure 11. Cumulative covering factors for impact parameters less than R without (*left*) and with (*right*) some threshold cut on the column densities (for Si ions, $\log N_{th} = 13$; for C ions, $\log N_{th} = 13.8$; for O VI, $\log N_{th} = 14.5$, and for H I, $\log N_{th} = 17.6$, see text for more detail and Paper I). Confidence intervals (vertical bars) are at the 68% level and data points are the median values. On the left panel, the solid lines are polynomial fits to median values of f_c for Si III, O VI, C II–C IV, Si II–Si IV (i.e., taking the mean value of f_c between these two ions at a given R). On the right panel, the orange line is a polynomial fit to the mean values of f_c for C II, C IV, Si II, Si III, and Si IV while the gray line is polynomial fit to the median values of f_c for O VI.

With that in mind, we first consider the left panel of Fig. 11, i.e., where all the absorbers irrespective of their absorption strengths are taken into account to estimate the cumulative covering factors. We fitted 4 low-degree polynomials to the data: Si III, O VI, and treating in pair C II–C IV and Si II–Si IV as they appear to follow each other reasonably well, respectively. For C II–C IV and Si II–Si IV, we fit the mean covering factors of each ionic pair. For O VI, we only fitted data beyond 200 kpc owing to the smaller size sample (there are only 3 data points within 200 kpc and 11 in total, see Fig. 8). It is striking how the cumulative covering factors of Si III and O VI vary with R quite differently from each other and from the other ions. The cumulative covering factor of Si III increases with R , reaches a maximum somewhere between 250 and 300 kpc, and then decreases, but still remains much higher than f_c of C II–C IV or Si II–Si IV. The cumulative covering factor of O VI monotonically increases with R up to $R \sim 569$ kpc. In contrast, while the cumulative covering factors of C II–C IV or Si II–Si IV are offset from each other, they both monotonically decrease with R . There seems to be a plateau in C II–C IV covering factor beyond 400 kpc, which is not observed for Si II or Si IV.

Turning to the right panel of Fig. 11 where we show f_c for a given column density threshold that changes with species (see above), the relation between f_c and R is quite different. For all the ions, the cumulative covering factors monotonically decrease with increasing R . For C II, C IV, Si II, Si III, and Si IV, the covering factors are essentially the same within 1σ , and the orange line in Fig. 11 shows a second-degree polynomial fit to the

mean values of f_c between these different ions. Ignoring data at $R < 200$ kpc owing to the small sample size, O VI has a similar evolution of f_c with R , but overall f_c is tentatively a factor ~ 1.5 times larger than for the other ions at any R .

The contrast between the two panels of Fig. 11 strongly suggests that the CGM of M31 has three main populations of absorbers: 1) the strong absorbers that are found mostly at $R \lesssim 100\text{--}150$ kpc ($0.3\text{--}0.5R_{vir}$) probing the denser regions and multiple gas-phase (singly to highly ionized gas) of the CGM, 2) weak absorbers probing the diffuse CGM traced principally by Si III (but also observed in higher ions and more rarely in C II) that are found at any surveyed R but more frequent at $R \lesssim R_{vir}$, and 3) hotter, more diffuse CGM probed by O VI, O VI having the unique property compared to the ions that its column density remains largely invariant with the radius of the M31 CGM.

4.7. Ion ratios and their Relation with R

In §4.3, we show that the ratio of O I to Si ions provides a direct estimate of the ionization fraction of the CGM gas of M31. Using ratios of the main ions studied here (C II, C IV, Si II, Si III, Si IV, O VI), we can further constrain the ionization and physical conditions in the CGM of M31 and how they may change with R . To estimate the ionic ratios, we consider the component analysis of the absorption profiles, i.e., we compare the column densities estimated over the same velocity range. However, coincident velocities do not necessarily mean that they probe the same gas, especially if their ionization potentials are quite different (such as for C II and

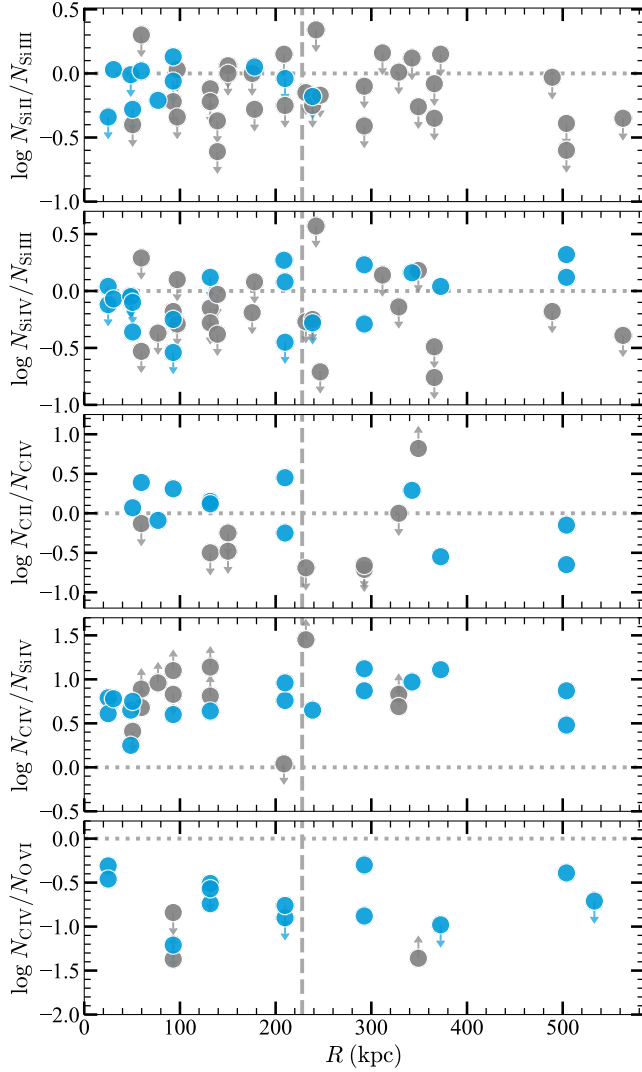


Figure 12. Logarithmic column density ratios of different ions as a function of the projected distances from M31 of the background QSOs. The column densities in individual components are compared to estimate the ionic ratios. Blue symbols indicate that both ions in the ratio are detected. Blue down or up arrows indicate that the absorption is saturated for the ion in the denominator or numerator of the ratio. Gray symbols indicate that one of the ions in the ratio is not detected at $> 2\sigma$. The components associated with the MS have again been removed. The dashed vertical lines mark R_{200} .

C IV). In Fig. 12, we show the results for several ion ratios as a function of R .

4.7.1. The Si II/Si III and Si IV/Si III ratios

The Si II/Si III and Si IV/Si III ratios are particularly useful because they trace different ionization levels independently of relative elemental abundances. The ionization potentials for these ions are 8.1–16.3 eV for

Si II, 16.3–33.5 eV for Si III, and 33.5–45.1 eV for Si IV. The top two panels of Fig. 12 show the ratios Si II/Si III and Si IV/Si III as a function of R . In both panels, there are many upper limits and there is no evidence of any correlation with R , except perhaps for the Si II/Si III ratio where the only detections of Si II are at $R \lesssim R_{200}$ (see also Fig. 9).

With so many upper limits, we use the Kaplan-Meier estimator (see §4.2) to estimate the mean of these ratios: $\langle \log N_{\text{SiII}}/N_{\text{SiIII}} \rangle = (-0.50 \pm 0.04) \pm 0.23$ (mean, error on the mean from the Kaplan-Meier estimator, and standard deviation for 44 data points with 38 upper limits) and $\langle \log N_{\text{SiIV}}/N_{\text{SiIII}} \rangle = (-0.49 \pm 0.07) \pm 0.20$ (43 data points with 32 upper limits). There are only 4/44 components where $\log N_{\text{SiII}}/N_{\text{SiIII}} \simeq 0$ and 8/43 where $\log N_{\text{SiIV}}/N_{\text{SiIII}} \gtrsim 0$. In the latter cases, Si IV could be produced by another mechanism such as collisional ionization. Among the three Si ions in our survey, Si III is the dominant ion at any R from M31 in the ionizing energy range 8.1–45.1 eV. Ions (of any element) with ionizing energies in the range 16.3–33.5 eV are therefore expected to be dominant ions at least for processes that are dominated by photoionization.

The Si II/Si III ratio has previously been used to constrain the properties of the photoionized gas. According to photoionization modeling produced by Oppenheimer et al. (2018a), an ionic ratio of $\langle \log N_{\text{SiII}}/N_{\text{SiIII}} \rangle = (-0.50 \pm 0.04) \pm 0.23$ would imply gas density in the range $-3 \lesssim \log n_{\text{H}} \lesssim -2.5$ and a temperature of the gas around 10^4 K (see Fig. 16 in Oppenheimer et al. 2018a).

4.7.2. The C II/C IV ratio

For the C II/C IV ratio the ionizing energy ranges are well separated with 11.3–24.3 eV for C II and 47.9–64.4 eV for C IV. In fact with an ionization potential above the He II ionization edge at 54.4 eV, C IV can be also produced not just photoionization but also by collisional ionization. Therefore C II and C IV are unlikely to probe the same ionization mechanisms or be in a gas with the same density. We note that C II has ionization energies that overlap with Si III and larger than those of Si II, which certainly explain the presence of C II beyond R_{200} where Si II is systematically not detected.

The third panel of Fig. 12 shows the C II/C IV ratios. There is again no strong relationship between C II/C IV and R , but $\log N_{\text{CII}}/N_{\text{CIV}} \gtrsim 0$ is more frequently observed at $R < R_{200}$ (6/12) than at $R > R_{200}$ (2/9), consistent with the observation made in §4.4 that the gas becomes more highly ionized as R increases. With the survival analysis (considering the only lower limit as a detection), we find $\langle \log N_{\text{CII}}/N_{\text{CIV}} \rangle = (-0.21 \pm 0.11) \pm 0.40$ (21 data points with 8 upper limits). Con-

sidering data at $R < R_{200}$, we have $\langle \log N_{\text{C II}}/N_{\text{C IV}} \rangle = (-0.07 \pm 0.10) \pm 0.28$ (12 data points with 4 upper limits), while at $R \geq R_{200}$, we find $\langle \log N_{\text{C II}}/N_{\text{C IV}} \rangle = (-0.33 \pm 0.18) \pm 0.22$ (9 data points with 4 upper limits), confirming again that the gas is more ionized and also more highly ionized at $R > R_{200}$.

4.7.3. The C IV/Si IV ratio

For the C IV/Si IV ratio, different species are compared, but as we discuss in §4.2, the relative abundances of C and Si are consistent with the solar ratio owing to little evidence of any strong dust depletion or nucleosynthesis effects, i.e., these effects should not affect the observed ratio of C IV/Si IV. Si IV and C IV have near adjacent ionization energies 33.5–45.1 eV to 47.9–64.4 eV, respectively. Both photoionization and collisional ionization processes can be important at these ionizing energies, but if $\log N_{\text{C IV}}/N_{\text{Si IV}} > 0$, then the ionization from hot stars is unimportant (see Fig. 13 in Lehner et al. 2011), which is nearly always the case, as illustrated in Fig. 12. A harder photoionizing spectrum or collisional ionization must be at play to explain the origin of these ions.

Fig. 12 suggest a moderate correlation between $\log N_{\text{C IV}}/N_{\text{Si IV}}$ and R . If the two data points beyond 400 kpc are removed (and treating the limits as actual values), a Spearman rank order implies a monotonic correlation between $\log N_{\text{C IV}}/N_{\text{Si IV}}$ and R with a correlation coefficient $r_s = +0.45$ and $p = 0.019$ for the gas at $R < 1.2R_{\text{vir}}$. Considering the entire sample, the Spearman rank test yield $r_s = 0.34$ and $p = 0.07$. This is again consistent with our earlier conclusion that the gas becomes more highly ionized as R increases. With the survival analysis (considering the 3 upper limits as detections),⁷ we find $\langle \log N_{\text{C IV}}/N_{\text{Si IV}} \rangle = (+0.87 \pm 0.07) \pm 0.24$ (29 data points with 9 lower limits). This is about a factor 1.9 larger than the mean derived for the broad C IV and Si IV components in the Milky Way disk and low-halo (Lehner et al. 2011), which is about 1σ larger.

4.7.4. The C IV/O VI ratio

Finally, in the last panel of Fig. 12, we show the C IV/O VI ratio as a function of R . As for the C IV/Si IV ratio, different species are compared, and for the same reasons, the relative dust depletion or nucleosynthesis effects should be negligible. With 113.9–138.1 eV ionizing energies needed to produce O VI, this is the highest high ion in the sample and as we demonstrated

in the previous section the O VI properties (covering factor and column density as a function of R) are quite unique. Not surprisingly Fig. 12 does not reveal any relation between $\log N_{\text{C IV}}/N_{\text{O VI}}$ and R .

If we treat the two lower limits as detections, then the survival analysis yields $\langle \log N_{\text{C IV}}/N_{\text{O VI}} \rangle = (-0.93 \pm 0.11) \pm 0.32$ (16 data points with 6 upper limits). The mean and range of $\log N_{\text{C IV}}/N_{\text{O VI}}$ are smaller than observed in the Milky Way disk and low halo where the full range varies from -1 to $+1$ dex (see, e.g., Fig. 14 of Lehner et al. 2011). This demonstrates that the highly ionized gas in the 113.9–138.1 eV range is much more important than in the 47.9–64.4 eV range at any R of the M31 CGM.

4.8. Metal and Baryon Mass of the M31 CGM

With a better understanding of the column density variation with R , we can estimate with more confidence the metal and baryon mass of the M31 CGM than in our original survey where we had very little information between 50 and 300 kpc (LHW15). The metal mass can be directly estimated from the column densities of the metal ions. With the silicon ions, we have information on its three dominant ionization stages in the $T < 7 \times 10^4$ K ionized gas (ionizing energies in the range 8–45 eV, see §4.5), so we can obtain a direct measured metal mass without any major ionization corrections. Following LHW15 (and see also Peebles et al. 2014), the metal mass of the cool photoionized CGM is

$$M_Z^{\text{cool}} = 2\pi \mu_{\text{Si}}^{-1} m_{\text{Si}} \int R N_{\text{Si}}(R) dR,$$

where $\mu_{\text{Si}} = 0.064$ is the solar mass fraction of metals in silicon (i.e., $12 + \log(\text{Si}/\text{H})_{\odot} = 7.51$ and $Z_{\odot} = 0.0142$ from Asplund et al. 2009), $m_{\text{Si}} = 28m_p$, and for $N_{\text{Si}}(R)$ we use the hyperbola (“H model”, Eqn. F1), single power-law (“SPL model”, Eqn. F2), and GP models that we determine in §4.5 and Appendix F (see Fig. 10).

A direct method to estimate the total mass is to convert the total observed column density of Si to total hydrogen column density via $N_{\text{H}} = N_{\text{HI}} + N_{\text{HII}} = N_{\text{Si}} (\text{Si}/\text{H})_{\odot}^{-1} (Z/Z_{\odot})^{-1}$. The baryonic mass of the CGM of M31 is then:

$$M_g^{\text{cool}} = 2\pi m_{\text{H}} \mu f_c \left(\frac{\text{Si}}{\text{H}} \right)_{\odot}^{-1} \left(\frac{Z}{Z_{\odot}} \right)^{-1} \int R N_{\text{Si}}(R) dR,$$

where $\mu \simeq 1.4$ (to correct for the presence of He), $m_{\text{H}} = 1.67 \times 10^{-24}$ g is the hydrogen mass, f_c is covering fraction (that is 1 over the considered radii), and $\log(\text{Si}/\text{H})_{\odot} = -4.49$ is the solar abundance of Si. Inserting the values for each parameter, M_g^{cool} can be simply written in terms of M_Z^{cool} : $M_g^{\text{cool}} \simeq 10^2 (Z/Z_{\odot})^{-1} M_Z^{\text{cool}}$.

⁷ If these 3 upper limits are included or excluded from the sample, the means are essentially the same.

In Table 6, we summarize the estimated metal mass over different regions of the CGM for the three models of $N_{\text{Si}}(R)$, within R_{200} (first entry), within R_{vir} (second entry), within $1/2R_{\text{vir}}$ (third entry), between $1/2R_{\text{vir}}$ and R_{vir} (fourth entry), and within 360 kpc (fifth entry), which corresponds to the radius where at least one of the Si ions is always detected (beyond that, the number of detections drastically plummets). A key difference between the H/SPL models and the GP model is that the range of values for the H/SPL models is derived using the low (dotted) and high (dashed) curves in Fig. 10 while for the GP models we actually use the standard deviations from the low and high models (i.e., the top and bottom of the shaded blue curve in Fig. 10). Hence it is not surprising that the mass ranges for the GP model are larger. Nevertheless there is a large overlap between the three models. As the GP results overlap with the other models and provide empirical confidence intervals, we adopt them for the remaining of the paper. At R_{vir} , the metal and cool gas masses are therefore $(2.0 \pm 0.5) \times 10^7$ and $2 \times 10^9 (Z/Z_{\odot})^{-1} M_{\odot}$, respectively. Owing to the new functional form of $N_{\text{Si}}(R)$ and how the lower limits are treated, this explains the factor 1.4 times increase in the metal mass compared to that derived in LHW15.

These masses do not include the more highly ionized gas traced by O VI or C IV. Even though the sample with O VI is smaller than C IV, we use O VI to probe the higher ionization gas phase because as we show above the properties of O VI (column density and covering fraction as a function of R) are quite different from all the other ions, including C IV, which behaves more like the other, lower ions. Furthermore, Lehner et al. (2011) using $1.5\text{--}3 \text{ km s}^{-1}$ resolution UV spectra show that C IV can probe cool and hotter gas while the profiles of N V and O VI are typically broad and more consistent with hotter gas. Since O VI is always detected and there is little evidence for variation with R (see Fig. 8), we can simply use the mean column density $\log N_{\text{O VI}} = 14.46 \pm 0.10$ (error on the mean using the survival method for censoring) to estimate the baryon mass assuming a spherical distribution:

$$M_{\text{g}}^{\text{warm}} = \pi r^2 m_{\text{H}} \mu f_{\text{c}} \frac{N_{\text{O VI}}}{f_{\text{O VI}}^i} \left(\frac{\text{O}}{\text{H}}\right)_{\odot}^{-1} \left(\frac{Z}{Z_{\odot}}\right)^{-1},$$

where the O VI ionization fraction is $f_{\text{O VI}}^i \lesssim 0.2$ (see §4.3), $f_{\text{c}} = 1$ for O VI at any R (see Fig. 8). At R_{vir} , we find $M_{\text{g}}^{\text{warm}} \gtrsim 9.3 \times 10^9 (Z/Z_{\odot})^{-1} M_{\odot}$ or $M_{\text{g}}^{\text{warm}} \gtrsim 4.4 M_{\text{g}}^{\text{cool}}$ (assuming the metallicity is about similar in the cooler and hotter gas-phases). At R_{200} , we find $M_{\text{g}}^{\text{warm}} \gtrsim 5.5 \times 10^9 (Z/Z_{\odot})^{-1} M_{\odot}$ (assuming the metallicity is similar in the cooler and hotter gas-phases). These are lower limits because the fraction of O VI could

be much smaller than 20% and the metallicity of the cool or warm ionized gas is also likely to less than solar (see below). In terms of metal mass in the highly ionized gas-phase, we have $M_{\text{g}}^{\text{warm}} \simeq 10^2 (Z/Z_{\odot})^{-1} M_{\text{Z}}^{\text{warm}}$ and hence also $M_{\text{Z}}^{\text{warm}} \gtrsim 4.4 M_{\text{Z}}^{\text{cool}}$. Since O VI is detected out to the maximum surveyed radius of 569 kpc, and at that radius (i.e., $1.9R_{\text{vir}}$), $M_{\text{g}}^{\text{warm}} \gtrsim 34 \times 10^9 (Z/Z_{\odot})^{-1} M_{\odot}$.

By combining both the cool and hot gas-phase masses, we can find the baryon mass for gas in the temperature range $\sim 10^3\text{--}10^{5.5} \text{ K}$ at R_{vir} :

$$M_{\text{g}} = M_{\text{g}}^{\text{cool}} + M_{\text{g}}^{\text{warm}} \\ \gtrsim 1.1 \times 10^{10} \left(\frac{Z}{Z_{\odot}}\right)^{-1} M_{\odot}.$$

Within R_{200} , the total mass $M_{\text{g}} \gtrsim 7.2 \times 10^9 M_{\odot}$. As the stellar mass of M31 is about $10^{11} M_{\odot}$ (e.g., Geehan et al. 2006; Tamm et al. 2012), the mass of the diffuse weakly and highly ionized CGM of M31 within $1R_{\text{vir}}$ is therefore at least 10% of the stellar mass of M31 and could be significantly larger than 10%.

This estimate does not take into account the hot ($T \gtrsim 10^6 \text{ K}$) coronal gas. The diffuse X-ray emission is observed to extend to about 30–70 kpc around a handful of massive, non-starbursting galaxies (Anderson & Bregman 2011; Bregman et al. 2018) or in stacked images of galaxies (Anderson et al. 2013; Bregman et al. 2018), but beyond 50 kpc, the CGM is too diffuse to be traced with X-ray imaging, even though a large mass could be present. Using the results summarized recently by Bregman et al. (2018), the hot gas mass of spiral galaxy halos is in the range $M_{\text{g}}^{\text{hot}} \simeq 1\text{--}10 \times 10^9 M_{\odot}$ within 50 kpc. For M31, $M_{\text{g}} = M_{\text{g}}^{\text{cool}} + M_{\text{g}}^{\text{warm}} \gtrsim 0.4 \times 10^9 M_{\odot}$ within 50 kpc. Extrapolating the X-ray results to R_{vir} , Bregman et al. (2018) find masses of the hot X-ray gas similar to the stellar masses of these galaxies in the range $M_{\text{g}}^{\text{hot}} \simeq 1\text{--}10 \times 10^{11} M_{\odot}$. For the MW hot halo within $1R_{\text{vir}}$, Gupta et al. (2017) (but see also Gupta et al. 2012, 2014; Wang & Yao 2012; Henley et al. 2014) derive $3\text{--}10 \times 10^{10} M_{\odot}$, i.e., on the low side of the mass range listed in Bregman et al. (2018). The hot gas could therefore dominate the mass of the CGM of M31. There are, however, two caveats to that latter conclusion. First, if $f_{\text{O VI}} \ll 0.2$, then $M_{\text{g}}^{\text{warm}}$ could be become much larger. Second, the metallicity of the hot X-ray gas ranges from 0.1 to $0.5Z_{\odot}$ with a mean metallicity of $0.3Z_{\odot}$ (Bregman et al. 2018; Gupta et al. 2017), while for the cooler gas we have conservatively adopted a solar abundance. If instead we adopt a $0.3Z_{\odot}$ metallicity (consistent with the rough limits set in §§4.1, 4.2), then $M_{\text{g}} \simeq 3.7 \times 10^{10} M_{\odot}$ at R_{vir} , which is now comparable to the hot halo mass of the MW. If we adopt the average metallicity de-

rived for the X-ray gas, then $M_g^{\text{cool}} + M_g^{\text{warm}}$ would be comparable to the hot gas mass if $M_g^{\text{hot}} \sim 5 \times 10^{10} M_\odot$ at R_{vir} for M31. Depending on the true metallicities and the actual state of ionization, the cool and warm gas in the M31 halo could therefore contribute to a substantial enhancement of the total baryonic mass compared to our conservative assumptions.

4.9. Mapping the Metal Surface Densities in the CGM of M31

Thus far, we have ignored the distribution of the targets in azimuthal angle (Φ) relative to the projected minor and major axes of M31, where different physical processes may occur. In Fig. 13, we show the distribution of the column densities of each ion in the X–Y plane near M31 where the circles represent detections and downward triangles are non-detections. Multiple colors in a given circle indicate several components along that sightline for that ion. In that figure, we also show the projected minor and major axes of M31 (dashed lines). The overall trends that are readily apparent from Fig. 13 are the ones already described in the previous sections: 1) overall the column density decreases with increasing R , 2) the decrease in N is much stronger for low ions than high ions, 3) Si III and O VI are observed at any R while singly ionized species tend to be more frequently observed at small impact parameters. This figure (and Fig. 9) also reveals that absorption with two or more components is observed more frequently at $R < 200$ kpc: using Si III, 64%–86% of the sightlines have at least 2 velocity components at $R < 200$ kpc, while this drops to 14%–31% at $R > 200$ kpc (68% confidence intervals using the Wilson score interval); similar results are found using the other ions. However, the complexity of the velocity profiles does not change with Φ .

Considering various radius ranges (e.g., 25–50 kpc, 50–100 kpc, etc.) up to $1R_{\text{vir}}$, there is no indication that the column densities strongly depend on Φ . Considering Si III first, it is equally detected along the projected major and minor axes and in-between (wherever there is a sightline) and overall the strength of the absorption mostly depends on R , not Φ . Considering the other ions, they all show a mixture of detections and non-detections, and the non-detections (that are mostly beyond 50 kpc) are not preferentially observed along a certain axis or one of the regions shown in Fig. 13. We therefore find no strong evidence of an azimuthal dependence in the column densities.

Beyond $\gtrsim 1.1R_{\text{vir}}$, the situation is different with all but one detection (in C IV and O VI only) being near the southern projected major axis and about 52° east off near the $X = 0$ kpc axis. There is detection in this

region of Si III, C IV, Si IV, O VI, and also C II. That is the main region where C II is detected beyond 200 kpc. In contrast, between the $X = 0$ kpc axis and southern projected minor axis, the only region where there are several QSOs beyond R_{vir} , there is no detection in any of the ions (excluding O VI because there is no *FUSE* observations in these directions). Although that direction is suspiciously in the direction of the MS, it is very unlikely to be additional contamination from the MS because 1) the velocities would be off from those expected of the MS in these directions (see Fig. 3 and also §4.10), and 2) there is no overall decrease of the column densities as $|b_{\text{MS}}|$ increases, a trend observed for the components identified as the MS components (see Fig. 4). In fact, regarding the second point, the opposite trend is observed with the highest column densities being more frequently at $|b_{\text{MS}}| \gtrsim 15^\circ$ than near the MS main axis ($b_{\text{MS}} \sim 0^\circ$). Therefore while at $R < R_{\text{vir}}$ there is no apparent trend between N and Φ for any ions (although we keep in mind that the azimuthal information for O VI is minimal), most of the detections at $R > R_{\text{vir}}$ are near the southern projected major axis and 52° east off of that axis.

The fact that the gas is observed mainly in a specific region of the CGM beyond R_{vir} suggests an IGM filament feeding the CGM of M31, as is observed in some cosmological simulations. In particular, [Nuza et al. \(2014\)](#) study the gas distribution in simulated recreations of MW and M31 using a constrained cosmological simulation of the Local Group from the Constrained Local UniversE Simulations (CLUES) project. In their Figures 3 and 6, they show different velocity and density projection maps where the central galaxy (M31 or MW) is edge-on. They find that some of the gas in the CGM can flow in a filament-like structure, coming from outside the virial radius all the way down to the galactic disk.

4.10. Mapping the Velocities in the CGM of M31

How the velocity field of the gas is distributed in R and Φ beyond 25–50 kpc is a key diagnostic of accretion and feedback. However, a statistical survey using one sightline per galaxy (such as COS-Halos) cannot address this problem because it observes many galaxies in an essential random mix of orientations and inclinations, which necessarily washes out any coherent velocity structures. An experiment like Project AMIGA is needed to access information about large-scale flows in a sizable sample of lines of sight for a single galaxy. The velocity information remains limited because we have only the (projected) radial velocity along pencil beams piercing the CGM at various R and Φ . Nevertheless as we show be-

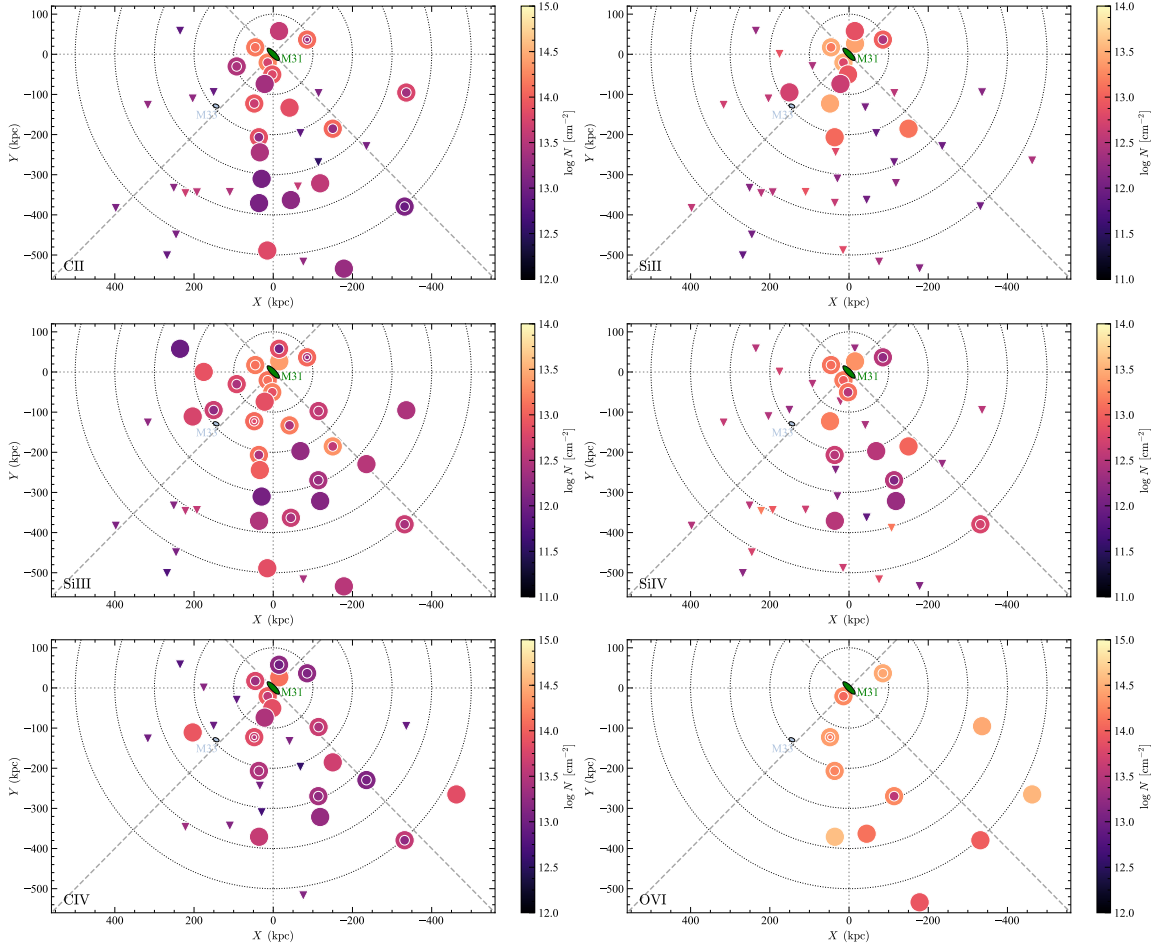


Figure 13. Positions of the Project AMIGA targets relative to the M31, where the axes show the physical impact parameter from the center of M31 (north is up, east to the left). Dotted circles are centered on M31 to mark 100 kpc intervals. The dashed lines represent the projected minor and major axes of M31 and the thin dotted lines are $\pm 45^\circ$ from the major/minor axes (which by definition of the coordinate systems also correspond to the vertical and horizontal zero-axis). Each panel corresponds to a different ion. In each panel, the column densities of each velocity component are shown and color coded according the vertical color bar. Circles represent detections while triangles are non-detections. Circles with several color indicate the observed absorption along the sightlines have more than one component.

low some trends are apparent thanks to the large size of the sample. We use here the v_{M31} peculiar velocities as defined by Eqn. 2. By definition, in the M31 velocity frame, an absorber with no peculiar velocity relative to M31's bulk motion has $v_{\text{M31}} = 0 \text{ km s}^{-1}$. In §3.2, we show that the M31 peculiar velocities of the absorbers seen toward the QSOs and the velocities of the M31 dwarf satellites largely overlap. We now review how the velocities of the absorbers are distributed in the CGM of M31 over the entire surveyed range of R .

In Figs. 14 and 15, we show the distribution of the M31 peculiar velocities of the individual components identified for each ion and column-density-weighted average velocities of each ion, respectively. Circles with several colors indicate that the observed absorption appears in more than one component. Both Figs. 14 and 15 demon-

strate that in many cases there is some overlap in the velocities between low ions (Si II, C II, Si III) and higher ions (Si IV, C IV, O VI). This strongly implies that the CGM of M31 has multiple gas-phases with overlapping kinematics when they are observed in projection (a property also readily observed from the normalized profiles shown in Fig. 2 and as supplemental material in Appendix G). There are also some rarer cases where there is no velocity correspondence in the velocities between Si III and higher ions (see, e.g., near $X \simeq -335$ $Y \simeq -95$ kpc), indicating that the observed absorption in each ion is dominated by a single phase—that is, the components are likely to be distinct single-phase objects.

The full range of velocities associated with the CGM of M31 are between $-249 \leq v_{\text{M31}} \leq +175 \text{ km s}^{-1}$ for Si III, but for all the other ions it is $-53 \lesssim$

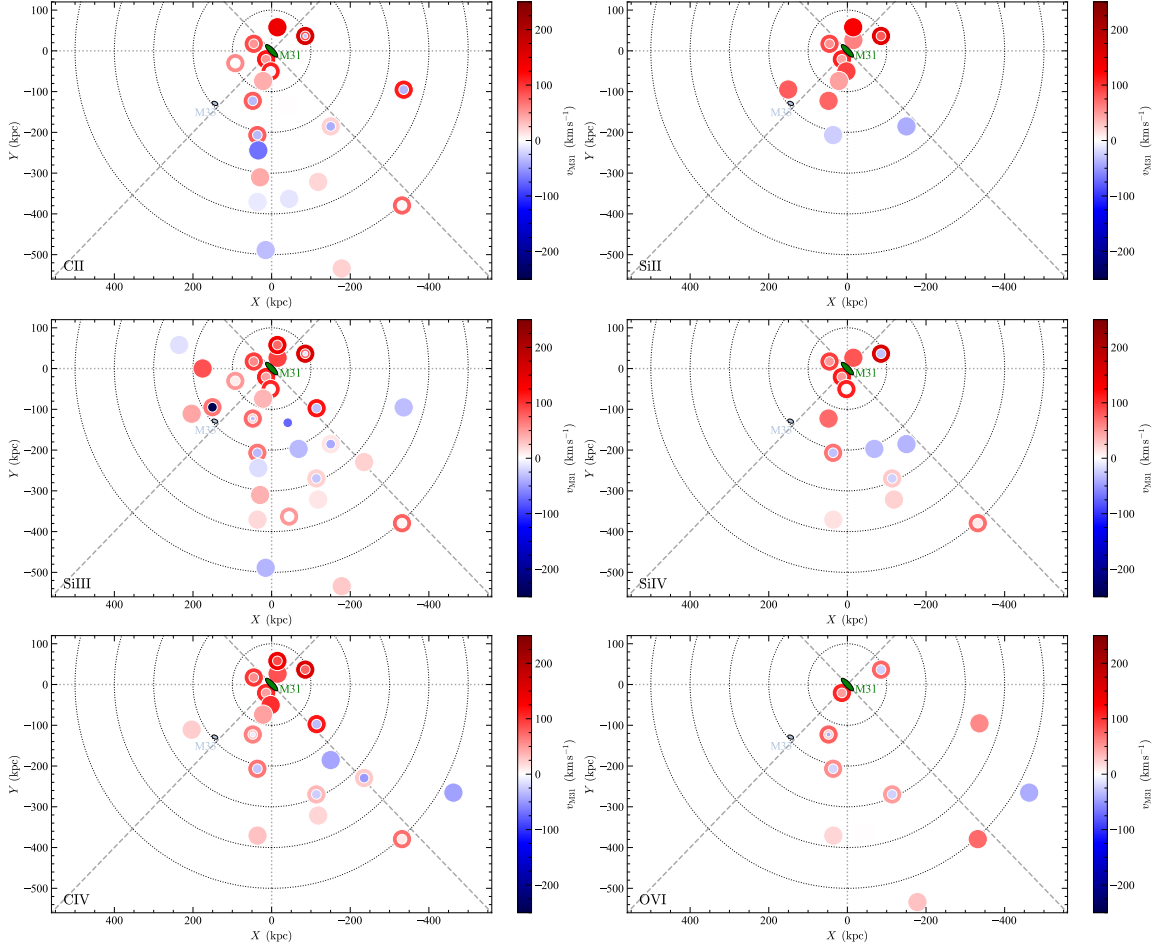


Figure 14. Similar to Fig. 13, but we now show the distribution of the M31 velocities for each component observed for each ion. Circles with several color indicate the observed absorption along the sightlines have more than one components. By definition, in the M31 velocity frame, an absorber with no peculiar velocity relative to M31’s bulk motion has $v_{\text{M31}} = 0 \text{ km s}^{-1}$.

$v_{\text{M31}} \leq +175 \text{ km s}^{-1}$. Furthermore there is only one absorber/component of Si III that has $v_{\text{M31}} = -249 \text{ km s}^{-1}$. We emphasize that the rarity of velocity $v_{\text{M31}} < -249 \text{ km s}^{-1}$ (corresponding to $v_{\text{LSR}} < -510 \text{ km s}^{-1}$ in the direction of this sightline) is not an artifact since velocities below these values are not contaminated by any foreground gaseous features.

We show in §3.2 that the velocity dispersion of the M31 dwarf satellites have a velocity dispersion that is larger (110 km s^{-1} for the dwarfs vs. 68 km s^{-1} for the Si III absorbers) and the M31 dwarfs have some velocities in the velocity range contaminated by the MW and MS. While the CGM gas velocity field distribution may not follow that of the dwarf satellites, it remains plausible that some of the absorption from the extended region of the M31 CGM could be lost owing to contamination from the MW or MS. Therefore we may not be fully probing the entire velocity distribution of the M31 CGM. However, as discussed in §2.5, there is no evidence that the velocity distributions of the Si III component

in and outside the MS contamination zone are different (see also Figs. 1 and 14), and hence it is quite possible that at least the MS contamination does not affect much the velocity distribution of the M31 CGM. With these caveats, we now proceed describing the apparent trends of the velocity distribution in the CGM of M31.

From Fig. 14, the first apparent property was already noted in the previous section: the velocity complexity (and hence full-width) of the absorption profiles increases with decreasing R (see §4.9). Within $R \lesssim 100 \text{ kpc}$ or $\lesssim 200 \text{ kpc}$, about 75% of the Si III absorbers have at least two components (at the COS G130M-G160M resolution). This drops to about 33% at $200 < R \lesssim 569 \text{ kpc}$.

The second property evident from either Fig. 14 or Fig. 15 is that the M31 peculiar velocities are larger at $R \lesssim 100 \text{ kpc}$ than at higher R . Table 7 lists the average M31 velocities, their standard deviations, and their interquartile ranges (IQRs) for the individual components and averaged components in three samples; the

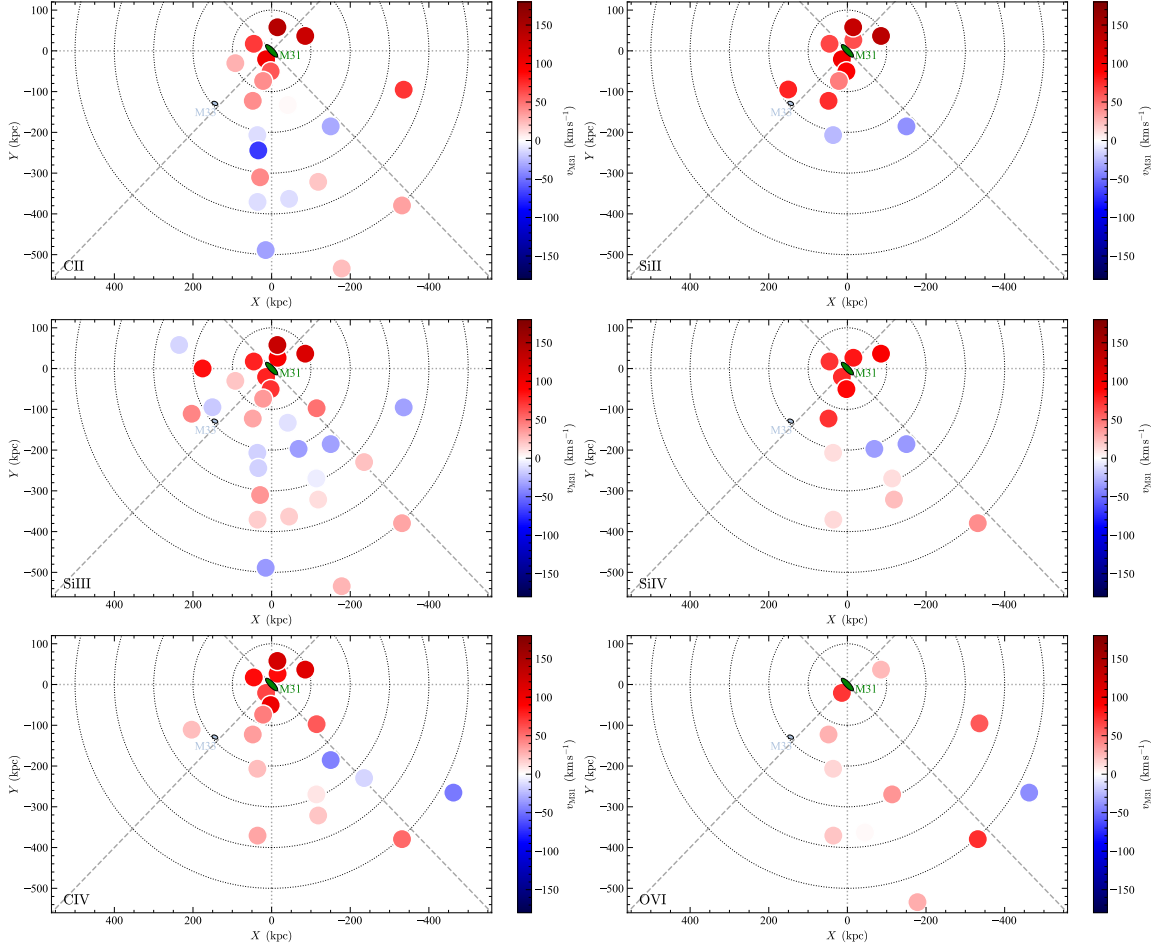


Figure 15. Same as Fig. 14, but for the average velocities.

full AMIGA set, the subset with $R \leq 100$ kpc, and the subset with $R > 100$ kpc. From this table and for all the ions besides O VI, $\langle v_{M31} \rangle = 90 \text{ km s}^{-1}$ at $R \leq 100$ kpc, while at $R > 100$ kpc, $\langle v_{M31} \rangle = 20 \text{ km s}^{-1}$, a factor 4.5 times smaller. There are only two data points for O VI, at $R \leq 100$ kpc, but the average at $R > 100$ kpc is $\langle v_{M31} \rangle = 22 \text{ km s}^{-1}$, following a similar pattern as observed for the other ions. For all the ions but C II, the velocity dispersions or IQRs are smaller at $R \leq 100$ kpc than at $R > 100$ kpc.

The third property observed in Fig. 14 or Fig. 15 is that at $R \leq 100$ kpc, there is no evidence for negative M31 velocities, while at $R > 100$ kpc, about 40% of the Si III sample has blueshifted v_{M31} velocities. This partially explains the previous result, but even if we consider the absolute velocities, $\langle |v_{M31}| \rangle = 40 \text{ km s}^{-1}$ at $R > 100$ kpc, implying $\langle |v_{M31}(R > 100)| \rangle = 0.44 \langle |v_{M31}(R \leq 100)| \rangle$, i.e., in absolute terms or not, v_{M31} is smaller at $R > 100$ kpc than at $R \leq 100$ kpc. Therefore at $R > 100$ kpc, not only are the peculiar velocities of the CGM gas less extreme, but they are

also more uniformly distributed around the bulk motion of M31. At $R < 100$ kpc, the peculiar velocities of the CGM gas are more extreme and systematically redshifted relative to the bulk motion of M31.

The fourth property appears in Fig. 7 where we compare v_{M31} velocities of the M31 dwarfs and Si III absorbers, which shows that overall the velocities of the satellites and the CGM gas do not follow each other. As noted in §3.3 (see also Table 4), some velocity components seen in absorption toward the QSOs are found with $\Delta_{\text{sep}} < 1$ and have $\delta v < v_{\text{esc,dwarf}}$. However, the last two trends found for the CGM gas are not observed for the dwarfs. Fig. 7 shows that both blue- and redshifted v_{M31} velocities are observed at any R and v_{M31} above and below 50 km s^{-1} are also observed at any R . More quantitatively, at $R > 100$ kpc or $R \leq 100$ kpc, $\langle v_{M31,\text{dwarf}} \rangle \simeq 34 \text{ km s}^{-1}$ ($\langle |v_{M31,\text{dwarf}}| \rangle \simeq 102 \text{ km s}^{-1}$), remarkably contrasting with the properties of the CGM gas described in the previous two paragraphs. These findings strongly suggests that the velocity fields of the dwarfs and CGM gas are decoupled. We infer from

this decoupling that (1) gas bound to satellites does not make a significant contribution to CGM gas observed in this way, and (2) the velocities of gas removed from satellites via tidal or ram-pressure interactions, if it is present, becomes decoupled from the dwarf that brought it in (as one might expect from its definition as unbound to the satellites).

The fifth property is more readily apparent considering the average velocities shown in Fig. 15 where considering the CGM gas in different annuli, there is an apparent change in the sign of the average v_{M31} velocities with on average a positive velocity in at $R < 200$ kpc, negative velocity in $200 < R < 300$ kpc, and again positive velocity in $300 < R < 400$ kpc. This is more evident with Si III where the sample of absorbers is larger, but taking the average velocities in the different annuli, the same pattern is observed for C II, Si III, Si IV, and C IV. Beyond $\gtrsim 1.1R_{\text{vir}}$ (330 kpc), there is the region of gas that we have identified in §4.9 that is observed between near the southern projected major axis and about 52° east off near the $X = 0$ kpc axis. In that region v_{M31} is predominantly positive.

We emphasize again that the MS contamination does not really alter these properties and neither is the source of these properties. As shown in Fig. 1 (see also §2.5), the MS contamination dominantly occurs in the region $X < 0$ for any Y . There is no evidence that these properties change with Φ and in particular between the quadrants $X < 0$ and $X > 0$ (see §2.5). Absorption occurring in the velocity range $-50 \lesssim v_{M31} \lesssim +150 \text{ km s}^{-1}$ is also not contaminated by the MS.

5. DISCUSSION

The major goal of Project AMIGA is to determine the global distribution of the gas phases and metals through the entire CGM of a representative galaxy. With a large sample of QSOs accumulated over many surveys, and newly observed by *HST*/COS, we are able to probe multiple sightlines that pierce M31 at different radii and azimuthal angles. Undertaking this study in the UV has been critical since only in this wavelength band there are the diagnostics and spectral resolution to constrain the physical properties of the multiple gas-phases existing in the CGM over $10^4\text{--}5.5$ K (for $z = 0$, the hottest phase can only be probed with X-ray observations). With 25 sightlines within about $1.1R_{\text{vir}}$ and 43 within 569 kpc ($\lesssim 1.9R_{\text{vir}}$) of M31, the size of the sample and the information as a function of R and Φ are unparalleled. We will now consider the broad patterns and conclusions we can draw from this unique dataset.

5.1. Pervasive Metals in the CGM of M31

A key finding of Project AMIGA is the ubiquitous presence of metals in the CGM of M31. While the search for H I with $\log N_{\text{HI}} \gtrsim 17.5$ in the CGM of M31 toward pointed radio observations has been unsuccessful in the current sample (Paper I and see Fig. 1), the covering factor of Si III (29 sightlines) is essentially 100% out to $1.2R_{\text{vir}}$, while O VI associated with M31 is detected toward all 11 sightlines with FUSE data, all the way out to $1.9R_{\text{vir}}$, the maximum radius of our survey (see §§4.4, 4.6). From the ionization range probed by Project AMIGA, we further show that Si III and O VI are key probes of the diffuse gas (see §4.7). With information from Si II, Si III, and Si IV, we demonstrate that Si III is the dominant ion in the ionizing energy range 8–45 eV (see §4.7.1). The fact that Si III and O VI have such high covering factors suggests that these ions are not produced in small clumps within a hotter medium; instead it must be more pervasively distributed.

The finding of pervasive metals in the CGM of M31 is a strong indication of ongoing and past gas outflows that ejected metals well beyond their formation site. Based on a specific star-formation rate of $\text{SFR}/M_\star = (5 \pm 1) \times 10^{-12} \text{ yr}^{-1}$ (using the stellar mass M_\star and SFR from Geehan et al. 2006; Kang et al. 2009), M31 is not currently in an active star-forming episode. In fact, Williams et al. (2017) show that the bulk of star formation occurred in the first ~ 6 billion years and the last strong episode happened over ~ 2 billion years ago (see also Fig. 6 in Telford et al. 2019 for a metal production model of M31). Hence most of the metals seen in the CGM of M31 have most likely been ejected by previous star-forming episodes and/or stripped from its dwarfs and more massive companions. However, the fact that metals are detected beyond R_{vir} , and, that beyond R_{vir} they are found predominantly in a certain direction, also suggests that some of the metals may be coming from the Local group medium, possibly recycling metals from the MW or M31 (see §4.9), or from an IGM filament in that particular direction.

In §4.8, we estimate that the mass of metals $M_Z^{\text{cool}} = (2.0 \pm 0.5) \times 10^7 M_\odot$ within R_{vir} for the predominantly photoionized gas probed by Si II, Si III, and Si IV. For the gas probed by O VI, we find that $M_Z^{\text{warm}} > 4.4M_Z^{\text{cool}} \gtrsim 9 \times 10^7 M_\odot$ at R_{vir} (this is a lower limit because the fractional amount of O VI is an upper limit, see §4.8). The sum of these two phases yields a lower limit to the CGM metal mass because the hotter phase probed by the X-ray and metals bound in dust are not included. If the hot baryon mass of M31 is not too different from that estimated for the MW (see §4.8), then we expect $M_Z^{\text{hot}} \approx M_Z^{\text{warm}}$. The CLUES simulation of the Local group estimates that the mass of the hot ($> 10^5$

K) gas is a factor 3 larger than the cooler ($< 10^5$ K) gas (Nuza et al. 2014). The dust CGM mass remains quite uncertain, but could be at the level of $5 \times 10^7 M_\odot$ according to estimates around $0.1\text{--}1L^*$ galaxies (Ménard et al. 2010; Peebles et al. 2014; Peek et al. 2015). Hence the total metal mass of the CGM of M31 out to R_{vir} could be as large as $M_Z^{\text{CGM}} \gtrsim 2.5 \times 10^8 M_\odot$.

The stellar mass of M31 is $(1.5 \pm 0.2) \times 10^{11} M_\odot$ (e.g., Williams et al. 2017). Using this result, Telford et al. (2019) estimated that the current metal mass in stars is $3.9 \times 10^8 M_\odot$, i.e., about the same amount that is found in the entire CGM of M31 up to R_{vir} . Telford et al. (2019) also estimated the metal mass of the gas in the disk of M31 to be around $(0.8\text{--}3.2) \times 10^7 M_\odot$, while Draine et al. (2014) estimated the dust mass in the disk to be around $5.4 \times 10^7 M_\odot$, yielding a total metal mass in the disk of M31 of about $M_Z^{\text{disk}} \simeq 5 \times 10^8 M_\odot$. Therefore M31 has in its CGM within R_{vir} at least 50% of the present-day metal mass in its disk. As we show in §4.4 and §4.8 and discuss above, metals are also found beyond R_{vir} , especially in the more highly ionized phase traced by O VI (and even higher ions). These metals could come from M31 or being recycled in the Local group from the MW or dwarf galaxies.

5.2. Comparison with COS-Halos Galaxies

The Project AMIGA experiment is quite different from most of the surveys of the CGM of galaxies done so far. Outside the local universe, surveys of the CGM of galaxies involve assembling samples of CGM gas in aggregate by using one sightline per galaxy (see §1), and in some nearby cases up to 3–4 sightlines (e.g., Bowen et al. 2016; Keeney et al. 2017). By assembling a sizable sample of absorbers associated with galaxies in a particular sub-population (e.g. L^* , sub- L^* , passive or star-forming galaxies), one can then assess how the column densities change with radii around that kind of galaxy, and from this estimate average surface densities, mass budgets, etc. can then be evaluated. By contrast, Project AMIGA has assembled almost as many sightlines surrounding M31 as COS-Halos had for its full sample of 44 galaxies. We can now make a direct comparison between these two types of experiments. For this comparison, we use the COS-Halos survey of $0.3 < L/L^* < 2$ galaxies at $z \simeq 0.2$, which selected galaxies within about 160 kpc from the sightline (Tumlinson et al. 2011, 2013; Werk et al. 2013, 2014). The full mass range of the COS-Halos galaxies is quite large, $11.5 \lesssim \log M_{200} \lesssim 13.7$, but most of the star-forming galaxies are in the range $11.5 \lesssim \log M_{200} \lesssim 12.5$ and most of the passive quiescent galaxies have $13.0 \lesssim \log M_{200} \lesssim 13.7$. As a reminder, M31 has $\log M_{200} = 12.1$ (see §1).

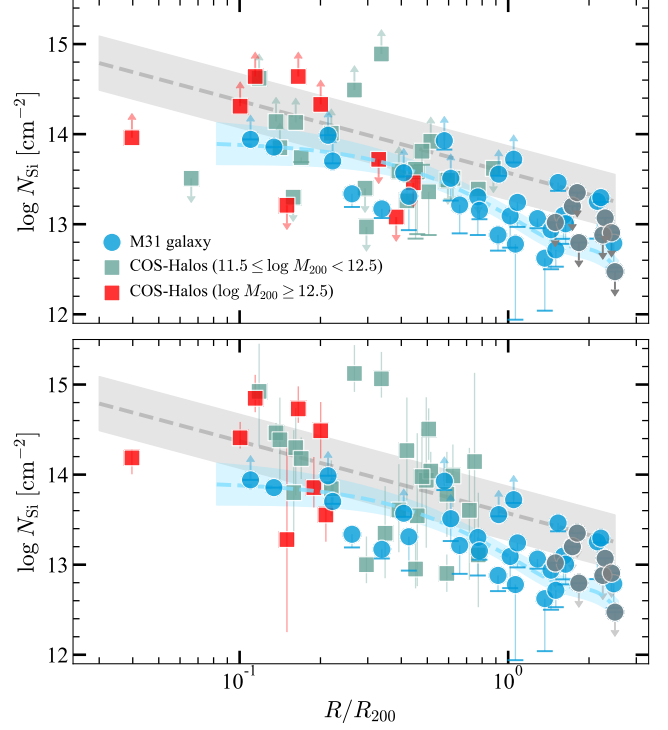


Figure 16. Comparison of the total column densities of Si from M31 and the COS-Halos galaxies as a function of R/R_{200} . *Top panel:* N_{Si} are directly constrained by the estimates on $N_{\text{Si II}}$, $N_{\text{Si III}}$, and $N_{\text{Si IV}}$ from the observations for both Project AMIGA and COS-Halos (Werk et al. 2013). The error bars are less than the size of the square and the vertical bars include the range of possible values if the non-detections are either near their 3σ upper limits or so low as to be negligible. *Bottom panel:* same as top panel but N_{Si} for the COS-Halos data is derived from Cloudy photoionization models (Werk et al. 2014). The gray dashed line and shaded region represent the best fit between N_{Si} and R/R_{200} and its dispersion using COS-Halos modeled data. The blue area shows the full range of the GP model of the Project AMIGA data (see §4.5).

5.2.1. Column Densities of Si vs. R

In Fig. 16, we show the total column densities of Si as a function of R/R_{200} for the COS-Halos galaxies and M31. For the COS-Halos survey, each data point corresponds to an absorber at some impact parameter from a galaxy, while for M31, each data point is an absorber probing the CGM at a different impact parameter from the same galaxy. For COS-Halos, we consider two cases: 1) the column densities of Si estimated in a similar fashion as those for M31; and 2) the column densities of Si estimated from photoionization modeling. For case 2) we use the results from Werk et al. (2014) (see also Prochaska et al. 2017b), which were used to determine the metal mass of the CGM of the COS-Halos galaxies

in Peeples et al. (2014). For case 1), we use the results from Werk et al. (2013) and follow the procedure in §4.5 to estimate N_{Si} from the column densities of Si II, Si III, and Si IV. We require that all three Si ions are available, except in the cases where there are only lower limits for two ions (typically Si II and Si III) since in that case the resulting column density is a lower limit that encompasses any missing column density from the remaining Si ion (typically Si IV). The sample size in case 1) is 35, while it is 33 in case 2) with some overlap between the two subsamples. In Fig. 16, we also show the modeled column density of Si as a function of R , in gray for COS-Halos and blue for M31 (we show the adopted GP model, see §4.5).

A striking difference between the COS-Halos and M31 data immediately apparent from Fig. 16 is that, at $R/R_{200} \lesssim 0.3$, there is a large amount of very high Si column densities in COS-Halos that are absent in Project AMIGA. The reason that the COS-Halos Si column densities have higher lower limits than those of M31 is because the weak transitions of Si II are saturated in COS-Halos, a situation not observed in M31 toward any of the sightlines—the lower limits of Si arise only because Si III is saturated. These high Si column densities also correspond to the very strong N_{HI} ($\log N_{\text{HI}} \gtrsim 18$) absorbers observed in COS-Halos, but again not in M31 (Paper I). However, while for H I, the beam dilution could have affected somewhat the interpretation of the difference between COS-Halos (H I absorption) and M31 (H I emission), for the metal ions this is not an issue. Therefore the higher frequency of saturated weak Si II transitions in COS-Halos compared to M31 is a real effect, not an artifact.

Besides this difference, the estimated Si column densities from the observations in the COS-Halos and Project AMIGA surveys are distributed with a similar scatter at larger impact parameters ($R/R_{200} \gtrsim 0.4$) where the gas is more ionized (see top panel in Fig. 16). The photoionization-modeled COS-Halos Si displayed on the bottom panel have some higher values than observed in the top panel, but in the impact parameter region $0.4 \lesssim R/R_{200} \lesssim 0.8$ where they are observed, there are also several lower limits. Beyond $R > 0.9R_{200}$, there is no COS-Halos observation (owing to the design of the survey). The extrapolated model to the COS-Halos observations shown in gray in Fig. 16 is a factor 2–4 higher than the models of the Project AMIGA data shown in blue depending on R/R_{200} .

A likely explanation for the higher column density absorbers is that some of these COS-Halos absorbers could be fully or partly associated with a closer galaxy than the initially targeted COS-Halos galaxies where

the gas can contain more neutral and weakly ionized gas. Indeed, while the COS-Halos galaxies were selected to have no bright companion, that selection did not preclude fainter nearby companions such as dwarf satellites (see Tumlinson et al. 2013). Galaxy observation follow-up by Werk et al. (2012) found several $L > 0.1L^*$ galaxies within 160 kpc of the targeted COS-Halos galaxy. Comparing the results from other surveys of galaxies/absorbers at low redshift (Stocke et al. 2013; Bowen et al. 2002), Bregman et al. (2018) also noted a higher preponderance of high H I column density absorbers in the COS-Halos survey. However, the higher COS-Halos column densities at large radii could also be an effect of evolution in the typical CGM, as COS-Halos probed a slightly higher cosmological redshift. It is also possible that the M31 CGM is less rich in ionized gas at these radii than the typical L^* galaxy at $z \sim 0.2$, because of its star formation history or environment.

5.2.2. CGM Mass Comparison

Among a key physical parameter of the CGM is its mass, which is obtained from the column density distribution of the gas and assuming a certain geometry of the gas. For M31, we cannot derive the baryonic mass of CGM gas without assuming a metallicity since the H I column density remains unknown toward all the targets in our sample (but see §4.1, 4.8). However, the metal mass of the cool gas probed by Si II, Si III, and Si IV can be straightforwardly estimated directly from the observations without any ionization modeling (see top panel of Fig. 16).

Even though both Peeples et al. (2014) and Werk et al. (2014) use the Si column densities derived from photoionization models, as illustrated in Fig. 16, this would not change the outcome that the metal mass of the cool CGM gas derived from the COS-Halos survey is about a factor 2–3 higher than the metal mass derived in Project AMIGA. This is because there are 7 COS-Halos Si column densities at $R/R_{200} < 0.3$ that are much higher owing to saturation in the weak Si II transitions (see above), driving the overall model of $N_{\text{Si}}(R)$ substantially higher. The fact that these high N_{Si} are not found in the CGM of M31 or lower redshift galaxies at similar impact parameters (e.g., Bowen et al. 2002; Stocke et al. 2013) suggests a source of high-column H I and Si II absorbers in the COS-Halos sample that could be recent outflows, strong accretion/recycling, or gas associated with closer satellites to the sightline. With only 5 targets within $R/R_{200} < 0.3$ and none below $R/R_{200} < 0.1$ for M31, it would be quite useful to target more QSOs in the inner region of the CGM of M31 to better determine how $N_{\text{Si}}(R)$ varies with R at small impact parameters.

For the warm-hot gas probed by O VI, the COS-Halos star-forming galaxies have $\langle N_{\text{O VI}} \rangle = 10^{14.5} \text{ cm}^{-2}$, a detection rate close to 100%, and no large variation of $N_{\text{O VI}}$ with R (Tumlinson et al. 2011). For M31, we have a similar average O VI column density, hit rate, and little evidence for any large variation of $N_{\text{O VI}}$ with R (see §4.8). This implies that the masses of the warm-hot CGM of M31 and COS-Halos star-forming galaxies are similar. M31 has a specific SFR that is a factor $\gtrsim 10$ lower than the COS-Halos star-forming galaxies, but its halo mass is on the higher side of the COS-Halos star-forming galaxies (but lower than the COS-Halos quiescent galaxies). As discussed in §5.3.3 in more detail, M31 and the COS-Halos star-forming galaxies have halo masses in the range $M_{200} \simeq 10^{11.7} - 10^{12.3} M_{\odot}$, corresponding to a virial temperature range that overlaps with the temperature at which the ionization fraction of O VI peaks, which may naturally explaining some of the properties of the O VI in the CGM of “ L^* ” galaxies (Oppenheimer et al. 2018b). It is also possible that some O VI arises in photoionized gas or combinations of different phases (see §5.3.3).

Based on the comparison above, we find that the O VI is less subject to the uncertainty in the association of the absorber to the correct galaxy owing to its column density being less dependent on R (see also §5.3). Therefore this leads to similar metal masses of the CGM of the $z \sim 0.2$ COS-Halos galaxies and M31 for the O VI gas-phase. For the lower ions, their column densities are more dependent on R (see also §5.3). Therefore the association of the absorber to the correct galaxy is more critical to derive an accurate column density profile with R and hence derive an accurate CGM metal mass. However, we note that despite these uncertainties the metal mass of the cool CGM of the COS-Halos galaxies is only a factor 2–3 higher than that derived for M31.

5.3. A Changing CGM with Radius

A key discovery from Project AMIGA is that the properties of the CGM of M31 change with R . This is reminiscent of our earlier survey (LHW15), but the increase in the size sample has transformed some of the tentative results of our earlier survey into robust findings. In particular the radius around $R \sim 100$ –150 kpc appears critical in view of several properties changing near this threshold radius:

1. For any ions, the frequency of strong absorption is larger at $R \lesssim 100$ –150 kpc than at larger R .
2. The column densities of Si and C ions change by a factor > 5 –10 between about 25 kpc and 150 kpc, while they change only by a factor $\lesssim 2$ between 150 kpc and 300 kpc.

3. The detection rate of singly ionized species (C II, Si II) is close to 100% at $R < 150$ kpc, but sharply decreases beyond (see Fig. 9), and therefore the gas has a more complex gas-phase structure at $R < 150$ kpc.

4. The peculiar velocities of the CGM gas are more extreme and systematically redshifted relative to the bulk motion of M31 at $R \lesssim 100$ kpc, while at $R \gtrsim 100$ kpc, the peculiar velocities of the CGM gas are less extreme and more uniformly distributed around the bulk motion of M31.

There are also two other significant regions: 1) beyond $R_{200} \simeq 230$ kpc the gas is becoming more ionized and more highly ionized than at lower R (e.g., there is a near total absence of Si II absorption beyond R_{200} —see Fig. 9, or, a higher C II/C IV ratio on average at $R \gtrsim R_{200}$ than at lower R —see §4.7.2); and 2) beyond $1.1R_{\text{vir}}$ the gas is not detected in all the directions away from M31, as it is at smaller radii, but only in a cone near the southern projected major axis and about 52° east off the $X = 0$ kpc axis (see §4.9).

The overall picture that can be drawn out from these properties is that the inner regions of the CGM of M31 are more dynamic and complex, while the more diffuse regions at $R \gtrsim 0.5R_{\text{vir}}$ are more static and simpler. Zoom-in cosmological simulations capture in more detail and more accurately the structures of the CGM than large-scale cosmological simulations thanks to their higher mass and spatial resolution. Below we use several results from zoom simulations to gain some insights on these observed changes with R . However, the results laid out in §4 also now provide a new testbed for zoom simulations, so that not only qualitative but also quantitative comparison can be undertaken. We note that most of the zoom simulations discussed here have only a single massive halo. However, according to the ELVIS simulations of Local group analogs (Garrison-Kimmel et al. 2014), there should be no major difference at least within about R_{vir} for the distribution of the gas between isolated and paired galaxies.

5.3.1. Visualization and Origins of the CGM Variation

To help visualize the properties described above and gain some insights into the possible origins of these trends, we begin by qualitatively examining two zoom simulations. First, we consider the Local group zoom simulations from the CLUES project (Nuza et al. 2014) where the gas distribution around MW and M31-like galaxies is studied. This paper does not show the distribution of the individual ions, but examines the two main gas-phases above and below 10^5 K in an environment that is a constrained analog to the Local group. Interestingly, considering Fig. 3 (simulated M31) or Fig. 6

(simulated MW) in Nuza et al., the region within 100–150 kpc appears more complex, with a large covering factor for both cool and hot gas phases and higher velocities than at larger radii. In these simulations, this is a result of the combined effects of cooling and supernova heating affecting the closer regions of the CGM of M31. This simulation also provides an explanation for the gas observed beyond $1.1R_{\text{vir}}$ that is preferentially observed in a limited region of the CGM of M31 (see Fig. 13 and see middle right panel of their Fig. 3) whereby the $\lesssim 10^5$ K gas might be accreting onto the CGM of M31. We also note that Nuza et al. (2014) find a mass for the $\lesssim 10^5$ K CGM gas of $1.7 \times 10^{10} M_{\odot}$, broadly consistent with our findings (see §4.8). More quantitative comparisons between the CLUES (or Local group analog simulations like ELVIS-FIRE simulations, Garrison-Kimmel et al. 2014, 2019) and Project AMIGA results are beyond the scope of this paper, but they would be valuable to undertake in the future.

Second, we consider the zoom Eris2 simulation of a massive, star-forming galaxy at $z = 2.8$ presented in Shen et al. (2013). The Eris2 galaxy being $z = 2.8$ and with a star-formation rate of $20 M_{\odot} \text{ yr}^{-1}$ is nothing like M31, but this paper shows the distribution of the gas around the central galaxy using some of the same ions that are studied in Project AMIGA, specifically Si II, Si IV, C II, C IV, and O VI (see their Figs. 3a and 4a, b). Because Eris2 is so different from M31, we would naively expect their CGM properties to be different, and yet: 1) Eris2 is surrounded by a large diffuse O VI halo with a near unity covering factor all the way out to about $3R_{\text{vir}}$; 2) the covering factor of absorbing material in the CGM of Eris2 declines less rapidly with impact parameter for C IV or O VI compared to C II, Si II, or Si IV; 3) beyond R_{vir} , the covering factor of Si II drops more sharply than C II. There are also key differences, like the strongest absorption in any of these ions being observed in the bipolar outflows perpendicular to the plane of the disk, which is unsurprisingly not observed in M31 since it currently has a low star-formation rate (e.g., Williams et al. 2017). However, the broad picture of the CGM of M31 and the simulated Eris2 galaxy are remarkably similar. This implies that some of the properties of the CGM may depend more on the micro-physics producing the various gas-phases than the large-scale physical processes (outflow, accretion) that vary substantially over time. In fact, the Eris2 simulation shows that inflows and outflows coexist and are both traced by diffuse O VI; In Eris2, a high covering factor of strong O VI absorbers seems to be the least unambiguous tracer of large-scale outflows.

5.3.2. Quantitative Comparison in the CGM Variation between Observations and Simulations

Two simulations of M31-like galaxies in different environments at widely separated epochs show some similarity with some of the observed trends in the CGM of M31. We now take one step further by quantitatively comparing the column density variation of the different ions as a function of R in three different zoom-in cosmological simulations, two being led by members of the Project AMIGA team (FIRE and FOGGIE collaborations), and a zoom-in simulation from the Evolution and Assembly of GaLaxies and their Environments (EAGLE) simulation project (Oppenheimer et al. 2018a; Schaye et al. 2015; Crain et al. 2015).

• Comparison with FIRE-2 Zoom Simulations

We first compare our observations with column densities modeled using cosmological zoom-in simulations from the FIRE project⁸. Details of the simulation setup and CGM modeling methods are presented in Ji et al. (2019). Briefly, the outputs analyzed here are FIRE-2 simulations evolved with the GIZMO code using the meshless finite mass (MFM) solver (Hopkins 2015). The simulations include a detailed model for stellar feedback including core-collapse and Type Ia SNe, stellar winds from OB and AGB stars, photoionization, and radiation pressure (for details, see Hopkins et al. 2018). We focus on the “m12i” FIRE halo, which has a mass $M_{\text{vir}} \approx 1.2M_{200} \approx 1.2 \times 10^{12} M_{\odot}$ at $z = 0$, which is comparable to the halo mass of M31. However, neither the SFR history nor the present-day SFR are similar. The “m12i” FIRE halo has a factor 10–12 higher SFR (see Fig. 3 in Hopkins et al. 2019) than the present-day SFR of M31 of $0.5 M_{\odot} \text{ yr}^{-1}$ (e.g. Kang et al. 2009). We compare Project AMIGA to FIRE-2 simulations with two different sets of physical ingredients. The “MHD” run includes magnetic fields, anisotropic thermal conduction and viscosity, and the “CR” run includes all these processes plus the “full physics” treatment of stellar cosmic rays. The CR simulation assumes a diffusion coefficient $\kappa_{\parallel} = 3 \times 10^{29} \text{ cm}^2 \text{ s}^{-1}$, which was calibrated to be consistent with observational constraints from γ -ray emission of the MW and some other nearby galaxies (Hopkins et al. 2019; Chan et al. 2019). Ji et al. (2019) showed cosmic rays can potentially provide a large or even dominant non-thermal fraction of the total pressure support in the CGM of low-redshift $\sim L^*$ galaxies. As a result, in the fiducial CR run analyzed here, the volume-filling CGM is much cooler ($\sim 10^4 - 10^5$ K) and

⁸ FIRE project website: <http://fire.northwestern.edu>

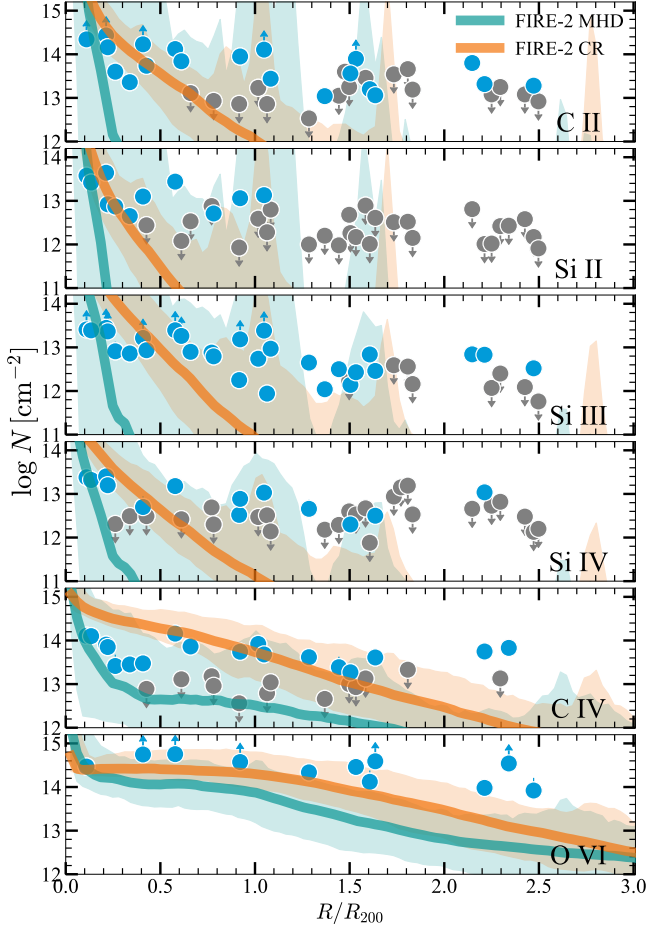


Figure 17. Comparison of ion column density profiles between Project AMIGA (total column densities) and FIRE-2 simulations, where “MHD” and “CR” runs. Thick curves show median values of an ensemble of sightlines produced from simulations, and shaded regions show the full range across all model sightlines.

is thus photoionized in regions where in the run without CRs prefers by hot gas that is more collisionally ionized.

The column densities are generated as discussed in Ji et al. (2019). For the ionization modeling, a hybrid treatment combining the FG09 (Faucher-Giguère et al. 2009) and HM12 (Haardt & Madau 2012) UV background models is used.⁹

⁹ We use this mixture because, based on the recent UV background analysis of Faucher-Giguère (2020), the FG09 model is in better agreement with the most up-to-date low-redshift empirical constraints at energies relevant for low and intermediate ions (C II, Si II, Si III, Si IV, and C IV). However, the HM12 model is likely more accurate for high ions such as O VI because the FG09 model used a crude AGN spectral model which under-predicted the higher-energy part of the UV/X-ray background. Ji et al. (2019) shows how some ion columns depend on the assumed UV background model.

In Fig. 17, we compare the ion column densities from FIRE-2 simulations with observationally-derived total column densities around M31 as a function of R/R_{200} . The green and orange curves show the median simulated column densities for the MHD and CR runs, respectively, while the shaded regions show the full range of columns for all sightlines at a given impact parameter (the lowest values are truncated to match the scales that are adequate for the observations, see Ji et al. 2019 for the full range of values). The CR run produces higher column densities and better agreement with observations than the MHD run for all ions presented. The much higher column densities of low/intermediate ions (C II, Si II, Si III, and Si IV) in the CR run owing to the more volume-filling and uniform cool phase, which produces higher median values of ion column densities and smaller variations across different sightlines. In contrast, in the MHD run the cool phase is pressure confined by the hot phase to compact and dense regions, leading to smaller median columns but larger scatter for the low and intermediate ions. We note, however, that even in the CR runs the predicted column densities are lower than observations at the larger impact parameters $R \gtrsim 0.5R_{200}$. This might be due to insufficient resolution to resolve fine-scale structure in outer halos, or it may indicate that feedback effects are more important at large radii than in the present simulations. This difference is quite notable owing to the fact that the star formation of the “m12i” galaxy has been continuous with a SFR in the range $5\text{--}20 M_{\odot} \text{ yr}^{-1}$ (Hopkins et al. 2019) over the last ~ 8 billion years while M31 had only a continuous SFR around $6\text{--}8 M_{\odot} \text{ yr}^{-1}$ over its first 5 billion years while over the last 8 billion years it had only two short bursts of star formation about 4 and 2 billion years ago (Williams et al. 2017). While there are some discrepancies, the simulations also follow some similar trends: 1) the simulated column densities of the low ions decrease more rapidly with R than the high ions, 2) O VI is observed beyond $1.7R_{200}$ where there is no substantial amount of low/intermediate ions, and 3) a larger scatter is observed in the column densities of the low and intermediate ions than O VI.

In the FIRE-2 simulations, both collisional ionization and photoionization can contribute significantly to the simulated O VI columns, typically with an increasing contribution from photoionization with increasing impact parameter, driven by decreasing gas densities. In the MHD run, most of the O VI in the inner halo ($R \lesssim 0.5R_{200}$) is produced by collisional ionization, but photoionization can dominate at larger impact parameters. In the CR run, collisional ionization and photoionization contribute comparably to the O VI mass at

radii $50 < R < 200$ kpc (Ji et al. 2019). The actual origins of the CGM in terms of gas flows in FIRE-2 simulations without magnetic fields or cosmic rays were analyzed in Hafen et al. (2019a), although the results are expected to be similar for simulations with MHD only. In these simulations, O VI exists as part of a well-mixed hot halo, with contributions from all the primary channels of CGM mass growth: IGM accretion, wind, and contributions from satellite halos (reminiscent of the Eris2 simulations, see above and Shen et al. 2013). The metals responsible for O VI absorption originate primarily in winds, but IGM accretion may contribute a large fraction of total gas mass traced by O VI since the halo is well-mixed and IGM accretion contributes $\gtrsim 60\%$ of the total CGM mass. In the simulations, the hot halo gas persists in the CGM for billions of years, and the gas that leaves the CGM does so primarily by accreting onto the central galaxy (Hafen et al. 2019b).

• *Comparison with FOGGIE Simulations*

We also compare the observed total column densities to the Milky-Way like-mass “Tempest” ($M_{200} \approx 4.2 \times 10^{11} M_{\odot}$) halo from the FOGGIE simulations,¹⁰ which has a halo mass of $M_{200} \approx 4.2 \times 10^{11} M_{\odot}$ (Peeples et al. 2019). We use the $z = 0$ output (see Zheng et al. 2020 for simulation details), but because of the size difference between M31 and the Tempest galaxy, we again scale all distances by R_{200} ($R_{200} = 159$ kpc for the simulated halo compared to 230 kpc for M31). The only “feedback” included in this FOGGIE run is thermal explosion-driven SNe outflows. While this feedback is limited in scope compared to FIRE, FOGGIE achieves higher mass resolution than FIRE-2 by using a “forced refinement” scheme that applies a fixed computational cell size of $\sim 381h^{-1}$ pc within a moving cube centered on the galaxy that is $\sim 200h^{-1}$ ckpc on a side. This refinement scheme enforces constant *spatial resolution* on the CGM, resulting in a variable and very small mass resolution in the low density gas, with typical cell masses of ($\lesssim 1\text{--}100 M_{\odot}$). The individual small-scale structures that contribute to the observed absorption profiles can therefore be resolved. These small-scale structures that become only apparent in high-resolution simulations are hosts to a significant amount of cool gas, enhancing the column densities in especially the low ionization state of the gas (Peeples et al. 2019; Corlies et al. 2020, and see also van de Voort et al. 2019; Hummels et al. 2019; Rhodin et al. 2019).

As for the FIRE-2 simulations, we compare the total Project AMIGA column densities to FOGGIE because

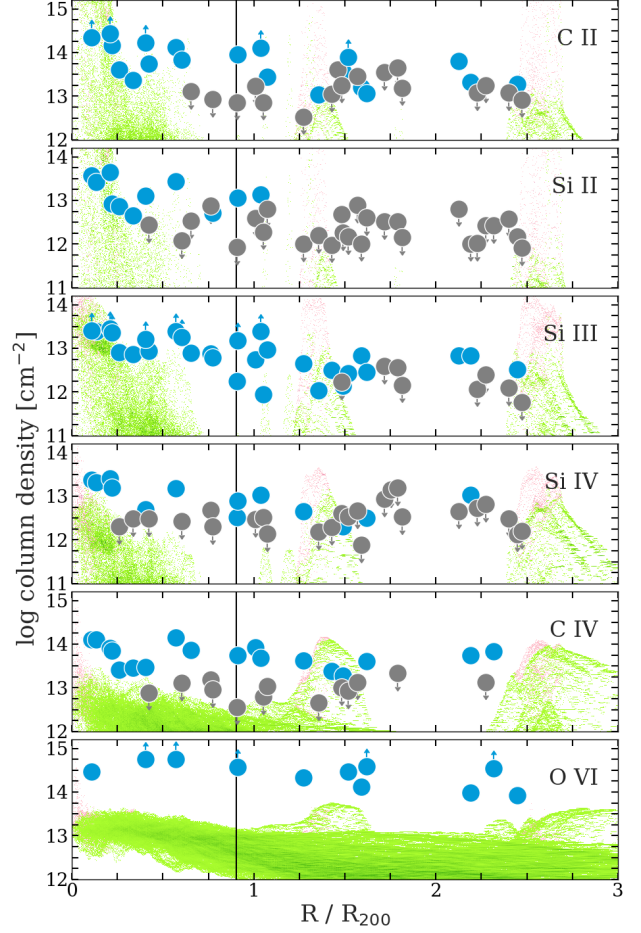


Figure 18. Comparison of ion column density profiles between Project AMIGA (total column densities) and the “Tempest” halo from the FOGGIE simulations. The pink and green shaded areas are projected total column densities from the simulated halo with and without galaxy/satellite contributions, respectively, while the rest of the figure is analogous to Fig. 8. The vertical line shows the extent of the forced resolution cube in the FOGGIE simulation.

in the simulation we do not (yet) separate individual components, but look at the projected column densities through the halo. We note that the CGM is not necessarily self-similar, so some differences between the simulation predictions and M31 observations at rescaled impact parameter could be due to the halo mass difference. This is especially so since the halo mass range $M_h \approx 3 \times 10^{11}\text{--}10^{12} M_{\odot}$ corresponds to the expected transition between cold and hot accretion (e.g., Birnboim & Dekel 2003; Keres et al. 2003; Faucher-Giguère et al. 2011; Stern et al. 2020).

In Fig. 18, we compare the simulated and observed column densities for each ion probed by our survey. The pink and green shaded areas are the data points from

¹⁰ FOGGIE project website: <http://foggie.science>

the simulation (with and without satellite contribution, respectively) and show the total column density in projection through the halo. The scatter in the simulated data points comes from variation in the structures along the mock sightline and most of the scatter is in fact below 10^{11} cm^{-2} . The peaks in the column densities are due to small satellites in the halo, which enhance primarily the low-ion column densities. We show the green points to highlight the difference between the mock column densities with and without satellites. For the high ionization lines the difference is negligible, while the difference in the low ions is significant.

Overall, the metal line column densities are systematically lower than in the observations at any R . Only at $R \lesssim 0.3R_{200}$, there is some overlap for the singly ionized species between the FOGGIE simulation and observations. However, the discrepancy is particularly striking for Si III and the high ions. This can be understood by the current feedback implementation in FOGGIE, which does not expel enough metals from the stellar disk into the CGM (Hamilton-Campos et al. 2020) to be consistent with known galactic metal budgets (Peeples et al. 2014). This effect is expected to be stronger for the high ions than the low ions, due to the additional heating and ionization of the CGM that would be expected from stronger feedback, and indeed the discrepancy between the simulation and observations is larger for the high ions (and Si III) than for the singly ionized species. However, while the absolute scale of the column densities is off, there are also some similarities between the simulation and observations in the behavior of the relative scale of the column density profiles with R : 1) the column densities of the low ions drop more rapidly with R than the high ions; 2) despite the inadequate feedback in the current simulations, the O VI-bearing gas (and C IV to a lesser extent) is observed well-beyond R_{200} ; 3) a large scatter is observed in the column densities of the low and intermediate ions than O VI. It is striking that the overall slope of the O VI profile resembles the observations but at significantly lower absolute column density. In the FOGGIE simulation, the low ions tracing mainly dense, cool gas are preferentially found in the disk or satellites, while the hotter gas traced by the higher ions is more homogeneously distributed in the halo.

- *Comparison with EAGLE Simulations*

Finally, we compare our results with the EAGLE zoom-in simulations (EAGLE *Recal-L025N0752* high-resolution volume) discussed in length in Oppenheimer et al. (2018a). The EAGLE simulations have successfully reproduced a variety of galaxy observables (e.g., Crain et al. 2015; Schaye et al. 2015) and achieved

“broad but imperfect” agreement with some of the extant CGM observations (e.g., Turner et al. 2016; Rahmati & Oppenheimer 2018; Oppenheimer et al. 2018a; Lehner et al. 2019; Wotta et al. 2019).

Oppenheimer et al. (2018a) aimed to directly study the multiphase CGM traced by low metal ions and to compare with the COS-Halos survey (see §5.2). As such, they explored the circumgalactic metal content traced by the same ions explored in Project AMIGA in the CGM galaxies with masses that comprise that of M31. Overall Oppenheimer et al. find agreement between the simulated and COS-Halos samples for Si II, Si III, Si IV, and C II within a factor two or so and larger disagreement with O VI, where the column density is systematically lower. With Project AMIGA, we can directly compare the results with one of the EAGLE galaxies that has a mass very close to M31 and also compare the column densities beyond 160 kpc, the maximum radius of the COS-Halos survey (Tumlinson et al. 2013; Werk et al. 2013). We refer the reader to Oppenheimer et al. (2016), Rahmati & Oppenheimer (2018), and Oppenheimer et al. (2018a) for more detail on the EAGLE zoom-in simulations. We also refer the reader to Fig. 1 in Oppenheimer et al. (2018a) where in the middle column they show the column density map for galaxy halo mass of $\log M_{200} = 12.2$ at $z \simeq 0.2$, which qualitatively shows similar trends described in §5.3.1.

In Fig. 19, we compare the EAGLE and observed column densities as a function of the impact parameter out to R_{vir} . As in the previous two figures, the blue and gray circles are detections and non-detections in the halo of M31. The green curve in each panel represents the mean column density for each ion as a function of the impact parameter for the EAGLE galaxy with $\log M_{200} = 12.1$ at $z = 0$. In contrast to FIRE-2 or FOGGIE simulations, the EAGLE simulations appear to produce a better agreement between N and R for low and intermediate ions (Si II, Si III, Si IV), and C IV out to larger impact parameters. However, as already noted in Oppenheimer et al. (2018a), this agreement is offset by producing too much column density for the low and intermediate ions at small impact parameters (see, e.g., Si II, which is not affected by lower limits, is clearly overproduced at $R \lesssim 80$ kpc). The flat profile of O VI, with very little dependence on R , is similar to the observations and other models, but overall the EAGLE O VI column densities are a factor 0.2–0.6 dex smaller than observed. Oppenheimer et al. (2018a) (and also Oppenheimer et al. 2016) already noted that issue from their comparison with the COS-Halos galaxies (see also §5.2), requiring additional source(s) of ionization for the O VI such as AGN flickering (Oppenheimer & Schaye

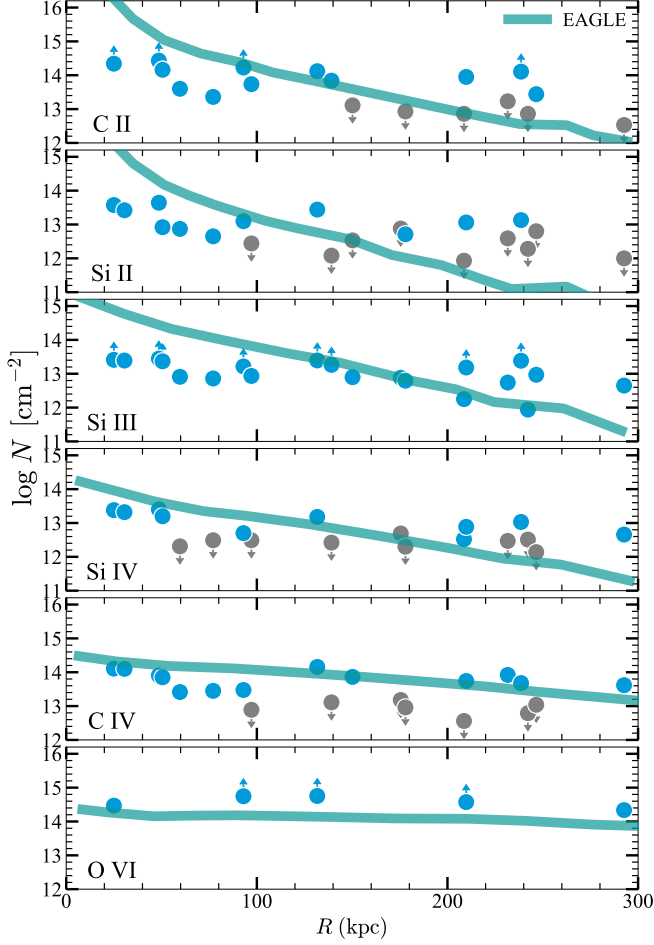


Figure 19. Comparison of ion column density profiles between Project AMIGA and EAGLE zoom-in simulation of a galaxy with $\log M_{200} \simeq 12.1$ at $z = 0$ (from the models presented in Oppenheimer et al. 2018a). For the EAGLE simulation, the mean column densities are shown. Note that here we only plot the column density profiles out to about R_{vir} .

2013a; Oppenheimer et al. 2018b) or possibly CRs as shown for the FIRE-2 simulations (see Ji et al. 2019 and above). While the results are shown only to R_{vir} , as in the other simulations and M31, O VI is also observed well beyond R_{vir} in the EAGLE simulations (see Fig. 1 in Oppenheimer et al. 2018a).

5.3.3. Insights from the Observation/Simulation Comparison

The comparison with the simulations shows that the CGM is changing in zoom-in simulations on length scales roughly similar to those observed in M31. The low ions and high ions follow substantially different profiles with radius, in both data and simulations. In the zoom-in simulations described above, the inner regions of the CGM of galaxies are more directly affected by large-

scale feedback and recycling processes between the disk and CGM of galaxies. Therefore it is not surprising that the M31 CGM within 100–150 kpc shows a large variation in column density profiles with R , a more complex gas-phase structure, and larger peculiar velocities even though the current star formation rate is low. While both accretion and large-scale outflow coexist in the CGM and are responsible for the gas flow properties, stellar feedback is required to produce substantial amount of metals in the CGM at large impact parameters (see Figs. 17, 18, 19). M31 has currently a low SFR, but it had several episodes of bursting star formation in the past (e.g., Williams et al. 2017), likely ejecting a large portion of its metals in the CGM during these episodes.

Various models simulating different galaxy masses at different epochs, with distinct SFRs or feedback processes can reproduce at some level the diffuse O VI observed beyond R_{vir} . All the simulations we have reviewed produce O VI profiles that are flatter than the low ions and which extend to beyond R_{vir} with significant column density. While the galaxy halo masses are different, they are all roughly in the range of about $10^{11.5} - 10^{12.3} M_{\odot}$, which is a mass range where their virial temperatures overlap with the temperature at which the ionization fraction of O VI peaks (Oppenheimer et al. 2016). Using the EAGLE simulations, Oppenheimer et al. (2016) show that the virial temperature of the galaxy halos can explain the presence of strong O VI in the CGM of star-forming galaxies with $M_{200} \simeq 10^{11.5} - 10^{12.3} M_{\odot}$ and the absence of strong O VI in the CGM of quiescent galaxies that have overall higher halo masses ($M_{200} 10^{12.5} - 10^{13.5} M_{\odot}$) and hence higher virial temperatures, i.e., halo mass, not SFR largely drives the presence of strong O VI in the CGM of galaxies (cf. §5.2). Production the O VI in volume-filling virialized gas could explain why O VI is widely spread in the CGM of simulated galaxies and the real M31. Additional ionization mechanisms from cosmic rays (Ji et al. 2019 and see Fig. 17) or fluctuating AGNs (Oppenheimer & Schaye 2013a; Oppenheimer et al. 2018b) can further boost the O VI production, but halo masses with their virial temperatures close to the temperature at which the ionization fraction of O VI peaks appear to provide a natural source for the diffuse, extended O VI in the CGM of L^* galaxies. Conversely, a number of studies have shown that significant O VI can arise in active outflows, with the outflow column densities varying strongly with the degree of feedback (Hummels et al. 2013; Hafen et al. 2019a). Right now, no clear observational test can distinguish O VI in warm virialized gas and direct outflows. However, any model that attempts

to distinguish them will be constrained by the flat profile and low scatter seen by Project AMIGA.

On the other hand, the cooler, diffuse ionized gas probed predominantly by Si III, and also low ions (C II, Si II) at smaller impact parameters, is not well-reproduced in the simulations. In the FIRE-2 and FOGGIE simulations, the column densities of Si III and low ions within $\lesssim 0.3R_{200}$ are reasonably matched, but their covering fractions drop sharply and much more rapidly than observed for M31 when $R > 0.3R_{200}$. Only near satellite galaxies within $0.3R_{200}$ do the column densities of these ions increase. This is, however, not a fair comparison as M31 lacks gas-rich satellites within this radius. Furthermore the near unity covering factor of Si III out to $1.65R_{200}$ in the CGM of M31 could not be explained by dwarf satellites anyway. For the EAGLE simulation, this problem is not as extreme as in the other simulations, but EAGLE does overproduce low and intermediate ions in the inner regions ($\lesssim 0.3R_{200}$) of the CGM. Possibly maintaining a high resolution out to R_{vir} would be needed to accurately model the small-scale structures of the cool gas content and preserve it over longer periods of time (Hummels et al. 2019; Peebles et al. 2019; van de Voort et al. 2019).

While the observations of M31 and simulations discussed above show some discrepancy, there is an overall trend that is universally observed: when the ionization energies increase from the singly-ionized species (Si II, C II) to intermediate ions (Si III, Si IV) to C IV to O VI, the column density dispersions and dependence on R decrease. While the larger scatter in the low and intermediate column densities compared to O VI was observed previously (e.g., Werk et al. 2013; Liang et al. 2016), that trend with R was not as obvious owing to a larger scatter at any R , in part caused by neighboring galaxies or different galaxy masses (Oppenheimer et al. 2018a). This general trend is the primary point of agreement between the observations and simulations, especially considering that the simulations were not tuned to match the CGM properties. This trend most likely arises from the physical conditions of the gas: in the inner regions of the CGM the gas takes on a density that favors the production of the low and intermediate ions. At these densities O VI would need to be collisionally ionized or distributed in pockets of low-density photoionized gas. In the outer regions of the CGM, the overall gas must have a much lower density where O VI and weak Si III and nearly no singly ionized species can be produced predominantly by photoionization processes. This basic structure of the CGM appears in broad agreement between Project AMIGA, statistical sampling of many

galaxies like COS-Halos, and three different suites of simulations.

5.4. Implications for the MW CGM

Based the findings from Project AMIGA, it is likely that the MW has not only an extended hot CGM (Gupta et al. 2014, 2017), but also an extended CGM of cool (Si II, Si III, Si IV) and warm-hot (C IV, O VI) gas that extends all the way to about 300 kpc (R_{vir}), and even farther away for the O VI. In fact, the MW and M31 O VI CGMs most likely already overlap as it can be seen, e.g., in the CLUES simulations of the Local group (Nuza et al. 2014) since the distance between M31 and MW is only 752 kpc.

A large covering factor of the CGM of M31 is not detected at high peculiar velocities (see Fig. 15), and in fact beyond 100 kpc, the velocities v_{M31} are scattered around 20 km s^{-1} . Even within 100 kpc, the average velocity is about 90 km s^{-1} , which would barely constitute a HVC studied in the MW. In the MW most of the absorption within $\pm 90 \text{ km s}^{-1}$ relative to the systemic velocity of the MW in a given direction is dominated by the disk, i.e., material within a few hundreds of pc from the galactic plane. Because the HVC velocities are high enough to separate them from the disk absorption, HVCs in the MW have been studied for many years to determine the “halo” properties of the MW (e.g. Wakker & van Woerden 1997; Putman et al. 2012; Richter et al. 2017). However, we know now that the distances of these HVCs, including the predominantly ionized HVCs, are not at 100s of kpc from the MW, but most of them are within 15–20 kpc from the sun (e.g. Wakker 2001; Wakker et al. 2008; Thom et al. 2008; Lehner & Howk 2011; Lehner et al. 2012), i.e., in a radius not even explored by Project AMIGA and many other surveys of the galaxy CGM at higher redshifts (e.g., Werk et al. 2013; Liang & Chen 2014; Borthakur et al. 2016; Burchett et al. 2016). Only the MS allows us to probe the interaction between the MW and the Magellanic clouds in the CGM of the MW out to about 50–100 kpc (e.g., D’Onghia & Fox 2016). The results from Project AMIGA strongly suggest that the CGM of the MW is hidden in the low velocity absorption arising from its disk (see also Zheng et al. 2015). To complicate the matter, the column densities of the low, intermediate ions, and C IV drop substantially beyond 100–150 kpc (see, e.g., Figs. 8, 10). Owing to its strength and little dependence on R , O VI is among the best ultraviolet diagnostic of the extended CGM (see also the recent FOGGIE simulation results by Zheng et al. 2020).

6. SUMMARY

With Project AMIGA, we have surveyed the CGM of a galaxy with an unprecedented number of background targets (43) piercing it at various azimuths and impact parameters, 25 from $0.08R_{\text{vir}}$ to about $1.1R_{\text{vir}}$ and the additional 18 between $1.1 < R/R_{\text{vir}} \lesssim 1.9$. The 43 QSOs were all observed with COS G130M/G160M or G130M (providing in particular O I, C II, C IV, Si II, Si III, Si IV) and 11 were also observed with *FUSE* (providing O VI). The resolution of the COS G130M/G160M and the SNRs have been key for the success of this program. All the data were uniformly reduced and analyzed. For the 43 QSOs in our sample, we have identified all the absorption features in their spectra to determine if any transitions used to probe the CGM of M31 could be contaminated. We provide the entire line identification in Appendix A. While we survey only a single galaxy, M31, the uniqueness of our experiment has allowed us to gain a wealth of new information that can be summarized as follows.

1. Ionized gas traced by Si III and O VI have near unity covering factor all the way out to $1.2R_{\text{vir}}$ and $1.9R_{\text{vir}}$, respectively. All the other ions have their covering factors monotonically decreasing as R increases.
2. We do not find that the properties of the CGM of M31 strongly depend on the azimuth with respect to the major and minor axes, but several properties of the CGM depend on the projected distance.
3. The gas has a more complex gas-phase structure at $R \lesssim 0.5R_{\text{vir}}$ with high covering factors of all the ions. At larger R , the gas becomes more highly ionized, with a paucity of singly ionized species. Stronger absorbers are also observed closer to M31 with the column densities of all the ions but O VI decreasing sharply as R increases up to $R \lesssim 0.5R_{\text{vir}}$; beyond $R \gtrsim 0.5R_{\text{vir}}$ the column densities decrease much more mildly with increasing R .
4. The velocity structure of the absorption profiles is more complex with $R \lesssim 0.5R_{\text{vir}}$ where frequently more than one velocity component is observed, while at larger R , the absorption profiles predominantly show only one velocity component (at the COS resolution). The peculiar velocities of the CGM gas are also more extreme and systematically redshifted by about $+90 \text{ km s}^{-1}$ relative to the bulk motion of M31 at $R \lesssim 0.5R_{\text{vir}}$. On the other hand, at $R \gtrsim 0.5R_{\text{vir}}$, the peculiar velocities are both blue- and redshifted relative to the bulk motion of M31 and only by $10\text{--}20 \text{ km s}^{-1}$ on average.
5. Cosmological zoom-in simulations $\sim L^*$ galaxies (individual galaxies or galaxies in Local group analogs) show that O VI does extend well beyond R_{vir} as observed for M31. On the other hand, cosmological zoom-in simulations do not reproduce well the column density profiles of the low ions (Si II, C II) or intermediate ions (Si III, Si IV). All the zoom in simulations explored in this work show some common traits with the observations of the CGM of M31: 1) the column densities of O VI do not vary much with R while those of the lower ions have a strong dependence with R ; 2) the scatter in the column densities at R is smaller in O VI than any lower ions; 3) O VI is observed at $R \gg R_{\text{vir}}$. In other words, the dispersion and the dependence of the column densities on the impact parameter decline going from singly through doubly to highly ionized species.
6. We estimate that the mass of the cool metal mass probed by Si II, Si III, and Si IV of the CGM within R_{vir} is $2 \times 10^7 M_{\odot}$ and by O VI is $> 8 \times 10^7 M_{\odot}$. The total metal mass could be as large as $\gtrsim 2.5 \times 10^8 M_{\odot}$ if the dust and hot X-ray gas are accounted for. Since the total metal mass in the disk of M31 is about $M_Z^{\text{disk}} \simeq 5 \times 10^8 M_{\odot}$, the CGM of M31 has at least 50% of the present-day metal mass of its disk and possibly much more.
7. We estimate the baryon mass of the $\sim 10^4\text{--}10^{5.5} \text{ K}$ gas is $\gtrsim 3.7 \times 10^{10} (Z/0.3 Z_{\odot})^{-1} M_{\odot}$ at R_{vir} . The dependence on the largely unknown metallicity of the CGM makes the baryon mass estimate uncertain, but it is broadly comparable to other recent observational results or estimates in zoom-in simulations.
8. We study if any of the M31 dwarf satellites could give rise to some of the observed absorption associated with the CGM of M31. We find it is plausible that few absorbers within close spatial and velocity proximity of the dwarfs could be associated with the CGM of dwarfs if they have a gaseous CGM. However, these are Sph galaxies, which have had their gas stripped via ram-pressure and unlikely to have much gas left in their CGM. And, indeed, none of the properties of the absorbers in close proximity to these dwarf galaxies show any peculiarity that would associate them to the CGM of the satellites rather than the CGM of M31.

ACKNOWLEDGEMENTS

We thank David Nidever for sharing his original fits of the MS H I emission and Ben Oppenheimer for sharing the EAGLE simulations shown in Fig. 19. Support for this research was provided by NASA through grant HST-GO-14268 from the Space Telescope Science Institute, which is operated by the Association of Universities for Research in Astronomy, Incorporated, under NASA contract NAS5-26555. CAFG and ZH were also

supported by NSF through grants AST-1517491, AST-1715216, and CAREER award AST-1652522; by NASA through grants NNX15AB22G and 17-ATP17-0067; by STScI through grants HST-GO-14681.011 and HST-AR-14293.001-A; and by a Cottrell Scholar Award from the Research Corporation for Science Advancement. Based on observations made with the NASA-CNES-CSA Far Ultraviolet Spectroscopic Explorer, which was operated

for NASA by the Johns Hopkins University under NASA contract NAS5-32985.

Software: Astropy (Astropy Collaboration et al. 2018), emcee (Foreman-Mackey et al. 2013), Matplotlib (Hunter 2007), PyIGM (Prochaska et al. 2017a)

Facilities: HST(COS); HST(STIS); FUSE

REFERENCES

- Akerman, C. J., Carigi, L., Nissen, P. E., Pettini, M., & Asplund, M. 2004, *A&A*, 414, 931
- Anderson, M. E., & Bregman, J. N. 2011, *ApJ*, 737, 22
- Anderson, M. E., Bregman, J. N., & Dai, X. 2013, *ApJ*, 762, 106
- Anglés-Alcázar, D., Faucher-Giguère, C.-A., Kereš, D., et al. 2017, *MNRAS*, 470, 4698
- Asplund, M., Grevesse, N., Sauval, A. J., & Scott, P. 2009, *ARA&A*, 47, 481
- Astropy Collaboration, Price-Whelan, A. M., Sipőcz, B. M., et al. 2018, *AJ*, 156, 123
- Bechtold, J., Crotts, A. P. S., Duncan, R. C., & Fang, Y. 1994, *ApJL*, 437, L83
- Berg, M. A., Howk, J. C., Lehner, N., et al. 2019, *ApJ*, 883, 5
- Birnboim, Y., & Dekel, A. 2003, *MNRAS*, 345, 349
- Bordoloi, R., Tumlinson, J., Werk, J. K., et al. 2014, *ApJ*, 796, 136
- Borthakur, S., Heckman, T., Tumlinson, J., et al. 2016, *ApJ*, 833, 259
- Bowen, D. V., Chelouche, D., Jenkins, E. B., et al. 2016, *ApJ*, 826, 50
- Bowen, D. V., Pettini, M., & Blades, J. C. 2002, *ApJ*, 580, 169
- Bregman, J. N., Anderson, M. E., Miller, M. J., et al. 2018, *ApJ*, 862, 3
- Brown, T. M., Ferguson, H. C., Smith, E., et al. 2004, *AJ*, 127, 2738
- Buitinck, L., Louppe, G., Blondel, M., et al. 2013, in *ECML PKDD Workshop: Languages for Data Mining and Machine Learning*, 108–122
- Burchett, J. N., Tripp, T. M., Bordoloi, R., et al. 2016, *ApJ*, 832, 124
- Bustard, C., Pardy, S. A., D’Onghia, E., Zweibel, E. G., & Gallagher, J. S., I. 2018, *ApJ*, 863, 49
- Cameron, E. 2011, *PASA*, 28, 128
- Cescutti, G., Matteucci, F., McWilliam, A., & Chiappini, C. 2009, *A&A*, 505, 605
- Chan, T., Kereš, D., Hopkins, P., et al. 2019, *Monthly Notices of the Royal Astronomical Society*, 488, 3716
- Chemin, L., Carignan, C., & Foster, T. 2009, *ApJ*, 705, 1395
- Chen, H.-W., Johnson, S. D., Straka, L. A., et al. 2019, *MNRAS*, 484, 431
- Collins, M. L. M., Chapman, S. C., Rich, R. M., et al. 2013, *ApJ*, 768, 172
- Corbelli, E. 2003, *MNRAS*, 342, 199
- Corlies, L., Peebles, M. S., Tumlinson, J., et al. 2020, *arXiv e-prints*, arXiv:1811.05060
- Courteau, S., & van den Bergh, S. 1999, *AJ*, 118, 337
- Crain, R. A., Schaye, J., Bower, R. G., et al. 2015, *MNRAS*, 450, 1937
- Crighton, N. H. M., Hennawi, J. F., & Prochaska, J. X. 2013, *ApJL*, 776, L18
- de Vaucouleurs, G., de Vaucouleurs, A., Corwin, Jr., H. G., et al. 1991, *Third Reference Catalogue of Bright Galaxies. Volume I: Explanations and references. Volume II: Data for galaxies between 0^h and 12^h. Volume III: Data for galaxies between 12^h and 24^h*. (Springer, New York, NY (USA))
- D’Onghia, E., & Fox, A. J. 2016, *ARA&A*, 54, 363
- Draine, B. T., Aniano, G., Krause, O., et al. 2014, *ApJ*, 780, 172
- Ellison, S. L., Ibata, R., Pettini, M., et al. 2004, *A&A*, 414, 79
- Fabbian, D., Khomenko, E., Moreno-Inertis, F., & Nordlund, Å. 2010, *ApJ*, 724, 1536
- Faucher-Giguère, C.-A. 2020, *MNRAS*, 259
- Faucher-Giguère, C.-A., Kereš, D., & Ma, C.-P. 2011, *MNRAS*, 417, 2982
- Faucher-Giguère, C.-A., Lidz, A., Zaldarriaga, M., & Hernquist, L. 2009, *ApJ*, 703, 1416
- Feigelson, E. D., & Nelson, P. I. 1985, *ApJ*, 293, 192
- Field, G. B. 1971, *ApJ*, 165, 29
- Fischer, W. J., et al. 2019, *Cosmic Origins Spectrograph Instrument Handbook*, version 18.0 edn., STScI, Baltimore: STScI
- Fitzpatrick, E. L., & Spitzer, Jr., L. 1997, *ApJ*, 475, 623
- Foreman-Mackey, D., Hogg, D. W., Lang, D., & Goodman, J. 2013, *PASP*, 125, 306

- Fox, A. J., Savage, B. D., & Wakker, B. P. 2005, *AJ*, 130, 2418
- Fox, A. J., Wakker, B. P., Barger, K. A., et al. 2014, *ApJ*, 787, 147
- Garrison-Kimmel, S., Boylan-Kolchin, M., Bullock, J. S., & Lee, K. 2014, *MNRAS*, 438, 2578
- Garrison-Kimmel, S., Hopkins, P. F., Wetzel, A., et al. 2019, *MNRAS*, 487, 1380
- Geehan, J. J., Fardal, M. A., Babul, A., & Guhathakurta, P. 2006, *MNRAS*, 366, 996
- Gilbert, K. M., Tollerud, E., Beaton, R. L., et al. 2018, *ApJ*, 852, 128
- Gnat, O., & Sternberg, A. 2007, *ApJS*, 168, 213
- Grebel, E. K., Gallagher, John S., I., & Harbeck, D. 2003, *AJ*, 125, 1926
- Green, J. C., Froning, C. S., Osterman, S., et al. 2012, *ApJ*, 744, 60
- Gupta, A., Mathur, S., Galeazzi, M., & Krongold, Y. 2014, *Ap&SS*, 352, 775
- Gupta, A., Mathur, S., & Krongold, Y. 2017, *ApJ*, 836, 243
- Gupta, A., Mathur, S., Krongold, Y., Nicastro, F., & Galeazzi, M. 2012, *ApJL*, 756, L8
- Haardt, F., & Madau, P. 2012, *ApJ*, 746, 125
- Hafen, Z., Faucher-Giguère, C.-A., Anglés-Alcázar, D., et al. 2017, *MNRAS*, 469, 2292
- Hafen, Z., Faucher-Giguere, C. A., Angles-Alcazar, D., et al. 2019a, *arXiv e-prints*, [arXiv:1910.01123](https://arxiv.org/abs/1910.01123)
- Hafen, Z., Faucher-Giguère, C.-A., Anglés-Alcázar, D., et al. 2019b, *MNRAS*, 488, 1248
- Hamilton-Campos, K. A., Simons, R., Peeples, M., & Tumlinson, J. 2020, in *American Astronomical Society Meeting Abstracts*, Vol. 52, American Astronomical Society Meeting Abstracts, 207.07
- Henley, D. B., Shelton, R. L., & Kwak, K. 2014, *ApJ*, 791, 41
- Hopkins, P. F. 2015, *MNRAS*, 450, 53
- Hopkins, P. F., Kereš, D., Oñorbe, J., et al. 2014, *MNRAS*, 445, 581
- Hopkins, P. F., Wetzel, A., Kereš, D., et al. 2018, *MNRAS*, 480, 800
- Hopkins, P. F., Chan, T., Garrison-Kimmel, S., et al. 2019, *arXiv preprint arXiv:1905.04321*
- Howk, J. C., Wotta, C. B., Berg, M. A., et al. 2017, *ApJ*, 846, 141
- Hummels, C. B., Bryan, G. L., Smith, B. D., & Turk, M. J. 2013, *MNRAS*, 430, 1548
- Hummels, C. B., Smith, B. D., Hopkins, P. F., et al. 2019, *ApJ*, 882, 156
- Hunter, J. D. 2007, *Computing in Science and Engineering*, 9, 90
- Isobe, T., Feigelson, E. D., & Nelson, P. I. 1986, *ApJ*, 306, 490
- Jenkins, E. B. 2009, *ApJ*, 700, 1299
- Ji, S., Chan, T., Hummels, C. B., et al. 2019, *arXiv preprint arXiv:1909.00003*
- Johnson, S. D., Chen, H.-W., & Mulchaey, J. S. 2015, *MNRAS*, 449, 3263
- Kacprzak, G. G., Pointon, S. K., Nielsen, N. M., et al. 2019, *ApJ*, 886, 91
- Kalberla, P. M. W., Burton, W. B., Hartmann, D., et al. 2005, *A&A*, 440, 775
- Kalberla, P. M. W., McClure-Griffiths, N. M., Pisano, D. J., et al. 2010, *A&A*, 521, A17
- Kam, S. Z., Carignan, C., Chemin, L., et al. 2017, *AJ*, 154, 41
- Kang, Y., Bianchi, L., & Rey, S.-C. 2009, *ApJ*, 703, 614
- Keeney, B. A., Stocke, J. T., Rosenberg, J. L., et al. 2013, *ApJ*, 765, 27
- Keeney, B. A., Stocke, J. T., Danforth, C. W., et al. 2017, *ApJS*, 230, 6
- Keres, D., Yun, M. S., & Young, J. S. 2003, *ApJ*, 582, 659
- Klypin, A. A., Trujillo-Gomez, S., & Primack, J. 2011, *ApJ*, 740, 102
- Kulkarni, V. P., Cashman, F. H., Lopez, S., et al. 2019, *ApJ*, 886, 83
- Lehner, N., & Howk, J. C. 2011, *Science*, 334, 955
- Lehner, N., Howk, J. C., Thom, C., et al. 2012, *MNRAS*, 424, 2896
- Lehner, N., Howk, J. C., & Wakker, B. P. 2015, *ApJ*, 804, 79
- Lehner, N., Jenkins, E. B., Gry, C., et al. 2003, *ApJ*, 595, 858
- Lehner, N., Keenan, F. P., & Sembach, K. R. 2001, *MNRAS*, 323, 904
- Lehner, N., O’Meara, J. M., Fox, A. J., et al. 2014, *ApJ*, 788, 119
- Lehner, N., Wotta, C. B., Howk, J. C., et al. 2018, *ApJ*, 866, 33
- . 2019, *ApJ*, 887, 5
- Lehner, N., Zech, W. F., Howk, J. C., & Savage, B. D. 2011, *ApJ*, 727, 46
- Lehner, N., Howk, J. C., Tripp, T. M., et al. 2013, *ApJ*, 770, 138
- Liang, C. J., & Chen, H.-W. 2014, *MNRAS*, 445, 2061
- Liang, C. J., Kravtsov, A. V., & Agertz, O. 2016, *MNRAS*, 458, 1164
- Lopez, S., Reimers, D., Gregg, M. D., et al. 2005, *ApJ*, 626, 767
- Lopez, S., Tejos, N., Barrientos, L. F., et al. 2020, *MNRAS*, 491, 4442

- Martin, C. L., Scannapieco, E., Ellison, S. L., et al. 2010, *ApJ*, 721, 174
- Martin, N. F., Chambers, K. C., Collins, M. L. M., et al. 2014, *ApJL*, 793, L14
- Martin, N. F., Ibata, R. A., Lewis, G. F., et al. 2016, *ApJ*, 833, 167
- Martin, N. F., Weisz, D. R., Albers, S. M., et al. 2017, *ApJ*, 850, 16
- Mattsson, L. 2010, *A&A*, 515, A68
- Mayer, L., Mastropietro, C., Wadsley, J., Stadel, J., & Moore, B. 2006, *MNRAS*, 369, 1021
- McConnachie, A. W. 2012, *AJ*, 144, 4
- McConnachie, A. W., Irwin, M. J., Ferguson, A. M. N., et al. 2005, *MNRAS*, 356, 979
- McMillan, P. J. 2011, *MNRAS*, 414, 2446
- Ménard, B., Scranton, R., Fukugita, M., & Richards, G. 2010, *MNRAS*, 405, 1025
- Moos, H. W., Cash, W. C., Cowie, L. L., et al. 2000, *ApJ*, 538, L1
- Muzahid, S., Kacprzak, G. G., Charlton, J. C., & Churchill, C. W. 2016, *ApJ*, 823, 66
- Muzahid, S., Kacprzak, G. G., Churchill, C. W., et al. 2015, *ApJ*, 811, 132
- Nidever, D. L., Majewski, S. R., & Butler Burton, W. 2008, *ApJ*, 679, 432
- Nidever, D. L., Majewski, S. R., Butler Burton, W., & Nigra, L. 2010, *ApJ*, 723, 1618
- Nuza, S. E., Parisi, F., Scannapieco, C., et al. 2014, *MNRAS*, 441, 2593
- Oppenheimer, B. D., & Schaye, J. 2013a, *MNRAS*, 434, 1063
- . 2013b, *MNRAS*, 434, 1043
- Oppenheimer, B. D., Schaye, J., Crain, R. A., Werk, J. K., & Richings, A. J. 2018a, *MNRAS*, 481, 835
- Oppenheimer, B. D., Segers, M., Schaye, J., Richings, A. J., & Crain, R. A. 2018b, *MNRAS*, 474, 4740
- Oppenheimer, B. D., Crain, R. A., Schaye, J., et al. 2016, *MNRAS*, 460, 2157
- Pedregosa, F., Varoquaux, G., Gramfort, A., et al. 2011, *Journal of Machine Learning Research*, 12, 2825
- Peek, J. E. G., Ménard, B., & Corrales, L. 2015, *ApJ*, 813, 7
- Peeples, M. S., Werk, J. K., Tumlinson, J., et al. 2014, *ApJ*, 786, 54
- Peeples, M. S., Corlies, L., Tumlinson, J., et al. 2019, *ApJ*, 873, 129
- Péroux, C., Rahmani, H., Arrigoni Battaia, F., & Augustin, R. 2018, *MNRAS*, 479, L50
- Poisson, M., Bustos, C., López Fuentes, M., Mandrini, C. H., & Cristiani, G. D. 2019, *arXiv e-prints*, arXiv:1911.00901
- Prochaska, J. X., Tejos, N., Wotta, C. B., et al. 2017a, *pygmpy*: Initial release for publications, UCSC, doi:10.5281/zenodo.1045480
- Prochaska, J. X., Werk, J. K., Worseck, G., et al. 2017b, *ApJ*, 837, 169
- Putman, M. E., Peek, J. E. G., & Jounge, M. R. 2012, *ARA&A*, 50, 491
- Putman, M. E., Staveley-Smith, L., Freeman, K. C., Gibson, B. K., & Barnes, D. G. 2003, *ApJ*, 586, 170
- Rahmati, A., & Oppenheimer, B. D. 2018, *MNRAS*, 476, 4865
- Rauch, M., Sargent, W. L. W., Barlow, T. A., & Carswell, R. F. 2001, *ApJ*, 562, 76
- Rhodin, N. H. P., Agertz, O., Christensen, L., Renaud, F., & Fynbo, J. P. U. 2019, *MNRAS*, 488, 3634
- Ribaudo, J., Lehner, N., Howk, J. C., et al. 2011, *ApJ*, 743, 207
- Richter, P., Nuza, S. E., Fox, A. J., et al. 2017, *A&A*, 607, A48
- Riess, A. G., Fliri, J., & Valls-Gabaud, D. 2012, *ApJ*, 745, 156
- Riley, A., et al. 2019, *STIS Instrument Handbook*, version 11.0 edn., STScI, Baltimore: STScI
- Rosenwasser, B., Muzahid, S., Charlton, J. C., et al. 2018, *MNRAS*, 476, 2258
- Rubin, K. H. R., O’Meara, J. M., Cooksey, K. L., et al. 2018, *ApJ*, 859, 146
- Savage, B. D., Kim, T.-S., Wakker, B. P., et al. 2014, *ApJS*, 212, 8
- Savage, B. D., & Sembach, K. R. 1991, *ApJ*, 379, 245
- . 1996, *ARA&A*, 34, 279
- Schaye, J., Crain, R. A., Bower, R. G., et al. 2015, *MNRAS*, 446, 521
- Schönrich, R., Binney, J., & Dehnen, W. 2010, *MNRAS*, 403, 1829
- Shen, S., Madau, P., Guedes, J., et al. 2013, *ApJ*, 765, 89
- Shull, J. M., Jones, J. R., Danforth, C. W., & Collins, J. A. 2009, *ApJ*, 699, 754
- Smette, A., Surdej, J., Shaver, P. A., et al. 1992, *ApJ*, 389, 39
- Stern, J., Fielding, D., Faucher-Giguère, C.-A., & Quataert, E. 2020, *MNRAS*, 492, 6042
- Stocke, J. T., Keeney, B. A., Danforth, C. W., et al. 2013, *ApJ*, 763, 148
- Suresh, J., Nelson, D., Genel, S., Rubin, K. H. R., & Hernquist, L. 2019, *MNRAS*, 483, 4040
- Tamm, A., Tempel, E., Tenjes, P., Tihhonova, O., & Tuvikene, T. 2012, *A&A*, 546, A4
- Telford, O. G., Werk, J. K., Dalcanton, J. J., & Williams, B. F. 2019, *ApJ*, 877, 120

- The LUVOIR Team. 2019, arXiv e-prints, arXiv:1912.06219
- Thom, C., Peek, J. E. G., Putman, M. E., et al. 2008, *ApJ*, 684, 364
- Thom, C., Werk, J. K., Tumlinson, J., et al. 2011, *ApJ*, 736, 1
- Thom, C., Tumlinson, J., Werk, J. K., et al. 2012, *ApJL*, 758, L41
- Tripp, T. M., Sembach, K. R., Bowen, D. V., et al. 2008, *ApJS*, 177, 39
- Tripp, T. M., Meiring, J. D., Prochaska, J. X., et al. 2011, *Science*, 334, 952
- Tumlinson, J., Peebles, M. S., & Werk, J. K. 2017, *ARA&A*, 55, 389
- Tumlinson, J., Thom, C., Werk, J. K., et al. 2011, *Science*, 334, 948
- . 2013, *ApJ*, 777, 59
- Turner, M. L., Schaye, J., Crain, R. A., Theuns, T., & Wendt, M. 2016, *MNRAS*, 462, 2440
- van de Voort, F., Springel, V., Mandelker, N., van den Bosch, F. C., & Pakmor, R. 2019, *MNRAS*, 482, L85
- van der Marel, R. P., Fardal, M., Besla, G., et al. 2012, *ApJ*, 753, 8
- van der Marel, R. P., & Guhathakurta, P. 2008, *ApJ*, 678, 187
- Veljanoski, J., Mackey, A. D., Ferguson, A. M. N., et al. 2014, *MNRAS*, 442, 2929
- Wakker, B. P. 2001, *ApJS*, 136, 463
- . 2006, *ApJS*, 163, 282
- Wakker, B. P., Hernandez, A. K., French, D. M., et al. 2015, *ApJ*, 814, 40
- Wakker, B. P., & van Woerden, H. 1997, *ARA&A*, 35, 217
- Wakker, B. P., York, D. G., Wilhelm, R., et al. 2008, *ApJ*, 672, 298
- Wakker, B. P., Savage, B. D., Sembach, K. R., et al. 2003, *ApJS*, 146, 1
- Wang, Q. D., & Yao, Y. 2012, arXiv e-prints, arXiv:1211.4834
- Watkins, L. L., Evans, N. W., & An, J. H. 2010, *MNRAS*, 406, 264
- Watts, D. G., & Bacon, D. W. 1974, *Technometrics*, 16, 369
- Welty, D. E., Hobbs, L. M., Lauroesch, J. T., et al. 1999, *ApJS*, 124, 465
- Welty, D. E., Lauroesch, J. T., Blades, J. C., Hobbs, L. M., & York, D. G. 1997, *ApJ*, 489, 672
- Werk, J. K., Prochaska, J. X., Thom, C., et al. 2012, *ApJS*, 198, 3
- . 2013, *ApJS*, 204, 17
- Werk, J. K., Prochaska, J. X., Tumlinson, J., et al. 2014, *ApJ*, 792, 8
- Williams, B. F., Dolphin, A. E., Dalcanton, J. J., et al. 2017, *ApJ*, 846, 145
- Woodgate, B. E., Kimble, R. A., Bowers, C. W., et al. 1998, *PASP*, 110, 1183
- Wotta, C. B., Lehner, N., Howk, J. C., et al. 2019, *ApJ*, 872, 81
- Wotta, C. B., Lehner, N., Howk, J. C., O’Meara, J. M., & Prochaska, J. X. 2016, *ApJ*, 831, 95
- Zahedy, F. S., Chen, H.-W., Johnson, S. D., et al. 2019, *MNRAS*, 484, 2257
- Zahedy, F. S., Chen, H.-W., Rauch, M., Wilson, M. L., & Zabludoff, A. 2016, *MNRAS*, 458, 2423
- Zech, W. F., Lehner, N., Howk, J. C., Dixon, W. V. D., & Brown, T. M. 2008, *ApJ*, 679, 460
- Zheng, Y., Peebles, M. S., O’Shea, B. W., et al. 2020, arXiv e-prints, arXiv:2001.07736
- Zheng, Y., Putman, M. E., Peek, J. E. G., & Joung, M. R. 2015, *ApJ*, 807, 103

Table 1. Sample Summary

Target	z_{em}	RA	Dec	l_{MS}	b_{MS}	R	X	Y	PID	COS Grating	SNR
		($^{\circ}$)	($^{\circ}$)	($^{\circ}$)	($^{\circ}$)	(kpc)	(kpc)	(kpc)			
RX_J0048.3+3941	0.134	12.079	39.687	-125.0	24.8	25.0	14.1	-20.7	11632	G130M-G160M	31.5
HS0033+4300	0.120	9.096	43.278	-129.1	22.7	30.5	-15.2	26.5	11632	G130M-G160M	5.9
HS0058+4213	0.190	15.380	42.493	-128.1	27.3	48.6	45.4	17.3	11632	G130M-G160M	8.1
RX_J0043.6+3725	0.080	10.927	37.422	-122.6	23.7	50.5	2.5	-50.5	14268	G130M-G160M	17.9
Zw535.012	0.048	9.087	45.665	-131.7	22.9	59.7	-14.7	57.8	14268	G130M-G160M	17.8
RX_J0050.8+3536	0.058	12.711	35.612	-120.5	25.0	77.1	21.6	-74.0	14268	G130M-G160M	18.7
IRAS_F00040+4325	0.163	1.652	43.708	-130.1	17.4	93.0	-85.5	36.5	14268	G130M-G160M	24.9
RXS_J0118.8+3836	0.216	19.706	38.606	-123.7	30.7	97.2	92.3	-30.2	14268	G130M-G160M	14.4
MRK352	0.015	14.972	31.827	-116.1	26.5	131.7	48.0	-122.7	14268	G130M-G160M	12.2
RX_J0028.1+3103	0.500	7.045	31.063	-116.3	19.7	139.1	-41.1	-132.9	14268	G130M-G160M	13.6
KAZ238	0.043	0.242	33.344	-119.7	14.5	150.2	-114.4	-97.3	14268	G130M-G160M	11.5
FBS0150+396	0.212	28.278	39.929	-125.9	37.2	175.5	175.5	0.2	14268	G130M-G160M	10.3
3C48.0	0.367	24.422	33.160	-117.3	34.6	177.9	150.6	-94.9	14268	G130M-G160M	16.6
4C25.01	0.284	4.916	26.048	-111.4	17.0	208.7	-68.6	-197.1	14268	G130M-G160M	18.6
PG0052+251	0.155	13.717	25.427	-109.2	24.7	209.8	36.3	-206.7	14268	G130M-G160M	28.6
RXS_J0155.6+3115	0.135	28.900	31.255	-115.0	38.4	231.6	203.4	-110.8	14268	G130M-G160M	17.2
RBS2055	0.038	357.970	26.326	-113.2	11.0	238.6	-150.3	-185.4	14268	G130M-G160M	22.3
3C66A	0.444	35.665	43.035	-131.3	41.9	242.2	235.2	57.9	12612	G130M-G160M	21.4
RX_J0053.7+2232	0.148	13.442	22.539	-106.2	23.9	246.6	33.9	-244.2	14268	G130M-G160M	14.2
MRK335	0.026	1.581	20.203	-106.3	12.6	292.6	-113.8	-269.6	11524	G130M-G160M	29.8
MRK1148	0.064	12.978	17.433	-100.8	22.5	311.6	29.3	-310.3	14268	G130M-G160M	20.9
RBS2005	0.120	351.476	21.887	-110.5	4.0	328.6	-235.3	-229.5	14268	G130M-G160M	16.2
RX_J0023.5+1547	0.412	5.877	15.796	-100.8	15.5	335.9	-62.2	-330.1	14071	G130M	6.4
MRK1179	0.038	38.343	27.937	-111.0	46.7	341.0	316.6	-126.6	14268	G130M-G160M	9.5
PG0003+158	0.451	1.497	16.164	-102.3	11.5	342.5	-118.4	-321.4	12038	G130M-G160M	21.4
UGC12163	0.025	340.664	29.725	-121.2	-2.5	349.2	-335.9	-95.3	12212	G130M-G160M	9.9
SDSSJ011623.06+142940.6	0.394	19.096	14.495	-96.2	27.6	360.7	109.7	-343.6	13774	G130M-G160M	7.7
PG0026+129	0.142	7.307	13.268	-97.9	16.2	365.8	-44.5	-363.1	12569	G130M	16.9
MRK1502	0.061	13.396	12.693	-95.7	21.8	372.4	35.8	-370.7	12569	G130M-G160M	23.2
SDSSJ014143.20+134032.0	0.045	25.430	13.676	-93.7	33.4	394.8	192.7	-344.5	12275	G130M	4.6
MRK1501	0.089	2.629	10.975	-96.9	11.2	403.3	-107.4	-388.8	12569	G130M	3.4
IRAS01477+1254	0.147	27.618	13.150	-92.6	35.4	411.6	221.8	-346.7	11727	G130M-G160M	4.9
SDSSJ015952.95+134554.3	0.504	29.971	13.765	-92.7	37.7	417.3	251.1	-333.3	12603	G130M	11.2
3C454.3	0.859	343.491	16.148	-107.5	-5.0	444.1	-345.5	-279.0	13398	G130M-G160M	6.6
SDSSJ225738.20+134045.0	0.595	344.409	13.679	-104.9	-5.0	462.5	-339.9	-313.7	11598	G130M-G160M	7.9
PG0044+030	0.623	11.775	3.332	-86.6	17.7	489.0	15.1	-488.8	12275	G130M	8.4
NGC7469	0.016	345.815	8.874	-99.9	-5.3	503.9	-331.6	-379.4	12212	G130M-G160M	32.7
PHL1226	0.404	28.617	4.805	-82.5	34.1	512.4	245.4	-449.8	12536	G130M	8.8
UM228	0.098	5.254	0.880	-86.3	10.7	522.8	-75.9	-517.3	13017	G130M-G160M	7.3
MRK304	0.066	334.301	14.239	-109.0	-13.9	533.1	-462.4	-265.2	12569	G130M-G160M	23.9
MRK595	0.027	40.395	7.187	-80.6	46.0	552.4	397.6	-383.5	12275	G130M	11.1
PG2349-014	0.174	357.984	-1.154	-86.6	3.2	562.9	-178.3	-534.0	12569	G130M	27.1
MRK1014	0.163	29.959	0.395	-76.9	33.9	568.7	268.1	-501.5	12569	G130M	24.3

NOTE—The 18 sightlines from our large *HST* program have the PID 14268; for the supplemental archival 25 other targets, the *HST* PID is listed. All the projected distances are computed using the three dimensional separation (coordinates of the target and distance of M31 assumed to be 752 kpc). The coordinates l_{MS} and b_{MS} are the MS longitudes and latitudes as defined by Nidever et al. (2008). The SNR is given per COS resolution element (assuming $R \sim 17,000$) and estimated in the continuum near Si III $\lambda 1206$.

Table 2. Summary of the Results

Target	Ion	v_1	v_2	v	σ_v	$\log N$	$\sigma_{\log N}^1$	$\sigma_{\log N}^2$	f_N	f_{MS}
		(km s ⁻¹)	(km s ⁻¹)	(km s ⁻¹)	(km s ⁻¹)	[cm ⁻²]				
RX_J0048.3+3941	Al II	-480.0	-320.0	-397.2	19.6	11.92	0.15	0.23	0	-1
RX_J0048.3+3941	C II	-480.0	-320.0	-381.4	1.2	14.15	0.01	0.01	-2	-1
RX_J0048.3+3941	C IV	-480.0	-320.0	-390.8	5.3	13.25	0.05	0.05	0	-1
RX_J0048.3+3941	Fe II	-480.0	-320.0	-432.9	25.2	13.40	0.15	0.23	0	-1
RX_J0048.3+3941	N I	-480.0	-320.0	12.88	0.18	0.30	-1	-1
RX_J0048.3+3941	N V	-480.0	-320.0	12.77	0.18	0.30	-1	-1
RX_J0048.3+3941	O I	-480.0	-320.0	13.47	0.18	0.30	-1	-1
RX_J0048.3+3941	O VI	-480.0	-320.0	-375.5	6.2	13.85	0.05	0.06	0	-1
RX_J0048.3+3941	S II	-480.0	-320.0	13.74	0.18	0.30	-1	-1
RX_J0048.3+3941	Si II	-480.0	-320.0	-374.0	2.4	12.93	0.02	0.02	0	-1
RX_J0048.3+3941	Si III	-480.0	-320.0	-376.0	1.6	13.06	0.02	0.02	-2	-1
RX_J0048.3+3941	Si IV	-480.0	-320.0	12.39	0.18	0.30	-1	-1
RX_J0048.3+3941	Al II	-300.0	-210.0	11.68	0.18	0.30	-1	0
RX_J0048.3+3941	C II	-300.0	-210.0	-239.0	3.7	13.73	0.06	0.07	-2	0
RX_J0048.3+3941	C IV	-300.0	-210.0	-242.8	0.5	13.95	0.01	0.01	0	0
RX_J0048.3+3941	Fe II	-300.0	-210.0	13.18	0.18	0.30	-1	0
RX_J0048.3+3941	N I	-300.0	-210.0	12.74	0.18	0.30	-1	0
RX_J0048.3+3941	N V	-300.0	-210.0	-245.7	6.1	12.95	0.09	0.11	0	0
RX_J0048.3+3941	O I	-300.0	-210.0	13.34	0.18	0.30	-1	0
RX_J0048.3+3941	O VI	-300.0	-210.0	-243.7	1.5	14.26	0.03	0.03	0	0
RX_J0048.3+3941	S II	-300.0	-210.0	13.60	0.18	0.30	-1	0
RX_J0048.3+3941	Si II	-300.0	-210.0	-247.9	2.9	12.78	0.04	0.05	0	0
RX_J0048.3+3941	Si III	-300.0	-210.0	-245.4	0.6	13.12	0.01	0.01	-2	0
RX_J0048.3+3941	Si IV	-300.0	-210.0	-241.4	0.8	13.16	0.02	0.02	0	0
RX_J0048.3+3941	Al II	-210.0	-140.0	-176.4	1.9	12.39	0.04	0.05	0	0
RX_J0048.3+3941	C II	-210.0	-140.0	-176.8	0.9	14.22	0.03	0.04	-2	0
RX_J0048.3+3941	C IV	-210.0	-140.0	-186.3	0.8	13.59	0.02	0.02	0	0
RX_J0048.3+3941	Fe II	-210.0	-140.0	-180.4	6.9	13.31	0.13	0.18	0	0
RX_J0048.3+3941	N I	-210.0	-140.0	12.69	0.18	0.30	-1	0
RX_J0048.3+3941	N V	-210.0	-140.0	12.59	0.18	0.30	-1	0
RX_J0048.3+3941	O I	-210.0	-140.0	-172.6	9.5	13.34	0.16	0.27	0	0
RX_J0048.3+3941	O VI	-210.0	-140.0	-184.6	1.4	14.05	0.03	0.03	0	0
RX_J0048.3+3941	S II	-210.0	-140.0	13.73	0.18	0.30	-1	0
RX_J0048.3+3941	Si II	-210.0	-140.0	-182.4	1.4	13.50	0.03	0.03	0	0
RX_J0048.3+3941	Si III	-210.0	-140.0	-180.4	0.5	13.10	0.01	0.01	-2	0
RX_J0048.3+3941	Si IV	-210.0	-140.0	-178.4	0.8	12.98	0.02	0.02	0	0
HS0033+4300	Al II	-440.0	-335.0	12.29	0.18	0.30	-1	-1
HS0033+4300	C II	-440.0	-335.0	-385.4	18.7	14.12	0.07	0.09	0	-1
HS0033+4300	C IV	-440.0	-335.0	13.06	0.18	0.30	-1	-1
HS0033+4300	Fe II	-440.0	-335.0	13.73	0.18	0.30	-1	-1
HS0033+4300	N I	-440.0	-335.0	13.65	0.18	0.30	-1	-1
HS0033+4300	N V	-440.0	-335.0	13.53	0.18	0.30	-1	-1
HS0033+4300	O I	-440.0	-335.0	14.03	0.18	0.30	-1	-1
HS0033+4300	P II	-440.0	-335.0	14.60	0.18	0.30	-1	-1
HS0033+4300	S II	-440.0	-335.0	14.47	0.18	0.30	-1	-1
HS0033+4300	Si II	-440.0	-335.0	12.59	0.18	0.30	-1	-1
HS0033+4300	Si III	-440.0	-335.0	-385.6	14.4	12.90	0.17	0.28	0	-1
HS0033+4300	Si IV	-440.0	-335.0	-379.0	12.1	13.26	0.15	0.23	0	-1
HS0033+4300	Al II	-300.0	-150.0	12.37	0.18	0.30	-1	0
HS0033+4300	C IV	-300.0	-150.0	-215.8	3.0	14.10	0.04	0.05	0	0
HS0033+4300	Fe II	-300.0	-150.0	13.80	0.18	0.30	-1	0
HS0033+4300	N I	-300.0	-150.0	13.74	0.18	0.30	-1	0

Table 2 continued

Table 2 (*continued*)

Target	Ion	v_1	v_2	v	σ_v	$\log N$	$\sigma_{\log N}^1$	$\sigma_{\log N}^2$	f_N	f_{MS}
		(km s ⁻¹)	(km s ⁻¹)	(km s ⁻¹)	(km s ⁻¹)	[cm ⁻²]				
HS0033+4300	N v	-300.0	-150.0	13.62	0.18	0.30	-1	0
HS0033+4300	O I	-300.0	-150.0	14.10	0.18	0.30	-1	0
HS0033+4300	P II	-300.0	-150.0	14.68	0.18	0.30	-1	0
HS0033+4300	S II	-300.0	-150.0	14.52	0.18	0.30	-1	0
HS0033+4300	Si II	-300.0	-150.0	-239.3	16.4	13.42	0.13	0.20	0	0
HS0033+4300	Si III	-300.0	-150.0	-208.2	10.4	13.39	0.06	0.07	0	0
HS0033+4300	Si IV	-300.0	-150.0	-219.3	7.7	13.32	0.07	0.09	0	0
HS0058+4213	Al II	-275.0	-215.0	12.18	0.18	0.30	-1	0
HS0058+4213	C II	-275.0	-215.0	-236.9	2.6	14.16	0.09	0.11	-2	0
HS0058+4213	C IV	-275.0	-215.0	-232.7	6.3	13.33	0.12	0.17	0	0
HS0058+4213	Fe II	-275.0	-215.0	13.63	0.18	0.30	-1	0
HS0058+4213	N I	-275.0	-215.0	13.34	0.18	0.30	-1	0
HS0058+4213	N v	-275.0	-215.0	13.17	0.18	0.30	-1	0
HS0058+4213	O I	-275.0	-215.0	13.67	0.18	0.30	-1	0
HS0058+4213	P II	-275.0	-215.0	14.25	0.18	0.30	-1	0
HS0058+4213	S II	-275.0	-215.0	14.11	0.18	0.30	-1	0
HS0058+4213	Si II	-275.0	-215.0	-236.0	3.5	13.47	0.08	0.10	0	0
HS0058+4213	Si III	-275.0	-215.0	-230.6	3.7	13.12	0.05	0.06	-2	0
HS0058+4213	Si IV	-275.0	-215.0	-239.1	3.0	13.08	0.08	0.10	0	0
HS0058+4213	Al II	-215.0	-170.0	12.13	0.18	0.30	-1	0
HS0058+4213	C II	-215.0	-170.0	-199.5	4.4	14.10	0.04	0.05	-2	0
HS0058+4213	C IV	-215.0	-170.0	-191.3	1.8	13.77	0.06	0.07	0	0
HS0058+4213	Fe II	-215.0	-170.0	13.58	0.18	0.30	-1	0
HS0058+4213	N I	-215.0	-170.0	13.27	0.18	0.30	-1	0
HS0058+4213	N v	-215.0	-170.0	13.12	0.18	0.30	-1	0
HS0058+4213	O I	-215.0	-170.0	13.60	0.18	0.30	-1	0
HS0058+4213	P II	-215.0	-170.0	14.18	0.18	0.30	-1	0
HS0058+4213	S II	-215.0	-170.0	14.06	0.18	0.30	-1	0
HS0058+4213	Si II	-215.0	-170.0	-197.2	2.5	13.16	0.03	0.04	0	0
HS0058+4213	Si III	-215.0	-170.0	-193.7	2.7	13.17	0.03	0.03	-2	0
HS0058+4213	Si IV	-215.0	-170.0	-195.1	2.0	13.12	0.07	0.08	0	0
RX_J0043.6+3725	Al II	-350.0	-250.0	11.91	0.18	0.30	-1	0
RX_J0043.6+3725	C II	-350.0	-250.0	-295.7	2.5	13.79	0.04	0.04	0	0
RX_J0043.6+3725	C IV	-350.0	-250.0	12.92	0.18	0.30	-1	0
RX_J0043.6+3725	Fe II	-350.0	-250.0	13.64	0.18	0.30	-1	0
RX_J0043.6+3725	N I	-350.0	-250.0	13.11	0.18	0.30	-1	0
RX_J0043.6+3725	N v	-350.0	-250.0	12.98	0.18	0.30	-1	0
RX_J0043.6+3725	O I	-350.0	-250.0	13.30	0.18	0.30	-1	0
RX_J0043.6+3725	P II	-350.0	-250.0	13.87	0.18	0.30	-1	0
RX_J0043.6+3725	S II	-350.0	-250.0	13.93	0.18	0.30	-1	0
RX_J0043.6+3725	Si II	-350.0	-250.0	12.47	0.18	0.30	-1	0
RX_J0043.6+3725	Si III	-350.0	-250.0	-290.9	2.5	12.87	0.04	0.04	0	0
RX_J0043.6+3725	Si IV	-350.0	-250.0	-291.2	13.7	12.51	0.16	0.26	0	0
RX_J0043.6+3725	Al II	-250.0	-120.0	11.98	0.18	0.30	-1	0
RX_J0043.6+3725	C II	-250.0	-120.0	-181.1	2.8	13.92	0.03	0.04	0	0
RX_J0043.6+3725	C IV	-250.0	-120.0	-188.5	2.5	13.85	0.03	0.03	0	0
RX_J0043.6+3725	Fe II	-250.0	-120.0	13.72	0.18	0.30	-1	0
RX_J0043.6+3725	N I	-250.0	-120.0	13.18	0.18	0.30	-1	0
RX_J0043.6+3725	N v	-250.0	-120.0	13.03	0.18	0.30	-1	0
RX_J0043.6+3725	O I	-250.0	-120.0	13.35	0.18	0.30	-1	0
RX_J0043.6+3725	P II	-250.0	-120.0	13.93	0.18	0.30	-1	0
RX_J0043.6+3725	S II	-250.0	-120.0	13.98	0.18	0.30	-1	0
RX_J0043.6+3725	Si II	-250.0	-120.0	-197.8	8.0	12.92	0.09	0.11	0	0

Table 2 *continued*

Table 2 (*continued*)

Target	Ion	v_1	v_2	v	σ_v	$\log N$	$\sigma_{\log N}^1$	$\sigma_{\log N}^2$	f_N	f_{MS}
		(km s ⁻¹)	(km s ⁻¹)	(km s ⁻¹)	(km s ⁻¹)	[cm ⁻²]				
RX_J0043.6+3725	Si III	-250.0	-120.0	-184.1	1.8	13.20	0.02	0.03	-2	0
RX_J0043.6+3725	Si IV	-250.0	-120.0	-180.4	4.6	13.10	0.05	0.06	0	0
Zw535.012	Al II	-450.0	-320.0	12.23	0.18	0.30	-1	-1
Zw535.012	C II	-450.0	-320.0	13.11	0.18	0.30	-1	-1
Zw535.012	C IV	-450.0	-320.0	13.11	0.18	0.30	-1	-1
Zw535.012	Fe II	-450.0	-320.0	13.59	0.18	0.30	-1	-1
Zw535.012	N I	-450.0	-320.0	13.18	0.18	0.30	-1	-1
Zw535.012	N V	-450.0	-320.0	12.99	0.18	0.30	-1	-1
Zw535.012	O I	-450.0	-320.0	13.31	0.18	0.30	-1	-1
Zw535.012	P II	-450.0	-320.0	13.90	0.18	0.30	-1	-1
Zw535.012	S II	-450.0	-320.0	13.82	0.18	0.30	-1	-1
Zw535.012	Si II	-450.0	-320.0	12.55	0.18	0.30	-1	-1
Zw535.012	Si III	-450.0	-320.0	-372.7	8.7	12.49	0.09	0.12	0	-1
Zw535.012	Si IV	-450.0	-320.0	12.55	0.18	0.30	-1	-1
Zw535.012	Al II	-250.0	-200.0	12.01	0.18	0.30	-1	0
Zw535.012	C II	-250.0	-200.0	12.86	0.18	0.30	-1	0
Zw535.012	C IV	-250.0	-200.0	-215.3	7.2	12.99	0.16	0.26	0	0
Zw535.012	Fe II	-250.0	-200.0	13.42	0.18	0.30	-1	0
Zw535.012	N I	-250.0	-200.0	12.97	0.18	0.30	-1	0
Zw535.012	N V	-250.0	-200.0	12.77	0.18	0.30	-1	0
Zw535.012	O I	-250.0	-200.0	13.07	0.18	0.30	-1	0
Zw535.012	P II	-250.0	-200.0	13.64	0.18	0.30	-1	0
Zw535.012	S II	-250.0	-200.0	13.58	0.18	0.30	-1	0
Zw535.012	Si II	-250.0	-200.0	12.32	0.18	0.30	-1	0
Zw535.012	Si III	-250.0	-200.0	-230.4	5.9	12.02	0.15	0.22	0	0
Zw535.012	Si IV	-250.0	-200.0	12.31	0.18	0.30	-1	0
Zw535.012	Al II	-200.0	-150.0	12.02	0.18	0.30	-1	0
Zw535.012	C II	-200.0	-150.0	-163.1	1.9	13.60	0.05	0.06	0	0
Zw535.012	C IV	-200.0	-150.0	-165.8	4.4	13.21	0.11	0.15	0	0
Zw535.012	Fe II	-200.0	-150.0	13.41	0.18	0.30	-1	0
Zw535.012	N I	-200.0	-150.0	12.96	0.18	0.30	-1	0
Zw535.012	N V	-200.0	-150.0	12.77	0.18	0.30	-1	0
Zw535.012	O I	-200.0	-150.0	13.07	0.18	0.30	-1	0
Zw535.012	P II	-200.0	-150.0	13.65	0.18	0.30	-1	0
Zw535.012	S II	-200.0	-150.0	13.57	0.18	0.30	-1	0
Zw535.012	Si II	-200.0	-150.0	-173.3	0.7	12.87	0.02	0.02	0	0
Zw535.012	Si III	-200.0	-150.0	-167.6	1.2	12.85	0.04	0.04	0	0
Zw535.012	Si IV	-200.0	-150.0	12.32	0.18	0.30	-1	0
RX_J0050.8+3536	Al II	-300.0	-190.0	12.05	0.18	0.30	-1	0
RX_J0050.8+3536	C II	-300.0	-190.0	-244.0	7.5	13.36	0.10	0.12	0	0
RX_J0050.8+3536	C IV	-300.0	-190.0	-237.1	4.7	13.45	0.06	0.07	0	0
RX_J0050.8+3536	Fe II	-300.0	-190.0	13.64	0.18	0.30	-1	0
RX_J0050.8+3536	N I	-300.0	-190.0	13.12	0.18	0.30	-1	0
RX_J0050.8+3536	N V	-300.0	-190.0	12.95	0.18	0.30	-1	0
RX_J0050.8+3536	O I	-300.0	-190.0	13.37	0.18	0.30	-1	0
RX_J0050.8+3536	P II	-300.0	-190.0	13.86	0.18	0.30	-1	0
RX_J0050.8+3536	S II	-300.0	-190.0	13.87	0.18	0.30	-1	0
RX_J0050.8+3536	Si II	-300.0	-190.0	-237.4	11.9	12.65	0.14	0.20	0	0
RX_J0050.8+3536	Si III	-300.0	-190.0	-247.3	2.6	12.86	0.04	0.04	0	0
RX_J0050.8+3536	Si IV	-300.0	-190.0	12.49	0.18	0.30	-1	0
IRAS_F00040+4325	Al II	-460.0	-400.0	11.82	0.18	0.30	-1	-1
IRAS_F00040+4325	C II	-460.0	-400.0	12.84	0.18	0.30	-1	-1
IRAS_F00040+4325	C IV	-460.0	-400.0	12.65	0.18	0.30	-1	-1

Table 2 *continued*

Table 2 (*continued*)

Target	Ion	v_1	v_2	v	σ_v	$\log N$	$\sigma_{\log N}^1$	$\sigma_{\log N}^2$	f_N	f_{MS}
		(km s ⁻¹)	(km s ⁻¹)	(km s ⁻¹)	(km s ⁻¹)	[cm ⁻²]				
IRAS.F00040+4325	Fe II	-460.0	-400.0	13.29	0.18	0.30	-1	-1
IRAS.F00040+4325	N I	-460.0	-400.0	12.76	0.18	0.30	-1	-1
IRAS.F00040+4325	N V	-460.0	-400.0	13.00	0.18	0.30	-1	-1
IRAS.F00040+4325	O I	-460.0	-400.0	13.19	0.18	0.30	-1	-1
IRAS.F00040+4325	O VI	-460.0	-400.0	13.88	0.18	0.30	-1	-1
IRAS.F00040+4325	P II	-460.0	-400.0	13.77	0.18	0.30	-1	-1
IRAS.F00040+4325	S II	-460.0	-400.0	13.66	0.18	0.30	-1	-1
IRAS.F00040+4325	Si II	-460.0	-400.0	-427.9	6.4	11.94	0.14	0.21	0	-1
IRAS.F00040+4325	Si III	-460.0	-400.0	-426.4	4.3	11.99	0.10	0.12	0	-1
IRAS.F00040+4325	Si IV	-460.0	-400.0	12.05	0.18	0.30	-1	-1
IRAS.F00040+4325	Al II	-390.0	-279.0	11.98	0.18	0.30	-1	0
IRAS.F00040+4325	C II	-390.0	-279.0	-344.9	9.2	13.23	0.11	0.14	0	0
IRAS.F00040+4325	C IV	-390.0	-279.0	13.08	0.18	0.30	-1	0
IRAS.F00040+4325	Fe II	-390.0	-279.0	13.45	0.18	0.30	-1	0
IRAS.F00040+4325	N I	-390.0	-279.0	12.89	0.18	0.30	-1	0
IRAS.F00040+4325	N V	-390.0	-279.0	12.84	0.18	0.30	-1	0
IRAS.F00040+4325	O I	-390.0	-279.0	13.33	0.18	0.30	-1	0
IRAS.F00040+4325	O VI	-390.0	-279.0	-337.0	177.0	14.45	0.14	0.21	0	0
IRAS.F00040+4325	P II	-390.0	-279.0	13.90	0.18	0.30	-1	0
IRAS.F00040+4325	S II	-390.0	-279.0	13.80	0.18	0.30	-1	0
IRAS.F00040+4325	Si II	-390.0	-279.0	12.28	0.18	0.30	-1	0
IRAS.F00040+4325	Si III	-390.0	-279.0	-327.2	3.7	12.50	0.05	0.06	0	0
IRAS.F00040+4325	Si IV	-390.0	-279.0	-344.1	13.2	12.25	0.16	0.25	0	0
IRAS.F00040+4325	Al II	-281.0	-195.0	11.91	0.18	0.30	-1	0
IRAS.F00040+4325	C II	-281.0	-195.0	-223.6	3.4	13.54	0.05	0.06	0	0
IRAS.F00040+4325	C IV	-281.0	-195.0	-238.0	3.8	13.23	0.06	0.07	0	0
IRAS.F00040+4325	Fe II	-281.0	-195.0	13.42	0.18	0.30	-1	0
IRAS.F00040+4325	N I	-281.0	-195.0	12.82	0.18	0.30	-1	0
IRAS.F00040+4325	N V	-281.0	-195.0	12.79	0.18	0.30	-1	0
IRAS.F00040+4325	O I	-281.0	-195.0	-228.1	5.5	13.67	0.08	0.10	0	0
IRAS.F00040+4325	O VI	-281.0	-195.0	-239.4	18.2	14.44	0.10	0.13	-2	0
IRAS.F00040+4325	P II	-281.0	-195.0	13.85	0.18	0.30	-1	0
IRAS.F00040+4325	S II	-281.0	-195.0	13.74	0.18	0.30	-1	0
IRAS.F00040+4325	Si II	-281.0	-195.0	-232.8	7.3	12.44	0.12	0.16	0	0
IRAS.F00040+4325	Si III	-281.0	-195.0	-234.3	3.8	12.31	0.06	0.07	0	0
IRAS.F00040+4325	Si IV	-281.0	-195.0	12.13	0.18	0.30	-1	0
IRAS.F00040+4325	Al II	-195.0	-125.0	11.86	0.18	0.30	-1	0
IRAS.F00040+4325	C II	-195.0	-125.0	-153.6	0.9	14.07	0.02	0.02	-2	0
IRAS.F00040+4325	C IV	-195.0	-125.0	-154.3	3.8	13.11	0.07	0.08	0	0
IRAS.F00040+4325	Fe II	-195.0	-125.0	13.39	0.18	0.30	-1	0
IRAS.F00040+4325	N I	-195.0	-125.0	12.78	0.18	0.30	-1	0
IRAS.F00040+4325	N V	-195.0	-125.0	12.74	0.18	0.30	-1	0
IRAS.F00040+4325	O I	-195.0	-125.0	-159.9	5.6	13.51	0.11	0.14	0	0
IRAS.F00040+4325	O VI	-195.0	-125.0	13.95	0.18	0.30	-1	0
IRAS.F00040+4325	S II	-195.0	-125.0	13.69	0.18	0.30	-1	0
IRAS.F00040+4325	Si II	-195.0	-125.0	-159.8	2.9	12.99	0.06	0.07	0	0
IRAS.F00040+4325	Si III	-195.0	-125.0	-154.0	0.7	13.05	0.02	0.02	-2	0
IRAS.F00040+4325	Si IV	-195.0	-125.0	-152.6	4.2	12.51	0.08	0.09	0	0
RXS_J0118.8+3836	Al II	-300.0	-245.0	12.11	0.18	0.30	-1	0
RXS_J0118.8+3836	C II	-300.0	-245.0	-272.3	3.7	13.46	0.10	0.14	0	0
RXS_J0118.8+3836	C IV	-300.0	-245.0	12.90	0.18	0.30	-1	0
RXS_J0118.8+3836	Fe II	-300.0	-245.0	13.75	0.18	0.30	-1	0
RXS_J0118.8+3836	N I	-300.0	-245.0	13.08	0.18	0.30	-1	0

Table 2 *continued*

Table 2 (*continued*)

Target	Ion	v_1	v_2	v	σ_v	$\log N$	$\sigma_{\log N}^1$	$\sigma_{\log N}^2$	f_N	f_{MS}
		(km s ⁻¹)	(km s ⁻¹)	(km s ⁻¹)	(km s ⁻¹)	[cm ⁻²]				
RXS_J0118.8+3836	N v	-300.0	-245.0	12.93	0.18	0.30	-1	0
RXS_J0118.8+3836	O I	-300.0	-245.0	13.48	0.18	0.30	-1	0
RXS_J0118.8+3836	S II	-300.0	-245.0	13.76	0.18	0.30	-1	0
RXS_J0118.8+3836	Si II	-300.0	-245.0	12.44	0.18	0.30	-1	0
RXS_J0118.8+3836	Si III	-300.0	-245.0	-265.2	1.8	12.78	0.05	0.06	0	0
RXS_J0118.8+3836	Si IV	-300.0	-245.0	12.49	0.18	0.30	-1	0
RXS_J0118.8+3836	Al II	-245.0	-190.0	12.13	0.18	0.30	-1	0
RXS_J0118.8+3836	C II	-245.0	-190.0	-216.1	4.7	13.41	0.11	0.15	0	0
RXS_J0118.8+3836	C IV	-245.0	-190.0	12.89	0.18	0.30	-1	0
RXS_J0118.8+3836	Fe II	-245.0	-190.0	13.74	0.18	0.30	-1	0
RXS_J0118.8+3836	N I	-245.0	-190.0	13.08	0.18	0.30	-1	0
RXS_J0118.8+3836	N v	-245.0	-190.0	12.94	0.18	0.30	-1	0
RXS_J0118.8+3836	O I	-245.0	-190.0	13.48	0.18	0.30	-1	0
RXS_J0118.8+3836	S II	-245.0	-190.0	13.78	0.18	0.30	-1	0
RXS_J0118.8+3836	Si II	-245.0	-190.0	12.44	0.18	0.30	-1	0
RXS_J0118.8+3836	Si III	-245.0	-190.0	-224.5	3.6	12.41	0.09	0.11	0	0
RXS_J0118.8+3836	Si IV	-245.0	-190.0	12.51	0.18	0.30	-1	0
MRK352	Al II	-350.0	-267.0	12.29	0.18	0.30	-1	0
MRK352	C II	-350.0	-267.0	-305.2	6.7	13.65	0.11	0.16	0	0
MRK352	C IV	-350.0	-267.0	-282.2	4.1	13.50	0.06	0.07	0	0
MRK352	Fe II	-350.0	-267.0	13.80	0.18	0.30	-1	0
MRK352	N I	-350.0	-267.0	13.32	0.18	0.30	-1	0
MRK352	N v	-350.0	-267.0	12.68	0.18	0.30	-1	0
MRK352	O I	-350.0	-267.0	14.08	0.18	0.30	-1	0
MRK352	O VI	-350.0	-267.0	-310.9	5.5	14.24	0.08	0.11	0	0
MRK352	S II	-350.0	-267.0	13.94	0.18	0.30	-1	0
MRK352	Si II	-350.0	-267.0	12.72	0.18	0.30	-1	0
MRK352	Si III	-350.0	-267.0	-302.9	3.4	12.84	0.06	0.08	0	0
MRK352	Si IV	-350.0	-267.0	12.69	0.18	0.30	-1	0
MRK352	Al II	-267.0	-225.0	12.16	0.18	0.30	-1	0
MRK352	C II	-267.0	-225.0	13.16	0.18	0.30	-1	0
MRK352	C IV	-267.0	-225.0	-242.6	1.1	13.66	0.04	0.04	0	0
MRK352	Fe II	-267.0	-225.0	13.65	0.18	0.30	-1	0
MRK352	N I	-267.0	-225.0	13.17	0.18	0.30	-1	0
MRK352	N v	-267.0	-225.0	12.53	0.18	0.30	-1	0
MRK352	O I	-267.0	-225.0	13.94	0.18	0.30	-1	0
MRK352	O VI	-267.0	-225.0	-243.9	3.7	14.17	0.05	0.06	0	0
MRK352	S II	-267.0	-225.0	13.76	0.18	0.30	-1	0
MRK352	Si II	-267.0	-225.0	12.58	0.18	0.30	-1	0
MRK352	Si III	-267.0	-225.0	-244.2	1.7	12.80	0.06	0.07	0	0
MRK352	Si IV	-267.0	-225.0	12.52	0.18	0.30	-1	0
MRK352	Al II	-227.0	-155.0	12.25	0.18	0.30	-1	0
MRK352	C II	-227.0	-155.0	-192.1	3.3	13.94	0.07	0.08	0	0
MRK352	C IV	-227.0	-155.0	-209.7	2.0	13.82	0.13	0.13	0	0
MRK352	Fe II	-227.0	-155.0	13.78	0.18	0.30	-1	0
MRK352	N I	-227.0	-155.0	13.28	0.18	0.30	-1	0
MRK352	N v	-227.0	-155.0	12.67	0.18	0.30	-1	0
MRK352	O I	-227.0	-155.0	14.06	0.18	0.30	-1	0
MRK352	O VI	-227.0	-155.0	-193.8	4.7	14.39	0.05	0.05	-2	0
MRK352	S II	-227.0	-155.0	14.13	0.18	0.30	-1	0
MRK352	Si II	-227.0	-155.0	-196.3	3.9	13.44	0.08	0.09	0	0
MRK352	Si III	-227.0	-155.0	-197.5	2.1	13.06	0.06	0.07	-2	0
MRK352	Si IV	-227.0	-155.0	-198.1	3.8	13.18	0.07	0.09	0	0

Table 2 *continued*

Table 2 (*continued*)

Target	Ion	v_1	v_2	v	σ_v	$\log N$	$\sigma_{\log N}^1$	$\sigma_{\log N}^2$	f_N	f_{MS}
		(km s ⁻¹)	(km s ⁻¹)	(km s ⁻¹)	(km s ⁻¹)	[cm ⁻²]				
RX_J0028.1+3103	Al II	-405.0	-335.0	12.01	0.18	0.30	-1	0
RX_J0028.1+3103	C II	-405.0	-335.0	13.10	0.18	0.30	-1	0
RX_J0028.1+3103	C IV	-405.0	-335.0	13.11	0.18	0.30	-1	0
RX_J0028.1+3103	N I	-405.0	-335.0	13.15	0.18	0.30	-1	0
RX_J0028.1+3103	N V	-405.0	-335.0	12.99	0.18	0.30	-1	0
RX_J0028.1+3103	O I	-405.0	-335.0	-385.5	11.9	13.69	0.18	0.30	-1	0
RX_J0028.1+3103	S II	-405.0	-335.0	13.94	0.18	0.30	-1	0
RX_J0028.1+3103	Si II	-405.0	-335.0	12.08	0.18	0.30	-1	0
RX_J0028.1+3103	Si III	-405.0	-335.0	-361.9	5.0	12.45	0.09	0.12	0	0
RX_J0028.1+3103	Si IV	-405.0	-335.0	12.42	0.18	0.30	-1	0
RX_J0028.1+3103	Al II	-335.0	-235.0	12.10	0.18	0.30	-1	0
RX_J0028.1+3103	C II	-335.0	-235.0	-284.1	3.3	13.84	0.06	0.06	0	0
RX_J0028.1+3103	C IV	-335.0	-235.0	13.19	0.18	0.30	-1	0
RX_J0028.1+3103	Fe II	-335.0	-235.0	14.39	0.18	0.30	-1	0
RX_J0028.1+3103	N I	-335.0	-235.0	13.23	0.18	0.30	-1	0
RX_J0028.1+3103	N V	-335.0	-235.0	13.09	0.18	0.30	-1	0
RX_J0028.1+3103	O I	-335.0	-235.0	13.71	0.18	0.30	-1	0
RX_J0028.1+3103	S II	-335.0	-235.0	14.01	0.18	0.30	-1	0
RX_J0028.1+3103	Si II	-335.0	-235.0	12.58	0.18	0.30	-1	0
RX_J0028.1+3103	Si III	-335.0	-235.0	-284.9	1.9	13.19	0.04	0.04	-2	0
RX_J0028.1+3103	Si IV	-335.0	-235.0	12.81	0.18	0.30	-1	0
KAZ238	Al II	-455.0	-410.0	12.25	0.18	0.30	-1	-1
KAZ238	C II	-455.0	-410.0	13.11	0.18	0.30	-1	-1
KAZ238	C IV	-455.0	-410.0	12.94	0.18	0.30	-1	-1
KAZ238	N I	-455.0	-410.0	13.15	0.18	0.30	-1	-1
KAZ238	N V	-455.0	-410.0	13.04	0.18	0.30	-1	-1
KAZ238	S II	-455.0	-410.0	14.23	0.18	0.30	-1	-1
KAZ238	S III	-455.0	-410.0	13.92	0.18	0.30	-1	-1
KAZ238	Si II	-455.0	-410.0	12.53	0.18	0.30	-1	-1
KAZ238	Si III	-455.0	-410.0	-432.1	3.4	12.43	0.12	0.16	0	-1
KAZ238	Al II	-370.0	-305.0	12.34	0.18	0.30	-1	0
KAZ238	C II	-370.0	-305.0	13.20	0.18	0.30	-1	0
KAZ238	C IV	-370.0	-305.0	-333.7	4.2	13.45	0.09	0.11	0	0
KAZ238	N I	-370.0	-305.0	13.25	0.18	0.30	-1	0
KAZ238	N V	-370.0	-305.0	13.11	0.18	0.30	-1	0
KAZ238	S III	-370.0	-305.0	14.00	0.18	0.30	-1	0
KAZ238	Si II	-370.0	-305.0	12.61	0.18	0.30	-1	0
KAZ238	Si III	-370.0	-305.0	-332.6	5.2	12.55	0.10	0.14	0	0
KAZ238	Al II	-225.0	-150.0	12.33	0.18	0.30	-1	0
KAZ238	C II	-225.0	-150.0	13.17	0.18	0.30	-1	0
KAZ238	C IV	-225.0	-150.0	-187.6	3.3	13.65	0.07	0.08	0	0
KAZ238	N I	-225.0	-150.0	13.28	0.18	0.30	-1	0
KAZ238	N V	-225.0	-150.0	13.18	0.18	0.30	-1	0
KAZ238	S II	-225.0	-150.0	14.33	0.18	0.30	-1	0
KAZ238	S III	-225.0	-150.0	14.08	0.18	0.30	-1	0
KAZ238	Si II	-225.0	-150.0	12.64	0.18	0.30	-1	0
KAZ238	Si III	-225.0	-150.0	-186.2	5.4	12.64	0.09	0.12	0	0
FBS0150+396	Al II	-210.0	-135.0	12.49	0.18	0.30	-1	0
FBS0150+396	C IV	-210.0	-135.0	13.18	0.18	0.30	-1	0
FBS0150+396	Fe II	-210.0	-135.0	13.62	0.18	0.30	-1	0
FBS0150+396	N I	-210.0	-135.0	13.17	0.18	0.30	-1	0
FBS0150+396	O I	-210.0	-135.0	13.76	0.18	0.30	-1	0
FBS0150+396	S II	-210.0	-135.0	14.07	0.18	0.30	-1	0

Table 2 *continued*

Table 2 (*continued*)

Target	Ion	v_1	v_2	v	σ_v	$\log N$	$\sigma_{\log N}^1$	$\sigma_{\log N}^2$	f_N	f_{MS}
		(km s ⁻¹)	(km s ⁻¹)	(km s ⁻¹)	(km s ⁻¹)	[cm ⁻²]				
FBS0150+396	Si II	-210.0	-135.0	12.88	0.18	0.30	-1	0
FBS0150+396	Si III	-210.0	-135.0	-170.6	3.8	12.88	0.08	0.10	0	0
FBS0150+396	Si IV	-210.0	-135.0	12.69	0.18	0.30	-1	0
3C48.0	Al II	-535.0	-485.0	11.76	0.18	0.30	-1	0
3C48.0	C II	-535.0	-485.0	12.93	0.18	0.30	-1	0
3C48.0	Fe II	-535.0	-485.0	13.49	0.18	0.30	-1	0
3C48.0	N I	-535.0	-485.0	13.01	0.18	0.30	-1	0
3C48.0	N V	-535.0	-485.0	12.91	0.18	0.30	-1	0
3C48.0	O I	-535.0	-485.0	13.80	0.18	0.30	-1	0
3C48.0	S II	-535.0	-485.0	14.02	0.18	0.30	-1	0
3C48.0	Si II	-535.0	-485.0	11.94	0.18	0.30	-1	0
3C48.0	Si III	-535.0	-485.0	-507.6	3.9	12.22	0.11	0.15	0	0
3C48.0	Si IV	-535.0	-485.0	12.30	0.18	0.30	-1	0
3C48.0	Al II	-235.0	-140.0	12.01	0.18	0.30	-1	0
3C48.0	C IV	-235.0	-140.0	12.96	0.18	0.30	-1	0
3C48.0	Fe II	-235.0	-140.0	13.71	0.18	0.30	-1	0
3C48.0	N I	-235.0	-140.0	13.17	0.18	0.30	-1	0
3C48.0	N V	-235.0	-140.0	13.35	0.18	0.30	-1	0
3C48.0	O I	-235.0	-140.0	13.94	0.18	0.30	-1	0
3C48.0	S II	-235.0	-140.0	13.97	0.18	0.30	-1	0
3C48.0	Si II	-235.0	-140.0	-172.2	10.9	12.71	0.13	0.19	0	0
3C48.0	Si III	-235.0	-140.0	-183.7	2.2	12.66	0.10	0.10	0	0
4C25.01	Al II	-390.0	-335.0	11.98	0.18	0.30	-1	-1
4C25.01	C II	-390.0	-335.0	12.86	0.18	0.30	-1	-1
4C25.01	C IV	-390.0	-335.0	12.56	0.18	0.30	-1	-1
4C25.01	Fe II	-390.0	-335.0	13.37	0.18	0.30	-1	-1
4C25.01	N I	-390.0	-335.0	13.01	0.18	0.30	-1	-1
4C25.01	N V	-390.0	-335.0	12.87	0.18	0.30	-1	-1
4C25.01	S II	-390.0	-335.0	13.78	0.18	0.30	-1	-1
4C25.01	Si II	-390.0	-335.0	11.93	0.18	0.30	-1	-1
4C25.01	Si III	-390.0	-335.0	-367.4	6.1	12.06	0.14	0.20	0	-1
4C25.01	Si IV	-390.0	-335.0	12.37	0.18	0.30	-1	-1
4C25.01	Al II	-335.0	-280.0	11.99	0.18	0.30	-1	0
4C25.01	C II	-335.0	-280.0	-311.3	6.1	13.01	0.18	0.30	-1	0
4C25.01	C IV	-335.0	-280.0	12.56	0.18	0.30	-1	0
4C25.01	Fe II	-335.0	-280.0	13.47	0.18	0.30	-1	0
4C25.01	N I	-335.0	-280.0	13.01	0.18	0.30	-1	0
4C25.01	N V	-335.0	-280.0	12.86	0.18	0.30	-1	0
4C25.01	O I	-335.0	-280.0	13.29	0.18	0.30	-1	0
4C25.01	S II	-335.0	-280.0	13.78	0.18	0.30	-1	0
4C25.01	Si II	-335.0	-280.0	12.40	0.18	0.30	-1	0
4C25.01	Si III	-335.0	-280.0	-313.3	4.2	12.25	0.10	0.12	0	0
4C25.01	Si IV	-335.0	-280.0	-312.8	6.1	12.52	0.14	0.21	0	0
PG0052+251	Al II	-347.0	-230.0	-275.1	14.0	12.14	0.14	0.22	0	0
PG0052+251	C II	-347.0	-230.0	-291.4	2.3	13.86	0.03	0.03	0	0
PG0052+251	C IV	-347.0	-230.0	-285.6	3.8	13.41	0.05	0.05	0	0
PG0052+251	Fe II	-347.0	-230.0	13.49	0.18	0.30	-1	0
PG0052+251	N I	-347.0	-230.0	12.88	0.18	0.30	-1	0
PG0052+251	N V	-347.0	-230.0	12.83	0.18	0.30	-1	0
PG0052+251	O I	-347.0	-230.0	-263.1	17.2	13.45	0.15	0.22	0	0
PG0052+251	O VI	-347.0	-230.0	-278.5	5.7	14.31	0.06	0.07	-2	0
PG0052+251	S II	-347.0	-230.0	13.81	0.18	0.30	-1	0
PG0052+251	Si II	-347.0	-230.0	-282.6	2.3	13.06	0.03	0.03	0	0

Table 2 *continued*

Table 2 (*continued*)

Target	Ion	v_1	v_2	v	σ_v	$\log N$	$\sigma_{\log N}^1$	$\sigma_{\log N}^2$	f_N	f_{MS}
		(km s ⁻¹)	(km s ⁻¹)	(km s ⁻¹)	(km s ⁻¹)	[cm ⁻²]				
PG0052+251	Si III	-347.0	-230.0	-292.1	1.0	13.10	0.02	0.02	-2	0
PG0052+251	Si IV	-347.0	-230.0	-287.8	4.3	12.65	0.06	0.07	0	0
PG0052+251	Al II	-230.0	-150.0	11.93	0.18	0.30	-1	0
PG0052+251	C II	-230.0	-150.0	-178.3	6.1	13.22	0.09	0.12	0	0
PG0052+251	C IV	-230.0	-150.0	-191.4	2.0	13.47	0.04	0.04	0	0
PG0052+251	Fe II	-230.0	-150.0	13.41	0.18	0.30	-1	0
PG0052+251	N I	-230.0	-150.0	12.79	0.18	0.30	-1	0
PG0052+251	N V	-230.0	-150.0	12.74	0.18	0.30	-1	0
PG0052+251	O I	-230.0	-150.0	13.26	0.18	0.30	-1	0
PG0052+251	O VI	-230.0	-150.0	-201.4	3.9	14.23	0.06	0.08	-2	0
PG0052+251	S II	-230.0	-150.0	13.72	0.18	0.30	-1	0
PG0052+251	Si II	-230.0	-150.0	12.18	0.18	0.30	-1	0
PG0052+251	Si III	-230.0	-150.0	-191.2	2.6	12.43	0.05	0.05	0	0
PG0052+251	Si IV	-230.0	-150.0	-189.6	3.3	12.51	0.06	0.06	0	0
RXS_J0155.6+3115	Al II	-270.0	-140.0	12.40	0.18	0.30	-1	0
RXS_J0155.6+3115	C II	-270.0	-140.0	13.23	0.18	0.30	-1	0
RXS_J0155.6+3115	C IV	-270.0	-140.0	-210.0	3.5	13.92	0.05	0.05	0	0
RXS_J0155.6+3115	Fe II	-270.0	-140.0	13.93	0.18	0.30	-1	0
RXS_J0155.6+3115	N I	-270.0	-140.0	13.23	0.18	0.30	-1	0
RXS_J0155.6+3115	N V	-270.0	-140.0	13.16	0.18	0.30	-1	0
RXS_J0155.6+3115	O I	-270.0	-140.0	13.93	0.18	0.30	-1	0
RXS_J0155.6+3115	S II	-270.0	-140.0	14.13	0.18	0.30	-1	0
RXS_J0155.6+3115	Si II	-270.0	-140.0	12.59	0.18	0.30	-1	0
RXS_J0155.6+3115	Si III	-270.0	-140.0	-190.3	5.8	12.74	0.06	0.07	0	0
RXS_J0155.6+3115	Si IV	-270.0	-140.0	12.47	0.18	0.30	-1	0
RBS2055	Al II	-470.0	-385.0	11.97	0.18	0.30	-1	-1
RBS2055	C II	-470.0	-385.0	-408.0	5.6	13.42	0.08	0.09	0	-1
RBS2055	C IV	-470.0	-385.0	-430.3	5.3	13.19	0.09	0.12	0	-1
RBS2055	Fe II	-470.0	-385.0	-435.1	8.7	13.26	0.18	0.30	-1	-1
RBS2055	N I	-470.0	-385.0	12.99	0.18	0.30	-1	-1
RBS2055	N V	-470.0	-385.0	12.76	0.18	0.30	-1	-1
RBS2055	O I	-470.0	-385.0	13.26	0.18	0.30	-1	-1
RBS2055	S II	-470.0	-385.0	13.41	0.18	0.30	-1	-1
RBS2055	Si II	-470.0	-385.0	-404.6	3.5	12.26	0.05	0.05	0	-1
RBS2055	Si III	-470.0	-385.0	-422.7	1.0	13.13	0.02	0.02	-2	-1
RBS2055	Si IV	-470.0	-385.0	-429.4	4.0	12.83	0.07	0.08	0	-1
RBS2055	Al II	-380.0	-300.0	-329.9	6.0	12.32	0.10	0.13	0	0
RBS2055	C II	-380.0	-300.0	-330.6	1.2	14.04	0.03	0.03	-2	0
RBS2055	C IV	-380.0	-300.0	-335.1	1.7	13.68	0.03	0.04	0	0
RBS2055	Fe II	-380.0	-300.0	13.09	0.18	0.30	-1	0
RBS2055	N I	-380.0	-300.0	12.98	0.18	0.30	-1	0
RBS2055	N V	-380.0	-300.0	12.74	0.18	0.30	-1	0
RBS2055	O I	-380.0	-300.0	-330.7	6.0	13.60	0.10	0.12	0	0
RBS2055	S II	-385.0	-300.0	13.43	0.18	0.30	-1	0
RBS2055	Si II	-380.0	-300.0	-330.5	1.9	13.13	0.04	0.04	0	0
RBS2055	Si III	-380.0	-300.0	-333.2	0.8	13.31	0.02	0.02	-2	0
RBS2055	Si IV	-380.0	-300.0	-327.8	2.6	13.03	0.04	0.05	0	0
RBS2055	Al II	-300.0	-225.0	11.94	0.18	0.30	-1	0
RBS2055	C II	-300.0	-225.0	-269.4	5.9	13.26	0.10	0.13	0	0
RBS2055	C IV	-300.0	-225.0	13.10	0.18	0.30	-1	0
RBS2055	Fe II	-300.0	-225.0	13.06	0.18	0.30	-1	0
RBS2055	N I	-300.0	-225.0	12.97	0.18	0.30	-1	0
RBS2055	N V	-300.0	-225.0	12.74	0.18	0.30	-1	0

Table 2 continued

Table 2 (*continued*)

Target	Ion	v_1	v_2	v	σ_v	$\log N$	$\sigma_{\log N}^1$	$\sigma_{\log N}^2$	f_N	f_{MS}
		(km s ⁻¹)	(km s ⁻¹)	(km s ⁻¹)	(km s ⁻¹)	[cm ⁻²]				
RBS2055	O I	-300.0	-225.0	13.28	0.18	0.30	-1	0
RBS2055	S II	-300.0	-225.0	13.38	0.18	0.30	-1	0
RBS2055	Si II	-300.0	-225.0	12.33	0.18	0.30	-1	0
RBS2055	Si III	-300.0	-225.0	-278.6	2.8	12.58	0.05	0.05	0	0
RBS2055	Si IV	-300.0	-225.0	12.33	0.18	0.30	-1	0
3C66A	Al II	-295.0	-215.0	11.93	0.18	0.30	-1	0
3C66A	C II	-295.0	-215.0	12.86	0.18	0.30	-1	0
3C66A	C IV	-295.0	-215.0	12.79	0.18	0.30	-1	0
3C66A	Fe II	-295.0	-215.0	13.37	0.18	0.30	-1	0
3C66A	N I	-295.0	-215.0	12.92	0.18	0.30	-1	0
3C66A	N V	-295.0	-215.0	12.76	0.18	0.30	-1	0
3C66A	O I	-295.0	-215.0	-251.0	8.6	13.40	0.18	0.30	-1	0
3C66A	S II	-295.0	-215.0	-242.5	10.1	13.82	0.18	0.31	-1	0
3C66A	Si II	-295.0	-215.0	12.28	0.18	0.30	-1	0
3C66A	Si III	-295.0	-215.0	-257.3	3.5	11.94	0.14	0.15	0	0
3C66A	Si IV	-295.0	-215.0	12.51	0.18	0.30	-1	0
RX_J0053.7+2232	Al II	-370.0	-305.0	12.24	0.18	0.30	-1	-1
RX_J0053.7+2232	C II	-370.0	-305.0	-320.1	7.3	13.44	0.13	0.19	0	-1
RX_J0053.7+2232	C IV	-370.0	-305.0	13.04	0.18	0.30	-1	-1
RX_J0053.7+2232	Fe II	-370.0	-305.0	13.65	0.18	0.30	-1	-1
RX_J0053.7+2232	N I	-370.0	-305.0	13.11	0.18	0.30	-1	-1
RX_J0053.7+2232	N V	-370.0	-305.0	13.05	0.18	0.30	-1	-1
RX_J0053.7+2232	O I	-370.0	-305.0	13.77	0.18	0.30	-1	-1
RX_J0053.7+2232	S II	-370.0	-305.0	14.02	0.18	0.30	-1	-1
RX_J0053.7+2232	S III	-370.0	-305.0	13.78	0.18	0.30	-1	-1
RX_J0053.7+2232	Si II	-370.0	-305.0	-335.1	3.8	12.62	0.09	0.11	0	-1
RX_J0053.7+2232	Si III	-370.0	-305.0	-332.1	1.8	12.90	0.05	0.05	0	-1
RX_J0053.7+2232	Si IV	-370.0	-305.0	12.14	0.18	0.30	-1	-1
RX_J0053.7+2232	Al II	-305.0	-200.0	12.36	0.18	0.30	-1	0
RX_J0053.7+2232	C II	-305.0	-200.0	13.33	0.18	0.30	-1	0
RX_J0053.7+2232	C IV	-305.0	-200.0	13.14	0.18	0.30	-1	0
RX_J0053.7+2232	Fe II	-305.0	-200.0	13.76	0.18	0.30	-1	0
RX_J0053.7+2232	N I	-305.0	-200.0	13.23	0.18	0.30	-1	0
RX_J0053.7+2232	N V	-305.0	-200.0	13.16	0.18	0.30	-1	0
RX_J0053.7+2232	O I	-305.0	-200.0	13.88	0.18	0.30	-1	0
RX_J0053.7+2232	S II	-305.0	-200.0	14.15	0.18	0.30	-1	0
RX_J0053.7+2232	S III	-305.0	-200.0	13.89	0.18	0.30	-1	0
RX_J0053.7+2232	Si II	-305.0	-200.0	12.80	0.18	0.30	-1	0
RX_J0053.7+2232	Si III	-305.0	-200.0	-267.0	3.3	12.97	0.05	0.05	0	0
RX_J0053.7+2232	Si IV	-305.0	-200.0	12.26	0.18	0.30	-1	0
MRK335	Al II	-450.0	-372.0	11.69	0.18	0.30	-1	-1
MRK335	C II	-450.0	-372.0	-405.5	2.9	13.25	0.06	0.06	0	-1
MRK335	C IV	-450.0	-372.0	12.60	0.18	0.30	-1	-1
MRK335	Fe II	-450.0	-372.0	13.23	0.18	0.30	-1	-1
MRK335	N I	-450.0	-372.0	12.79	0.18	0.30	-1	-1
MRK335	N V	-450.0	-372.0	12.42	0.18	0.30	-1	-1
MRK335	O I	-450.0	-372.0	-416.3	8.7	13.31	0.14	0.22	0	-1
MRK335	O VI	-450.0	-372.0	12.84	0.18	0.30	-1	-1
MRK335	S II	-450.0	-372.0	13.42	0.18	0.30	-1	-1
MRK335	Si II	-450.0	-372.0	-412.2	1.9	12.32	0.04	0.04	0	-1
MRK335	Si III	-450.0	-372.0	-409.4	1.7	12.49	0.03	0.04	0	-1
MRK335	Si IV	-450.0	-372.0	-414.9	8.6	12.33	0.13	0.19	0	-1
MRK335	Al II	-372.0	-310.0	11.64	0.18	0.30	-1	-1

Table 2 continued

Table 2 (*continued*)

Target	Ion	v_1	v_2	v	σ_v	$\log N$	$\sigma_{\log N}^1$	$\sigma_{\log N}^2$	f_N	f_{MS}
		(km s ⁻¹)	(km s ⁻¹)	(km s ⁻¹)	(km s ⁻¹)	[cm ⁻²]				
MRK335	C II	-372.0	-310.0	-336.8	1.4	13.40	0.04	0.04	0	-1
MRK335	C IV	-372.0	-310.0	-331.6	3.5	13.00	0.07	0.08	0	-1
MRK335	Fe II	-372.0	-310.0	12.96	0.18	0.30	-1	-1
MRK335	N I	-372.0	-310.0	12.73	0.18	0.30	-1	-1
MRK335	N V	-372.0	-310.0	12.36	0.18	0.30	-1	-1
MRK335	O I	-372.0	-310.0	-337.0	3.9	13.51	0.08	0.10	0	-1
MRK335	O VI	-372.0	-310.0	-335.0	2.0	13.49	0.04	0.05	0	-1
MRK335	S II	-372.0	-310.0	13.37	0.18	0.30	-1	-1
MRK335	Si II	-372.0	-310.0	-339.9	1.3	12.32	0.03	0.03	0	-1
MRK335	Si III	-372.0	-310.0	-339.7	0.8	12.75	0.02	0.02	0	-1
MRK335	Si IV	-372.0	-310.0	-343.2	4.4	12.44	0.10	0.12	0	-1
MRK335	Al II	-310.0	-273.0	11.53	0.18	0.30	-1	0
MRK335	C II	-310.0	-273.0	12.53	0.18	0.30	-1	0
MRK335	C IV	-310.0	-273.0	-293.8	1.8	13.24	0.07	0.08	0	0
MRK335	Fe II	-310.0	-273.0	12.87	0.18	0.30	-1	0
MRK335	N I	-310.0	-273.0	12.64	0.18	0.30	-1	0
MRK335	N V	-310.0	-273.0	12.23	0.18	0.30	-1	0
MRK335	O I	-310.0	-273.0	13.01	0.18	0.30	-1	0
MRK335	O VI	-310.0	-273.0	-291.5	0.9	13.54	0.03	0.04	0	0
MRK335	S II	-310.0	-273.0	13.24	0.18	0.30	-1	0
MRK335	Si II	-310.0	-273.0	12.00	0.18	0.30	-1	0
MRK335	Si III	-310.0	-273.0	-297.3	0.8	12.41	0.04	0.04	0	0
MRK335	Si IV	-310.0	-273.0	-290.6	4.3	12.12	0.14	0.21	0	0
MRK335	Al II	-273.0	-190.0	11.71	0.18	0.30	-1	0
MRK335	C II	-273.0	-190.0	12.72	0.18	0.30	-1	0
MRK335	C IV	-273.0	-190.0	-234.2	2.1	13.38	0.03	0.04	0	0
MRK335	Fe II	-273.0	-190.0	13.04	0.18	0.30	-1	0
MRK335	N I	-273.0	-190.0	-231.0	10.3	12.88	0.15	0.24	-1	0
MRK335	N V	-273.0	-190.0	12.42	0.18	0.30	-1	0
MRK335	O I	-273.0	-190.0	13.20	0.18	0.30	-1	0
MRK335	O VI	-273.0	-190.0	-221.0	0.6	14.26	0.01	0.01	0	0
MRK335	Si II	-273.0	-190.0	12.18	0.18	0.30	-1	0
MRK335	Si III	-273.0	-190.0	-246.9	3.7	12.28	0.06	0.06	0	0
MRK335	Si IV	-273.0	-190.0	-242.4	5.8	12.51	0.09	0.11	0	0
MRK1148	Al II	-220.0	-180.0	11.64	0.18	0.30	-1	0
MRK1148	C II	-220.0	-180.0	-193.7	3.3	13.04	0.10	0.13	0	0
MRK1148	C IV	-220.0	-180.0	12.66	0.18	0.30	-1	0
MRK1148	Fe II	-220.0	-180.0	13.33	0.18	0.30	-1	0
MRK1148	N I	-220.0	-180.0	12.86	0.18	0.30	-1	0
MRK1148	N V	-220.0	-180.0	12.69	0.18	0.30	-1	0
MRK1148	O I	-220.0	-180.0	12.82	0.18	0.30	-1	0
MRK1148	S II	-220.0	-180.0	13.61	0.18	0.30	-1	0
MRK1148	Si II	-220.0	-180.0	12.20	0.18	0.30	-1	0
MRK1148	Si III	-220.0	-180.0	-197.9	3.1	12.04	0.11	0.14	0	0
MRK1148	Si IV	-220.0	-180.0	12.18	0.18	0.30	-1	0
RBS2005	Al II	-420.0	-375.0	12.01	0.18	0.30	-1	-1
RBS2005	C II	-420.0	-375.0	-402.1	3.3	13.26	0.10	0.13	0	-1
RBS2005	C IV	-420.0	-375.0	-402.5	5.0	12.97	0.14	0.21	0	-1
RBS2005	Fe II	-420.0	-375.0	13.53	0.18	0.30	-1	-1
RBS2005	N I	-420.0	-375.0	13.00	0.18	0.30	-1	-1
RBS2005	N V	-420.0	-375.0	12.89	0.18	0.30	-1	-1
RBS2005	O I	-420.0	-375.0	13.68	0.18	0.30	-1	-1
RBS2005	S II	-420.0	-375.0	13.83	0.18	0.30	-1	-1

Table 2 *continued*

Table 2 (*continued*)

Target	Ion	v_1	v_2	v	σ_v	$\log N$	$\sigma_{\log N}^1$	$\sigma_{\log N}^2$	f_N	f_{MS}
		(km s ⁻¹)	(km s ⁻¹)	(km s ⁻¹)	(km s ⁻¹)	[cm ⁻²]				
RBS2005	Si II	-420.0	-375.0	11.98	0.18	0.30	-1	-1
RBS2005	Si III	-420.0	-375.0	-396.3	1.2	12.84	0.04	0.04	0	-1
RBS2005	Si IV	-420.0	-375.0	-411.8	8.3	12.29	0.16	0.25	0	-1
RBS2005	Al II	-375.0	-310.0	12.09	0.18	0.30	-1	-1
RBS2005	C II	-375.0	-310.0	-353.9	7.5	13.19	0.13	0.18	0	-1
RBS2005	C IV	-375.0	-310.0	-339.2	6.2	13.12	0.12	0.16	0	-1
RBS2005	N I	-375.0	-310.0	13.08	0.18	0.30	-1	-1
RBS2005	N V	-375.0	-310.0	12.97	0.18	0.30	-1	-1
RBS2005	O I	-375.0	-310.0	13.74	0.18	0.30	-1	-1
RBS2005	S II	-375.0	-310.0	13.93	0.18	0.30	-1	-1
RBS2005	Si II	-375.0	-310.0	12.07	0.18	0.30	-1	-1
RBS2005	Si III	-375.0	-310.0	-350.2	2.0	12.81	0.04	0.05	0	-1
RBS2005	Si IV	-375.0	-310.0	12.29	0.18	0.30	-1	-1
RBS2005	Al II	-310.0	-220.0	12.19	0.18	0.30	-1	0
RBS2005	C II	-310.0	-220.0	13.05	0.18	0.30	-1	0
RBS2005	C IV	-310.0	-220.0	-263.2	11.9	13.05	0.16	0.24	0	0
RBS2005	Fe II	-310.0	-220.0	13.68	0.18	0.30	-1	0
RBS2005	N I	-310.0	-220.0	13.15	0.18	0.30	-1	0
RBS2005	N V	-310.0	-220.0	13.05	0.18	0.30	-1	0
RBS2005	O I	-310.0	-220.0	13.82	0.18	0.30	-1	0
RBS2005	S II	-310.0	-220.0	14.00	0.18	0.30	-1	0
RBS2005	Si II	-310.0	-220.0	12.51	0.18	0.30	-1	0
RBS2005	Si III	-310.0	-220.0	-266.9	5.4	12.50	0.08	0.10	0	0
RBS2005	Si IV	-310.0	-220.0	12.36	0.18	0.30	-1	0
RX_J0023.5+1547	C II	-420.0	-290.0	13.60	0.18	0.30	-1	-1
RX_J0023.5+1547	N I	-420.0	-290.0	-348.9	16.6	13.83	0.18	0.30	-1	-1
RX_J0023.5+1547	N V	-420.0	-290.0	13.88	0.18	0.30	-1	-1
RX_J0023.5+1547	Si III	-420.0	-290.0	-356.5	15.8	13.17	0.09	0.11	-2	-1
MRK1179	Al II	-325.0	-275.0	12.22	0.18	0.30	-1	0
MRK1179	C II	-325.0	-275.0	13.25	0.18	0.30	-1	0
MRK1179	C IV	-325.0	-275.0	13.00	0.18	0.30	-1	0
MRK1179	N I	-325.0	-275.0	13.48	0.18	0.30	-1	0
MRK1179	N V	-325.0	-275.0	12.94	0.18	0.30	-1	0
MRK1179	O I	-325.0	-275.0	13.61	0.18	0.30	-1	0
MRK1179	Si II	-325.0	-275.0	12.68	0.18	0.30	-1	0
MRK1179	Si III	-325.0	-275.0	12.23	0.18	0.30	-1	0
MRK1179	Si IV	-325.0	-275.0	12.60	0.18	0.30	-1	0
PG0003+158	Al II	-460.0	-368.0	11.84	0.18	0.30	-1	-1
PG0003+158	C II	-460.0	-368.0	-403.9	1.8	13.34	0.10	0.10	0	-1
PG0003+158	C IV	-460.0	-368.0	-401.7	2.1	13.56	0.03	0.03	0	-1
PG0003+158	Fe II	-460.0	-368.0	13.46	0.18	0.30	-1	-1
PG0003+158	N I	-460.0	-368.0	12.96	0.18	0.30	-1	-1
PG0003+158	N V	-460.0	-368.0	12.77	0.18	0.30	-1	-1
PG0003+158	O I	-460.0	-368.0	13.42	0.18	0.30	-1	-1
PG0003+158	S II	-460.0	-368.0	13.71	0.18	0.30	-1	-1
PG0003+158	Si II	-460.0	-368.0	-387.4	5.1	12.39	0.06	0.07	0	-1
PG0003+158	Si III	-460.0	-368.0	-404.9	1.5	12.89	0.03	0.03	0	-1
PG0003+158	Si IV	-460.0	-368.0	-403.6	5.3	12.71	0.07	0.09	0	-1
PG0003+158	Al II	-368.0	-275.0	-318.7	7.9	12.06	0.12	0.17	0	-1
PG0003+158	C II	-368.0	-275.0	-325.2	1.1	14.01	0.02	0.02	-2	-1
PG0003+158	C IV	-368.0	-275.0	-336.8	1.6	13.66	0.02	0.03	0	-1
PG0003+158	Fe II	-368.0	-275.0	13.46	0.18	0.30	-1	-1
PG0003+158	N I	-368.0	-275.0	12.95	0.18	0.30	-1	-1

Table 2 continued

Table 2 (*continued*)

Target	Ion	v_1	v_2	v	σ_v	$\log N$	$\sigma_{\log N}^1$	$\sigma_{\log N}^2$	f_N	f_{MS}
		(km s ⁻¹)	(km s ⁻¹)	(km s ⁻¹)	(km s ⁻¹)	[cm ⁻²]				
PG0003+158	O I	-368.0	-275.0	-324.0	2.8	14.16	0.05	0.05	0	-1
PG0003+158	S II	-368.0	-275.0	13.91	0.18	0.30	-1	-1
PG0003+158	Si II	-368.0	-275.0	-322.7	2.6	13.28	0.04	0.05	0	-1
PG0003+158	Si III	-368.0	-275.0	-331.7	1.0	13.11	0.02	0.02	-2	-1
PG0003+158	Si IV	-368.0	-275.0	-340.9	5.7	12.73	0.07	0.08	0	-1
PG0003+158	Al II	-275.0	-205.0	11.77	0.18	0.30	-1	0
PG0003+158	C II	-275.0	-205.0	-236.5	2.0	13.56	0.04	0.04	0	0
PG0003+158	C IV	-275.0	-205.0	-235.4	2.1	13.27	0.05	0.05	0	0
PG0003+158	N I	-275.0	-205.0	12.90	0.18	0.30	-1	0
PG0003+158	N V	-275.0	-205.0	12.72	0.18	0.30	-1	0
PG0003+158	O I	-275.0	-205.0	13.37	0.18	0.30	-1	0
PG0003+158	S II	-275.0	-205.0	13.65	0.18	0.30	-1	0
PG0003+158	Si II	-275.0	-205.0	12.26	0.18	0.30	-1	0
PG0003+158	Si III	-275.0	-205.0	-244.6	2.2	12.14	0.10	0.10	0	0
PG0003+158	Si IV	-275.0	-205.0	-233.1	8.1	12.30	0.15	0.22	0	0
UGC12163	Al II	-475.0	-375.0	12.25	0.18	0.30	-1	-1
UGC12163	C II	-475.0	-375.0	-425.2	5.0	14.05	0.10	0.13	0	-1
UGC12163	C IV	-475.0	-375.0	-424.5	5.8	13.52	0.08	0.11	0	-1
UGC12163	Fe II	-475.0	-375.0	13.89	0.18	0.30	-1	-1
UGC12163	Mg II	-475.0	-375.0	15.58	0.18	0.30	-1	-1
UGC12163	N I	-475.0	-375.0	13.41	0.18	0.30	-1	-1
UGC12163	N V	-475.0	-375.0	13.28	0.18	0.30	-1	-1
UGC12163	O I	-475.0	-375.0	14.08	0.18	0.30	-1	-1
UGC12163	O VI	-475.0	-375.0	13.57	0.18	0.30	-1	-1
UGC12163	P II	-475.0	-375.0	14.48	0.18	0.30	-1	-1
UGC12163	S II	-475.0	-375.0	14.09	0.18	0.30	-1	-1
UGC12163	S III	-475.0	-375.0	14.17	0.18	0.30	-1	-1
UGC12163	Si II	-475.0	-375.0	-414.7	9.1	12.47	0.12	0.17	0	-1
UGC12163	Si III	-475.0	-375.0	-425.5	21.4	13.45	0.06	0.07	-2	-1
UGC12163	Si IV	-475.0	-375.0	-426.0	6.2	13.15	0.09	0.12	0	-1
UGC12163	Al II	-375.0	-310.0	12.14	0.18	0.30	-1	0
UGC12163	C II	-375.0	-310.0	-353.0	7.3	13.35	0.13	0.20	0	0
UGC12163	C IV	-375.0	-310.0	13.01	0.18	0.30	-1	0
UGC12163	Fe II	-375.0	-310.0	13.77	0.18	0.30	-1	0
UGC12163	N I	-375.0	-310.0	13.32	0.18	0.30	-1	0
UGC12163	N V	-375.0	-310.0	12.99	0.18	0.30	-1	0
UGC12163	O I	-375.0	-310.0	13.95	0.18	0.30	-1	0
UGC12163	O VI	-375.0	-310.0	13.46	0.18	0.30	-1	0
UGC12163	S II	-375.0	-310.0	14.01	0.18	0.30	-1	0
UGC12163	Si II	-375.0	-310.0	12.17	0.18	0.30	-1	0
UGC12163	Si III	-375.0	-310.0	-349.8	6.2	12.43	0.13	0.18	0	0
UGC12163	Si IV	-375.0	-310.0	12.61	0.18	0.30	-1	0
UGC12163	Al II	-310.0	-220.0	12.23	0.18	0.30	-1	0
UGC12163	C II	-310.0	-220.0	13.23	0.18	0.30	-1	0
UGC12163	C IV	-310.0	-220.0	13.10	0.18	0.30	-1	0
UGC12163	Fe II	-310.0	-220.0	13.84	0.18	0.30	-1	0
UGC12163	N I	-310.0	-220.0	13.36	0.18	0.30	-1	0
UGC12163	N V	-310.0	-220.0	13.07	0.18	0.30	-1	0
UGC12163	O I	-310.0	-220.0	13.74	0.18	0.30	-1	0
UGC12163	O VI	-310.0	-220.0	-259.1	19.9	14.46	0.04	0.04	0	0
UGC12163	P II	-310.0	-220.0	14.40	0.18	0.30	-1	0
UGC12163	S II	-310.0	-220.0	14.07	0.18	0.30	-1	0
UGC12163	S III	-310.0	-220.0	14.14	0.18	0.30	-1	0

Table 2 continued

Table 2 (*continued*)

Target	Ion	v_1	v_2	v	σ_v	$\log N$	$\sigma_{\log N}^1$	$\sigma_{\log N}^2$	f_N	f_{MS}
		(km s ⁻¹)	(km s ⁻¹)	(km s ⁻¹)	(km s ⁻¹)	[cm ⁻²]				
UGC12163	Si II	-310.0	-220.0	12.75	0.18	0.30	-1	0
UGC12163	Si III	-310.0	-220.0	12.29	0.18	0.30	-1	0
UGC12163	Si IV	-310.0	-220.0	12.70	0.18	0.30	-1	0
UGC12163	Al II	-220.0	-180.0	12.01	0.18	0.30	-1	0
UGC12163	C II	-220.0	-180.0	-203.8	3.3	13.75	0.09	0.12	-2	0
UGC12163	C IV	-220.0	-180.0	12.93	0.18	0.30	-1	0
UGC12163	Fe II	-220.0	-180.0	13.68	0.18	0.30	-1	0
UGC12163	N I	-220.0	-180.0	13.20	0.18	0.30	-1	0
UGC12163	N V	-220.0	-180.0	12.87	0.18	0.30	-1	0
UGC12163	O I	-220.0	-180.0	-207.5	2.5	14.21	0.19	0.34	0	0
UGC12163	O VI	-220.0	-180.0	13.33	0.18	0.30	-1	0
UGC12163	P II	-220.0	-180.0	14.16	0.18	0.30	-1	0
UGC12163	S II	-220.0	-180.0	-203.4	3.3	14.24	0.10	0.13	0	0
UGC12163	S III	-220.0	-180.0	13.98	0.18	0.30	-1	0
UGC12163	Si II	-220.0	-180.0	12.55	0.18	0.30	-1	0
UGC12163	Si III	-220.0	-180.0	12.10	0.18	0.30	-1	0
UGC12163	Si IV	-220.0	-180.0	12.53	0.18	0.30	-1	0
SDSSJ011623.06+142940.6	Al II	-340.0	-240.0	12.15	0.18	0.30	-1	-1
SDSSJ011623.06+142940.6	C II	-340.0	-240.0	13.46	0.18	0.30	-1	-1
SDSSJ011623.06+142940.6	C IV	-340.0	-240.0	13.13	0.18	0.30	-1	-1
SDSSJ011623.06+142940.6	Fe II	-340.0	-240.0	13.78	0.18	0.30	-1	-1
SDSSJ011623.06+142940.6	N I	-340.0	-240.0	13.50	0.18	0.30	-1	-1
SDSSJ011623.06+142940.6	N V	-340.0	-240.0	13.37	0.18	0.30	-1	-1
SDSSJ011623.06+142940.6	S II	-340.0	-240.0	14.31	0.18	0.30	-1	-1
SDSSJ011623.06+142940.6	Si II	-340.0	-240.0	12.89	0.18	0.30	-1	-1
SDSSJ011623.06+142940.6	Si III	-340.0	-240.0	-288.6	6.1	12.97	0.11	0.14	0	-1
SDSSJ011623.06+142940.6	Si IV	-340.0	-240.0	12.67	0.18	0.30	-1	-1
PG0026+129	C II	-330.0	-260.0	-294.5	5.0	13.39	0.10	0.13	0	-1
PG0026+129	Fe II	-330.0	-260.0	13.52	0.18	0.30	-1	-1
PG0026+129	N I	-330.0	-260.0	13.03	0.18	0.30	-1	-1
PG0026+129	N V	-330.0	-260.0	12.97	0.18	0.30	-1	-1
PG0026+129	O I	-330.0	-260.0	13.60	0.18	0.30	-1	-1
PG0026+129	O VI	-330.0	-260.0	13.85	0.18	0.30	-1	-1
PG0026+129	S II	-330.0	-260.0	13.87	0.18	0.30	-1	-1
PG0026+129	Si II	-330.0	-260.0	12.01	0.18	0.30	-1	-1
PG0026+129	Si III	-330.0	-260.0	-286.2	2.0	12.75	0.04	0.05	0	-1
PG0026+129	Si IV	-330.0	-260.0	-291.7	3.1	12.45	0.07	0.08	0	-1
PG0026+129	C II	-260.0	-210.0	-247.1	6.0	13.20	0.12	0.17	0	0
PG0026+129	Fe II	-260.0	-210.0	13.46	0.18	0.30	-1	0
PG0026+129	N I	-260.0	-210.0	12.95	0.18	0.30	-1	0
PG0026+129	N V	-260.0	-210.0	12.89	0.18	0.30	-1	0
PG0026+129	O I	-260.0	-210.0	13.51	0.18	0.30	-1	0
PG0026+129	O VI	-260.0	-210.0	-232.9	54.2	14.12	0.16	0.26	0	0
PG0026+129	S II	-260.0	-210.0	13.80	0.18	0.30	-1	0
PG0026+129	Si II	-260.0	-210.0	12.29	0.18	0.30	-1	0
PG0026+129	Si III	-260.0	-210.0	-236.3	1.6	12.64	0.05	0.05	0	0
PG0026+129	Si IV	-260.0	-210.0	11.88	0.18	0.30	-1	0
PG0026+129	C II	-210.0	-155.0	13.00	0.18	0.30	-1	0
PG0026+129	Fe II	-210.0	-155.0	13.49	0.18	0.30	-1	0
PG0026+129	N I	-210.0	-155.0	12.97	0.18	0.30	-1	0
PG0026+129	N V	-210.0	-155.0	12.92	0.18	0.30	-1	0
PG0026+129	O I	-210.0	-155.0	13.52	0.18	0.30	-1	0
PG0026+129	O VI	-210.0	-155.0	13.80	0.18	0.30	-1	0

Table 2 continued

Table 2 (*continued*)

Target	Ion	v_1	v_2	v	σ_v	$\log N$	$\sigma_{\log N}^1$	$\sigma_{\log N}^2$	f_N	f_{MS}
		(km s ⁻¹)	(km s ⁻¹)	(km s ⁻¹)	(km s ⁻¹)	[cm ⁻²]				
PG0026+129	S II	-210.0	-155.0	13.81	0.18	0.30	-1	0
PG0026+129	Si II	-210.0	-155.0	12.32	0.18	0.30	-1	0
PG0026+129	Si III	-210.0	-155.0	-184.8	2.8	12.40	0.08	0.09	0	0
PG0026+129	Si IV	-210.0	-155.0	11.91	0.18	0.30	-1	0
MRK1502	Al II	-250.0	-130.0	11.85	0.18	0.30	-1	0
MRK1502	C II	-250.0	-130.0	-229.6	16.3	13.06	0.12	0.17	0	0
MRK1502	C IV	-250.0	-130.0	-187.0	2.2	13.61	0.03	0.03	0	0
MRK1502	Fe II	-250.0	-130.0	13.30	0.18	0.30	-1	0
MRK1502	N I	-250.0	-130.0	13.32	0.18	0.30	-1	0
MRK1502	N V	-250.0	-130.0	12.88	0.18	0.30	-1	0
MRK1502	O I	-250.0	-130.0	13.33	0.18	0.30	-1	0
MRK1502	O VI	-250.0	-130.0	-197.8	21.4	14.59	0.03	0.04	-2	0
MRK1502	S II	-250.0	-130.0	13.72	0.18	0.30	-1	0
MRK1502	Si II	-250.0	-130.0	12.61	0.18	0.30	-1	0
MRK1502	Si III	-250.0	-130.0	-200.0	6.2	12.46	0.07	0.08	0	0
MRK1502	Si IV	-250.0	-130.0	-204.3	14.0	12.50	0.14	0.21	0	0
SDSSJ014143.20+134032.0	C II	-330.0	-280.0	13.54	0.18	0.30	-1	0
SDSSJ014143.20+134032.0	Fe II	-330.0	-280.0	14.10	0.18	0.30	-1	0
SDSSJ014143.20+134032.0	N I	-330.0	-280.0	13.64	0.18	0.30	-1	0
SDSSJ014143.20+134032.0	N V	-330.0	-280.0	13.47	0.18	0.30	-1	0
SDSSJ014143.20+134032.0	O I	-330.0	-280.0	13.95	0.18	0.30	-1	0
SDSSJ014143.20+134032.0	S II	-330.0	-280.0	14.39	0.18	0.30	-1	0
SDSSJ014143.20+134032.0	Si II	-330.0	-280.0	12.51	0.18	0.30	-1	0
SDSSJ014143.20+134032.0	Si III	-330.0	-280.0	12.59	0.18	0.30	-1	0
SDSSJ014143.20+134032.0	Si IV	-330.0	-280.0	12.94	0.18	0.30	-1	0
MRK1501	C II	-405.0	-300.0	-346.9	2.0	14.21	0.04	0.04	-2	-1
MRK1501	N I	-405.0	-300.0	13.93	0.18	0.30	-1	-1
MRK1501	N V	-405.0	-300.0	13.78	0.18	0.30	-1	-1
MRK1501	O I	-405.0	-300.0	14.10	0.18	0.30	-1	-1
MRK1501	S II	-405.0	-300.0	14.69	0.18	0.30	-1	-1
MRK1501	Si II	-405.0	-300.0	-343.0	14.1	13.49	0.09	0.12	-2	-1
MRK1501	Si III	-405.0	-300.0	-351.9	59.2	13.46	0.12	0.16	-2	-1
MRK1501	Si IV	-405.0	-300.0	13.15	0.18	0.30	-1	-1
IRAS01477+1254	Al II	-325.0	-275.0	12.56	0.18	0.30	-1	0
IRAS01477+1254	C II	-325.0	-275.0	13.66	0.18	0.30	-1	0
IRAS01477+1254	C IV	-325.0	-275.0	13.33	0.18	0.30	-1	0
IRAS01477+1254	N I	-325.0	-275.0	13.61	0.18	0.30	-1	0
IRAS01477+1254	N V	-325.0	-275.0	13.48	0.18	0.30	-1	0
IRAS01477+1254	O I	-325.0	-275.0	14.26	0.18	0.30	-1	0
IRAS01477+1254	S II	-325.0	-275.0	14.41	0.18	0.30	-1	0
IRAS01477+1254	Si II	-325.0	-275.0	12.52	0.18	0.30	-1	0
IRAS01477+1254	Si III	-325.0	-275.0	12.56	0.18	0.30	-1	0
IRAS01477+1254	Si IV	-325.0	-275.0	13.19	0.18	0.30	-1	0
SDSSJ015952.95+134554.3	C II	-330.0	-280.0	13.19	0.18	0.30	-1	0
SDSSJ015952.95+134554.3	N I	-330.0	-280.0	13.19	0.18	0.30	-1	0
SDSSJ015952.95+134554.3	N V	-330.0	-280.0	13.07	0.18	0.30	-1	0
SDSSJ015952.95+134554.3	O I	-330.0	-280.0	13.83	0.18	0.30	-1	0
SDSSJ015952.95+134554.3	S II	-330.0	-280.0	13.99	0.18	0.30	-1	0
SDSSJ015952.95+134554.3	Si II	-330.0	-280.0	12.15	0.18	0.30	-1	0
SDSSJ015952.95+134554.3	Si III	-330.0	-280.0	12.16	0.18	0.30	-1	0
SDSSJ015952.95+134554.3	Si IV	-330.0	-280.0	12.53	0.18	0.30	-1	0
3C454.3	Al II	-445.0	-260.0	-357.9	13.2	12.71	0.10	0.13	0	-1
3C454.3	C II	-445.0	-260.0	-363.1	6.1	14.65	0.03	0.03	-2	-1

Table 2 *continued*

Table 2 (*continued*)

Target	Ion	v_1	v_2	v	σ_v	$\log N$	$\sigma_{\log N}^1$	$\sigma_{\log N}^2$	f_N	f_{MS}
		(km s ⁻¹)	(km s ⁻¹)	(km s ⁻¹)	(km s ⁻¹)	[cm ⁻²]				
3C454.3	C IV	-430.0	-260.0	-339.0	4.0	14.05	0.04	0.04	0	-1
3C454.3	N I	-445.0	-260.0	14.30	0.18	0.30	-1	-1
3C454.3	N V	-445.0	-260.0	13.55	0.18	0.30	-1	-1
3C454.3	S II	-445.0	-260.0	14.51	0.18	0.30	-1	-1
3C454.3	Si II	-445.0	-260.0	-366.8	7.2	13.77	0.06	0.07	0	-1
3C454.3	Si III	-445.0	-230.0	-340.1	45.3	13.88	0.03	0.03	-2	-1
3C454.3	Si IV	-445.0	-260.0	-334.3	11.9	13.73	0.09	0.12	0	-1
SDSSJ225738.20+134045.0	Al II	-450.0	-298.0	12.41	0.18	0.30	-1	-1
SDSSJ225738.20+134045.0	C II	-450.0	-298.0	-351.6	4.3	14.42	0.06	0.07	0	-1
SDSSJ225738.20+134045.0	C IV	-450.0	-298.0	-361.5	4.3	14.16	0.05	0.06	0	-1
SDSSJ225738.20+134045.0	Fe II	-450.0	-298.0	14.04	0.18	0.30	-1	-1
SDSSJ225738.20+134045.0	N I	-450.0	-298.0	13.65	0.18	0.30	-1	-1
SDSSJ225738.20+134045.0	N V	-450.0	-298.0	13.42	0.18	0.30	-1	-1
SDSSJ225738.20+134045.0	O I	-450.0	-298.0	14.13	0.18	0.30	-1	-1
SDSSJ225738.20+134045.0	S II	-450.0	-298.0	14.39	0.18	0.30	-1	-1
SDSSJ225738.20+134045.0	Si II	-450.0	-298.0	-360.2	3.8	13.39	0.05	0.05	0	-1
SDSSJ225738.20+134045.0	Si III	-450.0	-298.0	-359.6	7.3	13.71	0.02	0.02	-2	-1
SDSSJ225738.20+134045.0	Si IV	-450.0	-298.0	-349.1	5.5	13.66	0.06	0.07	0	-1
PG0044+030	C II	-350.0	-265.0	-300.1	3.7	13.91	0.07	0.08	0	-1
PG0044+030	N I	-350.0	-265.0	13.47	0.18	0.30	-1	-1
PG0044+030	N V	-350.0	-265.0	13.51	0.18	0.30	-1	-1
PG0044+030	O I	-350.0	-265.0	-287.3	12.0	13.83	0.15	0.23	0	-1
PG0044+030	S II	-350.0	-265.0	14.16	0.18	0.30	-1	-1
PG0044+030	Si II	-350.0	-265.0	-291.9	3.0	13.03	0.06	0.06	0	-1
PG0044+030	Si III	-350.0	-265.0	-303.5	3.4	13.18	0.07	0.08	-2	-1
PG0044+030	Si IV	-350.0	-265.0	12.68	0.18	0.30	-1	-1
PG0044+030	C II	-255.0	-175.0	-218.5	4.2	13.80	0.08	0.10	0	0
PG0044+030	N I	-255.0	-175.0	13.46	0.18	0.30	-1	0
PG0044+030	N V	-255.0	-175.0	13.51	0.18	0.30	-1	0
PG0044+030	O I	-255.0	-175.0	13.68	0.18	0.30	-1	0
PG0044+030	S II	-255.0	-175.0	14.16	0.18	0.30	-1	0
PG0044+030	Si II	-255.0	-175.0	12.81	0.18	0.30	-1	0
PG0044+030	Si III	-255.0	-175.0	-221.1	5.4	12.84	0.10	0.13	0	0
PG0044+030	Si IV	-255.0	-175.0	12.66	0.18	0.30	-1	0
NGC7469	Al II	-400.0	-268.0	-334.2	4.1	12.45	0.05	0.05	0	-1
NGC7469	C II	-400.0	-268.0	-337.6	0.8	14.44	0.01	0.01	-2	-1
NGC7469	C IV	-400.0	-268.0	-329.4	0.8	13.92	0.01	0.01	0	-1
NGC7469	Fe II	-400.0	-268.0	13.46	0.18	0.30	-1	-1
NGC7469	N I	-400.0	-268.0	12.84	0.18	0.30	-1	-1
NGC7469	N V	-400.0	-268.0	12.40	0.18	0.30	-1	-1
NGC7469	O I	-400.0	-268.0	-341.2	1.6	14.35	0.02	0.02	0	-1
NGC7469	O VI	-400.0	-268.0	-312.4	4.7	13.95	0.05	0.06	0	-1
NGC7469	S II	-400.0	-268.0	13.58	0.18	0.30	-1	-1
NGC7469	Si II	-400.0	-268.0	-342.7	2.1	13.50	0.03	0.03	0	-1
NGC7469	Si III	-400.0	-268.0	-332.7	5.9	13.76	0.01	0.01	-2	-1
NGC7469	Si IV	-400.0	-268.0	-326.2	1.0	13.36	0.01	0.01	0	-1
NGC7469	Al II	-268.0	-210.0	-244.2	4.2	11.71	0.11	0.14	0	0
NGC7469	C II	-268.0	-210.0	-251.2	2.5	13.08	0.05	0.06	0	0
NGC7469	C IV	-268.0	-210.0	-243.6	1.0	13.23	0.02	0.03	0	0
NGC7469	Fe II	-268.0	-210.0	13.29	0.18	0.30	-1	0
NGC7469	N I	-268.0	-210.0	12.65	0.18	0.30	-1	0
NGC7469	N V	-268.0	-210.0	12.21	0.18	0.30	-1	0
NGC7469	O I	-268.0	-210.0	13.10	0.18	0.30	-1	0

Table 2 *continued*

Table 2 (*continued*)

Target	Ion	v_1	v_2	v	σ_v	$\log N$	$\sigma_{\log N}^1$	$\sigma_{\log N}^2$	f_N	f_{MS}
		(km s ⁻¹)	(km s ⁻¹)	(km s ⁻¹)	(km s ⁻¹)	[cm ⁻²]				
NGC7469	S II	-268.0	-210.0	13.36	0.18	0.30	-1	0
NGC7469	Si II	-268.0	-210.0	12.03	0.18	0.30	-1	0
NGC7469	Si III	-268.0	-210.0	-247.6	0.8	12.63	0.02	0.02	0	0
NGC7469	Si IV	-268.0	-210.0	-243.1	1.5	12.75	0.04	0.04	0	0
NGC7469	Al II	-202.0	-150.0	11.55	0.18	0.30	-1	0
NGC7469	C II	-202.0	-150.0	-176.2	3.4	12.94	0.09	0.11	0	0
NGC7469	C IV	-202.0	-150.0	-181.8	0.4	13.59	0.02	0.02	0	0
NGC7469	Fe II	-202.0	-150.0	13.26	0.18	0.30	-1	0
NGC7469	N I	-202.0	-150.0	12.63	0.18	0.30	-1	0
NGC7469	O I	-202.0	-150.0	13.06	0.18	0.30	-1	0
NGC7469	O VI	-202.0	-150.0	-179.2	0.9	13.98	0.03	0.03	0	0
NGC7469	S II	-202.0	-150.0	13.79	0.18	0.30	-1	0
NGC7469	Si II	-202.0	-150.0	12.01	0.18	0.30	-1	0
NGC7469	Si III	-202.0	-150.0	-176.6	0.9	12.40	0.03	0.03	0	0
NGC7469	Si IV	-202.0	-150.0	-182.2	1.0	12.72	0.03	0.03	0	0
PHL1226	C II	-290.0	-250.0	13.08	0.18	0.30	-1	0
PHL1226	N V	-290.0	-250.0	13.24	0.18	0.30	-1	0
PHL1226	S II	-290.0	-250.0	13.88	0.18	0.30	-1	0
PHL1226	Si II	-290.0	-250.0	12.02	0.18	0.30	-1	0
PHL1226	Si III	-290.0	-250.0	12.07	0.18	0.30	-1	0
PHL1226	Si IV	-290.0	-250.0	12.73	0.18	0.30	-1	0
UM228	Al II	-300.0	-250.0	12.40	0.18	0.30	-1	0
UM228	C II	-300.0	-250.0	13.25	0.18	0.30	-1	0
UM228	C IV	-300.0	-250.0	13.13	0.18	0.30	-1	0
UM228	N I	-300.0	-250.0	13.45	0.18	0.30	-1	0
UM228	N V	-300.0	-250.0	13.33	0.18	0.30	-1	0
UM228	S II	-300.0	-250.0	14.28	0.18	0.30	-1	0
UM228	S III	-300.0	-250.0	14.24	0.18	0.30	-1	0
UM228	Si II	-300.0	-250.0	12.42	0.18	0.30	-1	0
UM228	Si III	-300.0	-250.0	12.40	0.18	0.30	-1	0
UM228	Si IV	-300.0	-250.0	12.82	0.18	0.30	-1	0
MRK304	Al II	-408.0	-255.0	11.93	0.18	0.30	-1	-1
MRK304	C II	-408.0	-255.0	-357.4	5.2	13.57	0.04	0.05	0	-1
MRK304	C IV	-408.0	-255.0	-325.5	2.7	13.83	0.03	0.03	0	-1
MRK304	Fe II	-408.0	-255.0	13.45	0.18	0.30	-1	-1
MRK304	N I	-408.0	-255.0	13.08	0.18	0.30	-1	-1
MRK304	N V	-408.0	-255.0	12.91	0.18	0.30	-1	-1
MRK304	O I	-408.0	-255.0	13.45	0.18	0.30	-1	-1
MRK304	O VI	-408.0	-255.0	-318.8	8.6	14.54	0.05	0.06	-2	-1
MRK304	S II	-408.0	-255.0	13.77	0.18	0.30	-1	-1
MRK304	Si II	-408.0	-255.0	12.43	0.18	0.30	-1	-1
MRK304	Si III	-408.0	-255.0	-342.4	1.3	13.30	0.02	0.02	-2	-1
MRK304	Si IV	-408.0	-255.0	-345.1	4.8	12.99	0.04	0.05	0	-1
MRK595	C II	-330.0	-280.0	13.08	0.18	0.30	-1	0
MRK595	Fe II	-330.0	-280.0	13.65	0.18	0.30	-1	0
MRK595	N I	-330.0	-280.0	13.18	0.18	0.30	-1	0
MRK595	N V	-330.0	-280.0	12.73	0.18	0.30	-1	0
MRK595	O I	-330.0	-280.0	13.59	0.18	0.30	-1	0
MRK595	S II	-330.0	-280.0	13.65	0.18	0.30	-1	0
MRK595	Si II	-330.0	-280.0	12.58	0.18	0.30	-1	0
MRK595	Si III	-330.0	-280.0	12.09	0.18	0.30	-1	0
MRK595	Si IV	-330.0	-280.0	12.48	0.18	0.30	-1	0
PG2349-014	C II	-380.0	-320.0	-336.6	1.8	13.74	0.04	0.04	0	-1

Table 2 continued

Table 2 (*continued*)

Target	Ion	v_1	v_2	v	σ_v	$\log N$	$\sigma_{\log N}^1$	$\sigma_{\log N}^2$	f_N	f_{MS}
		(km s ⁻¹)	(km s ⁻¹)	(km s ⁻¹)	(km s ⁻¹)	[cm ⁻²]				
PG2349-014	Fe II	-380.0	-320.0	13.56	0.18	0.30	-1	-1
PG2349-014	N I	-380.0	-320.0	12.90	0.18	0.30	-1	-1
PG2349-014	N V	-380.0	-320.0	12.80	0.18	0.30	-1	-1
PG2349-014	O I	-380.0	-320.0	13.44	0.18	0.30	-1	-1
PG2349-014	O VI	-380.0	-320.0	-344.6	7.6	13.87	0.12	0.18	-2	-1
PG2349-014	S II	-380.0	-320.0	13.71	0.18	0.30	-1	-1
PG2349-014	Si II	-380.0	-320.0	-342.4	1.0	12.85	0.02	0.03	0	-1
PG2349-014	Si III	-380.0	-320.0	-338.7	0.6	13.07	0.02	0.02	-2	-1
PG2349-014	Si IV	-380.0	-320.0	-344.2	1.8	12.86	0.05	0.05	0	-1
PG2349-014	C II	-320.0	-280.0	-298.1	0.6	14.09	0.03	0.03	-2	-1
PG2349-014	Fe II	-320.0	-280.0	13.45	0.18	0.30	-1	-1
PG2349-014	N I	-320.0	-280.0	12.81	0.18	0.30	-1	-1
PG2349-014	N V	-320.0	-280.0	12.71	0.18	0.30	-1	-1
PG2349-014	O I	-320.0	-280.0	-302.0	2.2	13.85	0.08	0.09	0	-1
PG2349-014	O VI	-320.0	-280.0	-304.2	8.2	13.93	0.18	0.31	0	-1
PG2349-014	S II	-320.0	-280.0	13.61	0.18	0.30	-1	-1
PG2349-014	Si II	-320.0	-280.0	-295.7	1.0	13.36	0.04	0.04	-2	-1
PG2349-014	Si III	-320.0	-280.0	-300.1	0.6	13.33	0.03	0.03	-2	-1
PG2349-014	Si IV	-320.0	-280.0	-298.7	0.6	13.16	0.02	0.02	0	-1
PG2349-014	C II	-280.0	-250.0	-265.7	0.7	13.68	0.04	0.04	-2	-1
PG2349-014	Fe II	-280.0	-250.0	13.41	0.18	0.30	-1	-1
PG2349-014	N I	-280.0	-250.0	12.76	0.18	0.30	-1	-1
PG2349-014	N V	-280.0	-250.0	12.64	0.18	0.30	-1	-1
PG2349-014	O I	-280.0	-250.0	13.27	0.18	0.30	-1	-1
PG2349-014	O VI	-280.0	-250.0	-265.2	3.7	13.82	0.09	0.11	-2	-1
PG2349-014	S II	-280.0	-250.0	13.55	0.18	0.30	-1	-1
PG2349-014	Si II	-280.0	-250.0	-269.7	1.5	12.95	0.07	0.08	0	-1
PG2349-014	Si III	-280.0	-250.0	-265.1	0.4	13.12	0.02	0.02	-2	-1
PG2349-014	Si IV	-280.0	-250.0	-267.8	0.8	12.84	0.04	0.04	0	-1
PG2349-014	C II	-250.0	-190.0	-225.5	2.9	13.44	0.06	0.07	0	-1
PG2349-014	Fe II	-250.0	-190.0	13.55	0.18	0.30	-1	-1
PG2349-014	N I	-250.0	-190.0	12.90	0.18	0.30	-1	-1
PG2349-014	N V	-250.0	-190.0	12.79	0.18	0.30	-1	-1
PG2349-014	O I	-250.0	-190.0	13.44	0.18	0.30	-1	-1
PG2349-014	O VI	-250.0	-190.0	-223.9	5.4	14.39	0.04	0.04	-2	-1
PG2349-014	S II	-250.0	-190.0	13.71	0.18	0.30	-1	-1
PG2349-014	Si II	-250.0	-190.0	-222.6	6.3	12.42	0.13	0.18	0	-1
PG2349-014	Si III	-250.0	-190.0	-226.0	0.7	13.07	0.02	0.02	-2	-1
PG2349-014	Si IV	-250.0	-190.0	-227.4	2.4	12.76	0.05	0.06	0	-1
PG2349-014	C II	-190.0	-145.0	-173.0	2.6	13.28	0.08	0.10	0	0
PG2349-014	Fe II	-190.0	-145.0	13.50	0.18	0.30	-1	0
PG2349-014	N I	-190.0	-145.0	12.86	0.18	0.30	-1	0
PG2349-014	N V	-190.0	-145.0	12.74	0.18	0.30	-1	0
PG2349-014	O I	-190.0	-145.0	13.37	0.18	0.30	-1	0
PG2349-014	O VI	-190.0	-145.0	-166.2	9.8	13.92	0.17	0.29	0	0
PG2349-014	Si II	-190.0	-145.0	12.17	0.18	0.30	-1	0
PG2349-014	Si III	-190.0	-145.0	-169.8	1.1	12.52	0.04	0.04	0	0
PG2349-014	Si IV	-190.0	-145.0	12.13	0.18	0.30	-1	0
MRK1014	C II	-325.0	-275.0	12.92	0.18	0.30	-1	0
MRK1014	N I	-325.0	-275.0	12.92	0.18	0.30	-1	0
MRK1014	N V	-325.0	-275.0	12.87	0.18	0.30	-1	0
MRK1014	O I	-325.0	-275.0	13.46	0.18	0.30	-1	0
MRK1014	S II	-325.0	-275.0	13.77	0.18	0.30	-1	0

Table 2 continued

Table 2 (*continued*)

Target	Ion	v_1	v_2	v	σ_v	$\log N$	$\sigma_{\log N}^1$	$\sigma_{\log N}^2$	f_N	f_{MS}
		(km s ⁻¹)	(km s ⁻¹)	(km s ⁻¹)	(km s ⁻¹)	[cm ⁻²]				
MRK1014	Si II	-325.0	-275.0	11.91	0.18	0.30	-1	0
MRK1014	Si III	-325.0	-275.0	11.76	0.18	0.30	-1	0
MRK1014	Si IV	-325.0	-275.0	12.20	0.18	0.30	-1	0

NOTE—The velocities v_1 and v_2 correspond to the integration of the absorption component. The 1σ errors $\sigma_{\log N}^1$ and $\sigma_{\log N}^2$ are the positive and negative errors, respectively, on the logarithm of the column density. The flag f_N has the following definition: 0 = detection (not saturated or contaminated); -1 = upper limit; -2 = lower limit (due to saturation of the line). The flag f_{MS} has the following definition: 0 = not contaminated by the MS; -1 = contaminated by the MS (see §2.5).

APPENDIX

Table 3. Summary of the M31 Dwarf Galaxies

Name	Type	l_{MS}	b_{MS}	v_{LSR}	D_{dwarf}	R	X	Y	M_*	M_{200}	R_{200}	v_{200}
		($^{\circ}$)	($^{\circ}$)	(km s^{-1})	(kpc)	(kpc)	(kpc)	(kpc)	($10^5 M_{\odot}$)	($10^8 M_{\odot}$)	(kpc)	(km s^{-1})
M32	cE	-126.5	23.8	-194.6	805.0	5.3	-0.1	-5.3	3200.0	852.2	92.8	88.9
NGC 205	dE/dSph	-127.5	23.4	-241.3	824.0	8.0	-5.8	5.5	3300.0	864.8	93.2	89.3
And IX	dSph	-129.0	25.7	-203.5	766.0	35.3	24.3	25.6	1.5	21.5	27.2	26.1
And XVII	dSph	-130.3	22.9	-246.3	794.0	42.3	-13.2	40.2	2.6	28.0	29.7	28.5
And I	dSph	-123.4	24.2	-372.0	745.0	43.0	7.6	-42.3	39.0	102.7	45.8	43.9
And XXVII	dSph	-131.5	23.1	-534.2	828.0	55.5	-12.2	54.1	1.2	19.3	26.3	25.2
And III	dSph	-121.9	22.0	-341.5	748.0	65.2	-18.9	-62.4	8.3	48.9	35.8	34.3
And X	dSph	-130.8	28.2	-160.0	701.0	73.5	55.4	48.3	1.0	17.4	25.3	24.3
And XXV	dSph	-133.1	21.9	-101.8	813.0	79.0	-28.3	73.8	6.8	44.4	34.7	33.2
And XV	dSph	-123.3	29.8	-336.9	631.0	89.7	81.4	-37.7	4.9	38.0	32.9	31.5
NGC 185	dE/dSph	-134.7	23.4	-198.0	617.0	93.1	-8.2	92.8	680.0	405.1	72.4	69.4
NGC 147	dE/dSph	-134.8	22.4	-187.0	676.0	97.5	-20.8	95.3	620.0	387.6	71.4	68.4
And XXVI	dSph	-134.3	20.8	-255.1	762.0	97.8	-41.8	88.4	0.6	13.9	23.5	22.5
And XI	dSph	-118.7	23.9	-416.6	759.0	98.4	9.8	-97.9	0.5	12.6	22.8	21.8
And XIX	dSph	-120.8	18.6	-106.7	933.0	101.2	-62.4	-79.6	4.3	35.7	32.2	30.9
And V	dSph	-134.1	28.6	-398.9	773.0	105.3	60.9	85.9	3.9	34.0	31.7	30.4
And XXIV	dSph	-132.7	30.2	-124.7	600.0	107.7	80.8	71.2	0.9	17.1	25.2	24.2
Cas II	dSph	-136.1	23.0	-133.7	681.0	110.8	-13.1	110.0	1.4	20.8	26.9	25.8
And XIII	dSph	-117.7	24.9	-192.5	912.0	110.9	25.1	-108.1	0.4	11.5	22.1	21.2
And XXI	dSph	-129.3	15.1	-355.1	859.0	118.0	-115.5	23.8	7.6	46.9	35.3	33.8
And XX	dSph	-121.4	16.2	-450.6	802.0	121.1	-94.5	-75.9	0.3	9.8	20.9	20.0
And XXIII	dSph	-124.0	32.7	-236.3	769.0	121.6	118.9	-25.6	11.0	56.0	37.4	35.9
And II	dSph	-117.8	30.1	-192.5	652.0	135.2	92.5	-98.6	76.0	141.5	51.0	48.9
Cas III	dSph	-138.2	22.9	-365.2	772.0	135.7	-13.8	135.0	71.1	137.1	50.5	48.3
And XXIX	dSph	-117.3	13.5	-188.8	731.0	179.7	-123.7	-130.4	1.8	23.5	28.0	26.8
And XXII	dSph	-111.4	32.2	-130.6	794.0	210.1	130.5	-164.7	0.3	10.5	21.5	20.6
And VII	dSph	-138.6	12.1	-299.8	762.0	211.5	-157.1	141.5	95.0	157.5	52.9	50.6
IC 10	dIrr	-146.6	20.7	-340.0	794.0	240.1	-38.0	237.1	860.0	453.5	75.2	72.0
Lac I	dSph	-131.0	4.6	-188.0	756.0	255.4	-252.4	38.9	40.9	105.1	46.2	44.3
And VI	dSph	-111.6	10.5	-348.8	783.0	258.2	-153.1	-207.9	28.0	87.6	43.5	41.6
LGS 3	dIrr/dSph	-105.1	26.2	-286.8	769.0	259.8	65.4	-251.4	9.6	52.4	36.6	35.1
Per I	dSph	-132.2	49.4	-328.6	785.0	337.5	331.3	64.4	11.3	56.7	37.6	36.0

NOTE—Galaxy parameters are from [McConnachie \(2012\)](#), [Martin et al. \(2014, 2016\)](#) and references therein.

Table 4. QSO Absorbers within R_{200} of M31 Dwarf Galaxies

Dwarf	QSO	$v_{\text{LSR, Si III}}$	Δ_{sep}	v_{esc}	δv
		(km s $^{-1}$)		(km s $^{-1}$)	(km s $^{-1}$)
M32	RX_J0048.3+3941	−550.4	0.23	187.3	55.1
M32	RX_J0048.3+3941	−485.4	0.23	187.3	9.9
M32	HS0033+4300	−513.2	0.38	144.3	7.9
M32	HS0058+4213	−535.6	0.55	120.1	42.9
M32	HS0058+4213	−498.7	0.55	120.1	6.0
M32	RX_J0043.6+3725	−595.9	0.49	127.3	101.9
M32	RX_J0043.6+3725	−489.1	0.49	127.3	4.9
M32	Zw535.012	−535.4	0.70	106.4	27.8
M32	Zw535.012	−472.6	0.70	106.4	35.0
M32	RX_J0050.8+3536	−552.3	0.78	100.9	65.1
NGC 205	RX_J0048.3+3941	−550.4	0.35	150.5	10.6
NGC 205	RX_J0048.3+3941	−485.4	0.35	150.5	54.4
NGC 205	HS0033+4300	−513.2	0.25	179.8	36.7
NGC 205	HS0058+4213	−535.6	0.56	119.0	1.6
NGC 205	HS0058+4213	−498.7	0.56	119.0	38.5
NGC 205	RX_J0043.6+3725	−595.9	0.61	114.7	57.3
NGC 205	RX_J0043.6+3725	−489.1	0.61	114.7	49.5
NGC 205	Zw535.012	−535.4	0.57	118.4	16.8
NGC 205	Zw535.012	−472.6	0.57	118.4	79.6
NGC 205	RX_J0050.8+3536	−552.3	0.90	94.1	20.5
NGC 205	IRAS_F00040+4325	−632.2	0.92	93.3	70.1
NGC 205	IRAS_F00040+4325	−539.3	0.92	93.3	22.8
NGC 205	IRAS_F00040+4325	−459.0	0.92	93.3	103.1
And IX	HS0058+4213	−535.6	0.84	28.5	32.2
And IX	HS0058+4213	−498.7	0.84	28.5	4.7
And XVII	HS0033+4300	−513.2	0.46	41.8	37.4
And XVII	Zw535.012	−535.4	0.60	36.9	17.5
And XVII	Zw535.012	−472.6	0.60	36.9	80.3
And I	RX_J0048.3+3941	−550.4	0.49	62.5	127.8
And I	RX_J0048.3+3941	−485.4	0.49	62.5	192.8
And I	RX_J0043.6+3725	−595.9	0.21	96.1	81.1
And I	RX_J0043.6+3725	−489.1	0.21	96.1	187.9
And I	RX_J0050.8+3536	−552.3	0.76	50.5	117.9
And XXVII	Zw535.012	−535.4	0.17	61.2	304.5
And XXVII	Zw535.012	−472.6	0.17	61.2	367.3
And III	RX_J0043.6+3725	−595.9	0.69	41.4	48.2
And III	RX_J0043.6+3725	−489.1	0.69	41.4	155.0
And XXV	Zw535.012	−535.4	0.61	42.7	132.0
And XXV	Zw535.012	−472.6	0.61	42.7	69.2
And XV	RXS_J0118.8+3836	−570.2	0.40	49.6	70.0
And XV	RXS_J0118.8+3836	−529.5	0.40	49.6	110.7
NGC 185	HS0033+4300	−513.2	0.92	72.3	13.4
NGC 185	Zw535.012	−535.4	0.49	99.1	33.3
NGC 185	Zw535.012	−472.6	0.49	99.1	29.5
NGC 147	HS0033+4300	−513.2	0.97	69.5	26.8
NGC 147	Zw535.012	−535.4	0.53	93.8	46.7
NGC 147	Zw535.012	−472.6	0.53	93.8	16.1
And XXI	IRAS_F00040+4325	−632.2	0.92	35.2	25.0
And XXI	IRAS_F00040+4325	−539.3	0.92	35.2	117.9
And XXI	IRAS_F00040+4325	−459.0	0.92	35.2	198.2
And XXIII	RXS_J0118.8+3836	−570.2	0.72	42.2	23.0
And XXIII	RXS_J0118.8+3836	−529.5	0.72	42.2	17.7
And II	MRK352	−607.9	0.99	49.0	104.2
And II	MRK352	−549.2	0.99	49.0	45.5
And II	MRK352	−502.5	0.99	49.0	1.2
And VI	RBS2055	−638.2	0.52	57.6	19.9
And VI	RBS2055	−583.6	0.52	57.6	74.5
LGS 3	RX_J0053.7+2232	−572.0	0.88	37.4	28.0

NOTE—The match between dwarfs and QSO absorbers was made so that the projected separation between the dwarf and QSO is within R_{200} of the dwarf, i.e., $\Delta_{\text{sep}} = r/R_{200}^{\text{dwarf}} \leq 1$ (where r is the projected distance between the QSO and dwarf). Here v_{esc} is the escape velocity of the dwarf at the projected distance of the QSO assuming a point-like mass with halo mass listed in Table 3. The velocity separation between the QSO absorber and the dwarf is $\delta v = |v_{\text{M31, Si III}} - v_{\text{M31, dwarf}}|$.

Table 5. Strength and Abundance of Key Ions

Ion	$f\lambda$	$[X/H]_{\odot}$
C II $\lambda 1334$	171	−3.57
C IV $\lambda 1550$	147	−3.31
C IV $\lambda 1548$	294	−3.57
Si II $\lambda 1526$	203	−4.49
Si II $\lambda 1190$	348	−4.49
Si II $\lambda 1193$	695	−4.49
Si II $\lambda 1260$	1487	−4.49
Si III $\lambda 1206$	1967	−4.49
Si IV $\lambda 1402$	358	−4.49
Si IV $\lambda 1393$	715	−4.49
O VI $\lambda 1031$	137	−3.31

NOTE— $[X/H]_{\odot}$ is the solar abundance of the element X, i.e., C, O, or Si (solar abundances from [Asplund et al. 2009](#)).

Table 6. Metal mass of the Cool CGM of M31

Range	M_Z	M_Z	M_Z
	H Model	SPL Model	GP Model
(kpc)	($10^7 M_{\odot}$)	($10^7 M_{\odot}$)	($10^7 M_{\odot}$)
5–230	1.5–2.1	1.4–1.7	1.2–2.1
5–300	2.0–2.6	1.8–2.0	1.5–2.5
5–150	1.0–1.5	1.0–1.2	0.73–1.4
150–300	1.0–1.1	0.77–0.78	0.72–1.1
5–360	2.5–3.0	2.1–2.3	1.7–2.9

NOTE— M_Z corresponds to the metal mass traced by Si II, Si III, and Si IV. The H Model corresponds to the low and high hyperbola models, the SPL model represents the high and low the single-power law models, and the GP model encompasses the range allowed by the errors from the low and high model (see §4.5 and Appendix F).

Table 7. Summary of the Velocities of the CGM of M31

Ion	Region	$\langle v_{\text{M31}} \rangle$	IQR
		(km s ⁻¹)	(km s ⁻¹)
Individual Components			
C II	All R	31.3 ± 52.3	$[-6.5, 68.0]$
C II	$R \leq 100$ kpc	80.6 ± 39.9	$[37.9, 101.1]$
C II	$R > 100$ kpc	4.7 ± 36.6	$[-21.2, 24.9]$
Si II	All R	65.7 ± 53.1	$[53.8, 95.2]$
Si II	$R \leq 100$ kpc	90.6 ± 32.3	$[67.2, 117.8]$
Si II	$R > 100$ kpc	22.3 ± 54.5	$[-27.0, 76.8]$
Si III	All R	26.8 ± 45.5	$[-10.1, 54.7]$
Si III	$R \leq 100$ kpc	77.9 ± 34.1	$[59.9, 95.9]$
Si III	$R > 100$ kpc	7.4 ± 32.3	$[-12.4, 36.1]$
Si IV	All R	39.5 ± 43.1	$[8.3, 71.0]$
Si IV	$R \leq 100$ kpc	82.2 ± 7.5	$[76.3, 88.4]$
Si IV	$R > 100$ kpc	12.8 ± 33.7	$[-0.6, 26.9]$
C IV	All R	42.6 ± 47.3	$[10.8, 70.2]$
C IV	$R \leq 100$ kpc	88.3 ± 23.8	$[71.1, 102.1]$
C IV	$R > 100$ kpc	13.5 ± 33.4	$[4.9, 40.4]$
O VI	All R	28.9 ± 30.8	$[13.1, 43.0]$
Averaged Components			
C II	All R	34.2 ± 58.9	$[-23.0, 68.1]$
C II	$R \leq 100$ kpc	67.0 ± 55.3	$[22.7, 92.4]$
C II	$R > 100$ kpc	10.5 ± 49.3	$[-33.2, 37.2]$
Si II	All R	68.1 ± 50.6	$[54.2, 98.7]$
Si II	$R \leq 100$ kpc	86.4 ± 35.1	$[61.5, 111.2]$
Si II	$R > 100$ kpc	22.3 ± 54.5	$[-27.0, 76.8]$
Si III	All R	25.3 ± 67.3	$[-18.9, 66.9]$
Si III	$R \leq 100$ kpc	69.3 ± 48.1	$[43.8, 103.3]$
Si III	$R > 100$ kpc	4.1 ± 64.9	$[-24.0, 47.7]$
Si IV	All R	39.6 ± 55.4	$[-2.5, 78.8]$
Si IV	$R \leq 100$ kpc	69.9 ± 56.2	$[52.3, 112.4]$
Si IV	$R > 100$ kpc	14.9 ± 40.4	$[-22.9, 50.3]$
C IV	All R	43.3 ± 55.7	$[8.4, 84.4]$
C IV	$R \leq 100$ kpc	91.3 ± 33.7	$[69.9, 107.4]$
C IV	$R > 100$ kpc	14.0 ± 45.2	$[-8.0, 52.8]$
O VI	All R	27.9 ± 44.0	$[-9.8, 68.5]$

NOTE—Average, standard deviation, and IQR velocity range are listed for the individual components and averaged M31 velocity components.

A. LINE IDENTIFICATION

In Table A1, we provide the line identification for each absorption feature detected at about the 2σ level (the line list is complete at this level, but can include also less significant absorption). The table is ordered by alphabetical order of the QSO name and for each QSO in order of increasing observed wavelength (second column). In this table, we define the various types of absorption features as follows (third column): “ISMLG” is any ISM/CGM/IGM absorption from the Local group environment (mostly the MW and M31); “IGMABS” is any intervening IGM/CGM absorber at $\Delta v > 3000 \text{ km s}^{-1}$ from the QSO redshift; “PROXIMATE” is a proximate/associated absorber at $500 < \Delta v < 3000 \text{ km s}^{-1}$ from the QSO redshift; “INTRINSIC” is an absorber at $\Delta v < 500 \text{ km s}^{-1}$ from the QSO redshift. Any “UNIDENTIFIED” feature at the $> 2\sigma$ level is marked with that denomination. Finally, “OTHER” includes known fixed-pattern noise feature (“FPN”), special case of fixed-pattern noise feature occurring near the edge of the COS detector (“EDGE”), or the 1043 Å detector flaw in the *FUSE* data that causes a fake line (“FLAW”). FPN, EDGE, and FLAW all appear in the fourth column, which is otherwise used to list the atom or ion detected. The fifth column gives the rest wavelength of the atom/ion. The sixth column provides the information regarding frame into which the velocity (sixth column) and redshift (seventh column) are defined (“L”: LSR frame—any absorption at $|v_{\text{LSR}}| \leq 700 \text{ km s}^{-1}$, and otherwise “H”: heliocentric frame). Finally the last two columns give the approximate equivalent widths (W_λ) and errors that are only provided as guidelines, i.e., these should not be used for quantitative scientific purposes since the continuum placement is only approximate. We finally note that the H_2 lines are not individually measured, but are based on a model of the H_2 absorption (see Wakker 2006), which is the reason for not providing an error on W_λ .

The process for identifying the absorption lines in the COS spectra is reviewed in §2.3. As discussed in this section, some of the QSOs do not have the full FUV wavelength coverage or their redshifts put $\text{Ly}\alpha$ beyond the observed wavelength. There are seven such cases that are reviewed below:

- 3C454.3: With $z_{\text{em}} = 0.859$, the highest redshift $\text{Ly}\alpha$ absorber would be at 2259 Å. However, there are also COS G225M and FOS G190H/G270H data that help disentangle any possible $\text{Ly}\beta$ from $\text{Ly}\alpha$. In the velocity range $-700 \leq v_{\text{LSR}} \leq -150 \text{ km s}^{-1}$, there is detection of absorption in several ions, with all the velocity profiles being consistent, suggesting no contamination in the surveyed velocity range $-700 \leq v_{\text{LSR}} \leq -150 \text{ km s}^{-1}$.
- PG0044+030: With $z_{\text{em}} = 0.859$, the highest redshift $\text{Ly}\alpha$ absorber would be at 1973 Å. The FOS G190H/G270H data helps securely identifying $\text{Ly}\beta$ above 1347 Å in the G130M spectrum. Many lines between 1215 and 1347 Å are clearly identified as higher redshift Lyman series and metal lines, leaving just 5 absorption features identified as $\text{Ly}\alpha$, which is about the expected number of absorbers given the SNR in the COS spectrum of this target. In the velocity range $-700 \leq v_{\text{LSR}} \leq -150 \text{ km s}^{-1}$, there is detection of absorption in several ions, with all the velocity profiles being consistent, suggesting no contamination in the surveyed velocity range.
- PHL1226: This target has only COS G130M observations, and since $z_{\text{em}} = 0.404$, the highest redshift $\text{Ly}\alpha$ absorber would be at 1705 Å. There are 11 lines that are listed as $\text{Ly}\alpha$ in Table A1, which might be $\text{Ly}\beta$. However, some are very unlikely $\text{Ly}\beta$ as they are so strong that $\text{Ly}\gamma$ and/or metal lines would be expected to be detected and are not. In all but Si III there is no detection in the velocity range $-700 \leq v_{\text{LSR}} \leq -150 \text{ km s}^{-1}$. The absorption at -332 km s^{-1} from Si III $\lambda 1206$ is, however, clearly identified as O I $\lambda 1039$ associated with the super Lyman limit system at $z = 0.15974$.
- RX_J0023.5+1547: This target has also only COS G130M observations, and since $z_{\text{em}} = 0.412$, the highest redshift $\text{Ly}\alpha$ absorber would be at 1716 Å. There are 7 lines that are listed as $\text{Ly}\alpha$ in Table A1, which could be $\text{Ly}\beta$. Given the SNR of the COS spectrum, the expected number of $\text{Ly}\alpha$ lines between 1215 and 1460 Å is 15, while we identify 13. On the other hand, the expected number of $\text{Ly}\beta$ is 4, and only 1 is identified. This is well within the possible cosmic variance, but it is possible that 2–3 lines that are identified as $\text{Ly}\alpha$ could actually be $\text{Ly}\beta$. In the velocity range $-700 \leq v_{\text{LSR}} \leq -150 \text{ km s}^{-1}$, only Si III is detected, but there is no likely contamination of this absorption feature.
- RX_J0028.1+3103: This target has also COS G130M and G160M observations, but since $z_{\text{em}} = 0.500$, the highest redshift $\text{Ly}\alpha$ absorber would be at 1823 Å. Only one possible $\text{Ly}\beta$ identified as $\text{Ly}\alpha$ is above the spectral limit of 1792 Å. In the velocity range $-700 \leq v_{\text{LSR}} \leq -150 \text{ km s}^{-1}$, two components are detected, with one observed in C II, Si III, Si IV, and a weaker one only in Si III. Based on our line identification, there is no likely contamination of the weaker Si III absorption.

- SDSSJ015952.95+134554.3: This target has also only COS G130M observations, and since $z_{\text{em}} = 0.504$, the highest redshift Ly α absorber would be at 1828 Å. Given the SNR of the COS spectrum, we expect about 21 Ly α and 7 Ly β while 19 and 2 are listed in Table A1, respectively. So it is possible that 2–3 lines identified as Ly α could actually be Ly β . There is no detection of Si III (or other ions) in the velocity range $-700 \leq v_{\text{LSR}} \leq -150 \text{ km s}^{-1}$, and hence no contamination issue.
- SDSSJ225738.20+134045.0: This target has also COS G130M and G160M observations, but since $z_{\text{em}} = 0.595$, the highest redshift Ly α absorber would be at 1938 Å. There are 3 Ly α with no corresponding Ly β that possibly could be Ly β , but it is very unlikely to be the case for the 3 identified Ly α . In the velocity range $-700 \leq v_{\text{LSR}} \leq -150 \text{ km s}^{-1}$, there is detection of absorption in several ions, with all the velocity profiles being consistent, suggesting no contamination in the surveyed velocity range.

B. VISUALLY IDENTIFYING CONTAMINATION

In order to visually assess possible line contamination as well as conflicts in independent line identifications, we have designed the “conflict plot” that is shown in Fig. A1. In this plot, the locations on the x -axis are scaled according to $\log \lambda_{\text{obs}}$ and the y -axis scale is proportional to $\log(1+z)$. The diagonal lines represent loci of different transitions and how their observed wavelengths change with z . The diagonal lines are color coded depending on whether they trace metal transitions (gray), H $_2$ (green), or H I (blue). We identify some of the transitions at the top and on the sides of the plot. Any absorption feature that is identified in the COS spectrum is identified by a gray filled circle. Although not shown here, an independent line identification would be represented with a different symbol, immediately identifying the similarities and differences between two independent line identifications. The red horizontal lines represent redshift systems with any line (usually Ly α) that has $W_\lambda \geq 100 \text{ mÅ}$; systems with Ly α having strengths below this threshold do not have lines that stretch across the whole plot, but can have short line segments that cover just Ly β and Ly γ . Some of the common interstellar lines appear along the yellow and orange lines that represent a blue shift of -500 and -150 km s^{-1} , respectively (i.e., within the velocity range where we observe M31 CGM gas). For Project AMIGA, we mostly concentrate on transitions at $\lambda > 1145 \text{ Å}$ that are available in the COS G130M and G160M wavelength bandpass. However, if there are *FUSE* data, which provide wavelength coverage $\lambda < 1145 \text{ Å}$, we also use those.

In this figure, potential conflicts are readily detected at the intersection of the horizontal red line, a gray/green/blue sloping line, and the vertical orange/yellow line. If for one of the line of interest, there is a gray circle at $z > 0.01$ at the one of the intersection, there is a potential contamination in the velocity range $-700 \leq v_{\text{LSR}} \leq -150 \text{ km s}^{-1}$ that needs to be checked. For each sightline, in our sample, we have produced these conflict plots to easily identify any potential contamination of the absorption in the velocity range $-700 \leq v_{\text{LSR}} \leq -150 \text{ km s}^{-1}$.

For the specific example shown in Fig. A1, there are two potential conflicts for the components identified in the velocity $-700 \leq v_{\text{LSR}} \leq -150 \text{ km s}^{-1}$. One is near the N I $\lambda 1134.1$ line, where an O VI absorber at $z = 0.09753$ is present at 1132.58 (shifted by -400 km s^{-1} relative to N I, see Table A1). However, there is no contamination near N I $\lambda 1199.1$ in the velocity range $-700 \leq v_{\text{LSR}} \leq -150 \text{ km s}^{-1}$, so we know there is no N I absorption. The second conflict is for C II $\lambda 1334$ where Ly α at $z = 0.09723$ contaminates the -140 km s^{-1} C II component. Although there are several weaker Lyman series transitions that could have been used to correct for that contamination (which we did in some other cases), in this case we have also *FUSE* observations that provide C II $\lambda 1036$ where the absorption is not contaminated in this component.

C. COMPARISON BETWEEN COS G130M/G160M AND STIS E140M SPECTRA

For three targets (MRK335, UGC12163, and NGC7469) in our sample we have higher resolution STIS E140M spectra. Using the same integration velocity ranges that we used for COS (which is justified since the spectra were initially all aligned), we estimate the velocities and column densities in the STIS E140M spectra. The results are summarized in Table A2. In the footnote of this table we also list the SNRs in the continuum near C II and Si III since not only resolution but also SNRs can explain some of the differences. The STIS data have systematically lower SNRs than the COS spectra. Fox et al. (2005) show that in low SNR STIS E140M spectra (4–9 per resolution element), the AOD method can overestimate the apparent column densities by a factor 0.1–0.4 dex, especially when the absorption is weak. As for the COS spectra, we use the original binning sampling of the data to estimate the column densities. Binning by 2 or 3 pixels the STIS spectra did not change the results in contrast to the study of Fox et al. (2005), but in this study, the simulated spectra were affected only by Poisson noise while the STIS E140M are affected by both Poisson and fixed-pattern noises.

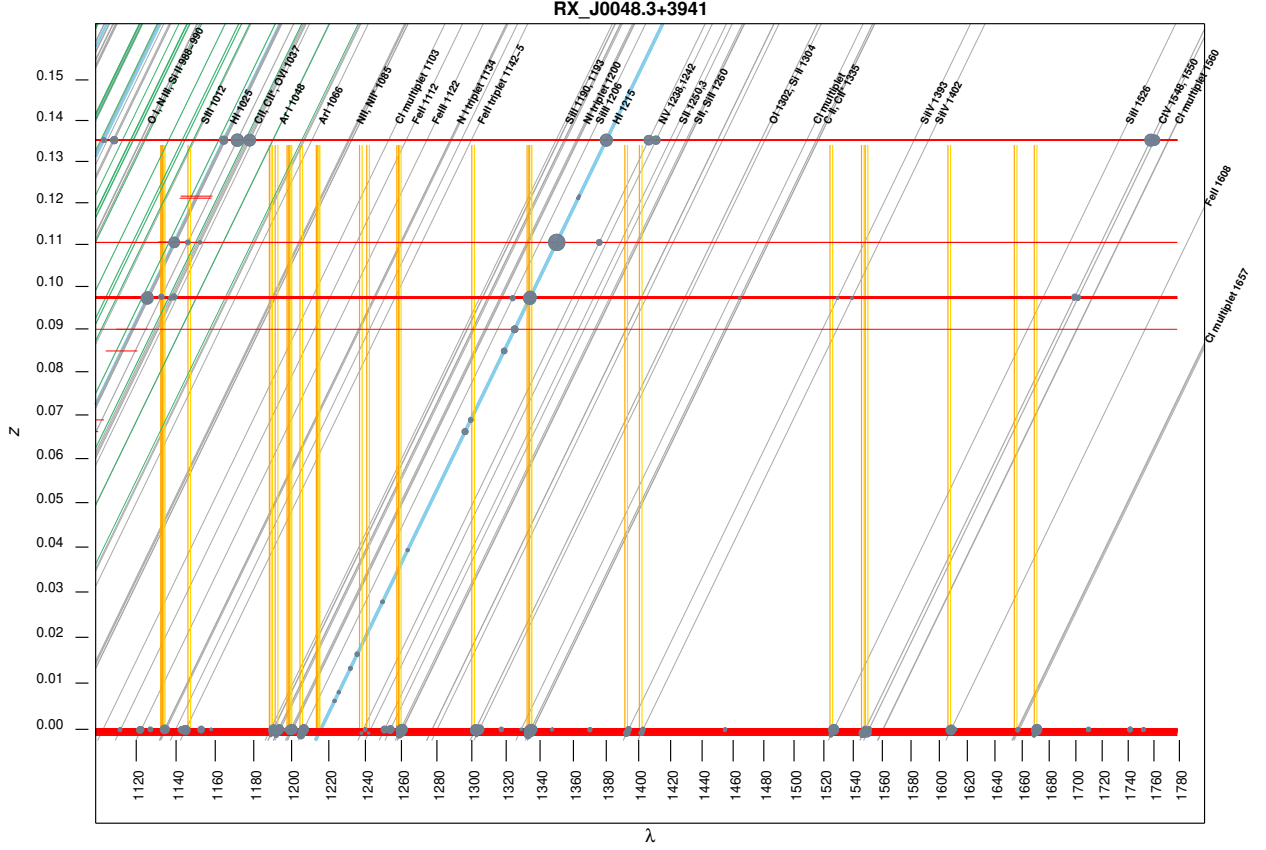


Figure A1. Example of conflict plot used to determine potential contamination in the velocity range $-700 \lesssim v_{\text{LSR}} \lesssim -150$ km s^{-1} . Locations on the x -axis are scaled according to $\log \lambda_{\text{obs}}$, but the markers show the wavelength. The y -axis scale is proportional to $\log(1+z)$, but the markers show z . The diagonal lines represent loci of different transitions and how their observed wavelengths change with z . The gray lines correspond to metal transitions, while the green ones indicate H_2 transitions. Lyman series lines of H I are shown in blue. Some of the transitions are identified near the top and on the sides of the plot. Absorption features identified in the UV spectrum are shown with gray dots with varying sizes proportional to $\sqrt{W_\lambda}$. The red horizontal lines represent redshift systems with any line (usually $\text{Ly}\alpha$) that has $W_\lambda \geq 100$ mÅ; systems with $\text{Ly}\alpha$ having strengths below this threshold do not have lines that stretch across the whole plot, but do have short line segments that cover just $\text{Ly}\beta$ and $\text{Ly}\gamma$. Most of the lines of interests appear along the yellow and orange lines that represent a blue shift of -500 and -150 km s^{-1} , respectively. Potential conflicts arise at the intersection of the horizontal red line, a gray/green/blue sloping line, and the vertical orange/yellow line.

As illustrated in Fig. A2 (and see also normalized profiles in the supplemental figures) with the spectra of MRK335 where we show for C II and Si III the COS and STIS spectra, more components can be revealed in the higher resolution spectrum and the components appear sharper and deeper in the higher resolution spectrum. However, the STIS spectrum is also much noisier. For MRK335, the absorption in all the components are weak with a peak absorption depth at the 20% level in C II and 30–40% in Si III. Within about the $1\text{--}2\sigma$ errors the column densities between COS and STIS are in agreement even though additional components are revealed in the STIS spectrum. The column densities derived from the STIS spectrum are systematically higher, but this effect is consistent with the lower SNRs in the STIS data that was observed by Fox et al. (2005). For UGC12163, with a peak absorption depth at 60% in C II and 90% in Si III in the component at -425 km s^{-1} in the COS spectrum (see supplemental figures), the absorption in these two transitions is marked as saturated. The STIS Si III reaches zero-flux level, confirming complete saturation in Si III. The STIS apparent column density of C II is 0.09 dex higher than the estimated lower limit from the COS spectrum, but in agreement within the 1σ error, implying that the adopted peak optical depth of $\tau_a > 0.9$ is about right for saturation in the COS spectra (see §2.4.2). The other components toward UGC12163 are weak and the STIS upper limits are in agreement with the COS detection. Toward NGC7469, the most negative absorption is again the strongest component and both COS C II and Si III were correctly identified as saturated (even though again

these do not reach zero-flux levels, while they do in the STIS spectrum). The other two components in the spectra of NGC7469 are very weak. For Si III, the SNR effect is observed with the STIS spectrum having 0.1–0.2 dex higher than the column densities derived in the very high SNR COS spectrum. On the other hand, the SNR near C II is higher in the STIS spectrum and for the component at -251 km s^{-1} , the column densities derived from the COS and STIS spectra are in excellent agreement (see Table A2).

While the sample with both STIS and COS spectra is small, the comparison shows that there is overall a good agreement in the column densities derived from the STIS and COS data and our conservative choice of $\tau_a \sim 0.9$ as the threshold for saturation in the COS data is adequate.

D. CONFRONTING THE AOD RESULTS WITH A LINE-PROFILE FITTING ANALYSIS

For the most blended profiles (6 targets in our sample), we also use a Voigt profile fit (PF) analysis to separate the absorption profiles into individual components with the goal to assess differences in column density estimates between the PF and AOD methods. With the PF method, we model the absorption profile as individual components using a modified version of the software described in [Fitzpatrick & Spitzer \(1997\)](#) (and see also [Lehner et al. 2011](#) for the updates). The best-fit values describing the gas are determined by comparing the model profiles convolved with the COS G130M or G160M (and STIS E140M when available) instrumental line-spread function (LSF) of the data. The COS and STIS LSFs are not purely Gaussian and we adopt the tabulated COS LSFs from the COS and STIS instrument handbooks ([Riley et al. 2019](#); [Fischer et al. 2019](#)). As the COS LSFs vary with the FUV lifetime positions, we use the COS LSFs at the appropriate lifetime positions.¹¹ Three parameters N_i , b_i , and v_i for each component, i , are input as initial guesses and were subsequently varied to minimize χ^2 . The fitting process enables us to find the best fit of the component structure using the data from one or more transitions of the same ionic species simultaneously. However, all the ions are fitted independently (i.e., we did not assume a common component structure for all the ions a priori). When STIS E140M data are available we also fit the COS and STIS independently to assess how different these are (see also Appendix C). We apply this method to C II, C IV, Si II, Si III, Si IV, and O VI if it is available.

We always start each fit with the smallest number of components that reasonably model the profiles, and add more components as needed. We do not fix any of the input parameters, i.e., each input parameter is allowed to freely vary. This procedure is repeated for each profile until the best fit is achieved. We finally bear in mind that even though the χ^2 goodness of fit may be good, the PF method may still not assess correctly the saturation level especially since the COS resolution is relatively crude for PF. In low SNR or complicated profile, a broad component may also be fitted principally to reduce the χ^2 while several narrower components could be more adequate and physically more appropriate (see also [Lehner et al. 2011](#)). This is a limitation of the profile fitting especially when the spectral resolution is only $\sim 17 \text{ km s}^{-1}$ and/or the SNR is low. For C IV and Si IV we fit all the components including the MW low velocity components since those are not saturated, while for the other ions, we only fit the high-velocity components since the low velocity components are saturated.

The results from component fitting are provided in Table A3. In Fig. A2, we show an example of PF where both COS and STIS observations are available (in the supplemental material, we show the PFs for the 6 targets). Considering first the COS data only, although C II and Si II are fitted independently, the velocity centroids of C II and Si II match each other. The two components seen in C II and Si II are also observed in Si III at the same velocities. However, only the component at -330 km s^{-1} is observed in C IV (and possibly Si IV). Two additional components are observed in Si III but not in C II or Si II. These additional components seen in Si III are also observed in C IV, but shifted in velocity; an additional component is also observed at -227 km s^{-1} only C IV. This demonstrates a clear change in the gas properties with velocity. The STIS E140M observations show additional components, but the results are far more uncertain (especially in the narrow components) owing to the lower SNR of the STIS data (for STIS column densities with less than 0.15 dex, those are quite consistent with the COS derived column densities).

Much of these conclusions regarding the velocity structures and how the ionization properties change in the different components can be drawn from the AOD analysis by comparing the velocity profiles and derived averaged velocities in each determined components. The six targets that we model with Voigt PFs have the most complex velocity structure in our sample and therefore a comparison with the AOD results provides a way to assess how similar or dissimilar are the results between the AOD and PF analyses in the worst case scenarios. For C II, C IV, Si II, Si III, and Si IV, we use the information in Tables 2 and A3 to match the component. For 78% (69/88) of the components, we can match

¹¹ For targets obtained at different lifetime positions, we adopt the one with the longest exposure time, but we note that the results would not change quantitatively if we adopted another lifetime position (less than 0.02–0.04 dex on the column densities).

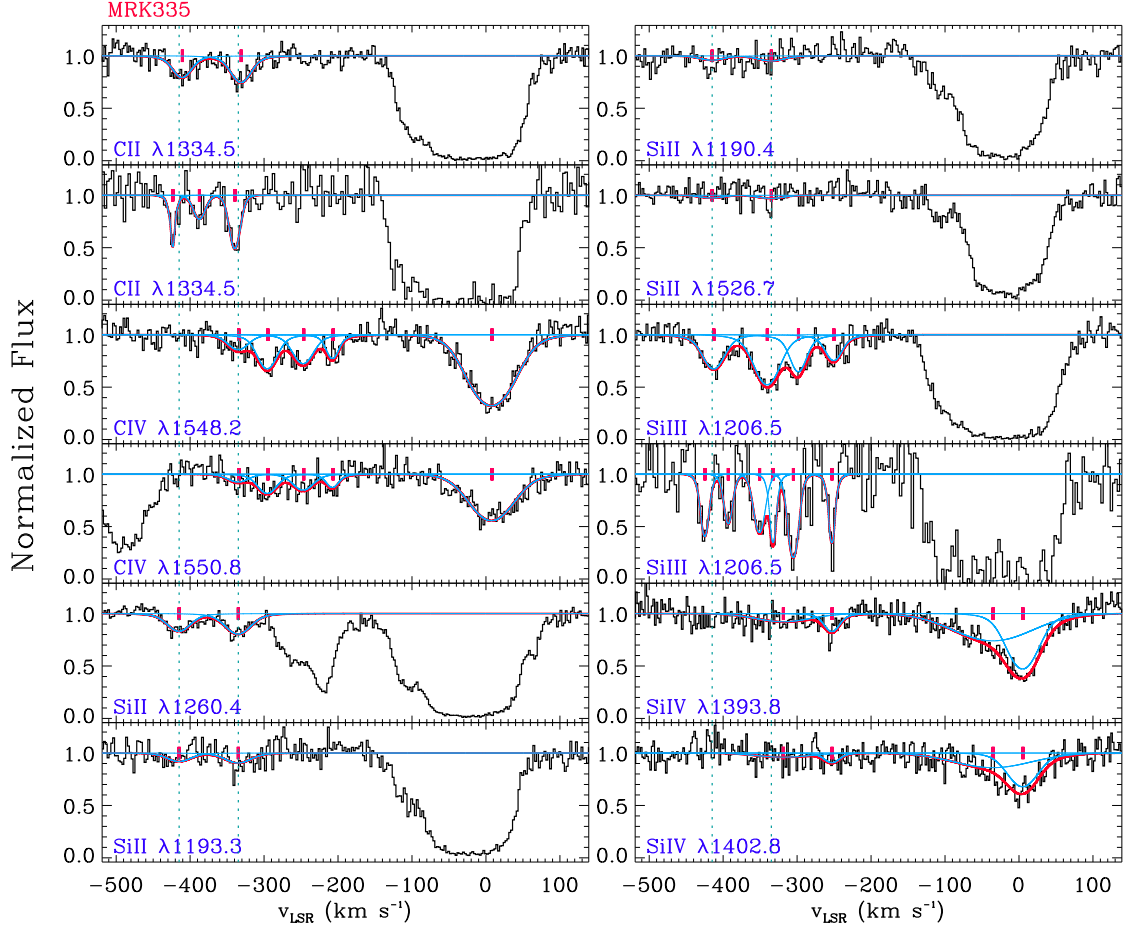


Figure A2. Example of normalized absorption lines as a function of the LSR velocity toward MRK335 with a Voigt PF model to the data. The red tick-marks show the velocity centroids. In each panel, the red line shows the resulting PF while the blue line show the individual components. The green vertical dotted lines show the velocity centroids of Si II. When the same ions appear twice (here C II and Si III), the top and bottom panel shows the COS and STIS data, respectively. Note that the higher resolution of STIS E140M shows additional components in C II and Si III, but the low SNR near Si III makes the results very uncertain.

them directly. For another 8, we coadd two components in the PF or AOD to match the AOD or PF results, and therefore in total we have 88% matched AOD and PF components. For 3% (3/88) and 9% (8/88) of the components, the PF fits yield extremely narrow ($b < 4 \text{ km s}^{-1}$) or broad ($b \gtrsim 45 \text{ km s}^{-1}$) components, respectively; in these cases, the results are deemed uncertain because they appear in low SNR spectra and/or complicated profiles (see above). In particular, the majority of broad components (7/8) appear in Si III and Si IV with no counterpart broad components in C IV.

For the matched components, the PF and AOD velocity centroids are in good agreement with a difference on average of $0.4\text{--}2.8 \text{ km s}^{-1}$ (and dispersion around the mean of $3\text{--}6 \text{ km s}^{-1}$) depending on the ions. In the Fig. A3, we show the comparison of the column densities for the individual components derived from the PF (y -axis) and AOD (x -axis) methods. Within 1σ error, the majority of the data are within the 1:1 relationship. There is a slight systematic since $\langle \log N_{\text{PF}} - \log N_{\text{AOD}} \rangle \simeq +0.06 \pm 0.10$ for C II, Si II, C IV, S IV; for Si III that difference is somewhat larger with $+0.09 \pm 0.10$ dex, but within 1σ dispersion in agreement with the 1:1 relationship. This systematic can be understood as follows: 1) in blended absorption some extra absorption can be present in the wings of the profiles that is taken into account in the PF but not necessarily in the AOD method (this effect is more important for weak absorption features); 2) the width in the AOD integration is fixed, while in the PF it is a free parameter, which can increase the column if the width is larger than used in the AOD. Another systematic observed from Fig. A3 is that the errors in the PF method are on average about $+0.07 \pm 0.15$ dex larger than those of the AOD. Several effects can explain this

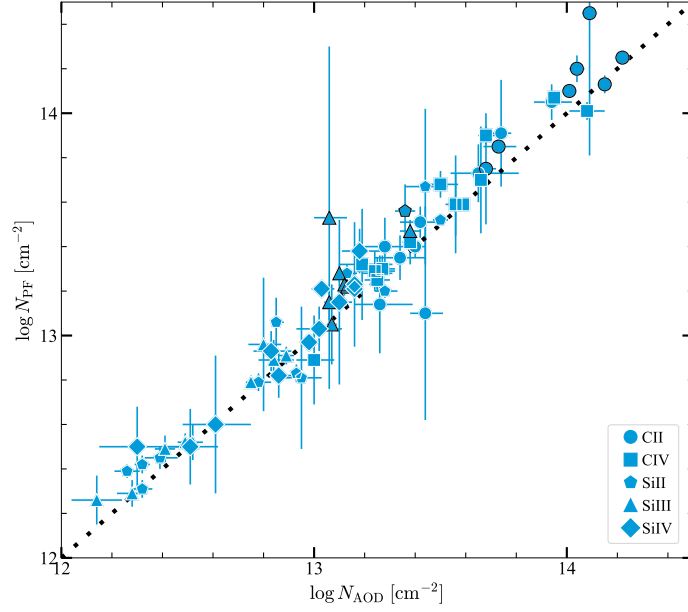


Figure A3. Comparison of the column densities derived using the AOD and PF methods for the matched components. Black outlined circles indicate that the absorption is flagged as saturated using the AOD method.

systematic: 1) broad shallow components can arise in PF but not in AOD (e.g., for Si IV, removing any components with $b > 40 \text{ km s}^{-1}$ from the sample would change the error difference from 0.08 to 0.04 dex); 2) PF of saturated components (removing Si III saturated components from the sample would change the systematic from 0.08 to 0.04 dex—as noted above, with the AOD we, however, consider saturated components as lower limits only, which is likely to be the case also for the PF results); 3) in the PF, all the components influence the error in each component (typically relatively well-separated and not too shallow absorbing components lead to similar errors as, e.g., C II, Si II, and Si III shown in Fig. A2, see Table A3).

In conclusion, while there are some systematic differences between the AOD and PF derived column densities, those are on average small (less than 15%). Furthermore and importantly the targets considered in this section have the most complicated blending of components in our sample. Since a great part of this small systematic arises owing to the profiles being heavily blended, a majority of our sample is not affected by those.

E. M33 IN THE CGM OF M31

M33 is separated from M31 by about 190 kpc (see Fig. 1) and is the third most massive galaxy in the Local group, but has still a mass about 20 times lower than M31 (Corbelli 2003). It is considered a dwarf spiral galaxy, but its stellar mass of $(3\text{--}6) \times 10^9 M_\odot$ (Corbelli 2003) is at least 10 times larger than the next two most massive satellites (M32 and NGC205) of M31 (see Table 3), making M33 quite unique. Kam et al. (2017) show that the halo mass could be as large as $5.2 \times 10^{11} M_\odot$ within a virial radius of 168 kpc, but this would imply a very low baryonic mass fraction, suggesting a more plausible M33 virial radius (and hence halo mass) that is much smaller.

While M33 appears quite unique as a dwarf spiral galaxy, there are two main reasons that the CGM of M33 is unlikely to affect much the observed absorption observed toward the QSOs in our sample. First, the systemic velocity of M33 is -180 km s^{-1} and the rotation velocity range is from -300 to -75 km s^{-1} . Therefore, a large fraction of the M33 CGM absorption may actually be lost in the MW HVC and disk absorption ($v_{\text{LSR}} > -150 \text{ km s}^{-1}$). Second, checking the column density maps shown in Fig. 13, there is no apparent trend between N and the projected distance from M33, and, furthermore the two closest sightlines to M33 show a lack of strong absorption from singly ionized species. To show explicitly this lack of trend, we plot in Fig. A4 the column densities of the various ions in our sample as a function of the projected distance from M33 (R_{M33}). Contrary to Fig. 8, there is no trend between N and R_{M33} . Furthermore, non-detections and detections are found at any projected distances from M33. All these strongly suggest that the CGM of M33 does not contribute significantly to the observed absorption associated with the CGM of M31.

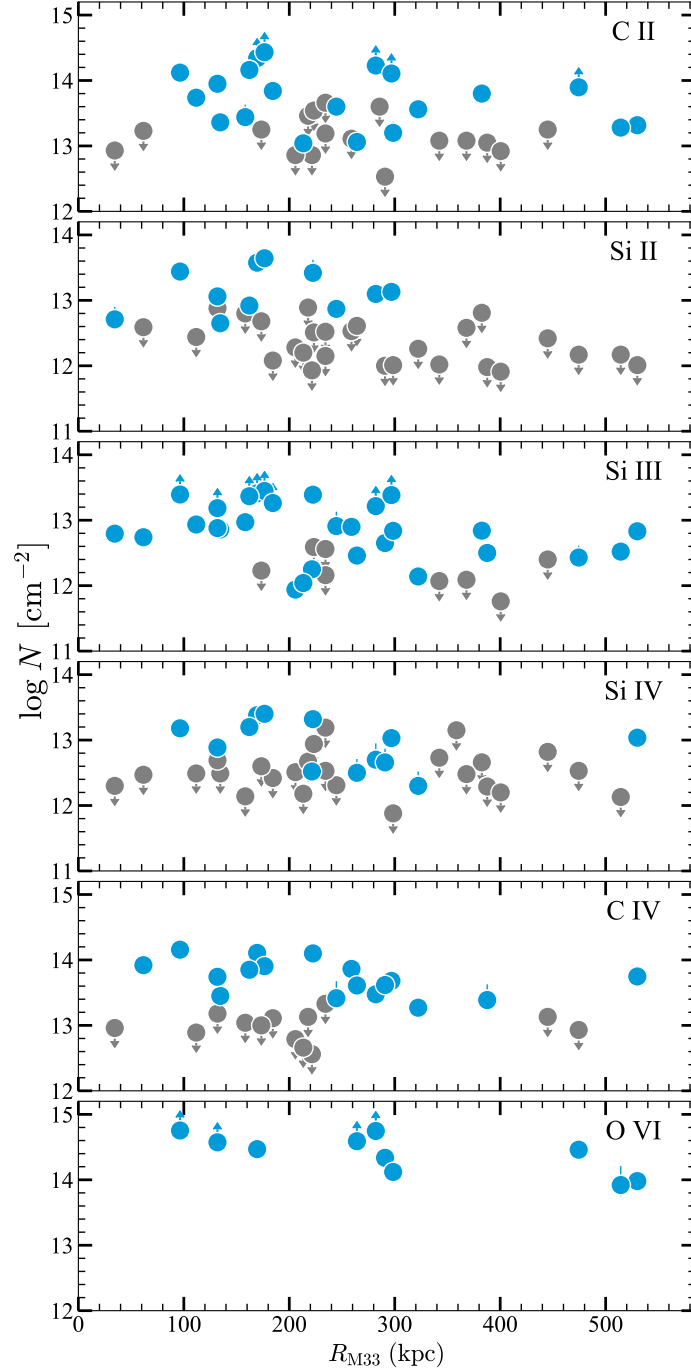


Figure A4. Logarithm of the total column densities of the detected ions as a function of R . Blue circles are detections, while gray circles with downward arrows are non-detections. A blue circle with an upward arrow denotes that the absorption is saturated, resulting into a lower limit.

F. MODELING THE COLUMN DENSITY OF SI AS A FUNCTION OF R

To model the functional form of N_{Si} with R (see §4.5), we consider three models, a hyperbolic (H) model, single-power law (SPL) model, and a Gaussian Process (GP) model. Since our sample contains both lower and upper limits, we first need to determine how to treat censored points in the fit. Beyond 360 kpc, 8/10 data are upper limits but there is only 1 upper limit at $R < 360$ kpc. Upper limits correspond to non-detection of any Si ions, and hence the value of N_{Si} can only decrease. We have assessed the effect of these upper limits on the fit by refitting with these

values decreased by a factor 2, 4, and 10; the overall effect on the fits is small. We adopt a factor 10 decrease for all the models. The lower limits are mostly observed at $R \lesssim 140$ kpc (only 2 are observed at $R > 140$ kpc, see Fig. 10). As discussed in §2.4.2, none of the absorption of Si III associated with the CGM of M31 reaches the zero-flux level. We estimate that the lower limits at $R > 50$ kpc should be increased by 0.1 dex while for the two inner lower limits, the increase is larger, and likely as large as 0.3 to 0.6 dex; we consider these two extrema in the fit. Finally, for data with vertical-ticked bars in Fig. 10, we take the mean value between the high and low values.

For the H model, we first use the smaller correction on the inner region lower limits and consider the two populations of data below and above $R_{\text{th}} = 130$ kpc and fit each population with a linear fit. We note R_{th} can vary between 90 and 130 kpc without varying the fit results. We find $N_{\text{Si}}/(10^{14}\text{cm}^{-2}) = -1.76 \times 10^{-2} R + 1.80$ at $R_{\text{th}} < 130$ kpc and $N_{\text{Si}}/(10^{14}\text{cm}^{-2}) = -3.25 \times 10^{-4} R + 0.204$ at $R_{\text{th}} \geq 130$ kpc. The two lines intersect at $R_0 = 92$ kpc and $N_{\text{Si}}^0 = 2.0 \times 10^{13} \text{cm}^{-2}$. If stronger correction on the lower limits is applied, then we find $N_{\text{Si}}/(10^{14}\text{cm}^{-2}) = -3.43 \times 10^{-2} R + 3.26$ at $R_{\text{th}} < 130$ kpc and $N_{\text{Si}}/(10^{14}\text{cm}^{-2}) = -3.24 \times 10^{-4} R + 0.204$ at $R_{\text{th}} \geq 130$ kpc. The two lines intersect at $R_0 = 90$ kpc and $N_{\text{Si}}^0 = 1.7 \times 10^{13} \text{cm}^{-2}$. As expected, the effect of the different corrections on the lower limits is much stronger on the fit at $R < 130$ kpc. The two regimes can be then modeled with a single hyperbola (e.g., [Watts & Bacon 1974](#)):

$$N_{\text{Si}}/(10^{14} \text{cm}^{-2}) = N_{\text{Si}}^0/(10^{14} \text{cm}^{-2}) + \beta_1(R - R_0) + \beta_2[(R - R_0)^2 + \delta^2/4]^{0.5}, \quad (\text{F1})$$

where $\beta_1 = (\alpha_1 + \alpha_2)/2$ ($\alpha_{1,2}$ being the slopes of each straight-line), $\beta_2 = (\alpha_2 - \alpha_1)/2$, and the radius of curvature at $R = R_0$ being proportional to δ (an adjustable parameter that allows one to exactly follow the lines right to the intersection point— $\delta = 0$ or smoothly merge the two asymptotes— $\delta > 0$). We adopt $\delta = 30$. The dotted and dashed orange curves in Fig. 10 show the models where the lower limits at $R < 50$ kpc are increased by a factor 0.3 or 0.6 dex, respectively.

The second model is the SPL, which can be written as:

$$N_{\text{Si}} = N_{\text{Si}}^0 R^\beta (\text{cm}^{-2}), \quad (\text{F2})$$

where here $N_{\text{Si}}^0 = 10^{15.91} \text{cm}^{-2}$ and $\beta = -1.23$ and $N_{\text{Si}}^0 = 10^{16.16} \text{cm}^{-2}$ and $\beta = -1.33$ corresponding to lower limits at $R < 50$ kpc being increased by a factor 0.3 or 0.6 dex, respectively. These two fits are shown in Fig. 10 with the dotted and dashed green lines, respectively.

Finally, we use the GP model, which is a generic supervised learning method designed to solve a regression, here between $\log N$ and R . The major advantages of this method are that the prediction interpolates the observations in a non-parametric way and is probabilistic so that empirical confidence intervals can be computed. We use the Python `SCIKIT-LEARN` GAUSSIAN PROCESS REGRESSION ([Pedregosa et al. 2011](#); [Buitinck et al. 2013](#)) to model the data with a squared-exponential kernel (with a length-scale of 0.1 and lower and upper bounds on length-scale from 0.01 to 130). Changing the length-scale has little effect on the model, but changing the bounds changes the smoothness of the model (a small length-scale value means that function values can change quickly while large values characterize functions that change only slowly). The use of a more complex kernel like a Matern kernel would yield similar results when using similar bounds. We treat all the data with the same weight using an error of 0.3 dex on the column density. This is larger than the typical measurements (0.05–0.15 dex) in our sample except for some of the data with vertical-ticked bars in Fig. 10. This error can be understood as a prior factor to smooth out the scatter of the data; empirically, 0.3 dex is the minimal value to make the model converge.¹² The effect of an increase on the error on each data point would flatten the relationship with a somewhat larger deviation. The same weight is justified in order to not favor detections versus upper or lower limits. With these assumptions, we model the data and show the mean values of the predictive distribution from the GP models in Fig. 10 with the dotted and dashed blue curves corresponding again to the cases where the lower limits at $R < 50$ kpc are increased by a factor 0.3 or 0.6 dex, respectively. The blue area around each curve show the standard deviation determined by the GP model.

G. SUPPLEMENTAL FIGURES

As part of the supplemental figures associated with this work, we provide for each absorber a figure as shown in Fig. 2 where we plot the normalized profiles of metal-line transitions for which we estimated the column densities.

¹² Including another term in the kernel (e.g., adding another squared-exponential kernel to the original kernel) would produce a similar model with a larger standard deviation; in that case the error on each data point would have actually no effect on the model.

Each color corresponds to a component and the velocity range of the absorption over which the velocity profile is integrated to derive the column densities and kinematics.

In a separate file, we also provide a figure as shown in Fig. A2, which shows the normalized profiles and the Voigt profile fitting. The profile fitting is done for 6 QSOs where the absorption components in the velocity range $-700 \leq v_{\text{LSR}} \leq -150 \text{ km s}^{-1}$ are more severely blended.

Table A1. Line List Identification

Target	λ_{obs}	Type	Ion	λ_{rest}	Frame	cz	z	W_{λ}	$\sigma_{W_{\lambda}}$
	(Å)			(Å)		(km s ⁻¹)		(mÅ)	(mÅ)
3C454.3	1144.95	ISMLG	Fe II	1144.9	L	2.0	-0.00002	309.4	96.6
3C454.3	1146.29	IGMABS	H I	1025.7	H	35240.0	0.11758	260.5	71.2
3C454.3	1152.82	ISMLG	P II	1152.8	L	-1.0	-0.00002	166.3	38.3
3C454.3	1153.25	IGMABS	O VI	1031.9	H	35246.0	0.11758	155.6	30.3
3C454.3	1158.39	IGMABS	O III	832.9	H	117142.0	0.39074	142.0	28.6
3C454.3	1159.58	IGMABS	O VI	1037.6	H	35239.0	0.11758	93.0	44.3
3C454.3	1182.72	IGMABS	H I	1025.7	H	45885.0	0.15307	63.0	27.3
3C454.3	1183.43	IGMABS	H I	1025.7	H	46094.0	0.15376	548.3	24.0
3C454.3	1183.77	IGMABS	H I	1025.7	H	46192.0	0.15408	296.1	22.1
3C454.3	1188.85	ISMLG	Si II	1190.4	L	-393.0	-0.00127	121.2	22.0
3C454.3	1189.16	ISMLG	Si II	1190.4	L	-317.0	-0.00106	140.3	26.0
3C454.3	1190.41	ISMLG	Si II	1190.4	L	-3.0	-0.00002	412.4	22.7
3C454.3	1190.60	IGMABS	O VI	1031.9	H	46098.0	0.15376	294.6	20.5
3C454.3	1190.91	IGMABS	O VI	1031.9	H	46187.0	0.15408	74.6	21.6
3C454.3	1191.76	ISMLG	Si II	1193.2	L	-384.0	-0.00127	131.3	21.1
3C454.3	1192.03	ISMLG	Si II	1193.2	L	-316.0	-0.00106	155.6	26.2
3C454.3	1193.25	ISMLG	Si II	1193.2	L	-10.0	-0.00002	413.6	26.4
3C454.3	1193.97	ISMLG	C I	1193.9	L	-6.0	-0.00002	74.3	29.0
3C454.3	1195.68	IGMABS	C II	1036.3	H	46096.0	0.15376	92.6	23.3
3C454.3	1197.19	IGMABS	O VI	1037.6	H	46105.0	0.15376	153.0	22.0
3C454.3	1197.49	IGMABS	O VI	1037.6	H	46191.0	0.15408	53.3	16.0
3C454.3	1199.50	ISMLG	N I	1199.5	L	-12.0	-0.00002	430.9	101.7
3C454.3	1200.17	ISMLG	N I	1200.2	L	-12.0	-0.00002	308.8	96.3
3C454.3	1200.67	ISMLG	N I	1200.7	L	-11.0	-0.00002	311.2	96.7
3C454.3	1204.94	ISMLG	Si III	1206.5	L	-387.0	-0.00127	253.5	24.8
3C454.3	1205.21	ISMLG	Si III	1206.5	L	-320.0	-0.00106	321.6	19.8
3C454.3	1206.07	ISMLG	Si III	1206.5	L	-108.0	-0.00036	102.2	27.3
3C454.3	1206.50	ISMLG	Si III	1206.5	L	1.0	-0.00002	505.2	27.6
3C454.3	1229.18	IGMABS	H I	930.7	H	96124.0	0.32061	125.1	29.5
3C454.3	1238.49	IGMABS	H I	937.8	H	96123.0	0.32061	198.3	28.0
3C454.3	1239.94	ISMLG	Mg II	1239.9	L	2.0	-0.00002	44.0	23.8
3C454.3	1244.72	IGMABS	H I	1215.6	H	7165.0	0.02390	206.5	22.7
3C454.3	1246.39	IGMABS	H I	1215.6	H	7575.0	0.02527	204.1	33.0
3C454.3	1250.56	ISMLG	S II	1250.5	L	-4.0	-0.00002	210.0	21.7
3C454.3	1252.41	IGMABS	H I	1215.6	H	9060.0	0.03022	218.0	31.0
3C454.3	1253.78	ISMLG	S II	1253.8	L	-7.0	-0.00002	255.8	20.1
3C454.3	1254.25	IGMABS	H I	949.7	H	96120.0	0.32061	227.6	28.3
3C454.3	1257.19	IGMABS	C II	903.9	H	117144.0	0.39074	62.9	15.3
3C454.3	1258.81	ISMLG	Si II	1260.4	L	-384.0	-0.00127	215.5	15.6
3C454.3	1259.09	ISMLG	Si II	1260.4	L	-318.0	-0.00106	221.9	17.6
3C454.3	1259.48	ISMLG	S II	1259.5	L	-9.0	-0.00002	238.6	19.7
3C454.3	1260.42	ISMLG	Si II	1260.4	L	-1.0	-0.00002	476.3	19.6
3C454.3	1260.71	ISMLG	C I	1260.7	L	-5.0	-0.00002	94.6	16.1
3C454.3	1262.07	IGMABS	H I	1215.6	H	11443.0	0.03817	180.7	25.4
3C454.3	1262.74	IGMABS	H I	1215.6	H	11608.0	0.03872	414.4	22.2
3C454.3	1263.86	IGMABS	H I	1215.6	H	11883.0	0.03964	77.2	24.7
3C454.3	1277.22	ISMLG	C I	1277.2	L	-5.0	-0.00002	138.5	16.8
3C454.3	1277.50	ISMLG	C I*	1277.5	L	-3.0	-0.00002	70.8	17.7
3C454.3	1280.14	ISMLG	C I	1280.1	L	1.0	-0.00002	57.3	18.4
3C454.3	1284.35	IGMABS	H I	972.5	H	96120.0	0.32061	376.2	59.9

Table A1 continued

Table A1 (*continued*)

Target	λ_{obs}	Type	Ion	λ_{rest}	Frame	cz	z	W_{λ}	$\sigma_{W_{\lambda}}$
	(Å)			(Å)		(km s ⁻¹)		(mÅ)	(mÅ)
3C454.3	1302.11	ISMLG	O I	1302.1	L	-13.0	-0.00002	453.1	78.0
3C454.3	1303.34	IGMABS	H I	1215.6	H	21620.0	0.07212	230.6	62.0
3C454.3	1304.32	ISMLG	Si II	1304.3	L	-11.0	-0.00002	381.4	74.2
3C454.3	1316.65	IGMABS	H I	1215.6	H	24901.0	0.08306	155.3	26.9
3C454.3	1317.19	ISMLG	Ni II	1317.2	L	-6.0	-0.00002	48.3	18.3
3C454.3	1320.85	IGMABS	H I	949.7	H	117144.0	0.39074	79.5	17.1
3C454.3	1321.43	IGMABS	C III	977.0	H	105679.0	0.35253	408.0	30.1
3C454.3	1325.51	IGMABS	H I	1025.7	H	87619.0	0.29224	116.9	30.2
3C454.3	1328.81	ISMLG	C I	1328.8	L	-6.0	-0.00002	88.3	20.0
3C454.3	1329.07	ISMLG	C I*	1329.1	L	-11.0	-0.00002	106.8	24.7
3C454.3	1332.82	ISMLG	C II	1334.5	L	-384.0	-0.00127	282.9	19.6
3C454.3	1333.13	ISMLG	C II	1334.5	L	-315.0	-0.00106	92.2	10.0
3C454.3	1334.51	ISMLG	C II	1334.5	L	-6.0	-0.00002	522.5	22.7
3C454.3	1335.66	ISMLG	C II*	1335.7	L	-11.0	-0.00002	260.6	23.1
3C454.3	1337.54	IGMABS	H I	1215.6	H	30054.0	0.10025	287.6	21.5
3C454.3	1340.55	IGMABS	H I	1025.7	H	92016.0	0.30690	73.6	22.5
3C454.3	1347.22	ISMLG	Cl I	1347.2	L	-4.0	-0.00002	55.8	20.6
3C454.3	1352.20	IGMABS	H I	972.5	H	117034.0	0.39036	61.0	23.1
3C454.3	1352.56	IGMABS	H I	972.5	H	117144.0	0.39074	111.1	15.7
3C454.3	1354.58	IGMABS	H I	1025.7	H	96117.0	0.32061	364.2	29.2
3C454.3	1354.75	IGMABS	H I	1025.7	H	96167.0	0.32079	147.7	15.7
3C454.3	1358.33	IGMABS	H I	1215.6	H	35181.0	0.11735	213.7	16.6
3C454.3	1358.60	IGMABS	H I	1215.6	H	35248.0	0.11758	420.6	16.7
3C454.3	1358.78	IGMABS	C III	977.0	H	117142.0	0.39074	201.0	14.0
3C454.3	1362.78	IGMABS	O VI	1031.9	H	96119.0	0.32061	164.8	25.9
3C454.3	1370.09	ISMLG	Ni II	1370.1	L	-9.0	-0.00002	72.5	18.9
3C454.3	1370.31	IGMABS	O VI	1037.6	H	96122.0	0.32061	97.6	18.3
3C454.3	1375.91	IGMABS	H I	1025.7	H	102351.0	0.34140	115.4	19.9
3C454.3	1376.56	IGMABS	N III	989.7	H	117142.0	0.39074	86.8	19.9
3C454.3	1387.33	IGMABS	H I	1025.7	H	105690.0	0.35253	123.2	31.6
3C454.3	1388.64	IGMABS	C III	977.0	H	126301.0	0.42129	130.4	33.6
3C454.3	1391.99	IGMABS	Si III	1206.5	H	46091.0	0.15376	533.9	21.6
3C454.3	1393.77	ISMLG	Si IV	1393.7	L	1.0	-0.00002	325.5	30.2
3C454.3	1394.63	IGMABS	H I	1215.6	H	44132.0	0.14721	242.5	21.6
3C454.3	1395.72	IGMABS	O VI	1031.9	H	105689.0	0.35253	161.4	15.6
3C454.3	1396.27	IGMABS	O VI	1031.9	H	105847.0	0.35305	126.2	21.9
3C454.3	1400.99	ISMLG	Si IV	1402.7	L	-381.0	-0.00127	97.0	19.7
3C454.3	1401.31	ISMLG	Si IV	1402.7	L	-313.0	-0.00106	96.1	21.3
3C454.3	1401.76	IGMABS	H I	1215.6	H	45890.0	0.15307	262.7	23.2
3C454.3	1402.59	IGMABS	H I	1215.6	H	46095.0	0.15376	808.9	18.9
3C454.3	1402.78	ISMLG	Si IV	1402.7	L	1.0	-0.00002	446.4	30.0
3C454.3	1402.98	IGMABS	H I	1215.6	H	46191.0	0.15408	345.8	16.7
3C454.3	1403.41	IGMABS	O VI	1037.6	H	105685.0	0.35253	143.4	17.1
3C454.3	1403.95	IGMABS	O VI	1037.6	H	105841.0	0.35305	79.9	19.5
3C454.3	1406.81	IGMABS	N III	989.7	H	126305.0	0.42129	215.3	27.0
3C454.3	1418.98	IGMABS	H I	1215.6	H	50137.0	0.16724	50.0	28.4
3C454.3	1422.41	IGMABS	H I	1215.6	H	50982.0	0.17006	75.9	32.6
3C454.3	1426.13	IGMABS	H I	1025.7	H	117028.0	0.39036	263.7	23.8
3C454.3	1426.52	IGMABS	H I	1025.7	H	117142.0	0.39074	223.9	14.8
3C454.3	1426.87	IGMABS	H I	1025.7	H	117246.0	0.39109	110.1	18.6
3C454.3	1427.98	IGMABS	H I	1215.6	H	52358.0	0.17465	263.7	35.5
3C454.3	1435.12	IGMABS	O VI	1031.9	H	117135.0	0.39074	166.5	18.1
3C454.3	1435.51	IGMABS	H I	1215.6	H	54214.0	0.18084	75.2	24.8

Table A1 continued

Table A1 (*continued*)

Target	λ_{obs}	Type	Ion	λ_{rest}	Frame	cz	z	W_{λ}	$\sigma_{W_{\lambda}}$
	(Å)			(Å)		(km s ⁻¹)		(mÅ)	(mÅ)
3C454.3	1441.29	IGMABS	C II	1036.3	H	117145.0	0.39074	26.8	8.1
3C454.3	1443.06	IGMABS	O VI	1037.6	H	117142.0	0.39074	127.7	11.1
3C454.3	1449.41	IGMABS	H I	1025.7	H	123833.0	0.41307	63.0	17.0
3C454.3	1451.22	IGMABS	H I	1025.7	H	124364.0	0.41485	55.9	9.4
3C454.3	1454.05	IGMABS	H I	1215.6	H	58787.0	0.19609	184.4	11.6
3C454.3	1454.25	IGMABS	Si II	1260.4	H	46102.0	0.15376	107.7	9.9
3C454.3	1457.86	IGMABS	H I	1025.7	H	126303.0	0.42129	116.8	16.0
3C454.3	1466.66	IGMABS	O VI	1031.9	H	126296.0	0.42129	143.3	15.0
3C454.3	1470.75	IGMABS	H I	1215.6	H	62903.0	0.20982	63.0	15.4
3C454.3	1474.73	IGMABS	O VI	1037.6	H	126293.0	0.42129	101.0	9.7
3C454.3	1484.84	IGMABS	H I	1215.6	H	66380.0	0.22142	115.4	20.1
3C454.3	1491.46	IGMABS	C II	1334.5	H	35253.0	0.11758	88.1	18.2
3C454.3	1503.09	IGMABS	H I	1215.6	H	70879.0	0.23643	75.2	20.1
3C454.3	1509.70	IGMABS	H I	1215.6	H	72510.0	0.24187	54.4	12.2
3C454.3	1516.22	IGMABS	H I	937.8	H	184905.0	0.61678	74.2	17.4
3C454.3	1524.73	ISMLG	Si II	1526.7	L	-388.0	-0.00127	71.1	13.9
3C454.3	1525.10	ISMLG	Si II	1526.7	L	-316.0	-0.00106	59.9	12.9
3C454.3	1526.65	ISMLG	Si II	1526.7	L	-12.0	-0.00002	448.2	13.9
3C454.3	1533.30	IGMABS	H I	1215.6	H	78331.0	0.26128	36.8	11.6
3C454.3	1535.52	IGMABS	H I	949.7	H	184903.0	0.61678	88.9	12.8
3C454.3	1539.72	IGMABS	C II	1334.5	H	46094.0	0.15376	138.3	13.1
3C454.3	1542.19	IGMABS	H I	1215.6	H	80522.0	0.26859	113.8	16.2
3C454.3	1546.25	ISMLG	C IV	1548.2	L	-378.0	-0.00127	143.0	9.3
3C454.3	1546.53	ISMLG	C IV	1548.2	L	-324.0	-0.00106	157.4	10.6
3C454.3	1548.23	ISMLG	C IV	1548.2	L	4.0	-0.00002	462.4	15.0
3C454.3	1548.82	ISMLG	C IV	1550.7	L	-379.0	-0.00127	88.9	11.3
3C454.3	1549.09	ISMLG	C IV	1550.7	L	-327.0	-0.00106	96.2	12.5
3C454.3	1550.80	ISMLG	C IV	1550.7	L	3.0	-0.00002	261.0	18.2
3C454.3	1557.08	IGMABS	H I	1215.6	H	84195.0	0.28084	204.9	12.5
3C454.3	1560.24	ISMLG	C I	1560.3	L	-13.0	-0.00002	183.5	11.5
3C454.3	1560.65	ISMLG	C I*	1560.7	L	-11.0	-0.00002	85.4	10.6
3C454.3	1562.33	IGMABS	H I	1215.6	H	85490.0	0.28516	247.0	23.3
3C454.3	1567.56	IGMABS	H I	1215.6	H	86777.0	0.28946	45.6	11.2
3C454.3	1570.94	IGMABS	H I	1215.6	H	87613.0	0.29224	310.4	18.5
3C454.3	1572.42	IGMABS	H I	972.5	H	184919.0	0.61678	121.2	11.6
3C454.3	1572.56	IGMABS	H I	1215.6	H	88011.0	0.29357	98.0	8.6
3C454.3	1578.92	IGMABS	H I	1215.6	H	89579.0	0.29880	51.2	14.4
3C454.3	1588.76	IGMABS	H I	1215.6	H	92007.0	0.30690	341.0	18.7
3C454.3	1591.82	IGMABS	H I	1215.6	H	92762.0	0.30942	44.1	14.5
3C454.3	1593.37	IGMABS	Si III	1206.5	H	96130.0	0.32061	45.5	17.4
3C454.3	1598.95	IGMABS	H I	1215.6	H	94519.0	0.31528	285.1	20.6
3C454.3	1602.66	IGMABS	H I	1215.6	H	95433.0	0.31833	72.2	20.1
3C454.3	1603.27	IGMABS	H I	1215.6	H	95584.0	0.31883	101.4	20.3
3C454.3	1604.30	IGMABS	H I	1025.7	H	169103.0	0.56407	81.5	20.8
3C454.3	1604.81	IGMABS	H I	1025.7	H	169252.0	0.56455	185.1	20.0
3C454.3	1605.42	IGMABS	H I	1215.6	H	96115.0	0.32061	399.3	14.7
3C454.3	1605.64	IGMABS	H I	1215.6	H	96169.0	0.32079	342.2	13.8
3C454.3	1608.05	IGMABS	Si IV	1393.7	H	46092.0	0.15376	189.0	22.9
3C454.3	1608.40	ISMLG	Fe II	1608.4	L	-9.0	-0.00002	499.3	28.3
3C454.3	1626.37	IGMABS	H I	1025.7	H	175555.0	0.58560	204.5	55.2
3C454.3	1630.69	IGMABS	H I	1215.6	H	102348.0	0.34140	457.1	27.6
3C454.3	1633.69	IGMABS	H I	1215.6	H	103087.0	0.34386	63.7	19.7
3C454.3	1642.66	IGMABS	H I	1215.6	H	105299.0	0.35124	136.8	22.5

Table A1 continued

Table A1 (*continued*)

Target	λ_{obs}	Type	Ion	λ_{rest}	Frame	cz	z	W_{λ}	$\sigma_{W_{\lambda}}$
	(Å)			(Å)		(km s ⁻¹)		(mÅ)	(mÅ)
3C454.3	1643.65	IGMABS	H I	1215.6	H	105542.0	0.35205	168.0	17.4
3C454.3	1644.23	IGMABS	H I	1215.6	H	105687.0	0.35253	503.0	16.1
3C454.3	1644.86	IGMABS	H I	1215.6	H	105841.0	0.35305	190.5	21.9
3C454.3	1645.71	IGMABS	H I	1215.6	H	106051.0	0.35375	85.3	14.2
3C454.3	1656.87	ISMLG	C I	1656.9	L	-11.0	-0.00002	258.9	18.5
3C454.3	1657.84	ISMLG	C I*	1657.9	L	-11.0	-0.00002	60.1	16.2
3C454.3	1658.41	IGMABS	H I	1025.7	H	184918.0	0.61678	284.4	24.1
3C454.3	1668.64	ISMLG	Al II	1670.7	L	-385.0	-0.00127	121.5	19.6
3C454.3	1668.98	ISMLG	Al II	1670.7	L	-325.0	-0.00106	51.2	18.4
3C454.3	1670.71	ISMLG	Al II	1670.7	L	-13.0	-0.00002	474.8	22.7
3C454.3	1677.94	IGMABS	Si III	1206.5	H	117143.0	0.39074	62.9	13.5
3C454.3	1682.83	IGMABS	H I	1215.6	H	115205.0	0.38428	481.0	27.5
3C454.3	1685.65	IGMABS	H I	1215.6	H	115901.0	0.38660	447.4	24.2
3C454.3	1690.22	IGMABS	H I	1215.6	H	117028.0	0.39036	545.5	19.0
3C454.3	1690.68	IGMABS	H I	1215.6	H	117141.0	0.39074	613.6	15.3
3C454.3	1691.10	IGMABS	H I	1215.6	H	117245.0	0.39109	226.1	14.6
3C454.3	1694.26	IGMABS	H I	972.5	H	222477.0	0.74211	111.4	18.1
3C454.3	1694.69	IGMABS	H I	1215.6	H	118131.0	0.39404	164.7	22.5
3C454.3	1703.40	IGMABS	C IV	1548.2	H	30052.0	0.10025	91.4	28.9
3C454.3	1706.21	IGMABS	C IV	1550.7	H	30047.0	0.10025	64.9	21.7
3C454.3	1709.15	IGMABS	H I	937.8	H	246582.0	0.82253	58.9	14.8
3C454.3	1709.43	IGMABS	H I	1025.7	H	199829.0	0.66656	183.9	28.5
3C454.3	1716.60	IGMABS	H I	1215.6	H	123533.0	0.41206	164.1	26.5
3C454.3	1717.83	IGMABS	H I	1215.6	H	123836.0	0.41307	299.0	24.9
3C454.3	1719.99	IGMABS	H I	1215.6	H	124368.0	0.41485	349.4	25.4
3C454.3	1727.82	IGMABS	H I	1215.6	H	126299.0	0.42129	374.1	25.2
3C454.3	1729.29	IGMABS	H I	1215.6	H	126661.0	0.42250	78.5	25.0
3C454.3	1730.24	IGMABS	C IV	1548.2	H	35249.0	0.11758	148.2	25.7
3C454.3	1730.93	IGMABS	H I	949.7	H	246587.0	0.82253	76.5	21.7
3C454.3	1741.49	ISMLG	Ni II	1741.5	L	-11.0	-0.00002	96.3	24.8
3C454.3	1751.86	ISMLG	Ni II	1751.9	L	-9.0	-0.00002	97.4	27.1
3C454.3	1757.36	IGMABS	H I	1215.6	H	133584.0	0.44559	167.9	30.8
3C454.3	1767.70	IGMABS	H I	1215.6	H	136133.0	0.45409	168.0	35.3
3C454.3	1770.31	IGMABS	H I	1215.6	H	136777.0	0.45624	295.3	30.6
3C454.3	1772.46	IGMABS	H I	972.5	H	246584.0	0.82253	200.6	46.9
3C454.3	1786.26	IGMABS	C IV	1548.2	H	46096.0	0.15376	456.1	21.7
3C454.3	1786.94	IGMABS	H I	1025.7	H	222485.0	0.74211	374.5	25.8
3C454.3	1789.21	IGMABS	C IV	1550.7	H	46092.0	0.15376	296.5	27.0
3C454.3	1848.83	IGMABS	H I	1215.6	H	156141.0	0.52083	894.9	143.8
3C454.3	1859.84	IGMABS	H I	1215.6	H	158858.0	0.52989	506.7	102.0
3C454.3	1866.01	IGMABS	H I	1025.7	H	245594.0	0.81920	226.5	63.2
3C454.3	1869.43	IGMABS	H I	1025.7	H	246593.0	0.82253	542.2	90.0
3C454.3	1877.26	IGMABS	O VI	1031.9	H	245583.0	0.81920	283.5	57.1
3C454.3	1881.02	IGMABS	H I	1215.6	H	164080.0	0.54731	170.8	62.8
3C454.3	1901.39	IGMABS	H I	1215.6	H	169103.0	0.56407	264.3	36.6
3C454.3	1901.98	IGMABS	H I	1215.6	H	169248.0	0.56455	495.8	35.3
3C454.3	1927.57	IGMABS	H I	1215.6	H	175558.0	0.58560	470.7	71.6
3C454.3	1965.47	IGMABS	H I	1215.6	H	184907.0	0.61678	566.5	90.7
3C454.3	1994.77	IGMABS	H I	1215.6	H	192131.0	0.64088	344.2	44.7
3C454.3	2025.99	IGMABS	H I	1215.6	H	199830.0	0.66656	819.1	66.9
3C454.3	2074.53	IGMABS	H I	1215.6	H	211801.0	0.70649	223.7	87.6
3C454.3	2083.77	IGMABS	H I	1215.6	H	214079.0	0.71409	492.6	88.3
3C454.3	2093.95	IGMABS	C IV	1548.2	H	105678.0	0.35253	408.2	67.6

Table A1 *continued*

Table A1 (*continued*)

Target	λ_{obs}	Type	Ion	λ_{rest}	Frame	cz	z	W_{λ}	$\sigma_{W_{\lambda}}$
	(Å)			(Å)		(km s ⁻¹)		(mÅ)	(mÅ)
3C454.3	2097.44	IGMABS	C iv	1550.7	H	105679.0	0.35253	212.4	47.1
3C454.3	2117.84	IGMABS	H i	1215.6	H	222480.0	0.74211	1096.1	80.5
3C454.3	2152.54	IGMABS	C iv	1548.2	H	117023.0	0.39036	406.0	45.5
3C454.3	2153.10	IGMABS	C iv	1548.2	H	117131.0	0.39074	423.0	41.6
3C454.3	2156.12	IGMABS	C iv	1550.7	H	117023.0	0.39036	275.5	42.3
3C454.3	2156.70	IGMABS	C iv	1550.7	H	117135.0	0.39074	267.3	44.5
3C454.3	2204.83	IGMABS	H i	1215.6	H	243935.0	0.81368	258.4	62.5
3C454.3	2211.55	IGMABS	H i	1215.6	H	245591.0	0.81920	584.9	69.1
3C454.3	2215.60	IGMABS	H i	1215.6	H	246590.0	0.82253	820.4	46.4
3C454.3	2217.77	IGMABS	H i	1215.6	H	247125.0	0.82432	265.8	38.1
3C454.3	2315.42	UNIDENTIFIED	UNIND	1000.0	H	0.0	-1.00000	752.1	132.3
3C454.3	2323.70	UNIDENTIFIED	UNIND	1000.0	H	0.0	-1.00000	752.7	107.5
3C454.3	2344.20	ISMLG	Fe ii	2344.2	L	-2.0	-0.00002	350.8	91.8
3C454.3	2350.48	UNIDENTIFIED	UNIND	1000.0	H	0.0	-1.00000	514.0	135.4
3C454.3	2374.46	ISMLG	Fe ii	2374.4	L	0.0	-0.00002	348.3	93.5
3C454.3	2382.79	ISMLG	Fe ii	2382.7	L	3.0	-0.00002	590.0	87.0
3C454.3	2586.65	ISMLG	Fe ii	2586.6	L	0.0	-0.00002	445.8	73.5
3C454.3	2600.14	ISMLG	Fe ii	2600.1	L	-3.0	-0.00002	522.4	71.2
3C454.3	2792.71	ISMLG	Mg ii	2796.3	L	-391.0	-0.00127	330.1	0.1
3C454.3	2793.39	ISMLG	Mg ii	2796.3	L	-318.0	-0.00106	344.4	0.1
3C454.3	2796.38	ISMLG	Mg ii	2796.3	L	2.0	-0.00002	490.0	0.1
3C454.3	2799.85	ISMLG	Mg ii	2803.5	L	-394.0	-0.00127	259.5	0.1
3C454.3	2800.57	ISMLG	Mg ii	2803.5	L	-317.0	-0.00106	114.9	0.1
3C454.3	2803.54	ISMLG	Mg ii	2803.5	L	1.0	-0.00002	591.3	0.1
3C454.3	2852.93	PROXIMATE	H i	2852.9	L	-3.0	-0.00002	726.5	80.4
3C48.0	1051.63	PROXIMATE	NeVIII	770.4	H	109434.0	0.36503	422.9	252.3
3C48.0	1065.17	PROXIMATE	NeVIII	780.3	H	109436.0	0.36503	239.2	209.2
3C48.0	1075.25	PROXIMATE	O iv	787.7	H	109433.0	0.36503	263.4	160.1
3C48.0	1076.08	INTRINSIC	O iv	787.7	H	109750.0	0.36608	568.8	201.7
3C48.0	1134.13	ISMLG	N i	1134.1	L	-9.0	-0.00002	194.9	46.3
3C48.0	1134.37	ISMLG	N i	1134.4	L	-12.0	-0.00002	134.0	50.3
3C48.0	1134.95	ISMLG	N i	1134.9	L	-8.0	-0.00002	170.6	53.7
3C48.0	1136.97	PROXIMATE	O iii	832.9	H	109432.0	0.36503	70.7	27.8
3C48.0	1138.05	INTRINSIC	O iii	832.9	H	109823.0	0.36632	185.3	29.8
3C48.0	1143.19	ISMLG	Fe ii	1143.2	L	-8.0	-0.00002	146.3	19.7
3C48.0	1144.90	ISMLG	Fe ii	1144.9	L	-11.0	-0.00002	265.6	20.0
3C48.0	1145.81	IGMABS	H i	919.3	H	73847.0	0.24636	55.3	14.5
3C48.0	1147.86	IGMABS	H i	920.9	H	73859.0	0.24636	54.6	15.8
3C48.0	1150.57	IGMABS	H i	923.1	H	73855.0	0.24636	71.6	16.5
3C48.0	1152.83	ISMLG	P ii	1152.8	L	3.0	-0.00002	156.6	17.1
3C48.0	1154.39	IGMABS	H i	926.2	H	73850.0	0.24636	84.2	15.0
3C48.0	1160.06	IGMABS	H i	930.7	H	73859.0	0.24636	139.4	21.5
3C48.0	1163.97	IGMABS	H i	1025.7	H	40406.0	0.13479	40.7	15.6
3C48.0	1164.90	IGMABS	H i	1025.7	H	40678.0	0.13568	108.8	19.3
3C48.0	1168.54	IGMABS	H i	937.8	H	73761.0	0.24607	109.5	14.7
3C48.0	1168.84	IGMABS	H i	937.8	H	73858.0	0.24636	136.2	13.7
3C48.0	1171.61	IGMABS	C iii	977.0	H	59710.0	0.19913	33.4	13.1
3C48.0	1171.91	IGMABS	C iii	977.0	H	59800.0	0.19951	155.1	17.5
3C48.0	1172.39	IGMABS	C iii	977.0	H	59949.0	0.20000	88.5	13.9
3C48.0	1183.43	IGMABS	H i	949.7	H	73766.0	0.24607	150.2	10.2
3C48.0	1183.72	IGMABS	H i	949.7	H	73857.0	0.24636	210.6	10.3
3C48.0	1186.25	IGMABS	H i	1025.7	H	46917.0	0.15650	143.6	14.8
3C48.0	1190.42	ISMLG	Si ii	1190.4	L	0.0	-0.00002	427.9	10.7

Table A1 continued

Table A1 (*continued*)

Target	λ_{obs}	Type	Ion	λ_{rest}	Frame	cz	z	W_{λ}	$\sigma_{W_{\lambda}}$
	(Å)			(Å)		(km s ⁻¹)		(mÅ)	(mÅ)
3C48.0	1190.88	IGMABS	H I	926.2	H	85660.0	0.28570	70.7	10.8
3C48.0	1192.54	IGMABS	H I	1025.7	H	48757.0	0.16265	69.7	12.0
3C48.0	1193.30	ISMLG	Si II	1193.2	L	1.0	-0.00002	405.7	11.6
3C48.0	1196.70	IGMABS	H I	930.7	H	85662.0	0.28570	62.3	12.7
3C48.0	1199.54	ISMLG	N I	1199.5	L	-3.0	-0.00002	333.3	34.7
3C48.0	1200.19	ISMLG	N I	1200.2	L	-7.0	-0.00002	285.0	24.5
3C48.0	1200.69	ISMLG	N I	1200.7	L	-6.0	-0.00002	305.9	29.4
3C48.0	1205.77	IGMABS	H I	937.8	H	85663.0	0.28570	146.4	10.3
3C48.0	1206.10	ISMLG	Si III	1206.5	L	-99.0	-0.00033	113.3	7.7
3C48.0	1206.47	ISMLG	Si III	1206.5	L	-6.0	-0.00002	390.0	6.0
3C48.0	1206.81	ISMLG	Si III	1206.5	L	77.0	0.00028	70.8	8.9
3C48.0	1207.79	IGMABS	C III	977.0	H	70810.0	0.23622	41.7	14.6
3C48.0	1211.82	IGMABS	H I	972.5	H	73762.0	0.24607	174.5	16.7
3C48.0	1212.11	IGMABS	H I	972.5	H	73852.0	0.24636	205.4	19.8
3C48.0	1221.10	IGMABS	H I	949.7	H	85655.0	0.28570	121.8	18.9
3C48.0	1229.97	IGMABS	H I	1025.7	H	59697.0	0.19913	40.9	9.3
3C48.0	1230.34	IGMABS	H I	1025.7	H	59805.0	0.19951	101.5	9.9
3C48.0	1230.82	IGMABS	H I	1025.7	H	59946.0	0.20000	56.5	9.6
3C48.0	1237.45	IGMABS	O VI	1031.9	H	59709.0	0.19913	87.6	10.3
3C48.0	1237.78	IGMABS	O VI	1031.9	H	59803.0	0.19951	261.8	10.3
3C48.0	1238.26	IGMABS	O VI	1031.9	H	59943.0	0.20000	85.9	11.2
3C48.0	1240.97	IGMABS	H I	1025.7	H	62912.0	0.20985	115.1	15.0
3C48.0	1244.23	IGMABS	O VI	1037.6	H	59695.0	0.19913	55.4	10.9
3C48.0	1244.60	IGMABS	O VI	1037.6	H	59803.0	0.19951	171.9	10.9
3C48.0	1245.10	IGMABS	O VI	1037.6	H	59947.0	0.20000	53.5	10.7
3C48.0	1248.43	PROXIMATE	H I	914.5	H	109435.0	0.36503	32.4	10.3
3C48.0	1248.91	PROXIMATE	H I	914.9	H	109439.0	0.36503	35.5	9.0
3C48.0	1249.47	PROXIMATE	H I	915.3	H	109438.0	0.36503	35.1	10.1
3C48.0	1250.14	PROXIMATE	H I	915.8	H	109437.0	0.36503	50.8	9.4
3C48.0	1250.44	IGMABS	H I	972.5	H	85665.0	0.28570	183.7	7.1
3C48.0	1250.57	ISMLG	S II	1250.5	L	-3.0	-0.00002	187.4	6.8
3C48.0	1250.97	PROXIMATE	H I	916.4	H	109437.0	0.36503	90.0	10.4
3C48.0	1252.00	PROXIMATE	H I	917.1	H	109441.0	0.36503	74.6	11.1
3C48.0	1253.31	PROXIMATE	H I	918.1	H	109445.0	0.36503	76.7	9.0
3C48.0	1253.81	ISMLG	S II	1253.8	L	1.0	-0.00002	227.5	8.2
3C48.0	1254.97	PROXIMATE	H I	919.3	H	109444.0	0.36503	100.7	10.8
3C48.0	1257.17	PROXIMATE	H I	920.9	H	109444.0	0.36503	100.2	10.6
3C48.0	1257.85	INTRINSIC	H I	920.9	H	109663.0	0.36580	86.6	8.2
3C48.0	1258.12	INTRINSIC	H I	920.9	H	109751.0	0.36608	90.6	7.4
3C48.0	1259.52	ISMLG	S II	1259.5	L	0.0	-0.00002	246.6	8.1
3C48.0	1260.15	PROXIMATE	H I	923.1	H	109439.0	0.36503	308.2	8.5
3C48.0	1260.38	ISMLG	Si II	1260.4	L	-10.0	-0.00002	506.4	4.9
3C48.0	1260.83	INTRINSIC	H I	923.1	H	109663.0	0.36580	132.7	7.0
3C48.0	1261.10	INTRINSIC	H I	923.1	H	109750.0	0.36608	89.4	9.8
3C48.0	1264.34	PROXIMATE	H I	926.2	H	109439.0	0.36503	183.9	10.8
3C48.0	1265.06	INTRINSIC	H I	926.2	H	109670.0	0.36580	188.7	12.7
3C48.0	1265.31	INTRINSIC	H I	926.2	H	109752.0	0.36608	54.6	7.8
3C48.0	1266.83	IGMABS	H I	949.7	H	100092.0	0.33385	45.5	11.1
3C48.0	1267.46	INTRINSIC	H I	926.2	H	110447.0	0.36838	72.6	11.6
3C48.0	1270.52	PROXIMATE	H I	930.7	H	109441.0	0.36503	242.6	9.4
3C48.0	1271.24	INTRINSIC	H I	930.7	H	109671.0	0.36580	192.6	9.2
3C48.0	1271.48	INTRINSIC	H I	930.7	H	109749.0	0.36608	109.0	7.6
3C48.0	1273.64	INTRINSIC	H I	930.7	H	110446.0	0.36838	73.3	11.3

Table A1 continued

Table A1 (*continued*)

Target	λ_{obs}	Type	Ion	λ_{rest}	Frame	cz	z	W_{λ}	$\sigma_{W_{\lambda}}$
	(Å)			(Å)		(km s ⁻¹)		(mÅ)	(mÅ)
3C48.0	1274.11	PROXIMATE	S VI	933.3	H	109440.0	0.36503	146.9	10.8
3C48.0	1274.80	INTRINSIC	S VI	933.3	H	109662.0	0.36580	210.3	12.4
3C48.0	1277.26	ISMLG	C I	1277.2	L	4.0	-0.00002	94.6	12.1
3C48.0	1278.12	IGMABS	H I	1025.7	H	73770.0	0.24607	296.4	8.0
3C48.0	1278.38	IGMABS	H I	1025.7	H	73845.0	0.24636	295.2	10.3
3C48.0	1280.15	PROXIMATE	H I	937.8	H	109438.0	0.36503	322.6	19.4
3C48.0	1280.86	INTRINSIC	H I	937.8	H	109665.0	0.36580	219.8	12.2
3C48.0	1281.12	INTRINSIC	H I	937.8	H	109749.0	0.36608	160.8	12.3
3C48.0	1281.34	INTRINSIC	H I	937.8	H	109821.0	0.36632	73.2	12.0
3C48.0	1283.30	INTRINSIC	H I	937.8	H	110446.0	0.36838	46.2	14.3
3C48.0	1289.32	PROXIMATE	S VI	944.5	H	109440.0	0.36503	114.0	15.0
3C48.0	1290.03	INTRINSIC	S VI	944.5	H	109663.0	0.36580	103.9	13.0
3C48.0	1290.27	IGMABS	H I	972.5	H	97943.0	0.32670	55.3	10.2
3C48.0	1293.65	IGMABS	H I	1215.6	H	19231.0	0.06415	445.2	12.7
3C48.0	1296.42	PROXIMATE	H I	949.7	H	109430.0	0.36503	377.3	9.8
3C48.0	1297.17	INTRINSIC	H I	949.7	H	109667.0	0.36580	338.2	6.8
3C48.0	1297.22	IGMABS	H I	972.5	H	100086.0	0.33385	222.0	8.5
3C48.0	1297.45	INTRINSIC	H I	949.7	H	109757.0	0.36608	226.6	5.3
3C48.0	1297.66	INTRINSIC	H I	949.7	H	109822.0	0.36632	142.6	7.3
3C48.0	1299.64	INTRINSIC	H I	949.7	H	110448.0	0.36838	146.7	10.0
3C48.0	1302.13	ISMLG	O I	1302.1	L	-10.0	-0.00002	382.9	25.6
3C48.0	1303.77	IGMABS	H I	1215.6	H	21727.0	0.07247	382.6	22.2
3C48.0	1304.32	ISMLG	Si II	1304.3	L	-11.0	-0.00002	368.0	24.2
3C48.0	1311.85	IGMABS	H I	1215.6	H	23720.0	0.07912	87.8	13.2
3C48.0	1317.22	ISMLG	Ni II	1317.2	L	2.0	-0.00002	63.5	14.7
3C48.0	1318.78	IGMABS	H I	1025.7	H	85654.0	0.28570	292.8	13.7
3C48.0	1323.70	IGMABS	H I	1215.6	H	26641.0	0.08886	85.6	16.2
3C48.0	1327.54	PROXIMATE	H I	972.5	H	109433.0	0.36503	420.9	14.5
3C48.0	1328.30	INTRINSIC	H I	972.5	H	109666.0	0.36580	387.7	9.4
3C48.0	1328.57	INTRINSIC	H I	972.5	H	109750.0	0.36608	426.8	8.6
3C48.0	1328.80	INTRINSIC	H I	972.5	H	109822.0	0.36632	241.9	10.4
3C48.0	1328.85	ISMLG	C I	1328.8	L	4.0	-0.00002	58.0	9.5
3C48.0	1330.80	INTRINSIC	H I	972.5	H	110438.0	0.36838	140.6	12.5
3C48.0	1332.04	IGMABS	H I	1025.7	H	89528.0	0.29861	59.2	10.2
3C48.0	1333.66	PROXIMATE	C III	977.0	H	109433.0	0.36503	332.2	10.5
3C48.0	1334.42	INTRINSIC	C III	977.0	H	109666.0	0.36580	390.1	3.5
3C48.0	1334.51	ISMLG	C II	1334.5	L	-5.0	-0.00002	496.0	5.9
3C48.0	1334.85	ISMLG	C II	1334.5	L	71.0	0.00028	69.5	7.1
3C48.0	1335.69	ISMLG	C II*	1335.7	L	-4.0	-0.00002	204.0	9.7
3C48.0	1336.94	INTRINSIC	C III	977.0	H	110440.0	0.36838	92.4	11.0
3C48.0	1351.13	PROXIMATE	N III	989.7	H	109441.0	0.36503	86.9	12.3
3C48.0	1351.87	INTRINSIC	N III	989.7	H	109664.0	0.36580	72.7	12.7
3C48.0	1353.53	IGMABS	H I	1215.6	H	33997.0	0.11340	123.9	12.2
3C48.0	1356.56	IGMABS	H I	1215.6	H	34744.0	0.11589	190.0	10.7
3C48.0	1360.81	IGMABS	H I	1025.7	H	97938.0	0.32670	84.1	7.2
3C48.0	1361.09	IGMABS	H I	1025.7	H	98021.0	0.32697	70.0	9.7
3C48.0	1368.13	IGMABS	H I	1025.7	H	100078.0	0.33385	214.7	11.1
3C48.0	1369.06	IGMABS	O VI	1031.9	H	97942.0	0.32670	95.3	7.3
3C48.0	1369.33	IGMABS	O VI	1031.9	H	98023.0	0.32697	59.4	9.4
3C48.0	1370.11	ISMLG	Ni II	1370.1	L	-4.0	-0.00002	70.7	11.3
3C48.0	1376.63	IGMABS	O VI	1037.6	H	97948.0	0.32670	97.0	10.0
3C48.0	1379.24	IGMABS	H I	1215.6	H	40336.0	0.13455	142.1	9.8
3C48.0	1379.53	IGMABS	H I	1215.6	H	40408.0	0.13479	359.4	15.4

Table A1 continued

Table A1 (*continued*)

Target	λ_{obs}	Type	Ion	λ_{rest}	Frame	cz	z	W_{λ}	$\sigma_{W_{\lambda}}$
	(Å)			(Å)		(km s ⁻¹)		(mÅ)	(mÅ)
3C48.0	1380.62	IGMABS	H I	1215.6	H	40677.0	0.13568	297.0	12.9
3C48.0	1384.41	IGMABS	H I	1025.7	H	104835.0	0.34968	106.7	14.0
3C48.0	1389.87	IGMABS	H I	1025.7	H	106431.0	0.35500	134.6	15.2
3C48.0	1392.74	IGMABS	H I	1215.6	H	43666.0	0.14565	180.6	12.2
3C48.0	1393.70	ISMLG	Si IV	1393.7	L	-13.0	-0.00002	156.2	11.3
3C48.0	1398.35	IGMABS	H I	1215.6	H	45051.0	0.15027	83.2	16.9
3C48.0	1400.14	PROXIMATE	H I	1025.7	H	109433.0	0.36503	562.1	10.8
3C48.0	1400.93	INTRINSIC	H I	1025.7	H	109663.0	0.36580	467.7	6.3
3C48.0	1401.22	INTRINSIC	H I	1025.7	H	109748.0	0.36608	559.3	8.9
3C48.0	1401.47	INTRINSIC	H I	1025.7	H	109822.0	0.36632	378.8	8.5
3C48.0	1402.73	ISMLG	Si IV	1402.7	L	-10.0	-0.00002	82.8	11.0
3C48.0	1403.58	INTRINSIC	H I	1025.7	H	110438.0	0.36838	161.7	12.0
3C48.0	1405.92	IGMABS	H I	1215.6	H	46917.0	0.15650	409.4	11.8
3C48.0	1408.61	PROXIMATE	O VI	1031.9	H	109432.0	0.36503	609.2	10.7
3C48.0	1409.39	INTRINSIC	O VI	1031.9	H	109661.0	0.36580	632.3	7.2
3C48.0	1409.69	INTRINSIC	O VI	1031.9	H	109748.0	0.36608	482.5	6.1
3C48.0	1409.95	INTRINSIC	O VI	1031.9	H	109824.0	0.36632	836.9	9.3
3C48.0	1412.08	INTRINSIC	O VI	1031.9	H	110440.0	0.36838	51.0	9.6
3C48.0	1413.40	IGMABS	H I	1215.6	H	48762.0	0.16265	155.1	11.5
3C48.0	1415.65	IGMABS	H I	1215.6	H	49317.0	0.16450	100.0	12.3
3C48.0	1416.37	PROXIMATE	O VI	1037.6	H	109431.0	0.36503	610.0	12.8
3C48.0	1417.18	INTRINSIC	O VI	1037.6	H	109664.0	0.36580	597.2	7.3
3C48.0	1417.47	INTRINSIC	O VI	1037.6	H	109748.0	0.36608	526.5	6.2
3C48.0	1417.71	INTRINSIC	O VI	1037.6	H	109817.0	0.36632	582.2	8.0
3C48.0	1419.87	INTRINSIC	O VI	1037.6	H	110443.0	0.36838	68.0	12.7
3C48.0	1431.10	IGMABS	H I	1215.6	H	53126.0	0.17721	145.3	18.7
3C48.0	1454.86	ISMLG	Ni II	1454.8	L	4.0	-0.00002	66.0	14.6
3C48.0	1457.75	IGMABS	H I	1215.6	H	59698.0	0.19913	123.1	24.1
3C48.0	1458.21	IGMABS	H I	1215.6	H	59813.0	0.19951	356.8	8.6
3C48.0	1458.80	IGMABS	H I	1215.6	H	59958.0	0.20000	240.8	9.0
3C48.0	1467.11	IGMABS	H I	1215.6	H	62007.0	0.20683	87.9	17.0
3C48.0	1470.78	IGMABS	H I	1215.6	H	62912.0	0.20985	88.0	17.5
3C48.0	1477.60	IGMABS	H I	1215.6	H	64594.0	0.21546	54.1	15.8
3C48.0	1486.66	IGMABS	H I	1215.6	H	66827.0	0.22291	87.6	20.7
3C48.0	1490.84	IGMABS	H I	1215.6	H	67859.0	0.22635	122.8	16.2
3C48.0	1493.68	IGMABS	H I	1215.6	H	68558.0	0.22869	135.8	18.7
3C48.0	1502.13	ISMLG	Ni II	1502.1	L	-4.0	-0.00002	38.6	13.4
3C48.0	1502.83	IGMABS	H I	1215.6	H	70817.0	0.23622	133.4	17.7
3C48.0	1514.20	IGMABS	H I	1215.6	H	73620.0	0.24557	75.5	17.7
3C48.0	1514.81	IGMABS	H I	1215.6	H	73769.0	0.24607	574.6	10.4
3C48.0	1515.16	IGMABS	H I	1215.6	H	73857.0	0.24636	613.8	8.9
3C48.0	1519.04	IGMABS	H I	1215.6	H	74814.0	0.24955	100.8	17.7
3C48.0	1526.69	ISMLG	Si II	1526.7	L	-4.0	-0.00002	434.3	11.1
3C48.0	1538.35	IGMABS	H I	1215.6	H	79576.0	0.26544	31.4	14.7
3C48.0	1545.44	IGMABS	H I	1215.6	H	81324.0	0.27127	80.1	17.1
3C48.0	1548.17	ISMLG	C IV	1548.2	L	-8.0	-0.00002	230.7	17.3
3C48.0	1549.00	IGMABS	H I	1215.6	H	82201.0	0.27419	86.5	16.1
3C48.0	1550.72	ISMLG	C IV	1550.7	L	-12.0	-0.00002	129.9	19.3
3C48.0	1556.90	IGMABS	H I	1215.6	H	84150.0	0.28069	145.8	17.3
3C48.0	1560.31	ISMLG	C I	1560.3	L	0.0	-0.00002	76.1	17.3
3C48.0	1562.99	IGMABS	H I	1215.6	H	85651.0	0.28570	429.7	14.3
3C48.0	1563.64	IGMABS	H I	1215.6	H	85811.0	0.28623	152.4	20.7
3C48.0	1578.68	IGMABS	H I	1215.6	H	89521.0	0.29861	263.1	37.4

Table A1 continued

Table A1 (*continued*)

Target	λ_{obs}	Type	Ion	λ_{rest}	Frame	cz	z	W_{λ}	$\sigma_{W_{\lambda}}$
	(Å)			(Å)		(km s ⁻¹)		(mÅ)	(mÅ)
3C48.0	1583.96	IGMABS	H I	1215.6	H	90824.0	0.30296	161.7	38.9
3C48.0	1608.39	ISMLG	Fe II	1608.4	L	-12.0	-0.00002	407.9	34.5
3C48.0	1612.83	IGMABS	H I	1215.6	H	97942.0	0.32670	309.2	32.1
3C48.0	1613.16	IGMABS	H I	1215.6	H	98024.0	0.32697	335.7	30.6
3C48.0	1621.53	IGMABS	H I	1215.6	H	100087.0	0.33385	424.0	42.2
3C48.0	1640.76	IGMABS	H I	1215.6	H	104831.0	0.34968	483.4	18.1
3C48.0	1643.58	IGMABS	N V	1238.8	H	97950.0	0.32670	39.9	17.6
3C48.0	1647.23	IGMABS	H I	1215.6	H	106427.0	0.35500	624.9	22.9
3C48.0	1648.84	IGMABS	N V	1242.8	H	97945.0	0.32670	58.1	12.0
3C48.0	1654.82	PROXIMATE	H I	1215.6	H	108299.0	0.36125	200.9	22.3
3C48.0	1656.92	ISMLG	C I	1656.9	L	-2.0	-0.00002	110.8	16.0
3C48.0	1659.43	PROXIMATE	H I	1215.6	H	109434.0	0.36503	627.9	16.2
3C48.0	1660.36	INTRINSIC	H I	1215.6	H	109664.0	0.36580	566.0	10.3
3C48.0	1660.70	INTRINSIC	H I	1215.6	H	109748.0	0.36608	252.0	8.3
3C48.0	1660.99	INTRINSIC	H I	1215.6	H	109819.0	0.36632	440.5	11.3
3C48.0	1663.20	INTRINSIC	H I	1215.6	H	110363.0	0.36813	125.2	8.8
3C48.0	1663.50	INTRINSIC	H I	1215.6	H	110438.0	0.36838	148.7	11.3
3C48.0	1670.72	ISMLG	Al II	1670.7	L	-12.0	-0.00002	510.2	18.1
3C48.0	1680.14	OTHER	FPN	0.0	H	0.0	-1.00000	28.4	18.4
3C48.0	1683.55	OTHER	FPN	0.0	H	0.0	-1.00000	59.1	21.6
3C48.0	1691.01	PROXIMATE	N V	1238.8	H	109429.0	0.36503	463.4	23.9
3C48.0	1691.99	INTRINSIC	N V	1238.8	H	109667.0	0.36580	1065.0	27.6
3C48.0	1696.46	PROXIMATE	N V	1242.8	H	109432.0	0.36503	375.8	27.2
3C48.0	1697.44	INTRINSIC	N V	1242.8	H	109668.0	0.36580	781.3	23.9
3C48.0	1709.55	ISMLG	Ni II	1709.6	L	-10.0	-0.00002	94.7	29.8
3C48.0	1741.52	ISMLG	Ni II	1741.5	L	-6.0	-0.00002	100.5	42.2
3C48.0	1751.86	ISMLG	Ni II	1751.9	L	-10.0	-0.00002	67.6	36.5
3C48.0	2113.31	PROXIMATE	C IV	1548.2	H	109427.0	0.36503	600.5	218.3
3C48.0	2114.56	INTRINSIC	C IV	1548.2	H	109668.0	0.36580	1173.3	148.6
3C48.0	2116.85	PROXIMATE	C IV	1550.7	H	109432.0	0.36503	524.0	197.8
3C48.0	2118.04	INTRINSIC	C IV	1550.7	H	109661.0	0.36580	873.2	269.7
3C48.0	2118.52	INTRINSIC	C IV	1548.2	H	110436.0	0.36838	462.7	164.9
3C48.0	2122.03	INTRINSIC	H I	1550.7	H	110432.0	0.36838	74.6	190.8
3C66A	1142.37	ISMLG	Fe II	1142.3	L	2.0	-0.00003	93.8	19.5
3C66A	1143.24	ISMLG	Fe II	1143.2	L	3.0	-0.00003	229.2	20.8
3C66A	1144.90	ISMLG	Fe II	1144.9	L	-10.0	-0.00003	258.2	11.5
3C66A	1152.83	ISMLG	P II	1152.8	L	2.0	-0.00003	153.9	12.6
3C66A	1157.92	ISMLG	C I	1157.9	L	3.0	-0.00003	44.8	9.4
3C66A	1181.26	IGMABS	H I	1025.7	H	45461.0	0.15162	65.7	6.5
3C66A	1181.48	IGMABS	H I	1025.7	H	45525.0	0.15187	80.4	7.9
3C66A	1188.37	IGMABS	O VI	1031.9	H	45450.0	0.15162	31.2	7.8
3C66A	1188.82	ISMLG	C I	1188.8	L	-4.0	-0.00003	33.6	6.4
3C66A	1190.00	ISMLG	Si II	1190.4	L	-105.0	-0.00035	88.4	5.7
3C66A	1190.36	ISMLG	Si II	1190.4	L	-13.0	-0.00003	381.0	4.4
3C66A	1192.89	ISMLG	Si II	1193.2	L	-100.0	-0.00035	73.8	5.9
3C66A	1193.24	ISMLG	Si II	1193.2	L	-13.0	-0.00003	423.1	4.8
3C66A	1193.99	ISMLG	C I	1193.9	L	0.0	-0.00003	14.2	6.3
3C66A	1194.88	IGMABS	H I	972.5	H	68538.0	0.22859	44.6	7.6
3C66A	1197.19	ISMLG	Mn II	1197.1	L	2.0	-0.00003	57.5	7.5
3C66A	1199.52	ISMLG	N I	1199.5	L	-8.0	-0.00003	342.5	5.8
3C66A	1200.19	ISMLG	N I	1200.2	L	-8.0	-0.00003	325.0	5.7
3C66A	1200.68	ISMLG	N I	1200.7	L	-8.0	-0.00003	315.8	5.7
3C66A	1201.09	ISMLG	Mn II	1201.1	L	-6.0	-0.00003	55.8	7.6

Table A1 continued

Table A1 (*continued*)

Target	λ_{obs}	Type	Ion	λ_{rest}	Frame	cz	z	W_{λ}	$\sigma_{W_{\lambda}}$
	(Å)			(Å)		(km s ⁻¹)		(mÅ)	(mÅ)
3C66A	1205.45	IGMABS	H I	1025.7	H	52531.0	0.17519	63.7	7.6
3C66A	1205.88	IGMABS	H I	1025.7	H	52657.0	0.17562	140.5	7.5
3C66A	1206.08	ISMLG	Si III	1206.5	L	-105.0	-0.00035	117.8	5.4
3C66A	1206.45	ISMLG	Si III	1206.5	L	-11.0	-0.00003	501.0	6.0
3C66A	1208.09	IGMABS	H I	972.5	H	72612.0	0.24226	53.0	12.7
3C66A	1208.78	IGMABS	Si III	1206.5	H	566.0	0.00190	83.6	9.1
3C66A	1233.11	IGMABS	H I	1215.6	H	4301.0	0.01435	30.5	6.7
3C66A	1239.90	ISMLG	Mg II	1239.9	L	-6.0	-0.00003	45.9	5.4
3C66A	1240.38	ISMLG	Mg II	1240.3	L	-4.0	-0.00003	26.5	5.4
3C66A	1248.87	IGMABS	H I	1215.6	H	8188.0	0.02731	112.5	5.8
3C66A	1250.55	ISMLG	S II	1250.5	L	-7.0	-0.00003	219.9	5.3
3C66A	1253.77	ISMLG	S II	1253.8	L	-9.0	-0.00003	257.6	4.8
3C66A	1259.46	ISMLG	S II	1259.5	L	-14.0	-0.00003	269.6	4.4
3C66A	1259.98	ISMLG	Si II	1260.4	L	-105.0	-0.00035	126.3	4.6
3C66A	1260.38	ISMLG	Si II	1260.4	L	-10.0	-0.00003	459.7	2.9
3C66A	1260.74	ISMLG	C I	1260.7	L	1.0	-0.00003	91.8	4.1
3C66A	1266.28	IGMABS	H I	949.7	H	99917.0	0.33327	21.5	6.2
3C66A	1267.43	IGMABS	H I	1215.6	H	12765.0	0.04258	71.1	5.2
3C66A	1269.44	IGMABS	H I	1215.6	H	13259.0	0.04423	90.0	6.6
3C66A	1274.17	IGMABS	H I	1025.7	H	72614.0	0.24226	85.3	6.3
3C66A	1274.59	IGMABS	H I	1025.7	H	72737.0	0.24264	58.1	5.1
3C66A	1277.23	ISMLG	C I	1277.2	L	-3.0	-0.00003	126.0	5.7
3C66A	1278.00	IGMABS	H I	1215.6	H	15371.0	0.05127	288.7	5.9
3C66A	1278.27	IGMABS	H I	1215.6	H	15437.0	0.05149	199.3	5.9
3C66A	1280.15	ISMLG	C I	1280.1	L	3.0	-0.00003	51.4	4.6
3C66A	1280.63	IGMABS	H I	1215.6	H	16021.0	0.05344	91.4	7.0
3C66A	1282.28	IGMABS	O VI	1031.9	H	72732.0	0.24264	165.0	7.8
3C66A	1283.82	IGMABS	H I	1215.6	H	16806.0	0.05606	27.1	6.1
3C66A	1285.38	IGMABS	H I	1215.6	H	17191.0	0.05734	21.4	6.9
3C66A	1287.81	IGMABS	Si III	1206.5	H	20203.0	0.06735	91.4	7.5
3C66A	1289.34	IGMABS	O VI	1037.6	H	72729.0	0.24264	106.3	7.0
3C66A	1291.80	IGMABS	H I	972.5	H	98414.0	0.32830	52.7	8.2
3C66A	1293.61	IGMABS	H I	1215.6	H	19221.0	0.06412	51.6	8.6
3C66A	1296.63	IGMABS	H I	972.5	H	99905.0	0.33327	51.2	8.2
3C66A	1297.28	IGMABS	H I	1215.6	H	20125.0	0.06713	154.4	5.5
3C66A	1297.54	IGMABS	H I	1215.6	H	20190.0	0.06735	471.8	3.3
3C66A	1298.03	IGMABS	H I	1215.6	H	20311.0	0.06775	354.0	5.5
3C66A	1301.72	ISMLG	O I	1302.1	L	-104.0	-0.00035	71.5	5.9
3C66A	1302.14	ISMLG	O I	1302.1	L	-7.0	-0.00003	359.4	4.4
3C66A	1303.89	ISMLG	Si II	1304.3	L	-111.0	-0.00035	102.2	4.9
3C66A	1304.31	ISMLG	Si II	1304.3	L	-15.0	-0.00003	365.0	4.5
3C66A	1312.62	IGMABS	H I	1215.6	H	23909.0	0.07975	164.1	6.6
3C66A	1317.17	ISMLG	Ni II	1317.2	L	-10.0	-0.00003	81.9	7.9
3C66A	1323.53	IGMABS	H I	1215.6	H	26600.0	0.08873	408.1	8.7
3C66A	1328.83	ISMLG	C I	1328.8	L	0.0	-0.00003	76.2	6.3
3C66A	1329.08	ISMLG	C I*	1329.0	L	-2.0	-0.00003	29.8	5.8
3C66A	1334.08	ISMLG	C II	1334.5	L	-102.0	-0.00035	183.8	4.6
3C66A	1334.47	ISMLG	C II	1334.5	L	-13.0	-0.00003	464.3	3.7
3C66A	1335.66	ISMLG	C II*	1335.7	L	-10.0	-0.00003	318.2	6.1
3C66A	1337.06	IGMABS	C II	1334.5	H	569.0	0.00190	19.9	5.2
3C66A	1347.25	ISMLG	Cl I	1347.2	L	2.0	-0.00003	55.2	5.1
3C66A	1356.08	IGMABS	H I	1215.6	H	34627.0	0.11550	379.3	8.5
3C66A	1361.90	IGMABS	H I	1215.6	H	36061.0	0.12029	55.4	7.3

Table A1 continued

Table A1 (*continued*)

Target	λ_{obs}	Type	Ion	λ_{rest}	Frame	cz	z	W_{λ}	$\sigma_{W_{\lambda}}$
	(Å)			(Å)		(km s ⁻¹)		(mÅ)	(mÅ)
3C66A	1362.48	IGMABS	H I	1025.7	H	98426.0	0.32830	164.4	8.5
3C66A	1365.53	IGMABS	H I	1215.6	H	36956.0	0.12327	28.7	6.6
3C66A	1367.56	IGMABS	H I	1025.7	H	99912.0	0.33327	134.4	7.6
3C66A	1369.09	IGMABS	H I	1025.7	H	100356.0	0.33474	30.2	5.5
3C66A	1370.09	ISMLG	Ni II	1370.1	L	-9.0	-0.00003	84.2	5.9
3C66A	1370.71	IGMABS	O VI	1031.9	H	98423.0	0.32830	49.6	8.3
3C66A	1374.32	IGMABS	H I	1215.6	H	39125.0	0.13051	56.7	6.7
3C66A	1388.19	IGMABS	H I	1215.6	H	42545.0	0.14191	92.7	8.6
3C66A	1393.71	ISMLG	Si IV	1393.7	L	-12.0	-0.00003	132.3	7.5
3C66A	1399.99	IGMABS	H I	1215.6	H	45456.0	0.15162	271.4	5.8
3C66A	1400.30	IGMABS	H I	1215.6	H	45530.0	0.15187	277.1	3.3
3C66A	1400.74	IGMABS	H I	1215.6	H	45639.0	0.15224	130.9	7.5
3C66A	1402.70	ISMLG	Si IV	1402.7	L	-15.0	-0.00003	86.1	9.9
3C66A	1413.11	IGMABS	H I	1215.6	H	48689.0	0.16241	106.1	8.8
3C66A	1421.82	IGMABS	H I	1215.6	H	50838.0	0.16958	64.7	8.0
3C66A	1424.43	IGMABS	C II	1334.5	H	20195.0	0.06735	29.4	6.7
3C66A	1428.65	IGMABS	H I	1215.6	H	52522.0	0.17519	158.1	7.2
3C66A	1429.17	IGMABS	H I	1215.6	H	52650.0	0.17562	453.6	8.0
3C66A	1445.95	IGMABS	H I	1215.6	H	56788.0	0.18942	95.4	12.7
3C66A	1454.81	ISMLG	Ni II	1454.8	L	-6.0	-0.00003	55.1	7.6
3C66A	1493.11	IGMABS	H I	1215.6	H	68418.0	0.22822	63.3	8.8
3C66A	1493.56	IGMABS	H I	1215.6	H	68530.0	0.22859	159.2	11.2
3C66A	1500.24	IGMABS	H I	1215.6	H	70176.0	0.23408	98.1	11.0
3C66A	1510.17	IGMABS	H I	1215.6	H	72627.0	0.24226	427.9	9.7
3C66A	1510.64	IGMABS	H I	1215.6	H	72740.0	0.24264	239.3	7.6
3C66A	1526.67	ISMLG	Si II	1526.7	L	-7.0	-0.00003	491.2	9.9
3C66A	1533.26	IGMABS	H I	1215.6	H	78320.0	0.26125	154.6	12.9
3C66A	1547.66	ISMLG	C IV	1548.2	L	-105.0	-0.00035	58.2	11.8
3C66A	1548.12	ISMLG	C IV	1548.2	L	-15.0	-0.00003	176.7	12.0
3C66A	1550.24	ISMLG	C IV	1550.7	L	-104.0	-0.00035	39.4	11.7
3C66A	1550.79	ISMLG	C IV	1550.7	L	3.0	-0.00003	180.9	13.6
3C66A	1551.14	IGMABS	C IV	1548.2	H	568.0	0.00190	157.9	9.3
3C66A	1553.73	IGMABS	C IV	1550.7	H	571.0	0.00190	112.2	13.1
3C66A	1560.33	ISMLG	C I	1560.3	L	4.0	-0.00003	149.4	12.9
3C66A	1560.69	ISMLG	C I*	1560.7	L	-4.0	-0.00003	58.6	14.6
3C66A	1571.49	IGMABS	H I	1215.6	H	87748.0	0.29270	106.5	18.8
3C66A	1579.21	IGMABS	H I	1215.6	H	89651.0	0.29904	54.4	11.0
3C66A	1581.12	IGMABS	H I	1215.6	H	90122.0	0.30061	254.1	10.0
3C66A	1581.62	IGMABS	H I	1215.6	H	90246.0	0.30103	204.4	12.9
3C66A	1608.38	ISMLG	Fe II	1608.4	L	-14.0	-0.00003	436.7	13.2
3C66A	1614.77	IGMABS	H I	1215.6	H	98421.0	0.32830	548.9	22.6
3C66A	1620.82	IGMABS	H I	1215.6	H	99913.0	0.33327	466.3	20.7
3C66A	1622.60	IGMABS	H I	1215.6	H	100352.0	0.33474	231.7	20.6
3C66A	1656.93	ISMLG	C I	1656.9	L	1.0	-0.00003	173.4	17.1
3C66A	1670.71	ISMLG	Al II	1670.7	L	-13.0	-0.00003	521.9	16.8
3C66A	1709.60	ISMLG	Ni II	1709.6	L	0.0	-0.00003	71.4	18.7
3C66A	1741.48	ISMLG	Ni II	1741.5	L	-12.0	-0.00003	97.0	21.1
3C66A	1751.90	ISMLG	Ni II	1751.9	L	-3.0	-0.00003	80.7	27.4
3C66A	2026.39	ISMLG	Mg I	2026.4	L	-13.0	-0.00003	409.0	27.4
3C66A	2795.41	ISMLG	Mg II	2796.3	L	-101.0	-0.00035	378.8	2.3
3C66A	2796.35	ISMLG	Mg II	2796.3	L	0.0	-0.00003	721.9	2.4
3C66A	2802.58	ISMLG	Mg II	2803.5	L	-102.0	-0.00035	299.6	2.9
3C66A	2803.49	PROXIMATE	H I	2803.5	L	-4.0	-0.00003	868.2	2.2

Table A1 continued

Table A1 (*continued*)

Target	λ_{obs}	Type	Ion	λ_{rest}	Frame	cz	z	W_{λ}	$\sigma_{W_{\lambda}}$
	(Å)			(Å)		(km s ⁻¹)		(mÅ)	(mÅ)
4C25.01	1134.94	ISMLG	N I	1134.9	L	-11.0	-0.00004	306.5	79.8
4C25.01	1143.21	ISMLG	Fe II	1143.2	L	-5.0	-0.00004	193.8	21.4
4C25.01	1144.89	ISMLG	Fe II	1144.9	L	-13.0	-0.00004	232.1	21.6
4C25.01	1152.78	ISMLG	P II	1152.8	L	-9.0	-0.00004	95.5	17.5
4C25.01	1159.40	INTRINSIC	C II	903.6	H	84858.0	0.28303	96.3	22.3
4C25.01	1159.83	INTRINSIC	C II	903.9	H	84856.0	0.28303	87.4	16.9
4C25.01	1160.05	INTRINSIC	C II*	904.1	H	84854.0	0.28303	105.0	15.9
4C25.01	1160.49	INTRINSIC	C II*	904.4	H	84857.0	0.28303	70.5	13.9
4C25.01	1169.18	IGMABS	H I	1025.7	H	41929.0	0.13988	77.4	24.2
4C25.01	1172.45	INTRINSIC	H I	913.8	H	84844.0	0.28303	36.9	12.9
4C25.01	1172.73	INTRINSIC	H I	914.0	H	84847.0	0.28303	31.3	12.1
4C25.01	1173.03	INTRINSIC	H I	914.2	H	84841.0	0.28303	28.6	11.1
4C25.01	1173.44	INTRINSIC	H I	914.5	H	84855.0	0.28303	80.3	14.4
4C25.01	1173.88	INTRINSIC	H I	914.9	H	84854.0	0.28303	97.0	13.5
4C25.01	1174.40	INTRINSIC	H I	915.3	H	84851.0	0.28303	133.8	12.4
4C25.01	1175.05	INTRINSIC	H I	915.8	H	84858.0	0.28303	178.0	13.2
4C25.01	1175.81	INTRINSIC	H I	916.4	H	84851.0	0.28303	124.0	11.7
4C25.01	1176.78	INTRINSIC	H I	917.1	H	84854.0	0.28303	186.8	12.0
4C25.01	1178.01	INTRINSIC	H I	918.1	H	84856.0	0.28303	165.5	13.0
4C25.01	1179.55	INTRINSIC	H I	919.3	H	84850.0	0.28303	195.1	13.3
4C25.01	1181.63	INTRINSIC	H I	920.9	H	84853.0	0.28303	218.1	11.4
4C25.01	1184.45	INTRINSIC	H I	923.1	H	84856.0	0.28303	233.5	13.9
4C25.01	1188.37	INTRINSIC	H I	926.2	H	84848.0	0.28303	242.7	13.3
4C25.01	1189.98	ISMLG	Si II	1190.4	L	-108.0	-0.00035	80.0	8.0
4C25.01	1190.36	ISMLG	Si II	1190.4	L	-14.0	-0.00004	410.3	6.5
4C25.01	1190.67	ISMLG	Si II	1190.4	L	64.0	0.00022	49.5	7.1
4C25.01	1192.85	ISMLG	Si II	1193.2	L	-110.0	-0.00035	107.8	7.3
4C25.01	1193.23	ISMLG	Si II	1193.2	L	-14.0	-0.00004	424.7	5.7
4C25.01	1193.56	ISMLG	Si II	1193.2	L	68.0	0.00022	86.8	7.4
4C25.01	1194.18	INTRINSIC	H I	930.7	H	84849.0	0.28303	283.5	16.7
4C25.01	1197.08	INTRINSIC	S VI	933.3	H	84700.0	0.28250	32.1	8.1
4C25.01	1197.56	INTRINSIC	S VI	933.3	H	84854.0	0.28303	200.8	8.6
4C25.01	1199.50	ISMLG	N I	1199.5	L	-13.0	-0.00004	314.8	11.6
4C25.01	1199.81	ISMLG	N I	1199.5	L	65.0	0.00022	42.0	10.4
4C25.01	1200.18	ISMLG	N I	1200.2	L	-12.0	-0.00004	283.9	12.5
4C25.01	1200.65	ISMLG	N I	1200.7	L	-15.0	-0.00004	263.2	14.4
4C25.01	1203.22	INTRINSIC	H I	937.8	H	84846.0	0.28303	298.5	13.1
4C25.01	1205.02	ISMLG	Si III	1206.5	L	-369.0	-0.00123	34.9	8.1
4C25.01	1205.23	ISMLG	Si III	1206.5	L	-315.0	-0.00105	42.3	6.8
4C25.01	1205.63	ISMLG	Si III	1206.5	L	-217.0	-0.00072	27.9	8.0
4C25.01	1205.85	ISMLG	Si III	1206.5	L	-162.0	-0.00055	40.5	6.4
4C25.01	1206.06	ISMLG	Si III	1206.5	L	-109.0	-0.00035	143.4	6.0
4C25.01	1206.43	ISMLG	Si III	1206.5	L	-18.0	-0.00004	459.4	4.8
4C25.01	1206.78	ISMLG	Si III	1206.5	L	70.0	0.00022	114.9	6.5
4C25.01	1211.86	INTRINSIC	S VI	944.5	H	84852.0	0.28303	129.1	22.8
4C25.01	1218.54	INTRINSIC	H I	949.7	H	84848.0	0.28303	301.0	28.2
4C25.01	1219.71	IGMABS	H I	1215.6	H	996.0	0.00332	115.4	15.9
4C25.01	1232.74	IGMABS	H I	1025.7	H	60507.0	0.20187	99.2	11.9
4C25.01	1239.89	ISMLG	Mg II	1239.9	L	-8.0	-0.00004	23.7	7.8
4C25.01	1242.75	IGMABS	H I	1025.7	H	63432.0	0.21157	52.0	10.9
4C25.01	1247.26	INTRINSIC	H I	972.5	H	84686.0	0.28250	44.7	6.7
4C25.01	1247.77	INTRINSIC	H I	972.5	H	84844.0	0.28303	322.9	6.2
4C25.01	1248.09	INTRINSIC	H I	972.5	H	84943.0	0.28335	80.2	6.5

Table A1 continued

Table A1 (*continued*)

Target	λ_{obs}	Type	Ion	λ_{rest}	Frame	cz	z	W_{λ}	$\sigma_{W_{\lambda}}$
	(Å)			(Å)		(km s ⁻¹)		(mÅ)	(mÅ)
4C25.01	1248.66	INTRINSIC	H I	972.5	H	85118.0	0.28393	42.9	8.1
4C25.01	1250.54	ISMLG	S II	1250.5	L	-9.0	-0.00004	112.9	9.2
4C25.01	1253.01	INTRINSIC	C III	977.0	H	84686.0	0.28250	197.8	8.4
4C25.01	1253.52	INTRINSIC	C III	977.0	H	84842.0	0.28303	344.7	5.5
4C25.01	1253.79	ISMLG	S II	1253.8	L	-5.0	-0.00004	191.0	3.9
4C25.01	1253.85	INTRINSIC	C III	977.0	H	84944.0	0.28335	185.7	6.7
4C25.01	1253.99	IGMABS	H I	1215.6	H	9450.0	0.03152	101.0	5.5
4C25.01	1254.41	INTRINSIC	C III	977.0	H	85116.0	0.28393	164.1	8.2
4C25.01	1259.45	ISMLG	S II	1259.5	L	-15.0	-0.00004	177.7	7.1
4C25.01	1259.70	ISMLG	Si II	1260.4	L	-172.0	-0.00055	50.6	5.2
4C25.01	1260.00	ISMLG	Si II	1260.4	L	-101.0	-0.00035	152.6	5.0
4C25.01	1260.35	ISMLG	Si II	1260.4	L	-16.0	-0.00004	465.1	3.6
4C25.01	1260.71	ISMLG	Si II	1260.4	L	68.0	0.00022	93.0	5.5
4C25.01	1269.93	INTRINSIC	N III	989.7	H	84848.0	0.28303	225.8	7.0
4C25.01	1270.26	INTRINSIC	N III	989.7	H	84948.0	0.28335	43.4	8.0
4C25.01	1272.20	IGMABS	H I	1215.6	H	13940.0	0.04650	145.2	8.1
4C25.01	1275.80	IGMABS	H I	1215.6	H	14829.0	0.04946	179.3	16.8
4C25.01	1277.23	ISMLG	C I	1277.2	L	-3.0	-0.00004	36.3	9.0
4C25.01	1282.22	IGMABS	H I	1025.7	H	74967.0	0.25009	122.3	16.6
4C25.01	1291.85	IGMABS	H I	1025.7	H	77782.0	0.25944	81.7	12.0
4C25.01	1293.89	IGMABS	H I	1215.6	H	19288.0	0.06434	126.5	17.6
4C25.01	1299.05	IGMABS	H I	1215.6	H	20561.0	0.06859	120.8	13.5
4C25.01	1301.72	ISMLG	O I	1302.1	L	-103.0	-0.00035	80.6	8.0
4C25.01	1302.10	ISMLG	O I	1302.1	L	-15.0	-0.00004	418.8	7.8
4C25.01	1302.43	ISMLG	O I	1302.1	L	60.0	0.00022	54.4	7.7
4C25.01	1303.92	ISMLG	Si II	1304.3	L	-104.0	-0.00035	49.4	9.8
4C25.01	1304.30	ISMLG	Si II	1304.3	L	-17.0	-0.00004	372.2	7.9
4C25.01	1304.67	ISMLG	Si II	1304.3	L	68.0	0.00022	47.1	9.4
4C25.01	1314.26	PROXIMATE	H I	1025.7	H	84333.0	0.28129	35.6	10.8
4C25.01	1315.47	INTRINSIC	H I	1025.7	H	84686.0	0.28250	135.4	10.7
4C25.01	1316.04	INTRINSIC	H I	1025.7	H	84852.0	0.28303	423.3	7.6
4C25.01	1316.37	INTRINSIC	H I	1025.7	H	84950.0	0.28335	148.7	7.8
4C25.01	1316.97	INTRINSIC	H I	1025.7	H	85125.0	0.28393	111.5	8.8
4C25.01	1317.14	ISMLG	Ni II	1317.2	L	-17.0	-0.00004	60.6	9.3
4C25.01	1318.36	IGMABS	H I	1215.6	H	25325.0	0.08448	59.3	11.0
4C25.01	1323.45	INTRINSIC	O VI	1031.9	H	84694.0	0.28250	380.5	8.3
4C25.01	1323.99	INTRINSIC	O VI	1031.9	H	84849.0	0.28303	442.9	6.5
4C25.01	1324.33	INTRINSIC	O VI	1031.9	H	84949.0	0.28335	248.3	7.8
4C25.01	1324.92	INTRINSIC	O VI	1031.9	H	85121.0	0.28393	200.0	10.6
4C25.01	1328.81	ISMLG	C I	1328.8	L	-5.0	-0.00004	32.1	8.8
4C25.01	1329.64	INTRINSIC	C II	1036.3	H	84846.0	0.28303	87.3	9.0
4C25.01	1330.51	INTRINSIC	C II*	1037.0	H	84846.0	0.28303	81.7	5.9
4C25.01	1330.74	INTRINSIC	O VI	1037.6	H	84692.0	0.28250	345.1	7.8
4C25.01	1331.26	INTRINSIC	O VI	1037.6	H	84841.0	0.28303	418.1	7.7
4C25.01	1331.64	INTRINSIC	O VI	1037.6	H	84950.0	0.28335	165.2	8.1
4C25.01	1332.22	INTRINSIC	O VI	1037.6	H	85118.0	0.28393	128.9	11.2
4C25.01	1333.79	ISMLG	C II	1334.5	L	-166.0	-0.00055	57.3	6.3
4C25.01	1334.08	ISMLG	C II	1334.5	L	-102.0	-0.00035	185.4	4.5
4C25.01	1334.47	ISMLG	C II	1334.5	L	-14.0	-0.00004	454.6	3.3
4C25.01	1334.83	ISMLG	C II	1334.5	L	66.0	0.00022	133.3	5.7
4C25.01	1335.68	ISMLG	C II*	1335.7	L	-6.0	-0.00004	133.2	8.9
4C25.01	1338.62	IGMABS	H I	1215.6	H	30321.0	0.10114	50.8	8.1
4C25.01	1358.54	IGMABS	H I	1215.6	H	35232.0	0.11752	66.0	10.9

Table A1 continued

Table A1 (*continued*)

Target	λ_{obs}	Type	Ion	λ_{rest}	Frame	cz	z	W_{λ}	$\sigma_{W_{\lambda}}$
	(Å)			(Å)		(km s ⁻¹)		(mÅ)	(mÅ)
4C25.01	1363.58	IGMABS	H I	1215.6	H	36475.0	0.12167	390.1	8.0
4C25.01	1363.86	IGMABS	H I	1215.6	H	36545.0	0.12190	456.0	7.7
4C25.01	1364.41	IGMABS	H I	1215.6	H	36681.0	0.12235	232.6	10.7
4C25.01	1366.98	IGMABS	H I	1215.6	H	37313.0	0.12446	198.0	10.0
4C25.01	1368.30	IGMABS	H I	1215.6	H	37639.0	0.12555	76.7	12.0
4C25.01	1369.96	IGMABS	H I	1215.6	H	38048.0	0.12691	135.3	17.3
4C25.01	1380.79	IGMABS	H I	1215.6	H	40719.0	0.13582	44.0	10.1
4C25.01	1385.72	IGMABS	H I	1215.6	H	41934.0	0.13988	247.8	16.6
4C25.01	1393.30	ISMLG	Si IV	1393.7	L	-100.0	-0.00035	37.2	10.2
4C25.01	1393.70	ISMLG	Si IV	1393.7	L	-13.0	-0.00004	223.6	12.7
4C25.01	1398.62	IGMABS	H I	1215.6	H	45116.0	0.15049	59.4	11.5
4C25.01	1402.71	ISMLG	Si IV	1402.7	L	-13.0	-0.00004	167.5	13.9
4C25.01	1434.31	IGMABS	H I	1215.6	H	53919.0	0.17985	42.1	24.9
4C25.01	1447.28	IGMABS	H I	1215.6	H	57117.0	0.19052	66.1	11.7
4C25.01	1456.80	IGMABS	H I	1215.6	H	59465.0	0.19835	70.8	12.8
4C25.01	1461.08	IGMABS	H I	1215.6	H	60519.0	0.20187	323.8	9.6
4C25.01	1472.86	IGMABS	H I	1215.6	H	63426.0	0.21157	124.8	12.4
4C25.01	1479.21	IGMABS	H I	1215.6	H	64991.0	0.21679	102.3	13.5
4C25.01	1498.22	IGMABS	H I	1215.6	H	69679.0	0.23243	149.7	13.6
4C25.01	1500.75	IGMABS	H I	1215.6	H	70302.0	0.23450	55.6	13.1
4C25.01	1512.01	IGMABS	H I	1215.6	H	73080.0	0.24377	266.2	11.3
4C25.01	1513.05	IGMABS	H I	1215.6	H	73336.0	0.24462	83.8	12.2
4C25.01	1516.96	IGMABS	H I	1215.6	H	74301.0	0.24784	36.4	10.4
4C25.01	1518.39	IGMABS	H I	1215.6	H	74652.0	0.24901	289.4	13.5
4C25.01	1519.70	IGMABS	H I	1215.6	H	74975.0	0.25009	450.8	14.9
4C25.01	1526.17	ISMLG	Si II	1526.7	L	-106.0	-0.00035	48.9	8.6
4C25.01	1526.63	ISMLG	Si II	1526.7	L	-15.0	-0.00004	476.7	6.9
4C25.01	1526.94	IGMABS	H I	1215.6	H	76761.0	0.25605	141.1	7.6
4C25.01	1527.35	INTRINSIC	Si II	1190.4	H	84852.0	0.28303	62.0	7.9
4C25.01	1529.60	IGMABS	H I	1215.6	H	77417.0	0.25824	88.3	16.0
4C25.01	1531.05	INTRINSIC	Si II	1193.2	H	84857.0	0.28303	99.3	10.3
4C25.01	1531.06	IGMABS	H I	1215.6	H	77778.0	0.25944	99.3	10.6
4C25.01	1531.59	IGMABS	H I	1215.6	H	77907.0	0.25987	153.2	8.4
4C25.01	1532.56	INTRINSIC	Si II*	1194.5	H	84847.0	0.28303	67.1	8.2
4C25.01	1536.28	INTRINSIC	Si II*	1197.3	H	84846.0	0.28303	19.7	8.4
4C25.01	1547.95	INTRINSIC	Si III	1206.5	H	84843.0	0.28303	285.8	6.2
4C25.01	1548.16	ISMLG	C IV	1548.2	L	-9.0	-0.00004	191.2	4.9
4C25.01	1548.53	ISMLG	C IV	1548.2	L	63.0	0.00022	53.3	6.2
4C25.01	1550.72	ISMLG	C IV	1550.7	L	-11.0	-0.00004	182.1	9.6
4C25.01	1555.16	PROXIMATE	H I	1215.6	H	83720.0	0.27926	108.4	7.4
4C25.01	1557.62	PROXIMATE	H I	1215.6	H	84327.0	0.28129	237.8	8.3
4C25.01	1559.10	INTRINSIC	H I	1215.6	H	84692.0	0.28250	334.5	5.6
4C25.01	1559.74	INTRINSIC	H I	1215.6	H	84851.0	0.28303	512.0	3.8
4C25.01	1560.13	INTRINSIC	H I	1215.6	H	84947.0	0.28335	455.8	3.4
4C25.01	1560.84	INTRINSIC	H I	1215.6	H	85122.0	0.28393	258.8	6.0
4C25.01	1588.78	INTRINSIC	N V	1238.8	H	84690.0	0.28250	307.7	15.9
4C25.01	1589.42	INTRINSIC	N V	1238.8	H	84845.0	0.28303	416.9	11.5
4C25.01	1589.82	INTRINSIC	N V	1238.8	H	84940.0	0.28335	162.5	10.8
4C25.01	1590.56	INTRINSIC	N V	1238.8	H	85121.0	0.28393	166.5	14.5
4C25.01	1593.90	INTRINSIC	N V	1242.8	H	84691.0	0.28250	186.5	13.1
4C25.01	1594.53	INTRINSIC	N V	1242.8	H	84844.0	0.28303	350.1	12.5
4C25.01	1594.97	INTRINSIC	N V	1242.8	H	84950.0	0.28335	70.0	12.7
4C25.01	1595.70	INTRINSIC	N V	1242.8	H	85127.0	0.28393	74.8	15.9

Table A1 continued

Table A1 (*continued*)

Target	λ_{obs}	Type	Ion	λ_{rest}	Frame	cz	z	W_{λ}	$\sigma_{W_{\lambda}}$
	(Å)			(Å)		(km s ⁻¹)		(mÅ)	(mÅ)
4C25.01	1608.36	ISMLG	Fe II	1608.4	L	-17.0	-0.00004	373.7	23.7
4C25.01	1617.14	INTRINSIC	Si II	1260.4	H	84846.0	0.28303	110.6	24.9
4C25.01	1622.69	INTRINSIC	Si II*	1264.7	H	84849.0	0.28303	143.9	28.2
4C25.01	1656.91	ISMLG	C I	1656.9	L	-3.0	-0.00004	79.3	22.1
4C25.01	1670.20	ISMLG	Al II	1670.7	L	-105.0	-0.00035	66.4	19.3
4C25.01	1670.71	ISMLG	Al II	1670.7	L	-14.0	-0.00004	564.2	18.8
4C25.01	1673.55	INTRINSIC	Si II	1304.3	H	84851.0	0.28303	73.4	23.5
4C25.01	1712.20	INTRINSIC	C II	1334.5	H	84840.0	0.28303	102.4	26.0
4C25.01	1713.74	INTRINSIC	C II*	1335.7	H	84848.0	0.28303	170.2	22.2
4C25.01	1788.20	INTRINSIC	H I	1393.7	H	84843.0	0.28303	319.1	38.9
FBS0150+396	1142.26	ISMLG	Fe II	1142.3	L	-28.0	-0.00006	144.0	36.1
FBS0150+396	1143.12	ISMLG	Fe II	1143.2	L	-29.0	-0.00006	286.2	41.3
FBS0150+396	1144.84	ISMLG	Fe II	1144.9	L	-25.0	-0.00006	346.0	29.6
FBS0150+396	1152.75	ISMLG	P II	1152.8	L	-17.0	-0.00006	139.6	51.4
FBS0150+396	1159.20	IGMABS	C III	977.0	H	55900.0	0.18649	1931.7	173.6
FBS0150+396	1162.38	IGMABS	C III	977.0	H	56877.0	0.18973	859.3	149.7
FBS0150+396	1169.28	PROXIMATE	H I	972.5	H	60647.0	0.20230	198.5	75.6
FBS0150+396	1171.18	PROXIMATE	H I	972.5	H	61234.0	0.20426	207.0	89.3
FBS0150+396	1172.13	PROXIMATE	H I	972.5	H	61527.0	0.20524	76.1	56.8
FBS0150+396	1172.55	PROXIMATE	H I	972.5	H	61657.0	0.20568	142.2	63.0
FBS0150+396	1174.39	IGMABS	N III	989.7	H	55910.0	0.18649	1160.3	100.7
FBS0150+396	1174.66	PROXIMATE	C III	977.0	H	60645.0	0.20230	962.1	89.7
FBS0150+396	1174.99	PROXIMATE	C III	977.0	H	60745.0	0.20262	551.1	66.9
FBS0150+396	1175.43	PROXIMATE	C III	977.0	H	60881.0	0.20307	518.3	42.0
FBS0150+396	1175.80	PROXIMATE	C III	977.0	H	60993.0	0.20346	529.6	39.6
FBS0150+396	1176.60	PROXIMATE	C III	977.0	H	61241.0	0.20426	791.5	45.1
FBS0150+396	1177.02	PROXIMATE	C III	977.0	H	61367.0	0.20470	359.0	30.4
FBS0150+396	1177.53	PROXIMATE	C III	977.0	H	61524.0	0.20524	398.9	42.0
FBS0150+396	1177.97	PROXIMATE	C III	977.0	H	61659.0	0.20568	344.7	32.8
FBS0150+396	1178.28	PROXIMATE	C III	977.0	H	61756.0	0.20598	171.9	32.8
FBS0150+396	1179.54	IGMABS	O VI	1031.9	H	42884.0	0.14306	324.6	61.9
FBS0150+396	1190.02	PROXIMATE	N III	989.7	H	60644.0	0.20230	726.5	19.7
FBS0150+396	1190.34	PROXIMATE	N III	989.7	H	60741.0	0.20262	521.6	11.7
FBS0150+396	1190.80	PROXIMATE	N III	989.7	H	60879.0	0.20307	199.5	15.3
FBS0150+396	1191.18	PROXIMATE	N III	989.7	H	60994.0	0.20346	189.3	15.0
FBS0150+396	1191.95	PROXIMATE	N III	989.7	H	61228.0	0.20426	674.6	25.4
FBS0150+396	1192.41	PROXIMATE	N III	989.7	H	61367.0	0.20470	585.8	12.9
FBS0150+396	1192.93	PROXIMATE	N III	989.7	H	61526.0	0.20524	237.1	13.7
FBS0150+396	1193.25	ISMLG	Si II	1193.2	L	-10.0	-0.00006	531.4	33.3
FBS0150+396	1193.36	PROXIMATE	N III	989.7	H	61655.0	0.20568	315.6	20.1
FBS0150+396	1193.68	PROXIMATE	N III	989.7	H	61753.0	0.20598	171.2	15.4
FBS0150+396	1194.26	PROXIMATE	Si II*	992.6	H	60877.0	0.20307	73.5	12.9
FBS0150+396	1194.54	IGMABS	H I	1025.7	H	49341.0	0.16459	102.4	13.7
FBS0150+396	1195.00	PROXIMATE	N III*	991.5	H	61528.0	0.20524	38.4	9.6
FBS0150+396	1195.46	PROXIMATE	N III*	991.5	H	61666.0	0.20568	202.3	35.9
FBS0150+396	1195.75	PROXIMATE	N III*	991.5	H	61755.0	0.20598	145.2	28.1
FBS0150+396	1196.85	PROXIMATE	Si II*	992.6	H	61659.0	0.20568	58.3	11.0
FBS0150+396	1197.13	PROXIMATE	Si II*	992.6	H	61743.0	0.20598	70.6	10.2
FBS0150+396	1199.49	ISMLG	N I	1199.5	L	-15.0	-0.00006	364.6	32.9
FBS0150+396	1200.18	ISMLG	N I	1200.2	L	-11.0	-0.00006	345.6	32.1
FBS0150+396	1200.64	ISMLG	N I	1200.7	L	-18.0	-0.00006	317.1	28.4
FBS0150+396	1205.82	ISMLG	Si III	1206.5	L	-168.0	-0.00052	65.5	19.4
FBS0150+396	1206.08	ISMLG	Si III	1206.5	L	-104.0	-0.00034	51.5	15.1

Table A1 continued

Table A1 (*continued*)

Target	λ_{obs}	Type	Ion	λ_{rest}	Frame	cz	z	W_{λ}	$\sigma_{W_{\lambda}}$
	(Å)			(Å)		(km s ⁻¹)		(mÅ)	(mÅ)
FBS0150+396	1206.40	ISMLG	Si III	1206.5	L	-26.0	-0.00006	388.6	22.7
FBS0150+396	1224.38	IGMABS	O VI	1031.9	H	55912.0	0.18649	929.8	70.2
FBS0150+396	1227.72	IGMABS	O VI	1031.9	H	56882.0	0.18973	313.5	49.8
FBS0150+396	1231.11	IGMABS	O VI	1037.6	H	55905.0	0.18649	783.8	65.2
FBS0150+396	1233.23	PROXIMATE	H I	1025.7	H	60649.0	0.20230	527.2	48.0
FBS0150+396	1233.56	PROXIMATE	H I	1025.7	H	60747.0	0.20262	616.2	49.1
FBS0150+396	1234.01	PROXIMATE	H I	1025.7	H	60878.0	0.20307	224.6	40.1
FBS0150+396	1234.41	PROXIMATE	H I	1025.7	H	60994.0	0.20346	102.8	29.7
FBS0150+396	1235.23	PROXIMATE	H I	1025.7	H	61235.0	0.20426	365.4	39.5
FBS0150+396	1235.70	PROXIMATE	H I	1025.7	H	61373.0	0.20470	119.2	26.3
FBS0150+396	1236.26	PROXIMATE	H I	1025.7	H	61534.0	0.20524	74.8	22.8
FBS0150+396	1236.72	PROXIMATE	H I	1025.7	H	61670.0	0.20568	201.5	21.6
FBS0150+396	1237.02	PROXIMATE	H I	1025.7	H	61756.0	0.20598	134.1	19.9
FBS0150+396	1239.24	IGMABS	H I	1215.6	H	5812.0	0.01939	262.8	20.5
FBS0150+396	1240.66	PROXIMATE	O VI	1031.9	H	60642.0	0.20230	786.2	21.2
FBS0150+396	1240.99	PROXIMATE	O VI	1031.9	H	60738.0	0.20262	659.6	18.6
FBS0150+396	1241.49	PROXIMATE	O VI	1031.9	H	60881.0	0.20307	119.0	21.7
FBS0150+396	1241.86	PROXIMATE	O VI	1031.9	H	60989.0	0.20346	99.1	22.4
FBS0150+396	1242.72	PROXIMATE	O VI	1031.9	H	61239.0	0.20426	348.2	21.8
FBS0150+396	1243.16	PROXIMATE	O VI	1031.9	H	61368.0	0.20470	84.1	14.8
FBS0150+396	1243.71	PROXIMATE	O VI	1031.9	H	61527.0	0.20524	131.8	17.8
FBS0150+396	1244.19	PROXIMATE	O VI	1031.9	H	61668.0	0.20568	64.3	11.8
FBS0150+396	1244.48	PROXIMATE	O VI	1031.9	H	61752.0	0.20598	106.5	11.5
FBS0150+396	1245.15	IGMABS	H I	1215.6	H	7270.0	0.02425	51.3	10.0
FBS0150+396	1246.30	PROXIMATE	C II	1036.3	H	60738.0	0.20262	54.2	10.9
FBS0150+396	1247.51	PROXIMATE	O VI	1037.6	H	60643.0	0.20230	586.5	15.0
FBS0150+396	1247.85	PROXIMATE	O VI	1037.6	H	60742.0	0.20262	255.1	10.1
FBS0150+396	1248.33	PROXIMATE	O VI	1037.6	H	60881.0	0.20307	80.8	13.4
FBS0150+396	1248.74	PROXIMATE	O VI	1037.6	H	60998.0	0.20346	141.8	11.3
FBS0150+396	1249.54	PROXIMATE	O VI	1037.6	H	61229.0	0.20426	196.8	13.5
FBS0150+396	1250.01	PROXIMATE	O VI	1037.6	H	61364.0	0.20470	82.3	10.7
FBS0150+396	1250.52	ISMLG	S II	1250.5	L	-13.0	-0.00006	250.4	14.1
FBS0150+396	1251.03	PROXIMATE	O VI	1037.6	H	61659.0	0.20568	70.4	10.2
FBS0150+396	1251.36	PROXIMATE	O VI	1037.6	H	61756.0	0.20598	75.4	8.6
FBS0150+396	1253.76	ISMLG	S II	1253.8	L	-10.0	-0.00006	259.5	9.3
FBS0150+396	1256.74	IGMABS	H I	1215.6	H	10129.0	0.03379	72.5	13.8
FBS0150+396	1259.47	ISMLG	S II	1259.5	L	-11.0	-0.00006	323.0	14.4
FBS0150+396	1259.74	ISMLG	Si II	1260.4	L	-161.0	-0.00052	80.3	9.7
FBS0150+396	1259.96	ISMLG	Si II	1260.4	L	-109.0	-0.00034	41.2	8.7
FBS0150+396	1260.35	ISMLG	Si II	1260.4	L	-18.0	-0.00006	485.2	18.0
FBS0150+396	1284.39	IGMABS	H I	1215.6	H	16946.0	0.05653	156.5	38.3
FBS0150+396	1302.11	ISMLG	O I	1302.1	L	-14.0	-0.00006	379.8	18.6
FBS0150+396	1304.32	ISMLG	Si II	1304.3	L	-11.0	-0.00006	379.6	16.1
FBS0150+396	1307.64	IGMABS	H I	1215.6	H	22679.0	0.07565	111.4	22.0
FBS0150+396	1309.01	IGMABS	H I	1215.6	H	23019.0	0.07678	228.2	28.3
FBS0150+396	1317.16	ISMLG	Ni II	1317.2	L	-14.0	-0.00006	129.4	20.7
FBS0150+396	1321.60	IGMABS	H I	1215.6	H	26124.0	0.08714	323.7	36.0
FBS0150+396	1333.85	ISMLG	C II	1334.5	L	-153.0	-0.00052	130.4	25.9
FBS0150+396	1334.04	ISMLG	C II	1334.5	L	-112.0	-0.00034	116.7	15.9
FBS0150+396	1334.41	ISMLG	C II	1334.5	L	-28.0	-0.00006	525.2	28.5
FBS0150+396	1335.58	ISMLG	C II*	1335.7	L	-29.0	-0.00006	346.5	31.3
FBS0150+396	1344.93	IGMABS	H I	1215.6	H	31877.0	0.10633	112.4	24.1
FBS0150+396	1349.96	PROXIMATE	Fe III	1122.5	H	60742.0	0.20262	52.7	12.1

Table A1 continued

Table A1 (*continued*)

Target	λ_{obs}	Type	Ion	λ_{rest}	Frame	cz	z	W_{λ}	$\sigma_{W_{\lambda}}$
	(Å)			(Å)		(km s ⁻¹)		(mÅ)	(mÅ)
FBS0150+396	1351.82	PROXIMATE	Fe III	1122.5	H	61239.0	0.20426	62.6	12.8
FBS0150+396	1352.32	PROXIMATE	Fe III	1122.5	H	61371.0	0.20470	58.0	12.3
FBS0150+396	1353.41	PROXIMATE	Fe III	1122.5	H	61661.0	0.20568	105.3	8.5
FBS0150+396	1353.71	PROXIMATE	Fe III	1122.5	H	61744.0	0.20598	63.9	7.5
FBS0150+396	1360.97	IGMABS	H I	1215.6	H	35833.0	0.11953	105.5	14.3
FBS0150+396	1363.28	IGMABS	H I	1215.6	H	36401.0	0.12142	91.1	12.3
FBS0150+396	1368.36	IGMABS	H I	1215.6	H	37654.0	0.12560	58.6	12.0
FBS0150+396	1370.04	ISMLG	Ni II	1370.1	L	-19.0	-0.00006	60.2	10.5
FBS0150+396	1385.70	IGMABS	H I	1215.6	H	41931.0	0.13987	222.6	25.6
FBS0150+396	1389.58	IGMABS	H I	1215.6	H	42887.0	0.14306	263.8	26.7
FBS0150+396	1391.82	IGMABS	H I	1215.6	H	43440.0	0.14490	242.0	24.8
FBS0150+396	1393.64	ISMLG	Si IV	1393.7	L	-26.0	-0.00006	194.4	28.1
FBS0150+396	1402.65	ISMLG	Si IV	1402.7	L	-26.0	-0.00006	117.3	42.1
FBS0150+396	1412.86	IGMABS	H I	1215.6	H	48629.0	0.16221	114.7	23.9
FBS0150+396	1415.75	IGMABS	H I	1215.6	H	49342.0	0.16459	202.2	29.3
FBS0150+396	1431.48	IGMABS	Si III	1206.5	H	55905.0	0.18649	1013.0	48.3
FBS0150+396	1435.44	IGMABS	Si III	1206.5	H	56889.0	0.18973	471.6	48.9
FBS0150+396	1436.04	PROXIMATE	Si II	1193.2	H	60987.0	0.20346	133.1	33.2
FBS0150+396	1437.01	PROXIMATE	Si II	1193.2	H	61231.0	0.20426	120.5	27.0
FBS0150+396	1438.73	PROXIMATE	Si II	1193.2	H	61662.0	0.20568	105.1	20.8
FBS0150+396	1440.19	PROXIMATE	Si II*	1194.5	H	61662.0	0.20568	50.2	12.9
FBS0150+396	1440.51	PROXIMATE	Si II*	1197.3	H	60868.0	0.20307	76.2	13.6
FBS0150+396	1442.38	IGMABS	H I	1215.6	H	55908.0	0.18649	831.0	29.1
FBS0150+396	1443.66	PROXIMATE	Si II*	1197.3	H	61659.0	0.20568	94.5	13.4
FBS0150+396	1444.03	PROXIMATE	Si II*	1197.3	H	61750.0	0.20598	86.6	12.4
FBS0150+396	1446.32	IGMABS	H I	1215.6	H	56880.0	0.18973	247.5	24.5
FBS0150+396	1450.58	PROXIMATE	Si III	1206.5	H	60650.0	0.20230	1185.3	13.3
FBS0150+396	1450.96	PROXIMATE	Si III	1206.5	H	60743.0	0.20262	419.1	10.7
FBS0150+396	1451.51	PROXIMATE	Si III	1206.5	H	60879.0	0.20307	231.6	19.4
FBS0150+396	1451.98	PROXIMATE	Si III	1206.5	H	60997.0	0.20346	273.3	9.3
FBS0150+396	1452.97	PROXIMATE	Si III	1206.5	H	61243.0	0.20426	447.2	13.5
FBS0150+396	1453.46	PROXIMATE	Si III	1206.5	H	61365.0	0.20470	147.4	13.0
FBS0150+396	1454.13	PROXIMATE	Si III	1206.5	H	61532.0	0.20524	100.1	11.9
FBS0150+396	1454.68	PROXIMATE	Si III	1206.5	H	61668.0	0.20568	227.3	9.1
FBS0150+396	1455.02	PROXIMATE	Si III	1206.5	H	61754.0	0.20598	154.1	8.5
FBS0150+396	1457.78	IGMABS	H I	1215.6	H	59705.0	0.19916	30.3	10.6
FBS0150+396	1461.60	PROXIMATE	H I	1215.6	H	60647.0	0.20230	1054.3	9.8
FBS0150+396	1461.99	PROXIMATE	H I	1215.6	H	60743.0	0.20262	788.0	6.6
FBS0150+396	1462.53	PROXIMATE	H I	1215.6	H	60878.0	0.20307	197.4	14.3
FBS0150+396	1463.01	PROXIMATE	H I	1215.6	H	60995.0	0.20346	130.7	13.3
FBS0150+396	1463.98	PROXIMATE	H I	1215.6	H	61235.0	0.20426	575.3	14.6
FBS0150+396	1464.52	PROXIMATE	H I	1215.6	H	61367.0	0.20470	136.7	12.5
FBS0150+396	1465.17	PROXIMATE	H I	1215.6	H	61529.0	0.20524	154.7	10.1
FBS0150+396	1465.71	PROXIMATE	H I	1215.6	H	61661.0	0.20568	367.1	7.3
FBS0150+396	1466.07	PROXIMATE	H I	1215.6	H	61751.0	0.20598	156.2	9.4
FBS0150+396	1469.86	IGMABS	N V	1238.8	H	55912.0	0.18649	553.2	24.0
FBS0150+396	1473.87	IGMABS	N V	1238.8	H	56881.0	0.18973	488.4	21.6
FBS0150+396	1474.58	IGMABS	N V	1242.8	H	55909.0	0.18649	794.7	28.5
FBS0150+396	1478.58	IGMABS	N V	1242.8	H	56874.0	0.18973	358.8	26.3
FBS0150+396	1489.43	PROXIMATE	N V	1238.8	H	60647.0	0.20230	821.1	12.1
FBS0150+396	1489.84	PROXIMATE	N V	1238.8	H	60746.0	0.20262	313.7	10.2
FBS0150+396	1490.34	PROXIMATE	N V	1238.8	H	60868.0	0.20307	120.1	16.9
FBS0150+396	1490.85	PROXIMATE	N V	1238.8	H	60991.0	0.20346	138.3	12.4

Table A1 continued

Table A1 (*continued*)

Target	λ_{obs}	Type	Ion	λ_{rest}	Frame	cz	z	W_{λ}	$\sigma_{W_{\lambda}}$
	(Å)			(Å)		(km s ⁻¹)		(mÅ)	(mÅ)
FBS0150+396	1491.88	PROXIMATE	N v	1238.8	H	61239.0	0.20426	356.1	11.5
FBS0150+396	1492.39	PROXIMATE	N v	1238.8	H	61363.0	0.20470	172.6	8.8
FBS0150+396	1493.62	PROXIMATE	N v	1238.8	H	61662.0	0.20568	143.6	10.2
FBS0150+396	1494.02	PROXIMATE	N v	1238.8	H	61757.0	0.20598	123.3	12.4
FBS0150+396	1494.21	PROXIMATE	N v	1242.8	H	60644.0	0.20230	797.9	13.0
FBS0150+396	1494.61	PROXIMATE	N v	1242.8	H	60742.0	0.20262	232.8	10.9
FBS0150+396	1495.19	PROXIMATE	N v	1242.8	H	60881.0	0.20307	101.8	11.6
FBS0150+396	1495.64	PROXIMATE	N v	1242.8	H	60990.0	0.20346	71.4	11.8
FBS0150+396	1496.64	PROXIMATE	N v	1242.8	H	61231.0	0.20426	219.1	16.6
FBS0150+396	1497.19	PROXIMATE	N v	1242.8	H	61363.0	0.20470	68.1	9.8
FBS0150+396	1498.45	PROXIMATE	N v	1242.8	H	61667.0	0.20568	74.8	10.8
FBS0150+396	1498.80	PROXIMATE	N v	1242.8	H	61751.0	0.20598	59.6	8.8
FBS0150+396	1515.39	PROXIMATE	Si II	1260.4	H	60644.0	0.20230	93.5	10.4
FBS0150+396	1515.84	PROXIMATE	Si II	1260.4	H	60750.0	0.20262	67.8	9.4
FBS0150+396	1516.37	PROXIMATE	Si II	1260.4	H	60876.0	0.20307	81.1	8.4
FBS0150+396	1516.85	PROXIMATE	Si II	1260.4	H	60991.0	0.20346	76.6	9.9
FBS0150+396	1517.90	PROXIMATE	Si II	1260.4	H	61241.0	0.20426	199.2	10.5
FBS0150+396	1518.42	PROXIMATE	Si II	1260.4	H	61365.0	0.20470	105.7	8.8
FBS0150+396	1519.10	PROXIMATE	Si II	1260.4	H	61528.0	0.20524	35.7	8.1
FBS0150+396	1519.69	PROXIMATE	Si II	1260.4	H	61668.0	0.20568	151.7	7.7
FBS0150+396	1520.04	PROXIMATE	Si II	1260.4	H	61749.0	0.20598	93.2	7.8
FBS0150+396	1520.99	PROXIMATE	Si II*	1264.7	H	60742.0	0.20262	103.7	9.2
FBS0150+396	1521.55	PROXIMATE	Si II*	1264.7	H	60874.0	0.20307	38.7	9.5
FBS0150+396	1522.03	PROXIMATE	Si II*	1264.7	H	60987.0	0.20346	40.7	9.6
FBS0150+396	1523.07	PROXIMATE	Si II*	1264.7	H	61236.0	0.20426	209.3	11.6
FBS0150+396	1523.64	PROXIMATE	Si II*	1264.7	H	61369.0	0.20470	91.6	8.0
FBS0150+396	1524.85	PROXIMATE	Si II*	1264.7	H	61657.0	0.20568	129.9	9.2
FBS0150+396	1525.26	PROXIMATE	Si II*	1264.7	H	61755.0	0.20598	162.7	9.2
FBS0150+396	1525.89	ISMLG	Si II	1526.7	L	-161.0	-0.00052	35.7	7.5
FBS0150+396	1526.59	ISMLG	Si II	1526.7	L	-23.0	-0.00006	457.4	8.7
FBS0150+396	1547.36	ISMLG	C IV	1548.2	L	-164.0	-0.00052	73.2	17.1
FBS0150+396	1548.08	ISMLG	C IV	1548.2	L	-24.0	-0.00006	198.8	20.1
FBS0150+396	1549.97	ISMLG	C IV	1550.7	L	-156.0	-0.00052	34.4	14.7
FBS0150+396	1550.69	ISMLG	C IV	1550.7	L	-17.0	-0.00006	103.9	16.3
FBS0150+396	1560.19	ISMLG	C I	1560.3	L	-22.0	-0.00006	78.8	16.0
FBS0150+396	1571.35	UNIDENTIFIED	UNIND	1000.0	H	0.0	-1.00000	75.6	19.1
FBS0150+396	1584.05	UNIDENTIFIED	UNIND	1000.0	H	0.0	-1.00000	222.3	35.5
FBS0150+396	1585.23	UNIDENTIFIED	UNIND	1000.0	H	0.0	-1.00000	292.2	42.2
FBS0150+396	1604.93	PROXIMATE	C II	1334.5	H	60743.0	0.20262	103.5	21.6
FBS0150+396	1605.89	PROXIMATE	C II*	1335.7	H	60641.0	0.20230	89.6	21.8
FBS0150+396	1606.35	PROXIMATE	C II*	1335.7	H	60745.0	0.20262	133.5	25.9
FBS0150+396	1608.37	ISMLG	Fe II	1608.4	L	-15.0	-0.00006	435.3	25.0
FBS0150+396	1609.05	PROXIMATE	C II	1334.5	H	61668.0	0.20568	133.3	22.7
FBS0150+396	1610.47	PROXIMATE	C II*	1335.7	H	61670.0	0.20568	242.9	36.3
FBS0150+396	1653.65	IGMABS	Si IV	1393.7	H	55902.0	0.18649	1870.0	93.8
FBS0150+396	1664.37	IGMABS	Si IV	1402.7	H	55907.0	0.18649	1310.4	117.0
FBS0150+396	1670.65	ISMLG	Al II	1670.7	L	-25.0	-0.00006	497.7	72.6
FBS0150+396	1675.72	PROXIMATE	Si IV	1393.7	H	60648.0	0.20230	1436.3	63.2
FBS0150+396	1676.17	PROXIMATE	Si IV	1393.7	H	60745.0	0.20262	653.5	33.8
FBS0150+396	1676.80	PROXIMATE	Si IV	1393.7	H	60881.0	0.20307	298.2	60.6
FBS0150+396	1677.33	PROXIMATE	Si IV	1393.7	H	60995.0	0.20346	172.3	46.5
FBS0150+396	1678.47	PROXIMATE	Si IV	1393.7	H	61240.0	0.20426	520.2	40.3
FBS0150+396	1679.03	PROXIMATE	Si IV	1393.7	H	61360.0	0.20470	190.5	37.9

Table A1 continued

Table A1 (*continued*)

Target	λ_{obs}	Type	Ion	λ_{rest}	Frame	cz	z	W_{λ}	$\sigma_{W_{\lambda}}$
	(Å)			(Å)		(km s ⁻¹)		(mÅ)	(mÅ)
FBS0150+396	1679.80	PROXIMATE	Si iv	1393.7	H	61526.0	0.20524	96.8	26.9
FBS0150+396	1680.44	PROXIMATE	Si iv	1393.7	H	61664.0	0.20568	275.2	29.0
FBS0150+396	1680.81	PROXIMATE	Si iv	1393.7	H	61744.0	0.20598	215.2	22.8
FBS0150+396	1686.53	PROXIMATE	Si iv	1402.7	H	60643.0	0.20230	1080.0	29.2
FBS0150+396	1687.00	PROXIMATE	Si iv	1402.7	H	60743.0	0.20262	436.5	22.5
FBS0150+396	1687.60	PROXIMATE	Si iv	1402.7	H	60872.0	0.20307	189.2	26.1
FBS0150+396	1688.20	PROXIMATE	Si iv	1402.7	H	60999.0	0.20346	103.3	22.7
FBS0150+396	1689.33	PROXIMATE	Si iv	1402.7	H	61242.0	0.20426	366.1	22.4
FBS0150+396	1689.91	PROXIMATE	Si iv	1402.7	H	61365.0	0.20470	177.2	18.9
FBS0150+396	1690.67	PROXIMATE	Si iv	1402.7	H	61529.0	0.20524	56.4	17.7
FBS0150+396	1691.31	PROXIMATE	Si iv	1402.7	H	61663.0	0.20568	184.6	15.0
FBS0150+396	1691.68	PROXIMATE	Si iv	1402.7	H	61743.0	0.20598	175.3	15.7
FBS0150+396	1709.49	ISMLG	Ni ii	1709.6	L	-21.0	-0.00006	31.2	28.8
FBS0150+396	1741.45	ISMLG	H i	1741.5	L	-18.0	-0.00006	128.6	32.9
HS0033+4300	1143.16	ISMLG	Fe ii	1143.2	L	-19.0	-0.00005	74.7	28.2
HS0033+4300	1144.84	ISMLG	Fe ii	1144.9	L	-26.0	-0.00005	253.5	33.6
HS0033+4300	1148.90	INTRINSIC	H i	1025.7	H	36001.0	0.12008	162.4	19.0
HS0033+4300	1149.14	INTRINSIC	H i	1025.7	H	36071.0	0.12033	252.7	18.0
HS0033+4300	1149.81	INTRINSIC	H i	1025.7	H	36269.0	0.12095	543.2	18.2
HS0033+4300	1150.69	PROXIMATE	H i	1025.7	H	36524.0	0.12184	430.9	19.4
HS0033+4300	1152.72	ISMLG	P ii	1152.8	L	-25.0	-0.00005	145.0	28.9
HS0033+4300	1155.83	INTRINSIC	O vi	1031.9	H	35996.0	0.12008	274.6	15.4
HS0033+4300	1156.10	INTRINSIC	O vi	1031.9	H	36075.0	0.12033	460.9	12.9
HS0033+4300	1156.74	INTRINSIC	O vi	1031.9	H	36262.0	0.12095	779.9	14.6
HS0033+4300	1157.66	PROXIMATE	O vi	1031.9	H	36528.0	0.12184	543.3	13.0
HS0033+4300	1158.12	PROXIMATE	O vi	1031.9	H	36662.0	0.12230	291.2	14.6
HS0033+4300	1162.21	INTRINSIC	O vi	1037.6	H	35999.0	0.12008	225.6	13.2
HS0033+4300	1162.47	INTRINSIC	O vi	1037.6	H	36074.0	0.12033	466.5	12.4
HS0033+4300	1163.12	INTRINSIC	O vi	1037.6	H	36260.0	0.12095	673.3	12.1
HS0033+4300	1164.04	PROXIMATE	O vi	1037.6	H	36526.0	0.12184	507.4	13.0
HS0033+4300	1164.54	PROXIMATE	O vi	1037.6	H	36670.0	0.12230	187.2	15.5
HS0033+4300	1189.92	ISMLG	Si ii	1190.4	L	-125.0	-0.00041	185.6	26.1
HS0033+4300	1190.36	ISMLG	Si ii	1190.4	L	-15.0	-0.00005	409.2	27.1
HS0033+4300	1192.80	ISMLG	Si ii	1193.2	L	-123.0	-0.00041	203.3	26.4
HS0033+4300	1193.19	ISMLG	Si ii	1193.2	L	-26.0	-0.00005	450.3	25.2
HS0033+4300	1193.94	ISMLG	C i	1193.9	L	-13.0	-0.00005	36.9	26.5
HS0033+4300	1199.45	ISMLG	N i	1199.5	L	-26.0	-0.00005	423.9	37.9
HS0033+4300	1200.11	ISMLG	N i	1200.2	L	-27.0	-0.00005	400.8	32.1
HS0033+4300	1200.60	ISMLG	N i	1200.7	L	-26.0	-0.00005	308.3	27.3
HS0033+4300	1204.98	ISMLG	Si iii	1206.5	L	-377.0	-0.00126	107.9	35.0
HS0033+4300	1205.66	ISMLG	Si iii	1206.5	L	-208.0	-0.00071	205.4	27.6
HS0033+4300	1205.99	ISMLG	Si iii	1206.5	L	-128.0	-0.00041	183.3	26.0
HS0033+4300	1206.39	ISMLG	Si iii	1206.5	L	-26.0	-0.00005	437.9	38.3
HS0033+4300	1221.68	IGMABS	H i	1215.6	H	1482.0	0.00494	105.8	52.7
HS0033+4300	1240.00	IGMABS	H i	1215.6	H	6000.0	0.02001	75.3	29.0
HS0033+4300	1250.49	ISMLG	S ii	1250.5	L	-21.0	-0.00005	207.7	30.8
HS0033+4300	1253.69	ISMLG	S ii	1253.8	L	-27.0	-0.00005	259.7	30.8
HS0033+4300	1258.79	ISMLG	Si ii	1260.4	L	-389.0	-0.00126	93.6	28.0
HS0033+4300	1259.43	ISMLG	S ii	1259.5	L	-21.0	-0.00005	246.9	23.1
HS0033+4300	1259.90	ISMLG	Si ii	1260.4	L	-124.0	-0.00041	290.0	20.0
HS0033+4300	1260.35	ISMLG	Si ii	1260.4	L	-18.0	-0.00005	521.9	23.9
HS0033+4300	1261.81	IGMABS	H i	1215.6	H	11379.0	0.03796	52.6	25.2
HS0033+4300	1262.11	IGMABS	H i	1215.6	H	11453.0	0.03820	69.7	29.0

Table A1 continued

Table A1 (*continued*)

Target	λ_{obs}	Type	Ion	λ_{rest}	Frame	cz	z	W_{λ}	$\sigma_{W_{\lambda}}$
	(Å)			(Å)		(km s ⁻¹)		(mÅ)	(mÅ)
HS0033+4300	1264.38	IGMABS	H I	1215.6	H	12012.0	0.04007	89.5	30.5
HS0033+4300	1301.63	ISMLG	O I	1302.1	L	-123.0	-0.00041	242.6	26.5
HS0033+4300	1302.11	ISMLG	O I	1302.1	L	-13.0	-0.00005	437.7	31.0
HS0033+4300	1303.85	ISMLG	Si II	1304.3	L	-118.0	-0.00041	134.2	31.4
HS0033+4300	1304.25	ISMLG	Si II	1304.3	L	-27.0	-0.00005	381.6	28.3
HS0033+4300	1325.22	IGMABS	H I	1215.6	H	27017.0	0.09012	138.0	42.9
HS0033+4300	1332.82	ISMLG	C II	1334.5	L	-384.0	-0.00126	195.7	31.0
HS0033+4300	1333.60	ISMLG	C II	1334.5	L	-209.0	-0.00071	219.9	24.4
HS0033+4300	1334.00	ISMLG	C II	1334.5	L	-119.0	-0.00041	319.1	18.3
HS0033+4300	1334.47	ISMLG	C II	1334.5	L	-15.0	-0.00005	577.9	24.7
HS0033+4300	1335.58	ISMLG	C II*	1335.7	L	-28.0	-0.00005	289.3	30.8
HS0033+4300	1346.60	IGMABS	H I	1215.6	H	32289.0	0.10771	90.2	27.2
HS0033+4300	1361.65	INTRINSIC	H I	1215.6	H	35999.0	0.12008	168.8	8.6
HS0033+4300	1361.95	INTRINSIC	H I	1215.6	H	36074.0	0.12033	380.8	7.8
HS0033+4300	1362.71	INTRINSIC	H I	1215.6	H	36260.0	0.12095	776.9	7.5
HS0033+4300	1363.79	PROXIMATE	H I	1215.6	H	36527.0	0.12184	542.7	7.4
HS0033+4300	1364.34	PROXIMATE	H I	1215.6	H	36664.0	0.12230	179.7	9.3
HS0033+4300	1370.01	ISMLG	Ni II	1370.1	L	-27.0	-0.00005	79.6	17.5
HS0033+4300	1387.58	INTRINSIC	N V	1238.8	H	36001.0	0.12008	231.5	16.5
HS0033+4300	1387.86	INTRINSIC	N V	1238.8	H	36068.0	0.12033	302.6	12.9
HS0033+4300	1388.67	INTRINSIC	N V	1238.8	H	36262.0	0.12095	771.8	15.1
HS0033+4300	1389.77	PROXIMATE	N V	1238.8	H	36530.0	0.12184	274.5	25.2
HS0033+4300	1390.29	PROXIMATE	N V	1238.8	H	36655.0	0.12230	141.5	22.7
HS0033+4300	1392.06	INTRINSIC	N V	1242.8	H	36003.0	0.12008	93.1	11.3
HS0033+4300	1392.38	INTRINSIC	N V	1242.8	H	36082.0	0.12033	257.5	13.0
HS0033+4300	1393.13	INTRINSIC	N V	1242.8	H	36262.0	0.12095	735.8	14.0
HS0033+4300	1394.24	PROXIMATE	N V	1242.8	H	36531.0	0.12184	279.3	31.0
HS0033+4300	1394.83	PROXIMATE	N V	1242.8	H	36671.0	0.12230	71.0	18.9
HS0033+4300	1401.74	ISMLG	Si IV	1402.7	L	-221.0	-0.00071	66.8	27.4
HS0033+4300	1402.65	ISMLG	Si IV	1402.7	L	-26.0	-0.00005	92.5	28.9
HS0033+4300	1454.78	ISMLG	Ni II	1454.8	L	-13.0	-0.00005	70.7	19.3
HS0033+4300	1526.08	ISMLG	Si II	1526.7	L	-122.0	-0.00041	165.7	18.2
HS0033+4300	1526.57	ISMLG	Si II	1526.7	L	-27.0	-0.00005	487.2	19.5
HS0033+4300	1547.11	ISMLG	C IV	1548.2	L	-211.0	-0.00071	273.9	22.6
HS0033+4300	1548.07	ISMLG	C IV	1548.2	L	-27.0	-0.00005	195.7	23.5
HS0033+4300	1549.68	ISMLG	C IV	1550.7	L	-213.0	-0.00071	161.1	19.2
HS0033+4300	1550.70	ISMLG	C IV	1550.7	L	-15.0	-0.00005	55.0	22.3
HS0033+4300	1608.30	ISMLG	Fe II	1608.4	L	-28.0	-0.00005	350.1	34.6
HS0033+4300	1656.86	ISMLG	C I	1656.9	L	-13.0	-0.00005	75.5	35.2
HS0033+4300	1670.08	ISMLG	Al II	1670.7	L	-126.0	-0.00041	155.5	31.5
HS0033+4300	1670.64	ISMLG	Al II	1670.7	L	-27.0	-0.00005	523.3	27.4
HS0033+4300	1734.11	INTRINSIC	C IV	1548.2	H	35998.0	0.12008	120.9	15.8
HS0033+4300	1734.49	INTRINSIC	C IV	1548.2	H	36072.0	0.12033	155.0	11.8
HS0033+4300	1735.47	INTRINSIC	C IV	1548.2	H	36262.0	0.12095	806.5	15.0
HS0033+4300	1736.89	PROXIMATE	C IV	1548.2	H	36537.0	0.12184	418.4	19.9
HS0033+4300	1737.36	INTRINSIC	C IV	1550.7	H	36069.0	0.12033	174.0	11.3
HS0033+4300	1738.36	INTRINSIC	C IV	1550.7	H	36262.0	0.12095	691.7	27.1
HS0033+4300	1739.78	PROXIMATE	C IV	1550.7	H	36537.0	0.12184	258.2	18.9
HS0033+4300	1741.40	ISMLG	H I	1741.5	L	-27.0	-0.00005	55.3	14.9
HS0058+4213	1139.76	IGMABS	O VI	1031.9	H	31326.0	0.10452	98.1	32.1
HS0058+4213	1143.14	ISMLG	Fe II	1143.2	L	-22.0	-0.00007	163.5	30.6
HS0058+4213	1144.84	ISMLG	Fe II	1144.9	L	-25.0	-0.00007	295.7	30.7
HS0058+4213	1146.04	IGMABS	O VI	1037.6	H	31325.0	0.10452	68.1	32.8

Table A1 continued

Table A1 (*continued*)

Target	λ_{obs}	Type	Ion	λ_{rest}	Frame	cz	z	W_{λ}	$\sigma_{W_{\lambda}}$
	(Å)			(Å)		(km s ⁻¹)		(mÅ)	(mÅ)
HS0058+4213	1148.82	PROXIMATE	H I	972.5	H	54342.0	0.18125	205.3	31.5
HS0058+4213	1152.48	PROXIMATE	H I	972.5	H	55469.0	0.18499	80.3	19.0
HS0058+4213	1152.72	ISMLG	P II	1152.8	L	-25.0	-0.00007	165.6	28.2
HS0058+4213	1154.13	PROXIMATE	C III	977.0	H	54346.0	0.18125	151.1	24.9
HS0058+4213	1154.50	IGMABS	H I	1025.7	H	37639.0	0.12557	199.2	22.2
HS0058+4213	1156.52	INTRINSIC	H I	972.5	H	56715.0	0.18921	248.1	27.5
HS0058+4213	1161.51	IGMABS	O VI	1031.9	H	37647.0	0.12557	90.9	25.2
HS0058+4213	1161.84	INTRINSIC	C III	977.0	H	56711.0	0.18921	55.4	21.6
HS0058+4213	1165.66	IGMABS	H I	1025.7	H	40899.0	0.13641	136.4	18.5
HS0058+4213	1165.91	IGMABS	H I	1025.7	H	40972.0	0.13668	339.9	29.3
HS0058+4213	1167.89	IGMABS	O VI	1037.6	H	37640.0	0.12557	68.6	26.7
HS0058+4213	1172.97	IGMABS	O VI	1031.9	H	40975.0	0.13668	177.7	36.3
HS0058+4213	1186.64	IGMABS	H I	1025.7	H	47032.0	0.15687	116.4	23.1
HS0058+4213	1189.47	ISMLG	Si II	1190.4	L	-239.0	-0.00077	67.3	13.6
HS0058+4213	1189.63	ISMLG	Si II	1190.4	L	-198.0	-0.00064	46.1	14.0
HS0058+4213	1190.05	ISMLG	Si II	1190.4	L	-92.0	-0.00027	163.7	12.4
HS0058+4213	1190.37	ISMLG	Si II	1190.4	L	-12.0	-0.00007	352.1	14.2
HS0058+4213	1192.34	ISMLG	Si II	1193.2	L	-239.0	-0.00077	69.6	14.1
HS0058+4213	1192.51	ISMLG	Si II	1193.2	L	-196.0	-0.00064	78.6	16.7
HS0058+4213	1192.92	ISMLG	Si II	1193.2	L	-93.0	-0.00027	177.1	11.2
HS0058+4213	1193.24	ISMLG	Si II	1193.2	L	-12.0	-0.00007	339.8	15.2
HS0058+4213	1197.10	ISMLG	Mn II	1197.1	L	-22.0	-0.00007	49.9	22.5
HS0058+4213	1199.19	ISMLG	N I	1199.5	L	-90.0	-0.00027	88.0	16.3
HS0058+4213	1199.50	ISMLG	N I	1199.5	L	-13.0	-0.00007	397.2	22.5
HS0058+4213	1200.18	ISMLG	N I	1200.2	L	-12.0	-0.00007	364.6	17.5
HS0058+4213	1200.65	ISMLG	N I	1200.7	L	-14.0	-0.00007	360.5	18.3
HS0058+4213	1205.60	ISMLG	Si III	1206.5	L	-224.0	-0.00077	132.2	10.9
HS0058+4213	1205.70	ISMLG	Si III	1206.5	L	-198.0	-0.00064	128.2	9.8
HS0058+4213	1205.92	ISMLG	Si III	1206.5	L	-143.0	-0.00050	77.2	13.2
HS0058+4213	1206.13	ISMLG	Si III	1206.5	L	-92.0	-0.00027	180.2	11.8
HS0058+4213	1206.45	ISMLG	Si III	1206.5	L	-11.0	-0.00007	364.9	15.3
HS0058+4213	1211.65	PROXIMATE	H I	1025.7	H	54341.0	0.18125	435.7	76.1
HS0058+4213	1219.80	INTRINSIC	H I	1025.7	H	56723.0	0.18921	307.4	84.7
HS0058+4213	1221.48	IGMABS	H I	1215.6	H	1433.0	0.00478	234.1	30.8
HS0058+4213	1222.82	PROXIMATE	O VI	1031.9	H	55459.0	0.18499	158.6	22.3
HS0058+4213	1224.01	IGMABS	H I	1215.6	H	2056.0	0.00686	176.7	24.2
HS0058+4213	1225.70	PROXIMATE	O VI	1037.6	H	54343.0	0.18125	180.7	30.1
HS0058+4213	1226.86	IGMABS	H I	1215.6	H	2760.0	0.00920	249.2	22.2
HS0058+4213	1227.79	IGMABS	H I	1215.6	H	2988.0	0.00997	83.3	16.6
HS0058+4213	1228.23	IGMABS	H I	1215.6	H	3097.0	0.01033	111.0	20.7
HS0058+4213	1229.58	PROXIMATE	O VI	1037.6	H	55462.0	0.18499	85.9	15.2
HS0058+4213	1250.49	ISMLG	S II	1250.5	L	-21.0	-0.00007	249.4	16.5
HS0058+4213	1253.71	ISMLG	S II	1253.8	L	-23.0	-0.00007	268.9	16.1
HS0058+4213	1259.44	ISMLG	S II	1259.5	L	-18.0	-0.00007	387.6	16.4
HS0058+4213	1259.82	ISMLG	Si II	1260.4	L	-143.0	-0.00050	57.4	11.1
HS0058+4213	1260.04	ISMLG	Si II	1260.4	L	-92.0	-0.00027	200.8	7.4
HS0058+4213	1260.37	ISMLG	Si II	1260.4	L	-12.0	-0.00007	401.8	9.1
HS0058+4213	1260.70	ISMLG	C I	1260.7	L	-8.0	-0.00007	89.7	13.9
HS0058+4213	1264.31	IGMABS	H I	1215.6	H	11994.0	0.04001	53.3	20.0
HS0058+4213	1297.50	IGMABS	H I	1215.6	H	20179.0	0.06731	76.8	18.4
HS0058+4213	1301.76	ISMLG	O I	1302.1	L	-93.0	-0.00027	173.8	12.4
HS0058+4213	1302.12	ISMLG	O I	1302.1	L	-11.0	-0.00007	345.3	16.9
HS0058+4213	1303.38	ISMLG	Si II	1304.3	L	-228.0	-0.00077	61.8	24.3

Table A1 continued

Table A1 (*continued*)

Target	λ_{obs}	Type	Ion	λ_{rest}	Frame	cz	z	W_{λ}	$\sigma_{W_{\lambda}}$
	(Å)			(Å)		(km s ⁻¹)		(mÅ)	(mÅ)
HS0058+4213	1303.96	ISMLG	Si II	1304.3	L	-93.0	-0.00027	115.5	16.8
HS0058+4213	1304.33	ISMLG	Si II	1304.3	L	-10.0	-0.00007	341.5	14.1
HS0058+4213	1317.10	ISMLG	Ni II	1317.2	L	-26.0	-0.00007	107.6	19.2
HS0058+4213	1331.04	IGMABS	H I	1215.6	H	28451.0	0.09490	306.8	23.8
HS0058+4213	1333.47	ISMLG	C II	1334.5	L	-238.0	-0.00077	140.3	10.8
HS0058+4213	1333.68	ISMLG	C II	1334.5	L	-191.0	-0.00064	146.5	12.3
HS0058+4213	1333.89	ISMLG	C II	1334.5	L	-145.0	-0.00050	96.1	13.9
HS0058+4213	1334.12	ISMLG	C II	1334.5	L	-94.0	-0.00027	224.8	8.8
HS0058+4213	1334.49	ISMLG	C II	1334.5	L	-9.0	-0.00007	416.5	14.4
HS0058+4213	1335.63	ISMLG	C II*	1335.7	L	-17.0	-0.00007	382.4	16.5
HS0058+4213	1336.08	IGMABS	H I	1215.6	H	29693.0	0.09904	145.1	21.0
HS0058+4213	1342.73	IGMABS	H I	1215.6	H	31334.0	0.10452	387.8	27.7
HS0058+4213	1348.00	IGMABS	H I	1215.6	H	32634.0	0.10886	198.9	32.3
HS0058+4213	1367.90	IGMABS	H I	1215.6	H	37542.0	0.12523	126.2	22.1
HS0058+4213	1368.33	IGMABS	H I	1215.6	H	37646.0	0.12557	374.5	23.8
HS0058+4213	1370.04	ISMLG	Ni II	1370.1	L	-21.0	-0.00007	90.2	19.3
HS0058+4213	1378.05	IGMABS	H I	1215.6	H	40043.0	0.13357	145.1	26.2
HS0058+4213	1381.50	IGMABS	H I	1215.6	H	40894.0	0.13641	329.9	17.4
HS0058+4213	1381.83	IGMABS	H I	1215.6	H	40977.0	0.13668	613.5	17.4
HS0058+4213	1389.81	IGMABS	H I	1215.6	H	42943.0	0.14324	56.2	17.5
HS0058+4213	1390.25	IGMABS	H I	1215.6	H	43053.0	0.14361	148.9	22.4
HS0058+4213	1392.68	ISMLG	Si IV	1393.7	L	-232.0	-0.00077	74.1	14.2
HS0058+4213	1392.83	ISMLG	Si IV	1393.7	L	-199.0	-0.00064	64.3	11.8
HS0058+4213	1393.68	ISMLG	Si IV	1393.7	L	-18.0	-0.00007	119.9	15.4
HS0058+4213	1401.69	ISMLG	Si IV	1402.7	L	-231.0	-0.00077	35.2	13.4
HS0058+4213	1401.85	ISMLG	Si IV	1402.7	L	-196.0	-0.00064	42.0	11.5
HS0058+4213	1402.72	ISMLG	Si IV	1402.7	L	-11.0	-0.00007	71.4	18.1
HS0058+4213	1406.37	IGMABS	H I	1215.6	H	47028.0	0.15687	344.1	18.2
HS0058+4213	1417.57	IGMABS	H I	1215.6	H	49790.0	0.16608	70.3	9.3
HS0058+4213	1417.92	IGMABS	H I	1215.6	H	49877.0	0.16637	116.2	17.9
HS0058+4213	1423.06	IGMABS	H I	1215.6	H	51143.0	0.17060	26.1	11.7
HS0058+4213	1429.58	IGMABS	H I	1215.6	H	52751.0	0.17596	100.3	11.6
HS0058+4213	1434.73	INTRINSIC	Si III	1206.5	H	56711.0	0.18921	36.9	8.3
HS0058+4213	1436.01	PROXIMATE	H I	1215.6	H	54338.0	0.18125	481.8	12.0
HS0058+4213	1440.55	PROXIMATE	H I	1215.6	H	55457.0	0.18499	243.0	7.8
HS0058+4213	1445.69	INTRINSIC	H I	1215.6	H	56724.0	0.18921	548.8	10.2
HS0058+4213	1454.76	ISMLG	Ni II	1454.8	L	-17.0	-0.00007	74.4	11.5
HS0058+4213	1463.39	PROXIMATE	N V	1238.8	H	54345.0	0.18125	296.4	21.5
HS0058+4213	1468.01	PROXIMATE	N V	1238.8	H	55463.0	0.18499	52.6	17.6
HS0058+4213	1468.06	PROXIMATE	N V	1242.8	H	54338.0	0.18125	229.4	18.4
HS0058+4213	1472.74	PROXIMATE	N V	1242.8	H	55466.0	0.18499	58.7	16.0
HS0058+4213	1525.55	ISMLG	Si II	1526.7	L	-227.0	-0.00077	63.0	15.8
HS0058+4213	1526.23	ISMLG	Si II	1526.7	L	-93.0	-0.00027	158.2	14.6
HS0058+4213	1526.66	ISMLG	Si II	1526.7	L	-10.0	-0.00007	431.5	17.3
HS0058+4213	1547.05	ISMLG	C IV	1548.2	L	-224.0	-0.00077	96.7	14.8
HS0058+4213	1547.24	ISMLG	C IV	1548.2	L	-187.0	-0.00064	157.6	16.0
HS0058+4213	1548.12	ISMLG	C IV	1548.2	L	-16.0	-0.00007	173.3	27.4
HS0058+4213	1549.55	ISMLG	C IV	1550.7	L	-238.0	-0.00077	69.3	17.6
HS0058+4213	1549.80	ISMLG	C IV	1550.7	L	-189.0	-0.00064	98.3	18.1
HS0058+4213	1550.70	ISMLG	C IV	1550.7	L	-16.0	-0.00007	81.9	26.0
HS0058+4213	1608.32	ISMLG	Fe II	1608.4	L	-24.0	-0.00007	463.5	33.4
HS0058+4213	1633.47	UNIDENTIFIED	UNIND	1000.0	H	0.0	-1.00000	198.6	33.0
HS0058+4213	1656.88	ISMLG	C I	1656.9	L	-10.0	-0.00007	107.4	36.4

Table A1 *continued*

Table A1 (*continued*)

Target	λ_{obs}	Type	Ion	λ_{rest}	Frame	cz	z	W_{λ}	$\sigma_{W_{\lambda}}$
	(Å)			(Å)		(km s ⁻¹)		(mÅ)	(mÅ)
HS0058+4213	1669.50	ISMLG	Al II	1670.7	L	-231.0	-0.00077	61.7	24.5
HS0058+4213	1670.28	ISMLG	Al II	1670.7	L	-92.0	-0.00027	169.6	23.7
HS0058+4213	1670.70	ISMLG	Al II	1670.7	L	-16.0	-0.00007	500.6	34.6
HS0058+4213	1709.47	ISMLG	Ni II	1709.6	L	-23.0	-0.00007	119.8	43.7
HS0058+4213	1710.03	IGMABS	C IV	1548.2	H	31336.0	0.10452	210.3	47.1
HS0058+4213	1712.88	IGMABS	C IV	1550.7	H	31336.0	0.10452	127.5	63.6
HS0058+4213	1742.62	IGMABS	C IV	1548.2	H	37646.0	0.12557	169.8	46.2
HS0058+4213	1745.51	IGMABS	H I	1550.7	H	37644.0	0.12557	99.3	54.0
IRAS01477+1254	1175.54	INTRINSIC	H I	1025.7	H	43788.0	0.14605	1362.4	162.2
IRAS01477+1254	1176.35	INTRINSIC	H I	1025.7	H	44024.0	0.14684	804.9	108.5
IRAS01477+1254	1182.65	INTRINSIC	O VI	1031.9	H	43788.0	0.14605	478.4	75.7
IRAS01477+1254	1183.48	INTRINSIC	O VI	1031.9	H	44028.0	0.14684	306.0	66.0
IRAS01477+1254	1187.72	INTRINSIC	C II	1036.3	H	43793.0	0.14605	1123.7	90.1
IRAS01477+1254	1188.52	INTRINSIC	C II	1036.3	H	44023.0	0.14684	1078.6	90.4
IRAS01477+1254	1189.20	INTRINSIC	O VI	1037.6	H	43795.0	0.14605	363.0	66.5
IRAS01477+1254	1190.05	ISMLG	Si II	1190.4	L	-92.0	-0.00033	117.9	40.3
IRAS01477+1254	1190.43	ISMLG	Si II	1190.4	L	4.0	-0.00001	345.3	45.6
IRAS01477+1254	1192.90	ISMLG	Si II	1193.2	L	-98.0	-0.00033	143.3	40.3
IRAS01477+1254	1193.31	ISMLG	Si II	1193.2	L	6.0	-0.00001	347.9	38.8
IRAS01477+1254	1199.58	ISMLG	N I	1199.5	L	7.0	-0.00001	262.1	116.8
IRAS01477+1254	1200.23	ISMLG	N I	1200.2	L	3.0	-0.00001	142.7	89.4
IRAS01477+1254	1200.69	ISMLG	N I	1200.7	L	-4.0	-0.00001	215.8	93.8
IRAS01477+1254	1206.49	ISMLG	Si III	1206.5	L	-2.0	-0.00001	580.7	63.0
IRAS01477+1254	1236.64	IGMABS	H I	1215.6	H	5172.0	0.01725	191.6	55.5
IRAS01477+1254	1242.32	INTRINSIC	N II	1083.9	H	43787.0	0.14605	829.5	65.0
IRAS01477+1254	1243.15	INTRINSIC	N II	1083.9	H	44016.0	0.14684	479.3	44.5
IRAS01477+1254	1244.31	IGMABS	H I	1215.6	H	7062.0	0.02356	255.8	45.8
IRAS01477+1254	1247.63	IGMABS	H I	1215.6	H	7881.0	0.02629	288.9	72.2
IRAS01477+1254	1250.57	ISMLG	S II	1250.5	L	-1.0	-0.00001	76.9	37.5
IRAS01477+1254	1253.76	ISMLG	S II	1253.8	L	-11.0	-0.00001	177.4	37.0
IRAS01477+1254	1259.52	ISMLG	S II	1259.5	L	-1.0	-0.00001	240.2	44.0
IRAS01477+1254	1260.03	ISMLG	Si II	1260.4	L	-94.0	-0.00033	173.5	23.2
IRAS01477+1254	1260.39	ISMLG	Si II	1260.4	L	-7.0	-0.00001	559.0	42.6
IRAS01477+1254	1276.46	IGMABS	H I	1215.6	H	14991.0	0.05000	161.5	45.0
IRAS01477+1254	1286.50	INTRINSIC	Fe III	1122.5	H	43792.0	0.14605	794.4	57.2
IRAS01477+1254	1287.36	INTRINSIC	Fe III	1122.5	H	44023.0	0.14684	368.6	42.8
IRAS01477+1254	1293.49	IGMABS	H I	1215.6	H	19190.0	0.06401	462.0	53.6
IRAS01477+1254	1294.22	IGMABS	H I	1215.6	H	19372.0	0.06462	500.5	54.3
IRAS01477+1254	1301.70	ISMLG	O I	1302.1	L	-107.0	-0.00033	215.2	65.6
IRAS01477+1254	1302.15	ISMLG	O I	1302.1	L	-5.0	-0.00001	331.0	68.7
IRAS01477+1254	1303.89	ISMLG	Si II	1304.3	L	-110.0	-0.00033	131.3	70.9
IRAS01477+1254	1304.33	ISMLG	Si II	1304.3	L	-9.0	-0.00001	273.6	76.9
IRAS01477+1254	1305.70	IGMABS	H I	1215.6	H	22202.0	0.07406	314.1	88.7
IRAS01477+1254	1309.86	IGMABS	H I	1215.6	H	23228.0	0.07748	142.0	93.2
IRAS01477+1254	1334.06	ISMLG	C II	1334.5	L	-105.0	-0.00033	207.9	50.9
IRAS01477+1254	1334.49	ISMLG	C II	1334.5	L	-10.0	-0.00001	450.9	55.8
IRAS01477+1254	1335.70	ISMLG	C II*	1335.7	L	-2.0	-0.00001	237.6	40.6
IRAS01477+1254	1344.65	IGMABS	H I	1215.6	H	31806.0	0.10609	404.6	53.6
IRAS01477+1254	1347.95	UNIDENTIFIED	UNIND	1000.0	H	0.0	-1.00000	1732.8	103.0
IRAS01477+1254	1364.30	INTRINSIC	Si II	1190.4	H	43791.0	0.14605	1152.7	71.0
IRAS01477+1254	1365.22	INTRINSIC	Si II	1190.4	H	44024.0	0.14684	483.7	53.0
IRAS01477+1254	1367.61	INTRINSIC	Si II	1193.2	H	43795.0	0.14605	1057.5	69.0
IRAS01477+1254	1368.55	INTRINSIC	Si II	1193.2	H	44031.0	0.14684	375.2	42.4

Table A1 continued

Table A1 (*continued*)

Target	λ_{obs}	Type	Ion	λ_{rest}	Frame	cz	z	W_{λ}	$\sigma_{W_{\lambda}}$
	(Å)			(Å)		(km s ⁻¹)		(mÅ)	(mÅ)
IRAS01477+1254	1382.70	INTRINSIC	Si III	1206.5	H	43784.0	0.14605	1336.8	73.9
IRAS01477+1254	1383.67	INTRINSIC	Si III	1206.5	H	44023.0	0.14684	638.4	56.2
IRAS01477+1254	1393.22	INTRINSIC	H I	1215.6	H	43786.0	0.14605	1337.3	72.5
IRAS01477+1254	1394.18	INTRINSIC	H I	1215.6	H	44022.0	0.14684	894.1	36.2
IRAS01477+1254	1402.76	ISMLG	Si IV	1402.7	L	-3.0	-0.00001	185.6	57.5
IRAS01477+1254	1419.79	INTRINSIC	N V	1238.8	H	43793.0	0.14605	197.8	60.7
IRAS01477+1254	1424.37	INTRINSIC	N V	1242.8	H	43798.0	0.14605	146.8	45.4
IRAS01477+1254	1444.53	INTRINSIC	Si II	1260.4	H	43790.0	0.14605	1285.9	53.6
IRAS01477+1254	1445.50	INTRINSIC	Si II	1260.4	H	44021.0	0.14684	545.3	38.5
IRAS01477+1254	1492.36	INTRINSIC	O I	1302.1	H	43788.0	0.14605	791.7	79.7
IRAS01477+1254	1493.38	INTRINSIC	O I	1302.1	H	44021.0	0.14684	371.9	53.5
IRAS01477+1254	1494.92	INTRINSIC	Si II	1304.3	H	43795.0	0.14605	823.8	74.9
IRAS01477+1254	1495.91	INTRINSIC	Si II	1304.3	H	44022.0	0.14684	268.1	51.2
IRAS01477+1254	1526.19	ISMLG	Si II	1526.7	L	-102.0	-0.00033	183.0	50.4
IRAS01477+1254	1526.69	ISMLG	Si II	1526.7	L	-4.0	-0.00001	357.8	51.8
IRAS01477+1254	1529.50	INTRINSIC	C II	1334.5	H	43797.0	0.14605	1440.6	77.0
IRAS01477+1254	1530.51	INTRINSIC	C II	1334.5	H	44026.0	0.14684	1403.6	76.5
IRAS01477+1254	1548.20	ISMLG	C IV	1548.2	L	0.0	-0.00001	287.4	58.2
IRAS01477+1254	1550.75	ISMLG	C IV	1550.7	L	-6.0	-0.00001	131.3	52.3
IRAS01477+1254	1597.39	INTRINSIC	Si IV	1393.7	H	43799.0	0.14605	987.4	109.5
IRAS01477+1254	1598.41	INTRINSIC	Si IV	1393.7	H	44020.0	0.14684	462.9	82.5
IRAS01477+1254	1670.26	ISMLG	Al II	1670.7	L	-94.0	-0.00033	214.6	85.0
IRAS01477+1254	1670.77	ISMLG	Al II	1670.7	L	-4.0	-0.00001	426.3	86.2
IRAS01477+1254	1749.73	INTRINSIC	Si II	1526.7	H	43793.0	0.14605	1251.2	169.8
IRAS01477+1254	1750.91	INTRINSIC	Si II	1526.7	H	44026.0	0.14684	611.9	116.9
IRAS01477+1254	1774.35	INTRINSIC	C IV	1548.2	H	43790.0	0.14605	1477.5	305.1
IRAS01477+1254	1775.54	INTRINSIC	C IV	1548.2	H	44021.0	0.14684	601.7	212.7
IRAS01477+1254	1777.28	INTRINSIC	C IV	1550.7	H	43785.0	0.14605	1100.9	216.5
IRAS01477+1254	1778.51	PROXIMATE	H I	1550.7	H	44025.0	0.14684	236.5	103.2
IRAS_F00040+4325	1020.46	ISMLG	Si II	1020.6	L	-69.0	-0.00022	182.1	58.5
IRAS_F00040+4325	1020.66	ISMLG	Si II	1020.6	L	-12.0	-0.00003	258.1	64.8
IRAS_F00040+4325	1030.83	ISMLG	O VI	1031.9	L	-319.0	-0.00107	104.5	68.3
IRAS_F00040+4325	1031.44	ISMLG	Cl I	1031.5	L	-20.0	-0.00003	66.1	58.3
IRAS_F00040+4325	1031.69	ISMLG	O VI	1031.9	L	-70.0	-0.00022	70.1	55.5
IRAS_F00040+4325	1031.86	ISMLG	O VI	1031.9	L	-18.0	-0.00003	88.9	67.0
IRAS_F00040+4325	1035.80	ISMLG	C II	1036.3	L	-156.0	-0.00050	132.2	38.6
IRAS_F00040+4325	1036.12	ISMLG	C II	1036.3	L	-62.0	-0.00022	223.3	38.4
IRAS_F00040+4325	1036.31	ISMLG	C II	1036.3	L	-9.0	-0.00003	339.3	45.7
IRAS_F00040+4325	1047.96	ISMLG	Ar I	1048.2	L	-73.0	-0.00022	90.4	45.5
IRAS_F00040+4325	1048.16	ISMLG	Ar I	1048.2	L	-17.0	-0.00003	117.2	61.9
IRAS_F00040+4325	1055.20	ISMLG	Fe II	1055.2	L	-19.0	-0.00003	87.6	61.7
IRAS_F00040+4325	1063.13	ISMLG	Fe II	1063.1	L	-12.0	-0.00003	275.2	40.1
IRAS_F00040+4325	1063.91	ISMLG	Fe II	1063.9	L	-19.0	-0.00003	120.2	53.1
IRAS_F00040+4325	1066.60	ISMLG	Ar I	1066.6	L	-17.0	-0.00003	266.1	53.3
IRAS_F00040+4325	1091.64	IGMABS	H I	972.5	H	36715.0	0.12249	151.1	54.8
IRAS_F00040+4325	1096.83	ISMLG	Fe II	1096.8	L	-14.0	-0.00003	185.7	55.5
IRAS_F00040+4325	1121.93	ISMLG	Fe II	1121.9	L	-11.0	-0.00003	242.2	73.0
IRAS_F00040+4325	1122.46	ISMLG	Fe III	1122.5	L	-17.0	-0.00003	65.4	52.8
IRAS_F00040+4325	1125.38	ISMLG	Fe II	1125.4	L	-17.0	-0.00003	133.2	60.6
IRAS_F00040+4325	1133.59	ISMLG	Fe II	1133.6	L	-19.0	-0.00003	65.6	53.8
IRAS_F00040+4325	1133.93	ISMLG	N I	1134.1	L	-62.0	-0.00022	112.8	42.4
IRAS_F00040+4325	1134.11	ISMLG	N I	1134.1	L	-15.0	-0.00003	198.5	44.9
IRAS_F00040+4325	1134.35	ISMLG	N I	1134.4	L	-16.0	-0.00003	271.5	47.4

Table A1 continued

Table A1 (*continued*)

Target	λ_{obs}	Type	Ion	λ_{rest}	Frame	cz	z	W_{λ}	$\sigma_{W_{\lambda}}$
	(Å)			(Å)		(km s ⁻¹)		(mÅ)	(mÅ)
IRAS_F00040+4325	1134.73	ISMLG	N I	1134.9	L	-66.0	-0.00022	62.6	24.5
IRAS_F00040+4325	1134.94	ISMLG	N I	1134.9	L	-12.0	-0.00003	229.0	24.8
IRAS_F00040+4325	1142.31	ISMLG	Fe II	1142.3	L	-14.0	-0.00003	44.5	11.0
IRAS_F00040+4325	1143.16	ISMLG	Fe II	1143.2	L	-17.0	-0.00003	157.4	10.4
IRAS_F00040+4325	1144.68	ISMLG	Fe II	1144.9	L	-69.0	-0.00022	78.2	10.1
IRAS_F00040+4325	1144.89	ISMLG	Fe II	1144.9	L	-12.0	-0.00003	237.0	8.4
IRAS_F00040+4325	1145.15	ISMLG	Fe II	1144.9	L	56.0	0.00018	22.3	10.9
IRAS_F00040+4325	1150.16	IGMABS	H I	1025.7	H	36370.0	0.12131	38.6	9.2
IRAS_F00040+4325	1150.31	IGMABS	H I	1025.7	H	36414.0	0.12145	35.3	8.8
IRAS_F00040+4325	1151.37	IGMABS	H I	1025.7	H	36723.0	0.12249	180.3	11.5
IRAS_F00040+4325	1152.77	ISMLG	P II	1152.8	L	-14.0	-0.00003	177.0	10.6
IRAS_F00040+4325	1157.24	IGMABS	O VI	1031.9	H	36407.0	0.12145	80.4	12.5
IRAS_F00040+4325	1157.86	ISMLG	C I	1157.9	L	-13.0	-0.00003	50.8	10.1
IRAS_F00040+4325	1158.32	IGMABS	O VI	1031.9	H	36721.0	0.12249	102.5	9.4
IRAS_F00040+4325	1159.40	IGMABS	H I	1025.7	H	39071.0	0.13036	222.0	14.3
IRAS_F00040+4325	1163.64	IGMABS	O VI	1037.6	H	36411.0	0.12145	74.3	11.0
IRAS_F00040+4325	1164.70	IGMABS	O VI	1037.6	H	36717.0	0.12249	88.8	13.4
IRAS_F00040+4325	1166.46	IGMABS	O VI	1031.9	H	39085.0	0.13036	89.1	16.5
IRAS_F00040+4325	1172.89	IGMABS	O VI	1037.6	H	39085.0	0.13036	37.0	10.9
IRAS_F00040+4325	1178.15	IGMABS	H I	1025.7	H	44551.0	0.14863	63.1	8.6
IRAS_F00040+4325	1188.58	ISMLG	C I	1188.8	L	-64.0	-0.00022	19.3	3.9
IRAS_F00040+4325	1188.76	ISMLG	C I	1188.8	L	-19.0	-0.00003	41.7	5.2
IRAS_F00040+4325	1189.77	ISMLG	Si II	1190.4	L	-162.0	-0.00050	37.1	4.7
IRAS_F00040+4325	1190.14	ISMLG	Si II	1190.4	L	-69.0	-0.00022	181.0	3.6
IRAS_F00040+4325	1190.37	ISMLG	Si II	1190.4	L	-12.0	-0.00003	258.4	3.2
IRAS_F00040+4325	1190.62	ISMLG	Si II	1190.4	L	50.0	0.00018	43.0	4.0
IRAS_F00040+4325	1192.36	ISMLG	Si II	1193.2	L	-233.0	-0.00078	23.9	4.6
IRAS_F00040+4325	1192.64	ISMLG	Si II	1193.2	L	-163.0	-0.00050	66.9	5.1
IRAS_F00040+4325	1193.01	ISMLG	Si II	1193.2	L	-71.0	-0.00022	214.9	3.0
IRAS_F00040+4325	1193.24	ISMLG	Si II	1193.2	L	-13.0	-0.00003	256.4	2.8
IRAS_F00040+4325	1193.48	ISMLG	Si II	1193.2	L	49.0	0.00018	57.3	3.5
IRAS_F00040+4325	1197.11	ISMLG	Mn II	1197.1	L	-18.0	-0.00003	25.4	4.5
IRAS_F00040+4325	1199.28	ISMLG	N I	1199.5	L	-68.0	-0.00022	139.1	4.2
IRAS_F00040+4325	1199.51	ISMLG	N I	1199.5	L	-10.0	-0.00003	267.8	3.3
IRAS_F00040+4325	1199.96	ISMLG	N I	1200.2	L	-66.0	-0.00022	123.5	3.7
IRAS_F00040+4325	1200.16	ISMLG	N I	1200.2	L	-16.0	-0.00003	260.5	2.9
IRAS_F00040+4325	1200.44	ISMLG	N I	1200.7	L	-67.0	-0.00022	148.3	3.0
IRAS_F00040+4325	1200.67	ISMLG	N I	1200.7	L	-11.0	-0.00003	229.5	2.7
IRAS_F00040+4325	1201.02	ISMLG	Mn II	1201.1	L	-24.0	-0.00003	22.5	4.5
IRAS_F00040+4325	1204.78	ISMLG	Si III	1206.5	L	-427.0	-0.00144	20.8	4.6
IRAS_F00040+4325	1205.21	ISMLG	Si III	1206.5	L	-321.0	-0.00107	56.3	4.6
IRAS_F00040+4325	1205.56	ISMLG	Si III	1206.5	L	-234.0	-0.00078	41.4	4.6
IRAS_F00040+4325	1205.88	ISMLG	Si III	1206.5	L	-154.0	-0.00050	127.2	3.5
IRAS_F00040+4325	1206.22	ISMLG	Si III	1206.5	L	-71.0	-0.00022	258.4	2.8
IRAS_F00040+4325	1206.45	ISMLG	Si III	1206.5	L	-12.0	-0.00003	280.1	3.5
IRAS_F00040+4325	1206.71	ISMLG	Si III	1206.5	L	51.0	0.00018	80.8	4.7
IRAS_F00040+4325	1239.85	ISMLG	Mg II	1239.9	L	-18.0	-0.00003	40.2	6.1
IRAS_F00040+4325	1250.49	ISMLG	S II	1250.5	L	-20.0	-0.00003	223.5	4.6
IRAS_F00040+4325	1253.50	ISMLG	S II	1253.8	L	-72.0	-0.00022	55.9	4.9
IRAS_F00040+4325	1253.72	ISMLG	S II	1253.8	L	-20.0	-0.00003	243.5	4.3
IRAS_F00040+4325	1259.21	ISMLG	S II	1259.5	L	-73.0	-0.00022	78.3	5.3
IRAS_F00040+4325	1259.43	ISMLG	S II	1259.5	L	-20.0	-0.00003	261.9	3.6
IRAS_F00040+4325	1259.76	ISMLG	Si II	1260.4	L	-157.0	-0.00050	74.4	4.6

Table A1 continued

Table A1 (*continued*)

Target	λ_{obs}	Type	Ion	λ_{rest}	Frame	cz	z	W_{λ}	$\sigma_{W_{\lambda}}$
	(Å)			(Å)		(km s ⁻¹)		(mÅ)	(mÅ)
IRAS_F00040+4325	1260.12	ISMLG	Si II	1260.4	L	-72.0	-0.00022	228.8	3.5
IRAS_F00040+4325	1260.37	ISMLG	Si II	1260.4	L	-11.0	-0.00003	370.2	2.8
IRAS_F00040+4325	1260.65	ISMLG	Si II	1260.4	L	55.0	0.00018	87.1	4.0
IRAS_F00040+4325	1265.21	IGMABS	H I	1215.6	H	12218.0	0.04075	50.2	5.8
IRAS_F00040+4325	1265.52	IGMABS	H I	1215.6	H	12294.0	0.04101	41.2	6.0
IRAS_F00040+4325	1270.61	IGMABS	H I	1215.6	H	13550.0	0.04520	43.3	6.7
IRAS_F00040+4325	1276.95	ISMLG	C I	1277.2	L	-69.0	-0.00022	65.0	6.4
IRAS_F00040+4325	1277.20	ISMLG	C I	1277.2	L	-9.0	-0.00003	82.6	7.0
IRAS_F00040+4325	1279.85	ISMLG	C I	1280.1	L	-66.0	-0.00022	27.4	7.2
IRAS_F00040+4325	1280.09	ISMLG	C I	1280.1	L	-11.0	-0.00003	33.8	7.7
IRAS_F00040+4325	1282.19	IGMABS	H I	1215.6	H	16405.0	0.05472	57.9	8.3
IRAS_F00040+4325	1283.95	IGMABS	H I	1215.6	H	16839.0	0.05617	17.0	9.5
IRAS_F00040+4325	1301.21	ISMLG	O I	1302.1	L	-222.0	-0.00078	32.1	6.4
IRAS_F00040+4325	1301.86	ISMLG	O I	1302.1	L	-70.0	-0.00022	145.3	4.8
IRAS_F00040+4325	1302.12	ISMLG	O I	1302.1	L	-11.0	-0.00003	346.3	3.9
IRAS_F00040+4325	1302.41	ISMLG	O I	1302.1	L	57.0	0.00018	49.7	4.6
IRAS_F00040+4325	1304.05	ISMLG	Si II	1304.3	L	-73.0	-0.00022	129.1	5.2
IRAS_F00040+4325	1304.32	ISMLG	Si II	1304.3	L	-11.0	-0.00003	319.7	4.6
IRAS_F00040+4325	1304.60	ISMLG	Si II	1304.3	L	54.0	0.00018	33.2	4.7
IRAS_F00040+4325	1307.09	IGMABS	H I	1215.6	H	22544.0	0.07520	40.0	6.7
IRAS_F00040+4325	1313.28	IGMABS	H I	1215.6	H	24070.0	0.08029	54.5	10.0
IRAS_F00040+4325	1317.17	ISMLG	Ni II	1317.2	L	-11.0	-0.00003	65.4	11.4
IRAS_F00040+4325	1325.88	IGMABS	H I	1215.6	H	27178.0	0.09065	61.1	12.8
IRAS_F00040+4325	1328.54	ISMLG	C I	1328.8	L	-65.0	-0.00022	33.6	7.2
IRAS_F00040+4325	1328.79	ISMLG	C I	1328.8	L	-9.0	-0.00003	61.0	7.1
IRAS_F00040+4325	1330.21	IGMABS	H I	1215.6	H	28247.0	0.09422	46.8	9.8
IRAS_F00040+4325	1333.07	ISMLG	C II	1334.5	L	-329.0	-0.00107	49.1	7.4
IRAS_F00040+4325	1333.54	ISMLG	C II	1334.5	L	-223.0	-0.00078	66.3	6.0
IRAS_F00040+4325	1333.85	ISMLG	C II	1334.5	L	-154.0	-0.00050	163.2	5.4
IRAS_F00040+4325	1334.25	ISMLG	C II	1334.5	L	-63.0	-0.00022	239.2	3.6
IRAS_F00040+4325	1334.49	ISMLG	C II	1334.5	L	-10.0	-0.00003	383.6	3.6
IRAS_F00040+4325	1334.79	ISMLG	C II	1334.5	L	58.0	0.00018	88.1	4.9
IRAS_F00040+4325	1335.62	ISMLG	C II*	1335.7	L	-20.0	-0.00003	295.7	6.0
IRAS_F00040+4325	1341.29	IGMABS	H I	1215.6	H	30979.0	0.10333	225.1	7.9
IRAS_F00040+4325	1347.16	ISMLG	Cl I	1347.2	L	-19.0	-0.00003	40.1	6.8
IRAS_F00040+4325	1363.15	IGMABS	H I	1215.6	H	36368.0	0.12131	68.3	4.9
IRAS_F00040+4325	1363.31	IGMABS	H I	1215.6	H	36409.0	0.12145	63.1	4.1
IRAS_F00040+4325	1364.58	IGMABS	H I	1215.6	H	36722.0	0.12249	327.6	4.7
IRAS_F00040+4325	1370.06	ISMLG	Ni II	1370.1	L	-16.0	-0.00003	59.9	7.0
IRAS_F00040+4325	1374.14	IGMABS	H I	1215.6	H	39080.0	0.13036	515.2	8.9
IRAS_F00040+4325	1389.27	IGMABS	N V	1238.8	H	36409.0	0.12145	27.6	6.0
IRAS_F00040+4325	1390.55	IGMABS	N V	1238.8	H	36717.0	0.12249	23.5	4.7
IRAS_F00040+4325	1393.06	ISMLG	Si IV	1393.7	L	-150.0	-0.00050	34.1	4.9
IRAS_F00040+4325	1393.43	ISMLG	Si IV	1393.7	L	-70.0	-0.00022	37.4	4.7
IRAS_F00040+4325	1393.67	ISMLG	Si IV	1393.7	L	-19.0	-0.00003	95.1	5.2
IRAS_F00040+4325	1395.03	IGMABS	N V	1242.8	H	36721.0	0.12249	18.4	5.1
IRAS_F00040+4325	1396.36	IGMABS	H I	1215.6	H	44559.0	0.14863	160.7	6.4
IRAS_F00040+4325	1399.08	IGMABS	H I	1215.6	H	45231.0	0.15088	45.1	7.4
IRAS_F00040+4325	1401.23	IGMABS	H I	1215.6	H	45760.0	0.15264	98.4	4.5
IRAS_F00040+4325	1401.53	IGMABS	H I	1215.6	H	45834.0	0.15288	28.9	4.7
IRAS_F00040+4325	1402.68	ISMLG	Si IV	1402.7	L	-19.0	-0.00003	47.6	4.4
IRAS_F00040+4325	1405.11	PROXIMATE	H I	1215.6	H	46718.0	0.15584	67.3	5.1
IRAS_F00040+4325	1411.98	PROXIMATE	H I	1215.6	H	48412.0	0.16149	62.7	4.5

Table A1 continued

Table A1 (*continued*)

Target	λ_{obs}	Type	Ion	λ_{rest}	Frame	cz	z	W_{λ}	$\sigma_{W_{\lambda}}$
	(Å)			(Å)		(km s ⁻¹)		(mÅ)	(mÅ)
IRAS_F00040+4325	1454.78	ISMLG	Ni II	1454.8	L	-12.0	-0.00003	27.9	5.8
IRAS_F00040+4325	1526.33	ISMLG	Si II	1526.7	L	-74.0	-0.00022	188.7	6.3
IRAS_F00040+4325	1526.65	ISMLG	Si II	1526.7	L	-12.0	-0.00003	351.3	5.5
IRAS_F00040+4325	1526.95	ISMLG	Si II	1526.7	L	48.0	0.00018	25.7	7.4
IRAS_F00040+4325	1532.48	ISMLG	P II	1532.5	L	-11.0	-0.00003	24.0	8.2
IRAS_F00040+4325	1546.51	ISMLG	C IV	1548.2	L	-329.0	-0.00107	47.4	9.0
IRAS_F00040+4325	1547.03	ISMLG	C IV	1548.2	L	-227.0	-0.00078	46.2	9.7
IRAS_F00040+4325	1547.43	ISMLG	C IV	1548.2	L	-149.0	-0.00050	43.7	9.1
IRAS_F00040+4325	1548.12	ISMLG	C IV	1548.2	L	-17.0	-0.00003	51.9	8.2
IRAS_F00040+4325	1550.73	ISMLG	C IV	1550.7	L	-10.0	-0.00003	74.3	11.5
IRAS_F00040+4325	1559.99	ISMLG	C I	1560.3	L	-62.0	-0.00022	57.3	8.0
IRAS_F00040+4325	1560.27	ISMLG	C I	1560.3	L	-8.0	-0.00003	95.8	7.6
IRAS_F00040+4325	1608.06	ISMLG	Fe II	1608.4	L	-72.0	-0.00022	79.8	13.8
IRAS_F00040+4325	1608.39	ISMLG	Fe II	1608.4	L	-11.0	-0.00003	373.6	10.0
IRAS_F00040+4325	1608.74	ISMLG	Fe II	1608.4	L	54.0	0.00018	53.0	11.9
IRAS_F00040+4325	1656.59	ISMLG	C I	1656.9	L	-60.0	-0.00022	88.4	10.2
IRAS_F00040+4325	1656.87	ISMLG	C I	1656.9	L	-11.0	-0.00003	131.9	12.3
IRAS_F00040+4325	1670.39	ISMLG	Al II	1670.7	L	-71.0	-0.00022	213.2	11.2
IRAS_F00040+4325	1670.72	ISMLG	Al II	1670.7	L	-12.0	-0.00003	340.9	10.6
IRAS_F00040+4325	1671.07	ISMLG	Al II	1670.7	L	51.0	0.00018	46.6	12.2
IRAS_F00040+4325	1709.49	ISMLG	Ni II	1709.6	L	-20.0	-0.00003	60.8	16.4
IRAS_F00040+4325	1736.25	IGMABS	C IV	1548.2	H	36414.0	0.12145	58.7	17.5
IRAS_F00040+4325	1737.87	IGMABS	C IV	1548.2	H	36727.0	0.12249	143.2	18.1
IRAS_F00040+4325	1739.14	IGMABS	C IV	1550.7	H	36413.0	0.12145	59.0	16.0
IRAS_F00040+4325	1740.76	IGMABS	C IV	1550.7	H	36727.0	0.12249	90.6	15.5
IRAS_F00040+4325	1741.47	ISMLG	Ni II	1741.5	L	-14.0	-0.00003	74.5	17.9
IRAS_F00040+4325	1751.85	ISMLG	H I	1751.9	L	-12.0	-0.00003	52.0	20.5
KAZ238	1143.18	ISMLG	Fe II	1143.2	L	-12.0	-0.00003	94.4	27.3
KAZ238	1144.86	ISMLG	Fe II	1144.9	L	-21.0	-0.00003	314.8	42.5
KAZ238	1152.78	ISMLG	P II	1152.8	L	-10.0	-0.00003	108.1	28.9
KAZ238	1156.17	UNIDENTIFIED	UNIND	1000.0	H	0.0	-1.00000	457.7	55.0
KAZ238	1157.97	UNIDENTIFIED	UNIND	1000.0	H	0.0	-1.00000	338.1	42.4
KAZ238	1161.24	UNIDENTIFIED	UNIND	1000.0	H	0.0	-1.00000	353.0	51.2
KAZ238	1166.45	UNIDENTIFIED	UNIND	1000.0	H	0.0	-1.00000	475.4	60.7
KAZ238	1169.64	INTRINSIC	Fe III	1122.5	H	12583.0	0.04197	251.2	37.1
KAZ238	1170.42	INTRINSIC	Fe III	1122.5	H	12791.0	0.04267	96.9	26.9
KAZ238	1170.60	INTRINSIC	Fe III	1122.5	H	12840.0	0.04284	111.6	21.8
KAZ238	1170.81	INTRINSIC	Fe III	1122.5	H	12897.0	0.04300	126.5	18.7
KAZ238	1171.26	INTRINSIC	Fe III	1122.5	H	13015.0	0.04341	204.1	26.0
KAZ238	1176.92	UNIDENTIFIED	UNIND	1000.0	H	0.0	-1.00000	527.7	39.8
KAZ238	1190.34	ISMLG	Si II	1190.4	L	-19.0	-0.00003	375.1	18.2
KAZ238	1193.21	ISMLG	Si II	1193.2	L	-20.0	-0.00003	378.0	19.3
KAZ238	1194.65	INTRINSIC	Fe II	1144.9	H	13015.0	0.04341	104.8	22.9
KAZ238	1199.48	ISMLG	N I	1199.5	L	-17.0	-0.00003	324.9	14.7
KAZ238	1200.17	ISMLG	N I	1200.2	L	-14.0	-0.00003	345.1	19.0
KAZ238	1200.62	ISMLG	N I	1200.7	L	-21.0	-0.00003	350.9	20.3
KAZ238	1201.03	ISMLG	Mn II	1201.1	L	-22.0	-0.00003	40.6	13.2
KAZ238	1204.77	ISMLG	Si III	1206.5	L	-430.0	-0.00143	40.2	14.1
KAZ238	1205.15	ISMLG	Si III	1206.5	L	-337.0	-0.00110	64.4	15.1
KAZ238	1205.77	ISMLG	Si III	1206.5	L	-181.0	-0.00063	89.1	17.3
KAZ238	1206.42	ISMLG	Si III	1206.5	L	-21.0	-0.00003	359.2	17.3
KAZ238	1224.27	IGMABS	H I	1215.6	H	2121.0	0.00707	232.2	31.2
KAZ238	1234.05	IGMABS	H I	1215.6	H	4534.0	0.01512	59.9	11.1

Table A1 continued

Table A1 (*continued*)

Target	λ_{obs}	Type	Ion	λ_{rest}	Frame	cz	z	W_{λ}	$\sigma_{W_{\lambda}}$
	(Å)			(Å)		(km s ⁻¹)		(mÅ)	(mÅ)
KAZ238	1234.29	IGMABS	H I	1215.6	H	4591.0	0.01531	87.1	11.7
KAZ238	1235.39	IGMABS	H I	1215.6	H	4862.0	0.01622	629.7	19.9
KAZ238	1237.40	IGMABS	H I	1215.6	H	5360.0	0.01788	200.2	27.4
KAZ238	1240.36	INTRINSIC	Si II	1190.4	H	12578.0	0.04197	216.4	19.5
KAZ238	1241.21	INTRINSIC	Si II	1190.4	H	12793.0	0.04267	70.1	10.0
KAZ238	1241.41	INTRINSIC	Si II	1190.4	H	12842.0	0.04284	184.7	11.1
KAZ238	1241.60	INTRINSIC	Si II	1190.4	H	12890.0	0.04300	240.8	10.2
KAZ238	1242.07	INTRINSIC	Si II	1190.4	H	13010.0	0.04341	309.4	17.6
KAZ238	1243.37	INTRINSIC	Si II	1193.2	H	12581.0	0.04197	192.2	20.8
KAZ238	1244.19	INTRINSIC	Si II	1193.2	H	12789.0	0.04267	62.9	12.9
KAZ238	1244.39	INTRINSIC	Si II	1193.2	H	12837.0	0.04284	85.9	9.5
KAZ238	1244.62	INTRINSIC	Si II	1193.2	H	12897.0	0.04300	478.0	16.0
KAZ238	1245.10	INTRINSIC	Si II	1193.2	H	13016.0	0.04341	334.8	12.7
KAZ238	1250.52	ISMLG	S II	1250.5	L	-15.0	-0.00003	148.8	17.1
KAZ238	1250.73	INTRINSIC	N I	1199.5	H	12792.0	0.04267	40.2	9.0
KAZ238	1250.93	INTRINSIC	N I	1199.5	H	12841.0	0.04284	60.4	10.8
KAZ238	1251.13	INTRINSIC	N I	1199.5	H	12892.0	0.04300	64.7	11.1
KAZ238	1251.44	INTRINSIC	N I	1200.2	H	12793.0	0.04267	54.9	8.7
KAZ238	1251.61	INTRINSIC	N I	1199.5	H	13011.0	0.04341	150.6	16.5
KAZ238	1251.63	INTRINSIC	N I	1200.2	H	12841.0	0.04284	150.6	16.5
KAZ238	1251.83	INTRINSIC	N I	1200.2	H	12891.0	0.04300	61.7	10.9
KAZ238	1251.94	INTRINSIC	N I	1200.7	H	12790.0	0.04267	51.4	11.0
KAZ238	1252.14	INTRINSIC	N I	1200.7	H	12842.0	0.04284	75.0	10.8
KAZ238	1252.32	INTRINSIC	N I	1200.2	H	13012.0	0.04341	139.2	13.1
KAZ238	1252.34	INTRINSIC	N I	1200.7	H	12892.0	0.04300	145.6	12.2
KAZ238	1252.83	INTRINSIC	N I	1200.7	H	13014.0	0.04341	140.6	13.6
KAZ238	1253.76	ISMLG	S II	1253.8	L	-11.0	-0.00003	255.8	17.8
KAZ238	1257.09	INTRINSIC	Si III	1206.5	H	12572.0	0.04197	443.5	19.5
KAZ238	1257.98	INTRINSIC	Si III	1206.5	H	12793.0	0.04267	197.3	13.8
KAZ238	1258.18	INTRINSIC	Si III	1206.5	H	12841.0	0.04284	311.6	13.7
KAZ238	1258.38	INTRINSIC	Si III	1206.5	H	12891.0	0.04300	826.0	10.8
KAZ238	1258.85	INTRINSIC	Si III	1206.5	H	13009.0	0.04341	548.8	21.6
KAZ238	1259.47	ISMLG	S II	1259.5	L	-11.0	-0.00003	201.6	17.8
KAZ238	1260.35	ISMLG	Si II	1260.4	L	-16.0	-0.00003	447.0	16.4
KAZ238	1266.69	INTRINSIC	H I	1215.6	H	12582.0	0.04197	475.7	17.7
KAZ238	1267.54	INTRINSIC	H I	1215.6	H	12792.0	0.04267	216.6	22.9
KAZ238	1267.75	INTRINSIC	H I	1215.6	H	12843.0	0.04284	261.9	21.5
KAZ238	1267.94	INTRINSIC	H I	1215.6	H	12890.0	0.04300	595.7	8.2
KAZ238	1268.44	INTRINSIC	H I	1215.6	H	13013.0	0.04341	980.7	8.9
KAZ238	1277.20	ISMLG	C I	1277.2	L	-10.0	-0.00003	40.9	16.0
KAZ238	1291.89	INTRINSIC	N V	1238.8	H	12842.0	0.04284	58.1	14.8
KAZ238	1302.08	ISMLG	O I	1302.1	L	-21.0	-0.00003	388.3	19.0
KAZ238	1304.28	ISMLG	Si II	1304.3	L	-20.0	-0.00003	339.1	14.8
KAZ238	1307.77	INTRINSIC	S II	1253.8	H	12902.0	0.04300	50.6	16.5
KAZ238	1308.24	INTRINSIC	S II	1253.8	H	13016.0	0.04341	77.2	13.2
KAZ238	1313.30	INTRINSIC	Si II	1260.4	H	12578.0	0.04197	304.3	31.0
KAZ238	1314.17	INTRINSIC	S II	1259.5	H	13009.0	0.04341	199.4	19.4
KAZ238	1314.41	INTRINSIC	Si II	1260.4	H	12841.0	0.04284	151.7	16.1
KAZ238	1314.62	INTRINSIC	Si II	1260.4	H	12890.0	0.04300	599.9	23.6
KAZ238	1315.15	INTRINSIC	Si II	1260.4	H	13017.0	0.04341	462.4	22.0
KAZ238	1317.16	ISMLG	Ni II	1317.2	L	-12.0	-0.00003	46.7	23.8
KAZ238	1334.46	ISMLG	C II	1334.5	L	-16.0	-0.00003	441.7	14.5
KAZ238	1335.67	ISMLG	C II*	1335.7	L	-8.0	-0.00003	192.4	15.5

Table A1 continued

Table A1 (*continued*)

Target	λ_{obs}	Type	Ion	λ_{rest}	Frame	cz	z	W_{λ}	$\sigma_{W_{\lambda}}$
	(Å)			(Å)		(km s ⁻¹)		(mÅ)	(mÅ)
KAZ238	1342.08	UNIDENTIFIED	UNIND	1000.0	H	0.0	-1.00000	244.6	29.8
KAZ238	1350.65	UNIDENTIFIED	UNIND	1000.0	H	0.0	-1.00000	277.4	26.8
KAZ238	1352.68	UNIDENTIFIED	UNIND	1000.0	H	0.0	-1.00000	354.1	31.2
KAZ238	1355.01	UNIDENTIFIED	UNIND	1000.0	H	0.0	-1.00000	301.3	29.8
KAZ238	1357.73	INTRINSIC	O I	1302.1	H	12793.0	0.04267	113.4	15.3
KAZ238	1358.14	INTRINSIC	O I	1302.1	H	12885.0	0.04300	62.1	16.9
KAZ238	1358.70	INTRINSIC	O I	1302.1	H	13015.0	0.04341	226.5	28.1
KAZ238	1360.06	INTRINSIC	Si II	1304.3	H	12799.0	0.04267	115.0	15.7
KAZ238	1360.23	INTRINSIC	Si II	1304.3	H	12840.0	0.04284	66.2	14.5
KAZ238	1360.51	INTRINSIC	Si II	1304.3	H	12902.0	0.04300	131.0	21.1
KAZ238	1361.00	INTRINSIC	Si II	1304.3	H	13015.0	0.04341	184.7	22.1
KAZ238	1370.07	ISMLG	Ni II	1370.1	L	-14.0	-0.00003	48.7	16.6
KAZ238	1381.54	UNIDENTIFIED	UNIND	1000.0	H	0.0	-1.00000	365.5	34.1
KAZ238	1390.53	INTRINSIC	C II	1334.5	H	12580.0	0.04197	242.0	18.4
KAZ238	1391.47	INTRINSIC	C II	1334.5	H	12790.0	0.04267	206.1	19.4
KAZ238	1391.69	INTRINSIC	C II	1334.5	H	12840.0	0.04284	303.4	15.4
KAZ238	1391.94	INTRINSIC	C II	1334.5	H	12895.0	0.04300	925.4	19.2
KAZ238	1392.46	INTRINSIC	C II	1334.5	H	13012.0	0.04341	613.7	16.2
KAZ238	1393.70	ISMLG	Si IV	1393.7	L	-12.0	-0.00003	153.2	17.4
KAZ238	1402.73	ISMLG	Si IV	1402.7	L	-10.0	-0.00003	113.9	19.0
KAZ238	1452.25	INTRINSIC	Si IV	1393.7	H	12581.0	0.04197	456.5	78.4
KAZ238	1453.21	INTRINSIC	Si IV	1393.7	H	12788.0	0.04267	117.1	17.3
KAZ238	1453.46	INTRINSIC	Si IV	1393.7	H	12842.0	0.04284	224.3	15.9
KAZ238	1453.69	INTRINSIC	Si IV	1393.7	H	12891.0	0.04300	700.6	54.4
KAZ238	1454.25	INTRINSIC	Si IV	1393.7	H	13010.0	0.04341	102.3	16.5
KAZ238	1461.67	INTRINSIC	Si IV	1402.7	H	12586.0	0.04197	318.0	32.5
KAZ238	1462.62	INTRINSIC	Si IV	1402.7	H	12789.0	0.04267	93.3	17.2
KAZ238	1462.86	INTRINSIC	Si IV	1402.7	H	12843.0	0.04284	219.4	17.1
KAZ238	1463.09	INTRINSIC	Si IV	1402.7	H	12890.0	0.04300	138.1	12.9
KAZ238	1463.68	INTRINSIC	Si IV	1402.7	H	13018.0	0.04341	139.3	20.9
KAZ238	1478.33	UNIDENTIFIED	UNIND	1000.0	H	0.0	-1.00000	104.2	25.4
KAZ238	1487.39	UNIDENTIFIED	UNIND	1000.0	H	0.0	-1.00000	125.4	22.8
KAZ238	1492.16	UNIDENTIFIED	UNIND	1000.0	H	0.0	-1.00000	102.8	23.9
KAZ238	1526.60	ISMLG	Si II	1526.7	L	-21.0	-0.00003	430.2	26.3
KAZ238	1546.44	ISMLG	C IV	1548.2	L	-342.0	-0.00110	112.6	31.9
KAZ238	1547.22	ISMLG	C IV	1548.2	L	-190.0	-0.00063	92.9	26.3
KAZ238	1548.09	ISMLG	C IV	1548.2	L	-21.0	-0.00003	186.3	28.6
KAZ238	1548.99	ISMLG	C IV	1550.7	L	-346.0	-0.00110	101.4	32.7
KAZ238	1549.86	ISMLG	C IV	1550.7	L	-178.0	-0.00063	71.9	21.2
KAZ238	1550.68	ISMLG	C IV	1550.7	L	-20.0	-0.00003	173.8	27.1
KAZ238	1592.10	INTRINSIC	Si II	1526.7	H	12841.0	0.04284	106.1	35.6
KAZ238	1592.39	INTRINSIC	Si II	1526.7	H	12897.0	0.04300	265.3	25.1
KAZ238	1592.95	INTRINSIC	Si II	1526.7	H	13007.0	0.04341	334.9	35.5
KAZ238	1608.39	ISMLG	Fe II	1608.4	L	-12.0	-0.00003	358.9	133.7
KAZ238	1614.52	INTRINSIC	C IV	1548.2	H	12842.0	0.04284	392.6	109.3
KAZ238	1614.77	INTRINSIC	C IV	1548.2	H	12891.0	0.04300	645.1	125.2
KAZ238	1617.20	INTRINSIC	C IV	1550.7	H	12839.0	0.04284	236.4	64.4
KAZ238	1617.48	INTRINSIC	C IV	1550.7	H	12895.0	0.04300	419.5	65.1
KAZ238	1670.72	ISMLG	Al II	1670.7	L	-13.0	-0.00003	504.8	53.1
KAZ238	1742.07	INTRINSIC	Al II	1670.7	H	12791.0	0.04267	131.5	51.3
KAZ238	1742.34	INTRINSIC	Al II	1670.7	H	12839.0	0.04284	143.4	44.5
KAZ238	1742.70	INTRINSIC	Al II	1670.7	H	12903.0	0.04300	209.3	39.9
KAZ238	1743.30	PROXIMATE	H I	1670.7	H	13011.0	0.04341	425.6	60.2

Table A1 continued

Table A1 (*continued*)

Target	λ_{obs}	Type	Ion	λ_{rest}	Frame	cz	z	W_{λ}	$\sigma_{W_{\lambda}}$
	(Å)			(Å)		(km s ⁻¹)		(mÅ)	(mÅ)
MRK1014	1152.77	ISMLG	P II	1152.8	L	-12.0	-0.00002	130.7	18.8
MRK1014	1175.66	IGMABS	H I	1025.7	H	43823.0	0.14618	351.2	12.1
MRK1014	1182.75	IGMABS	O VI	1031.9	H	43816.0	0.14618	31.9	9.0
MRK1014	1190.17	ISMLG	Si II	1190.4	L	-62.0	-0.00020	97.0	5.4
MRK1014	1190.39	ISMLG	Si II	1190.4	L	-5.0	-0.00002	267.1	4.7
MRK1014	1193.03	ISMLG	Si II	1193.2	L	-66.0	-0.00020	90.6	6.2
MRK1014	1193.27	ISMLG	Si II	1193.2	L	-5.0	-0.00002	310.1	6.3
MRK1014	1199.29	ISMLG	N I	1199.5	L	-65.0	-0.00020	41.0	8.2
MRK1014	1199.54	ISMLG	N I	1199.5	L	-2.0	-0.00002	196.7	7.6
MRK1014	1200.23	ISMLG	N I	1200.2	L	2.0	-0.00002	179.4	6.7
MRK1014	1200.70	ISMLG	N I	1200.7	L	-3.0	-0.00002	195.1	9.1
MRK1014	1206.00	ISMLG	Si III	1206.5	L	-124.0	-0.00041	102.9	6.1
MRK1014	1206.24	ISMLG	Si III	1206.5	L	-66.0	-0.00020	134.9	3.6
MRK1014	1206.49	ISMLG	Si III	1206.5	L	-3.0	-0.00002	468.7	5.9
MRK1014	1244.37	IGMABS	H I	1215.6	H	7077.0	0.02361	111.5	11.3
MRK1014	1246.33	IGMABS	H I	1215.6	H	7560.0	0.02522	394.9	8.4
MRK1014	1249.80	IGMABS	H I	1215.6	H	8418.0	0.02808	153.0	12.4
MRK1014	1250.56	ISMLG	S II	1250.5	L	-4.0	-0.00002	95.1	7.4
MRK1014	1253.79	ISMLG	S II	1253.8	L	-3.0	-0.00002	144.7	7.9
MRK1014	1259.49	ISMLG	S II	1259.5	L	-6.0	-0.00002	149.3	7.0
MRK1014	1260.13	ISMLG	Si II	1260.4	L	-69.0	-0.00020	114.6	4.9
MRK1014	1260.39	ISMLG	Si II	1260.4	L	-8.0	-0.00002	385.8	4.7
MRK1014	1260.75	ISMLG	C I	1260.7	L	3.0	-0.00002	54.9	6.3
MRK1014	1263.55	IGMABS	H I	1215.6	H	11808.0	0.03939	52.0	10.5
MRK1014	1265.61	IGMABS	H I	1215.6	H	12315.0	0.04108	202.1	9.3
MRK1014	1267.92	IGMABS	H I	1215.6	H	12886.0	0.04298	252.0	10.0
MRK1014	1277.21	ISMLG	C I	1277.2	L	-8.0	-0.00002	35.0	7.9
MRK1014	1289.95	IGMABS	H I	1215.6	H	18319.0	0.06110	96.3	10.2
MRK1014	1291.74	IGMABS	H I	1215.6	H	18760.0	0.06258	93.1	12.9
MRK1014	1301.86	ISMLG	O I	1302.1	L	-70.0	-0.00020	88.7	8.0
MRK1014	1302.17	ISMLG	O I	1302.1	L	0.0	-0.00002	296.7	10.9
MRK1014	1304.06	ISMLG	Si II	1304.3	L	-72.0	-0.00020	65.0	9.9
MRK1014	1304.38	ISMLG	Si II	1304.3	L	2.0	-0.00002	274.8	10.7
MRK1014	1309.85	IGMABS	H I	1215.6	H	23225.0	0.07747	72.8	24.9
MRK1014	1327.51	IGMABS	H I	1215.6	H	27581.0	0.09200	476.4	14.0
MRK1014	1333.98	ISMLG	C II	1334.5	L	-125.0	-0.00041	56.6	7.7
MRK1014	1334.20	ISMLG	C II	1334.5	L	-74.0	-0.00020	182.4	5.3
MRK1014	1334.48	ISMLG	C II	1334.5	L	-12.0	-0.00002	449.2	8.1
MRK1014	1335.67	ISMLG	C II*	1335.7	L	-8.0	-0.00002	108.6	10.2
MRK1014	1337.58	IGMABS	H I	1215.6	H	30064.0	0.10028	38.6	12.2
MRK1014	1339.27	IGMABS	H I	1215.6	H	30482.0	0.10168	77.8	13.6
MRK1014	1344.09	IGMABS	H I	1215.6	H	31669.0	0.10564	210.8	14.9
MRK1014	1349.15	IGMABS	H I	1215.6	H	32916.0	0.10980	44.9	12.6
MRK1014	1382.81	IGMABS	Si III	1206.5	H	43811.0	0.14618	42.0	11.1
MRK1014	1393.38	IGMABS	H I	1215.6	H	43825.0	0.14618	580.5	7.0
MRK1014	1393.69	ISMLG	Si IV	1393.7	L	-14.0	-0.00002	186.4	7.4
MRK1014	1399.98	IGMABS	H I	1215.6	H	45453.0	0.15161	101.1	8.7
MRK1014	1402.77	ISMLG	Si IV	1402.7	L	-1.0	-0.00002	104.7	6.3
MRK1014	1403.13	PROXIMATE	H I	1215.6	H	46228.0	0.15420	110.0	8.6
MRK1014	1414.42	INTRINSIC	H I	1215.6	H	49013.0	0.16349	45.7	7.3
MRK1148	1143.20	ISMLG	Fe II	1143.2	L	-8.0	-0.00002	66.4	8.9
MRK1148	1144.76	ISMLG	Fe II	1144.9	L	-47.0	-0.00017	126.8	7.3
MRK1148	1144.91	ISMLG	Fe II	1144.9	L	-8.0	-0.00002	98.6	9.3

Table A1 continued

Table A1 (*continued*)

Target	λ_{obs}	Type	Ion	λ_{rest}	Frame	cz	z	W_{λ}	$\sigma_{W_{\lambda}}$
	(Å)			(Å)		(km s ⁻¹)		(mÅ)	(mÅ)
MRK1148	1152.66	ISMLG	P II	1152.8	L	-41.0	-0.00017	28.3	8.1
MRK1148	1152.80	ISMLG	P II	1152.8	L	-5.0	-0.00002	75.9	10.6
MRK1148	1157.87	ISMLG	C I	1157.9	L	-11.0	-0.00002	46.2	9.6
MRK1148	1188.81	ISMLG	C I	1188.8	L	-6.0	-0.00002	48.9	6.7
MRK1148	1190.23	ISMLG	Si II	1190.4	L	-48.0	-0.00017	176.8	4.3
MRK1148	1190.38	ISMLG	Si II	1190.4	L	-9.0	-0.00002	212.8	5.3
MRK1148	1193.10	ISMLG	Si II	1193.2	L	-49.0	-0.00017	190.1	3.6
MRK1148	1193.26	ISMLG	Si II	1193.2	L	-7.0	-0.00002	209.0	4.6
MRK1148	1193.96	ISMLG	C I	1193.9	L	-9.0	-0.00002	25.5	6.0
MRK1148	1199.36	ISMLG	N I	1199.5	L	-48.0	-0.00017	112.1	5.1
MRK1148	1199.54	ISMLG	N I	1199.5	L	-2.0	-0.00002	151.6	4.9
MRK1148	1200.05	ISMLG	N I	1200.2	L	-42.0	-0.00017	140.7	4.7
MRK1148	1200.22	ISMLG	N I	1200.2	L	-1.0	-0.00002	154.3	5.5
MRK1148	1200.53	ISMLG	N I	1200.7	L	-45.0	-0.00017	110.6	4.7
MRK1148	1200.68	ISMLG	N I	1200.7	L	-8.0	-0.00002	118.8	5.9
MRK1148	1205.70	ISMLG	Si III	1206.5	L	-199.0	-0.00065	14.8	5.9
MRK1148	1206.33	ISMLG	Si III	1206.5	L	-42.0	-0.00017	178.9	5.2
MRK1148	1206.47	ISMLG	Si III	1206.5	L	-8.0	-0.00002	240.3	4.3
MRK1148	1239.74	ISMLG	Mg II	1239.9	L	-45.0	-0.00017	10.8	5.3
MRK1148	1239.90	ISMLG	Mg II	1239.9	L	-7.0	-0.00002	19.6	5.0
MRK1148	1250.38	ISMLG	S II	1250.5	L	-48.0	-0.00017	34.4	5.1
MRK1148	1250.55	ISMLG	S II	1250.5	L	-7.0	-0.00002	66.0	5.4
MRK1148	1253.62	ISMLG	S II	1253.8	L	-44.0	-0.00017	69.5	4.8
MRK1148	1253.77	ISMLG	S II	1253.8	L	-9.0	-0.00002	74.5	4.3
MRK1148	1259.34	ISMLG	S II	1259.5	L	-42.0	-0.00017	82.9	4.6
MRK1148	1259.49	ISMLG	S II	1259.5	L	-7.0	-0.00002	101.0	4.3
MRK1148	1260.22	ISMLG	Si II	1260.4	L	-47.0	-0.00017	227.1	2.7
MRK1148	1260.39	ISMLG	Si II	1260.4	L	-7.0	-0.00002	208.4	3.3
MRK1148	1260.69	ISMLG	C I	1260.7	L	-10.0	-0.00002	49.0	4.2
MRK1148	1266.09	IGMABS	H I	1215.6	H	12435.0	0.04148	53.9	8.9
MRK1148	1277.20	ISMLG	C I	1277.2	L	-10.0	-0.00002	73.3	4.9
MRK1148	1280.09	ISMLG	C I	1280.1	L	-9.0	-0.00002	40.1	6.1
MRK1148	1283.64	INTRINSIC	Si III	1206.5	H	19167.0	0.06395	20.6	6.2
MRK1148	1284.36	PROXIMATE	H I	1215.6	H	16941.0	0.05651	58.3	7.0
MRK1148	1285.83	PROXIMATE	H I	1215.6	H	17301.0	0.05771	77.6	7.2
MRK1148	1288.78	PROXIMATE	H I	1215.6	H	18029.0	0.06014	34.2	4.9
MRK1148	1293.41	INTRINSIC	H I	1215.6	H	19171.0	0.06395	261.7	2.4
MRK1148	1301.96	ISMLG	O I	1302.1	L	-49.0	-0.00017	188.3	2.2
MRK1148	1302.15	ISMLG	O I	1302.1	L	-5.0	-0.00002	250.1	2.0
MRK1148	1304.15	ISMLG	Si II	1304.3	L	-50.0	-0.00017	155.1	1.8
MRK1148	1304.33	ISMLG	Si II	1304.3	L	-9.0	-0.00002	165.3	2.4
MRK1148	1317.16	ISMLG	Ni II	1317.2	L	-12.0	-0.00002	31.7	6.2
MRK1148	1318.05	INTRINSIC	N V	1238.8	H	19174.0	0.06395	30.3	5.5
MRK1148	1328.79	ISMLG	C I	1328.8	L	-10.0	-0.00002	36.8	7.2
MRK1148	1333.68	ISMLG	C II	1334.5	L	-192.0	-0.00065	12.3	4.3
MRK1148	1334.35	ISMLG	C II	1334.5	L	-40.0	-0.00017	271.8	4.5
MRK1148	1334.51	ISMLG	C II	1334.5	L	-5.0	-0.00002	250.7	4.5
MRK1148	1335.52	ISMLG	C II*	1335.7	L	-43.0	-0.00017	19.6	4.4
MRK1148	1335.66	ISMLG	C II*	1335.7	L	-10.0	-0.00002	98.5	4.9
MRK1148	1347.22	ISMLG	Cl I	1347.2	L	-5.0	-0.00002	23.1	6.9
MRK1148	1393.71	ISMLG	Si IV	1393.7	L	-10.0	-0.00002	86.1	6.8
MRK1148	1393.95	ISMLG	Si IV	1393.7	L	41.0	0.00012	34.1	6.6
MRK1148	1402.75	ISMLG	Si IV	1402.7	L	-5.0	-0.00002	70.5	8.9

Table A1 continued

Table A1 (*continued*)

Target	λ_{obs}	Type	Ion	λ_{rest}	Frame	cz	z	W_{λ}	$\sigma_{W_{\lambda}}$
	(Å)			(Å)		(km s ⁻¹)		(mÅ)	(mÅ)
MRK1148	1526.45	ISMLG	Si II	1526.7	L	-50.0	-0.00017	255.6	5.7
MRK1148	1526.69	ISMLG	Si II	1526.7	L	-3.0	-0.00002	151.9	8.6
MRK1148	1548.15	ISMLG	C IV	1548.2	L	-10.0	-0.00002	79.4	8.3
MRK1148	1548.39	ISMLG	C IV	1548.2	L	36.0	0.00012	102.2	9.2
MRK1148	1550.74	ISMLG	C IV	1550.7	L	-8.0	-0.00002	60.6	7.7
MRK1148	1551.00	ISMLG	C IV	1550.7	L	42.0	0.00012	45.9	8.9
MRK1148	1560.32	ISMLG	C I	1560.3	L	2.0	-0.00002	57.7	11.8
MRK1148	1608.15	ISMLG	Fe II	1608.4	L	-56.0	-0.00017	161.0	11.5
MRK1148	1608.45	ISMLG	Fe II	1608.4	L	-1.0	-0.00002	161.1	14.7
MRK1148	1647.19	INTRINSIC	C IV	1548.2	H	19167.0	0.06395	138.9	7.0
MRK1148	1649.92	INTRINSIC	C IV	1550.7	H	19165.0	0.06395	126.5	7.0
MRK1148	1656.88	ISMLG	C I	1656.9	L	-8.0	-0.00002	71.7	6.5
MRK1148	1670.49	ISMLG	Al II	1670.7	L	-54.0	-0.00017	242.3	6.4
MRK1148	1670.79	ISMLG	H I	1670.7	L	0.0	-0.00002	201.6	9.3
MRK1179	1134.94	ISMLG	N I	1134.9	L	-12.0	-0.00002	181.0	93.5
MRK1179	1143.21	ISMLG	Fe II	1143.2	L	-5.0	-0.00002	93.0	59.8
MRK1179	1144.89	ISMLG	Fe II	1144.9	L	-12.0	-0.00002	248.6	50.6
MRK1179	1188.78	ISMLG	C I	1188.8	L	-14.0	-0.00002	68.8	21.3
MRK1179	1189.89	ISMLG	Si II	1190.4	L	-133.0	-0.00042	111.2	22.8
MRK1179	1190.37	ISMLG	Si II	1190.4	L	-12.0	-0.00002	418.9	18.6
MRK1179	1192.79	ISMLG	Si II	1193.2	L	-126.0	-0.00042	171.0	22.9
MRK1179	1193.24	ISMLG	Si II	1193.2	L	-11.0	-0.00002	382.6	19.5
MRK1179	1199.50	ISMLG	N I	1199.5	L	-12.0	-0.00002	268.9	22.7
MRK1179	1200.17	ISMLG	N I	1200.2	L	-14.0	-0.00002	254.2	21.9
MRK1179	1200.67	ISMLG	N I	1200.7	L	-11.0	-0.00002	276.3	26.1
MRK1179	1205.97	ISMLG	Si III	1206.5	L	-132.0	-0.00042	218.5	20.8
MRK1179	1206.46	ISMLG	Si III	1206.5	L	-10.0	-0.00002	482.0	16.3
MRK1179	1219.82	IGMABS	H I	1215.6	H	1023.0	0.00341	154.7	46.1
MRK1179	1222.03	IGMABS	H I	1215.6	H	1567.0	0.00523	246.3	36.0
MRK1179	1223.81	IGMABS	H I	1215.6	H	2007.0	0.00669	102.2	22.9
MRK1179	1225.26	IGMABS	Si III	1206.5	H	4661.0	0.01553	80.5	21.9
MRK1179	1226.48	IGMABS	H I	1215.6	H	2665.0	0.00889	138.0	21.3
MRK1179	1234.55	IGMABS	H I	1215.6	H	4656.0	0.01553	309.0	13.3
MRK1179	1245.63	IGMABS	H I	1215.6	H	7387.0	0.02464	49.6	11.9
MRK1179	1247.89	IGMABS	H I	1215.6	H	7945.0	0.02650	72.5	9.9
MRK1179	1249.61	PROXIMATE	Si III	1206.5	H	10711.0	0.03574	53.9	8.4
MRK1179	1250.57	ISMLG	S II	1250.5	L	-1.0	-0.00002	123.6	6.2
MRK1179	1250.83	PROXIMATE	H I	1215.6	H	8670.0	0.02892	135.7	4.5
MRK1179	1252.22	INTRINSIC	Si III	1206.5	H	11361.0	0.03790	61.8	6.7
MRK1179	1253.79	ISMLG	S II	1253.8	L	-3.0	-0.00002	150.6	6.5
MRK1179	1258.21	PROXIMATE	H I	1215.6	H	10491.0	0.03499	227.0	6.2
MRK1179	1258.83	PROXIMATE	H I	1215.6	H	10643.0	0.03550	136.4	2.7
MRK1179	1259.11	PROXIMATE	H I	1215.6	H	10714.0	0.03574	522.6	3.8
MRK1179	1259.32	PROXIMATE	H I	1215.6	H	10766.0	0.03591	196.2	1.9
MRK1179	1259.47	ISMLG	S II	1259.5	L	-11.0	-0.00002	192.8	3.3
MRK1179	1259.90	ISMLG	Si II	1260.4	L	-125.0	-0.00042	198.8	4.2
MRK1179	1260.38	ISMLG	Si II	1260.4	L	-9.0	-0.00002	480.6	2.5
MRK1179	1260.73	ISMLG	C I	1260.7	L	0.0	-0.00002	77.8	3.5
MRK1179	1261.74	INTRINSIC	H I	1215.6	H	11361.0	0.03790	361.6	4.6
MRK1179	1277.25	ISMLG	C I	1277.2	L	0.0	-0.00002	65.1	9.2
MRK1179	1280.08	ISMLG	C I	1280.1	L	-13.0	-0.00002	38.6	11.8
MRK1179	1282.80	PROXIMATE	N V	1238.8	H	10643.0	0.03550	61.5	8.2
MRK1179	1283.06	PROXIMATE	N V	1238.8	H	10707.0	0.03574	218.9	7.4

Table A1 continued

Table A1 (*continued*)

Target	λ_{obs}	Type	Ion	λ_{rest}	Frame	cz	z	W_{λ}	$\sigma_{W_{\lambda}}$
	(Å)			(Å)		(km s ⁻¹)		(mÅ)	(mÅ)
MRK1179	1283.32	PROXIMATE	N v	1238.8	H	10768.0	0.03591	76.6	6.1
MRK1179	1285.79	INTRINSIC	N v	1238.8	H	11366.0	0.03790	135.0	11.0
MRK1179	1286.93	PROXIMATE	N v	1242.8	H	10645.0	0.03550	44.0	8.3
MRK1179	1287.19	PROXIMATE	N v	1242.8	H	10706.0	0.03574	174.1	8.4
MRK1179	1287.43	PROXIMATE	N v	1242.8	H	10764.0	0.03591	102.7	7.2
MRK1179	1289.89	INTRINSIC	N v	1242.8	H	11359.0	0.03790	108.9	12.3
MRK1179	1301.64	ISMLG	O i	1302.1	L	-123.0	-0.00042	170.7	18.2
MRK1179	1302.14	ISMLG	O i	1302.1	L	-7.0	-0.00002	330.0	12.8
MRK1179	1304.34	ISMLG	Si ii	1304.3	L	-6.0	-0.00002	338.1	16.8
MRK1179	1317.17	ISMLG	Ni ii	1317.2	L	-11.0	-0.00002	80.2	32.1
MRK1179	1333.94	ISMLG	C ii	1334.5	L	-134.0	-0.00042	292.2	18.1
MRK1179	1334.47	ISMLG	C ii	1334.5	L	-14.0	-0.00002	572.3	16.5
MRK1179	1335.70	ISMLG	C ii*	1335.7	L	-1.0	-0.00002	170.9	21.0
MRK1179	1347.24	ISMLG	Cl i	1347.2	L	0.0	-0.00002	56.5	14.7
MRK1179	1370.11	ISMLG	Ni ii	1370.1	L	-4.0	-0.00002	40.0	18.7
MRK1179	1393.69	ISMLG	Si iv	1393.7	L	-14.0	-0.00002	118.5	25.2
MRK1179	1402.77	ISMLG	Si iv	1402.7	L	-2.0	-0.00002	72.1	25.6
MRK1179	1446.60	INTRINSIC	Si iv	1393.7	H	11366.0	0.03790	92.0	20.2
MRK1179	1455.98	INTRINSIC	Si iv	1402.7	H	11370.0	0.03790	59.1	18.5
MRK1179	1526.05	ISMLG	Si ii	1526.7	L	-129.0	-0.00042	107.2	32.3
MRK1179	1526.65	ISMLG	Si ii	1526.7	L	-11.0	-0.00002	458.3	28.8
MRK1179	1548.15	ISMLG	C iv	1548.2	L	-10.0	-0.00002	198.1	28.6
MRK1179	1550.75	ISMLG	C iv	1550.7	L	-6.0	-0.00002	178.1	34.1
MRK1179	1560.26	ISMLG	C i	1560.3	L	-9.0	-0.00002	95.9	23.0
MRK1179	1560.68	ISMLG	C i*	1560.6	L	0.0	-0.00002	59.6	22.9
MRK1179	1603.16	PROXIMATE	C iv	1548.2	H	10642.0	0.03550	108.1	12.3
MRK1179	1603.52	PROXIMATE	C iv	1548.2	H	10710.0	0.03574	191.5	8.2
MRK1179	1603.80	PROXIMATE	C iv	1548.2	H	10766.0	0.03591	88.9	9.8
MRK1179	1606.14	PROXIMATE	C iv	1550.7	H	10702.0	0.03574	121.3	12.3
MRK1179	1606.48	PROXIMATE	C iv	1550.7	H	10767.0	0.03591	57.7	9.5
MRK1179	1606.86	INTRINSIC	C iv	1548.2	H	11358.0	0.03790	352.5	16.1
MRK1179	1608.40	ISMLG	Fe ii	1608.4	L	-10.0	-0.00002	277.1	18.4
MRK1179	1609.53	INTRINSIC	C iv	1550.7	H	11356.0	0.03790	294.8	21.8
MRK1179	1656.94	ISMLG	C i	1656.9	L	2.0	-0.00002	183.5	39.9
MRK1179	1670.73	ISMLG	H i	1670.7	L	-11.0	-0.00002	441.2	45.7
MRK1501	1189.00	ISMLG	Si ii	1190.4	L	-357.0	-0.00120	237.3	69.5
MRK1501	1190.33	ISMLG	Si ii	1190.4	L	-22.0	-0.00006	318.8	71.5
MRK1501	1191.87	ISMLG	Si ii	1193.2	L	-358.0	-0.00120	128.8	72.1
MRK1501	1193.20	ISMLG	Si ii	1193.2	L	-22.0	-0.00006	372.2	92.6
MRK1501	1199.47	ISMLG	N i	1199.5	L	-21.0	-0.00006	263.8	75.9
MRK1501	1200.15	ISMLG	N i	1200.2	L	-18.0	-0.00006	268.8	88.1
MRK1501	1200.63	ISMLG	N i	1200.7	L	-19.0	-0.00006	226.3	86.1
MRK1501	1205.09	ISMLG	Si iii	1206.5	L	-350.0	-0.00120	243.7	68.7
MRK1501	1205.45	ISMLG	Si iii	1206.5	L	-261.0	-0.00088	79.4	67.9
MRK1501	1206.43	ISMLG	Si iii	1206.5	L	-19.0	-0.00006	351.4	62.7
MRK1501	1206.75	ISMLG	Si iii	1206.5	L	62.0	0.00023	335.9	54.5
MRK1501	1250.54	ISMLG	S ii	1250.5	L	-8.0	-0.00006	92.4	52.7
MRK1501	1252.98	IGMABS	H i	1215.6	H	9201.0	0.03069	284.9	55.4
MRK1501	1253.78	ISMLG	S ii	1253.8	L	-7.0	-0.00006	165.3	55.3
MRK1501	1255.99	IGMABS	H i	1215.6	H	9944.0	0.03317	162.7	57.3
MRK1501	1258.96	ISMLG	Si ii	1260.4	L	-347.0	-0.00120	191.6	37.9
MRK1501	1259.48	ISMLG	S ii	1259.5	L	-9.0	-0.00006	195.2	49.0
MRK1501	1260.34	ISMLG	Si ii	1260.4	L	-20.0	-0.00006	439.6	46.1

Table A1 continued

Table A1 (*continued*)

Target	λ_{obs}	Type	Ion	λ_{rest}	Frame	cz	z	W_{λ}	$\sigma_{W_{\lambda}}$
	(Å)			(Å)		(km s ⁻¹)		(mÅ)	(mÅ)
MRK1501	1260.70	ISMLG	Si II	1260.4	L	66.0	0.00023	180.5	43.1
MRK1501	1276.31	IGMABS	H I	1215.6	H	14954.0	0.04988	97.2	41.7
MRK1501	1300.65	ISMLG	O I	1302.1	L	-349.0	-0.00120	65.5	38.4
MRK1501	1302.07	ISMLG	O I	1302.1	L	-23.0	-0.00006	411.3	36.2
MRK1501	1304.30	ISMLG	Si II	1304.3	L	-17.0	-0.00006	390.7	39.0
MRK1501	1309.46	IGMABS	H I	1215.6	H	23130.0	0.07715	266.7	51.1
MRK1501	1312.60	INTRINSIC	Si III	1206.5	H	26364.0	0.08794	105.4	36.0
MRK1501	1322.58	INTRINSIC	H I	1215.6	H	26364.0	0.08794	558.2	9.6
MRK1501	1323.01	INTRINSIC	H I	1215.6	H	26471.0	0.08830	289.8	8.8
MRK1501	1324.23	INTRINSIC	H I	1215.6	H	26772.0	0.08930	305.5	13.3
MRK1501	1326.83	PROXIMATE	H I	1215.6	H	27414.0	0.09144	31.1	9.2
MRK1501	1328.78	ISMLG	C I	1328.8	L	-11.0	-0.00006	73.7	12.8
MRK1501	1332.99	ISMLG	C II	1334.5	L	-346.0	-0.00120	213.9	11.3
MRK1501	1333.34	ISMLG	C II	1334.5	L	-268.0	-0.00088	90.2	13.8
MRK1501	1334.45	ISMLG	C II	1334.5	L	-19.0	-0.00006	448.7	10.4
MRK1501	1334.88	ISMLG	C II	1334.5	L	77.0	0.00023	155.1	14.6
MRK1501	1335.66	ISMLG	C II*	1335.7	L	-11.0	-0.00006	154.8	14.6
MRK1501	1393.70	ISMLG	Si IV	1393.7	L	-13.0	-0.00006	188.8	69.5
MRK1501	2793.08	ISMLG	Mg II	2796.3	L	-351.0	-0.00120	511.9	3.3
MRK1501	2796.15	ISMLG	Mg II	2796.3	L	-22.0	-0.00006	1072.0	2.3
MRK1501	2800.30	ISMLG	Mg II	2803.5	L	-345.0	-0.00120	216.7	3.7
MRK1501	2803.30	ISMLG	H I	2803.5	L	-24.0	-0.00006	1011.9	3.3
MRK1502	1020.67	ISMLG	Si II	1020.6	L	-7.0	-0.00003	206.0	37.1
MRK1502	1031.29	ISMLG	O VI	1031.9	L	-184.0	-0.00063	171.4	23.1
MRK1502	1031.93	ISMLG	O VI	1031.9	L	1.0	-0.00003	89.1	22.5
MRK1502	1036.30	ISMLG	C II	1036.3	L	-11.0	-0.00003	-3714.1	20.5
MRK1502	1037.59	ISMLG	O VI	1037.6	L	-7.0	-0.00003	169.0	30.0
MRK1502	1039.19	ISMLG	O I	1039.2	L	-13.0	-0.00003	289.4	24.7
MRK1502	1048.19	ISMLG	Ar I	1048.2	L	-10.0	-0.00003	104.2	18.5
MRK1502	1066.63	ISMLG	Ar I	1066.6	L	-9.0	-0.00003	93.1	21.0
MRK1502	1088.11	PROXIMATE	O VI	1031.9	H	16323.0	0.05445	135.0	15.7
MRK1502	1094.02	INTRINSIC	O VI	1031.9	H	18038.0	0.06019	178.5	5.2
MRK1502	1094.12	PROXIMATE	O VI	1037.6	H	16324.0	0.05445	178.5	5.2
MRK1502	1094.80	INTRINSIC	O VI	1031.9	H	18266.0	0.06092	122.7	11.5
MRK1502	1095.53	INTRINSIC	O VI	1031.9	H	18478.0	0.06164	116.0	11.1
MRK1502	1096.84	ISMLG	Fe II	1096.8	L	-10.0	-0.00003	108.0	10.7
MRK1502	1100.06	INTRINSIC	O VI	1037.6	H	18041.0	0.06019	151.8	13.8
MRK1502	1100.83	INTRINSIC	O VI	1037.6	H	18265.0	0.06092	95.6	27.4
MRK1502	1101.55	INTRINSIC	O VI	1037.6	H	18471.0	0.06164	80.1	18.8
MRK1502	1122.49	ISMLG	Fe III	1122.5	L	-10.0	-0.00003	112.0	27.7
MRK1502	1133.64	ISMLG	Fe II	1133.6	L	-8.0	-0.00003	44.6	19.5
MRK1502	1134.12	ISMLG	N I	1134.1	L	-11.0	-0.00003	112.1	19.7
MRK1502	1134.38	ISMLG	N I	1134.4	L	-10.0	-0.00003	104.4	15.4
MRK1502	1134.96	ISMLG	N I	1134.9	L	-5.0	-0.00003	153.7	17.5
MRK1502	1143.18	ISMLG	Fe II	1143.2	L	-11.0	-0.00003	127.5	32.8
MRK1502	1144.90	ISMLG	Fe II	1144.9	L	-11.0	-0.00003	155.6	19.8
MRK1502	1152.77	ISMLG	P II	1152.8	L	-12.0	-0.00003	66.8	11.7
MRK1502	1157.90	ISMLG	C I	1157.9	L	-2.0	-0.00003	31.8	9.3
MRK1502	1178.86	OTHER	FPN	0.0	H	0.0	-1.00000	38.8	7.5
MRK1502	1188.81	ISMLG	C I	1188.8	L	-5.0	-0.00003	53.3	5.7
MRK1502	1190.37	ISMLG	Si II	1190.4	L	-12.0	-0.00003	342.2	7.0
MRK1502	1193.24	ISMLG	Si II	1193.2	L	-13.0	-0.00003	391.0	5.2
MRK1502	1193.99	ISMLG	C I	1193.9	L	-1.0	-0.00003	19.2	2.9

Table A1 continued

Table A1 (*continued*)

Target	λ_{obs}	Type	Ion	λ_{rest}	Frame	cz	z	W_{λ}	$\sigma_{W_{\lambda}}$
	(Å)			(Å)		(km s ⁻¹)		(mÅ)	(mÅ)
MRK1502	1197.15	ISMLG	Mn II	1197.1	L	-8.0	-0.00003	21.4	5.5
MRK1502	1199.52	ISMLG	N I	1199.5	L	-7.0	-0.00003	224.6	17.4
MRK1502	1200.18	ISMLG	N I	1200.2	L	-10.0	-0.00003	228.7	19.4
MRK1502	1200.67	ISMLG	N I	1200.7	L	-9.0	-0.00003	197.5	19.1
MRK1502	1201.07	ISMLG	Mn II	1201.1	L	-12.0	-0.00003	32.9	6.8
MRK1502	1205.54	ISMLG	Si III	1206.5	L	-238.0	-0.00075	17.4	5.0
MRK1502	1205.76	ISMLG	Si III	1206.5	L	-184.0	-0.00063	19.4	4.9
MRK1502	1206.04	ISMLG	Si III	1206.5	L	-115.0	-0.00037	48.4	6.4
MRK1502	1206.45	ISMLG	Si III	1206.5	L	-11.0	-0.00003	486.0	5.6
MRK1502	1239.92	ISMLG	Mg II	1239.9	L	-1.0	-0.00003	25.2	5.7
MRK1502	1240.39	ISMLG	Mg II	1240.3	L	-2.0	-0.00003	29.3	5.8
MRK1502	1250.57	ISMLG	S II	1250.5	L	-3.0	-0.00003	86.8	4.5
MRK1502	1252.40	IGMABS	H I	1215.6	H	9058.0	0.03021	19.7	4.2
MRK1502	1252.63	IGMABS	H I	1215.6	H	9114.0	0.03040	35.9	4.9
MRK1502	1253.78	ISMLG	S II	1253.8	L	-7.0	-0.00003	116.0	5.0
MRK1502	1259.47	ISMLG	S II	1259.5	L	-11.0	-0.00003	135.5	4.1
MRK1502	1259.93	ISMLG	Si II	1260.4	L	-116.0	-0.00037	40.4	3.9
MRK1502	1260.38	ISMLG	Si II	1260.4	L	-11.0	-0.00003	450.7	3.3
MRK1502	1260.71	ISMLG	C I	1260.7	L	-5.0	-0.00003	37.1	2.0
MRK1502	1272.20	PROXIMATE	Si III	1206.5	H	16325.0	0.05445	15.2	2.7
MRK1502	1276.46	ISMLG	C I	1276.4	L	-5.0	-0.00003	16.1	3.2
MRK1502	1277.25	ISMLG	C I	1277.2	L	2.0	-0.00003	42.2	1.9
MRK1502	1277.70	IGMABS	H I	1215.6	H	15298.0	0.05103	96.9	3.7
MRK1502	1280.13	ISMLG	C I	1280.1	L	-1.0	-0.00003	36.2	2.2
MRK1502	1281.10	PROXIMATE	H I	1215.6	H	16135.0	0.05382	78.2	2.7
MRK1502	1281.47	PROXIMATE	H I	1215.6	H	16226.0	0.05412	123.2	2.3
MRK1502	1281.87	PROXIMATE	H I	1215.6	H	16324.0	0.05445	146.2	2.9
MRK1502	1284.56	PROXIMATE	H I	1215.6	H	16988.0	0.05667	42.5	2.4
MRK1502	1288.57	INTRINSIC	H I	1215.6	H	17978.0	0.05997	38.2	1.3
MRK1502	1288.85	INTRINSIC	H I	1215.6	H	18046.0	0.06019	15.5	1.1
MRK1502	1289.73	INTRINSIC	H I	1215.6	H	18264.0	0.06092	27.4	1.5
MRK1502	1302.12	ISMLG	O I	1302.1	L	-11.0	-0.00003	371.4	10.1
MRK1502	1304.33	ISMLG	Si II	1304.3	L	-9.0	-0.00003	274.2	11.7
MRK1502	1305.52	PROXIMATE	N V	1238.8	H	16140.0	0.05382	88.9	10.8
MRK1502	1306.28	PROXIMATE	N V	1238.8	H	16325.0	0.05445	99.0	4.9
MRK1502	1309.70	PROXIMATE	N V	1242.8	H	16137.0	0.05382	78.1	9.2
MRK1502	1310.48	PROXIMATE	N V	1242.8	H	16326.0	0.05445	87.7	4.0
MRK1502	1313.39	INTRINSIC	N V	1238.8	H	18045.0	0.06019	41.3	3.5
MRK1502	1314.31	INTRINSIC	N V	1238.8	H	18269.0	0.06092	43.4	3.2
MRK1502	1317.17	ISMLG	Ni II	1317.2	L	-10.0	-0.00003	26.2	4.0
MRK1502	1317.61	INTRINSIC	N V	1242.8	H	18046.0	0.06019	19.3	3.8
MRK1502	1318.52	INTRINSIC	N V	1242.8	H	18264.0	0.06092	18.6	4.8
MRK1502	1328.83	ISMLG	C I	1328.8	L	-1.0	-0.00003	55.4	5.4
MRK1502	1333.44	ISMLG	C II	1334.5	L	-245.0	-0.00075	33.8	4.4
MRK1502	1333.67	ISMLG	C II	1334.5	L	-193.0	-0.00063	28.8	4.4
MRK1502	1334.03	ISMLG	C II	1334.5	L	-113.0	-0.00037	48.0	4.4
MRK1502	1334.47	ISMLG	C II	1334.5	L	-14.0	-0.00003	530.5	4.9
MRK1502	1335.70	ISMLG	C II*	1335.7	L	-1.0	-0.00003	107.7	4.9
MRK1502	1347.25	ISMLG	Cl I	1347.2	L	2.0	-0.00003	64.3	7.2
MRK1502	1370.10	ISMLG	Ni II	1370.1	L	-8.0	-0.00003	46.6	7.6
MRK1502	1393.72	ISMLG	Si IV	1393.7	L	-9.0	-0.00003	148.3	9.6
MRK1502	1402.76	ISMLG	Si IV	1402.7	L	-4.0	-0.00003	94.4	10.1
MRK1502	1469.65	PROXIMATE	Si IV	1393.7	H	16323.0	0.05445	38.8	4.7

Table A1 continued

Table A1 (*continued*)

Target	λ_{obs}	Type	Ion	λ_{rest}	Frame	cz	z	W_{λ}	$\sigma_{W_{\lambda}}$
	(Å)			(Å)		(km s ⁻¹)		(mÅ)	(mÅ)
MRK1502	1479.15	PROXIMATE	Si iv	1402.7	H	16323.0	0.05445	27.8	3.8
MRK1502	1526.63	ISMLG	Si ii	1526.7	L	-15.0	-0.00003	369.4	8.1
MRK1502	1547.21	ISMLG	C iv	1548.2	L	-192.0	-0.00063	119.6	9.1
MRK1502	1547.67	ISMLG	C iv	1548.2	L	-104.0	-0.00037	35.0	7.0
MRK1502	1548.14	ISMLG	C iv	1548.2	L	-12.0	-0.00003	179.9	8.8
MRK1502	1549.78	ISMLG	C iv	1550.7	L	-194.0	-0.00063	78.6	7.3
MRK1502	1550.73	ISMLG	C iv	1550.7	L	-9.0	-0.00003	98.5	9.5
MRK1502	1560.30	ISMLG	C i	1560.3	L	-2.0	-0.00003	58.1	8.0
MRK1502	1608.41	ISMLG	Fe ii	1608.4	L	-9.0	-0.00003	261.4	11.6
MRK1502	1611.14	ISMLG	Fe ii	1611.2	L	-11.0	-0.00003	48.4	10.7
MRK1502	1627.23	IGMABS	C iv	1548.2	H	15302.0	0.05103	100.6	9.4
MRK1502	1629.93	IGMABS	C iv	1550.7	H	15300.0	0.05103	63.4	9.0
MRK1502	1631.99	PROXIMATE	C iv	1548.2	H	16224.0	0.05412	73.6	7.0
MRK1502	1632.49	PROXIMATE	C iv	1548.2	H	16320.0	0.05445	161.4	6.5
MRK1502	1634.72	PROXIMATE	C iv	1550.7	H	16227.0	0.05412	62.1	5.9
MRK1502	1635.23	PROXIMATE	C iv	1550.7	H	16325.0	0.05445	130.3	6.9
MRK1502	1641.37	INTRINSIC	C iv	1548.2	H	18041.0	0.06019	60.0	6.8
MRK1502	1644.11	INTRINSIC	C iv	1550.7	H	18043.0	0.06019	26.4	7.3
MRK1502	1656.91	ISMLG	C i	1656.9	L	-4.0	-0.00003	102.0	11.4
MRK1502	1670.71	ISMLG	Al ii	1670.7	L	-14.0	-0.00003	480.5	14.4
MRK1502	1709.54	ISMLG	Ni ii	1709.6	L	-12.0	-0.00003	40.4	13.1
MRK1502	1741.53	ISMLG	H i	1741.5	L	-4.0	-0.00003	53.2	12.2
MRK304	1020.66	ISMLG	Si ii	1020.6	L	-12.0	-0.00003	244.1	25.4
MRK304	1030.67	ISMLG	O vi	1031.9	L	-366.0	-0.00119	80.5	17.1
MRK304	1030.82	ISMLG	O vi	1031.9	L	-322.0	-0.00107	114.6	13.2
MRK304	1031.89	ISMLG	O vi	1031.9	L	-10.0	-0.00003	232.8	27.4
MRK304	1035.21	ISMLG	C ii	1036.3	L	-326.0	-0.00107	42.4	16.9
MRK304	1035.94	ISMLG	C ii	1036.3	L	-113.0	-0.00038	100.9	16.0
MRK304	1036.29	ISMLG	C ii	1036.3	L	-13.0	-0.00003	478.5	22.6
MRK304	1039.19	ISMLG	O i	1039.2	L	-10.0	-0.00003	329.8	32.5
MRK304	1048.17	ISMLG	Ar i	1048.2	L	-15.0	-0.00003	126.2	26.3
MRK304	1066.61	ISMLG	Ar i	1066.6	L	-14.0	-0.00003	293.8	27.0
MRK304	1083.94	ISMLG	N ii	1083.9	L	-15.0	-0.00003	429.1	88.6
MRK304	1087.80	IGMABS	O vi	1031.9	H	16231.0	0.05414	293.0	26.4
MRK304	1088.48	IGMABS	O vi	1031.9	H	16430.0	0.05478	109.3	23.9
MRK304	1092.71	INTRINSIC	H i	1025.7	H	19580.0	0.06529	328.8	26.9
MRK304	1093.79	IGMABS	O vi	1037.6	H	16230.0	0.05414	245.0	33.6
MRK304	1096.82	ISMLG	Fe ii	1096.8	L	-15.0	-0.00003	260.1	34.2
MRK304	1099.26	INTRINSIC	O vi	1031.9	H	19563.0	0.06529	235.7	25.6
MRK304	1112.00	ISMLG	Fe ii	1112.0	L	-12.0	-0.00003	120.3	22.6
MRK304	1121.92	ISMLG	Fe ii	1121.9	L	-14.0	-0.00003	170.4	24.9
MRK304	1122.50	ISMLG	Fe iii	1122.5	L	-6.0	-0.00003	246.3	27.8
MRK304	1125.40	ISMLG	Fe ii	1125.4	L	-13.0	-0.00003	96.8	29.1
MRK304	1133.62	ISMLG	Fe ii	1133.6	L	-11.0	-0.00003	53.0	21.9
MRK304	1134.12	ISMLG	N i	1134.1	L	-12.0	-0.00003	214.5	20.0
MRK304	1134.37	ISMLG	N i	1134.4	L	-12.0	-0.00003	182.0	18.8
MRK304	1134.94	ISMLG	N i	1134.9	L	-11.0	-0.00003	220.5	22.4
MRK304	1139.79	ISMLG	C i	1139.7	L	-1.0	-0.00003	37.3	17.0
MRK304	1142.32	ISMLG	Fe ii	1142.3	L	-12.0	-0.00003	58.7	11.5
MRK304	1143.20	ISMLG	Fe ii	1143.2	L	-8.0	-0.00003	153.8	13.3
MRK304	1144.90	ISMLG	Fe ii	1144.9	L	-11.0	-0.00003	273.2	9.1
MRK304	1152.79	ISMLG	P ii	1152.8	L	-7.0	-0.00003	128.3	11.0
MRK304	1157.90	ISMLG	C i	1157.9	L	-3.0	-0.00003	39.1	7.2

Table A1 continued

Table A1 (*continued*)

Target	λ_{obs}	Type	Ion	λ_{rest}	Frame	cz	z	W_{λ}	$\sigma_{W_{\lambda}}$
	(Å)			(Å)		(km s ⁻¹)		(mÅ)	(mÅ)
MRK304	1188.80	ISMLG	C I	1188.8	L	-8.0	-0.00003	50.1	6.1
MRK304	1190.37	ISMLG	Si II	1190.4	L	-12.0	-0.00003	496.6	7.0
MRK304	1190.72	ISMLG	Si II	1190.4	L	77.0	0.00027	30.1	5.1
MRK304	1193.24	ISMLG	Si II	1193.2	L	-12.0	-0.00003	502.6	6.6
MRK304	1193.59	ISMLG	Si II	1193.2	L	76.0	0.00027	66.7	5.3
MRK304	1193.99	ISMLG	C I	1193.9	L	-2.0	-0.00003	28.9	6.0
MRK304	1197.15	ISMLG	Mn II	1197.1	L	-8.0	-0.00003	27.3	5.9
MRK304	1199.49	ISMLG	N I	1199.5	L	-14.0	-0.00003	376.9	9.1
MRK304	1200.18	ISMLG	N I	1200.2	L	-11.0	-0.00003	344.8	8.0
MRK304	1200.65	ISMLG	N I	1200.7	L	-15.0	-0.00003	288.5	7.6
MRK304	1201.06	ISMLG	Mn II	1201.1	L	-15.0	-0.00003	30.3	5.9
MRK304	1205.04	ISMLG	Si III	1206.5	L	-364.0	-0.00119	114.2	3.4
MRK304	1205.17	ISMLG	Si III	1206.5	L	-331.0	-0.00107	119.0	3.9
MRK304	1206.04	ISMLG	Si III	1206.5	L	-114.0	-0.00038	54.2	4.7
MRK304	1206.45	ISMLG	Si III	1206.5	L	-12.0	-0.00003	494.5	3.5
MRK304	1206.83	ISMLG	Si III	1206.5	L	83.0	0.00027	208.8	4.6
MRK304	1238.78	ISMLG	N V	1238.8	L	-10.0	-0.00003	70.2	6.9
MRK304	1239.90	ISMLG	Mg II	1239.9	L	-6.0	-0.00003	39.3	5.5
MRK304	1240.37	ISMLG	Mg II	1240.3	L	-6.0	-0.00003	26.4	5.6
MRK304	1242.48	IGMABS	H I	1215.6	H	6613.0	0.02206	77.4	7.2
MRK304	1250.54	ISMLG	S II	1250.5	L	-9.0	-0.00003	144.9	6.3
MRK304	1253.75	ISMLG	S II	1253.8	L	-12.0	-0.00003	202.6	6.1
MRK304	1258.88	ISMLG	Si II	1260.4	L	-368.0	-0.00119	12.9	3.4
MRK304	1259.05	ISMLG	Si II	1260.4	L	-327.0	-0.00107	19.2	3.3
MRK304	1259.45	ISMLG	S II	1259.5	L	-15.0	-0.00003	230.2	5.9
MRK304	1260.37	ISMLG	Si II	1260.4	L	-13.0	-0.00003	510.0	3.0
MRK304	1260.72	ISMLG	C I	1260.7	L	-4.0	-0.00003	92.8	3.1
MRK304	1277.21	ISMLG	C I	1277.2	L	-8.0	-0.00003	83.2	3.9
MRK304	1280.10	ISMLG	C I	1280.1	L	-8.0	-0.00003	36.6	4.8
MRK304	1281.49	IGMABS	H I	1215.6	H	16232.0	0.05414	115.7	6.2
MRK304	1282.27	IGMABS	H I	1215.6	H	16423.0	0.05478	148.0	7.5
MRK304	1285.78	PROXIMATE	H I	1215.6	H	17289.0	0.05767	132.0	7.5
MRK304	1289.85	PROXIMATE	H I	1215.6	H	18294.0	0.06102	90.3	8.1
MRK304	1295.04	INTRINSIC	H I	1215.6	H	19574.0	0.06529	405.4	4.8
MRK304	1296.79	INTRINSIC	H I	1215.6	H	20005.0	0.06673	58.2	4.9
MRK304	1302.13	ISMLG	O I	1302.1	L	-9.0	-0.00003	463.1	3.0
MRK304	1304.31	ISMLG	Si II	1304.3	L	-14.0	-0.00003	420.3	3.8
MRK304	1305.87	IGMABS	N V	1238.8	H	16226.0	0.05414	66.9	4.3
MRK304	1306.70	IGMABS	N V	1238.8	H	16427.0	0.05478	74.3	4.7
MRK304	1310.10	IGMABS	N V	1242.8	H	16233.0	0.05414	120.2	7.2
MRK304	1310.28	PROXIMATE	N V	1238.8	H	17292.0	0.05767	74.5	5.9
MRK304	1310.91	IGMABS	N V	1242.8	H	16428.0	0.05478	105.1	6.2
MRK304	1314.43	PROXIMATE	N V	1238.8	H	18297.0	0.06102	306.4	11.1
MRK304	1314.47	PROXIMATE	N V	1242.8	H	17288.0	0.05767	113.9	6.9
MRK304	1317.20	ISMLG	Ni II	1317.2	L	-4.0	-0.00003	33.6	7.2
MRK304	1318.64	PROXIMATE	N V	1242.8	H	18294.0	0.06102	124.1	7.7
MRK304	1328.83	ISMLG	C I	1328.8	L	0.0	-0.00003	69.9	4.0
MRK304	1329.10	ISMLG	C I*	1329.1	L	0.0	-0.00003	48.1	4.6
MRK304	1332.88	ISMLG	C II	1334.5	L	-371.0	-0.00119	37.2	3.8
MRK304	1333.09	ISMLG	C II	1334.5	L	-323.0	-0.00107	47.9	4.1
MRK304	1334.46	ISMLG	C II	1334.5	L	-16.0	-0.00003	544.7	2.7
MRK304	1334.90	ISMLG	C II	1334.5	L	83.0	0.00027	191.7	3.8
MRK304	1335.67	ISMLG	C II*	1335.7	L	-8.0	-0.00003	236.7	6.1

Table A1 continued

Table A1 (*continued*)

Target	λ_{obs}	Type	Ion	λ_{rest}	Frame	cz	z	W_{λ}	$\sigma_{W_{\lambda}}$
	(Å)			(Å)		(km s ⁻¹)		(mÅ)	(mÅ)
MRK304	1347.20	ISMLG	Cl I	1347.2	L	-10.0	-0.00003	56.4	7.5
MRK304	1370.07	ISMLG	Ni II	1370.1	L	-14.0	-0.00003	53.7	6.0
MRK304	1392.03	ISMLG	Si IV	1393.7	L	-372.0	-0.00119	37.8	4.3
MRK304	1392.25	ISMLG	Si IV	1393.7	L	-324.0	-0.00107	42.6	5.1
MRK304	1393.71	ISMLG	Si IV	1393.7	L	-11.0	-0.00003	353.7	7.7
MRK304	1394.11	ISMLG	Si IV	1393.7	L	75.0	0.00027	48.4	5.6
MRK304	1401.04	ISMLG	Si IV	1402.7	L	-370.0	-0.00119	21.9	5.2
MRK304	1401.30	ISMLG	Si IV	1402.7	L	-316.0	-0.00107	32.6	5.6
MRK304	1402.74	ISMLG	Si IV	1402.7	L	-7.0	-0.00003	230.8	8.4
MRK304	1403.17	ISMLG	Si IV	1402.7	L	84.0	0.00027	42.7	6.4
MRK304	1454.80	ISMLG	Ni II	1454.8	L	-8.0	-0.00003	30.5	9.3
MRK304	1526.64	ISMLG	Si II	1526.7	L	-14.0	-0.00003	525.8	9.6
MRK304	1546.31	ISMLG	C IV	1548.2	L	-367.0	-0.00119	74.2	7.9
MRK304	1546.55	ISMLG	C IV	1548.2	L	-321.0	-0.00107	114.6	6.1
MRK304	1548.17	ISMLG	C IV	1548.2	L	-7.0	-0.00003	497.1	11.2
MRK304	1548.60	ISMLG	C IV	1548.2	L	77.0	0.00027	118.7	8.0
MRK304	1548.88	ISMLG	C IV	1550.7	L	-367.0	-0.00119	52.7	7.6
MRK304	1549.13	ISMLG	C IV	1550.7	L	-319.0	-0.00107	89.3	8.4
MRK304	1550.74	ISMLG	C IV	1550.7	L	-8.0	-0.00003	357.9	14.0
MRK304	1551.23	ISMLG	C IV	1550.7	L	87.0	0.00027	60.4	9.8
MRK304	1560.26	ISMLG	C I	1560.3	L	-9.0	-0.00003	80.5	8.9
MRK304	1560.68	ISMLG	C *	1560.6	L	-1.0	-0.00003	36.1	8.5
MRK304	1608.38	ISMLG	Fe II	1608.4	L	-13.0	-0.00003	365.7	11.9
MRK304	1611.19	ISMLG	Fe II	1611.2	L	-2.0	-0.00003	40.5	12.0
MRK304	1631.98	IGMABS	C IV	1548.2	H	16223.0	0.05414	153.2	12.8
MRK304	1632.99	IGMABS	C IV	1548.2	H	16419.0	0.05478	133.7	11.6
MRK304	1634.76	IGMABS	C IV	1550.7	H	16234.0	0.05414	144.4	13.5
MRK304	1635.71	IGMABS	C IV	1550.7	H	16418.0	0.05478	74.9	10.9
MRK304	1637.56	PROXIMATE	C IV	1548.2	H	17303.0	0.05767	118.7	14.1
MRK304	1640.28	PROXIMATE	C IV	1550.7	H	17301.0	0.05767	82.7	13.1
MRK304	1642.62	PROXIMATE	C IV	1548.2	H	18284.0	0.06102	251.6	19.5
MRK304	1645.40	PROXIMATE	C IV	1550.7	H	18291.0	0.06102	134.3	15.9
MRK304	1656.91	ISMLG	C I	1656.9	L	-3.0	-0.00003	121.3	8.1
MRK304	1657.35	ISMLG	C *	1657.3	L	-5.0	-0.00003	22.6	7.4
MRK304	1657.90	ISMLG	C I*	1657.9	L	-2.0	-0.00003	23.3	8.0
MRK304	1670.70	ISMLG	Al II	1670.7	L	-15.0	-0.00003	533.4	9.6
MRK304	1671.22	ISMLG	Al II	1670.7	L	78.0	0.00027	80.2	11.2
MRK304	1709.54	ISMLG	Ni II	1709.6	L	-12.0	-0.00003	70.4	16.9
MRK304	1741.49	ISMLG	Ni II	1741.5	L	-10.0	-0.00003	88.3	16.6
MRK304	1751.90	ISMLG	H I	1751.9	L	-4.0	-0.00003	64.8	14.9
MRK335	916.88	ISMLG	H I	918.1	L	-407.0	-0.00136	252.0	13.2
MRK335	917.11	ISMLG	H I	918.1	L	-332.0	-0.00115	188.1	7.1
MRK335	917.24	ISMLG	H I	918.1	L	-292.0	-0.00100	130.3	5.7
MRK335	917.75	ISMLG	H I	918.1	L	-124.0	-0.00037	153.9	6.6
MRK335	917.94	ISMLG	H I	918.1	L	-61.0	-0.00017	198.3	5.1
MRK335	918.10	ISMLG	H I	919.3	L	-409.0	-0.00136	228.6	6.7
MRK335	918.12	ISMLG	H I	918.1	L	-3.0	0.00003	282.1	5.6
MRK335	918.33	ISMLG	H I	919.3	L	-332.0	-0.00115	185.9	6.0
MRK335	918.46	ISMLG	H I	919.3	L	-291.0	-0.00100	32.9	9.5
MRK335	919.01	ISMLG	H I	919.3	L	-110.0	-0.00037	132.4	7.3
MRK335	919.17	ISMLG	H I	919.3	L	-60.0	-0.00017	232.7	5.1
MRK335	919.36	ISMLG	H I	919.3	L	2.0	0.00003	266.3	5.8
MRK335	919.71	ISMLG	H I	920.9	L	-410.0	-0.00136	189.2	5.7

Table A1 continued

Table A1 (*continued*)

Target	λ_{obs}	Type	Ion	λ_{rest}	Frame	cz	z	W_{λ}	$\sigma_{W_{\lambda}}$
	(Å)			(Å)		(km s ⁻¹)		(mÅ)	(mÅ)
MRK335	919.73	ISMLG	O I	919.9	L	-61.0	-0.00017	177.7	6.1
MRK335	919.91	ISMLG	O I	919.9	L	-3.0	0.00003	183.5	7.6
MRK335	919.94	ISMLG	H I	920.9	L	-333.0	-0.00115	124.8	4.9
MRK335	920.06	ISMLG	H I	920.9	L	-294.0	-0.00100	94.2	6.0
MRK335	920.58	ISMLG	H I	920.9	L	-126.0	-0.00037	109.4	5.6
MRK335	920.77	ISMLG	H I	920.9	L	-62.0	-0.00017	215.7	4.2
MRK335	920.96	ISMLG	H I	920.9	L	-2.0	0.00003	281.3	4.8
MRK335	921.69	ISMLG	O I	921.8	L	-54.0	-0.00017	84.3	7.8
MRK335	921.88	ISMLG	O I	921.8	L	7.0	0.00003	196.8	6.1
MRK335	921.90	ISMLG	H I	923.1	L	-406.0	-0.00136	195.3	7.3
MRK335	922.02	ISMLG	O I	922.2	L	-60.0	-0.00017	150.8	5.9
MRK335	922.12	ISMLG	H I	923.1	L	-335.0	-0.00115	142.1	6.4
MRK335	922.21	ISMLG	O I	922.2	L	2.0	0.00003	166.5	7.6
MRK335	922.25	ISMLG	H I	923.1	L	-291.0	-0.00100	74.4	7.0
MRK335	922.77	ISMLG	H I	923.1	L	-124.0	-0.00037	157.6	5.6
MRK335	922.97	ISMLG	H I	923.1	L	-58.0	-0.00017	208.0	3.8
MRK335	923.16	ISMLG	H I	923.1	L	4.0	0.00003	287.2	6.1
MRK335	924.78	ISMLG	O I	924.9	L	-56.0	-0.00017	108.1	8.0
MRK335	924.95	ISMLG	H I	926.2	L	-414.0	-0.00136	203.4	5.7
MRK335	924.95	ISMLG	O I	924.9	L	0.0	0.00003	179.5	6.7
MRK335	925.19	ISMLG	H I	926.2	L	-335.0	-0.00115	166.6	4.8
MRK335	925.26	ISMLG	O I	925.4	L	-60.0	-0.00017	166.6	5.7
MRK335	925.32	ISMLG	H I	926.2	L	-294.0	-0.00100	89.8	5.2
MRK335	925.44	ISMLG	H I	926.2	L	-254.0	-0.00087	67.4	5.2
MRK335	925.44	ISMLG	O I	925.4	L	-1.0	0.00003	106.3	8.3
MRK335	925.86	ISMLG	H I	926.2	L	-118.0	-0.00037	118.8	4.9
MRK335	926.05	ISMLG	H I	926.2	L	-58.0	-0.00017	212.8	4.3
MRK335	926.23	ISMLG	H I	926.2	L	3.0	0.00003	263.1	5.6
MRK335	929.34	ISMLG	O I	929.5	L	-59.0	-0.00017	103.7	6.8
MRK335	929.46	ISMLG	H I	930.7	L	-414.0	-0.00136	250.9	5.8
MRK335	929.52	ISMLG	O I	929.5	L	-1.0	0.00003	259.7	5.0
MRK335	929.72	ISMLG	H I	930.7	L	-331.0	-0.00115	183.4	3.8
MRK335	929.85	ISMLG	H I	930.7	L	-290.0	-0.00100	94.9	4.4
MRK335	929.97	ISMLG	H I	930.7	L	-252.0	-0.00087	40.0	6.0
MRK335	930.10	ISMLG	O I	930.2	L	-51.0	-0.00017	84.0	8.3
MRK335	930.25	ISMLG	O I	930.2	L	-1.0	0.00003	194.0	6.0
MRK335	930.37	ISMLG	H I	930.7	L	-122.0	-0.00037	175.2	4.3
MRK335	930.56	ISMLG	H I	930.7	L	-60.0	-0.00017	196.0	4.7
MRK335	936.45	ISMLG	O I	936.6	L	-57.0	-0.00017	158.8	6.2
MRK335	936.51	ISMLG	H I	937.8	L	-412.0	-0.00136	204.5	6.6
MRK335	936.63	ISMLG	O I	936.6	L	-1.0	0.00003	261.6	4.2
MRK335	936.75	ISMLG	H I	937.8	L	-337.0	-0.00115	205.8	3.5
MRK335	936.89	ISMLG	H I	937.8	L	-292.0	-0.00100	111.1	4.5
MRK335	937.02	ISMLG	H I	937.8	L	-249.0	-0.00087	71.2	5.4
MRK335	937.42	ISMLG	H I	937.8	L	-123.0	-0.00037	138.9	4.9
MRK335	937.61	ISMLG	H I	937.8	L	-61.0	-0.00017	191.1	5.1
MRK335	937.83	ISMLG	H I	937.8	L	8.0	0.00003	339.6	7.9
MRK335	945.19	ISMLG	C I	945.1	L	-1.0	0.00003	80.1	7.9
MRK335	948.44	ISMLG	H I	949.7	L	-410.0	-0.00136	215.3	5.4
MRK335	948.49	ISMLG	O I	948.6	L	-62.0	-0.00017	211.3	6.0
MRK335	948.68	ISMLG	H I	949.7	L	-336.0	-0.00115	189.1	4.8
MRK335	948.68	ISMLG	O I	948.6	L	0.0	0.00003	242.8	7.8
MRK335	948.82	ISMLG	H I	949.7	L	-291.0	-0.00100	117.6	5.0

Table A1 continued

Table A1 (*continued*)

Target	λ_{obs}	Type	Ion	λ_{rest}	Frame	cz	z	W_{λ}	$\sigma_{W_{\lambda}}$
	(Å)			(Å)		(km s ⁻¹)		(mÅ)	(mÅ)
MRK335	948.94	ISMLG	H I	949.7	L	-252.0	-0.00087	62.6	5.5
MRK335	949.08	ISMLG	H I	949.7	L	-211.0	-0.00067	18.9	7.4
MRK335	949.38	ISMLG	H I	949.7	L	-116.0	-0.00037	149.9	4.3
MRK335	950.71	ISMLG	O I	950.8	L	-55.0	-0.00017	75.9	8.9
MRK335	950.88	ISMLG	O I	950.8	L	-1.0	0.00003	117.9	10.4
MRK335	952.12	ISMLG	N I	952.3	L	-56.0	-0.00017	41.9	9.1
MRK335	952.22	ISMLG	N I	952.4	L	-60.0	-0.00017	86.5	8.3
MRK335	952.32	ISMLG	N I	952.3	L	4.0	0.00003	155.8	8.1
MRK335	952.36	ISMLG	N I	952.5	L	-50.0	-0.00017	140.3	7.2
MRK335	952.42	ISMLG	N I	952.4	L	2.0	0.00003	128.3	9.1
MRK335	952.52	ISMLG	N I	952.5	L	0.0	0.00003	71.5	10.4
MRK335	953.25	ISMLG	N I	953.4	L	-53.0	-0.00017	86.8	9.4
MRK335	953.44	ISMLG	N I	953.4	L	7.0	0.00003	200.5	6.6
MRK335	953.46	ISMLG	N I	953.6	L	-61.0	-0.00017	160.1	9.3
MRK335	953.65	ISMLG	N I	953.6	L	0.0	0.00003	135.0	11.2
MRK335	953.79	ISMLG	N I	953.9	L	-56.0	-0.00017	124.4	7.9
MRK335	953.92	ISMLG	N I	954.1	L	-57.0	-0.00017	186.9	5.6
MRK335	953.97	ISMLG	N I	953.9	L	1.0	0.00003	197.1	8.6
MRK335	954.09	ISMLG	N I	954.1	L	-3.0	0.00003	114.5	8.1
MRK335	963.64	ISMLG	P II	963.8	L	-50.0	-0.00017	60.7	5.7
MRK335	963.79	ISMLG	P II	963.8	L	-3.0	0.00003	205.6	4.9
MRK335	963.83	ISMLG	N I	963.9	L	-50.0	-0.00017	174.6	5.8
MRK335	963.98	ISMLG	N I	963.9	L	-2.0	0.00003	138.5	8.8
MRK335	964.44	ISMLG	N I	964.6	L	-58.0	-0.00017	110.2	6.5
MRK335	964.62	ISMLG	N I	964.6	L	-1.0	0.00003	108.4	6.9
MRK335	964.85	ISMLG	N I	965.0	L	-58.0	-0.00017	-20.4	5.2
MRK335	965.03	ISMLG	N I	965.0	L	-4.0	0.00003	8205.2	4.9
MRK335	971.19	ISMLG	H I	972.5	L	-414.0	-0.00136	244.9	5.8
MRK335	971.44	ISMLG	H I	972.5	L	-337.0	-0.00115	204.6	4.4
MRK335	971.54	ISMLG	O I	971.7	L	-62.0	-0.00017	230.1	5.3
MRK335	971.59	ISMLG	H I	972.5	L	-293.0	-0.00100	138.7	4.3
MRK335	971.73	ISMLG	H I	972.5	L	-250.0	-0.00087	135.9	3.9
MRK335	971.74	ISMLG	O I	971.7	L	1.0	0.00003	254.8	6.6
MRK335	971.85	ISMLG	H I	972.5	L	-212.0	-0.00067	89.4	4.5
MRK335	972.16	ISMLG	H I	972.5	L	-116.0	-0.00037	140.8	4.2
MRK335	975.69	ISMLG	C III	977.0	L	-409.0	-0.00136	112.0	8.6
MRK335	975.92	ISMLG	C III	977.0	L	-337.0	-0.00115	143.4	4.7
MRK335	976.07	ISMLG	C III	977.0	L	-290.0	-0.00100	133.1	4.4
MRK335	976.25	ISMLG	O I	976.4	L	-62.0	-0.00017	196.7	6.5
MRK335	976.44	ISMLG	O I	976.4	L	-2.0	0.00003	250.7	6.9
MRK335	976.63	ISMLG	C III	977.0	L	-118.0	-0.00037	127.1	4.3
MRK335	976.83	ISMLG	C III	977.0	L	-58.0	-0.00017	212.4	4.1
MRK335	977.00	ISMLG	C III	977.0	L	-5.0	0.00003	293.5	6.1
MRK335	988.57	ISMLG	O I	988.7	L	-61.0	-0.00017	143.7	8.1
MRK335	988.76	ISMLG	O I	988.7	L	-6.0	0.00003	148.4	8.7
MRK335	989.68	ISMLG	Si II	989.8	L	-58.0	-0.00017	192.7	7.3
MRK335	989.87	ISMLG	Si II	989.8	L	-1.0	0.00003	174.5	9.1
MRK335	1004.64	ISMLG	Cl I	1004.6	L	-7.0	0.00003	4.5	3.9
MRK335	1012.50	ISMLG	S III	1012.4	L	1.0	0.00003	75.6	3.6
MRK335	1020.51	ISMLG	Si II	1020.6	L	-55.0	-0.00017	42.6	3.4
MRK335	1020.70	ISMLG	Si II	1020.6	L	0.0	0.00003	120.2	2.9
MRK335	1024.31	ISMLG	H I	1025.7	L	-412.0	-0.00136	280.0	1.7
MRK335	1024.57	ISMLG	H I	1025.7	L	-336.0	-0.00115	201.1	1.3

Table A1 continued

Table A1 (*continued*)

Target	λ_{obs}	Type	Ion	λ_{rest}	Frame	cz	z	W_{λ}	$\sigma_{W_{\lambda}}$
	(Å)			(Å)		(km s ⁻¹)		(mÅ)	(mÅ)
MRK335	1024.72	ISMLG	H I	1025.7	L	-291.0	-0.00100	171.8	1.2
MRK335	1024.87	ISMLG	H I	1025.7	L	-249.0	-0.00087	123.8	1.1
MRK335	1025.00	ISMLG	H I	1025.7	L	-210.0	-0.00067	132.2	1.6
MRK335	1025.31	ISMLG	H I	1025.7	L	-120.0	-0.00037	104.2	2.2
MRK335	1030.77	ISMLG	O VI	1031.9	L	-337.0	-0.00115	32.8	3.2
MRK335	1030.92	ISMLG	O VI	1031.9	L	-293.0	-0.00100	54.6	2.7
MRK335	1031.06	ISMLG	O VI	1031.9	L	-252.0	-0.00087	34.3	2.4
MRK335	1031.20	ISMLG	O VI	1031.9	L	-210.0	-0.00067	74.6	2.1
MRK335	1031.53	ISMLG	O VI	1031.9	L	-116.0	-0.00037	23.9	3.0
MRK335	1031.75	ISMLG	O VI	1031.9	L	-52.0	-0.00017	26.1	3.3
MRK335	1031.93	ISMLG	O VI	1031.9	L	2.0	0.00003	80.2	4.0
MRK335	1032.42	IGMABS	H I	1025.7	H	1959.0	0.00652	25.2	3.2
MRK335	1034.90	ISMLG	C II	1036.3	L	-416.0	-0.00136	21.0	4.1
MRK335	1035.93	ISMLG	C II	1036.3	L	-117.0	-0.00037	90.0	2.3
MRK335	1036.13	ISMLG	C II	1036.3	L	-59.0	-0.00017	218.5	1.5
MRK335	1036.31	ISMLG	C II	1036.3	L	-7.0	0.00003	357.8	1.3
MRK335	1036.74	ISMLG	O VI	1037.6	L	-253.0	-0.00087	25.0	2.2
MRK335	1036.89	ISMLG	O VI	1037.6	L	-211.0	-0.00067	54.8	2.2
MRK335	1037.42	ISMLG	O VI	1037.6	L	-58.0	-0.00017	31.4	3.9
MRK335	1037.64	ISMLG	O VI	1037.6	L	6.0	0.00003	51.5	4.1
MRK335	1039.03	ISMLG	O I	1039.2	L	-58.0	-0.00017	172.5	2.5
MRK335	1039.24	ISMLG	O I	1039.2	L	2.0	0.00003	156.3	3.1
MRK335	1040.04	OTHER	FLAW	0.0	H	0.0	-1.00000	15.9	3.9
MRK335	1047.14	PROXIMATE	H I	1025.7	H	6260.0	0.02087	39.8	5.0
MRK335	1048.04	ISMLG	Ar I	1048.2	L	-53.0	-0.00017	41.0	2.1
MRK335	1048.19	ISMLG	Ar I	1048.2	L	-7.0	0.00003	84.7	1.7
MRK335	1055.08	ISMLG	Fe II	1055.2	L	-51.0	-0.00017	17.5	2.0
MRK335	1055.24	ISMLG	Fe II	1055.2	L	-5.0	0.00003	20.2	1.7
MRK335	1062.15	ISMLG	Fe II	1062.1	L	0.0	0.00003	8.6	1.7
MRK335	1063.00	ISMLG	Fe II	1063.1	L	-51.0	-0.00017	61.6	1.1
MRK335	1063.17	ISMLG	Fe II	1063.1	L	-3.0	0.00003	107.1	1.4
MRK335	1063.99	ISMLG	Fe II	1063.9	L	5.0	0.00003	6.8	1.4
MRK335	1066.66	ISMLG	Ar I	1066.6	L	1.0	0.00003	78.9	1.9
MRK335	1071.03	ISMLG	Cl II	1071.0	L	-2.0	0.00003	7.7	2.5
MRK335	1075.48	OTHER	EDGE	0.0	H	0.0	-1.00000	105.1	6.9
MRK335	1081.87	ISMLG	Fe II	1081.8	L	-1.0	0.00003	20.4	4.9
MRK335	1083.77	ISMLG	N II	1083.9	L	-62.0	-0.00017	164.6	15.1
MRK335	1083.99	ISMLG	N II	1083.9	L	0.0	0.00003	304.0	15.8
MRK335	1096.69	ISMLG	Fe II	1096.8	L	-51.0	-0.00017	33.2	2.3
MRK335	1096.85	ISMLG	Fe II	1096.8	L	-7.0	0.00003	76.9	3.2
MRK335	1112.07	ISMLG	Fe II	1112.0	L	6.0	0.00003	14.8	3.2
MRK335	1121.74	ISMLG	Fe II	1121.9	L	-62.0	-0.00017	27.8	3.4
MRK335	1121.96	ISMLG	Fe II	1121.9	L	-4.0	0.00003	57.9	3.7
MRK335	1122.33	ISMLG	Fe III	1122.5	L	-50.0	-0.00017	42.7	3.7
MRK335	1122.55	ISMLG	Fe III	1122.5	L	6.0	0.00003	76.1	4.4
MRK335	1125.25	ISMLG	Fe II	1125.4	L	-52.0	-0.00017	25.2	3.1
MRK335	1125.44	ISMLG	Fe II	1125.4	L	-1.0	0.00003	56.3	3.8
MRK335	1133.68	ISMLG	Fe II	1133.6	L	4.0	0.00003	13.2	3.7
MRK335	1133.97	ISMLG	N I	1134.1	L	-51.0	-0.00017	95.6	3.3
MRK335	1134.19	ISMLG	N I	1134.1	L	7.0	0.00003	182.4	3.6
MRK335	1134.22	ISMLG	N I	1134.4	L	-50.0	-0.00017	225.4	3.7
MRK335	1134.40	ISMLG	N I	1134.4	L	-4.0	0.00003	133.8	3.0
MRK335	1134.78	ISMLG	N I	1134.9	L	-52.0	-0.00017	145.9	2.9

Table A1 continued

Table A1 (*continued*)

Target	λ_{obs}	Type	Ion	λ_{rest}	Frame	cz	z	W_{λ}	$\sigma_{W_{\lambda}}$
	(Å)			(Å)		(km s ⁻¹)		(mÅ)	(mÅ)
MRK335	1134.95	ISMLG	N I	1134.9	L	-7.0	0.00003	157.0	3.1
MRK335	1139.77	ISMLG	C I	1139.7	L	-6.0	0.00003	12.5	2.6
MRK335	1142.37	ISMLG	Fe II	1142.3	L	0.0	0.00003	14.8	3.9
MRK335	1143.01	ISMLG	Fe II	1143.2	L	-58.0	-0.00017	24.0	4.3
MRK335	1143.21	ISMLG	Fe II	1143.2	L	-3.0	0.00003	45.4	3.2
MRK335	1144.72	ISMLG	Fe II	1144.9	L	-57.0	-0.00017	124.9	6.3
MRK335	1144.90	ISMLG	Fe II	1144.9	L	-9.0	0.00003	122.6	6.4
MRK335	1152.59	ISMLG	P II	1152.8	L	-58.0	-0.00017	34.6	7.2
MRK335	1152.79	ISMLG	P II	1152.8	L	-8.0	0.00003	62.1	6.1
MRK335	1157.89	ISMLG	C I	1157.9	L	-6.0	0.00003	21.3	5.1
MRK335	1188.76	ISMLG	Si II	1190.4	L	-418.0	-0.00136	12.2	5.0
MRK335	1189.96	ISMLG	Si II	1190.4	L	-116.0	-0.00037	46.6	3.6
MRK335	1190.19	ISMLG	Si II	1190.4	L	-58.0	-0.00017	210.2	2.3
MRK335	1190.44	ISMLG	Si II	1190.4	L	6.0	0.00003	241.4	3.7
MRK335	1191.96	ISMLG	Si II	1193.2	L	-333.0	-0.00115	21.4	4.0
MRK335	1192.82	ISMLG	Si II	1193.2	L	-119.0	-0.00037	65.4	3.5
MRK335	1193.07	ISMLG	Si II	1193.2	L	-55.0	-0.00017	232.1	2.1
MRK335	1193.30	ISMLG	Si II	1193.2	L	3.0	0.00003	242.7	3.4
MRK335	1193.96	ISMLG	C I	1193.9	L	-8.0	0.00003	13.1	4.0
MRK335	1199.31	ISMLG	N I	1199.5	L	-60.0	-0.00017	182.5	6.7
MRK335	1199.55	ISMLG	N I	1199.5	L	-1.0	0.00003	206.1	7.7
MRK335	1200.00	ISMLG	N I	1200.2	L	-56.0	-0.00017	151.2	5.8
MRK335	1200.21	ISMLG	N I	1200.2	L	-4.0	0.00003	201.6	6.6
MRK335	1200.48	ISMLG	N I	1200.7	L	-57.0	-0.00017	181.7	6.6
MRK335	1200.72	ISMLG	N I	1200.7	L	3.0	0.00003	154.6	7.9
MRK335	1204.85	ISMLG	Si III	1206.5	L	-409.0	-0.00136	60.7	4.2
MRK335	1205.14	ISMLG	Si III	1206.5	L	-339.0	-0.00115	86.8	3.2
MRK335	1205.28	ISMLG	Si III	1206.5	L	-302.0	-0.00100	54.5	3.2
MRK335	1205.49	ISMLG	Si III	1206.5	L	-251.0	-0.00087	32.1	3.3
MRK335	1206.04	ISMLG	Si III	1206.5	L	-115.0	-0.00037	87.7	2.4
MRK335	1206.26	ISMLG	Si III	1206.5	L	-60.0	-0.00017	272.5	1.6
MRK335	1206.52	ISMLG	Si III	1206.5	L	4.0	0.00003	316.6	2.4
MRK335	1223.59	IGMABS	H I	1215.6	H	1954.0	0.00652	210.9	5.1
MRK335	1224.89	IGMABS	H I	1215.6	H	2274.0	0.00759	62.5	4.8
MRK335	1232.97	IGMABS	H I	1215.6	H	4266.0	0.01423	49.7	4.8
MRK335	1234.05	IGMABS	H I	1215.6	H	4533.0	0.01512	29.3	3.3
MRK335	1238.82	ISMLG	N V	1238.8	L	1.0	0.00003	34.5	2.6
MRK335	1239.89	ISMLG	Mg II	1239.9	L	-9.0	0.00003	8.6	1.5
MRK335	1241.04	PROXIMATE	H I	1215.6	H	6256.0	0.02087	124.0	3.1
MRK335	1250.38	ISMLG	S II	1250.5	L	-49.0	-0.00017	34.1	1.1
MRK335	1250.57	ISMLG	S II	1250.5	L	-3.0	0.00003	84.3	1.0
MRK335	1253.59	ISMLG	S II	1253.8	L	-50.0	-0.00017	64.2	1.4
MRK335	1253.79	ISMLG	S II	1253.8	L	-3.0	0.00003	82.8	1.1
MRK335	1258.68	ISMLG	Si II	1260.4	L	-414.0	-0.00136	30.2	2.8
MRK335	1259.00	ISMLG	Si II	1260.4	L	-337.0	-0.00115	23.1	2.8
MRK335	1259.30	ISMLG	S II	1259.5	L	-52.0	-0.00017	61.5	2.0
MRK335	1259.49	ISMLG	S II	1259.5	L	-8.0	0.00003	101.8	1.8
MRK335	1259.96	ISMLG	Si II	1260.4	L	-110.0	-0.00037	103.8	2.1
MRK335	1260.19	ISMLG	Si II	1260.4	L	-55.0	-0.00017	258.9	0.9
MRK335	1260.43	ISMLG	Si II	1260.4	L	3.0	0.00003	290.1	1.4
MRK335	1260.73	ISMLG	C I	1260.7	L	-1.0	0.00003	48.8	2.5
MRK335	1277.23	ISMLG	C I	1277.2	L	-4.0	0.00003	40.9	3.1
MRK335	1280.11	ISMLG	C I	1280.1	L	-6.0	0.00003	19.1	3.7

Table A1 continued

Table A1 (*continued*)

Target	λ_{obs}	Type	Ion	λ_{rest}	Frame	cz	z	W_{λ}	$\sigma_{W_{\lambda}}$
	(Å)			(Å)		(km s ⁻¹)		(mÅ)	(mÅ)
MRK335	1301.70	ISMLG	O I	1302.1	L	-108.0	-0.00037	49.0	7.8
MRK335	1301.93	ISMLG	O I	1302.1	L	-54.0	-0.00017	149.1	6.7
MRK335	1302.13	ISMLG	O I	1302.1	L	-9.0	0.00003	159.8	7.1
MRK335	1303.85	ISMLG	Si II	1304.3	L	-119.0	-0.00037	48.8	7.7
MRK335	1304.12	ISMLG	Si II	1304.3	L	-57.0	-0.00017	185.8	6.8
MRK335	1304.39	ISMLG	Si II	1304.3	L	4.0	0.00003	188.6	8.2
MRK335	1316.96	ISMLG	Ni II	1317.2	L	-58.0	-0.00017	14.4	3.8
MRK335	1317.18	ISMLG	Ni II	1317.2	L	-8.0	0.00003	27.4	4.3
MRK335	1328.84	ISMLG	C I	1328.8	L	3.0	0.00003	21.6	4.6
MRK335	1332.71	ISMLG	C II	1334.5	L	-409.0	-0.00136	34.8	3.7
MRK335	1333.06	ISMLG	C II	1334.5	L	-331.0	-0.00115	37.6	3.9
MRK335	1333.22	ISMLG	C II	1334.5	L	-294.0	-0.00100	13.1	3.1
MRK335	1334.00	ISMLG	C II	1334.5	L	-120.0	-0.00037	101.7	3.2
MRK335	1334.27	ISMLG	C II	1334.5	L	-60.0	-0.00017	273.3	1.6
MRK335	1334.55	ISMLG	C II	1334.5	L	4.0	0.00003	344.8	2.7
MRK335	1335.70	ISMLG	C II*	1335.7	L	-1.0	0.00003	118.4	4.2
MRK335	1347.19	ISMLG	Cl I	1347.2	L	-10.0	0.00003	20.3	4.6
MRK335	1369.90	ISMLG	Ni II	1370.1	L	-51.0	-0.00017	16.3	3.8
MRK335	1370.09	ISMLG	Ni II	1370.1	L	-9.0	0.00003	25.0	3.9
MRK335	1392.57	ISMLG	Si IV	1393.7	L	-255.0	-0.00087	23.1	5.2
MRK335	1393.24	ISMLG	Si IV	1393.7	L	-111.0	-0.00037	19.2	4.8
MRK335	1393.50	ISMLG	Si IV	1393.7	L	-56.0	-0.00017	73.6	5.1
MRK335	1393.77	ISMLG	Si IV	1393.7	L	2.0	0.00003	162.9	5.3
MRK335	1402.48	ISMLG	Si IV	1402.7	L	-62.0	-0.00017	41.5	5.5
MRK335	1402.76	ISMLG	Si IV	1402.7	L	-3.0	0.00003	94.8	5.5
MRK335	1526.14	ISMLG	Si II	1526.7	L	-111.0	-0.00037	37.2	4.0
MRK335	1526.42	ISMLG	Si II	1526.7	L	-57.0	-0.00017	224.7	4.0
MRK335	1526.73	ISMLG	Si II	1526.7	L	4.0	0.00003	310.8	4.6
MRK335	1546.08	ISMLG	C IV	1548.2	L	-411.0	-0.00136	23.0	4.9
MRK335	1546.45	ISMLG	C IV	1548.2	L	-340.0	-0.00115	41.4	6.3
MRK335	1546.68	ISMLG	C IV	1548.2	L	-295.0	-0.00100	52.9	4.9
MRK335	1546.91	ISMLG	C IV	1548.2	L	-250.0	-0.00087	60.1	5.5
MRK335	1547.12	ISMLG	C IV	1548.2	L	-210.0	-0.00067	33.3	5.6
MRK335	1547.59	ISMLG	C IV	1548.2	L	-119.0	-0.00037	14.2	5.0
MRK335	1547.89	ISMLG	C IV	1548.2	L	-61.0	-0.00017	39.9	5.9
MRK335	1548.25	ISMLG	C IV	1548.2	L	8.0	0.00003	244.0	6.9
MRK335	1549.01	ISMLG	C IV	1550.7	L	-342.0	-0.00115	34.4	5.4
MRK335	1549.25	ISMLG	C IV	1550.7	L	-296.0	-0.00100	48.2	5.6
MRK335	1549.48	ISMLG	C IV	1550.7	L	-252.0	-0.00087	34.8	5.5
MRK335	1549.68	ISMLG	C IV	1550.7	L	-212.0	-0.00067	25.7	5.6
MRK335	1550.46	ISMLG	C IV	1550.7	L	-61.0	-0.00017	31.2	6.2
MRK335	1550.80	ISMLG	C IV	1550.7	L	4.0	0.00003	161.0	8.2
MRK335	1560.31	ISMLG	C I	1560.3	L	0.0	0.00003	56.8	5.9
MRK335	1608.19	ISMLG	Fe II	1608.4	L	-49.0	-0.00017	120.1	8.0
MRK335	1608.40	ISMLG	Fe II	1608.4	L	-9.0	0.00003	189.0	8.7
MRK335	1656.90	ISMLG	C I	1656.9	L	-5.0	0.00003	66.5	8.1
MRK335	1670.16	ISMLG	Al II	1670.7	L	-112.0	-0.00037	68.3	8.0
MRK335	1670.50	ISMLG	Al II	1670.7	L	-52.0	-0.00017	257.9	4.8
MRK335	1670.82	ISMLG	H I	1670.7	L	5.0	0.00003	319.1	6.7
MRK352	1020.64	ISMLG	Si II	1020.6	L	-19.0	-0.00005	242.6	37.7
MRK352	1030.93	ISMLG	O VI	1031.9	L	-290.0	-0.00096	92.5	24.4
MRK352	1031.20	ISMLG	O VI	1031.9	L	-211.0	-0.00070	271.5	36.7
MRK352	1031.89	ISMLG	O VI	1031.9	L	-9.0	-0.00005	116.3	33.2

Table A1 continued

Table A1 (*continued*)

Target	λ_{obs}	Type	Ion	λ_{rest}	Frame	cz	z	W_{λ}	$\sigma_{W_{\lambda}}$
	(Å)			(Å)		(km s ⁻¹)		(mÅ)	(mÅ)
MRK352	1035.61	ISMLG	C II	1036.3	L	-211.0	-0.00070	80.8	24.4
MRK352	1035.96	ISMLG	C II	1036.3	L	-110.0	-0.00039	199.2	18.0
MRK352	1036.28	ISMLG	C II	1036.3	L	-15.0	-0.00005	485.6	23.3
MRK352	1039.18	ISMLG	O I	1039.2	L	-14.0	-0.00005	356.8	49.3
MRK352	1046.84	INTRINSIC	O VI	1031.9	H	4332.0	0.01445	268.5	27.3
MRK352	1048.17	ISMLG	Ar I	1048.2	L	-14.0	-0.00005	215.2	18.5
MRK352	1052.59	INTRINSIC	O VI	1037.6	H	4326.0	0.01445	170.6	30.5
MRK352	1066.62	ISMLG	Ar I	1066.6	L	-12.0	-0.00005	296.1	35.2
MRK352	1096.81	ISMLG	Fe II	1096.8	L	-17.0	-0.00005	318.1	44.5
MRK352	1143.14	ISMLG	Fe II	1143.2	L	-22.0	-0.00005	134.8	49.9
MRK352	1144.85	ISMLG	Fe II	1144.9	L	-24.0	-0.00005	399.8	44.5
MRK352	1152.76	ISMLG	P II	1152.8	L	-15.0	-0.00005	174.0	45.6
MRK352	1189.59	ISMLG	Si II	1190.4	L	-208.0	-0.00070	80.3	17.3
MRK352	1189.94	ISMLG	Si II	1190.4	L	-121.0	-0.00039	99.4	14.3
MRK352	1190.34	ISMLG	Si II	1190.4	L	-20.0	-0.00005	412.6	12.6
MRK352	1192.47	ISMLG	Si II	1193.2	L	-206.0	-0.00070	61.2	13.3
MRK352	1192.80	ISMLG	Si II	1193.2	L	-124.0	-0.00039	133.9	14.1
MRK352	1193.21	ISMLG	Si II	1193.2	L	-20.0	-0.00005	484.6	14.0
MRK352	1193.60	ISMLG	Si II	1193.2	L	79.0	0.00025	38.4	14.4
MRK352	1199.48	ISMLG	N I	1199.5	L	-17.0	-0.00005	416.3	38.8
MRK352	1200.16	ISMLG	N I	1200.2	L	-15.0	-0.00005	359.0	26.3
MRK352	1200.63	ISMLG	N I	1200.7	L	-20.0	-0.00005	347.7	27.9
MRK352	1205.31	ISMLG	Si III	1206.5	L	-297.0	-0.00096	100.8	14.1
MRK352	1205.64	ISMLG	Si III	1206.5	L	-213.0	-0.00070	214.8	14.2
MRK352	1206.06	ISMLG	Si III	1206.5	L	-108.0	-0.00039	183.9	12.2
MRK352	1206.42	ISMLG	Si III	1206.5	L	-19.0	-0.00005	461.9	11.3
MRK352	1206.81	ISMLG	Si III	1206.5	L	77.0	0.00025	121.6	11.2
MRK352	1239.87	ISMLG	Mg II	1239.9	L	-14.0	-0.00005	26.5	5.2
MRK352	1240.35	ISMLG	Mg II	1240.3	L	-10.0	-0.00005	11.8	4.5
MRK352	1250.51	ISMLG	S II	1250.5	L	-15.0	-0.00005	177.7	12.3
MRK352	1253.72	ISMLG	S II	1253.8	L	-19.0	-0.00005	246.8	12.5
MRK352	1259.17	ISMLG	Si II	1260.4	L	-297.0	-0.00096	105.1	7.7
MRK352	1259.43	ISMLG	S II	1259.5	L	-20.0	-0.00005	274.5	7.5
MRK352	1259.91	ISMLG	Si II	1260.4	L	-123.0	-0.00039	185.3	6.0
MRK352	1260.33	ISMLG	Si II	1260.4	L	-22.0	-0.00005	512.0	5.3
MRK352	1260.75	ISMLG	Si II	1260.4	L	78.0	0.00025	73.0	7.7
MRK352	1277.21	ISMLG	C I	1277.2	L	-9.0	-0.00005	57.9	19.5
MRK352	1302.09	ISMLG	O I	1302.1	L	-19.0	-0.00005	493.5	48.6
MRK352	1304.27	ISMLG	Si II	1304.3	L	-23.0	-0.00005	392.0	47.0
MRK352	1317.17	ISMLG	Ni II	1317.2	L	-10.0	-0.00005	74.1	27.4
MRK352	1328.79	ISMLG	C I	1328.8	L	-10.0	-0.00005	29.9	24.2
MRK352	1333.20	ISMLG	C II	1334.5	L	-299.0	-0.00096	108.0	18.6
MRK352	1333.63	ISMLG	C II	1334.5	L	-203.0	-0.00070	134.6	14.5
MRK352	1334.01	ISMLG	C II	1334.5	L	-117.0	-0.00039	220.2	12.0
MRK352	1334.46	ISMLG	C II	1334.5	L	-16.0	-0.00005	548.0	13.7
MRK352	1334.86	ISMLG	C II	1334.5	L	73.0	0.00025	142.0	16.1
MRK352	1335.65	ISMLG	C II*	1335.7	L	-13.0	-0.00005	192.8	21.3
MRK352	1370.02	ISMLG	Ni II	1370.1	L	-25.0	-0.00005	96.0	20.9
MRK352	1392.79	ISMLG	Si IV	1393.7	L	-209.0	-0.00070	106.3	21.4
MRK352	1393.64	ISMLG	Si IV	1393.7	L	-25.0	-0.00005	220.5	26.5
MRK352	1401.80	ISMLG	Si IV	1402.7	L	-207.0	-0.00070	42.1	20.7
MRK352	1402.71	ISMLG	Si IV	1402.7	L	-14.0	-0.00005	109.1	18.7
MRK352	1525.65	ISMLG	Si II	1526.7	L	-207.0	-0.00070	36.7	13.9

Table A1 continued

Table A1 (*continued*)

Target	λ_{obs}	Type	Ion	λ_{rest}	Frame	cz	z	W_{λ}	$\sigma_{W_{\lambda}}$
	(Å)			(Å)		(km s ⁻¹)		(mÅ)	(mÅ)
MRK352	1526.10	ISMLG	Si II	1526.7	L	-119.0	-0.00039	89.8	15.3
MRK352	1526.59	ISMLG	Si II	1526.7	L	-23.0	-0.00005	579.9	18.7
MRK352	1546.72	ISMLG	C IV	1548.2	L	-288.0	-0.00096	167.3	12.0
MRK352	1547.09	ISMLG	C IV	1548.2	L	-216.0	-0.00070	231.8	11.5
MRK352	1548.10	ISMLG	C IV	1548.2	L	-21.0	-0.00005	189.6	15.1
MRK352	1548.55	ISMLG	C IV	1548.2	L	66.0	0.00025	48.4	11.9
MRK352	1549.30	ISMLG	C IV	1550.7	L	-286.0	-0.00096	58.1	11.2
MRK352	1549.67	ISMLG	C IV	1550.7	L	-216.0	-0.00070	152.0	11.0
MRK352	1550.67	ISMLG	C IV	1550.7	L	-21.0	-0.00005	103.6	13.4
MRK352	1551.14	ISMLG	C IV	1550.7	L	68.0	0.00025	37.0	12.2
MRK352	1560.22	ISMLG	C I	1560.3	L	-17.0	-0.00005	73.5	13.5
MRK352	1608.40	ISMLG	Fe II	1608.4	L	-10.0	-0.00005	434.9	43.0
MRK352	1656.87	ISMLG	C I	1656.9	L	-10.0	-0.00005	185.9	50.1
MRK352	1670.70	PROXIMATE	H I	1670.7	L	-16.0	-0.00005	662.5	46.2
MRK595	1139.76	ISMLG	C I	1139.7	L	-8.0	-0.00003	49.2	22.2
MRK595	1143.23	ISMLG	Fe II	1143.2	L	2.0	-0.00003	122.0	25.6
MRK595	1144.53	ISMLG	Fe II	1144.9	L	-106.0	-0.00036	113.7	22.8
MRK595	1144.93	ISMLG	Fe II	1144.9	L	-3.0	-0.00003	203.4	23.5
MRK595	1152.82	ISMLG	P II	1152.8	L	0.0	-0.00003	119.0	17.7
MRK595	1188.77	ISMLG	C I	1188.8	L	-16.0	-0.00003	52.9	15.0
MRK595	1189.98	ISMLG	Si II	1190.4	L	-109.0	-0.00036	190.4	11.2
MRK595	1190.35	ISMLG	Si II	1190.4	L	-17.0	-0.00003	309.8	11.7
MRK595	1192.89	ISMLG	Si II	1193.2	L	-100.0	-0.00036	287.6	10.9
MRK595	1193.24	ISMLG	Si II	1193.2	L	-13.0	-0.00003	317.2	11.4
MRK595	1193.95	ISMLG	C I	1193.9	L	-10.0	-0.00003	31.0	15.3
MRK595	1197.13	ISMLG	Mn II	1197.1	L	-13.0	-0.00003	46.9	16.5
MRK595	1199.10	ISMLG	N I	1199.5	L	-112.0	-0.00036	121.2	20.1
MRK595	1199.53	ISMLG	N I	1199.5	L	-6.0	-0.00003	235.5	18.9
MRK595	1199.78	ISMLG	N I	1200.2	L	-112.0	-0.00036	97.3	13.6
MRK595	1200.20	ISMLG	N I	1200.2	L	-5.0	-0.00003	236.5	17.9
MRK595	1200.68	ISMLG	N I	1200.7	L	-7.0	-0.00003	194.8	18.3
MRK595	1201.10	ISMLG	Mn II	1201.1	L	-4.0	-0.00003	31.7	15.3
MRK595	1205.76	ISMLG	Si III	1206.5	L	-185.0	-0.00056	81.7	9.8
MRK595	1206.08	ISMLG	Si III	1206.5	L	-104.0	-0.00036	340.7	9.3
MRK595	1206.50	ISMLG	Si III	1206.5	L	0.0	-0.00003	383.4	11.4
MRK595	1232.44	IGMABS	H I	1215.6	H	4135.0	0.01379	33.4	10.1
MRK595	1232.91	IGMABS	H I	1215.6	H	4251.0	0.01418	31.4	11.4
MRK595	1239.91	ISMLG	Mg II	1239.9	L	-5.0	-0.00003	37.6	4.4
MRK595	1240.33	PROXIMATE	H I	1215.6	H	6082.0	0.02029	285.4	8.5
MRK595	1240.55	PROXIMATE	H I	1215.6	H	6136.0	0.02047	101.8	6.2
MRK595	1241.97	PROXIMATE	H I	1215.6	H	6486.0	0.02164	22.3	5.7
MRK595	1246.57	INTRINSIC	H I	1215.6	H	7620.0	0.02542	581.3	5.9
MRK595	1250.56	ISMLG	S II	1250.5	L	-5.0	-0.00003	128.7	3.6
MRK595	1253.78	ISMLG	S II	1253.8	L	-5.0	-0.00003	154.4	4.2
MRK595	1259.04	ISMLG	S II	1259.5	L	-113.0	-0.00036	54.7	5.6
MRK595	1259.48	ISMLG	S II	1259.5	L	-8.0	-0.00003	137.6	5.8
MRK595	1259.98	ISMLG	Si II	1260.4	L	-104.0	-0.00036	425.3	3.3
MRK595	1260.43	ISMLG	Si II	1260.4	L	1.0	-0.00003	361.1	4.4
MRK595	1260.70	ISMLG	C I	1260.7	L	-8.0	-0.00003	79.1	5.3
MRK595	1260.93	ISMLG	C I*	1260.9	L	-17.0	-0.00003	39.1	5.3
MRK595	1264.00	PROXIMATE	N V	1238.8	H	6094.0	0.02029	83.7	5.9
MRK595	1264.19	PROXIMATE	N V	1238.8	H	6139.0	0.02047	154.2	6.9
MRK595	1268.01	PROXIMATE	N V	1242.8	H	6080.0	0.02029	70.3	7.8

Table A1 continued

Table A1 (*continued*)

Target	λ_{obs}	Type	Ion	λ_{rest}	Frame	cz	z	W_{λ}	$\sigma_{W_{\lambda}}$
	(Å)			(Å)		(km s ⁻¹)		(mÅ)	(mÅ)
MRK595	1268.23	PROXIMATE	N v	1242.8	H	6133.0	0.02047	123.9	7.1
MRK595	1270.30	INTRINSIC	N v	1238.8	H	7618.0	0.02542	104.3	7.7
MRK595	1274.41	INTRINSIC	N v	1242.8	H	7623.0	0.02542	115.0	18.4
MRK595	1277.21	ISMLG	C I	1277.2	L	-7.0	-0.00003	75.2	10.5
MRK595	1277.44	ISMLG	C I*	1277.5	L	-17.0	-0.00003	68.0	10.3
MRK595	1277.67	UNIDENTIFIED	UNIND	1000.0	H	0.0	-1.00000	33.7	10.2
MRK595	1280.07	ISMLG	C I	1280.1	L	-15.0	-0.00003	43.6	15.2
MRK595	1283.13	OTHER	FPN	0.0	H	0.0	-1.00000	44.1	18.3
MRK595	1301.73	ISMLG	O I	1302.1	L	-101.0	-0.00036	282.3	11.5
MRK595	1302.11	ISMLG	O I	1302.1	L	-12.0	-0.00003	321.0	13.7
MRK595	1303.34	OTHER	FPN	0.0	H	0.0	-1.00000	55.5	16.8
MRK595	1303.90	ISMLG	Si II	1304.3	L	-107.0	-0.00036	124.9	12.3
MRK595	1304.32	ISMLG	Si II	1304.3	L	-11.0	-0.00003	276.7	14.7
MRK595	1317.20	ISMLG	Ni II	1317.2	L	-4.0	-0.00003	58.0	14.7
MRK595	1328.80	ISMLG	C I	1328.8	L	-7.0	-0.00003	48.3	13.1
MRK595	1329.05	ISMLG	C I*	1329.1	L	-11.0	-0.00003	45.1	14.3
MRK595	1334.05	ISMLG	C II	1334.5	L	-108.0	-0.00036	493.1	9.6
MRK595	1334.54	ISMLG	C II	1334.5	L	2.0	-0.00003	393.2	9.5
MRK595	1335.68	ISMLG	C II*	1335.7	L	-6.0	-0.00003	160.1	14.0
MRK595	1347.20	ISMLG	Cl I	1347.2	L	-10.0	-0.00003	48.8	15.2
MRK595	1370.08	ISMLG	Ni II	1370.1	L	-12.0	-0.00003	47.1	12.7
MRK595	1393.70	ISMLG	Si IV	1393.7	L	-14.0	-0.00003	159.0	20.9
MRK595	1402.78	ISMLG	H I	1402.7	L	1.0	-0.00003	52.0	19.6
NGC7469	914.39	ISMLG	H ₂	914.3	L	-3.0	0.00000	662.0	0.0
NGC7469	914.60	ISMLG	H ₂	914.6	L	-3.0	0.00000	438.2	0.0
NGC7469	915.39	ISMLG	H ₂	915.4	L	-3.0	0.00000	470.4	0.0
NGC7469	929.52	ISMLG	H ₂	929.5	L	-3.0	0.00000	822.4	0.0
NGC7469	929.68	ISMLG	H ₂	929.6	L	-3.0	0.00000	535.8	0.0
NGC7469	930.57	ISMLG	H ₂	930.5	L	-3.0	0.00000	600.0	0.0
NGC7469	946.38	ISMLG	H ₂	946.3	L	-3.0	0.00000	510.5	0.0
NGC7469	946.41	ISMLG	H ₂	946.4	L	-3.0	0.00000	1161.3	0.0
NGC7469	947.41	ISMLG	H ₂	947.4	L	-3.0	0.00000	742.3	0.0
NGC7469	954.40	ISMLG	H ₂	954.4	L	-3.0	0.00000	504.3	0.0
NGC7469	955.05	ISMLG	H ₂	955.0	L	-3.0	0.00000	402.9	0.0
NGC7469	962.97	ISMLG	H ₂	962.9	L	-3.0	0.00000	506.1	0.0
NGC7469	964.97	ISMLG	H ₂	964.9	L	-3.0	0.00000	1280.7	0.0
NGC7469	965.05	ISMLG	H ₂	965.0	L	-3.0	0.00000	881.0	0.0
NGC7469	966.08	ISMLG	H ₂	966.0	L	-3.0	0.00000	879.1	0.0
NGC7469	971.97	ISMLG	H ₂	971.9	L	-3.0	0.00000	648.8	0.0
NGC7469	972.62	ISMLG	H ₂	972.6	L	-3.0	0.00000	521.4	0.0
NGC7469	981.43	ISMLG	H ₂	981.4	L	-3.0	0.00000	687.4	0.0
NGC7469	982.06	ISMLG	H ₂	982.0	L	-3.0	0.00000	535.0	0.0
NGC7469	985.62	ISMLG	H ₂	985.6	L	-3.0	0.00000	1355.6	0.0
NGC7469	985.63	ISMLG	H ₂	985.6	L	-3.0	0.00000	905.6	0.0
NGC7469	986.79	ISMLG	H ₂	986.7	L	-3.0	0.00000	944.7	0.0
NGC7469	991.37	ISMLG	H ₂	991.3	L	-3.0	0.00000	804.9	0.0
NGC7469	992.00	ISMLG	H ₂	992.0	L	-3.0	0.00000	646.2	0.0
NGC7469	992.80	ISMLG	H ₂	992.8	L	-3.0	0.00000	424.0	0.0
NGC7469	1000.71	ISMLG	H ₂	1001.8	L	-333.0	-0.00110	19.0	0.0
NGC7469	1001.34	ISMLG	H ₂	1002.4	L	-333.0	-0.00110	35.4	0.0
NGC7469	1001.64	ISMLG	H ₂	1001.6	L	-3.0	0.00000	32.3	0.0
NGC7469	1001.81	ISMLG	H ₂	1001.8	L	-3.0	0.00000	859.7	0.0
NGC7469	1001.88	ISMLG	HD	1001.8	L	-2.0	-0.00000	167.3	16.0

Table A1 continued

Table A1 (*continued*)

Target	λ_{obs}	Type	Ion	λ_{rest}	Frame	cz	z	W_{λ}	$\sigma_{W_{\lambda}}$
	(Å)			(Å)		(km s ⁻¹)		(mÅ)	(mÅ)
NGC7469	1002.18	ISMLG	H ₂	1003.2	L	-333.0	-0.00110	21.9	0.0
NGC7469	1002.44	ISMLG	H ₂	1002.4	L	-3.0	0.00000	682.9	0.0
NGC7469	1002.87	ISMLG	H ₂	1003.9	L	-333.0	-0.00110	11.9	0.0
NGC7469	1003.28	ISMLG	H ₂	1003.2	L	-3.0	0.00000	467.7	0.0
NGC7469	1003.97	ISMLG	H ₂	1003.9	L	-3.0	0.00000	137.3	0.0
NGC7469	1004.27	ISMLG	H ₂	1005.3	L	-333.0	-0.00110	7.5	0.0
NGC7469	1005.29	ISMLG	H ₂	1006.4	L	-333.0	-0.00110	13.2	0.0
NGC7469	1005.38	ISMLG	H ₂	1005.3	L	-3.0	0.00000	117.9	0.0
NGC7469	1006.40	ISMLG	H ₂	1006.4	L	-3.0	0.00000	83.7	0.0
NGC7469	1007.26	ISMLG	H ₂	1008.3	L	-333.0	-0.00110	9.3	0.0
NGC7469	1007.38	ISMLG	H ₂	1008.4	L	-333.0	-0.00110	38.8	0.0
NGC7469	1007.43	ISMLG	H ₂	1008.5	L	-333.0	-0.00110	27.8	0.0
NGC7469	1007.92	ISMLG	H ₂	1009.0	L	-333.0	-0.00110	12.1	0.0
NGC7469	1008.37	ISMLG	H ₂	1008.3	L	-3.0	0.00000	80.1	0.0
NGC7469	1008.49	ISMLG	H ₂	1008.4	L	-3.0	0.00000	762.3	0.0
NGC7469	1008.54	ISMLG	H ₂	1008.5	L	-3.0	0.00000	1149.4	0.0
NGC7469	1008.65	ISMLG	H ₂	1009.7	L	-333.0	-0.00110	40.9	0.0
NGC7469	1009.01	ISMLG	H ₂	1010.1	L	-333.0	-0.00110	12.8	0.0
NGC7469	1009.03	ISMLG	H ₂	1009.0	L	-3.0	0.00000	139.8	0.0
NGC7469	1009.71	ISMLG	H ₂	1009.7	L	-3.0	0.00000	8.1	0.0
NGC7469	1009.76	ISMLG	H ₂	1009.7	L	-3.0	0.00000	807.6	0.0
NGC7469	1009.82	ISMLG	H ₂	1010.9	L	-333.0	-0.00110	16.4	0.0
NGC7469	1010.12	ISMLG	H ₂	1010.1	L	-3.0	0.00000	83.7	0.0
NGC7469	1010.93	ISMLG	H ₂	1010.9	L	-3.0	0.00000	156.4	0.0
NGC7469	1011.45	ISMLG	HD	1011.4	L	-3.0	-0.00000	26.5	5.8
NGC7469	1011.55	ISMLG	H ₂	1012.6	L	-333.0	-0.00110	19.0	0.0
NGC7469	1011.68	ISMLG	H ₂	1012.8	L	-333.0	-0.00110	21.0	0.0
NGC7469	1011.80	ISMLG	H ₂	1011.8	L	-3.0	0.00000	42.7	0.0
NGC7469	1012.16	ISMLG	H ₂	1012.1	L	-3.0	0.00000	109.6	0.0
NGC7469	1012.25	ISMLG	H ₂	1012.2	L	-3.0	0.00000	36.5	0.0
NGC7469	1012.31	ISMLG	H ₂	1013.4	L	-333.0	-0.00110	38.4	0.0
NGC7469	1012.50	ISMLG	S III	1012.4	L	2.0	-0.00000	80.2	2.6
NGC7469	1012.67	ISMLG	H ₂	1012.6	L	-3.0	0.00000	88.5	0.0
NGC7469	1012.80	ISMLG	H ₂	1012.8	L	-3.0	0.00000	952.2	0.0
NGC7469	1013.20	ISMLG	H ₂	1014.3	L	-333.0	-0.00110	23.2	0.0
NGC7469	1013.38	ISMLG	H ₂	1014.5	L	-333.0	-0.00110	7.4	0.0
NGC7469	1013.42	ISMLG	H ₂	1013.4	L	-3.0	0.00000	761.6	0.0
NGC7469	1013.85	ISMLG	H ₂	1014.9	L	-333.0	-0.00110	13.7	0.0
NGC7469	1014.32	ISMLG	H ₂	1014.3	L	-3.0	0.00000	504.4	0.0
NGC7469	1014.49	ISMLG	H ₂	1014.5	L	-3.0	0.00000	78.2	0.0
NGC7469	1014.96	ISMLG	H ₂	1014.9	L	-3.0	0.00000	147.3	0.0
NGC7469	1014.97	ISMLG	H ₂	1014.9	L	-3.0	0.00000	49.8	0.0
NGC7469	1015.33	ISMLG	H ₂	1016.4	L	-333.0	-0.00110	7.9	0.0
NGC7469	1016.29	ISMLG	H ₂	1017.4	L	-333.0	-0.00110	15.6	0.0
NGC7469	1016.45	ISMLG	H ₂	1016.4	L	-3.0	0.00000	125.3	0.0
NGC7469	1017.37	ISMLG	H ₂	1017.3	L	-3.0	0.00000	34.5	0.0
NGC7469	1017.41	ISMLG	H ₂	1017.4	L	-3.0	0.00000	86.5	0.0
NGC7469	1018.37	ISMLG	H ₂	1019.5	L	-333.0	-0.00110	9.5	0.0
NGC7469	1019.49	ISMLG	H ₂	1019.5	L	-3.0	0.00000	81.1	0.0
NGC7469	1020.54	ISMLG	Si II	1020.6	L	-45.0	-0.00013	43.5	4.4
NGC7469	1020.70	ISMLG	Si II	1020.6	L	1.0	-0.00000	129.2	2.6
NGC7469	1020.75	ISMLG	H ₂	1020.7	L	-3.0	0.00000	46.2	0.0
NGC7469	1021.46	ISMLG	HD	1021.4	L	0.0	-0.00000	46.7	4.6

Table A1 continued

Table A1 (*continued*)

Target	λ_{obs}	Type	Ion	λ_{rest}	Frame	cz	z	W_{λ}	$\sigma_{W_{\lambda}}$
	(Å)			(Å)		(km s ⁻¹)		(mÅ)	(mÅ)
NGC7469	1023.23	ISMLG	H ₂	1024.3	L	-333.0	-0.00110	20.9	0.0
NGC7469	1023.42	ISMLG	H ₂	1023.4	L	-3.0	0.00000	36.5	0.0
NGC7469	1023.85	ISMLG	H ₂	1024.9	L	-333.0	-0.00110	38.4	0.0
NGC7469	1024.36	ISMLG	H ₂	1024.3	L	-3.0	0.00000	998.3	0.0
NGC7469	1024.79	ISMLG	H ₂	1025.9	L	-333.0	-0.00110	23.9	0.0
NGC7469	1024.98	ISMLG	H ₂	1024.9	L	-3.0	0.00000	796.8	0.0
NGC7469	1025.39	ISMLG	H ₂	1026.5	L	-333.0	-0.00110	13.5	0.0
NGC7469	1025.92	ISMLG	H ₂	1025.9	L	-3.0	0.00000	539.7	0.0
NGC7469	1026.52	ISMLG	H ₂	1026.5	L	-3.0	0.00000	151.6	0.0
NGC7469	1026.96	ISMLG	H ₂	1028.1	L	-333.0	-0.00110	8.3	0.0
NGC7469	1027.84	ISMLG	H ₂	1028.9	L	-333.0	-0.00110	15.5	0.0
NGC7469	1028.09	ISMLG	H ₂	1028.1	L	-3.0	0.00000	134.9	0.0
NGC7469	1028.97	ISMLG	H ₂	1028.9	L	-3.0	0.00000	87.5	0.0
NGC7469	1030.05	ISMLG	H ₂	1031.1	L	-333.0	-0.00110	10.2	0.0
NGC7469	1030.66	ISMLG	O VI	1031.9	L	-368.0	-0.00122	20.7	3.8
NGC7469	1030.81	ISMLG	O VI	1031.9	L	-325.0	-0.00110	69.5	3.7
NGC7469	1030.95	ISMLG	O VI	1031.9	L	-284.0	-0.00095	39.6	3.0
NGC7469	1031.08	ISMLG	O VI	1031.9	L	-244.0	-0.00083	66.5	3.2
NGC7469	1031.18	ISMLG	H ₂	1031.1	L	-3.0	0.00000	82.9	0.0
NGC7469	1031.28	ISMLG	O VI	1031.9	L	-187.0	-0.00060	103.8	3.6
NGC7469	1031.77	ISMLG	O VI	1031.9	L	-47.0	-0.00013	22.7	3.8
NGC7469	1031.91	ISMLG	HD	1031.9	L	-1.0	-0.00000	48.6	3.5
NGC7469	1031.93	ISMLG	O VI	1031.9	L	-1.0	0.00000	48.6	3.5
NGC7469	1032.34	ISMLG	H ₂	1032.3	L	-3.0	0.00000	46.4	0.0
NGC7469	1035.06	ISMLG	C II	1036.3	L	-370.0	-0.00122	57.0	3.0
NGC7469	1035.17	ISMLG	H ₂	1035.1	L	-3.0	0.00000	38.4	0.0
NGC7469	1035.19	ISMLG	C II	1036.3	L	-333.0	-0.00110	114.9	3.0
NGC7469	1035.39	ISMLG	H ₂	1036.5	L	-333.0	-0.00110	20.4	0.0
NGC7469	1036.00	ISMLG	H ₂	1037.1	L	-333.0	-0.00110	37.8	0.0
NGC7469	1036.17	ISMLG	C II	1036.3	L	-47.0	-0.00013	145.4	1.6
NGC7469	1036.33	ISMLG	C II	1036.3	L	-1.0	-0.00000	175.6	1.2
NGC7469	1036.54	ISMLG	H ₂	1036.5	L	-3.0	0.00000	1017.8	0.0
NGC7469	1037.00	ISMLG	H ₂	1038.1	L	-333.0	-0.00110	23.5	0.0
NGC7469	1037.14	ISMLG	H ₂	1037.1	L	-3.0	0.00000	809.5	0.0
NGC7469	1037.46	ISMLG	O VI	1037.6	L	-46.0	-0.00013	87.6	3.4
NGC7469	1037.54	ISMLG	H ₂	1038.6	L	-333.0	-0.00110	13.1	0.0
NGC7469	1037.62	ISMLG	O VI	1037.6	L	0.0	-0.00000	71.0	3.6
NGC7469	1037.77	ISMLG	O VI	1037.6	L	45.0	0.00013	57.2	3.7
NGC7469	1038.15	ISMLG	H ₂	1038.1	L	-3.0	0.00000	553.2	0.0
NGC7469	1038.68	ISMLG	H ₂	1038.6	L	-3.0	0.00000	153.5	0.0
NGC7469	1039.09	ISMLG	O I	1039.2	L	-41.0	-0.00013	120.8	2.5
NGC7469	1039.21	ISMLG	H ₂	1040.3	L	-333.0	-0.00110	8.2	0.0
NGC7469	1039.23	ISMLG	O I	1039.2	L	0.0	-0.00000	113.5	2.5
NGC7469	1039.40	ISMLG	O I	1039.2	L	48.0	0.00013	32.4	3.9
NGC7469	1040.00	ISMLG	H ₂	1041.1	L	-333.0	-0.00110	14.8	0.0
NGC7469	1040.36	ISMLG	H ₂	1040.3	L	-3.0	0.00000	138.5	0.0
NGC7469	1040.49	PROXIMATE	H I	1025.7	H	4316.0	0.01439	32.0	3.4
NGC7469	1041.15	ISMLG	H ₂	1041.1	L	-3.0	0.00000	88.1	0.0
NGC7469	1041.94	PROXIMATE	O VI	1031.9	H	2910.0	0.00970	101.8	2.7
NGC7469	1042.24	PROXIMATE	O VI	1031.9	H	2997.0	0.01006	243.9	2.7
NGC7469	1042.34	ISMLG	H ₂	1043.5	L	-333.0	-0.00110	10.1	0.0
NGC7469	1042.83	ISMLG	HD	1042.8	L	-4.0	-0.00000	16.9	2.7
NGC7469	1043.49	ISMLG	H ₂	1043.5	L	-3.0	0.00000	83.8	0.0

Table A1 continued

Table A1 (*continued*)

Target	λ_{obs}	Type	Ion	λ_{rest}	Frame	cz	z	W_{λ}	$\sigma_{W_{\lambda}}$
	(Å)			(Å)		(km s ⁻¹)		(mÅ)	(mÅ)
NGC7469	1043.88	PROXIMATE	O VI	1031.9	H	3472.0	0.01156	43.2	3.0
NGC7469	1044.53	ISMLG	H ₂	1044.5	L	-3.0	0.00000	45.9	0.0
NGC7469	1046.78	PROXIMATE	O VI	1031.9	H	4316.0	0.01439	138.7	3.8
NGC7469	1046.89	PROXIMATE	O VI	1031.9	H	4346.0	0.01451	92.0	2.5
NGC7469	1047.11	INTRINSIC	O VI	1031.9	H	4411.0	0.01471	48.4	3.3
NGC7469	1047.54	ISMLG	H ₂	1047.5	L	-3.0	0.00000	38.5	0.0
NGC7469	1047.69	PROXIMATE	O VI	1037.6	H	2910.0	0.00970	36.1	3.1
NGC7469	1047.99	PROXIMATE	O VI	1037.6	H	2999.0	0.01006	178.3	2.6
NGC7469	1048.20	ISMLG	H ₂	1049.3	L	-333.0	-0.00110	18.7	0.0
NGC7469	1048.21	ISMLG	Ar I	1048.2	L	-3.0	-0.00000	105.9	2.5
NGC7469	1048.79	ISMLG	H ₂	1049.9	L	-333.0	-0.00110	35.6	0.0
NGC7469	1049.36	ISMLG	H ₂	1049.3	L	-3.0	0.00000	999.5	0.0
NGC7469	1049.87	ISMLG	H ₂	1051.0	L	-333.0	-0.00110	21.8	0.0
NGC7469	1049.95	ISMLG	H ₂	1049.9	L	-3.0	0.00000	793.9	0.0
NGC7469	1050.33	ISMLG	H ₂	1051.4	L	-333.0	-0.00110	11.8	0.0
NGC7469	1051.02	ISMLG	H ₂	1051.0	L	-3.0	0.00000	545.8	0.0
NGC7469	1051.49	ISMLG	H ₂	1051.4	L	-3.0	0.00000	154.8	0.0
NGC7469	1052.11	ISMLG	H ₂	1053.2	L	-333.0	-0.00110	7.5	0.0
NGC7469	1052.57	PROXIMATE	O VI	1037.6	H	4321.0	0.01439	122.6	3.9
NGC7469	1052.65	PROXIMATE	O VI	1037.6	H	4342.0	0.01451	87.3	2.7
NGC7469	1052.81	ISMLG	H ₂	1053.9	L	-333.0	-0.00110	13.5	0.0
NGC7469	1052.88	INTRINSIC	O VI	1037.6	H	4408.0	0.01471	43.6	3.5
NGC7469	1053.27	ISMLG	H ₂	1053.2	L	-3.0	0.00000	136.9	0.0
NGC7469	1053.96	ISMLG	H ₂	1053.9	L	-3.0	0.00000	88.0	0.0
NGC7469	1054.27	ISMLG	HD	1054.2	L	1.0	-0.00000	19.8	2.8
NGC7469	1055.11	ISMLG	Fe II	1055.2	L	-44.0	-0.00013	17.2	2.1
NGC7469	1055.26	ISMLG	Fe II	1055.2	L	-2.0	-0.00000	40.4	2.7
NGC7469	1055.30	ISMLG	H ₂	1056.4	L	-333.0	-0.00110	9.2	0.0
NGC7469	1056.46	ISMLG	H ₂	1056.4	L	-3.0	0.00000	85.5	0.0
NGC7469	1057.37	ISMLG	H ₂	1057.3	L	-3.0	0.00000	44.2	0.0
NGC7469	1060.57	ISMLG	H ₂	1060.5	L	-3.0	0.00000	37.0	0.0
NGC7469	1061.70	ISMLG	H ₂	1062.8	L	-333.0	-0.00110	15.6	0.0
NGC7469	1062.28	ISMLG	H ₂	1063.4	L	-333.0	-0.00110	31.3	0.0
NGC7469	1062.87	ISMLG	H ₂	1062.8	L	-3.0	0.00000	929.0	0.0
NGC7469	1063.42	ISMLG	H ₂	1064.6	L	-333.0	-0.00110	18.4	0.0
NGC7469	1063.45	ISMLG	H ₂	1063.4	L	-3.0	0.00000	738.3	0.0
NGC7469	1063.81	ISMLG	H ₂	1064.9	L	-333.0	-0.00110	9.6	0.0
NGC7469	1063.97	ISMLG	Fe II	1063.9	L	-1.0	-0.00000	30.5	3.7
NGC7469	1064.59	ISMLG	H ₂	1064.6	L	-3.0	0.00000	509.4	0.0
NGC7469	1064.98	ISMLG	H ₂	1064.9	L	-3.0	0.00000	146.1	0.0
NGC7469	1066.26	ISMLG	HD	1066.2	L	-4.0	-0.00000	22.5	4.1
NGC7469	1066.29	ISMLG	H ₂	1067.4	L	-333.0	-0.00110	11.0	0.0
NGC7469	1066.66	ISMLG	Ar I	1066.6	L	0.0	-0.00000	73.4	3.0
NGC7469	1066.89	ISMLG	H ₂	1066.9	L	-3.0	0.00000	128.5	0.0
NGC7469	1067.47	ISMLG	H ₂	1067.4	L	-3.0	0.00000	86.7	0.0
NGC7469	1068.95	ISMLG	H ₂	1070.1	L	-333.0	-0.00110	7.6	0.0
NGC7469	1070.13	ISMLG	H ₂	1070.1	L	-3.0	0.00000	82.7	0.0
NGC7469	1070.89	ISMLG	H ₂	1070.9	L	-3.0	0.00000	40.2	0.0
NGC7469	1074.30	ISMLG	H ₂	1074.3	L	-3.0	0.00000	33.2	0.0
NGC7469	1075.94	ISMLG	H ₂	1077.1	L	-333.0	-0.00110	11.1	0.0
NGC7469	1076.50	ISMLG	H ₂	1077.7	L	-333.0	-0.00110	24.1	0.0
NGC7469	1077.13	ISMLG	H ₂	1077.1	L	-3.0	0.00000	795.8	0.0
NGC7469	1077.69	ISMLG	H ₂	1077.7	L	-3.0	0.00000	632.0	0.0

Table A1 continued

Table A1 (*continued*)

Target	λ_{obs}	Type	Ion	λ_{rest}	Frame	cz	z	W_{λ}	$\sigma_{W_{\lambda}}$
	(Å)			(Å)		(km s ⁻¹)		(mÅ)	(mÅ)
NGC7469	1077.73	ISMLG	H ₂	1078.9	L	-333.0	-0.00110	13.4	0.0
NGC7469	1078.03	ISMLG	H ₂	1079.2	L	-333.0	-0.00110	6.7	0.0
NGC7469	1078.92	ISMLG	H ₂	1078.9	L	-3.0	0.00000	439.0	0.0
NGC7469	1079.21	ISMLG	H ₂	1079.2	L	-3.0	0.00000	140.1	0.0
NGC7469	1080.51	ISMLG	H ₂	1081.7	L	-333.0	-0.00110	7.7	0.0
NGC7469	1081.26	ISMLG	H ₂	1081.2	L	-3.0	0.00000	121.5	0.0
NGC7469	1081.70	ISMLG	H ₂	1081.7	L	-3.0	0.00000	83.8	0.0
NGC7469	1081.84	ISMLG	Fe II	1081.8	L	-8.0	-0.00000	34.4	4.3
NGC7469	1084.55	ISMLG	H ₂	1084.5	L	-3.0	0.00000	79.9	0.0
NGC7469	1085.14	ISMLG	H ₂	1085.1	L	-3.0	0.00000	32.8	0.0
NGC7469	1088.79	ISMLG	H ₂	1088.7	L	-3.0	0.00000	26.2	0.0
NGC7469	1090.98	ISMLG	H ₂	1092.1	L	-333.0	-0.00110	6.1	0.0
NGC7469	1091.52	ISMLG	H ₂	1092.7	L	-333.0	-0.00110	14.2	0.0
NGC7469	1091.93	ISMLG	HD	1091.9	L	-5.0	-0.00000	75.0	5.4
NGC7469	1092.18	ISMLG	H ₂	1092.1	L	-3.0	0.00000	599.4	0.0
NGC7469	1092.72	ISMLG	H ₂	1092.7	L	-3.0	0.00000	475.3	0.0
NGC7469	1092.84	ISMLG	H ₂	1094.0	L	-333.0	-0.00110	7.4	0.0
NGC7469	1094.04	ISMLG	H ₂	1094.0	L	-3.0	0.00000	334.3	0.0
NGC7469	1094.23	ISMLG	H ₂	1094.2	L	-3.0	0.00000	119.7	0.0
NGC7469	1096.43	ISMLG	H ₂	1096.4	L	-3.0	0.00000	110.3	0.0
NGC7469	1096.71	ISMLG	H ₂	1096.7	L	-3.0	0.00000	77.9	0.0
NGC7469	1096.85	ISMLG	Fe II	1096.8	L	-7.0	-0.00000	94.9	2.1
NGC7469	1099.78	ISMLG	H ₂	1099.7	L	-3.0	0.00000	74.0	0.0
NGC7469	1100.15	ISMLG	H ₂	1100.1	L	-3.0	0.00000	20.9	0.0
NGC7469	1103.63	ISMLG	C I	1103.6	L	-1.0	-0.00000	7.7	4.0
NGC7469	1104.07	ISMLG	H ₂	1104.0	L	-3.0	0.00000	16.0	0.0
NGC7469	1105.72	ISMLG	HD	1105.7	L	3.0	-0.00000	34.0	4.8
NGC7469	1106.29	ISMLG	C I	1106.3	L	-6.0	-0.00000	10.9	3.5
NGC7469	1108.12	ISMLG	H ₂	1108.1	L	-3.0	0.00000	349.1	0.0
NGC7469	1108.62	ISMLG	H ₂	1108.6	L	-3.0	0.00000	283.9	0.0
NGC7469	1109.61	ISMLG	C I	1109.6	L	-5.0	-0.00000	25.1	3.6
NGC7469	1110.05	ISMLG	H ₂	1110.0	L	-3.0	0.00000	201.8	0.0
NGC7469	1110.11	ISMLG	H ₂	1110.1	L	-3.0	0.00000	100.8	0.0
NGC7469	1111.42	ISMLG	C I	1111.4	L	0.0	-0.00000	21.9	3.9
NGC7469	1112.03	ISMLG	Fe II	1112.0	L	-4.0	-0.00000	44.9	3.0
NGC7469	1112.48	ISMLG	H ₂	1112.4	L	-3.0	0.00000	94.9	0.0
NGC7469	1112.57	ISMLG	H ₂	1112.5	L	-3.0	0.00000	65.2	0.0
NGC7469	1115.88	ISMLG	H ₂	1115.8	L	-3.0	0.00000	60.7	0.0
NGC7469	1116.00	ISMLG	H ₂	1116.0	L	-3.0	0.00000	7.4	0.0
NGC7469	1117.85	ISMLG	C I	1117.8	L	-5.0	-0.00000	20.9	4.9
NGC7469	1121.94	ISMLG	Fe II	1121.9	L	-9.0	-0.00000	102.1	3.5
NGC7469	1122.37	ISMLG	Fe III	1122.5	L	-41.0	-0.00013	43.4	3.2
NGC7469	1122.43	ISMLG	C I	1122.4	L	-2.0	-0.00000	50.7	4.0
NGC7469	1122.53	ISMLG	Fe III	1122.5	L	2.0	-0.00000	73.3	3.4
NGC7469	1125.28	ISMLG	Fe II	1125.4	L	-45.0	-0.00013	41.0	3.6
NGC7469	1125.43	ISMLG	Fe II	1125.4	L	-4.0	-0.00000	69.6	2.7
NGC7469	1127.08	ISMLG	Fe II	1127.0	L	-5.0	-0.00000	17.9	4.1
NGC7469	1129.17	ISMLG	C I	1129.3	L	-39.0	-0.00013	23.1	3.7
NGC7469	1133.65	ISMLG	Fe II	1133.6	L	-4.0	-0.00000	36.2	3.0
NGC7469	1134.00	ISMLG	N I	1134.1	L	-44.0	-0.00013	36.7	3.0
NGC7469	1134.14	ISMLG	N I	1134.1	L	-6.0	-0.00000	97.8	2.1
NGC7469	1134.26	ISMLG	N I	1134.4	L	-42.0	-0.00013	64.0	2.5
NGC7469	1134.40	ISMLG	N I	1134.4	L	-5.0	-0.00000	120.8	3.1

Table A1 continued

Table A1 (*continued*)

Target	λ_{obs}	Type	Ion	λ_{rest}	Frame	cz	z	W_{λ}	$\sigma_{W_{\lambda}}$
	(Å)			(Å)		(km s ⁻¹)		(mÅ)	(mÅ)
NGC7469	1134.83	ISMLG	N I	1134.9	L	-41.0	-0.00013	65.6	2.3
NGC7469	1134.95	ISMLG	N I	1134.9	L	-7.0	-0.00000	124.7	2.3
NGC7469	1139.80	ISMLG	C I	1139.7	L	1.0	-0.00000	27.3	4.0
NGC7469	1142.34	ISMLG	Fe II	1142.3	L	-7.0	-0.00000	41.1	8.4
NGC7469	1143.22	ISMLG	Fe II	1143.2	L	-2.0	-0.00000	85.6	8.8
NGC7469	1144.77	ISMLG	Fe II	1144.9	L	-43.0	-0.00013	70.2	8.0
NGC7469	1144.91	ISMLG	Fe II	1144.9	L	-7.0	-0.00000	120.8	6.6
NGC7469	1152.65	ISMLG	P II	1152.8	L	-44.0	-0.00013	23.4	5.2
NGC7469	1152.83	ISMLG	P II	1152.8	L	3.0	-0.00000	65.7	6.3
NGC7469	1155.80	ISMLG	C I	1155.8	L	-2.0	-0.00000	27.6	4.4
NGC7469	1157.92	ISMLG	C I	1157.9	L	2.0	-0.00000	42.2	4.1
NGC7469	1158.32	ISMLG	C I	1158.3	L	-2.0	-0.00000	15.7	4.5
NGC7469	1188.81	ISMLG	C I	1188.8	L	-6.0	-0.00000	30.2	2.9
NGC7469	1188.95	ISMLG	Si II	1190.4	L	-370.0	-0.00122	40.2	2.7
NGC7469	1189.09	ISMLG	Si II	1190.4	L	-333.0	-0.00110	60.0	2.9
NGC7469	1189.27	ISMLG	Si II	1190.4	L	-290.0	-0.00095	9.8	2.9
NGC7469	1190.23	ISMLG	Si II	1190.4	L	-46.0	-0.00013	162.8	2.2
NGC7469	1190.42	ISMLG	Si II	1190.4	L	0.0	-0.00000	144.9	1.6
NGC7469	1190.59	ISMLG	Si II	1190.4	L	45.0	0.00013	43.2	3.2
NGC7469	1191.82	ISMLG	Si II	1193.2	L	-369.0	-0.00122	47.5	2.7
NGC7469	1191.97	ISMLG	Si II	1193.2	L	-332.0	-0.00110	79.3	2.3
NGC7469	1192.14	ISMLG	Si II	1193.2	L	-290.0	-0.00095	28.7	2.9
NGC7469	1193.10	ISMLG	Si II	1193.2	L	-47.0	-0.00013	172.9	1.9
NGC7469	1193.29	ISMLG	Si II	1193.2	L	1.0	-0.00000	165.1	1.6
NGC7469	1193.47	ISMLG	Si II	1193.2	L	45.0	0.00013	58.2	3.2
NGC7469	1193.99	ISMLG	C I	1193.9	L	0.0	-0.00000	27.6	3.9
NGC7469	1197.19	ISMLG	Mn II	1197.1	L	2.0	-0.00000	16.3	3.2
NGC7469	1199.40	ISMLG	N I	1199.5	L	-38.0	-0.00013	84.4	2.3
NGC7469	1199.56	ISMLG	N I	1199.5	L	2.0	-0.00000	136.1	2.4
NGC7469	1200.06	ISMLG	N I	1200.2	L	-40.0	-0.00013	61.6	2.4
NGC7469	1200.23	ISMLG	N I	1200.2	L	1.0	-0.00000	130.8	2.4
NGC7469	1200.54	ISMLG	N I	1200.7	L	-42.0	-0.00013	57.3	2.7
NGC7469	1200.69	ISMLG	N I	1200.7	L	-6.0	-0.00000	113.5	2.5
NGC7469	1205.02	ISMLG	Si III	1206.5	L	-368.0	-0.00122	115.2	2.1
NGC7469	1205.20	ISMLG	Si III	1206.5	L	-323.0	-0.00110	180.9	1.5
NGC7469	1205.36	ISMLG	Si III	1206.5	L	-284.0	-0.00095	89.0	1.9
NGC7469	1205.49	ISMLG	Si III	1206.5	L	-252.0	-0.00083	57.8	2.9
NGC7469	1205.77	ISMLG	Si III	1206.5	L	-182.0	-0.00060	24.4	3.4
NGC7469	1206.32	ISMLG	Si III	1206.5	L	-44.0	-0.00013	158.8	2.3
NGC7469	1206.50	ISMLG	Si III	1206.5	L	0.0	-0.00000	187.6	1.0
NGC7469	1206.70	ISMLG	Si III	1206.5	L	50.0	0.00013	164.2	1.7
NGC7469	1227.47	PROXIMATE	H I	1215.6	H	2909.0	0.00970	67.8	2.6
NGC7469	1227.90	PROXIMATE	H I	1215.6	H	3015.0	0.01006	244.6	2.5
NGC7469	1229.72	PROXIMATE	H I	1215.6	H	3465.0	0.01156	32.0	2.9
NGC7469	1232.01	PROXIMATE	H I	1215.6	H	4029.0	0.01344	173.4	2.6
NGC7469	1233.17	PROXIMATE	H I	1215.6	H	4315.0	0.01439	75.1	2.1
NGC7469	1233.31	PROXIMATE	H I	1215.6	H	4349.0	0.01451	30.1	1.3
NGC7469	1233.56	INTRINSIC	H I	1215.6	H	4411.0	0.01471	28.1	1.6
NGC7469	1234.19	INTRINSIC	H I	1215.6	H	4568.0	0.01524	12.1	1.4
NGC7469	1237.04	INTRINSIC	H I	1215.6	H	5269.0	0.01758	13.4	1.6
NGC7469	1238.07	PROXIMATE	H I	1215.6	H	5525.0	0.01843	10.9	1.7
NGC7469	1239.93	ISMLG	Mg II	1239.9	L	2.0	-0.00000	17.0	1.9
NGC7469	1240.39	ISMLG	Mg II	1240.3	L	0.0	-0.00000	13.0	1.9

Table A1 continued

Table A1 (*continued*)

Target	λ_{obs}	Type	Ion	λ_{rest}	Frame	cz	z	W_{λ}	$\sigma_{W_{\lambda}}$
	(Å)			(Å)		(km s ⁻¹)		(mÅ)	(mÅ)
NGC7469	1250.39	ISMLG	S II	1250.5	L	-44.0	-0.00013	25.8	1.9
NGC7469	1250.59	ISMLG	S II	1250.5	L	2.0	-0.00000	81.9	1.5
NGC7469	1250.86	PROXIMATE	N V	1238.8	H	2915.0	0.00970	49.6	2.3
NGC7469	1251.31	PROXIMATE	N V	1238.8	H	3022.0	0.01006	173.0	2.8
NGC7469	1253.13	PROXIMATE	N V	1238.8	H	3462.0	0.01156	17.2	3.1
NGC7469	1253.61	ISMLG	S II	1253.8	L	-45.0	-0.00013	33.3	2.1
NGC7469	1253.81	ISMLG	S II	1253.8	L	2.0	-0.00000	78.2	1.9
NGC7469	1254.92	PROXIMATE	N V	1242.8	H	2922.0	0.00970	22.7	2.5
NGC7469	1255.33	PROXIMATE	N V	1242.8	H	3022.0	0.01006	122.2	2.5
NGC7469	1256.66	PROXIMATE	N V	1238.8	H	4317.0	0.01439	30.0	3.1
NGC7469	1257.15	PROXIMATE	N V	1242.8	H	3461.0	0.01156	20.9	2.9
NGC7469	1258.86	ISMLG	Si II	1260.4	L	-371.0	-0.00122	80.5	1.6
NGC7469	1259.03	ISMLG	Si II	1260.4	L	-332.0	-0.00110	106.6	1.3
NGC7469	1259.22	ISMLG	Si II	1260.4	L	-286.0	-0.00095	25.1	1.7
NGC7469	1259.34	ISMLG	S II	1259.5	L	-42.0	-0.00013	58.7	1.6
NGC7469	1259.50	ISMLG	S II	1259.5	L	-5.0	-0.00000	79.3	1.1
NGC7469	1260.23	ISMLG	Si II	1260.4	L	-46.0	-0.00013	143.7	1.5
NGC7469	1260.43	ISMLG	Si II	1260.4	L	1.0	-0.00000	191.4	0.7
NGC7469	1260.61	ISMLG	Si II	1260.4	L	45.0	0.00013	101.2	1.5
NGC7469	1260.72	ISMLG	C I	1260.7	L	-5.0	-0.00000	73.7	2.0
NGC7469	1260.93	ISMLG	C I*	1260.9	L	1.0	-0.00000	20.3	1.6
NGC7469	1261.13	ISMLG	C I*	1261.1	L	2.0	-0.00000	14.1	1.8
NGC7469	1261.41	ISMLG	C I**	1261.4	L	-3.0	-0.00000	10.4	1.8
NGC7469	1276.47	ISMLG	C I	1276.4	L	-2.0	-0.00000	20.8	2.8
NGC7469	1277.25	ISMLG	C I	1277.2	L	2.0	-0.00000	63.1	3.0
NGC7469	1277.52	ISMLG	C I*	1277.5	L	0.0	-0.00000	22.9	2.5
NGC7469	1279.89	ISMLG	C I*	1279.8	L	0.0	-0.00000	27.4	3.0
NGC7469	1280.14	ISMLG	C I	1280.1	L	0.0	-0.00000	39.6	2.6
NGC7469	1280.59	ISMLG	C I*	1280.5	L	-2.0	-0.00000	9.0	2.8
NGC7469	1300.55	ISMLG	O I	1302.1	L	-372.0	-0.00122	26.1	3.3
NGC7469	1300.72	ISMLG	O I	1302.1	L	-332.0	-0.00110	80.0	3.2
NGC7469	1300.94	ISMLG	O I	1302.1	L	-283.0	-0.00095	17.0	3.0
NGC7469	1301.39	ISMLG	O I	1302.1	L	-180.0	-0.00060	29.1	4.8
NGC7469	1301.97	ISMLG	O I	1302.1	L	-45.0	-0.00013	127.8	2.6
NGC7469	1302.17	ISMLG	O I	1302.1	L	1.0	-0.00000	209.9	2.0
NGC7469	1302.36	ISMLG	O I	1302.1	L	45.0	0.00013	69.7	3.4
NGC7469	1302.94	ISMLG	Si II	1304.3	L	-329.0	-0.00110	28.8	5.1
NGC7469	1304.19	ISMLG	Si II	1304.3	L	-40.0	-0.00013	68.7	3.5
NGC7469	1304.37	ISMLG	Si II	1304.3	L	-1.0	-0.00000	177.6	2.6
NGC7469	1304.57	ISMLG	Si II	1304.3	L	47.0	0.00013	37.5	4.4
NGC7469	1317.03	ISMLG	Ni II	1317.2	L	-42.0	-0.00013	14.0	3.7
NGC7469	1317.20	ISMLG	Ni II	1317.2	L	-4.0	-0.00000	35.0	3.8
NGC7469	1328.83	ISMLG	C I	1328.8	L	-1.0	-0.00000	51.1	3.6
NGC7469	1329.10	ISMLG	C I*	1329.1	L	1.0	-0.00000	33.7	2.8
NGC7469	1329.58	ISMLG	C I**	1329.5	L	1.0	-0.00000	19.3	3.4
NGC7469	1332.89	ISMLG	C II	1334.5	L	-370.0	-0.00122	92.3	2.6
NGC7469	1333.06	ISMLG	C II	1334.5	L	-331.0	-0.00110	116.6	2.0
NGC7469	1333.27	ISMLG	C II	1334.5	L	-284.0	-0.00095	37.5	2.8
NGC7469	1333.42	ISMLG	C II	1334.5	L	-250.0	-0.00083	24.0	3.2
NGC7469	1333.74	ISMLG	C II	1334.5	L	-177.0	-0.00060	19.6	4.7
NGC7469	1334.33	ISMLG	C II	1334.5	L	-46.0	-0.00013	165.2	1.9
NGC7469	1334.54	ISMLG	C II	1334.5	L	2.0	-0.00000	204.7	1.1
NGC7469	1334.75	ISMLG	C II	1334.5	L	48.0	0.00013	127.5	2.5

Table A1 continued

Table A1 (*continued*)

Target	λ_{obs}	Type	Ion	λ_{rest}	Frame	cz	z	W_{λ}	$\sigma_{W_{\lambda}}$
	(Å)			(Å)		(km s ⁻¹)		(mÅ)	(mÅ)
NGC7469	1335.52	ISMLG	C II*	1335.7	L	-43.0	-0.00013	42.6	3.2
NGC7469	1335.69	ISMLG	C II*	1335.7	L	-4.0	-0.00000	93.6	3.0
NGC7469	1347.22	ISMLG	Cl I	1347.2	L	-3.0	-0.00000	32.0	3.8
NGC7469	1369.94	ISMLG	Ni II	1370.1	L	-42.0	-0.00013	20.1	3.4
NGC7469	1370.12	ISMLG	Ni II	1370.1	L	-3.0	-0.00000	31.2	3.4
NGC7469	1392.04	ISMLG	Si IV	1393.7	L	-369.0	-0.00122	39.5	3.5
NGC7469	1392.26	ISMLG	Si IV	1393.7	L	-323.0	-0.00110	91.8	3.2
NGC7469	1392.44	ISMLG	Si IV	1393.7	L	-283.0	-0.00095	26.2	3.0
NGC7469	1392.62	ISMLG	Si IV	1393.7	L	-245.0	-0.00083	29.6	3.7
NGC7469	1392.94	ISMLG	Si IV	1393.7	L	-176.0	-0.00060	26.5	4.4
NGC7469	1393.55	ISMLG	Si IV	1393.7	L	-46.0	-0.00013	47.5	4.0
NGC7469	1393.76	ISMLG	Si IV	1393.7	L	0.0	-0.00000	106.7	3.2
NGC7469	1393.98	ISMLG	Si IV	1393.7	L	46.0	0.00013	61.3	3.7
NGC7469	1401.05	ISMLG	Si IV	1402.7	L	-368.0	-0.00122	23.0	3.5
NGC7469	1401.24	ISMLG	Si IV	1402.7	L	-327.0	-0.00110	42.9	3.1
NGC7469	1401.44	ISMLG	Si IV	1402.7	L	-285.0	-0.00095	22.2	3.2
NGC7469	1401.62	ISMLG	Si IV	1402.7	L	-246.0	-0.00083	27.8	3.9
NGC7469	1401.94	ISMLG	Si IV	1402.7	L	-179.0	-0.00060	31.6	3.2
NGC7469	1402.56	ISMLG	Si IV	1402.7	L	-46.0	-0.00013	23.4	4.1
NGC7469	1402.76	ISMLG	Si IV	1402.7	L	-3.0	-0.00000	74.9	3.6
NGC7469	1402.96	ISMLG	Si IV	1402.7	L	40.0	0.00013	39.2	3.3
NGC7469	1454.81	ISMLG	Ni II	1454.8	L	-8.0	-0.00000	23.7	4.9
NGC7469	1467.76	ISMLG	Ni II	1467.7	L	1.0	-0.00000	12.9	4.5
NGC7469	1524.84	ISMLG	Si II	1526.7	L	-366.0	-0.00122	18.9	4.5
NGC7469	1525.02	ISMLG	Si II	1526.7	L	-331.0	-0.00110	45.5	4.0
NGC7469	1525.20	ISMLG	Si II	1526.7	L	-296.0	-0.00095	16.0	4.8
NGC7469	1526.48	ISMLG	Si II	1526.7	L	-45.0	-0.00013	146.2	3.9
NGC7469	1526.71	ISMLG	Si II	1526.7	L	0.0	-0.00000	181.1	2.8
NGC7469	1526.92	ISMLG	Si II	1526.7	L	42.0	0.00013	29.5	4.7
NGC7469	1546.29	ISMLG	C IV	1548.2	L	-370.0	-0.00122	61.2	4.8
NGC7469	1546.52	ISMLG	C IV	1548.2	L	-326.0	-0.00110	128.1	3.8
NGC7469	1546.73	ISMLG	C IV	1548.2	L	-285.0	-0.00095	58.6	4.0
NGC7469	1546.93	ISMLG	C IV	1548.2	L	-246.0	-0.00083	54.4	5.5
NGC7469	1547.28	ISMLG	C IV	1548.2	L	-179.0	-0.00060	75.8	4.9
NGC7469	1547.96	ISMLG	C IV	1548.2	L	-46.0	-0.00013	75.9	5.0
NGC7469	1548.20	ISMLG	C IV	1548.2	L	0.0	-0.00000	108.7	3.8
NGC7469	1548.44	ISMLG	C IV	1548.2	L	47.0	0.00013	79.7	4.2
NGC7469	1548.86	ISMLG	C IV	1550.7	L	-370.0	-0.00122	28.1	4.6
NGC7469	1549.10	ISMLG	C IV	1550.7	L	-325.0	-0.00110	71.6	4.9
NGC7469	1549.49	ISMLG	C IV	1550.7	L	-250.0	-0.00083	21.4	5.3
NGC7469	1549.84	ISMLG	C IV	1550.7	L	-182.0	-0.00060	56.5	5.3
NGC7469	1550.55	ISMLG	C IV	1550.7	L	-46.0	-0.00013	40.0	4.7
NGC7469	1550.79	ISMLG	C IV	1550.7	L	1.0	-0.00000	67.8	4.1
NGC7469	1551.02	ISMLG	C IV	1550.7	L	45.0	0.00013	61.7	4.7
NGC7469	1560.32	ISMLG	C I	1560.3	L	3.0	-0.00000	56.9	3.4
NGC7469	1560.68	ISMLG	C I*	1560.6	L	0.0	-0.00000	29.5	3.7
NGC7469	1561.44	ISMLG	C I**	1561.4	L	0.0	-0.00000	16.6	3.4
NGC7469	1563.30	PROXIMATE	C IV	1548.2	H	2923.0	0.00970	106.4	6.0
NGC7469	1563.79	PROXIMATE	C IV	1548.2	H	3019.0	0.01006	247.4	4.1
NGC7469	1565.89	PROXIMATE	C IV	1550.7	H	2920.0	0.00970	71.8	4.8
NGC7469	1566.06	PROXIMATE	C IV	1548.2	H	3459.0	0.01156	74.5	3.9
NGC7469	1566.39	PROXIMATE	C IV	1550.7	H	3017.0	0.01006	207.2	3.9
NGC7469	1568.72	PROXIMATE	C IV	1550.7	H	3468.0	0.01156	38.5	4.6

Table A1 continued

Table A1 (*continued*)

Target	λ_{obs}	Type	Ion	λ_{rest}	Frame	cz	z	W_{λ}	$\sigma_{W_{\lambda}}$
	(Å)			(Å)		(km s ⁻¹)		(mÅ)	(mÅ)
NGC7469	1608.21	ISMLG	Fe II	1608.4	L	-44.0	-0.00013	68.0	10.8
NGC7469	1608.41	ISMLG	Fe II	1608.4	L	-7.0	-0.00000	222.1	11.4
NGC7469	1656.94	ISMLG	C I	1656.9	L	2.0	-0.00000	98.7	7.8
NGC7469	1657.40	ISMLG	C I*	1657.3	L	3.0	-0.00000	38.7	6.2
NGC7469	1657.92	ISMLG	C I*	1657.9	L	3.0	-0.00000	29.2	7.4
NGC7469	1658.13	ISMLG	C I**	1658.1	L	2.0	-0.00000	8.4	6.5
NGC7469	1668.74	ISMLG	Al II	1670.7	L	-368.0	-0.00122	36.7	6.1
NGC7469	1668.97	ISMLG	Al II	1670.7	L	-327.0	-0.00110	59.7	6.5
NGC7469	1670.53	ISMLG	Al II	1670.7	L	-46.0	-0.00013	160.4	5.9
NGC7469	1670.79	ISMLG	Al II	1670.7	L	0.0	-0.00000	209.3	3.6
NGC7469	1671.01	ISMLG	Al II	1670.7	L	40.0	0.00013	80.3	5.7
NGC7469	1709.61	ISMLG	Ni II	1709.6	L	1.0	-0.00000	41.0	9.5
NGC7469	1741.52	ISMLG	Ni II	1741.5	L	-5.0	-0.00000	58.9	9.8
NGC7469	2793.34	ISMLG	Mg II	2796.3	L	-324.0	-0.00110	323.4	146.0
NGC7469	2796.36	ISMLG	Mg II	2796.3	L	1.0	-0.00000	573.9	35.0
NGC7469	2800.51	ISMLG	Mg II	2803.5	L	-323.0	-0.00110	176.3	166.0
NGC7469	2803.13	ISMLG	Mg II	2803.5	L	-43.0	-0.00013	302.4	89.9
NGC7469	2803.55	ISMLG	Mg II	2803.5	L	2.0	-0.00000	639.6	35.3
NGC7469	2852.98	ISMLG	H I	2852.9	L	1.0	-0.00000	314.5	56.1
PG0003+158	1133.16	IGMABS	H I	972.5	H	49513.0	0.16514	480.9	66.2
PG0003+158	1134.20	ISMLG	N I	1134.1	L	10.0	-0.00002	177.2	45.6
PG0003+158	1134.43	ISMLG	N I	1134.4	L	5.0	-0.00002	137.9	40.3
PG0003+158	1134.97	ISMLG	N I	1134.9	L	-3.0	-0.00002	157.1	56.1
PG0003+158	1138.07	IGMABS	Fe III	844.2	H	104318.0	0.34787	188.8	21.0
PG0003+158	1138.41	IGMABS	C III	977.0	H	49521.0	0.16514	329.5	21.3
PG0003+158	1140.82	UNIDENTIFIED	UNIND	1000.0	H	0.0	-1.00000	55.2	17.2
PG0003+158	1142.41	ISMLG	Fe II	1142.3	L	11.0	-0.00002	53.2	15.8
PG0003+158	1143.24	ISMLG	Fe II	1143.2	L	4.0	-0.00002	102.7	16.0
PG0003+158	1144.93	ISMLG	Fe II	1144.9	L	-2.0	-0.00002	233.4	16.1
PG0003+158	1152.81	ISMLG	P II	1152.8	L	-3.0	-0.00002	92.5	11.2
PG0003+158	1154.50	IGMABS	O III	832.9	H	115743.0	0.38603	49.1	9.1
PG0003+158	1167.25	IGMABS	O III	832.9	H	120333.0	0.40135	64.1	7.3
PG0003+158	1184.32	IGMABS	O III	832.9	H	126477.0	0.42185	52.6	8.8
PG0003+158	1188.83	ISMLG	Si II	1190.4	L	-399.0	-0.00131	58.2	6.2
PG0003+158	1189.15	ISMLG	Si II	1190.4	L	-320.0	-0.00108	62.6	6.9
PG0003+158	1190.02	ISMLG	Si II	1190.4	L	-99.0	-0.00031	93.1	5.3
PG0003+158	1190.35	ISMLG	Si II	1190.4	L	-18.0	-0.00002	292.1	3.9
PG0003+158	1190.63	ISMLG	Si II	1190.4	L	54.0	0.00019	41.2	5.5
PG0003+158	1191.76	ISMLG	Si II	1193.2	L	-384.0	-0.00131	37.9	6.0
PG0003+158	1191.99	ISMLG	Si II	1193.2	L	-327.0	-0.00108	86.5	5.4
PG0003+158	1192.92	ISMLG	Si II	1193.2	L	-92.0	-0.00031	93.8	4.5
PG0003+158	1193.22	ISMLG	Si II	1193.2	L	-17.0	-0.00002	335.3	3.9
PG0003+158	1193.53	ISMLG	Si II	1193.2	L	61.0	0.00019	31.7	5.0
PG0003+158	1195.12	IGMABS	H I	1025.7	H	49509.0	0.16514	481.4	20.2
PG0003+158	1197.15	ISMLG	Mn II	1197.1	L	-9.0	-0.00002	25.3	6.6
PG0003+158	1199.47	ISMLG	N I	1199.5	L	-20.0	-0.00002	268.4	15.9
PG0003+158	1200.14	ISMLG	N I	1200.2	L	-21.0	-0.00002	271.2	16.3
PG0003+158	1200.63	ISMLG	N I	1200.7	L	-19.0	-0.00002	262.6	13.6
PG0003+158	1201.10	ISMLG	Mn II	1201.1	L	-3.0	-0.00002	11.8	6.0
PG0003+158	1202.22	IGMABS	O VI	1031.9	H	49474.0	0.16514	46.7	16.1
PG0003+158	1202.52	IGMABS	O VI	1031.9	H	49560.0	0.16514	74.9	16.9
PG0003+158	1204.90	ISMLG	Si III	1206.5	L	-399.0	-0.00131	125.9	5.0
PG0003+158	1205.14	ISMLG	Si III	1206.5	L	-338.0	-0.00108	173.3	4.2

Table A1 continued

Table A1 (*continued*)

Target	λ_{obs}	Type	Ion	λ_{rest}	Frame	cz	z	W_{λ}	$\sigma_{W_{\lambda}}$
	(Å)			(Å)		(km s ⁻¹)		(mÅ)	(mÅ)
PG0003+158	1205.52	IGMABS	H I	923.1	H	91700.0	0.30579	57.8	4.9
PG0003+158	1205.53	ISMLG	Si III	1206.5	L	-241.0	-0.00078	57.8	4.9
PG0003+158	1206.11	ISMLG	Si III	1206.5	L	-97.0	-0.00031	138.7	4.5
PG0003+158	1206.44	ISMLG	Si III	1206.5	L	-15.0	-0.00002	396.2	2.4
PG0003+158	1206.76	ISMLG	Si III	1206.5	L	64.0	0.00019	182.2	4.6
PG0003+158	1207.47	IGMABS	C II	1036.3	H	49507.0	0.16514	21.4	5.3
PG0003+158	1209.10	IGMABS	O VI	1037.6	H	49547.0	0.16514	79.7	20.8
PG0003+158	1209.45	IGMABS	H I	926.2	H	91672.0	0.30579	83.1	20.1
PG0003+158	1218.43	IGMABS	C II	903.9	H	104290.0	0.34787	69.9	21.4
PG0003+158	1219.08	IGMABS	H I	1215.6	H	841.0	0.00281	181.2	18.3
PG0003+158	1220.74	IGMABS	H I	1025.7	H	56999.0	0.19010	82.0	10.0
PG0003+158	1223.32	IGMABS	H I	1025.7	H	57753.0	0.19268	28.8	7.0
PG0003+158	1224.23	IGMABS	H I	937.8	H	91563.0	0.30540	31.9	5.8
PG0003+158	1224.55	IGMABS	H I	937.8	H	91666.0	0.30579	136.2	6.2
PG0003+158	1230.40	IGMABS	H I	937.8	H	93535.0	0.31209	37.7	5.9
PG0003+158	1232.35	IGMABS	H I	914.2	H	104293.0	0.34787	20.3	6.0
PG0003+158	1232.74	IGMABS	H I	914.5	H	104292.0	0.34787	21.9	6.0
PG0003+158	1233.21	IGMABS	H I	914.9	H	104296.0	0.34787	28.8	5.5
PG0003+158	1233.77	IGMABS	H I	915.3	H	104297.0	0.34787	30.0	5.8
PG0003+158	1234.46	IGMABS	H I	915.8	H	104304.0	0.34787	61.2	5.9
PG0003+158	1234.98	IGMABS	C II	903.9	H	109779.0	0.36617	30.4	5.4
PG0003+158	1235.24	IGMABS	H I	916.4	H	104292.0	0.34787	47.0	5.7
PG0003+158	1236.27	IGMABS	H I	917.1	H	104297.0	0.34787	58.4	5.5
PG0003+158	1237.54	IGMABS	H I	918.1	H	104295.0	0.34787	84.6	6.3
PG0003+158	1239.19	IGMABS	H I	919.3	H	104298.0	0.34787	100.6	5.4
PG0003+158	1239.79	IGMABS	H I	949.7	H	91556.0	0.30540	63.7	5.2
PG0003+158	1240.15	IGMABS	H I	949.7	H	91669.0	0.30579	184.9	5.2
PG0003+158	1241.36	IGMABS	H I	920.9	H	104296.0	0.34787	108.6	5.4
PG0003+158	1244.31	IGMABS	H I	923.1	H	104297.0	0.34787	131.6	5.1
PG0003+158	1246.12	IGMABS	H I	949.7	H	93555.0	0.31209	52.2	6.8
PG0003+158	1247.68	IGMABS	O VI	1031.9	H	62680.0	0.20905	63.5	5.7
PG0003+158	1248.46	IGMABS	H I	926.2	H	104299.0	0.34787	156.5	5.3
PG0003+158	1250.55	ISMLG	S II	1250.5	L	-7.0	-0.00002	99.0	5.1
PG0003+158	1253.76	ISMLG	S II	1253.8	L	-11.0	-0.00002	131.3	5.4
PG0003+158	1254.57	IGMABS	H I	930.7	H	104302.0	0.34787	235.2	6.1
PG0003+158	1256.01	IGMABS	H I	919.3	H	109781.0	0.36617	16.3	4.4
PG0003+158	1258.21	IGMABS	H I	920.9	H	109781.0	0.36617	29.0	4.8
PG0003+158	1258.80	ISMLG	Si II	1260.4	L	-387.0	-0.00131	44.4	3.9
PG0003+158	1259.06	ISMLG	Si II	1260.4	L	-324.0	-0.00108	121.4	4.2
PG0003+158	1259.47	ISMLG	S II	1259.5	L	-11.0	-0.00002	172.0	4.5
PG0003+158	1260.04	ISMLG	Si II	1260.4	L	-91.0	-0.00031	115.9	3.6
PG0003+158	1260.34	ISMLG	Si II	1260.4	L	-19.0	-0.00002	402.4	2.1
PG0003+158	1260.68	ISMLG	Si II	1260.4	L	62.0	0.00019	155.6	3.4
PG0003+158	1261.22	IGMABS	H I	923.1	H	109789.0	0.36617	57.7	5.1
PG0003+158	1264.08	IGMABS	H I	937.8	H	104303.0	0.34787	193.7	5.2
PG0003+158	1265.43	IGMABS	H I	926.2	H	109790.0	0.36617	41.2	5.6
PG0003+158	1267.76	IGMABS	H I	1215.6	H	12846.0	0.04285	104.8	6.6
PG0003+158	1268.12	IGMABS	H I	1215.6	H	12934.0	0.04314	38.2	5.2
PG0003+158	1269.66	IGMABS	H I	972.5	H	91592.0	0.30540	77.0	4.0
PG0003+158	1269.92	IGMABS	H I	972.5	H	91669.0	0.30579	266.4	3.8
PG0003+158	1271.59	IGMABS	H I	930.7	H	109785.0	0.36617	52.2	5.6
PG0003+158	1275.83	IGMABS	C III	977.0	H	91687.0	0.30579	57.6	5.1
PG0003+158	1276.05	IGMABS	H I	972.5	H	93560.0	0.31209	42.0	5.1

Table A1 continued

Table A1 (*continued*)

Target	λ_{obs}	Type	Ion	λ_{rest}	Frame	cz	z	W_{λ}	$\sigma_{W_{\lambda}}$
	(Å)			(Å)		(km s ⁻¹)		(mÅ)	(mÅ)
PG0003+158	1277.26	ISMLG	C I	1277.2	L	3.0	-0.00002	66.5	5.7
PG0003+158	1280.19	IGMABS	H I	949.7	H	104307.0	0.34787	229.5	5.9
PG0003+158	1281.26	IGMABS	H I	937.8	H	109795.0	0.36617	83.5	6.2
PG0003+158	1281.77	IGMABS	H I	1215.6	H	16300.0	0.05437	65.2	6.4
PG0003+158	1292.18	IGMABS	H I	1215.6	H	18868.0	0.06294	97.4	5.9
PG0003+158	1293.69	IGMABS	H I	923.1	H	120332.0	0.40135	54.4	7.0
PG0003+158	1296.65	IGMABS	H I	1215.6	H	19971.0	0.06662	58.3	16.0
PG0003+158	1297.00	IGMABS	H I	949.7	H	109615.0	0.36566	31.0	6.4
PG0003+158	1297.52	IGMABS	H I	949.7	H	109777.0	0.36617	146.2	15.5
PG0003+158	1297.98	IGMABS	H I	926.2	H	120326.0	0.40135	44.1	7.6
PG0003+158	1299.73	IGMABS	H I	937.8	H	115700.0	0.38603	70.3	16.3
PG0003+158	1300.50	ISMLG	O I	1302.1	L	-384.0	-0.00131	66.2	12.3
PG0003+158	1300.79	ISMLG	O I	1302.1	L	-316.0	-0.00108	81.5	11.6
PG0003+158	1301.44	IGMABS	H I	949.7	H	111014.0	0.37032	48.2	13.8
PG0003+158	1301.79	ISMLG	O I	1302.1	L	-86.0	-0.00031	35.4	5.8
PG0003+158	1302.12	ISMLG	O I	1302.1	L	-12.0	-0.00002	258.0	5.9
PG0003+158	1303.96	ISMLG	Si II	1304.3	L	-93.0	-0.00031	68.3	9.2
PG0003+158	1304.29	ISMLG	Si II	1304.3	L	-18.0	-0.00002	330.4	8.6
PG0003+158	1304.55	ISMLG	Si II	1304.3	L	42.0	0.00019	102.1	9.3
PG0003+158	1310.87	IGMABS	H I	972.5	H	104295.0	0.34787	238.6	8.8
PG0003+158	1313.29	IGMABS	H I	1215.6	H	24074.0	0.08030	23.6	8.5
PG0003+158	1314.21	IGMABS	H I	937.8	H	120327.0	0.40135	99.3	9.3
PG0003+158	1314.81	IGMABS	H I	1215.6	H	24447.0	0.08155	123.0	8.2
PG0003+158	1316.29	IGMABS	Si III	1206.5	H	27282.0	0.09096	111.3	5.6
PG0003+158	1316.36	IGMABS	H I	949.7	H	115726.0	0.38603	138.5	5.9
PG0003+158	1316.63	IGMABS	C III	977.0	H	104207.0	0.34761	135.0	5.0
PG0003+158	1316.91	IGMABS	C III	977.0	H	104294.0	0.34787	254.2	5.2
PG0003+158	1317.21	ISMLG	Ni II	1317.2	L	-2.0	-0.00002	49.4	5.2
PG0003+158	1323.34	IGMABS	H I	1025.7	H	86985.0	0.29016	175.1	8.5
PG0003+158	1326.03	IGMABS	H I	1215.6	H	27216.0	0.09078	380.0	4.1
PG0003+158	1326.25	IGMABS	H I	1215.6	H	27270.0	0.09096	336.5	3.0
PG0003+158	1326.61	IGMABS	H I	1215.6	H	27358.0	0.09126	173.8	5.3
PG0003+158	1327.62	IGMABS	H I	972.5	H	109456.0	0.36510	17.9	4.8
PG0003+158	1328.09	IGMABS	H I	972.5	H	109603.0	0.36566	65.6	6.1
PG0003+158	1328.68	IGMABS	H I	972.5	H	109784.0	0.36617	243.9	5.4
PG0003+158	1330.37	IGMABS	H I	1215.6	H	28286.0	0.09435	522.4	4.9
PG0003+158	1330.95	IGMABS	H I	949.7	H	120332.0	0.40135	160.0	4.4
PG0003+158	1331.29	IGMABS	O VI	1031.9	H	86971.0	0.29016	139.5	5.1
PG0003+158	1332.75	IGMABS	H I	972.5	H	111038.0	0.37032	79.5	4.0
PG0003+158	1332.76	ISMLG	C II	1334.5	L	-398.0	-0.00131	79.5	4.0
PG0003+158	1333.08	ISMLG	C II	1334.5	L	-325.0	-0.00108	140.1	4.1
PG0003+158	1333.45	ISMLG	C II	1334.5	L	-244.0	-0.00078	67.9	5.3
PG0003+158	1333.73	IGMABS	C III	977.0	H	109454.0	0.36510	174.9	4.3
PG0003+158	1334.08	IGMABS	N III	989.7	H	104278.0	0.34787	148.2	3.9
PG0003+158	1334.10	ISMLG	C II	1334.5	L	-98.0	-0.00031	148.2	3.9
PG0003+158	1334.46	ISMLG	C II	1334.5	L	-16.0	-0.00002	432.9	2.2
PG0003+158	1334.77	ISMLG	C II	1334.5	L	53.0	0.00019	227.8	3.7
PG0003+158	1335.67	ISMLG	C II*	1335.7	L	-9.0	-0.00002	150.2	6.3
PG0003+158	1338.69	IGMABS	O VI	1037.6	H	86986.0	0.29016	104.5	5.6
PG0003+158	1338.96	IGMABS	H I	1025.7	H	91553.0	0.30540	120.1	4.1
PG0003+158	1339.28	IGMABS	H I	1025.7	H	91645.0	0.30579	469.4	5.4
PG0003+158	1345.77	IGMABS	H I	1025.7	H	93542.0	0.31209	158.5	8.0
PG0003+158	1347.20	ISMLG	Cl I	1347.2	L	-9.0	-0.00002	35.5	4.6

Table A1 continued

Table A1 (*continued*)

Target	λ_{obs}	Type	Ion	λ_{rest}	Frame	cz	z	W_{λ}	$\sigma_{W_{\lambda}}$
	(Å)			(Å)		(km s ⁻¹)		(mÅ)	(mÅ)
PG0003+158	1347.43	IGMABS	O VI	1031.9	H	91660.0	0.30579	30.0	5.4
PG0003+158	1347.95	IGMABS	H I	972.5	H	115725.0	0.38603	158.1	5.2
PG0003+158	1348.24	IGMABS	H I	972.5	H	115814.0	0.38638	48.8	5.0
PG0003+158	1350.43	IGMABS	H I	949.7	H	126478.0	0.42185	98.1	7.3
PG0003+158	1351.23	IGMABS	N V	1238.8	H	27204.0	0.09078	23.2	5.7
PG0003+158	1351.61	IGMABS	N V	1238.8	H	27295.0	0.09096	18.0	5.2
PG0003+158	1351.89	IGMABS	N V	1238.8	H	27363.0	0.09126	21.8	5.1
PG0003+158	1352.27	IGMABS	N III	989.7	H	109784.0	0.36617	57.5	6.7
PG0003+158	1354.17	IGMABS	C III	977.0	H	115725.0	0.38603	91.6	6.2
PG0003+158	1354.83	IGMABS	O VI	1037.6	H	91651.0	0.30579	23.0	7.0
PG0003+158	1355.65	IGMABS	N V	1242.8	H	27220.0	0.09078	20.7	5.3
PG0003+158	1355.98	IGMABS	N V	1242.8	H	27301.0	0.09096	17.9	5.2
PG0003+158	1356.26	IGMABS	N V	1242.8	H	27369.0	0.09126	14.2	5.7
PG0003+158	1362.86	IGMABS	H I	972.5	H	120321.0	0.40135	235.7	7.0
PG0003+158	1366.52	IGMABS	H I	1215.6	H	37201.0	0.12409	112.5	7.7
PG0003+158	1369.17	IGMABS	C III	977.0	H	120328.0	0.40135	101.6	6.1
PG0003+158	1370.11	ISMLG	Ni II	1370.1	L	-4.0	-0.00002	30.4	5.9
PG0003+158	1378.22	IGMABS	H I	972.5	H	125055.0	0.41712	30.9	7.0
PG0003+158	1379.05	IGMABS	H I	1215.6	H	40290.0	0.13439	44.5	8.0
PG0003+158	1381.43	IGMABS	H I	972.5	H	126045.0	0.42045	72.4	7.3
PG0003+158	1382.17	IGMABS	H I	1025.7	H	104182.0	0.34761	71.4	6.3
PG0003+158	1382.60	IGMABS	H I	1025.7	H	104306.0	0.34787	304.8	3.6
PG0003+158	1382.93	IGMABS	H I	972.5	H	126506.0	0.42185	191.2	6.1
PG0003+158	1385.59	IGMABS	H I	1025.7	H	105182.0	0.35090	21.7	5.3
PG0003+158	1387.84	IGMABS	C III	977.0	H	126058.0	0.42045	38.0	7.0
PG0003+158	1389.20	IGMABS	C III	977.0	H	126476.0	0.42185	111.6	7.7
PG0003+158	1390.62	IGMABS	O VI	1031.9	H	104207.0	0.34761	193.8	6.1
PG0003+158	1390.91	IGMABS	O VI	1031.9	H	104290.0	0.34787	112.8	5.6
PG0003+158	1391.97	ISMLG	Si IV	1393.7	L	-385.0	-0.00131	44.7	6.5
PG0003+158	1392.26	ISMLG	Si IV	1393.7	L	-323.0	-0.00108	28.9	5.8
PG0003+158	1392.69	ISMLG	Si IV	1393.7	L	-231.0	-0.00078	19.1	5.2
PG0003+158	1393.38	ISMLG	Si IV	1393.7	L	-83.0	-0.00031	34.0	6.1
PG0003+158	1393.75	ISMLG	Si IV	1393.7	L	-2.0	-0.00002	137.5	5.7
PG0003+158	1394.02	ISMLG	Si IV	1393.7	L	56.0	0.00019	63.9	5.3
PG0003+158	1396.87	IGMABS	C II	1036.3	H	104297.0	0.34787	51.1	6.3
PG0003+158	1398.29	IGMABS	O VI	1037.6	H	104207.0	0.34761	116.8	6.1
PG0003+158	1398.57	IGMABS	O VI	1037.6	H	104289.0	0.34787	53.7	6.2
PG0003+158	1400.23	IGMABS	H I	1025.7	H	109461.0	0.36510	52.0	7.3
PG0003+158	1400.75	IGMABS	H I	1025.7	H	109612.0	0.36566	139.0	6.3
PG0003+158	1401.31	IGMABS	H I	1025.7	H	109774.0	0.36617	317.0	6.0
PG0003+158	1401.68	ISMLG	Si IV	1402.7	L	-233.0	-0.00078	33.9	5.7
PG0003+158	1402.37	ISMLG	Si IV	1402.7	L	-86.0	-0.00031	44.1	6.6
PG0003+158	1402.75	ISMLG	Si IV	1402.7	L	-6.0	-0.00002	72.0	5.7
PG0003+158	1403.02	ISMLG	Si IV	1402.7	L	53.0	0.00019	34.2	6.1
PG0003+158	1405.63	IGMABS	H I	1025.7	H	111036.0	0.37032	173.8	6.3
PG0003+158	1405.93	IGMABS	Si III	1206.5	H	49554.0	0.16514	37.0	5.5
PG0003+158	1408.11	IGMABS	O VI	1031.9	H	109288.0	0.36446	247.1	6.8
PG0003+158	1408.67	IGMABS	O VI	1031.9	H	109451.0	0.36510	243.1	5.2
PG0003+158	1409.35	IGMABS	O VI	1031.9	H	109647.0	0.36566	120.1	6.4
PG0003+158	1409.83	IGMABS	O VI	1031.9	H	109787.0	0.36617	134.5	7.7
PG0003+158	1410.65	IGMABS	H I	1215.6	H	48084.0	0.16039	15.3	6.0
PG0003+158	1411.61	IGMABS	H I	1215.6	H	48321.0	0.16118	13.1	6.2
PG0003+158	1414.17	IGMABS	O VI	1031.9	H	111048.0	0.37032	25.9	7.0

Table A1 continued

Table A1 (*continued*)

Target	λ_{obs}	Type	Ion	λ_{rest}	Frame	cz	z	W_{λ}	$\sigma_{W_{\lambda}}$
	(Å)			(Å)		(km s ⁻¹)		(mÅ)	(mÅ)
PG0003+158	1415.84	IGMABS	O VI	1037.6	H	109278.0	0.36446	104.4	5.5
PG0003+158	1416.43	IGMABS	H I	1215.6	H	49508.0	0.16514	768.5	5.1
PG0003+158	1417.09	IGMABS	O VI	1037.6	H	109640.0	0.36566	52.8	5.5
PG0003+158	1417.58	IGMABS	O VI	1037.6	H	109779.0	0.36617	70.4	6.8
PG0003+158	1421.70	IGMABS	H I	1025.7	H	115735.0	0.38603	284.8	4.9
PG0003+158	1422.02	IGMABS	H I	1025.7	H	115829.0	0.38638	104.8	5.9
PG0003+158	1426.31	IGMABS	H I	1215.6	H	51946.0	0.17327	35.9	6.6
PG0003+158	1429.79	IGMABS	H I	1215.6	H	52804.0	0.17613	349.3	7.9
PG0003+158	1430.32	IGMABS	O VI	1031.9	H	115742.0	0.38603	87.8	6.4
PG0003+158	1430.58	IGMABS	O VI	1031.9	H	115817.0	0.38638	72.2	6.7
PG0003+158	1437.38	IGMABS	H I	1025.7	H	120316.0	0.40135	400.6	8.1
PG0003+158	1438.21	IGMABS	O VI	1037.6	H	115741.0	0.38603	55.4	6.5
PG0003+158	1438.60	IGMABS	O VI	1037.6	H	115855.0	0.38638	56.1	7.6
PG0003+158	1446.05	IGMABS	O VI	1031.9	H	120309.0	0.40135	228.8	11.9
PG0003+158	1446.77	IGMABS	H I	1215.6	H	56990.0	0.19010	370.1	10.6
PG0003+158	1449.91	IGMABS	H I	1215.6	H	57765.0	0.19268	214.5	13.2
PG0003+158	1452.20	IGMABS	H I	1215.6	H	58331.0	0.19457	84.7	8.3
PG0003+158	1453.60	IGMABS	H I	1025.7	H	125057.0	0.41712	43.3	17.4
PG0003+158	1454.00	IGMABS	O VI	1037.6	H	120303.0	0.40135	117.2	16.6
PG0003+158	1454.81	ISMLG	Ni II	1454.8	L	-6.0	-0.00002	17.0	5.4
PG0003+158	1457.10	IGMABS	H I	1025.7	H	126080.0	0.42045	72.0	17.7
PG0003+158	1458.40	IGMABS	H I	1025.7	H	126462.0	0.42185	295.4	17.0
PG0003+158	1467.26	IGMABS	O VI	1031.9	H	126472.0	0.42185	183.0	7.3
PG0003+158	1468.55	IGMABS	Si II	1260.4	H	49504.0	0.16514	48.8	7.4
PG0003+158	1469.81	IGMABS	H I	1215.6	H	62671.0	0.20905	108.8	7.2
PG0003+158	1470.26	IGMABS	H I	1215.6	H	62784.0	0.20942	45.0	7.4
PG0003+158	1475.35	IGMABS	O VI	1037.6	H	126471.0	0.42185	116.1	7.6
PG0003+158	1489.66	IGMABS	H I	1215.6	H	67567.0	0.22538	39.1	7.5
PG0003+158	1500.86	IGMABS	H I	1215.6	H	70330.0	0.23459	47.0	5.8
PG0003+158	1506.15	IGMABS	H I	1215.6	H	71634.0	0.23894	26.2	4.6
PG0003+158	1506.99	IGMABS	H I	1215.6	H	71842.0	0.23964	184.1	6.6
PG0003+158	1522.86	IGMABS	H I	1215.6	H	75755.0	0.25269	55.9	8.0
PG0003+158	1524.71	ISMLG	Si II	1526.7	L	-393.0	-0.00131	25.7	7.1
PG0003+158	1525.05	ISMLG	Si II	1526.7	L	-326.0	-0.00108	46.6	7.5
PG0003+158	1526.23	ISMLG	Si II	1526.7	L	-93.0	-0.00031	83.0	5.4
PG0003+158	1526.61	ISMLG	Si II	1526.7	L	-18.0	-0.00002	387.2	3.6
PG0003+158	1526.99	ISMLG	Si II	1526.7	L	56.0	0.00019	69.2	5.8
PG0003+158	1546.09	ISMLG	C IV	1548.2	L	-409.0	-0.00131	144.5	8.0
PG0003+158	1546.52	ISMLG	C IV	1548.2	L	-326.0	-0.00108	120.7	6.9
PG0003+158	1547.01	ISMLG	C IV	1548.2	L	-232.0	-0.00078	72.5	7.2
PG0003+158	1548.19	ISMLG	C IV	1548.2	L	-4.0	-0.00002	176.6	6.6
PG0003+158	1548.51	ISMLG	C IV	1548.2	L	59.0	0.00019	126.2	6.0
PG0003+158	1548.76	ISMLG	C IV	1550.7	L	-390.0	-0.00131	58.7	6.1
PG0003+158	1549.05	ISMLG	C IV	1550.7	L	-335.0	-0.00108	69.2	6.7
PG0003+158	1549.60	ISMLG	C IV	1550.7	L	-229.0	-0.00078	34.1	6.4
PG0003+158	1550.81	ISMLG	C IV	1550.7	L	5.0	-0.00002	84.3	7.2
PG0003+158	1551.06	ISMLG	C IV	1550.7	L	55.0	0.00019	49.9	6.9
PG0003+158	1554.91	IGMABS	C II	1334.5	H	49506.0	0.16514	81.4	9.0
PG0003+158	1555.61	IGMABS	H I	1215.6	H	83831.0	0.27963	66.9	9.2
PG0003+158	1560.30	ISMLG	C I	1560.3	L	-2.0	-0.00002	82.4	7.2
PG0003+158	1568.41	IGMABS	H I	1215.6	H	86988.0	0.29016	394.8	8.4
PG0003+158	1580.49	IGMABS	H I	1215.6	H	89968.0	0.30010	65.5	11.0
PG0003+158	1586.94	IGMABS	H I	1215.6	H	91557.0	0.30540	372.9	10.1

Table A1 continued

Table A1 (*continued*)

Target	λ_{obs}	Type	Ion	λ_{rest}	Frame	cz	z	W_{λ}	$\sigma_{W_{\lambda}}$
	(Å)			(Å)		(km s ⁻¹)		(mÅ)	(mÅ)
PG0003+158	1587.42	IGMABS	H I	1215.6	H	91675.0	0.30579	712.6	10.5
PG0003+158	1591.89	IGMABS	H I	1215.6	H	92779.0	0.30948	68.7	15.5
PG0003+158	1595.07	IGMABS	H I	1215.6	H	93562.0	0.31209	473.4	15.0
PG0003+158	1608.42	ISMLG	Fe II	1608.4	L	-6.0	-0.00002	312.5	14.9
PG0003+158	1626.30	IGMABS	Si III	1206.5	H	104312.0	0.34787	100.3	10.7
PG0003+158	1628.65	IGMABS	H I	1215.6	H	101844.0	0.33971	53.9	11.3
PG0003+158	1632.32	IGMABS	C IV	1548.2	H	16288.0	0.05437	26.1	9.7
PG0003+158	1636.23	IGMABS	H I	1215.6	H	103712.0	0.34595	63.2	11.7
PG0003+158	1637.27	IGMABS	H I	1215.6	H	103969.0	0.34680	132.8	12.7
PG0003+158	1638.25	IGMABS	H I	1215.6	H	104211.0	0.34761	345.6	9.4
PG0003+158	1638.56	IGMABS	H I	1215.6	H	104288.0	0.34787	537.4	9.3
PG0003+158	1642.25	IGMABS	H I	1215.6	H	105197.0	0.35090	161.5	13.5
PG0003+158	1648.30	IGMABS	Si III	1206.5	H	109780.0	0.36617	116.3	14.2
PG0003+158	1649.95	IGMABS	H I	1215.6	H	107097.0	0.35724	150.3	14.3
PG0003+158	1650.78	IGMABS	H I	1215.6	H	107302.0	0.35792	149.8	15.0
PG0003+158	1656.85	ISMLG	C I	1656.9	L	-14.0	-0.00002	81.9	9.5
PG0003+158	1658.73	IGMABS	H I	1215.6	H	109262.0	0.36446	67.9	13.5
PG0003+158	1659.51	IGMABS	H I	1215.6	H	109453.0	0.36510	223.1	9.6
PG0003+158	1660.19	IGMABS	H I	1215.6	H	109621.0	0.36566	488.8	7.8
PG0003+158	1660.81	IGMABS	H I	1215.6	H	109776.0	0.36617	537.8	8.1
PG0003+158	1664.35	IGMABS	H I	1215.6	H	110647.0	0.36908	32.1	9.2
PG0003+158	1665.85	IGMABS	H I	1215.6	H	111018.0	0.37032	378.9	14.3
PG0003+158	1668.97	ISMLG	Al II	1670.7	L	-327.0	-0.00108	51.1	11.2
PG0003+158	1670.29	ISMLG	Al II	1670.7	L	-90.0	-0.00031	93.8	8.9
PG0003+158	1670.69	ISMLG	Al II	1670.7	L	-18.0	-0.00002	400.2	8.5
PG0003+158	1671.11	ISMLG	Al II	1670.7	L	57.0	0.00019	42.3	11.0
PG0003+158	1675.59	IGMABS	H I	1215.6	H	113420.0	0.37833	78.6	14.1
PG0003+158	1684.95	IGMABS	H I	1215.6	H	115729.0	0.38603	726.2	10.3
PG0003+158	1685.38	IGMABS	H I	1215.6	H	115832.0	0.38638	322.8	10.2
PG0003+158	1689.06	IGMABS	C IV	1548.2	H	27275.0	0.09096	176.6	12.1
PG0003+158	1689.44	IGMABS	C IV	1548.2	H	27350.0	0.09126	93.7	10.9
PG0003+158	1690.34	IGMABS	N V	1238.8	H	109267.0	0.36446	112.4	14.2
PG0003+158	1691.08	IGMABS	N V	1238.8	H	109445.0	0.36510	181.8	11.8
PG0003+158	1691.87	IGMABS	C IV	1550.7	H	27276.0	0.09096	111.9	11.9
PG0003+158	1692.30	IGMABS	C IV	1550.7	H	27357.0	0.09126	99.9	12.1
PG0003+158	1694.72	IGMABS	H I	1215.6	H	118137.0	0.39406	138.0	15.4
PG0003+158	1695.70	IGMABS	N V	1242.8	H	109248.0	0.36446	117.5	14.2
PG0003+158	1696.51	IGMABS	N V	1242.8	H	109444.0	0.36510	119.0	12.9
PG0003+158	1698.88	IGMABS	Si II	1260.4	H	104288.0	0.34787	71.7	13.2
PG0003+158	1703.58	IGMABS	H I	1215.6	H	120323.0	0.40135	718.5	11.1
PG0003+158	1709.56	ISMLG	Ni II	1709.6	L	-7.0	-0.00002	32.0	11.7
PG0003+158	1710.45	IGMABS	H I	1215.6	H	122017.0	0.40701	58.0	15.4
PG0003+158	1713.63	IGMABS	Si III	1206.5	H	126012.0	0.42045	113.6	13.1
PG0003+158	1715.51	IGMABS	Si III	1206.5	H	126478.0	0.42185	58.0	14.3
PG0003+158	1717.03	IGMABS	N V	1238.8	H	115727.0	0.38603	53.4	13.2
PG0003+158	1722.37	IGMABS	H I	1215.6	H	124955.0	0.41681	61.0	8.8
PG0003+158	1722.75	IGMABS	H I	1215.6	H	125049.0	0.41712	248.8	10.7
PG0003+158	1726.80	IGMABS	H I	1215.6	H	126048.0	0.42045	107.3	17.0
PG0003+158	1728.50	IGMABS	H I	1215.6	H	126467.0	0.42185	712.8	14.1
PG0003+158	1741.54	ISMLG	Ni II	1741.5	L	-2.0	-0.00002	53.1	8.0
PG0003+158	1751.87	ISMLG	Ni II	1751.9	L	-7.0	-0.00002	44.9	7.3
PG0003+158	1754.21	PROXIMATE	H I	1215.6	H	132808.0	0.44300	57.9	8.4
PG0003+158	1758.24	PROXIMATE	H I	1215.6	H	133802.0	0.44632	57.6	5.9

Table A1 continued

Table A1 (*continued*)

Target	λ_{obs}	Type	Ion	λ_{rest}	Frame	cz	z	W_{λ}	$\sigma_{W_{\lambda}}$
	(Å)			(Å)		(km s ⁻¹)		(mÅ)	(mÅ)
PG0003+158	1758.83	PROXIMATE	H I	1215.6	H	133947.0	0.44680	71.6	6.3
PG0003+158	2260.81	ISMLG	Fe II	2260.7	L	4.0	-0.00002	135.7	0.0
PG0003+158	2344.35	ISMLG	Fe II	2344.2	L	17.0	-0.00002	692.0	0.0
PG0003+158	2374.38	ISMLG	Fe II	2374.4	L	-10.0	-0.00002	410.4	0.0
PG0003+158	2382.77	ISMLG	Fe II	2382.7	L	1.0	-0.00002	803.7	0.0
PG0003+158	2586.79	ISMLG	Fe II	2586.6	L	17.0	-0.00002	438.7	0.0
PG0003+158	2600.14	ISMLG	Fe II	2600.1	L	-4.0	-0.00002	574.1	0.0
PG0003+158	2796.21	ISMLG	Mg II	2796.3	L	-16.0	-0.00002	1141.0	0.0
PG0003+158	2803.56	ISMLG	H I	2803.5	L	3.0	-0.00002	848.2	0.0
PG0026+129	1020.68	ISMLG	Si II	1020.6	L	-6.0	-0.00003	147.1	46.9
PG0026+129	1031.91	ISMLG	O VI	1031.9	L	-4.0	-0.00003	118.6	65.5
PG0026+129	1036.29	ISMLG	C II	1036.3	L	-14.0	-0.00003	476.9	68.9
PG0026+129	1037.00	ISMLG	C II*	1037.0	L	-6.0	-0.00003	431.9	59.4
PG0026+129	1048.19	ISMLG	Ar I	1048.2	L	-8.0	-0.00003	60.2	33.2
PG0026+129	1059.88	IGMABS	H I	1025.7	H	9984.0	0.03331	286.5	56.0
PG0026+129	1083.95	ISMLG	N II	1083.9	L	-13.0	-0.00003	531.7	292.3
PG0026+129	1142.31	ISMLG	Fe II	1142.3	L	-13.0	-0.00003	46.6	13.7
PG0026+129	1143.20	ISMLG	Fe II	1143.2	L	-7.0	-0.00003	116.1	16.9
PG0026+129	1144.91	ISMLG	Fe II	1144.9	L	-7.0	-0.00003	142.4	15.2
PG0026+129	1151.61	OTHER	FPN	0.0	H	0.0	-1.00000	39.1	14.9
PG0026+129	1152.79	ISMLG	P II	1152.8	L	-8.0	-0.00003	76.7	14.2
PG0026+129	1188.78	ISMLG	C I	1188.8	L	-15.0	-0.00003	28.4	6.2
PG0026+129	1190.35	ISMLG	Si II	1190.4	L	-17.0	-0.00003	345.6	9.1
PG0026+129	1193.23	ISMLG	Si II	1193.2	L	-16.0	-0.00003	378.1	9.4
PG0026+129	1197.18	ISMLG	Mn II	1197.1	L	-1.0	-0.00003	28.4	5.7
PG0026+129	1199.52	ISMLG	N I	1199.5	L	-9.0	-0.00003	215.8	12.3
PG0026+129	1200.21	ISMLG	N I	1200.2	L	-4.0	-0.00003	176.9	11.4
PG0026+129	1200.70	ISMLG	N I	1200.7	L	-3.0	-0.00003	180.0	15.1
PG0026+129	1201.09	ISMLG	Mn II	1201.1	L	-8.0	-0.00003	19.5	9.2
PG0026+129	1205.37	ISMLG	Si III	1206.5	L	-280.0	-0.00095	89.6	7.6
PG0026+129	1205.54	ISMLG	Si III	1206.5	L	-238.0	-0.00081	69.7	6.4
PG0026+129	1205.76	ISMLG	Si III	1206.5	L	-184.0	-0.00062	42.4	7.2
PG0026+129	1206.47	ISMLG	Si III	1206.5	L	-8.0	-0.00003	540.3	9.7
PG0026+129	1239.90	ISMLG	Mg II	1239.9	L	-6.0	-0.00003	22.5	8.3
PG0026+129	1240.33	ISMLG	Mg II	1240.3	L	-17.0	-0.00003	16.7	8.6
PG0026+129	1250.55	ISMLG	S II	1250.5	L	-8.0	-0.00003	86.7	8.2
PG0026+129	1253.74	ISMLG	S II	1253.8	L	-15.0	-0.00003	195.4	9.4
PG0026+129	1256.17	IGMABS	H I	1215.6	H	9988.0	0.03331	564.3	10.4
PG0026+129	1259.48	ISMLG	S II	1259.5	L	-9.0	-0.00003	146.2	7.8
PG0026+129	1260.35	ISMLG	Si II	1260.4	L	-17.0	-0.00003	470.3	9.0
PG0026+129	1260.70	ISMLG	C I	1260.7	L	-8.0	-0.00003	38.9	6.7
PG0026+129	1263.19	IGMABS	H I	1215.6	H	11719.0	0.03909	442.0	9.5
PG0026+129	1277.23	ISMLG	C I	1277.2	L	-4.0	-0.00003	50.2	13.7
PG0026+129	1284.34	IGMABS	H I	1215.6	H	16935.0	0.05649	128.0	18.6
PG0026+129	1291.36	IGMABS	H I	1215.6	H	18665.0	0.06226	60.3	14.1
PG0026+129	1302.12	ISMLG	O I	1302.1	L	-12.0	-0.00003	391.9	14.1
PG0026+129	1304.32	ISMLG	Si II	1304.3	L	-11.0	-0.00003	271.1	13.4
PG0026+129	1313.81	IGMABS	H I	1215.6	H	24202.0	0.08073	143.1	9.4
PG0026+129	1328.80	ISMLG	C I	1328.8	L	-7.0	-0.00003	30.2	8.5
PG0026+129	1332.92	IGMABS	H I	1215.6	H	28914.0	0.09645	105.1	9.6
PG0026+129	1333.22	ISMLG	C II	1334.5	L	-294.0	-0.00095	56.2	8.4
PG0026+129	1333.44	ISMLG	C II	1334.5	L	-246.0	-0.00081	49.1	7.6
PG0026+129	1333.69	ISMLG	C II	1334.5	L	-189.0	-0.00062	28.5	9.5

Table A1 continued

Table A1 (*continued*)

Target	λ_{obs}	Type	Ion	λ_{rest}	Frame	cz	z	W_{λ}	$\sigma_{W_{\lambda}}$
	(Å)			(Å)		(km s ⁻¹)		(mÅ)	(mÅ)
PG0026+129	1334.46	ISMLG	C II	1334.5	L	-16.0	-0.00003	520.6	9.0
PG0026+129	1335.65	ISMLG	C II*	1335.7	L	-13.0	-0.00003	132.3	11.8
PG0026+129	1341.45	IGMABS	H I	1215.6	H	31019.0	0.10347	67.6	10.5
PG0026+129	1343.66	IGMABS	H I	1215.6	H	31564.0	0.10529	80.1	9.4
PG0026+129	1345.73	IGMABS	H I	1215.6	H	32073.0	0.10698	73.2	10.1
PG0026+129	1347.20	ISMLG	Cl I	1347.2	L	-10.0	-0.00003	63.0	9.7
PG0026+129	1360.57	IGMABS	H I	1215.6	H	35733.0	0.11919	100.0	8.3
PG0026+129	1370.11	ISMLG	Ni II	1370.1	L	-4.0	-0.00003	28.7	8.2
PG0026+129	1373.27	IGMABS	H I	1215.6	H	38866.0	0.12964	47.9	6.6
PG0026+129	1392.42	ISMLG	Si IV	1393.7	L	-289.0	-0.00095	28.7	3.3
PG0026+129	1392.93	ISMLG	Si IV	1393.7	L	-179.0	-0.00062	23.4	3.4
PG0026+129	1393.69	ISMLG	Si IV	1393.7	L	-15.0	-0.00003	167.4	5.5
PG0026+129	1401.43	ISMLG	Si IV	1402.7	L	-287.0	-0.00095	29.4	6.8
PG0026+129	1402.72	ISMLG	Si IV	1402.7	L	-12.0	-0.00003	117.1	9.8
PG0026+129	2796.20	ISMLG	Mg II	2796.3	L	-17.0	-0.00003	1124.2	1.3
PG0026+129	2803.37	PROXIMATE	H I	2803.5	L	-17.0	-0.00003	1026.0	2.3
PG0044+030	1173.37	IGMABS	N IV	765.1	H	159947.0	0.53353	183.7	22.8
PG0044+030	1190.16	ISMLG	Si II	1190.4	L	-66.0	-0.00019	161.3	17.3
PG0044+030	1190.43	ISMLG	Si II	1190.4	L	4.0	0.00000	205.3	12.7
PG0044+030	1192.12	ISMLG	Si II	1193.2	L	-295.0	-0.00097	90.8	21.0
PG0044+030	1193.02	ISMLG	Si II	1193.2	L	-67.0	-0.00019	170.1	17.6
PG0044+030	1193.30	ISMLG	Si II	1193.2	L	2.0	0.00000	220.4	12.4
PG0044+030	1199.30	ISMLG	N I	1199.5	L	-63.0	-0.00019	112.9	17.2
PG0044+030	1199.54	ISMLG	N I	1199.5	L	-2.0	0.00000	178.3	13.1
PG0044+030	1199.97	ISMLG	N I	1200.2	L	-63.0	-0.00019	123.6	16.0
PG0044+030	1200.24	ISMLG	N I	1200.2	L	5.0	0.00000	154.9	13.3
PG0044+030	1200.45	ISMLG	N I	1200.7	L	-65.0	-0.00019	110.5	15.4
PG0044+030	1200.73	ISMLG	N I	1200.7	L	4.0	0.00000	142.1	15.5
PG0044+030	1204.99	IGMABS	H I	1025.7	H	52394.0	0.17474	125.0	20.4
PG0044+030	1205.33	ISMLG	Si III	1206.5	L	-291.0	-0.00097	191.6	16.9
PG0044+030	1205.64	ISMLG	Si III	1206.5	L	-214.0	-0.00071	86.2	13.8
PG0044+030	1205.92	ISMLG	Si III	1206.5	L	-144.0	-0.00045	49.5	16.6
PG0044+030	1206.21	ISMLG	Si III	1206.5	L	-72.0	-0.00019	261.4	13.1
PG0044+030	1206.50	ISMLG	Si III	1206.5	L	0.0	0.00000	257.4	9.6
PG0044+030	1206.76	ISMLG	Si III	1206.5	L	63.0	0.00022	140.8	16.3
PG0044+030	1207.99	IGMABS	O IV	787.7	H	159952.0	0.53353	235.3	13.7
PG0044+030	1208.21	IGMABS	O IV	787.7	H	160035.0	0.53381	114.9	13.0
PG0044+030	1221.39	IGMABS	H I	1215.6	H	1411.0	0.00471	213.1	37.3
PG0044+030	1222.86	IGMABS	H I	930.7	H	94089.0	0.31384	158.0	22.1
PG0044+030	1223.28	IGMABS	H I	930.7	H	94223.0	0.31426	161.3	25.2
PG0044+030	1232.14	IGMABS	H I	937.8	H	94091.0	0.31384	202.4	16.4
PG0044+030	1232.55	IGMABS	H I	937.8	H	94223.0	0.31426	213.4	19.4
PG0044+030	1232.71	IGMABS	H I	937.8	H	94275.0	0.31447	32.2	9.7
PG0044+030	1234.35	IGMABS	H I	1215.6	H	4608.0	0.01537	184.8	26.9
PG0044+030	1237.76	IGMABS	H I	1215.6	H	5448.0	0.01817	397.7	20.6
PG0044+030	1247.82	IGMABS	H I	949.7	H	94089.0	0.31384	182.4	15.7
PG0044+030	1248.25	IGMABS	H I	949.7	H	94224.0	0.31426	266.6	13.7
PG0044+030	1248.40	IGMABS	H I	949.7	H	94272.0	0.31447	61.9	8.4
PG0044+030	1248.72	IGMABS	O IV	787.7	H	175455.0	0.58523	273.7	18.7
PG0044+030	1250.57	ISMLG	S II	1250.5	L	-1.0	0.00000	54.1	23.8
PG0044+030	1253.79	ISMLG	S II	1253.8	L	-4.0	0.00000	80.2	26.6
PG0044+030	1259.22	ISMLG	Si II	1260.4	L	-286.0	-0.00097	131.0	12.2
PG0044+030	1259.51	ISMLG	S II	1259.5	L	-3.0	0.00000	156.1	12.0

Table A1 continued

Table A1 (*continued*)

Target	λ_{obs}	Type	Ion	λ_{rest}	Frame	cz	z	W_{λ}	$\sigma_{W_{\lambda}}$
	(Å)			(Å)		(km s ⁻¹)		(mÅ)	(mÅ)
PG0044+030	1260.13	ISMLG	Si II	1260.4	L	-69.0	-0.00019	242.2	10.4
PG0044+030	1260.42	ISMLG	Si II	1260.4	L	0.0	0.00000	223.6	6.8
PG0044+030	1265.57	IGMABS	H I	1215.6	H	12306.0	0.04105	170.9	25.5
PG0044+030	1277.31	IGMABS	O III	832.9	H	159943.0	0.53353	250.6	12.8
PG0044+030	1277.74	IGMABS	H I	972.5	H	94083.0	0.31384	246.2	11.2
PG0044+030	1278.18	IGMABS	H I	972.5	H	94216.0	0.31426	389.5	19.8
PG0044+030	1278.40	IGMABS	H I	972.5	H	94284.0	0.31447	112.4	10.0
PG0044+030	1279.69	IGMABS	H I	1215.6	H	15787.0	0.05266	46.2	16.1
PG0044+030	1283.64	IGMABS	C III	977.0	H	94084.0	0.31384	140.3	14.4
PG0044+030	1284.05	IGMABS	C III	977.0	H	94209.0	0.31426	117.1	10.8
PG0044+030	1284.27	IGMABS	C III	977.0	H	94278.0	0.31447	117.9	11.1
PG0044+030	1286.48	IGMABS	O III	832.9	H	163247.0	0.54456	103.0	17.9
PG0044+030	1300.88	ISMLG	O I	1302.1	L	-296.0	-0.00097	45.4	13.7
PG0044+030	1301.84	ISMLG	O I	1302.1	L	-75.0	-0.00019	225.8	12.7
PG0044+030	1302.17	ISMLG	O I	1302.1	L	1.0	0.00000	214.8	10.6
PG0044+030	1303.68	IGMABS	H I	1215.6	H	21703.0	0.07239	160.8	19.5
PG0044+030	1304.08	ISMLG	Si II	1304.3	L	-67.0	-0.00019	215.1	12.0
PG0044+030	1304.39	ISMLG	Si II	1304.3	L	4.0	0.00000	172.1	12.1
PG0044+030	1333.20	ISMLG	C II	1334.5	L	-298.0	-0.00097	142.1	17.6
PG0044+030	1333.54	ISMLG	C II	1334.5	L	-222.0	-0.00071	133.7	15.9
PG0044+030	1333.93	IGMABS	H I	920.9	H	134430.0	0.44840	52.0	15.1
PG0044+030	1334.22	ISMLG	C II	1334.5	L	-69.0	-0.00019	278.1	11.2
PG0044+030	1334.54	ISMLG	C II	1334.5	L	2.0	0.00000	262.8	9.8
PG0044+030	1334.78	ISMLG	C II	1334.5	L	55.0	0.00022	36.4	13.5
PG0044+030	1335.69	ISMLG	C II*	1335.7	L	-5.0	0.00000	139.2	21.1
PG0044+030	1337.08	IGMABS	H I	923.1	H	134424.0	0.44840	85.6	15.6
PG0044+030	1341.55	IGMABS	H I	926.2	H	134429.0	0.44840	110.1	17.3
PG0044+030	1346.71	IGMABS	H I	1215.6	H	32315.0	0.10779	101.8	22.3
PG0044+030	1347.63	IGMABS	H I	1025.7	H	94086.0	0.31384	336.2	16.3
PG0044+030	1348.06	IGMABS	H I	1025.7	H	94211.0	0.31426	115.2	13.7
PG0044+030	1348.10	IGMABS	H I	930.7	H	134428.0	0.44840	165.6	13.3
PG0044+030	1348.28	IGMABS	H I	1025.7	H	94276.0	0.31447	363.2	10.8
PG0044+030	1355.94	IGMABS	H I	1215.6	H	34591.0	0.11538	60.5	15.8
PG0044+030	1358.31	IGMABS	H I	937.8	H	134426.0	0.44840	213.1	21.9
PG0044+030	1375.60	IGMABS	H I	949.7	H	134424.0	0.44840	248.2	15.1
PG0044+030	1386.25	IGMABS	H I	1215.6	H	42066.0	0.14032	74.4	24.8
PG0044+030	1393.44	ISMLG	Si IV	1393.7	L	-68.0	-0.00019	68.0	19.4
PG0044+030	1393.78	ISMLG	Si IV	1393.7	L	4.0	0.00000	96.2	20.8
PG0044+030	1402.76	ISMLG	Si IV	1402.7	L	-3.0	0.00000	41.6	18.7
PG0044+030	1408.60	IGMABS	H I	972.5	H	134421.0	0.44840	395.2	24.5
PG0044+030	1408.90	IGMABS	H I	1025.7	H	111993.0	0.37355	138.3	17.6
PG0044+030	1409.87	IGMABS	H I	919.3	H	159955.0	0.53353	73.8	23.1
PG0044+030	1412.35	IGMABS	H I	920.9	H	159958.0	0.53353	74.5	20.7
PG0044+030	1415.10	IGMABS	C III	977.0	H	134422.0	0.44840	363.5	14.1
PG0044+030	1415.66	IGMABS	H I	923.1	H	159942.0	0.53353	104.9	18.9
PG0044+030	1417.04	IGMABS	H I	1215.6	H	49659.0	0.16565	160.2	23.7
PG0044+030	1420.07	IGMABS	H I	1215.6	H	50406.0	0.16814	299.1	25.4
PG0044+030	1420.42	IGMABS	H I	926.2	H	159957.0	0.53353	118.9	16.1
PG0044+030	1422.57	IGMABS	H I	1215.6	H	51024.0	0.17020	145.3	21.1
PG0044+030	1422.92	IGMABS	H I	1215.6	H	51110.0	0.17049	86.5	19.0
PG0044+030	1424.85	IGMABS	H I	1215.6	H	51585.0	0.17207	78.1	25.2
PG0044+030	1425.87	IGMABS	H I	923.1	H	163259.0	0.54456	66.4	21.7
PG0044+030	1427.35	IGMABS	H I	930.7	H	159955.0	0.53353	235.3	19.6

Table A1 *continued*

Table A1 (*continued*)

Target	λ_{obs}	Type	Ion	λ_{rest}	Frame	cz	z	W_{λ}	$\sigma_{W_{\lambda}}$
	(Å)			(Å)		(km s ⁻¹)		(mÅ)	(mÅ)
PG0044+030	1428.09	IGMABS	H I	1215.6	H	52385.0	0.17474	476.1	19.2
PG0044+030	1428.68	IGMABS	H I	1215.6	H	52531.0	0.17522	155.2	23.7
PG0044+030	1429.48	IGMABS	H I	1215.6	H	52728.0	0.17588	170.6	22.6
PG0044+030	1430.60	IGMABS	H I	926.2	H	163251.0	0.54456	94.0	19.3
PG0044+030	1431.67	IGMABS	H I	1215.6	H	53267.0	0.17768	65.5	21.9
PG0044+030	1437.58	IGMABS	H I	930.7	H	163250.0	0.54456	167.8	19.4
PG0044+030	1438.17	IGMABS	H I	937.8	H	159955.0	0.53353	294.2	22.9
PG0044+030	1446.57	IGMABS	H I	1215.6	H	56941.0	0.18993	191.6	24.1
PG0044+030	1448.48	IGMABS	H I	937.8	H	163249.0	0.54456	288.1	23.5
PG0044+030	1451.77	IGMABS	H I	1215.6	H	58224.0	0.19421	117.9	22.4
PG0044+030	1456.48	IGMABS	H I	949.7	H	159955.0	0.53353	427.9	18.6
PG0044+030	1456.73	IGMABS	H I	949.7	H	160034.0	0.53381	161.6	15.8
PG0044+030	1465.06	IGMABS	H I	1215.6	H	61502.0	0.20515	155.5	35.3
PG0044+030	1669.79	IGMABS	H I	1215.6	H	111988.0	0.37355	1081.5	164.2
PG0044+030	1760.78	IGMABS	H I	1215.6	H	134428.0	0.44840	849.4	144.2
PG0044+030	1785.14	IGMABS	H I	1215.6	H	140436.0	0.46844	1181.6	113.1
PG0044+030	1813.49	IGMABS	H I	1215.6	H	147425.0	0.49176	975.5	115.7
PG0044+030	1864.26	IGMABS	H I	1215.6	H	159947.0	0.53353	576.1	56.7
PG0044+030	1864.61	IGMABS	H I	1215.6	H	160033.0	0.53381	491.2	0.1
PG0044+030	1877.68	IGMABS	H I	1215.6	H	163255.0	0.54456	1133.5	83.0
PG0044+030	1890.04	IGMABS	H I	1215.6	H	166305.0	0.55473	449.1	104.3
PG0044+030	1927.12	IGMABS	H I	1215.6	H	175448.0	0.58523	867.8	64.8
PG0044+030	1930.47	IGMABS	H I	1215.6	H	176274.0	0.58799	533.9	77.2
PG0044+030	2242.41	IGMABS	C IV	1548.2	H	134426.0	0.44840	259.9	0.0
PG0044+030	2246.14	IGMABS	C IV	1550.7	H	134424.0	0.44840	188.0	0.0
PG0044+030	2374.48	ISMLG	Fe II	2374.4	L	2.0	0.00000	356.2	103.8
PG0044+030	2382.77	ISMLG	Fe II	2382.7	L	1.0	0.00000	478.3	103.3
PG0044+030	2586.64	ISMLG	Fe II	2586.6	L	-1.0	0.00000	466.3	89.5
PG0044+030	2600.21	ISMLG	Fe II	2600.1	L	4.0	0.00000	569.7	79.9
PG0044+030	2796.35	ISMLG	Mg II	2796.3	L	0.0	0.00000	414.9	98.0
PG0044+030	2803.47	PROXIMATE	H I	2803.5	L	-7.0	0.00000	857.4	103.3
PG0052+251	1020.68	ISMLG	Si II	1020.6	L	-7.0	-0.00003	219.7	26.3
PG0052+251	1031.90	ISMLG	O VI	1031.9	L	-8.0	-0.00003	84.7	22.1
PG0052+251	1035.94	ISMLG	C II	1036.3	L	-116.0	-0.00037	220.8	19.4
PG0052+251	1036.31	ISMLG	C II	1036.3	L	-8.0	-0.00003	532.8	19.4
PG0052+251	1037.00	ISMLG	C II*	1037.0	L	-6.0	-0.00003	261.4	23.5
PG0052+251	1039.21	ISMLG	O I	1039.2	L	-7.0	-0.00003	302.9	40.4
PG0052+251	1048.17	ISMLG	Ar I	1048.2	L	-14.0	-0.00003	167.8	21.7
PG0052+251	1066.61	ISMLG	Ar I	1066.6	L	-15.0	-0.00003	141.7	27.9
PG0052+251	1097.98	INTRINSIC	H I	949.7	H	46791.0	0.15609	125.5	29.8
PG0052+251	1122.49	ISMLG	Fe III	1122.5	L	-9.0	-0.00003	132.8	37.1
PG0052+251	1124.35	INTRINSIC	H I	972.5	H	46797.0	0.15609	177.8	26.2
PG0052+251	1134.12	ISMLG	N I	1134.1	L	-11.0	-0.00003	272.2	26.9
PG0052+251	1134.37	ISMLG	N I	1134.4	L	-11.0	-0.00003	280.9	28.0
PG0052+251	1134.94	ISMLG	N I	1134.9	L	-10.0	-0.00003	288.3	35.6
PG0052+251	1139.04	IGMABS	H I	1025.7	H	33119.0	0.11052	198.1	23.4
PG0052+251	1143.18	ISMLG	Fe II	1143.2	L	-11.0	-0.00003	112.3	13.7
PG0052+251	1144.89	ISMLG	Fe II	1144.9	L	-13.0	-0.00003	236.3	10.3
PG0052+251	1145.97	IGMABS	O VI	1031.9	H	33133.0	0.11052	56.2	13.9
PG0052+251	1149.77	IGMABS	H I	1025.7	H	36255.0	0.12092	74.0	13.7
PG0052+251	1152.82	ISMLG	P II	1152.8	L	2.0	-0.00003	95.2	11.5
PG0052+251	1157.06	IGMABS	H I	1025.7	H	38386.0	0.12807	115.4	11.6
PG0052+251	1157.37	IGMABS	H I	1025.7	H	38478.0	0.12835	113.0	10.4

Table A1 continued

Table A1 (*continued*)

Target	λ_{obs}	Type	Ion	λ_{rest}	Frame	cz	z	W_{λ}	$\sigma_{W_{\lambda}}$
	(Å)			(Å)		(km s ⁻¹)		(mÅ)	(mÅ)
PG0052+251	1185.82	INTRINSIC	H I	1025.7	H	46793.0	0.15609	230.4	5.6
PG0052+251	1188.82	ISMLG	C I	1188.8	L	-2.0	-0.00003	23.2	4.9
PG0052+251	1189.32	ISMLG	Si II	1190.4	L	-275.0	-0.00095	24.6	4.7
PG0052+251	1190.01	ISMLG	Si II	1190.4	L	-102.0	-0.00037	84.2	4.2
PG0052+251	1190.37	ISMLG	Si II	1190.4	L	-12.0	-0.00003	378.4	3.4
PG0052+251	1192.18	ISMLG	Si II	1193.2	L	-279.0	-0.00095	56.4	4.1
PG0052+251	1192.84	ISMLG	Si II	1193.2	L	-112.0	-0.00037	103.4	3.7
PG0052+251	1193.25	ISMLG	Si II	1193.2	L	-10.0	-0.00003	422.1	4.3
PG0052+251	1197.16	ISMLG	Mn II	1197.1	L	-7.0	-0.00003	24.6	4.9
PG0052+251	1199.51	ISMLG	N I	1199.5	L	-10.0	-0.00003	352.6	4.5
PG0052+251	1200.18	ISMLG	N I	1200.2	L	-10.0	-0.00003	333.3	4.0
PG0052+251	1200.67	ISMLG	N I	1200.7	L	-10.0	-0.00003	300.9	3.9
PG0052+251	1201.10	ISMLG	Mn II	1201.1	L	-5.0	-0.00003	27.1	5.4
PG0052+251	1205.35	ISMLG	Si III	1206.5	L	-286.0	-0.00095	159.7	4.6
PG0052+251	1205.72	ISMLG	Si III	1206.5	L	-193.0	-0.00064	39.2	5.3
PG0052+251	1206.08	ISMLG	Si III	1206.5	L	-105.0	-0.00037	91.2	4.2
PG0052+251	1206.47	ISMLG	Si III	1206.5	L	-8.0	-0.00003	481.2	3.4
PG0052+251	1224.41	IGMABS	H I	1215.6	H	2155.0	0.00719	107.8	7.1
PG0052+251	1228.96	IGMABS	H I	1215.6	H	3277.0	0.01093	72.0	7.6
PG0052+251	1239.93	ISMLG	Mg II	1239.9	L	0.0	-0.00003	24.4	5.2
PG0052+251	1240.40	ISMLG	Mg II	1240.3	L	2.0	-0.00003	8.8	5.1
PG0052+251	1250.58	ISMLG	S II	1250.5	L	1.0	-0.00003	77.9	3.7
PG0052+251	1253.78	ISMLG	S II	1253.8	L	-6.0	-0.00003	195.4	6.0
PG0052+251	1255.94	IGMABS	H I	1215.6	H	9930.0	0.03312	107.5	7.4
PG0052+251	1256.70	IGMABS	H I	1215.6	H	10118.0	0.03375	59.5	6.7
PG0052+251	1257.55	IGMABS	H I	1215.6	H	10327.0	0.03445	118.8	7.0
PG0052+251	1259.23	ISMLG	Si II	1260.4	L	-284.0	-0.00095	170.1	5.2
PG0052+251	1259.46	ISMLG	S II	1259.5	L	-15.0	-0.00003	330.9	5.3
PG0052+251	1259.94	ISMLG	Si II	1260.4	L	-113.0	-0.00037	182.0	4.5
PG0052+251	1260.39	ISMLG	Si II	1260.4	L	-8.0	-0.00003	484.2	3.5
PG0052+251	1260.72	ISMLG	C I	1260.7	L	-3.0	-0.00003	31.1	3.5
PG0052+251	1266.78	IGMABS	H I	1215.6	H	12603.0	0.04204	33.2	6.5
PG0052+251	1271.27	IGMABS	H I	1215.6	H	13711.0	0.04574	377.0	7.6
PG0052+251	1277.25	ISMLG	C I	1277.2	L	1.0	-0.00003	50.1	6.0
PG0052+251	1281.44	IGMABS	H I	1215.6	H	16220.0	0.05410	119.0	11.8
PG0052+251	1289.20	IGMABS	H I	1215.6	H	18134.0	0.06049	42.2	9.4
PG0052+251	1292.64	IGMABS	H I	1215.6	H	18981.0	0.06331	282.7	8.8
PG0052+251	1294.65	IGMABS	H I	1215.6	H	19476.0	0.06496	46.2	9.0
PG0052+251	1300.95	ISMLG	O I	1302.1	L	-281.0	-0.00095	22.9	7.5
PG0052+251	1301.69	ISMLG	O I	1302.1	L	-110.0	-0.00037	112.4	5.5
PG0052+251	1302.12	ISMLG	O I	1302.1	L	-12.0	-0.00003	403.8	4.7
PG0052+251	1303.16	ISMLG	Si II	1304.3	L	-278.0	-0.00095	27.1	5.4
PG0052+251	1303.91	ISMLG	Si II	1304.3	L	-106.0	-0.00037	48.4	5.1
PG0052+251	1304.33	ISMLG	Si II	1304.3	L	-10.0	-0.00003	353.8	4.2
PG0052+251	1317.23	ISMLG	Ni II	1317.2	L	2.0	-0.00003	16.7	7.8
PG0052+251	1328.83	ISMLG	C I	1328.8	L	-1.0	-0.00003	33.1	6.8
PG0052+251	1333.27	ISMLG	C II	1334.5	L	-283.0	-0.00095	115.0	6.9
PG0052+251	1334.03	ISMLG	C II	1334.5	L	-113.0	-0.00037	217.5	5.4
PG0052+251	1334.50	ISMLG	C II	1334.5	L	-8.0	-0.00003	549.6	4.9
PG0052+251	1335.71	ISMLG	C II*	1335.7	L	1.0	-0.00003	112.4	4.4
PG0052+251	1347.25	ISMLG	Cl I	1347.2	L	3.0	-0.00003	24.9	5.6
PG0052+251	1350.03	IGMABS	H I	1215.6	H	33133.0	0.11052	744.1	9.4
PG0052+251	1362.67	IGMABS	H I	1215.6	H	36251.0	0.12092	280.0	5.6

Table A1 continued

Table A1 (*continued*)

Target	λ_{obs}	Type	Ion	λ_{rest}	Frame	cz	z	W_{λ}	$\sigma_{W_{\lambda}}$
	(Å)			(Å)		(km s ⁻¹)		(mÅ)	(mÅ)
PG0052+251	1364.14	IGMABS	H I	1215.6	H	36614.0	0.12213	197.2	9.7
PG0052+251	1370.10	ISMLG	Ni II	1370.1	L	-7.0	-0.00003	28.0	4.1
PG0052+251	1371.36	IGMABS	H I	1215.6	H	38394.0	0.12807	348.2	6.4
PG0052+251	1371.70	IGMABS	H I	1215.6	H	38479.0	0.12835	348.3	4.8
PG0052+251	1379.46	IGMABS	H I	1215.6	H	40391.0	0.13473	60.9	6.5
PG0052+251	1380.17	IGMABS	H I	1215.6	H	40567.0	0.13532	98.1	6.9
PG0052+251	1387.93	IGMABS	H I	1215.6	H	42479.0	0.14170	72.7	7.4
PG0052+251	1392.44	ISMLG	Si IV	1393.7	L	-284.0	-0.00095	45.8	4.5
PG0052+251	1393.76	ISMLG	Si IV	1393.7	L	0.0	-0.00003	133.3	4.9
PG0052+251	1394.83	INTRINSIC	Si III	1206.5	H	46795.0	0.15609	69.7	5.6
PG0052+251	1401.44	ISMLG	Si IV	1402.7	L	-285.0	-0.00095	19.3	3.3
PG0052+251	1402.77	ISMLG	Si IV	1402.7	L	0.0	-0.00003	71.4	3.3
PG0052+251	1405.43	INTRINSIC	H I	1215.6	H	46795.0	0.15609	367.1	4.1
PG0052+251	1454.84	ISMLG	Ni II	1454.8	L	-1.0	-0.00003	12.8	4.3
PG0052+251	1525.29	ISMLG	Si II	1526.7	L	-277.0	-0.00095	26.3	7.5
PG0052+251	1526.14	ISMLG	Si II	1526.7	L	-111.0	-0.00037	70.0	8.7
PG0052+251	1526.66	ISMLG	Si II	1526.7	L	-10.0	-0.00003	428.0	6.6
PG0052+251	1546.70	ISMLG	C IV	1548.2	L	-291.0	-0.00095	78.5	9.9
PG0052+251	1547.19	ISMLG	C IV	1548.2	L	-197.0	-0.00064	93.7	8.7
PG0052+251	1548.19	ISMLG	C IV	1548.2	L	-2.0	-0.00003	148.6	11.0
PG0052+251	1549.30	ISMLG	C IV	1550.7	L	-286.0	-0.00095	66.4	10.3
PG0052+251	1549.82	ISMLG	C IV	1550.7	L	-185.0	-0.00064	60.6	9.8
PG0052+251	1550.74	ISMLG	C IV	1550.7	L	-8.0	-0.00003	66.6	9.3
PG0052+251	1560.31	ISMLG	C I	1560.3	L	1.0	-0.00003	54.8	10.0
PG0052+251	1608.41	ISMLG	Fe II	1608.4	L	-8.0	-0.00003	334.0	15.4
PG0052+251	1611.22	ISMLG	Fe II	1611.2	L	3.0	-0.00003	58.6	17.5
PG0052+251	1619.03	IGMABS	C IV	1548.2	H	13714.0	0.04574	86.1	21.1
PG0052+251	1621.72	IGMABS	C IV	1550.7	H	13714.0	0.04574	56.4	14.2
PG0052+251	1656.28	ISMLG	C I*	1656.2	L	2.0	-0.00003	21.9	14.0
PG0052+251	1656.93	ISMLG	C I	1656.9	L	0.0	-0.00003	48.5	13.8
PG0052+251	1669.23	ISMLG	Al II	1670.7	L	-279.0	-0.00095	55.5	15.8
PG0052+251	1670.22	ISMLG	Al II	1670.7	L	-102.0	-0.00037	83.3	14.4
PG0052+251	1670.71	ISMLG	Al II	1670.7	L	-14.0	-0.00003	513.8	16.1
PG0052+251	1709.53	ISMLG	Ni II	1709.6	L	-14.0	-0.00003	33.7	15.2
PG0052+251	1741.55	PROXIMATE	H I	1741.5	L	-1.0	-0.00003	43.9	12.7
PG2349-014	1020.67	ISMLG	Si II	1020.6	L	-7.0	-0.00001	142.1	19.2
PG2349-014	1030.74	ISMLG	O VI	1031.9	L	-345.0	-0.00117	52.6	18.1
PG2349-014	1030.93	ISMLG	O VI	1031.9	L	-290.0	-0.00093	148.8	20.2
PG2349-014	1031.26	ISMLG	O VI	1031.9	L	-192.0	-0.00063	104.8	19.7
PG2349-014	1035.17	ISMLG	C II	1036.3	L	-337.0	-0.00117	41.8	12.3
PG2349-014	1035.33	ISMLG	C II	1036.3	L	-292.0	-0.00093	147.2	18.1
PG2349-014	1036.31	ISMLG	C II	1036.3	L	-9.0	-0.00001	65.3	18.1
PG2349-014	1039.20	ISMLG	O I	1039.2	L	-8.0	-0.00001	184.2	30.6
PG2349-014	1048.21	ISMLG	Ar I	1048.2	L	-4.0	-0.00001	108.1	20.7
PG2349-014	1063.19	ISMLG	Fe II	1063.1	L	4.0	-0.00001	106.3	13.8
PG2349-014	1064.82	IGMABS	H I	1025.7	H	11428.0	0.03810	227.1	21.5
PG2349-014	1066.65	ISMLG	Ar I	1066.6	L	-3.0	-0.00001	133.6	17.7
PG2349-014	1096.89	ISMLG	Fe II	1096.8	L	3.0	-0.00001	95.4	15.3
PG2349-014	1121.44	ISMLG	Fe III	1122.5	L	-291.0	-0.00093	65.1	16.9
PG2349-014	1121.99	ISMLG	Fe II	1121.9	L	3.0	-0.00001	64.1	19.1
PG2349-014	1123.81	IGMABS	H I	1025.7	H	28669.0	0.09562	79.1	18.2
PG2349-014	1143.21	ISMLG	Fe II	1143.2	L	-5.0	-0.00001	76.8	17.3
PG2349-014	1144.93	ISMLG	Fe II	1144.9	L	-2.0	-0.00001	143.3	13.9

Table A1 continued

Table A1 (*continued*)

Target	λ_{obs}	Type	Ion	λ_{rest}	Frame	cz	z	W_{λ}	$\sigma_{W_{\lambda}}$
	(Å)			(Å)		(km s ⁻¹)		(mÅ)	(mÅ)
PG2349-014	1152.80	ISMLG	P II	1152.8	L	-4.0	-0.00001	86.6	15.5
PG2349-014	1189.06	ISMLG	Si II	1190.4	L	-342.0	-0.00117	36.4	4.8
PG2349-014	1189.27	ISMLG	Si II	1190.4	L	-289.0	-0.00093	89.2	6.7
PG2349-014	1190.42	ISMLG	Si II	1190.4	L	0.0	-0.00001	215.7	5.8
PG2349-014	1190.72	ISMLG	Si II	1190.4	L	77.0	0.00023	21.2	6.2
PG2349-014	1191.93	ISMLG	Si II	1193.2	L	-341.0	-0.00117	34.1	4.5
PG2349-014	1192.13	ISMLG	Si II	1193.2	L	-292.0	-0.00093	128.1	5.8
PG2349-014	1193.30	ISMLG	Si II	1193.2	L	3.0	-0.00001	210.1	6.9
PG2349-014	1193.58	ISMLG	Si II	1193.2	L	74.0	0.00023	44.4	7.1
PG2349-014	1199.54	ISMLG	N I	1199.5	L	-2.0	-0.00001	177.3	7.6
PG2349-014	1200.22	ISMLG	N I	1200.2	L	0.0	-0.00001	199.0	9.1
PG2349-014	1200.70	ISMLG	N I	1200.7	L	-3.0	-0.00001	187.4	10.4
PG2349-014	1205.09	ISMLG	Si III	1206.5	L	-350.0	-0.00117	122.2	3.5
PG2349-014	1205.35	ISMLG	Si III	1206.5	L	-286.0	-0.00093	342.3	2.8
PG2349-014	1205.72	ISMLG	Si III	1206.5	L	-194.0	-0.00063	138.6	4.5
PG2349-014	1206.47	ISMLG	Si III	1206.5	L	-7.0	-0.00001	317.1	3.8
PG2349-014	1206.80	ISMLG	Si III	1206.5	L	75.0	0.00023	174.9	3.9
PG2349-014	1224.92	IGMABS	H I	1215.6	H	2281.0	0.00761	191.5	6.5
PG2349-014	1239.90	ISMLG	Mg II	1239.9	L	-7.0	-0.00001	19.6	5.9
PG2349-014	1250.56	ISMLG	S II	1250.5	L	-5.0	-0.00001	94.1	6.9
PG2349-014	1252.53	IGMABS	Si III	1206.5	H	11437.0	0.03810	33.6	7.0
PG2349-014	1253.77	ISMLG	S II	1253.8	L	-8.0	-0.00001	130.2	6.1
PG2349-014	1258.97	ISMLG	Si II	1260.4	L	-344.0	-0.00117	60.9	4.2
PG2349-014	1259.22	ISMLG	Si II	1260.4	L	-286.0	-0.00093	183.7	6.0
PG2349-014	1259.47	ISMLG	S II	1259.5	L	-11.0	-0.00001	151.6	3.6
PG2349-014	1260.43	ISMLG	Si II	1260.4	L	2.0	-0.00001	305.4	5.6
PG2349-014	1260.74	ISMLG	Si II	1260.4	L	76.0	0.00023	82.1	4.9
PG2349-014	1261.98	IGMABS	H I	1215.6	H	11421.0	0.03810	427.7	7.6
PG2349-014	1270.98	IGMABS	H I	1215.6	H	13640.0	0.04550	58.6	8.0
PG2349-014	1300.88	ISMLG	O I	1302.1	L	-297.0	-0.00093	43.0	9.7
PG2349-014	1302.13	ISMLG	O I	1302.1	L	-9.0	-0.00001	239.8	12.8
PG2349-014	1303.07	ISMLG	Si II	1304.3	L	-298.0	-0.00093	90.6	9.0
PG2349-014	1303.42	IGMABS	H I	1215.6	H	21640.0	0.07218	215.9	10.3
PG2349-014	1304.35	ISMLG	Si II	1304.3	L	-5.0	-0.00001	186.6	8.5
PG2349-014	1304.67	ISMLG	Si II	1304.3	L	70.0	0.00023	31.4	9.6
PG2349-014	1327.61	IGMABS	H I	1215.6	H	27605.0	0.09208	91.4	12.2
PG2349-014	1331.91	IGMABS	H I	1215.6	H	28665.0	0.09562	242.6	9.2
PG2349-014	1333.00	ISMLG	C II	1334.5	L	-344.0	-0.00117	100.2	5.5
PG2349-014	1333.21	ISMLG	C II	1334.5	L	-296.0	-0.00093	215.9	5.8
PG2349-014	1333.71	ISMLG	C II	1334.5	L	-184.0	-0.00063	60.7	7.9
PG2349-014	1334.48	ISMLG	C II	1334.5	L	-11.0	-0.00001	318.1	6.9
PG2349-014	1334.89	ISMLG	C II	1334.5	L	80.0	0.00023	136.7	7.0
PG2349-014	1335.69	ISMLG	C II*	1335.7	L	-4.0	-0.00001	129.7	9.1
PG2349-014	1336.02	ISMLG	C II*	1335.7	L	70.0	0.00023	35.0	7.2
PG2349-014	1352.65	IGMABS	H I	1215.6	H	33780.0	0.11268	74.5	10.0
PG2349-014	1356.43	IGMABS	H I	1215.6	H	34713.0	0.11579	120.6	10.3
PG2349-014	1373.10	IGMABS	H I	1215.6	H	38823.0	0.12950	82.9	11.3
PG2349-014	1389.42	IGMABS	H I	1215.6	H	42849.0	0.14293	43.5	8.7
PG2349-014	1392.14	ISMLG	Si IV	1393.7	L	-348.0	-0.00117	47.7	5.4
PG2349-014	1392.41	ISMLG	Si IV	1393.7	L	-291.0	-0.00093	161.4	6.8
PG2349-014	1393.73	ISMLG	Si IV	1393.7	L	-7.0	-0.00001	130.2	7.2
PG2349-014	1394.08	ISMLG	Si IV	1393.7	L	68.0	0.00023	31.1	6.0
PG2349-014	1401.15	ISMLG	Si IV	1402.7	L	-346.0	-0.00117	25.5	5.1

Table A1 continued

Table A1 (*continued*)

Target	λ_{obs}	Type	Ion	λ_{rest}	Frame	cz	z	W_{λ}	$\sigma_{W_{\lambda}}$
	(Å)			(Å)		(km s ⁻¹)		(mÅ)	(mÅ)
PG2349–014	1401.42	ISMLG	Si iv	1402.7	L	−290.0	−0.00093	86.1	6.7
PG2349–014	1402.73	ISMLG	Si iv	1402.7	L	−9.0	−0.00001	69.1	7.6
PG2349–014	1403.11	ISMLG	Si iv	1402.7	L	72.0	0.00023	14.6	6.3
PG2349–014	1403.84	IGMABS	H i	1215.6	H	46405.0	0.15479	76.7	7.6
PG2349–014	1407.59	PROXIMATE	H i	1215.6	H	47328.0	0.15787	91.8	9.1
PHL1226	1183.49	IGMABS	Si ii	1020.6	H	47813.0	0.15949	80.3	12.5
PHL1226	1183.74	IGMABS	Si ii	1020.6	H	47888.0	0.15974	79.9	12.1
PHL1226	1188.01	IGMABS	H i	1025.7	H	47432.0	0.15819	56.0	12.9
PHL1226	1188.62	IGMABS	H i	1025.7	H	47610.0	0.15879	277.2	11.1
PHL1226	1188.87	IGMABS	H i	1025.7	H	47684.0	0.15904	282.2	7.8
PHL1226	1189.31	IGMABS	H i	1025.7	H	47812.0	0.15949	1155.4	11.6
PHL1226	1189.54	IGMABS	H i	1025.7	H	47880.0	0.15974	1344.0	13.1
PHL1226	1189.83	IGMABS	H i	1025.7	H	47965.0	0.16000	847.6	10.8
PHL1226	1190.08	IGMABS	H i	1025.7	H	48038.0	0.16023	430.0	9.0
PHL1226	1190.37	ISMLG	Si ii	1190.4	L	−12.0	−0.00002	307.5	10.1
PHL1226	1192.98	ISMLG	Si ii	1193.2	L	−78.0	−0.00026	161.8	11.7
PHL1226	1193.26	ISMLG	Si ii	1193.2	L	−8.0	−0.00002	317.7	9.8
PHL1226	1196.53	IGMABS	O vi	1031.9	H	47819.0	0.15949	909.0	20.2
PHL1226	1196.74	IGMABS	O vi	1031.9	H	47882.0	0.15974	739.8	15.1
PHL1226	1197.03	IGMABS	O vi	1031.9	H	47965.0	0.16000	488.1	14.1
PHL1226	1197.27	IGMABS	O vi	1031.9	H	48035.0	0.16023	310.7	14.6
PHL1226	1198.41	IGMABS	H i	972.5	H	69626.0	0.23227	136.7	21.2
PHL1226	1198.67	IGMABS	H i	972.5	H	69706.0	0.23252	199.7	23.8
PHL1226	1198.80	IGMABS	H i	972.5	H	69748.0	0.23266	63.7	8.9
PHL1226	1199.51	ISMLG	N i	1199.5	L	−9.0	−0.00002	269.5	22.8
PHL1226	1200.19	ISMLG	N i	1200.2	L	−7.0	−0.00002	231.0	19.6
PHL1226	1200.69	ISMLG	N i	1200.7	L	−5.0	−0.00002	307.7	24.6
PHL1226	1201.62	IGMABS	C ii	1036.3	H	47814.0	0.15949	578.3	13.0
PHL1226	1201.85	IGMABS	C ii	1036.3	H	47881.0	0.15974	275.9	5.9
PHL1226	1202.15	IGMABS	C ii	1036.3	H	47967.0	0.16000	168.2	9.4
PHL1226	1203.11	IGMABS	O vi	1037.6	H	47814.0	0.15949	513.7	17.8
PHL1226	1203.34	IGMABS	O vi	1037.6	H	47883.0	0.15974	197.8	11.0
PHL1226	1203.63	IGMABS	O vi	1037.6	H	47966.0	0.16000	149.5	11.5
PHL1226	1203.90	IGMABS	O vi	1037.6	H	48043.0	0.16023	162.5	9.4
PHL1226	1204.18	IGMABS	C iii	977.0	H	69702.0	0.23252	99.8	5.5
PHL1226	1204.36	IGMABS	C iii	977.0	H	69759.0	0.23266	206.2	6.2
PHL1226	1205.19	IGMABS	O i	1039.2	H	47876.0	0.15974	180.0	14.4
PHL1226	1205.85	ISMLG	Si iii	1206.5	L	−162.0	−0.00058	61.8	14.5
PHL1226	1206.18	ISMLG	Si iii	1206.5	L	−80.0	−0.00026	167.2	8.5
PHL1226	1206.46	ISMLG	Si iii	1206.5	L	−9.0	−0.00002	401.1	11.4
PHL1226	1211.07	IGMABS	Si ii	1190.4	H	5202.0	0.01735	37.7	19.9
PHL1226	1211.49	IGMABS	Si ii	1190.4	H	5307.0	0.01771	105.8	24.9
PHL1226	1211.71	IGMABS	Si ii	1190.4	H	5363.0	0.01790	78.4	19.5
PHL1226	1219.93	IGMABS	N iii	989.7	H	69701.0	0.23252	79.5	11.3
PHL1226	1220.06	IGMABS	N iii	989.7	H	69743.0	0.23266	91.1	12.0
PHL1226	1221.90	IGMABS	H i	949.7	H	85908.0	0.28654	117.9	17.7
PHL1226	1222.65	IGMABS	H i	1215.6	H	1721.0	0.00574	343.3	19.1
PHL1226	1227.41	IGMABS	Si iii	1206.5	H	5196.0	0.01735	94.2	15.4
PHL1226	1227.86	IGMABS	Si iii	1206.5	H	5307.0	0.01771	154.1	8.5
PHL1226	1228.13	IGMABS	Si iii	1206.5	H	5374.0	0.01790	227.9	8.4
PHL1226	1228.30	IGMABS	Si iii	1206.5	H	5416.0	0.01809	156.3	9.0
PHL1226	1228.76	IGMABS	H i	930.7	H	95989.0	0.32020	45.9	13.1
PHL1226	1233.02	IGMABS	Fe ii	1063.1	H	47892.0	0.15974	77.8	11.1

Table A1 continued

Table A1 (*continued*)

Target	λ_{obs}	Type	Ion	λ_{rest}	Frame	cz	z	W_{λ}	$\sigma_{W_{\lambda}}$
	(Å)			(Å)		(km s ⁻¹)		(mÅ)	(mÅ)
PHL1226	1235.62	IGMABS	H I	1215.6	H	4920.0	0.01641	168.5	14.2
PHL1226	1236.10	IGMABS	H I	1215.6	H	5037.0	0.01680	67.5	6.4
PHL1226	1236.77	IGMABS	H I	1215.6	H	5203.0	0.01735	1171.2	9.5
PHL1226	1237.19	IGMABS	H I	1215.6	H	5308.0	0.01771	1199.8	9.0
PHL1226	1237.44	IGMABS	H I	1215.6	H	5368.0	0.01790	797.6	7.9
PHL1226	1237.66	IGMABS	H I	1215.6	H	5422.0	0.01809	406.2	6.4
PHL1226	1238.07	IGMABS	H I	937.8	H	95987.0	0.32020	84.3	10.8
PHL1226	1239.87	ISMLG	Mg II	1239.9	L	-14.0	-0.00002	32.3	10.7
PHL1226	1240.33	ISMLG	Mg II	1240.3	L	-16.0	-0.00002	21.0	9.9
PHL1226	1250.54	ISMLG	S II	1250.5	L	-9.0	-0.00002	122.3	11.0
PHL1226	1251.21	IGMABS	H I	972.5	H	85904.0	0.28654	145.8	13.7
PHL1226	1253.77	ISMLG	S II	1253.8	L	-7.0	-0.00002	210.4	11.7
PHL1226	1253.83	IGMABS	H I	949.7	H	95988.0	0.32020	210.4	11.7
PHL1226	1256.13	IGMABS	H I	1215.6	H	9977.0	0.03328	39.2	12.0
PHL1226	1256.89	IGMABS	N II	1083.9	H	47816.0	0.15949	455.7	10.6
PHL1226	1257.13	IGMABS	N II	1083.9	H	47884.0	0.15974	357.2	8.0
PHL1226	1259.48	ISMLG	S II	1259.5	L	-9.0	-0.00002	156.5	10.9
PHL1226	1260.10	ISMLG	Si II	1260.4	L	-77.0	-0.00026	95.1	4.0
PHL1226	1260.38	ISMLG	Si II	1260.4	L	-9.0	-0.00002	480.5	10.7
PHL1226	1260.72	ISMLG	C I	1260.7	L	-3.0	-0.00002	62.0	8.5
PHL1226	1263.97	IGMABS	H I	1025.7	H	69633.0	0.23227	208.5	11.2
PHL1226	1264.22	IGMABS	H I	1025.7	H	69707.0	0.23252	342.9	8.4
PHL1226	1264.37	IGMABS	H I	1025.7	H	69750.0	0.23266	218.9	7.3
PHL1226	1265.31	IGMABS	H I	1215.6	H	12240.0	0.04083	214.9	13.4
PHL1226	1270.97	IGMABS	H I	972.5	H	91995.0	0.30685	101.6	13.3
PHL1226	1271.83	IGMABS	O VI	1031.9	H	69696.0	0.23252	87.6	6.5
PHL1226	1272.03	IGMABS	O VI	1031.9	H	69753.0	0.23266	241.6	8.0
PHL1226	1273.82	IGMABS	H I	1215.6	H	14341.0	0.04784	37.5	15.5
PHL1226	1276.83	IGMABS	H I	1215.6	H	15084.0	0.05031	283.9	11.7
PHL1226	1277.23	ISMLG	C I	1277.2	L	-4.0	-0.00002	74.1	9.8
PHL1226	1278.19	IGMABS	H I	1215.6	H	15419.0	0.05143	229.0	14.7
PHL1226	1278.87	IGMABS	O VI	1037.6	H	69703.0	0.23252	67.7	6.9
PHL1226	1279.02	IGMABS	O VI	1037.6	H	69748.0	0.23266	139.8	9.1
PHL1226	1282.28	IGMABS	Si II	1260.4	H	5199.0	0.01735	75.7	12.5
PHL1226	1282.72	IGMABS	Si II	1260.4	H	5303.0	0.01771	110.9	9.8
PHL1226	1282.95	IGMABS	Si II	1260.4	H	5359.0	0.01790	151.2	9.8
PHL1226	1283.93	IGMABS	H I	972.5	H	95989.0	0.32020	234.7	11.8
PHL1226	1289.87	IGMABS	C III	977.0	H	95995.0	0.32020	145.3	13.3
PHL1226	1294.32	IGMABS	H I	1215.6	H	19396.0	0.06470	44.5	25.9
PHL1226	1300.92	IGMABS	H I	1215.6	H	21023.0	0.07012	152.0	24.5
PHL1226	1301.83	ISMLG	O I	1302.1	L	-77.0	-0.00026	97.3	13.3
PHL1226	1302.15	ISMLG	O I	1302.1	L	-4.0	-0.00002	337.2	22.1
PHL1226	1303.99	ISMLG	Si II	1304.3	L	-88.0	-0.00026	39.6	21.0
PHL1226	1304.37	ISMLG	Si II	1304.3	L	0.0	-0.00002	294.6	19.9
PHL1226	1305.93	IGMABS	H I	1215.6	H	22260.0	0.07425	240.6	31.6
PHL1226	1327.83	IGMABS	Fe II	1144.9	H	47890.0	0.15974	139.3	29.5
PHL1226	1334.18	ISMLG	C II	1334.5	L	-80.0	-0.00026	228.3	8.9
PHL1226	1334.52	ISMLG	C II	1334.5	L	-4.0	-0.00002	413.3	8.9
PHL1226	1335.69	ISMLG	C II*	1335.7	L	-3.0	-0.00002	163.8	13.9
PHL1226	1340.47	IGMABS	H I	1025.7	H	91992.0	0.30685	116.1	13.4
PHL1226	1342.91	IGMABS	H I	1215.6	H	31378.0	0.10467	188.5	15.1
PHL1226	1353.47	IGMABS	H I	1215.6	H	33983.0	0.11335	37.4	14.6
PHL1226	1354.15	IGMABS	H I	1025.7	H	95992.0	0.32020	397.8	14.9

Table A1 continued

Table A1 (*continued*)

Target	λ_{obs}	Type	Ion	λ_{rest}	Frame	cz	z	W_{λ}	$\sigma_{W_{\lambda}}$
	(Å)			(Å)		(km s ⁻¹)		(mÅ)	(mÅ)
PHL1226	1356.29	IGMABS	H I	1215.6	H	34677.0	0.11567	61.2	17.0
PHL1226	1357.67	IGMABS	C II	1334.5	H	5198.0	0.01735	161.2	15.7
PHL1226	1358.17	IGMABS	C II	1334.5	H	5309.0	0.01771	161.1	6.4
PHL1226	1358.42	IGMABS	C II	1334.5	H	5366.0	0.01790	253.0	11.9
PHL1226	1361.64	IGMABS	H I	1215.6	H	35996.0	0.12007	43.0	16.3
PHL1226	1362.11	IGMABS	H I	1215.6	H	36114.0	0.12046	24.2	10.9
PHL1226	1362.42	IGMABS	O VI	1031.9	H	96015.0	0.32020	99.0	12.4
PHL1226	1365.81	IGMABS	H I	1215.6	H	37025.0	0.12350	54.5	14.7
PHL1226	1369.93	IGMABS	O VI	1037.6	H	96014.0	0.32020	120.0	14.3
PHL1226	1377.42	IGMABS	H I	1215.6	H	39889.0	0.13306	197.8	19.5
PHL1226	1380.31	IGMABS	Si II	1190.4	H	47822.0	0.15949	329.6	12.4
PHL1226	1380.54	IGMABS	Si II	1190.4	H	47882.0	0.15974	328.5	8.5
PHL1226	1380.86	IGMABS	Si II	1190.4	H	47962.0	0.16000	109.0	8.9
PHL1226	1383.60	IGMABS	Si II	1193.2	H	47811.0	0.15949	453.2	10.4
PHL1226	1383.86	IGMABS	Si II	1193.2	H	47877.0	0.15974	363.0	8.7
PHL1226	1384.19	IGMABS	Si II	1193.2	H	47962.0	0.16000	158.7	10.0
PHL1226	1391.16	IGMABS	N I	1199.5	H	47888.0	0.15974	117.9	12.4
PHL1226	1391.95	IGMABS	N I	1200.2	H	47891.0	0.15974	107.8	11.9
PHL1226	1392.50	IGMABS	N I	1200.7	H	47886.0	0.15974	54.7	10.4
PHL1226	1393.75	ISMLG	Si IV	1393.7	L	-2.0	-0.00002	179.7	16.0
PHL1226	1398.09	IGMABS	Si III	1206.5	H	47607.0	0.15879	169.7	12.2
PHL1226	1398.39	IGMABS	Si III	1206.5	H	47682.0	0.15904	74.8	9.7
PHL1226	1398.92	IGMABS	Si III	1206.5	H	47813.0	0.15949	732.9	11.6
PHL1226	1399.19	IGMABS	Si III	1206.5	H	47881.0	0.15974	482.7	7.2
PHL1226	1399.52	IGMABS	Si III	1206.5	H	47961.0	0.16000	382.9	8.7
PHL1226	1399.82	IGMABS	Si III	1206.5	H	48037.0	0.16023	121.0	10.0
PHL1226	1402.73	ISMLG	Si IV	1402.7	L	-10.0	-0.00002	141.6	19.4
PHL1226	1407.98	IGMABS	H I	1215.6	H	47425.0	0.15819	186.9	25.4
PHL1226	1408.71	IGMABS	H I	1215.6	H	47605.0	0.15879	709.7	16.6
PHL1226	1409.01	IGMABS	H I	1215.6	H	47678.0	0.15904	526.6	9.0
PHL1226	1409.56	IGMABS	H I	1215.6	H	47814.0	0.15949	2335.5	20.9
PHL1226	1409.86	IGMABS	H I	1215.6	H	47889.0	0.15974	2299.8	21.3
PHL1226	1410.18	IGMABS	H I	1215.6	H	47967.0	0.16000	1530.5	18.1
PHL1226	1410.46	IGMABS	H I	1215.6	H	48036.0	0.16023	1401.8	20.7
PHL1226	1412.99	IGMABS	H I	1215.6	H	48661.0	0.16231	64.4	12.7
PHL1226	1413.19	IGMABS	H I	1215.6	H	48711.0	0.16248	82.9	9.6
PHL1226	1417.03	IGMABS	H I	1215.6	H	49657.0	0.16564	155.3	26.6
PHL1226	1436.39	IGMABS	N V	1238.8	H	47812.0	0.15949	200.1	17.3
PHL1226	1436.69	IGMABS	N V	1238.8	H	47883.0	0.15974	115.2	13.8
PHL1226	1437.01	IGMABS	N V	1238.8	H	47962.0	0.16000	114.9	14.0
PHL1226	1441.03	IGMABS	N V	1242.8	H	47817.0	0.15949	79.1	14.0
PHL1226	1441.30	IGMABS	N V	1242.8	H	47882.0	0.15974	53.0	13.0
PHL1226	1441.65	IGMABS	N V	1242.8	H	47966.0	0.16000	55.6	11.7
PHL1226	1460.60	IGMABS	Si II	1260.4	H	47613.0	0.15879	48.3	10.2
PHL1226	1461.44	IGMABS	Si II	1260.4	H	47812.0	0.15949	689.8	13.8
PHL1226	1461.77	IGMABS	Si II	1260.4	H	47891.0	0.15974	290.7	6.9
PHL1226	1462.09	PROXIMATE	H I	1260.4	H	47967.0	0.16000	217.9	11.1
RBS2005	1134.99	ISMLG	N I	1134.9	L	2.0	-0.00002	264.9	48.7
RBS2005	1142.36	ISMLG	Fe II	1142.3	L	-1.0	-0.00002	33.0	16.9
RBS2005	1143.22	ISMLG	Fe II	1143.2	L	-3.0	-0.00002	131.2	18.8
RBS2005	1144.62	ISMLG	Fe II	1144.9	L	-82.0	-0.00028	53.0	11.8
RBS2005	1144.93	ISMLG	Fe II	1144.9	L	-2.0	-0.00002	254.3	16.9
RBS2005	1152.83	ISMLG	P II	1152.8	L	3.0	-0.00002	93.8	13.8

Table A1 continued

Table A1 (*continued*)

Target	λ_{obs}	Type	Ion	λ_{rest}	Frame	cz	z	W_{λ}	$\sigma_{W_{\lambda}}$
	(Å)			(Å)		(km s ⁻¹)		(mÅ)	(mÅ)
RBS2005	1157.94	ISMLG	C I	1157.9	L	7.0	-0.00002	76.8	12.0
RBS2005	1158.34	ISMLG	C I	1158.3	L	5.0	-0.00002	64.4	13.0
RBS2005	1188.84	ISMLG	C I	1188.8	L	1.0	-0.00002	48.8	9.8
RBS2005	1190.08	ISMLG	Si II	1190.4	L	-85.0	-0.00028	115.0	8.1
RBS2005	1190.43	ISMLG	Si II	1190.4	L	4.0	-0.00002	421.1	8.7
RBS2005	1192.98	ISMLG	Si II	1193.2	L	-78.0	-0.00028	120.9	6.6
RBS2005	1193.31	ISMLG	Si II	1193.2	L	5.0	-0.00002	418.7	7.9
RBS2005	1197.21	ISMLG	Mn II	1197.1	L	6.0	-0.00002	19.9	11.2
RBS2005	1199.55	ISMLG	N I	1199.5	L	1.0	-0.00002	371.1	30.7
RBS2005	1200.23	ISMLG	N I	1200.2	L	3.0	-0.00002	386.3	30.6
RBS2005	1200.72	ISMLG	N I	1200.7	L	2.0	-0.00002	308.5	35.7
RBS2005	1201.11	ISMLG	Mn II	1201.1	L	-3.0	-0.00002	23.9	8.3
RBS2005	1204.89	ISMLG	Si III	1206.5	L	-401.0	-0.00135	107.9	6.6
RBS2005	1205.14	ISMLG	Si III	1206.5	L	-338.0	-0.00112	104.7	7.8
RBS2005	1205.40	ISMLG	Si III	1206.5	L	-273.0	-0.00093	61.0	10.1
RBS2005	1205.77	ISMLG	Si III	1206.5	L	-180.0	-0.00061	20.8	8.5
RBS2005	1206.15	ISMLG	Si III	1206.5	L	-86.0	-0.00028	164.9	8.1
RBS2005	1206.53	ISMLG	Si III	1206.5	L	8.0	-0.00002	502.5	7.2
RBS2005	1221.91	IGMABS	H I	1215.6	H	1539.0	0.00513	111.3	20.8
RBS2005	1229.64	IGMABS	H I	1215.6	H	3444.0	0.01149	398.0	16.6
RBS2005	1239.94	ISMLG	Mg II	1239.9	L	5.0	-0.00002	31.0	9.0
RBS2005	1240.40	ISMLG	Mg II	1240.3	L	1.0	-0.00002	29.0	8.9
RBS2005	1245.46	IGMABS	H I	1215.6	H	7345.0	0.02450	41.4	13.2
RBS2005	1248.45	IGMABS	H I	1215.6	H	8085.0	0.02697	130.1	12.8
RBS2005	1250.57	ISMLG	S II	1250.5	L	-2.0	-0.00002	138.1	11.2
RBS2005	1253.81	ISMLG	S II	1253.8	L	0.0	-0.00002	230.6	12.6
RBS2005	1259.54	ISMLG	S II	1259.5	L	4.0	-0.00002	328.3	11.6
RBS2005	1260.05	ISMLG	Si II	1260.4	L	-89.0	-0.00028	203.5	7.1
RBS2005	1260.46	ISMLG	Si II	1260.4	L	9.0	-0.00002	477.2	6.6
RBS2005	1260.74	ISMLG	C I	1260.7	L	0.0	-0.00002	88.8	6.5
RBS2005	1260.92	IGMABS	H I	1215.6	H	11160.0	0.03722	50.3	9.4
RBS2005	1266.87	IGMABS	H I	1215.6	H	12626.0	0.04212	331.0	13.5
RBS2005	1277.27	ISMLG	C I	1277.2	L	5.0	-0.00002	104.7	11.0
RBS2005	1277.51	ISMLG	C I*	1277.5	L	-1.0	-0.00002	53.1	10.8
RBS2005	1280.13	ISMLG	C I	1280.1	L	0.0	-0.00002	46.8	15.1
RBS2005	1283.26	IGMABS	H I	1215.6	H	16668.0	0.05560	151.5	23.6
RBS2005	1301.78	ISMLG	O I	1302.1	L	-90.0	-0.00028	185.5	30.1
RBS2005	1302.19	ISMLG	O I	1302.1	L	4.0	-0.00002	404.5	16.3
RBS2005	1303.99	ISMLG	Si II	1304.3	L	-87.0	-0.00028	66.5	17.4
RBS2005	1304.38	ISMLG	Si II	1304.3	L	2.0	-0.00002	362.0	18.1
RBS2005	1307.72	IGMABS	H I	1215.6	H	22700.0	0.07572	100.0	11.7
RBS2005	1316.62	IGMABS	H I	1215.6	H	24894.0	0.08304	133.0	18.6
RBS2005	1317.21	ISMLG	Ni II	1317.2	L	-1.0	-0.00002	36.1	14.9
RBS2005	1319.20	IGMABS	H I	1215.6	H	25531.0	0.08516	236.0	24.6
RBS2005	1328.83	ISMLG	C I	1328.8	L	0.0	-0.00002	54.3	12.6
RBS2005	1329.10	ISMLG	C I*	1329.1	L	-1.0	-0.00002	47.1	9.9
RBS2005	1331.76	IGMABS	H I	1215.6	H	28629.0	0.09550	89.4	11.6
RBS2005	1332.74	ISMLG	C II	1334.5	L	-403.0	-0.00135	42.3	8.2
RBS2005	1333.03	ISMLG	C II	1334.5	L	-338.0	-0.00112	47.0	9.2
RBS2005	1333.70	ISMLG	C II	1334.5	L	-188.0	-0.00061	47.5	9.5
RBS2005	1334.15	ISMLG	C II	1334.5	L	-86.0	-0.00028	234.9	6.4
RBS2005	1334.51	ISMLG	C II	1334.5	L	-5.0	-0.00002	435.6	4.1
RBS2005	1335.71	ISMLG	C II*	1335.7	L	1.0	-0.00002	219.4	9.8

Table A1 *continued*

Table A1 (*continued*)

Target	λ_{obs}	Type	Ion	λ_{rest}	Frame	cz	z	W_{λ}	$\sigma_{W_{\lambda}}$
	(Å)			(Å)		(km s ⁻¹)		(mÅ)	(mÅ)
RBS2005	1336.62	IGMABS	H I	1215.6	H	29826.0	0.09949	210.5	12.2
RBS2005	1347.23	ISMLG	Cl I	1347.2	L	-2.0	-0.00002	45.4	6.6
RBS2005	1370.12	ISMLG	Ni II	1370.1	L	-2.0	-0.00002	46.9	6.6
RBS2005	1391.84	ISMLG	Si IV	1393.7	L	-414.0	-0.00135	35.5	8.2
RBS2005	1392.48	ISMLG	Si IV	1393.7	L	-275.0	-0.00093	26.1	8.8
RBS2005	1393.39	ISMLG	Si IV	1393.7	L	-80.0	-0.00028	35.7	9.0
RBS2005	1393.77	ISMLG	Si IV	1393.7	L	2.0	-0.00002	259.8	8.6
RBS2005	1402.78	ISMLG	Si IV	1402.7	L	1.0	-0.00002	211.8	12.4
RBS2005	1454.84	ISMLG	Ni II	1454.8	L	-1.0	-0.00002	17.5	10.1
RBS2005	1526.29	ISMLG	Si II	1526.7	L	-81.0	-0.00028	132.6	10.7
RBS2005	1526.74	ISMLG	Si II	1526.7	L	6.0	-0.00002	407.8	12.8
RBS2005	1546.13	ISMLG	C IV	1548.2	L	-402.0	-0.00135	47.0	13.5
RBS2005	1546.47	ISMLG	C IV	1548.2	L	-335.0	-0.00112	73.3	15.2
RBS2005	1548.24	ISMLG	C IV	1548.2	L	6.0	-0.00002	317.5	16.6
RBS2005	1550.79	ISMLG	C IV	1550.7	L	2.0	-0.00002	292.1	15.7
RBS2005	1560.30	ISMLG	C I	1560.3	L	-2.0	-0.00002	72.8	11.1
RBS2005	1560.67	ISMLG	C I*	1560.6	L	-2.0	-0.00002	61.6	13.2
RBS2005	1608.02	ISMLG	Fe II	1608.4	L	-81.0	-0.00028	75.9	23.4
RBS2005	1608.44	ISMLG	Fe II	1608.4	L	-2.0	-0.00002	276.6	31.1
RBS2005	1656.97	ISMLG	C I	1656.9	L	7.0	-0.00002	135.9	25.1
RBS2005	1657.37	ISMLG	C I*	1657.3	L	-2.0	-0.00002	52.7	21.5
RBS2005	1670.29	ISMLG	Al II	1670.7	L	-89.0	-0.00028	123.4	24.8
RBS2005	1670.83	ISMLG	Al II	1670.7	L	8.0	-0.00002	531.9	26.0
RBS2005	1741.54	PROXIMATE	H I	1741.5	L	-3.0	-0.00002	57.4	14.3
RBS2055	1133.66	ISMLG	Fe II	1133.6	L	-1.0	0.00000	123.1	26.0
RBS2055	1134.17	ISMLG	N I	1134.1	L	2.0	0.00000	220.0	22.7
RBS2055	1134.43	ISMLG	N I	1134.4	L	5.0	0.00000	255.6	22.0
RBS2055	1134.76	ISMLG	N I	1134.9	L	-58.0	-0.00019	81.0	22.6
RBS2055	1135.00	ISMLG	N I	1134.9	L	5.0	0.00000	227.0	24.8
RBS2055	1143.23	ISMLG	Fe II	1143.2	L	1.0	0.00000	95.5	10.3
RBS2055	1144.70	ISMLG	Fe II	1144.9	L	-62.0	-0.00019	42.3	7.2
RBS2055	1144.92	ISMLG	Fe II	1144.9	L	-6.0	0.00000	228.1	9.0
RBS2055	1152.83	ISMLG	P II	1152.8	L	3.0	0.00000	92.4	10.4
RBS2055	1157.92	ISMLG	C I	1157.9	L	3.0	0.00000	25.2	7.9
RBS2055	1188.82	ISMLG	Si II	1190.4	L	-403.0	-0.00136	38.5	6.7
RBS2055	1189.10	ISMLG	Si II	1190.4	L	-331.0	-0.00109	55.2	5.8
RBS2055	1190.00	ISMLG	Si II	1190.4	L	-104.0	-0.00033	97.8	4.9
RBS2055	1190.19	ISMLG	Si II	1190.4	L	-57.0	-0.00019	167.6	2.7
RBS2055	1190.45	ISMLG	Si II	1190.4	L	9.0	0.00000	261.4	5.0
RBS2055	1191.67	ISMLG	Si II	1193.2	L	-407.0	-0.00136	22.2	6.3
RBS2055	1191.96	ISMLG	Si II	1193.2	L	-334.0	-0.00109	72.9	5.3
RBS2055	1192.17	ISMLG	Si II	1193.2	L	-281.0	-0.00092	21.4	5.5
RBS2055	1192.87	ISMLG	Si II	1193.2	L	-104.0	-0.00033	104.8	4.6
RBS2055	1193.06	ISMLG	Si II	1193.2	L	-57.0	-0.00019	150.8	2.2
RBS2055	1193.32	ISMLG	Si II	1193.2	L	9.0	0.00000	265.6	4.4
RBS2055	1197.19	ISMLG	Mn II	1197.1	L	2.0	0.00000	12.3	4.6
RBS2055	1199.32	ISMLG	N I	1199.5	L	-58.0	-0.00019	123.5	4.4
RBS2055	1199.56	ISMLG	N I	1199.5	L	4.0	0.00000	223.4	5.0
RBS2055	1200.00	ISMLG	N I	1200.2	L	-55.0	-0.00019	124.1	4.5
RBS2055	1200.23	ISMLG	N I	1200.2	L	1.0	0.00000	234.7	5.2
RBS2055	1200.48	ISMLG	N I	1200.7	L	-58.0	-0.00019	111.3	4.3
RBS2055	1200.72	ISMLG	N I	1200.7	L	3.0	0.00000	212.0	5.5
RBS2055	1201.10	ISMLG	Mn II	1201.1	L	-4.0	0.00000	16.2	5.3

Table A1 continued

Table A1 (*continued*)

Target	λ_{obs}	Type	Ion	λ_{rest}	Frame	cz	z	W_{λ}	$\sigma_{W_{\lambda}}$
	(Å)			(Å)		(km s ⁻¹)		(mÅ)	(mÅ)
RBS2055	1204.66	ISMLG	Si III	1206.5	L	-456.0	-0.00151	52.0	4.6
RBS2055	1204.85	ISMLG	Si III	1206.5	L	-410.0	-0.00136	139.1	4.1
RBS2055	1205.18	ISMLG	Si III	1206.5	L	-329.0	-0.00109	250.6	5.2
RBS2055	1205.39	ISMLG	Si III	1206.5	L	-275.0	-0.00092	53.4	5.4
RBS2055	1206.10	ISMLG	Si III	1206.5	L	-100.0	-0.00033	98.9	5.4
RBS2055	1206.27	ISMLG	Si III	1206.5	L	-57.0	-0.00019	168.6	2.7
RBS2055	1206.53	ISMLG	Si III	1206.5	L	8.0	0.00000	297.5	4.1
RBS2055	1222.28	IGMABS	H I	1215.6	H	1629.0	0.00543	91.3	9.0
RBS2055	1224.62	IGMABS	H I	1215.6	H	2207.0	0.00736	24.6	6.6
RBS2055	1238.83	ISMLG	N V	1238.8	L	3.0	0.00000	34.0	5.6
RBS2055	1248.31	IGMABS	H I	1215.6	H	8048.0	0.02685	38.8	4.9
RBS2055	1250.34	ISMLG	S II	1250.5	L	-58.0	-0.00019	35.0	3.1
RBS2055	1250.58	ISMLG	S II	1250.5	L	0.0	0.00000	110.1	2.8
RBS2055	1253.56	ISMLG	S II	1253.8	L	-58.0	-0.00019	40.5	2.2
RBS2055	1253.80	ISMLG	S II	1253.8	L	-1.0	0.00000	123.5	1.7
RBS2055	1258.72	ISMLG	Si II	1260.4	L	-405.0	-0.00136	34.7	1.9
RBS2055	1259.06	ISMLG	Si II	1260.4	L	-324.0	-0.00109	117.9	1.9
RBS2055	1259.28	ISMLG	S II	1259.5	L	-56.0	-0.00019	74.3	1.5
RBS2055	1259.50	ISMLG	S II	1259.5	L	-4.0	0.00000	139.4	1.2
RBS2055	1260.02	ISMLG	Si II	1260.4	L	-97.0	-0.00033	90.7	1.0
RBS2055	1260.17	ISMLG	Si II	1260.4	L	-60.0	-0.00019	184.3	0.7
RBS2055	1260.46	ISMLG	Si II	1260.4	L	9.0	0.00000	325.9	0.8
RBS2055	1260.75	ISMLG	C I	1260.7	L	3.0	0.00000	28.6	1.4
RBS2055	1261.49	INTRINSIC	H I	1215.6	H	11299.0	0.03769	85.3	2.1
RBS2055	1277.24	ISMLG	C I	1277.2	L	0.0	0.00000	62.1	5.9
RBS2055	1280.16	ISMLG	C I	1280.1	L	6.0	0.00000	26.5	6.1
RBS2055	1300.75	ISMLG	O I	1302.1	L	-327.0	-0.00109	28.5	5.2
RBS2055	1301.74	ISMLG	O I	1302.1	L	-99.0	-0.00033	85.7	3.7
RBS2055	1301.92	ISMLG	O I	1302.1	L	-56.0	-0.00019	141.7	2.6
RBS2055	1302.20	ISMLG	O I	1302.1	L	8.0	0.00000	285.5	3.9
RBS2055	1302.96	ISMLG	Si II	1304.3	L	-325.0	-0.00109	18.8	5.7
RBS2055	1303.96	ISMLG	Si II	1304.3	L	-95.0	-0.00033	34.7	4.2
RBS2055	1304.12	ISMLG	Si II	1304.3	L	-57.0	-0.00019	116.6	3.7
RBS2055	1304.40	ISMLG	Si II	1304.3	L	7.0	0.00000	259.7	4.1
RBS2055	1317.20	ISMLG	Ni II	1317.2	L	-4.0	0.00000	49.9	9.4
RBS2055	1328.85	ISMLG	C I	1328.8	L	5.0	0.00000	58.5	10.7
RBS2055	1332.72	ISMLG	C II	1334.5	L	-408.0	-0.00136	72.6	6.9
RBS2055	1333.07	ISMLG	C II	1334.5	L	-328.0	-0.00109	155.3	6.2
RBS2055	1333.32	ISMLG	C II	1334.5	L	-273.0	-0.00092	41.6	6.7
RBS2055	1334.09	ISMLG	C II	1334.5	L	-100.0	-0.00033	144.6	4.7
RBS2055	1334.27	ISMLG	C II	1334.5	L	-58.0	-0.00019	207.8	2.5
RBS2055	1334.56	ISMLG	C II	1334.5	L	7.0	0.00000	338.9	3.9
RBS2055	1335.45	ISMLG	C II*	1335.7	L	-58.0	-0.00019	38.2	6.0
RBS2055	1335.69	ISMLG	C II*	1335.7	L	-5.0	0.00000	160.0	6.4
RBS2055	1370.13	ISMLG	Ni II	1370.1	L	0.0	0.00000	48.3	6.5
RBS2055	1391.64	ISMLG	Si IV	1393.7	L	-456.0	-0.00151	27.4	6.1
RBS2055	1391.86	ISMLG	Si IV	1393.7	L	-408.0	-0.00136	44.8	8.0
RBS2055	1392.25	ISMLG	Si IV	1393.7	L	-325.0	-0.00109	89.2	7.9
RBS2055	1393.47	ISMLG	Si IV	1393.7	L	-62.0	-0.00019	43.2	6.6
RBS2055	1393.72	ISMLG	Si IV	1393.7	L	-8.0	0.00000	237.2	8.0
RBS2055	1400.65	ISMLG	Si IV	1402.7	L	-454.0	-0.00151	20.5	5.8
RBS2055	1401.25	ISMLG	Si IV	1402.7	L	-325.0	-0.00109	57.0	8.6
RBS2055	1402.75	ISMLG	Si IV	1402.7	L	-5.0	0.00000	193.9	9.6

Table A1 continued

Table A1 (*continued*)

Target	λ_{obs}	Type	Ion	λ_{rest}	Frame	cz	z	W_{λ}	$\sigma_{W_{\lambda}}$
	(Å)			(Å)		(km s ⁻¹)		(mÅ)	(mÅ)
RBS2055	1524.62	ISMLG	Si II	1526.7	L	-409.0	-0.00136	23.5	9.9
RBS2055	1525.05	ISMLG	Si II	1526.7	L	-325.0	-0.00109	37.7	8.5
RBS2055	1526.21	ISMLG	Si II	1526.7	L	-97.0	-0.00033	52.1	6.2
RBS2055	1526.42	ISMLG	Si II	1526.7	L	-57.0	-0.00019	169.4	5.8
RBS2055	1526.75	ISMLG	Si II	1526.7	L	8.0	0.00000	320.1	7.7
RBS2055	1545.87	ISMLG	C IV	1548.2	L	-451.0	-0.00151	28.3	6.3
RBS2055	1546.07	ISMLG	C IV	1548.2	L	-414.0	-0.00136	47.2	9.0
RBS2055	1546.48	ISMLG	C IV	1548.2	L	-334.0	-0.00109	178.3	10.0
RBS2055	1546.79	ISMLG	C IV	1548.2	L	-273.0	-0.00092	44.8	6.6
RBS2055	1547.89	ISMLG	C IV	1548.2	L	-61.0	-0.00019	43.8	8.5
RBS2055	1548.20	ISMLG	C IV	1548.2	L	0.0	0.00000	302.3	9.7
RBS2055	1548.68	ISMLG	C IV	1550.7	L	-407.0	-0.00136	50.5	9.8
RBS2055	1549.08	ISMLG	C IV	1550.7	L	-330.0	-0.00109	110.7	12.5
RBS2055	1549.34	ISMLG	C IV	1550.7	L	-279.0	-0.00092	28.2	7.9
RBS2055	1550.76	ISMLG	C IV	1550.7	L	-3.0	0.00000	220.3	11.1
RBS2055	1560.29	ISMLG	C I	1560.3	L	-4.0	0.00000	65.0	13.4
RBS2055	1608.14	ISMLG	Fe II	1608.4	L	-58.0	-0.00019	107.8	4.8
RBS2055	1608.41	ISMLG	Fe II	1608.4	L	-8.0	0.00000	306.4	4.6
RBS2055	1656.94	ISMLG	C I	1656.9	L	2.0	0.00000	121.3	14.6
RBS2055	1669.00	ISMLG	Al II	1670.7	L	-321.0	-0.00109	53.4	13.6
RBS2055	1670.26	ISMLG	Al II	1670.7	L	-95.0	-0.00033	75.6	10.6
RBS2055	1670.46	ISMLG	Al II	1670.7	L	-58.0	-0.00019	197.4	10.2
RBS2055	1670.83	ISMLG	Al II	1670.7	L	7.0	0.00000	365.5	12.8
RBS2055	1709.62	ISMLG	Ni II	1709.6	L	3.0	0.00000	38.5	13.4
RBS2055	1741.51	PROXIMATE	H I	1741.5	L	-8.0	0.00000	55.2	21.1
RXS_J0118.8+3836	1142.32	ISMLG	Fe II	1142.3	L	-11.0	-0.00003	81.4	29.3
RXS_J0118.8+3836	1143.18	ISMLG	Fe II	1143.2	L	-12.0	-0.00003	197.3	30.3
RXS_J0118.8+3836	1144.90	ISMLG	Fe II	1144.9	L	-10.0	-0.00003	324.6	25.2
RXS_J0118.8+3836	1152.77	ISMLG	P II	1152.8	L	-11.0	-0.00003	153.5	25.6
RXS_J0118.8+3836	1170.05	IGMABS	N II	1083.9	H	23799.0	0.07939	142.1	26.4
RXS_J0118.8+3836	1170.37	IGMABS	N II	1083.9	H	23888.0	0.07971	61.2	19.6
RXS_J0118.8+3836	1170.65	IGMABS	N II	1083.9	H	23965.0	0.07992	46.5	17.9
RXS_J0118.8+3836	1178.53	IGMABS	H I	1025.7	H	44662.0	0.14901	52.5	17.4
RXS_J0118.8+3836	1190.00	ISMLG	Si II	1190.4	L	-104.0	-0.00035	71.6	9.3
RXS_J0118.8+3836	1190.37	ISMLG	Si II	1190.4	L	-12.0	-0.00003	384.2	8.3
RXS_J0118.8+3836	1192.89	ISMLG	Si II	1193.2	L	-102.0	-0.00035	61.7	10.3
RXS_J0118.8+3836	1193.25	ISMLG	Si II	1193.2	L	-10.0	-0.00003	386.4	8.0
RXS_J0118.8+3836	1197.18	ISMLG	Mn II	1197.1	L	0.0	-0.00003	53.9	13.7
RXS_J0118.8+3836	1199.51	ISMLG	N I	1199.5	L	-10.0	-0.00003	376.4	11.8
RXS_J0118.8+3836	1200.19	ISMLG	N I	1200.2	L	-7.0	-0.00003	376.3	10.9
RXS_J0118.8+3836	1200.66	ISMLG	N I	1200.7	L	-12.0	-0.00003	368.8	11.9
RXS_J0118.8+3836	1205.45	ISMLG	Si III	1206.5	L	-261.0	-0.00087	87.5	9.0
RXS_J0118.8+3836	1205.60	ISMLG	Si III	1206.5	L	-224.0	-0.00075	39.1	8.3
RXS_J0118.8+3836	1206.08	ISMLG	Si III	1206.5	L	-103.0	-0.00035	115.2	10.6
RXS_J0118.8+3836	1206.45	ISMLG	Si III	1206.5	L	-12.0	-0.00003	352.7	8.9
RXS_J0118.8+3836	1207.72	IGMABS	H I	1025.7	H	53193.0	0.17741	117.4	22.3
RXS_J0118.8+3836	1221.70	IGMABS	O VI	1037.6	H	53187.0	0.17741	37.8	14.7
RXS_J0118.8+3836	1235.81	IGMABS	Fe II	1144.9	H	23795.0	0.07939	50.0	11.0
RXS_J0118.8+3836	1239.93	ISMLG	Mg II	1239.9	L	1.0	-0.00003	48.8	12.2
RXS_J0118.8+3836	1240.39	ISMLG	Mg II	1240.3	L	-2.0	-0.00003	24.7	8.6
RXS_J0118.8+3836	1243.03	IGMABS	H I	1215.6	H	6746.0	0.02250	31.0	10.3
RXS_J0118.8+3836	1245.23	IGMABS	H I	1215.6	H	7290.0	0.02432	335.8	12.2
RXS_J0118.8+3836	1247.51	IGMABS	H I	1215.6	H	7852.0	0.02619	166.2	12.9

Table A1 continued

Table A1 (*continued*)

Target	λ_{obs}	Type	Ion	λ_{rest}	Frame	cz	z	W_{λ}	$\sigma_{W_{\lambda}}$
	(Å)			(Å)		(km s ⁻¹)		(mÅ)	(mÅ)
RXS_J0118.8+3836	1250.57	ISMLG	S II	1250.5	L	-2.0	-0.00003	205.1	7.5
RXS_J0118.8+3836	1253.77	ISMLG	S II	1253.8	L	-7.0	-0.00003	269.3	6.8
RXS_J0118.8+3836	1256.30	IGMABS	H I	1215.6	H	10019.0	0.03342	29.8	8.0
RXS_J0118.8+3836	1256.72	IGMABS	H I	1215.6	H	10124.0	0.03377	22.8	7.6
RXS_J0118.8+3836	1259.47	ISMLG	S II	1259.5	L	-12.0	-0.00003	304.7	6.1
RXS_J0118.8+3836	1259.99	ISMLG	Si II	1260.4	L	-103.0	-0.00035	84.3	5.6
RXS_J0118.8+3836	1260.38	ISMLG	Si II	1260.4	L	-10.0	-0.00003	451.9	4.3
RXS_J0118.8+3836	1270.97	IGMABS	H I	1215.6	H	13637.0	0.04549	52.9	11.5
RXS_J0118.8+3836	1271.85	IGMABS	H I	1215.6	H	13855.0	0.04622	43.6	10.6
RXS_J0118.8+3836	1277.22	ISMLG	C I	1277.2	L	-6.0	-0.00003	72.9	12.7
RXS_J0118.8+3836	1279.73	IGMABS	H I	1215.6	H	15797.0	0.05269	55.4	19.4
RXS_J0118.8+3836	1284.93	IGMABS	Si II	1190.4	H	23802.0	0.07939	131.4	20.4
RXS_J0118.8+3836	1288.05	IGMABS	Si II	1193.2	H	23807.0	0.07939	166.6	16.6
RXS_J0118.8+3836	1288.41	IGMABS	Si II	1193.2	H	23898.0	0.07971	41.8	13.5
RXS_J0118.8+3836	1288.66	IGMABS	Si II	1193.2	H	23961.0	0.07992	59.2	15.7
RXS_J0118.8+3836	1302.12	ISMLG	O I	1302.1	L	-10.0	-0.00003	462.0	9.8
RXS_J0118.8+3836	1302.29	IGMABS	Si III	1206.5	H	23802.0	0.07939	88.3	8.0
RXS_J0118.8+3836	1302.68	IGMABS	Si III	1206.5	H	23898.0	0.07971	28.1	8.9
RXS_J0118.8+3836	1302.96	IGMABS	Si III	1206.5	H	23969.0	0.07992	196.7	23.0
RXS_J0118.8+3836	1304.32	ISMLG	Si II	1304.3	L	-11.0	-0.00003	353.9	9.7
RXS_J0118.8+3836	1311.60	IGMABS	H I	1215.6	H	23656.0	0.07891	38.2	13.7
RXS_J0118.8+3836	1312.19	IGMABS	H I	1215.6	H	23802.0	0.07939	860.0	14.2
RXS_J0118.8+3836	1312.57	IGMABS	H I	1215.6	H	23896.0	0.07971	825.9	10.6
RXS_J0118.8+3836	1312.83	IGMABS	H I	1215.6	H	23961.0	0.07992	1500.5	17.5
RXS_J0118.8+3836	1317.17	ISMLG	Ni II	1317.2	L	-10.0	-0.00003	75.1	20.8
RXS_J0118.8+3836	1333.35	ISMLG	C II	1334.5	L	-266.0	-0.00087	59.3	13.5
RXS_J0118.8+3836	1333.56	ISMLG	C II	1334.5	L	-219.0	-0.00075	49.7	11.5
RXS_J0118.8+3836	1334.05	ISMLG	C II	1334.5	L	-109.0	-0.00035	133.7	11.5
RXS_J0118.8+3836	1334.48	ISMLG	C II	1334.5	L	-12.0	-0.00003	481.5	10.9
RXS_J0118.8+3836	1335.69	ISMLG	C II*	1335.7	L	-4.0	-0.00003	227.6	12.8
RXS_J0118.8+3836	1337.06	IGMABS	H I	1215.6	H	29936.0	0.09986	34.8	16.7
RXS_J0118.8+3836	1359.48	IGMABS	H I	1215.6	H	35464.0	0.11829	32.8	18.1
RXS_J0118.8+3836	1360.51	IGMABS	Si II	1260.4	H	23805.0	0.07939	229.8	18.1
RXS_J0118.8+3836	1360.93	IGMABS	Si II	1260.4	H	23905.0	0.07971	52.0	11.3
RXS_J0118.8+3836	1361.16	IGMABS	Si II	1260.4	H	23960.0	0.07992	78.6	13.1
RXS_J0118.8+3836	1370.08	ISMLG	Ni II	1370.1	L	-11.0	-0.00003	98.0	14.8
RXS_J0118.8+3836	1393.71	ISMLG	Si IV	1393.7	L	-11.0	-0.00003	136.2	17.6
RXS_J0118.8+3836	1396.82	IGMABS	H I	1215.6	H	44672.0	0.14901	284.8	16.8
RXS_J0118.8+3836	1397.43	IGMABS	H I	1215.6	H	44823.0	0.14952	183.7	15.8
RXS_J0118.8+3836	1402.74	ISMLG	Si IV	1402.7	L	-7.0	-0.00003	61.9	20.1
RXS_J0118.8+3836	1405.53	IGMABS	O I	1302.1	H	23796.0	0.07939	78.6	18.2
RXS_J0118.8+3836	1407.89	IGMABS	Si II	1304.3	H	23794.0	0.07939	69.1	15.5
RXS_J0118.8+3836	1431.34	IGMABS	H I	1215.6	H	53185.0	0.17741	379.7	24.9
RXS_J0118.8+3836	1434.33	IGMABS	H I	1215.6	H	53924.0	0.17987	88.6	21.0
RXS_J0118.8+3836	1439.90	IGMABS	H I	1215.6	H	55297.0	0.18445	92.7	14.5
RXS_J0118.8+3836	1440.47	IGMABS	C II	1334.5	H	23798.0	0.07939	262.4	11.8
RXS_J0118.8+3836	1440.92	IGMABS	C II	1334.5	H	23899.0	0.07971	98.2	8.0
RXS_J0118.8+3836	1441.18	IGMABS	C II	1334.5	H	23957.0	0.07992	154.2	11.2
RXS_J0118.8+3836	1447.39	IGMABS	H I	1215.6	H	57144.0	0.19061	68.3	14.6
RXS_J0118.8+3836	1456.15	IGMABS	H I	1215.6	H	59304.0	0.19782	69.2	14.0
RXS_J0118.8+3836	1462.30	IGMABS	H I	1215.6	H	60821.0	0.20288	97.9	11.2
RXS_J0118.8+3836	1467.75	ISMLG	Ni II	1467.7	L	-1.0	-0.00003	16.9	11.2
RXS_J0118.8+3836	1504.38	IGMABS	Si IV	1393.7	H	23795.0	0.07939	176.0	13.8

Table A1 continued

Table A1 (*continued*)

Target	λ_{obs}	Type	Ion	λ_{rest}	Frame	cz	z	W_{λ}	$\sigma_{W_{\lambda}}$
	(Å)			(Å)		(km s ⁻¹)		(mÅ)	(mÅ)
RXS_J0118.8+3836	1514.14	IGMABS	Si iv	1402.7	H	23800.0	0.07939	109.6	15.5
RXS_J0118.8+3836	1526.20	ISMLG	Si ii	1526.7	L	-99.0	-0.00035	60.8	13.1
RXS_J0118.8+3836	1526.65	ISMLG	Si ii	1526.7	L	-11.0	-0.00003	425.6	10.0
RXS_J0118.8+3836	1548.16	ISMLG	C iv	1548.2	L	-9.0	-0.00003	161.7	19.2
RXS_J0118.8+3836	1550.72	ISMLG	C iv	1550.7	L	-11.0	-0.00003	117.7	23.7
RXS_J0118.8+3836	1560.24	ISMLG	C i	1560.3	L	-12.0	-0.00003	35.9	16.2
RXS_J0118.8+3836	1585.88	IGMABS	C iv	1548.2	H	7296.0	0.02432	68.7	29.7
RXS_J0118.8+3836	1608.43	ISMLG	Fe ii	1608.4	L	-5.0	-0.00003	327.4	41.0
RXS_J0118.8+3836	1647.95	IGMABS	Si ii	1526.7	H	23807.0	0.07939	117.2	34.6
RXS_J0118.8+3836	1656.92	ISMLG	C i	1656.9	L	-1.0	-0.00003	67.8	31.3
RXS_J0118.8+3836	1670.79	ISMLG	Al ii	1670.7	L	1.0	-0.00003	569.3	27.3
RXS_J0118.8+3836	1671.09	IGMABS	C iv	1548.2	H	23796.0	0.07939	322.0	23.6
RXS_J0118.8+3836	1673.84	IGMABS	C iv	1550.7	H	23790.0	0.07939	243.5	41.3
RXS_J0118.8+3836	1709.53	PROXIMATE	H i	1709.6	L	-14.0	-0.00003	85.0	30.9
RXS_J0155.6+3115	1134.95	ISMLG	N i	1134.9	L	-7.0	-0.00001	144.4	61.2
RXS_J0155.6+3115	1142.35	ISMLG	Fe ii	1142.3	L	-4.0	-0.00001	43.4	24.6
RXS_J0155.6+3115	1143.19	ISMLG	Fe ii	1143.2	L	-8.0	-0.00001	77.9	26.7
RXS_J0155.6+3115	1144.91	ISMLG	Fe ii	1144.9	L	-8.0	-0.00001	229.0	23.4
RXS_J0155.6+3115	1152.81	ISMLG	P ii	1152.8	L	-3.0	-0.00001	102.1	22.7
RXS_J0155.6+3115	1157.90	ISMLG	C i	1157.9	L	-3.0	-0.00001	35.8	15.1
RXS_J0155.6+3115	1160.50	PROXIMATE	H i	1025.7	H	39392.0	0.13139	201.3	12.7
RXS_J0155.6+3115	1160.65	PROXIMATE	H i	1025.7	H	39436.0	0.13154	131.6	12.6
RXS_J0155.6+3115	1161.87	PROXIMATE	H i	1025.7	H	39792.0	0.13271	135.7	12.2
RXS_J0155.6+3115	1162.08	PROXIMATE	H i	1025.7	H	39853.0	0.13292	81.9	11.2
RXS_J0155.6+3115	1163.92	PROXIMATE	O vi	1031.9	H	38348.0	0.12793	163.8	13.0
RXS_J0155.6+3115	1164.44	PROXIMATE	O vi	1031.9	H	38498.0	0.12844	168.9	17.9
RXS_J0155.6+3115	1166.89	PROXIMATE	O vi	1031.9	H	39208.0	0.13077	87.6	14.9
RXS_J0155.6+3115	1167.51	PROXIMATE	O vi	1031.9	H	39389.0	0.13139	247.9	9.2
RXS_J0155.6+3115	1167.68	PROXIMATE	O vi	1031.9	H	39438.0	0.13154	167.7	9.2
RXS_J0155.6+3115	1168.74	PROXIMATE	O vi	1031.9	H	39746.0	0.13258	221.1	6.2
RXS_J0155.6+3115	1168.87	PROXIMATE	O vi	1031.9	H	39783.0	0.13271	121.7	3.2
RXS_J0155.6+3115	1169.08	PROXIMATE	O vi	1031.9	H	39845.0	0.13292	249.5	8.6
RXS_J0155.6+3115	1170.35	PROXIMATE	O vi	1037.6	H	38351.0	0.12793	93.6	10.7
RXS_J0155.6+3115	1170.85	PROXIMATE	O vi	1037.6	H	38496.0	0.12844	77.9	12.5
RXS_J0155.6+3115	1173.96	PROXIMATE	O vi	1037.6	H	39394.0	0.13139	247.2	6.9
RXS_J0155.6+3115	1174.11	PROXIMATE	O vi	1037.6	H	39436.0	0.13154	134.8	5.6
RXS_J0155.6+3115	1175.18	PROXIMATE	O vi	1037.6	H	39746.0	0.13258	217.0	5.2
RXS_J0155.6+3115	1175.32	PROXIMATE	O vi	1037.6	H	39786.0	0.13271	144.0	3.7
RXS_J0155.6+3115	1175.52	PROXIMATE	O vi	1037.6	H	39844.0	0.13292	183.8	7.2
RXS_J0155.6+3115	1188.83	ISMLG	C i	1188.8	L	1.0	-0.00001	46.5	10.9
RXS_J0155.6+3115	1190.02	ISMLG	Si ii	1190.4	L	-100.0	-0.00034	121.7	8.7
RXS_J0155.6+3115	1190.39	ISMLG	Si ii	1190.4	L	-6.0	-0.00001	351.5	7.8
RXS_J0155.6+3115	1192.88	ISMLG	Si ii	1193.2	L	-103.0	-0.00034	122.6	8.6
RXS_J0155.6+3115	1193.26	ISMLG	Si ii	1193.2	L	-7.0	-0.00001	363.2	8.0
RXS_J0155.6+3115	1199.54	ISMLG	N i	1199.5	L	-3.0	-0.00001	294.2	19.0
RXS_J0155.6+3115	1200.20	ISMLG	N i	1200.2	L	-6.0	-0.00001	271.1	18.2
RXS_J0155.6+3115	1200.69	ISMLG	N i	1200.7	L	-4.0	-0.00001	268.9	21.4
RXS_J0155.6+3115	1205.72	ISMLG	Si iii	1206.5	L	-193.0	-0.00068	97.0	12.2
RXS_J0155.6+3115	1206.08	ISMLG	Si iii	1206.5	L	-104.0	-0.00034	192.9	8.1
RXS_J0155.6+3115	1206.47	ISMLG	Si iii	1206.5	L	-7.0	-0.00001	387.2	8.0
RXS_J0155.6+3115	1225.38	IGMABS	Si iii	1206.5	H	4690.0	0.01566	90.0	16.5
RXS_J0155.6+3115	1234.71	IGMABS	H i	1215.6	H	4696.0	0.01566	286.2	17.5
RXS_J0155.6+3115	1238.79	ISMLG	N v	1238.8	L	-7.0	-0.00001	57.8	14.7

Table A1 continued

Table A1 (*continued*)

Target	λ_{obs}	Type	Ion	λ_{rest}	Frame	cz	z	W_{λ}	$\sigma_{W_{\lambda}}$
	(Å)			(Å)		(km s ⁻¹)		(mÅ)	(mÅ)
RXS_J0155.6+3115	1239.94	ISMLG	Mg II	1239.9	L	4.0	-0.00001	22.5	10.4
RXS_J0155.6+3115	1245.26	IGMABS	H I	1215.6	H	7297.0	0.02434	78.8	16.6
RXS_J0155.6+3115	1250.56	ISMLG	S II	1250.5	L	-3.0	-0.00001	120.9	11.2
RXS_J0155.6+3115	1253.80	ISMLG	S II	1253.8	L	-1.0	-0.00001	188.8	12.2
RXS_J0155.6+3115	1255.37	IGMABS	H I	1215.6	H	9791.0	0.03266	601.2	15.7
RXS_J0155.6+3115	1259.49	ISMLG	S II	1259.5	L	-6.0	-0.00001	194.0	9.2
RXS_J0155.6+3115	1259.98	ISMLG	Si II	1260.4	L	-104.0	-0.00034	190.3	8.7
RXS_J0155.6+3115	1260.39	ISMLG	Si II	1260.4	L	-8.0	-0.00001	434.0	7.3
RXS_J0155.6+3115	1260.74	ISMLG	C I	1260.7	L	1.0	-0.00001	56.0	9.7
RXS_J0155.6+3115	1261.28	IGMABS	H I	1215.6	H	11248.0	0.03752	107.2	15.7
RXS_J0155.6+3115	1268.30	IGMABS	H I	1215.6	H	12978.0	0.04329	66.8	11.3
RXS_J0155.6+3115	1277.24	ISMLG	C I	1277.2	L	0.0	-0.00001	58.9	12.6
RXS_J0155.6+3115	1280.13	ISMLG	C I	1280.1	L	-2.0	-0.00001	40.9	15.1
RXS_J0155.6+3115	1301.69	ISMLG	O I	1302.1	L	-111.0	-0.00034	160.1	22.5
RXS_J0155.6+3115	1302.14	ISMLG	O I	1302.1	L	-6.0	-0.00001	392.8	20.0
RXS_J0155.6+3115	1303.92	ISMLG	Si II	1304.3	L	-104.0	-0.00034	78.6	22.6
RXS_J0155.6+3115	1304.34	ISMLG	Si II	1304.3	L	-8.0	-0.00001	287.3	18.9
RXS_J0155.6+3115	1306.18	IGMABS	H I	1215.6	H	22320.0	0.07445	156.5	28.6
RXS_J0155.6+3115	1317.18	ISMLG	Ni II	1317.2	L	-8.0	-0.00001	44.7	19.7
RXS_J0155.6+3115	1328.80	ISMLG	C I	1328.8	L	-8.0	-0.00001	80.7	17.5
RXS_J0155.6+3115	1330.83	IGMABS	H I	1215.6	H	28400.0	0.09473	235.4	22.1
RXS_J0155.6+3115	1334.06	ISMLG	C II	1334.5	L	-105.0	-0.00034	261.7	8.1
RXS_J0155.6+3115	1334.50	ISMLG	C II	1334.5	L	-7.0	-0.00001	413.0	7.4
RXS_J0155.6+3115	1335.70	ISMLG	C II*	1335.7	L	-1.0	-0.00001	200.9	12.1
RXS_J0155.6+3115	1342.48	IGMABS	H I	1215.6	H	31271.0	0.10431	175.6	17.6
RXS_J0155.6+3115	1344.58	IGMABS	H I	1215.6	H	31790.0	0.10604	300.2	16.4
RXS_J0155.6+3115	1347.22	ISMLG	Cl I	1347.2	L	-3.0	-0.00001	18.5	10.0
RXS_J0155.6+3115	1353.24	IGMABS	H I	1215.6	H	33925.0	0.11316	70.3	11.0
RXS_J0155.6+3115	1358.16	IGMABS	H I	1215.6	H	35138.0	0.11721	35.1	11.3
RXS_J0155.6+3115	1363.27	IGMABS	H I	1215.6	H	36398.0	0.12141	63.9	10.3
RXS_J0155.6+3115	1366.87	PROXIMATE	Si III	1206.5	H	39849.0	0.13292	56.8	9.4
RXS_J0155.6+3115	1370.12	ISMLG	Ni II	1370.1	L	-3.0	-0.00001	57.4	6.1
RXS_J0155.6+3115	1371.19	PROXIMATE	H I	1215.6	H	38354.0	0.12793	147.4	6.5
RXS_J0155.6+3115	1371.81	PROXIMATE	H I	1215.6	H	38505.0	0.12844	57.0	6.6
RXS_J0155.6+3115	1373.27	PROXIMATE	H I	1215.6	H	38864.0	0.12964	13.2	3.7
RXS_J0155.6+3115	1374.65	PROXIMATE	H I	1215.6	H	39205.0	0.13077	33.1	4.6
RXS_J0155.6+3115	1375.40	PROXIMATE	H I	1215.6	H	39390.0	0.13139	287.2	3.2
RXS_J0155.6+3115	1375.58	PROXIMATE	H I	1215.6	H	39435.0	0.13154	233.7	3.6
RXS_J0155.6+3115	1376.84	PROXIMATE	H I	1215.6	H	39746.0	0.13258	187.8	2.2
RXS_J0155.6+3115	1377.00	PROXIMATE	H I	1215.6	H	39786.0	0.13271	312.5	3.2
RXS_J0155.6+3115	1377.26	PROXIMATE	H I	1215.6	H	39849.0	0.13292	392.6	3.1
RXS_J0155.6+3115	1393.72	ISMLG	Si IV	1393.7	L	-8.0	-0.00001	154.8	12.3
RXS_J0155.6+3115	1397.30	PROXIMATE	N V	1238.8	H	38351.0	0.12793	99.0	12.9
RXS_J0155.6+3115	1397.92	PROXIMATE	N V	1238.8	H	38501.0	0.12844	38.1	12.9
RXS_J0155.6+3115	1401.60	PROXIMATE	N V	1238.8	H	39391.0	0.13139	129.3	6.0
RXS_J0155.6+3115	1401.78	PROXIMATE	N V	1238.8	H	39436.0	0.13154	139.4	5.6
RXS_J0155.6+3115	1401.78	PROXIMATE	N V	1242.8	H	38349.0	0.12793	139.4	5.6
RXS_J0155.6+3115	1402.40	PROXIMATE	N V	1242.8	H	38498.0	0.12844	29.3	7.7
RXS_J0155.6+3115	1402.73	ISMLG	Si IV	1402.7	L	-9.0	-0.00001	119.8	11.2
RXS_J0155.6+3115	1403.24	PROXIMATE	N V	1238.8	H	39789.0	0.13271	181.5	7.9
RXS_J0155.6+3115	1403.51	PROXIMATE	N V	1238.8	H	39853.0	0.13292	90.7	9.4
RXS_J0155.6+3115	1406.09	PROXIMATE	N V	1242.8	H	39389.0	0.13139	113.3	7.1
RXS_J0155.6+3115	1406.29	PROXIMATE	N V	1242.8	H	39436.0	0.13154	136.8	7.5

Table A1 continued

Table A1 (*continued*)

Target	λ_{obs}	Type	Ion	λ_{rest}	Frame	cz	z	W_{λ}	$\sigma_{W_{\lambda}}$
	(Å)			(Å)		(km s ⁻¹)		(mÅ)	(mÅ)
RXS_J0155.6+3115	1407.76	PROXIMATE	N v	1242.8	H	39792.0	0.13271	109.3	9.2
RXS_J0155.6+3115	1408.01	PROXIMATE	N v	1242.8	H	39851.0	0.13292	58.8	10.2
RXS_J0155.6+3115	1415.70	ISMLG	Ni II	1415.7	L	-3.0	-0.00001	49.6	13.7
RXS_J0155.6+3115	1526.17	ISMLG	Si II	1526.7	L	-106.0	-0.00034	71.7	20.4
RXS_J0155.6+3115	1526.66	ISMLG	Si II	1526.7	L	-9.0	-0.00001	424.3	18.9
RXS_J0155.6+3115	1547.17	ISMLG	C IV	1548.2	L	-200.0	-0.00068	210.4	22.7
RXS_J0155.6+3115	1547.65	ISMLG	C IV	1548.2	L	-107.0	-0.00034	64.7	20.3
RXS_J0155.6+3115	1548.16	ISMLG	C IV	1548.2	L	-9.0	-0.00001	198.6	22.3
RXS_J0155.6+3115	1549.74	ISMLG	C IV	1550.7	L	-200.0	-0.00068	127.4	23.7
RXS_J0155.6+3115	1550.79	ISMLG	C IV	1550.7	L	1.0	-0.00001	100.9	23.1
RXS_J0155.6+3115	1560.33	ISMLG	C I	1560.3	L	4.0	-0.00001	113.3	20.0
RXS_J0155.6+3115	1608.42	ISMLG	Fe II	1608.4	L	-6.0	-0.00001	299.3	38.4
RXS_J0155.6+3115	1656.95	ISMLG	C I	1656.9	L	4.0	-0.00001	141.6	33.3
RXS_J0155.6+3115	1670.22	ISMLG	Al II	1670.7	L	-103.0	-0.00034	105.5	36.1
RXS_J0155.6+3115	1670.75	ISMLG	Al II	1670.7	L	-8.0	-0.00001	470.1	34.7
RXS_J0155.6+3115	1741.55	ISMLG	Ni II	1741.5	L	-1.0	-0.00001	80.3	29.8
RXS_J0155.6+3115	1746.28	PROXIMATE	C IV	1548.2	H	38355.0	0.12793	88.6	24.7
RXS_J0155.6+3115	1749.21	PROXIMATE	C IV	1550.7	H	38359.0	0.12793	80.4	20.0
RXS_J0155.6+3115	1751.62	PROXIMATE	C IV	1548.2	H	39390.0	0.13139	198.0	11.9
RXS_J0155.6+3115	1751.88	PROXIMATE	C IV	1548.2	H	39439.0	0.13154	199.0	15.2
RXS_J0155.6+3115	1753.72	PROXIMATE	C IV	1548.2	H	39795.0	0.13271	238.9	13.6
RXS_J0155.6+3115	1754.02	PROXIMATE	C IV	1548.2	H	39854.0	0.13292	255.6	11.2
RXS_J0155.6+3115	1754.54	PROXIMATE	C IV	1550.7	H	39390.0	0.13139	195.8	10.6
RXS_J0155.6+3115	1754.79	PROXIMATE	C IV	1550.7	H	39438.0	0.13154	128.7	10.2
RXS_J0155.6+3115	1756.63	PROXIMATE	C IV	1550.7	H	39794.0	0.13271	154.8	10.2
RXS_J0155.6+3115	1756.89	PROXIMATE	H I	1550.7	H	39845.0	0.13292	200.2	12.4
RX_J0023.5+1547	1185.89	IGMABS	H I	1025.7	H	46813.0	0.15615	134.0	47.4
RX_J0023.5+1547	1190.39	ISMLG	Si II	1190.4	L	-7.0	-0.00002	341.0	36.8
RX_J0023.5+1547	1192.89	ISMLG	Si II	1193.2	L	-101.0	-0.00034	100.8	26.4
RX_J0023.5+1547	1193.26	ISMLG	Si II	1193.2	L	-8.0	-0.00002	404.9	30.3
RX_J0023.5+1547	1205.06	ISMLG	Si III	1206.5	L	-357.0	-0.00119	293.6	58.3
RX_J0023.5+1547	1206.08	ISMLG	Si III	1206.5	L	-103.0	-0.00034	190.0	29.8
RX_J0023.5+1547	1206.50	ISMLG	Si III	1206.5	L	-1.0	-0.00002	464.2	30.7
RX_J0023.5+1547	1237.08	IGMABS	H I	1215.6	H	5279.0	0.01761	532.7	39.3
RX_J0023.5+1547	1237.35	IGMABS	H I	1215.6	H	5346.0	0.01783	136.6	24.0
RX_J0023.5+1547	1250.54	ISMLG	S II	1250.5	L	-9.0	-0.00002	121.9	33.9
RX_J0023.5+1547	1253.77	ISMLG	S II	1253.8	L	-9.0	-0.00002	171.2	32.8
RX_J0023.5+1547	1259.50	ISMLG	S II	1259.5	L	-4.0	-0.00002	177.4	25.9
RX_J0023.5+1547	1259.99	ISMLG	Si II	1260.4	L	-102.0	-0.00034	170.1	17.2
RX_J0023.5+1547	1260.38	ISMLG	Si II	1260.4	L	-10.0	-0.00002	455.3	19.2
RX_J0023.5+1547	1260.73	ISMLG	C I	1260.7	L	-2.0	-0.00002	92.4	19.5
RX_J0023.5+1547	1277.26	ISMLG	C I	1277.2	L	3.0	-0.00002	65.2	23.5
RX_J0023.5+1547	1280.10	ISMLG	C I	1280.1	L	-8.0	-0.00002	35.5	29.1
RX_J0023.5+1547	1314.78	IGMABS	H I	1215.6	H	24442.0	0.08153	780.4	51.0
RX_J0023.5+1547	1334.10	ISMLG	C II	1334.5	L	-96.0	-0.00034	172.5	19.8
RX_J0023.5+1547	1334.51	ISMLG	C II	1334.5	L	-5.0	-0.00002	537.9	29.0
RX_J0023.5+1547	1335.71	ISMLG	C II*	1335.7	L	1.0	-0.00002	108.9	29.4
RX_J0023.5+1547	1392.00	IGMABS	H I	1215.6	H	43485.0	0.14505	117.8	35.4
RX_J0023.5+1547	1393.76	ISMLG	Si IV	1393.7	L	-1.0	-0.00002	120.5	30.6
RX_J0023.5+1547	1402.21	IGMABS	H I	1215.6	H	46003.0	0.15345	129.1	31.5
RX_J0023.5+1547	1402.76	ISMLG	Si IV	1402.7	L	-3.0	-0.00002	147.4	31.1
RX_J0023.5+1547	1404.97	IGMABS	H I	1215.6	H	46682.0	0.15572	75.2	21.8
RX_J0023.5+1547	1404.97	IGMABS	H I	1215.6	H	46682.0	0.15572	75.2	21.8

Table A1 continued

Table A1 (*continued*)

Target	λ_{obs}	Type	Ion	λ_{rest}	Frame	cz	z	W_{λ}	$\sigma_{W_{\lambda}}$
	(Å)			(Å)		(km s ⁻¹)		(mÅ)	(mÅ)
RX_J0023.5+1547	1405.06	IGMABS	H I	1215.6	H	46706.0	0.15579	80.0	17.6
RX_J0023.5+1547	1405.06	IGMABS	H I	1215.6	H	46706.0	0.15579	80.0	17.6
RX_J0023.5+1547	1405.50	IGMABS	H I	1215.6	H	46814.0	0.15615	404.4	26.5
RX_J0023.5+1547	1426.53	IGMABS	H I	1215.6	H	51999.0	0.17345	115.5	37.8
RX_J0023.5+1547	1432.01	IGMABS	H I	1215.6	H	53351.0	0.17796	68.0	35.4
RX_J0023.5+1547	1435.70	IGMABS	H I	1215.6	H	54261.0	0.18099	128.4	38.4
RX_J0023.5+1547	1441.91	IGMABS	H I	1215.6	H	55793.0	0.18611	178.5	38.8
RX_J0023.5+1547	1442.62	PROXIMATE	H I	1215.6	H	55968.0	0.18669	349.7	43.6
RX_J0028.1+3103	1138.56	IGMABS	H I	1025.7	H	32981.0	0.11003	315.3	32.7
RX_J0028.1+3103	1142.35	ISMLG	Fe II	1142.3	L	-4.0	0.00001	93.6	24.3
RX_J0028.1+3103	1143.23	ISMLG	Fe II	1143.2	L	0.0	0.00001	188.3	26.4
RX_J0028.1+3103	1143.47	PROXIMATE	N III	763.3	H	149290.0	0.49798	122.7	12.5
RX_J0028.1+3103	1143.65	PROXIMATE	N III	763.3	H	149362.0	0.49822	138.7	14.0
RX_J0028.1+3103	1143.94	INTRINSIC	N III	763.3	H	149477.0	0.49861	168.4	20.7
RX_J0028.1+3103	1144.69	ISMLG	Fe II	1144.9	L	-64.0	-0.00021	72.8	14.3
RX_J0028.1+3103	1144.97	ISMLG	Fe II	1144.9	L	8.0	0.00001	231.6	16.9
RX_J0028.1+3103	1145.44	IGMABS	O VI	1031.9	H	32979.0	0.11003	147.0	16.9
RX_J0028.1+3103	1146.16	PROXIMATE	N IV	765.1	H	149286.0	0.49798	334.4	11.3
RX_J0028.1+3103	1146.36	PROXIMATE	N IV	765.1	H	149363.0	0.49822	343.1	10.3
RX_J0028.1+3103	1146.67	INTRINSIC	N IV	765.1	H	149485.0	0.49861	442.4	14.4
RX_J0028.1+3103	1151.80	IGMABS	O VI	1037.6	H	32991.0	0.11003	82.4	21.3
RX_J0028.1+3103	1152.85	ISMLG	P II	1152.8	L	8.0	0.00001	100.3	20.1
RX_J0028.1+3103	1154.25	PROXIMATE	Ne VIII	770.4	H	149367.0	0.49822	253.6	16.7
RX_J0028.1+3103	1154.54	INTRINSIC	Ne VIII	770.4	H	149480.0	0.49861	207.2	19.2
RX_J0028.1+3103	1160.22	IGMABS	O IV	787.7	H	141771.0	0.47289	39.6	14.6
RX_J0028.1+3103	1169.11	PROXIMATE	Ne VIII	780.3	H	149366.0	0.49822	149.4	20.6
RX_J0028.1+3103	1169.40	INTRINSIC	Ne VIII	780.3	H	149478.0	0.49861	83.7	19.8
RX_J0028.1+3103	1169.40	IGMABS	C III	977.0	H	59030.0	0.19691	83.7	19.8
RX_J0028.1+3103	1169.77	IGMABS	O VI	1031.9	H	40045.0	0.13356	63.4	18.8
RX_J0028.1+3103	1178.13	UNIDENTIFIED	UNIND	1000.0	H	0.0	-1.00000	166.6	8.9
RX_J0028.1+3103	1178.39	PROXIMATE	SV	786.6	H	149294.0	0.49798	457.6	16.2
RX_J0028.1+3103	1178.58	PROXIMATE	SV	786.6	H	149366.0	0.49822	176.7	10.4
RX_J0028.1+3103	1179.23	PROXIMATE	O IV	787.7	H	149007.0	0.49704	126.7	14.2
RX_J0028.1+3103	1179.95	PROXIMATE	O IV	787.7	H	149283.0	0.49798	372.6	8.3
RX_J0028.1+3103	1180.15	PROXIMATE	O IV	787.7	H	149357.0	0.49822	500.3	5.8
RX_J0028.1+3103	1180.48	INTRINSIC	O IV	787.7	H	149485.0	0.49861	440.4	7.4
RX_J0028.1+3103	1188.85	ISMLG	C I	1188.8	L	4.0	0.00001	29.8	10.7
RX_J0028.1+3103	1189.96	ISMLG	Si II	1190.4	L	-115.0	-0.00038	39.9	8.8
RX_J0028.1+3103	1190.16	ISMLG	Si II	1190.4	L	-65.0	-0.00021	123.1	6.4
RX_J0028.1+3103	1190.45	ISMLG	Si II	1190.4	L	9.0	0.00001	301.3	8.0
RX_J0028.1+3103	1192.82	ISMLG	Si II	1193.2	L	-118.0	-0.00038	42.1	9.3
RX_J0028.1+3103	1193.01	ISMLG	Si II	1193.2	L	-69.0	-0.00021	152.0	7.8
RX_J0028.1+3103	1193.33	ISMLG	Si II	1193.2	L	11.0	0.00001	313.0	8.1
RX_J0028.1+3103	1195.47	UNIDENTIFIED	UNIND	1000.0	H	0.0	-1.00000	75.1	15.5
RX_J0028.1+3103	1197.21	ISMLG	Mn II	1197.1	L	8.0	0.00001	55.8	12.9
RX_J0028.1+3103	1199.53	ISMLG	N I	1199.5	L	-4.0	0.00001	346.3	21.1
RX_J0028.1+3103	1200.21	ISMLG	N I	1200.2	L	-4.0	0.00001	330.4	18.8
RX_J0028.1+3103	1200.70	ISMLG	N I	1200.7	L	-3.0	0.00001	303.2	15.9
RX_J0028.1+3103	1205.06	ISMLG	Si III	1206.5	L	-358.0	-0.00123	44.1	10.6
RX_J0028.1+3103	1205.35	ISMLG	Si III	1206.5	L	-285.0	-0.00094	214.3	11.2
RX_J0028.1+3103	1206.07	ISMLG	Si III	1206.5	L	-106.0	-0.00038	93.4	10.3
RX_J0028.1+3103	1206.23	ISMLG	Si III	1206.5	L	-66.0	-0.00021	171.3	6.3
RX_J0028.1+3103	1206.53	ISMLG	Si III	1206.5	L	6.0	0.00001	352.7	8.9

Table A1 continued

Table A1 (*continued*)

Target	λ_{obs}	Type	Ion	λ_{rest}	Frame	cz	z	W_{λ}	$\sigma_{W_{\lambda}}$
	(Å)			(Å)		(km s ⁻¹)		(mÅ)	(mÅ)
RX_J0028.1+3103	1222.44	IGMABS	H I	1025.7	H	57496.0	0.19178	33.3	12.5
RX_J0028.1+3103	1222.93	IGMABS	H I	1215.6	H	1790.0	0.00597	39.2	12.0
RX_J0028.1+3103	1239.91	ISMLG	Mg II	1239.9	L	-4.0	0.00001	131.6	8.4
RX_J0028.1+3103	1240.26	IGMABS	H I	1215.6	H	6063.0	0.02022	407.4	8.1
RX_J0028.1+3103	1240.93	IGMABS	H I	1215.6	H	6228.0	0.02078	430.5	6.9
RX_J0028.1+3103	1241.39	IGMABS	H I	1215.6	H	6342.0	0.02116	480.5	6.9
RX_J0028.1+3103	1241.82	IGMABS	H I	1215.6	H	6449.0	0.02151	92.5	7.0
RX_J0028.1+3103	1246.92	PROXIMATE	O III	832.9	H	149005.0	0.49704	159.2	12.1
RX_J0028.1+3103	1247.69	PROXIMATE	O III	832.9	H	149283.0	0.49798	241.5	7.1
RX_J0028.1+3103	1247.89	PROXIMATE	O III	832.9	H	149357.0	0.49822	418.4	7.8
RX_J0028.1+3103	1248.24	INTRINSIC	O III	832.9	H	149484.0	0.49861	284.6	6.3
RX_J0028.1+3103	1248.83	INTRINSIC	O II	833.3	H	149479.0	0.49861	94.7	12.1
RX_J0028.1+3103	1250.54	INTRINSIC	O II	834.4	H	149478.0	0.49861	126.8	6.0
RX_J0028.1+3103	1250.58	ISMLG	S II	1250.5	L	1.0	0.00001	169.4	8.7
RX_J0028.1+3103	1253.45	IGMABS	H I	1215.6	H	9317.0	0.03108	384.9	8.8
RX_J0028.1+3103	1253.79	ISMLG	S II	1253.8	L	-5.0	0.00001	250.1	7.7
RX_J0028.1+3103	1255.54	IGMABS	H I	949.7	H	96527.0	0.32195	40.6	10.1
RX_J0028.1+3103	1259.23	ISMLG	S II	1259.5	L	-67.0	-0.00021	60.1	6.3
RX_J0028.1+3103	1259.49	ISMLG	S II	1259.5	L	-6.0	0.00001	243.1	7.7
RX_J0028.1+3103	1259.94	ISMLG	Si II	1260.4	L	-114.0	-0.00038	94.0	7.6
RX_J0028.1+3103	1260.16	ISMLG	Si II	1260.4	L	-62.0	-0.00021	177.2	4.6
RX_J0028.1+3103	1260.46	ISMLG	Si II	1260.4	L	9.0	0.00001	375.5	5.4
RX_J0028.1+3103	1260.71	ISMLG	C I	1260.7	L	-6.0	0.00001	146.8	8.2
RX_J0028.1+3103	1277.30	ISMLG	C I	1277.2	L	12.0	0.00001	66.9	14.4
RX_J0028.1+3103	1280.18	ISMLG	C I	1280.1	L	10.0	0.00001	66.0	15.2
RX_J0028.1+3103	1285.65	IGMABS	H I	972.5	H	96519.0	0.32195	111.8	14.0
RX_J0028.1+3103	1285.92	IGMABS	H I	1215.6	H	17324.0	0.05779	73.9	14.4
RX_J0028.1+3103	1293.96	IGMABS	H I	1025.7	H	78399.0	0.26152	105.3	15.0
RX_J0028.1+3103	1296.03	IGMABS	H I	1215.6	H	19816.0	0.06610	247.8	22.5
RX_J0028.1+3103	1301.67	ISMLG	O I	1302.1	L	-115.0	-0.00038	81.0	13.5
RX_J0028.1+3103	1301.75	IGMABS	H I	1025.7	H	80677.0	0.26910	81.0	13.5
RX_J0028.1+3103	1301.88	ISMLG	O I	1302.1	L	-66.0	-0.00021	151.8	7.9
RX_J0028.1+3103	1302.20	ISMLG	O I	1302.1	L	8.0	0.00001	350.9	11.2
RX_J0028.1+3103	1304.08	ISMLG	Si II	1304.3	L	-68.0	-0.00021	63.5	10.9
RX_J0028.1+3103	1304.42	ISMLG	Si II	1304.3	L	12.0	0.00001	326.5	11.1
RX_J0028.1+3103	1305.32	IGMABS	H I	1215.6	H	22108.0	0.07374	97.5	15.5
RX_J0028.1+3103	1305.71	IGMABS	H I	1215.6	H	22205.0	0.07407	388.0	11.5
RX_J0028.1+3103	1312.28	IGMABS	H I	1215.6	H	23824.0	0.07947	97.2	17.8
RX_J0028.1+3103	1317.20	ISMLG	Ni II	1317.2	L	-4.0	0.00001	53.9	15.9
RX_J0028.1+3103	1328.87	ISMLG	C I	1328.8	L	9.0	0.00001	67.0	14.8
RX_J0028.1+3103	1330.51	IGMABS	H I	1025.7	H	89081.0	0.29717	136.7	18.7
RX_J0028.1+3103	1333.25	ISMLG	C II	1334.5	L	-288.0	-0.00094	93.8	11.1
RX_J0028.1+3103	1334.04	ISMLG	C II	1334.5	L	-110.0	-0.00038	118.9	9.3
RX_J0028.1+3103	1334.24	ISMLG	C II	1334.5	L	-66.0	-0.00021	190.0	5.4
RX_J0028.1+3103	1334.58	ISMLG	C II	1334.5	L	12.0	0.00001	375.3	8.4
RX_J0028.1+3103	1335.74	ISMLG	C II*	1335.7	L	7.0	0.00001	171.9	9.4
RX_J0028.1+3103	1336.87	IGMABS	H I	1215.6	H	29889.0	0.09970	103.9	13.1
RX_J0028.1+3103	1339.27	IGMABS	Si III	1206.5	H	32991.0	0.11003	74.7	12.4
RX_J0028.1+3103	1339.97	IGMABS	H I	923.1	H	135364.0	0.45151	34.3	9.4
RX_J0028.1+3103	1344.45	IGMABS	H I	926.2	H	135367.0	0.45151	44.4	14.5
RX_J0028.1+3103	1347.27	ISMLG	Cl I	1347.2	L	8.0	0.00001	45.9	12.3
RX_J0028.1+3103	1349.43	IGMABS	H I	1215.6	H	32986.0	0.11003	523.3	15.4
RX_J0028.1+3103	1350.97	IGMABS	H I	930.7	H	135352.0	0.45151	68.1	11.0

Table A1 continued

Table A1 (*continued*)

Target	λ_{obs}	Type	Ion	λ_{rest}	Frame	cz	z	W_{λ}	$\sigma_{W_{\lambda}}$
	(Å)			(Å)		(km s ⁻¹)		(mÅ)	(mÅ)
RX_J0028.1+3103	1353.62	PROXIMATE	C II	903.6	H	149295.0	0.49798	35.0	9.1
RX_J0028.1+3103	1353.84	PROXIMATE	C II	903.6	H	149368.0	0.49822	50.0	8.0
RX_J0028.1+3103	1354.10	PROXIMATE	C II	903.9	H	149285.0	0.49798	64.9	6.6
RX_J0028.1+3103	1354.17	INTRINSIC	C II	903.6	H	149476.0	0.49861	188.7	13.5
RX_J0028.1+3103	1354.34	PROXIMATE	C II	903.9	H	149365.0	0.49822	73.6	8.1
RX_J0028.1+3103	1354.70	INTRINSIC	C II	903.9	H	149484.0	0.49861	198.0	13.2
RX_J0028.1+3103	1355.97	IGMABS	H I	1025.7	H	96524.0	0.32195	236.2	13.8
RX_J0028.1+3103	1361.25	IGMABS	H I	937.8	H	135366.0	0.45151	111.4	16.1
RX_J0028.1+3103	1365.73	IGMABS	H I	1215.6	H	37007.0	0.12344	168.0	16.9
RX_J0028.1+3103	1370.17	ISMLG	Ni II	1370.1	L	9.0	0.00001	68.4	12.1
RX_J0028.1+3103	1370.59	INTRINSIC	H I	914.5	H	149478.0	0.49861	22.5	8.5
RX_J0028.1+3103	1371.11	INTRINSIC	H I	914.9	H	149481.0	0.49861	25.4	10.0
RX_J0028.1+3103	1371.73	INTRINSIC	H I	915.3	H	149483.0	0.49861	40.8	9.5
RX_J0028.1+3103	1372.16	IGMABS	H I	1215.6	H	38592.0	0.12873	51.6	10.1
RX_J0028.1+3103	1372.47	INTRINSIC	H I	915.8	H	149481.0	0.49861	52.9	9.9
RX_J0028.1+3103	1373.38	INTRINSIC	H I	916.4	H	149482.0	0.49861	64.7	11.9
RX_J0028.1+3103	1374.49	INTRINSIC	H I	917.1	H	149478.0	0.49861	93.0	12.6
RX_J0028.1+3103	1375.92	INTRINSIC	H I	918.1	H	149479.0	0.49861	77.7	9.2
RX_J0028.1+3103	1377.39	PROXIMATE	H I	919.3	H	149363.0	0.49822	28.9	9.2
RX_J0028.1+3103	1377.76	INTRINSIC	H I	919.3	H	149482.0	0.49861	82.4	11.0
RX_J0028.1+3103	1378.03	IGMABS	H I	1215.6	H	40040.0	0.13356	63.9	11.3
RX_J0028.1+3103	1378.58	IGMABS	H I	949.7	H	135364.0	0.45151	149.5	11.6
RX_J0028.1+3103	1379.15	IGMABS	H I	1215.6	H	40316.0	0.13448	35.9	9.3
RX_J0028.1+3103	1379.58	PROXIMATE	H I	920.9	H	149288.0	0.49798	40.9	9.0
RX_J0028.1+3103	1379.81	PROXIMATE	H I	920.9	H	149365.0	0.49822	33.6	7.8
RX_J0028.1+3103	1380.16	INTRINSIC	H I	920.9	H	149478.0	0.49861	104.8	10.0
RX_J0028.1+3103	1381.28	IGMABS	H I	937.8	H	141768.0	0.47289	35.9	9.2
RX_J0028.1+3103	1381.99	PROXIMATE	H I	923.1	H	149009.0	0.49704	32.2	8.0
RX_J0028.1+3103	1382.88	PROXIMATE	H I	923.1	H	149295.0	0.49798	33.8	7.3
RX_J0028.1+3103	1383.07	PROXIMATE	H I	923.1	H	149360.0	0.49822	60.3	8.9
RX_J0028.1+3103	1383.44	INTRINSIC	H I	923.1	H	149480.0	0.49861	136.1	10.7
RX_J0028.1+3103	1386.60	PROXIMATE	H I	926.2	H	149009.0	0.49704	100.2	12.7
RX_J0028.1+3103	1387.47	PROXIMATE	H I	926.2	H	149293.0	0.49798	89.8	9.5
RX_J0028.1+3103	1387.70	PROXIMATE	H I	926.2	H	149365.0	0.49822	78.7	8.7
RX_J0028.1+3103	1388.05	INTRINSIC	H I	926.2	H	149479.0	0.49861	159.2	11.6
RX_J0028.1+3103	1392.49	ISMLG	Si IV	1393.7	L	-274.0	-0.00094	64.3	11.0
RX_J0028.1+3103	1393.39	PROXIMATE	H I	930.7	H	149015.0	0.49704	188.1	11.5
RX_J0028.1+3103	1393.75	ISMLG	Si IV	1393.7	L	-1.0	0.00001	152.5	11.2
RX_J0028.1+3103	1394.25	PROXIMATE	H I	930.7	H	149292.0	0.49798	74.2	7.4
RX_J0028.1+3103	1394.46	PROXIMATE	H I	930.7	H	149360.0	0.49822	158.6	12.5
RX_J0028.1+3103	1394.84	INTRINSIC	H I	930.7	H	149483.0	0.49861	148.5	9.5
RX_J0028.1+3103	1398.19	PROXIMATE	S VI	933.3	H	149292.0	0.49798	86.1	9.2
RX_J0028.1+3103	1398.40	PROXIMATE	S VI	933.3	H	149360.0	0.49822	245.4	14.1
RX_J0028.1+3103	1398.78	INTRINSIC	S VI	933.3	H	149482.0	0.49861	87.0	9.6
RX_J0028.1+3103	1398.86	IGMABS	H I	949.7	H	141768.0	0.47289	83.0	9.8
RX_J0028.1+3103	1401.45	ISMLG	Si IV	1402.7	L	-283.0	-0.00094	55.6	11.4
RX_J0028.1+3103	1402.50	ISMLG	Si IV	1402.7	L	-59.0	-0.00021	48.3	11.8
RX_J0028.1+3103	1402.79	ISMLG	Si IV	1402.7	L	3.0	0.00001	118.9	10.8
RX_J0028.1+3103	1403.94	PROXIMATE	H I	937.8	H	149013.0	0.49704	162.3	14.1
RX_J0028.1+3103	1404.81	PROXIMATE	H I	937.8	H	149291.0	0.49798	136.9	9.6
RX_J0028.1+3103	1405.03	PROXIMATE	H I	937.8	H	149359.0	0.49822	124.6	7.3
RX_J0028.1+3103	1405.39	INTRINSIC	H I	937.8	H	149476.0	0.49861	223.9	12.0
RX_J0028.1+3103	1411.64	IGMABS	H I	972.5	H	135358.0	0.45151	252.3	13.3

Table A1 *continued*

Table A1 (*continued*)

Target	λ_{obs}	Type	Ion	λ_{rest}	Frame	cz	z	W_{λ}	$\sigma_{W_{\lambda}}$
	(Å)			(Å)		(km s ⁻¹)		(mÅ)	(mÅ)
RX_J0028.1+3103	1414.86	PROXIMATE	S VI	944.5	H	149285.0	0.49798	74.1	12.4
RX_J0028.1+3103	1415.11	PROXIMATE	S VI	944.5	H	149364.0	0.49822	179.1	19.3
RX_J0028.1+3103	1415.47	INTRINSIC	S VI	944.5	H	149478.0	0.49861	49.0	9.4
RX_J0028.1+3103	1417.36	IGMABS	H I	1215.6	H	49739.0	0.16591	40.2	13.1
RX_J0028.1+3103	1418.17	IGMABS	C III	977.0	H	135364.0	0.45151	174.2	17.3
RX_J0028.1+3103	1419.62	IGMABS	H I	1025.7	H	115127.0	0.38401	64.8	12.6
RX_J0028.1+3103	1420.94	IGMABS	H I	1215.6	H	50622.0	0.16886	66.4	13.5
RX_J0028.1+3103	1421.82	PROXIMATE	H I	949.7	H	149014.0	0.49704	256.1	14.6
RX_J0028.1+3103	1422.69	PROXIMATE	H I	949.7	H	149289.0	0.49798	281.3	11.4
RX_J0028.1+3103	1422.90	PROXIMATE	H I	949.7	H	149354.0	0.49822	230.8	8.9
RX_J0028.1+3103	1423.30	INTRINSIC	H I	949.7	H	149480.0	0.49861	275.4	12.7
RX_J0028.1+3103	1432.44	IGMABS	H I	972.5	H	141768.0	0.47289	53.6	11.3
RX_J0028.1+3103	1448.82	IGMABS	H I	1215.6	H	57495.0	0.19178	229.4	28.9
RX_J0028.1+3103	1454.82	ISMLG	Ni II	1454.8	L	-5.0	0.00001	24.8	10.5
RX_J0028.1+3103	1455.05	IGMABS	H I	1215.6	H	59033.0	0.19691	83.3	9.1
RX_J0028.1+3103	1455.94	PROXIMATE	H I	972.5	H	149012.0	0.49704	348.0	25.5
RX_J0028.1+3103	1456.83	PROXIMATE	H I	972.5	H	149288.0	0.49798	347.4	6.8
RX_J0028.1+3103	1457.06	PROXIMATE	H I	972.5	H	149358.0	0.49822	562.1	21.3
RX_J0028.1+3103	1457.44	INTRINSIC	H I	972.5	H	149476.0	0.49861	292.9	7.0
RX_J0028.1+3103	1462.66	PROXIMATE	C III	977.0	H	149014.0	0.49704	305.6	26.2
RX_J0028.1+3103	1463.55	PROXIMATE	C III	977.0	H	149288.0	0.49798	573.1	6.5
RX_J0028.1+3103	1463.78	PROXIMATE	C III	977.0	H	149358.0	0.49822	634.7	3.7
RX_J0028.1+3103	1464.17	INTRINSIC	C III	977.0	H	149478.0	0.49861	435.5	5.3
RX_J0028.1+3103	1464.59	IGMABS	H I	1215.6	H	61385.0	0.20476	98.2	8.9
RX_J0028.1+3103	1479.14	IGMABS	H I	1215.6	H	64973.0	0.21673	96.4	12.6
RX_J0028.1+3103	1481.75	PROXIMATE	N III	989.7	H	149004.0	0.49704	56.0	10.2
RX_J0028.1+3103	1482.70	PROXIMATE	N III	989.7	H	149292.0	0.49798	133.9	7.0
RX_J0028.1+3103	1482.94	PROXIMATE	N III	989.7	H	149364.0	0.49822	195.2	4.7
RX_J0028.1+3103	1483.33	INTRINSIC	N III	989.7	H	149481.0	0.49861	290.3	7.7
RX_J0028.1+3103	1488.84	IGMABS	H I	1025.7	H	135358.0	0.45151	406.6	13.0
RX_J0028.1+3103	1490.60	IGMABS	H I	1215.6	H	67801.0	0.22616	204.5	17.3
RX_J0028.1+3103	1497.84	IGMABS	O VI	1031.9	H	135356.0	0.45151	63.3	15.1
RX_J0028.1+3103	1510.78	IGMABS	H I	1025.7	H	141769.0	0.47289	197.8	12.0
RX_J0028.1+3103	1519.93	IGMABS	O VI	1031.9	H	141773.0	0.47289	34.5	9.7
RX_J0028.1+3103	1526.09	ISMLG	Si II	1526.7	L	-122.0	-0.00038	69.8	10.2
RX_J0028.1+3103	1526.38	ISMLG	Si II	1526.7	L	-65.0	-0.00021	146.6	7.4
RX_J0028.1+3103	1526.75	ISMLG	Si II	1526.7	L	8.0	0.00001	351.8	9.5
RX_J0028.1+3103	1528.29	IGMABS	O VI	1037.6	H	141768.0	0.47289	40.5	10.4
RX_J0028.1+3103	1533.24	IGMABS	H I	1215.6	H	78315.0	0.26123	65.2	10.5
RX_J0028.1+3103	1533.60	IGMABS	H I	1215.6	H	78403.0	0.26152	281.2	13.2
RX_J0028.1+3103	1534.59	IGMABS	H I	1215.6	H	78648.0	0.26234	273.5	15.0
RX_J0028.1+3103	1535.54	PROXIMATE	H I	1025.7	H	149008.0	0.49704	401.4	10.4
RX_J0028.1+3103	1536.51	PROXIMATE	H I	1025.7	H	149290.0	0.49798	469.0	7.9
RX_J0028.1+3103	1536.76	PROXIMATE	H I	1025.7	H	149363.0	0.49822	405.0	4.4
RX_J0028.1+3103	1537.16	INTRINSIC	H I	1025.7	H	149479.0	0.49861	417.0	7.6
RX_J0028.1+3103	1542.41	IGMABS	H I	1215.6	H	80576.0	0.26877	92.1	11.0
RX_J0028.1+3103	1542.80	IGMABS	H I	1215.6	H	80673.0	0.26910	396.6	8.9
RX_J0028.1+3103	1544.82	PROXIMATE	O VI	1031.9	H	149005.0	0.49704	40.4	11.3
RX_J0028.1+3103	1545.78	PROXIMATE	O VI	1031.9	H	149285.0	0.49798	491.7	7.2
RX_J0028.1+3103	1546.03	PROXIMATE	O VI	1031.9	H	149357.0	0.49822	618.1	4.7
RX_J0028.1+3103	1546.46	INTRINSIC	O VI	1031.9	H	149482.0	0.49861	718.5	7.7
RX_J0028.1+3103	1547.07	IGMABS	Si IV	1393.7	H	32976.0	0.11003	68.3	9.9
RX_J0028.1+3103	1547.90	ISMLG	C IV	1548.2	L	-60.0	-0.00021	66.8	7.8

Table A1 continued

Table A1 (*continued*)

Target	λ_{obs}	Type	Ion	λ_{rest}	Frame	cz	z	W_{λ}	$\sigma_{W_{\lambda}}$
	(Å)			(Å)		(km s ⁻¹)		(mÅ)	(mÅ)
RX_J0028.1+3103	1548.21	ISMLG	C iv	1548.2	L	0.0	0.00001	159.9	9.8
RX_J0028.1+3103	1550.47	ISMLG	C iv	1550.7	L	-61.0	-0.00021	59.1	10.4
RX_J0028.1+3103	1550.81	ISMLG	C iv	1550.7	L	7.0	0.00001	169.6	11.6
RX_J0028.1+3103	1552.40	PROXIMATE	C ii	1036.3	H	149287.0	0.49798	34.7	7.2
RX_J0028.1+3103	1552.67	PROXIMATE	C ii	1036.3	H	149366.0	0.49822	43.4	9.2
RX_J0028.1+3103	1553.06	INTRINSIC	C ii	1036.3	H	149480.0	0.49861	116.9	14.1
RX_J0028.1+3103	1554.31	PROXIMATE	O vi	1037.6	H	149286.0	0.49798	491.1	8.3
RX_J0028.1+3103	1554.57	PROXIMATE	O vi	1037.6	H	149359.0	0.49822	641.4	5.5
RX_J0028.1+3103	1554.98	INTRINSIC	O vi	1037.6	H	149478.0	0.49861	624.1	8.8
RX_J0028.1+3103	1555.33	IGMABS	H i	1215.6	H	83761.0	0.27940	99.2	10.9
RX_J0028.1+3103	1557.15	IGMABS	Si iv	1402.7	H	32993.0	0.11003	52.1	12.8
RX_J0028.1+3103	1560.36	ISMLG	C i	1560.3	L	10.0	0.00001	75.7	12.8
RX_J0028.1+3103	1576.93	IGMABS	H i	1215.6	H	89089.0	0.29717	329.0	27.4
RX_J0028.1+3103	1580.16	IGMABS	H i	1215.6	H	89887.0	0.29983	347.8	31.0
RX_J0028.1+3103	1592.52	INTRINSIC	S iv	1062.6	H	149480.0	0.49861	37.8	13.5
RX_J0028.1+3103	1604.31	IGMABS	H i	1215.6	H	95841.0	0.31969	115.7	21.9
RX_J0028.1+3103	1607.06	IGMABS	H i	1215.6	H	96520.0	0.32195	515.6	26.0
RX_J0028.1+3103	1608.11	ISMLG	Fe ii	1608.4	L	-63.0	-0.00021	110.2	15.4
RX_J0028.1+3103	1608.49	ISMLG	Fe ii	1608.4	L	8.0	0.00001	344.7	18.7
RX_J0028.1+3103	1623.19	IGMABS	H i	1215.6	H	100498.0	0.33523	119.4	29.7
RX_J0028.1+3103	1624.41	IGMABS	H i	1215.6	H	100797.0	0.33622	86.5	25.3
RX_J0028.1+3103	1639.65	IGMABS	H i	1215.6	H	104557.0	0.34876	73.9	26.7
RX_J0028.1+3103	1656.19	IGMABS	H i	1215.6	H	108635.0	0.36237	212.8	24.4
RX_J0028.1+3103	1656.98	ISMLG	C i	1656.9	L	10.0	0.00001	158.9	22.2
RX_J0028.1+3103	1662.47	IGMABS	H i	1215.6	H	110185.0	0.36754	217.2	27.8
RX_J0028.1+3103	1670.42	ISMLG	Al ii	1670.7	L	-65.0	-0.00021	139.6	14.5
RX_J0028.1+3103	1670.85	ISMLG	Al ii	1670.7	L	11.0	0.00001	401.6	17.3
RX_J0028.1+3103	1681.90	IGMABS	H i	1215.6	H	114976.0	0.38352	81.0	25.7
RX_J0028.1+3103	1682.50	IGMABS	H i	1215.6	H	115122.0	0.38401	231.0	24.6
RX_J0028.1+3103	1709.57	ISMLG	Ni ii	1709.6	L	-5.0	0.00001	82.3	26.6
RX_J0028.1+3103	1718.54	IGMABS	C iv	1548.2	H	32984.0	0.11003	291.9	31.5
RX_J0028.1+3103	1721.40	IGMABS	C iv	1550.7	H	32984.0	0.11003	162.4	29.6
RX_J0028.1+3103	1741.59	ISMLG	Ni ii	1741.5	L	7.0	0.00001	87.5	20.8
RX_J0028.1+3103	1751.89	ISMLG	Ni ii	1751.9	L	-5.0	0.00001	68.9	27.2
RX_J0028.1+3103	1764.56	IGMABS	H i	1215.6	H	135359.0	0.45151	744.0	45.8
RX_J0028.1+3103	1781.63	IGMABS	H i	1215.6	H	139571.0	0.46556	132.5	34.4
RX_J0028.1+3103	1790.11	IGMABS	H i	1215.6	H	141662.0	0.47253	177.7	38.9
RX_J0028.1+3103	1790.55	IGMABS	H i	1215.6	H	141768.0	0.47289	384.1	25.2
RX_J0028.1+3103	1790.90	IGMABS	H i	1215.6	H	141854.0	0.47318	216.3	34.0
RX_J0043.6+3725	1133.63	ISMLG	Fe ii	1133.6	L	-9.0	-0.00001	122.3	39.8
RX_J0043.6+3725	1134.15	ISMLG	N i	1134.1	L	-3.0	-0.00001	547.3	38.8
RX_J0043.6+3725	1134.41	ISMLG	N i	1134.4	L	-2.0	-0.00001	447.4	34.3
RX_J0043.6+3725	1134.96	ISMLG	N i	1134.9	L	-6.0	-0.00001	335.1	36.0
RX_J0043.6+3725	1142.33	ISMLG	Fe ii	1142.3	L	-9.0	-0.00001	104.4	20.7
RX_J0043.6+3725	1143.21	ISMLG	Fe ii	1143.2	L	-4.0	-0.00001	208.7	20.5
RX_J0043.6+3725	1144.92	ISMLG	Fe ii	1144.9	L	-5.0	-0.00001	326.2	17.0
RX_J0043.6+3725	1152.82	ISMLG	P ii	1152.8	L	2.0	-0.00001	234.9	19.4
RX_J0043.6+3725	1188.84	ISMLG	C i	1188.8	L	3.0	-0.00001	38.1	9.9
RX_J0043.6+3725	1190.37	ISMLG	Si ii	1190.4	L	-12.0	-0.00001	529.7	10.8
RX_J0043.6+3725	1192.17	ISMLG	Si ii	1193.2	L	-282.0	-0.00097	37.2	9.3
RX_J0043.6+3725	1192.51	ISMLG	Si ii	1193.2	L	-196.0	-0.00062	48.8	9.6
RX_J0043.6+3725	1193.26	ISMLG	Si ii	1193.2	L	-7.0	-0.00001	527.4	8.8
RX_J0043.6+3725	1197.20	ISMLG	Mn ii	1197.1	L	4.0	-0.00001	57.4	10.6

Table A1 continued

Table A1 (*continued*)

Target	λ_{obs}	Type	Ion	λ_{rest}	Frame	cz	z	W_{λ}	$\sigma_{W_{\lambda}}$
	(Å)			(Å)		(km s ⁻¹)		(mÅ)	(mÅ)
RX_J0043.6+3725	1199.54	ISMLG	N I	1199.5	L	-2.0	-0.00001	387.5	12.9
RX_J0043.6+3725	1200.21	ISMLG	N I	1200.2	L	-3.0	-0.00001	361.9	13.2
RX_J0043.6+3725	1200.69	ISMLG	N I	1200.7	L	-4.0	-0.00001	322.9	10.9
RX_J0043.6+3725	1201.12	ISMLG	Mn II	1201.1	L	1.0	-0.00001	38.3	15.5
RX_J0043.6+3725	1205.34	ISMLG	Si III	1206.5	L	-289.0	-0.00097	120.7	8.8
RX_J0043.6+3725	1205.77	ISMLG	Si III	1206.5	L	-183.0	-0.00062	200.3	9.6
RX_J0043.6+3725	1206.46	ISMLG	Si III	1206.5	L	-11.0	-0.00001	580.2	11.5
RX_J0043.6+3725	1222.19	IGMABS	H I	1215.6	H	1607.0	0.00536	109.0	16.9
RX_J0043.6+3725	1232.98	IGMABS	H I	1215.6	H	4269.0	0.01424	100.9	11.0
RX_J0043.6+3725	1239.92	ISMLG	Mg II	1239.9	L	-2.0	-0.00001	41.4	8.3
RX_J0043.6+3725	1240.37	ISMLG	Mg II	1240.3	L	-6.0	-0.00001	25.0	8.6
RX_J0043.6+3725	1250.58	ISMLG	S II	1250.5	L	0.0	-0.00001	213.6	9.6
RX_J0043.6+3725	1253.80	ISMLG	S II	1253.8	L	-2.0	-0.00001	249.2	8.0
RX_J0043.6+3725	1259.20	ISMLG	Si II	1260.4	L	-291.0	-0.00097	121.5	8.6
RX_J0043.6+3725	1259.49	ISMLG	S II	1259.5	L	-6.0	-0.00001	344.8	8.6
RX_J0043.6+3725	1260.38	ISMLG	Si II	1260.4	L	-11.0	-0.00001	606.1	9.2
RX_J0043.6+3725	1262.36	IGMABS	H I	1215.6	H	11515.0	0.03841	54.2	11.9
RX_J0043.6+3725	1277.22	ISMLG	C I	1277.2	L	-5.0	-0.00001	54.1	10.8
RX_J0043.6+3725	1298.88	IGMABS	H I	1215.6	H	20520.0	0.06845	127.9	16.1
RX_J0043.6+3725	1302.12	ISMLG	O I	1302.1	L	-11.0	-0.00001	489.0	9.4
RX_J0043.6+3725	1304.36	ISMLG	Si II	1304.3	L	-3.0	-0.00001	406.3	9.0
RX_J0043.6+3725	1310.96	INTRINSIC	H I	1215.6	H	23500.0	0.07839	45.5	5.2
RX_J0043.6+3725	1312.02	INTRINSIC	H I	1215.6	H	23760.0	0.07926	25.9	5.2
RX_J0043.6+3725	1313.08	INTRINSIC	H I	1215.6	H	24021.0	0.08013	103.3	5.8
RX_J0043.6+3725	1317.16	ISMLG	Ni II	1317.2	L	-12.0	-0.00001	93.1	7.3
RX_J0043.6+3725	1333.20	ISMLG	C II	1334.5	L	-298.0	-0.00097	98.6	7.7
RX_J0043.6+3725	1333.72	ISMLG	C II	1334.5	L	-182.0	-0.00062	142.0	7.4
RX_J0043.6+3725	1334.50	ISMLG	C II	1334.5	L	-8.0	-0.00001	641.9	6.7
RX_J0043.6+3725	1335.69	ISMLG	C II*	1335.7	L	-3.0	-0.00001	282.4	8.0
RX_J0043.6+3725	1370.09	ISMLG	Ni II	1370.1	L	-10.0	-0.00001	103.0	9.7
RX_J0043.6+3725	1392.91	ISMLG	Si IV	1393.7	L	-183.0	-0.00062	61.4	10.3
RX_J0043.6+3725	1393.72	ISMLG	Si IV	1393.7	L	-8.0	-0.00001	191.9	10.9
RX_J0043.6+3725	1401.88	ISMLG	Si IV	1402.7	L	-190.0	-0.00062	61.6	11.2
RX_J0043.6+3725	1402.75	ISMLG	Si IV	1402.7	L	-6.0	-0.00001	120.6	13.3
RX_J0043.6+3725	1454.81	ISMLG	Ni II	1454.8	L	-7.0	-0.00001	49.8	13.9
RX_J0043.6+3725	1526.66	ISMLG	Si II	1526.7	L	-9.0	-0.00001	545.6	13.2
RX_J0043.6+3725	1547.24	ISMLG	C IV	1548.2	L	-187.0	-0.00062	195.1	17.6
RX_J0043.6+3725	1548.20	ISMLG	C IV	1548.2	L	-1.0	-0.00001	241.8	18.8
RX_J0043.6+3725	1549.81	ISMLG	C IV	1550.7	L	-188.0	-0.00062	129.5	14.4
RX_J0043.6+3725	1550.77	ISMLG	C IV	1550.7	L	-1.0	-0.00001	154.0	18.3
RX_J0043.6+3725	1560.32	ISMLG	C I	1560.3	L	1.0	-0.00001	65.7	18.1
RX_J0043.6+3725	1608.40	ISMLG	Fe II	1608.4	L	-9.0	-0.00001	396.1	25.6
RX_J0043.6+3725	1656.87	ISMLG	C I	1656.9	L	-10.0	-0.00001	109.4	26.5
RX_J0043.6+3725	1670.72	ISMLG	Al II	1670.7	L	-11.0	-0.00001	550.1	15.5
RX_J0043.6+3725	1709.55	ISMLG	Ni II	1709.6	L	-9.0	-0.00001	68.2	26.2
RX_J0043.6+3725	1741.52	ISMLG	Ni II	1741.5	L	-6.0	-0.00001	109.7	33.9
RX_J0043.6+3725	1751.85	PROXIMATE	H I	1751.9	L	-11.0	-0.00001	111.4	31.2
RX_J0048.3+3941	952.31	ISMLG	N I	952.3	L	2.0	0.00000	147.6	21.0
RX_J0048.3+3941	952.42	ISMLG	N I	952.4	L	1.0	0.00000	153.0	20.6
RX_J0048.3+3941	953.25	ISMLG	N I	953.4	L	-52.0	-0.00015	108.4	24.7
RX_J0048.3+3941	953.43	ISMLG	N I	953.4	L	4.0	0.00000	174.8	22.9
RX_J0048.3+3941	953.51	ISMLG	N I	953.6	L	-46.0	-0.00015	134.0	19.6
RX_J0048.3+3941	953.67	ISMLG	N I	953.6	L	6.0	0.00000	188.5	22.0

Table A1 continued

Table A1 (*continued*)

Target	λ_{obs}	Type	Ion	λ_{rest}	Frame	cz	z	W_{λ}	$\sigma_{W_{\lambda}}$
	(Å)			(Å)		(km s ⁻¹)		(mÅ)	(mÅ)
RX_J0048.3+3941	953.81	ISMLG	N I	953.9	L	-50.0	-0.00015	138.5	20.0
RX_J0048.3+3941	953.99	ISMLG	N I	953.9	L	7.0	0.00000	211.6	23.4
RX_J0048.3+3941	954.11	ISMLG	N I	954.1	L	1.0	0.00000	78.9	23.8
RX_J0048.3+3941	964.00	ISMLG	N I	963.9	L	4.0	0.00000	142.4	31.2
RX_J0048.3+3941	964.64	ISMLG	N I	964.6	L	4.0	0.00000	117.2	28.4
RX_J0048.3+3941	965.05	ISMLG	N I	965.0	L	4.0	0.00000	161.9	31.2
RX_J0048.3+3941	975.61	ISMLG	C III	977.0	L	-433.0	-0.00145	78.2	27.8
RX_J0048.3+3941	975.80	ISMLG	C III	977.0	L	-374.0	-0.00126	140.0	25.3
RX_J0048.3+3941	975.96	ISMLG	C III	977.0	L	-324.0	-0.00108	131.5	20.1
RX_J0048.3+3941	976.09	ISMLG	C III	977.0	L	-284.0	-0.00095	105.6	22.0
RX_J0048.3+3941	1008.74	IGMABS	H I	919.3	H	29149.0	0.09723	16.6	11.1
RX_J0048.3+3941	1010.51	IGMABS	H I	920.9	H	29149.0	0.09723	16.3	8.6
RX_J0048.3+3941	1012.91	IGMABS	H I	923.1	H	29150.0	0.09723	47.4	9.6
RX_J0048.3+3941	1016.28	IGMABS	H I	926.2	H	29150.0	0.09723	29.8	8.5
RX_J0048.3+3941	1020.54	ISMLG	Si II	1020.6	L	-48.0	-0.00015	93.6	6.1
RX_J0048.3+3941	1020.71	ISMLG	Si II	1020.6	L	2.0	0.00000	123.3	5.5
RX_J0048.3+3941	1021.24	IGMABS	H I	930.7	H	29148.0	0.09723	63.0	11.5
RX_J0048.3+3941	1028.98	IGMABS	H I	937.8	H	29148.0	0.09723	96.3	10.4
RX_J0048.3+3941	1029.26	IGMABS	H I	937.8	H	29238.0	0.09753	52.4	8.7
RX_J0048.3+3941	1030.63	ISMLG	O VI	1031.9	L	-377.0	-0.00126	69.6	7.2
RX_J0048.3+3941	1030.82	ISMLG	O VI	1031.9	L	-322.0	-0.00108	34.8	5.9
RX_J0048.3+3941	1030.95	ISMLG	O VI	1031.9	L	-285.0	-0.00095	49.5	5.2
RX_J0048.3+3941	1031.31	ISMLG	O VI	1031.9	L	-178.0	-0.00060	122.4	7.2
RX_J0048.3+3941	1031.56	ISMLG	O VI	1031.9	L	-105.0	-0.00033	32.1	8.4
RX_J0048.3+3941	1031.77	ISMLG	O VI	1031.9	L	-47.0	-0.00015	37.4	6.8
RX_J0048.3+3941	1031.94	ISMLG	O VI	1031.9	L	5.0	0.00000	86.0	8.6
RX_J0048.3+3941	1035.04	ISMLG	C II	1036.3	L	-375.0	-0.00126	89.9	6.1
RX_J0048.3+3941	1035.50	ISMLG	C II	1036.3	L	-242.0	-0.00080	57.6	6.9
RX_J0048.3+3941	1035.72	ISMLG	C II	1036.3	L	-178.0	-0.00060	120.0	6.6
RX_J0048.3+3941	1035.98	ISMLG	C II	1036.3	L	-102.0	-0.00033	140.3	6.4
RX_J0048.3+3941	1036.18	ISMLG	C II	1036.3	L	-47.0	-0.00015	140.8	4.2
RX_J0048.3+3941	1036.36	ISMLG	C II	1036.3	L	8.0	0.00000	275.3	6.5
RX_J0048.3+3941	1036.86	ISMLG	C II*	1037.0	L	-46.0	-0.00015	101.0	4.3
RX_J0048.3+3941	1036.99	ISMLG	O VI	1037.6	L	-180.0	-0.00060	211.8	6.8
RX_J0048.3+3941	1037.04	ISMLG	C II*	1037.0	L	7.0	0.00000	202.8	6.5
RX_J0048.3+3941	1037.45	ISMLG	O VI	1037.6	L	-49.0	-0.00015	27.9	6.4
RX_J0048.3+3941	1037.59	ISMLG	O VI	1037.6	L	-8.0	0.00000	60.0	7.2
RX_J0048.3+3941	1038.89	ISMLG	O I	1039.2	L	-97.0	-0.00033	69.6	7.0
RX_J0048.3+3941	1039.07	ISMLG	O I	1039.2	L	-46.0	-0.00015	155.5	6.3
RX_J0048.3+3941	1039.26	ISMLG	O I	1039.2	L	9.0	0.00000	145.7	8.2
RX_J0048.3+3941	1042.10	IGMABS	H I	949.7	H	29154.0	0.09723	157.9	7.4
RX_J0048.3+3941	1042.38	IGMABS	H I	949.7	H	29240.0	0.09753	70.0	7.6
RX_J0048.3+3941	1048.05	ISMLG	Ar I	1048.2	L	-48.0	-0.00015	94.1	5.9
RX_J0048.3+3941	1048.20	ISMLG	Ar I	1048.2	L	-5.0	0.00000	105.5	5.8
RX_J0048.3+3941	1054.68	IGMABS	H I	949.7	H	33122.0	0.11048	36.6	8.9
RX_J0048.3+3941	1055.09	ISMLG	Fe II	1055.2	L	-48.0	-0.00015	40.7	6.7
RX_J0048.3+3941	1055.23	ISMLG	Fe II	1055.2	L	-8.0	0.00000	62.2	6.3
RX_J0048.3+3941	1056.59	INTRINSIC	H I	930.7	H	40533.0	0.13519	23.0	6.3
RX_J0048.3+3941	1059.58	INTRINSIC	S VI	933.3	H	40534.0	0.13519	53.6	8.9
RX_J0048.3+3941	1063.01	ISMLG	Fe II	1063.1	L	-48.0	-0.00015	111.4	5.6
RX_J0048.3+3941	1063.18	ISMLG	Fe II	1063.1	L	0.0	0.00000	145.2	5.9
RX_J0048.3+3941	1063.97	ISMLG	Fe II	1063.9	L	0.0	0.00000	35.4	8.0
RX_J0048.3+3941	1064.59	INTRINSIC	H I	937.8	H	40532.0	0.13519	31.2	8.0

Table A1 *continued*

Table A1 (*continued*)

Target	λ_{obs}	Type	Ion	λ_{rest}	Frame	cz	z	W_{λ}	$\sigma_{W_{\lambda}}$
	(Å)			(Å)		(km s ⁻¹)		(mÅ)	(mÅ)
RX_J0048.3+3941	1066.49	ISMLG	Ar I	1066.6	L	-47.0	-0.00015	55.5	6.1
RX_J0048.3+3941	1066.66	ISMLG	Ar I	1066.6	L	-1.0	0.00000	101.4	7.2
RX_J0048.3+3941	1067.08	IGMABS	H I	972.5	H	29145.0	0.09723	197.5	7.2
RX_J0048.3+3941	1067.40	IGMABS	H I	972.5	H	29241.0	0.09753	118.3	11.3
RX_J0048.3+3941	1072.04	IGMABS	C III	977.0	H	29155.0	0.09723	105.1	11.0
RX_J0048.3+3941	1072.21	INTRINSIC	S VI	944.5	H	40529.0	0.13519	45.1	4.6
RX_J0048.3+3941	1072.30	IGMABS	C III	977.0	H	29235.0	0.09753	105.2	10.0
RX_J0048.3+3941	1078.15	INTRINSIC	H I	949.7	H	40533.0	0.13519	64.8	13.1
RX_J0048.3+3941	1079.99	IGMABS	H I	972.5	H	33125.0	0.11048	99.7	12.1
RX_J0048.3+3941	1096.70	ISMLG	Fe II	1096.8	L	-48.0	-0.00015	89.8	5.8
RX_J0048.3+3941	1096.90	ISMLG	Fe II	1096.8	L	5.0	0.00000	102.1	7.0
RX_J0048.3+3941	1098.67	UNIDENTIFIED	UNIND	1000.0	H	0.0	-1.00000	34.0	10.8
RX_J0048.3+3941	1104.01	INTRINSIC	H I	972.5	H	40528.0	0.13519	57.9	9.6
RX_J0048.3+3941	1109.10	INTRINSIC	C III	977.0	H	40527.0	0.13519	131.1	9.2
RX_J0048.3+3941	1111.87	ISMLG	Fe II	1112.0	L	-48.0	-0.00015	25.9	5.5
RX_J0048.3+3941	1112.03	ISMLG	Fe II	1112.0	L	-5.0	0.00000	28.5	5.9
RX_J0048.3+3941	1121.80	ISMLG	Fe II	1121.9	L	-48.0	-0.00015	102.4	6.0
RX_J0048.3+3941	1121.95	ISMLG	Fe II	1121.9	L	-7.0	0.00000	70.3	6.2
RX_J0048.3+3941	1122.36	ISMLG	Fe III	1122.5	L	-44.0	-0.00015	26.8	5.6
RX_J0048.3+3941	1122.50	ISMLG	Fe III	1122.5	L	-5.0	0.00000	65.6	7.1
RX_J0048.3+3941	1125.46	IGMABS	H I	1025.7	H	29152.0	0.09723	358.4	10.4
RX_J0048.3+3941	1125.77	IGMABS	H I	1025.7	H	29241.0	0.09753	257.8	10.1
RX_J0048.3+3941	1127.07	ISMLG	Fe II	1127.0	L	-7.0	0.00000	50.6	12.2
RX_J0048.3+3941	1132.58	IGMABS	O VI	1031.9	H	29242.0	0.09753	67.7	12.1
RX_J0048.3+3941	1133.50	ISMLG	Fe II	1133.6	L	-43.0	-0.00015	39.6	6.7
RX_J0048.3+3941	1133.69	ISMLG	Fe II	1133.6	L	6.0	0.00000	52.8	6.6
RX_J0048.3+3941	1133.98	ISMLG	N I	1134.1	L	-48.0	-0.00015	111.1	5.3
RX_J0048.3+3941	1134.17	ISMLG	N I	1134.1	L	2.0	0.00000	179.1	5.9
RX_J0048.3+3941	1134.24	ISMLG	N I	1134.4	L	-45.0	-0.00015	119.0	5.2
RX_J0048.3+3941	1134.43	ISMLG	N I	1134.4	L	3.0	0.00000	127.0	5.9
RX_J0048.3+3941	1134.80	ISMLG	N I	1134.9	L	-47.0	-0.00015	70.1	5.5
RX_J0048.3+3941	1134.99	ISMLG	N I	1134.9	L	4.0	0.00000	106.1	6.5
RX_J0048.3+3941	1137.09	IGMABS	C II	1036.3	H	29146.0	0.09723	33.7	8.6
RX_J0048.3+3941	1138.82	IGMABS	O VI	1037.6	H	29240.0	0.09753	87.8	8.1
RX_J0048.3+3941	1139.06	IGMABS	H I	1025.7	H	33125.0	0.11048	279.2	10.3
RX_J0048.3+3941	1142.18	ISMLG	Fe II	1142.3	L	-50.0	-0.00015	48.0	5.7
RX_J0048.3+3941	1142.37	ISMLG	Fe II	1142.3	L	0.0	0.00000	46.7	6.6
RX_J0048.3+3941	1143.04	ISMLG	Fe II	1143.2	L	-50.0	-0.00015	117.6	6.1
RX_J0048.3+3941	1143.23	ISMLG	Fe II	1143.2	L	2.0	0.00000	67.5	6.6
RX_J0048.3+3941	1144.55	ISMLG	Fe II	1144.9	L	-101.0	-0.00033	54.9	7.2
RX_J0048.3+3941	1144.74	ISMLG	Fe II	1144.9	L	-52.0	-0.00015	211.2	5.7
RX_J0048.3+3941	1144.97	ISMLG	Fe II	1144.9	L	8.0	0.00000	133.7	6.3
RX_J0048.3+3941	1145.95	IGMABS	O VI	1031.9	H	33125.0	0.11048	51.1	7.5
RX_J0048.3+3941	1152.26	IGMABS	O VI	1037.6	H	33124.0	0.11048	24.2	5.6
RX_J0048.3+3941	1152.62	ISMLG	P II	1152.8	L	-52.0	-0.00015	77.7	4.6
RX_J0048.3+3941	1152.80	ISMLG	P II	1152.8	L	-5.0	0.00000	96.1	6.1
RX_J0048.3+3941	1157.92	ISMLG	C I	1157.9	L	3.0	0.00000	15.1	4.1
RX_J0048.3+3941	1164.41	INTRINSIC	H I	1025.7	H	40533.0	0.13519	163.0	10.5
RX_J0048.3+3941	1171.45	INTRINSIC	O VI	1031.9	H	40535.0	0.13519	384.2	11.3
RX_J0048.3+3941	1177.91	INTRINSIC	O VI	1037.6	H	40534.0	0.13519	340.2	9.5
RX_J0048.3+3941	1188.93	ISMLG	Si II	1190.4	L	-374.0	-0.00126	19.9	3.6
RX_J0048.3+3941	1189.48	ISMLG	Si II	1190.4	L	-235.0	-0.00080	34.6	3.5
RX_J0048.3+3941	1189.71	ISMLG	Si II	1190.4	L	-178.0	-0.00060	62.5	2.8

Table A1 continued

Table A1 (*continued*)

Target	λ_{obs}	Type	Ion	λ_{rest}	Frame	cz	z	W_{λ}	$\sigma_{W_{\lambda}}$
	(Å)			(Å)		(km s ⁻¹)		(mÅ)	(mÅ)
RX_J0048.3+3941	1190.01	ISMLG	Si II	1190.4	L	-101.0	-0.00033	147.1	2.7
RX_J0048.3+3941	1190.22	ISMLG	Si II	1190.4	L	-49.0	-0.00015	190.9	1.0
RX_J0048.3+3941	1190.44	ISMLG	Si II	1190.4	L	7.0	0.00000	201.7	2.7
RX_J0048.3+3941	1191.80	ISMLG	Si II	1193.2	L	-375.0	-0.00126	48.1	3.2
RX_J0048.3+3941	1192.30	ISMLG	Si II	1193.2	L	-249.0	-0.00080	33.8	2.7
RX_J0048.3+3941	1192.58	ISMLG	Si II	1193.2	L	-179.0	-0.00060	116.2	3.5
RX_J0048.3+3941	1192.89	ISMLG	Si II	1193.2	L	-101.0	-0.00033	164.0	2.5
RX_J0048.3+3941	1193.10	ISMLG	Si II	1193.2	L	-48.0	-0.00015	169.3	0.9
RX_J0048.3+3941	1193.32	ISMLG	Si II	1193.2	L	8.0	0.00000	207.8	2.6
RX_J0048.3+3941	1196.99	ISMLG	Mn II	1197.1	L	-49.0	-0.00015	18.4	3.1
RX_J0048.3+3941	1197.17	ISMLG	Mn II	1197.1	L	-5.0	0.00000	20.6	3.0
RX_J0048.3+3941	1199.14	ISMLG	N I	1199.5	L	-104.0	-0.00033	70.8	4.2
RX_J0048.3+3941	1199.34	ISMLG	N I	1199.5	L	-53.0	-0.00015	211.4	2.6
RX_J0048.3+3941	1199.58	ISMLG	N I	1199.5	L	7.0	0.00000	197.4	2.4
RX_J0048.3+3941	1200.02	ISMLG	N I	1200.2	L	-50.0	-0.00015	169.1	2.2
RX_J0048.3+3941	1200.26	ISMLG	N I	1200.2	L	8.0	0.00000	222.1	2.6
RX_J0048.3+3941	1200.52	ISMLG	N I	1200.7	L	-49.0	-0.00015	148.5	2.0
RX_J0048.3+3941	1200.74	ISMLG	N I	1200.7	L	9.0	0.00000	172.3	3.1
RX_J0048.3+3941	1200.92	ISMLG	Mn II	1201.1	L	-48.0	-0.00015	19.7	3.0
RX_J0048.3+3941	1201.10	ISMLG	Mn II	1201.1	L	-4.0	0.00000	11.3	3.4
RX_J0048.3+3941	1204.75	ISMLG	Si III	1206.5	L	-434.0	-0.00145	26.8	3.6
RX_J0048.3+3941	1204.97	ISMLG	Si III	1206.5	L	-379.0	-0.00126	130.5	3.1
RX_J0048.3+3941	1205.20	ISMLG	Si III	1206.5	L	-323.0	-0.00108	32.0	2.6
RX_J0048.3+3941	1205.37	ISMLG	Si III	1206.5	L	-282.0	-0.00095	54.9	2.9
RX_J0048.3+3941	1205.54	ISMLG	Si III	1206.5	L	-239.0	-0.00080	128.2	2.1
RX_J0048.3+3941	1205.77	ISMLG	Si III	1206.5	L	-182.0	-0.00060	158.6	2.4
RX_J0048.3+3941	1206.08	ISMLG	Si III	1206.5	L	-104.0	-0.00033	191.4	2.6
RX_J0048.3+3941	1206.31	ISMLG	Si III	1206.5	L	-48.0	-0.00015	169.8	1.0
RX_J0048.3+3941	1206.53	ISMLG	Si III	1206.5	L	8.0	0.00000	214.0	3.3
RX_J0048.3+3941	1223.12	IGMABS	H I	1215.6	H	1836.0	0.00613	25.7	5.9
RX_J0048.3+3941	1225.41	IGMABS	H I	1215.6	H	2401.0	0.00801	22.6	5.8
RX_J0048.3+3941	1231.73	IGMABS	H I	1215.6	H	3960.0	0.01321	33.7	5.7
RX_J0048.3+3941	1235.48	IGMABS	H I	1215.6	H	4886.0	0.01630	45.4	5.1
RX_J0048.3+3941	1237.83	ISMLG	N V	1238.8	L	-239.0	-0.00080	15.4	3.5
RX_J0048.3+3941	1239.74	ISMLG	Mg II	1239.9	L	-44.0	-0.00015	22.7	3.2
RX_J0048.3+3941	1239.92	ISMLG	Mg II	1239.9	L	-1.0	0.00000	24.4	3.3
RX_J0048.3+3941	1241.77	ISMLG	N V	1242.8	L	-249.0	-0.00080	12.2	4.1
RX_J0048.3+3941	1249.49	IGMABS	H I	1215.6	H	8340.0	0.02782	30.8	5.2
RX_J0048.3+3941	1250.39	ISMLG	S II	1250.5	L	-45.0	-0.00015	81.8	2.5
RX_J0048.3+3941	1250.55	ISMLG	S II	1250.5	L	-6.0	0.00000	100.9	2.6
RX_J0048.3+3941	1253.58	ISMLG	S II	1253.8	L	-53.0	-0.00015	109.9	2.6
RX_J0048.3+3941	1253.82	ISMLG	S II	1253.8	L	5.0	0.00000	132.0	2.3
RX_J0048.3+3941	1258.59	ISMLG	Si II	1260.4	L	-437.0	-0.00145	17.4	3.5
RX_J0048.3+3941	1258.85	ISMLG	Si II	1260.4	L	-374.0	-0.00126	75.0	3.0
RX_J0048.3+3941	1259.05	ISMLG	Si II	1260.4	L	-326.0	-0.00108	30.9	2.5
RX_J0048.3+3941	1259.32	ISMLG	S II	1259.5	L	-47.0	-0.00015	155.0	1.9
RX_J0048.3+3941	1259.52	ISMLG	S II	1259.5	L	0.0	0.00000	192.1	1.3
RX_J0048.3+3941	1259.68	ISMLG	Si II	1260.4	L	-177.0	-0.00060	206.2	2.6
RX_J0048.3+3941	1259.98	ISMLG	Si II	1260.4	L	-104.0	-0.00033	152.3	2.3
RX_J0048.3+3941	1260.21	ISMLG	Si II	1260.4	L	-50.0	-0.00015	192.4	0.7
RX_J0048.3+3941	1260.45	ISMLG	Si II	1260.4	L	7.0	0.00000	248.7	2.3
RX_J0048.3+3941	1260.76	ISMLG	C I	1260.7	L	5.0	0.00000	19.6	3.0
RX_J0048.3+3941	1263.48	IGMABS	H I	1215.6	H	11789.0	0.03932	22.3	3.8

Table A1 continued

Table A1 (*continued*)

Target	λ_{obs}	Type	Ion	λ_{rest}	Frame	cz	z	W_{λ}	$\sigma_{W_{\lambda}}$
	(Å)			(Å)		(km s ⁻¹)		(mÅ)	(mÅ)
RX_J0048.3+3941	1296.12	IGMABS	H I	1215.6	H	19839.0	0.06617	87.9	8.2
RX_J0048.3+3941	1299.39	IGMABS	H I	1215.6	H	20645.0	0.06886	52.7	6.7
RX_J0048.3+3941	1301.73	ISMLG	O I	1302.1	L	-101.0	-0.00033	168.3	4.8
RX_J0048.3+3941	1301.95	ISMLG	O I	1302.1	L	-49.0	-0.00015	222.9	1.8
RX_J0048.3+3941	1302.21	ISMLG	O I	1302.1	L	9.0	0.00000	219.3	5.2
RX_J0048.3+3941	1302.70	ISMLG	Si II	1304.3	L	-384.0	-0.00126	19.8	5.3
RX_J0048.3+3941	1303.30	ISMLG	Si II	1304.3	L	-247.0	-0.00080	37.5	6.5
RX_J0048.3+3941	1303.63	ISMLG	Si II	1304.3	L	-171.0	-0.00060	69.0	6.4
RX_J0048.3+3941	1303.93	ISMLG	Si II	1304.3	L	-102.0	-0.00033	106.9	5.5
RX_J0048.3+3941	1304.17	ISMLG	Si II	1304.3	L	-46.0	-0.00015	170.9	2.6
RX_J0048.3+3941	1304.41	ISMLG	Si II	1304.3	L	8.0	0.00000	191.3	4.5
RX_J0048.3+3941	1317.00	ISMLG	Ni II	1317.2	L	-50.0	-0.00015	26.1	3.6
RX_J0048.3+3941	1317.18	ISMLG	Ni II	1317.2	L	-8.0	0.00000	45.7	4.0
RX_J0048.3+3941	1318.81	IGMABS	H I	1215.6	H	25435.0	0.08484	76.4	7.5
RX_J0048.3+3941	1323.83	IGMABS	Si III	1206.5	H	29155.0	0.09723	61.3	4.8
RX_J0048.3+3941	1324.97	IGMABS	H I	1215.6	H	26954.0	0.08991	112.8	5.2
RX_J0048.3+3941	1328.85	ISMLG	C I	1328.8	L	4.0	0.00000	13.3	3.2
RX_J0048.3+3941	1332.59	ISMLG	C II	1334.5	L	-436.0	-0.00145	39.2	3.9
RX_J0048.3+3941	1332.86	ISMLG	C II	1334.5	L	-375.0	-0.00126	116.5	2.5
RX_J0048.3+3941	1333.09	ISMLG	C II	1334.5	L	-324.0	-0.00108	30.7	3.1
RX_J0048.3+3941	1333.26	ISMLG	C II	1334.5	L	-286.0	-0.00095	13.3	3.2
RX_J0048.3+3941	1333.45	ISMLG	C II	1334.5	L	-242.0	-0.00080	82.0	2.8
RX_J0048.3+3941	1333.74	ISMLG	C II	1334.5	L	-179.0	-0.00060	230.3	1.8
RX_J0048.3+3941	1333.88	IGMABS	H I	1215.6	H	29150.0	0.09723	400.1	1.2
RX_J0048.3+3941	1334.07	ISMLG	C II	1334.5	L	-104.0	-0.00033	333.1	0.8
RX_J0048.3+3941	1334.23	IGMABS	H I	1215.6	H	29238.0	0.09753	331.5	0.8
RX_J0048.3+3941	1334.32	ISMLG	C II	1334.5	L	-47.0	-0.00015	205.8	0.6
RX_J0048.3+3941	1334.57	ISMLG	C II	1334.5	L	9.0	0.00000	245.5	2.7
RX_J0048.3+3941	1335.52	ISMLG	C II*	1335.7	L	-42.0	-0.00015	89.8	2.7
RX_J0048.3+3941	1335.70	ISMLG	C II*	1335.7	L	-1.0	0.00000	172.6	2.7
RX_J0048.3+3941	1347.05	ISMLG	Cl I	1347.2	L	-43.0	-0.00015	8.1	3.0
RX_J0048.3+3941	1347.26	ISMLG	Cl I	1347.2	L	4.0	0.00000	19.0	3.6
RX_J0048.3+3941	1349.98	IGMABS	H I	1215.6	H	33122.0	0.11048	676.6	2.8
RX_J0048.3+3941	1362.89	IGMABS	H I	1215.6	H	36305.0	0.12110	19.2	3.1
RX_J0048.3+3941	1363.49	IGMABS	H I	1215.6	H	36452.0	0.12159	13.9	3.4
RX_J0048.3+3941	1369.94	ISMLG	Ni II	1370.1	L	-43.0	-0.00015	31.5	1.8
RX_J0048.3+3941	1370.10	ISMLG	Ni II	1370.1	L	-7.0	0.00000	32.7	1.8
RX_J0048.3+3941	1375.72	IGMABS	N V	1238.8	H	33129.0	0.11048	77.2	2.9
RX_J0048.3+3941	1380.02	INTRINSIC	H I	1215.6	H	40529.0	0.13519	367.8	2.4
RX_J0048.3+3941	1391.96	ISMLG	Si IV	1393.7	L	-388.0	-0.00126	14.2	2.4
RX_J0048.3+3941	1392.66	ISMLG	Si IV	1393.7	L	-237.0	-0.00080	93.2	2.6
RX_J0048.3+3941	1392.93	ISMLG	Si IV	1393.7	L	-179.0	-0.00060	56.5	2.5
RX_J0048.3+3941	1393.30	ISMLG	Si IV	1393.7	L	-99.0	-0.00033	30.2	2.8
RX_J0048.3+3941	1393.54	ISMLG	Si IV	1393.7	L	-48.0	-0.00015	45.9	2.3
RX_J0048.3+3941	1393.73	ISMLG	Si IV	1393.7	L	-7.0	0.00000	75.0	2.5
RX_J0048.3+3941	1401.67	ISMLG	Si IV	1402.7	L	-236.0	-0.00080	53.7	2.9
RX_J0048.3+3941	1401.96	ISMLG	Si IV	1402.7	L	-173.0	-0.00060	45.3	3.2
RX_J0048.3+3941	1402.32	ISMLG	Si IV	1402.7	L	-97.0	-0.00033	5.0	2.8
RX_J0048.3+3941	1402.54	ISMLG	Si IV	1402.7	L	-51.0	-0.00015	18.6	2.9
RX_J0048.3+3941	1402.74	ISMLG	Si IV	1402.7	L	-7.0	0.00000	43.3	2.6
RX_J0048.3+3941	1406.30	INTRINSIC	N V	1238.8	H	40530.0	0.13519	227.4	4.2
RX_J0048.3+3941	1410.83	INTRINSIC	N V	1242.8	H	40531.0	0.13519	169.9	4.2
RX_J0048.3+3941	1454.62	ISMLG	Ni II	1454.8	L	-46.0	-0.00015	22.9	3.4

Table A1 continued

Table A1 (*continued*)

Target	λ_{obs}	Type	Ion	λ_{rest}	Frame	cz	z	W_{λ}	$\sigma_{W_{\lambda}}$
	(Å)			(Å)		(km s ⁻¹)		(mÅ)	(mÅ)
RX_J0048.3+3941	1454.82	ISMLG	Ni II	1454.8	L	-5.0	0.00000	24.7	3.1
RX_J0048.3+3941	1464.30	IGMABS	C II	1334.5	H	29151.0	0.09723	14.9	4.3
RX_J0048.3+3941	1524.75	ISMLG	Si II	1526.7	L	-385.0	-0.00126	32.5	4.9
RX_J0048.3+3941	1525.79	ISMLG	Si II	1526.7	L	-180.0	-0.00060	72.8	5.1
RX_J0048.3+3941	1526.21	ISMLG	Si II	1526.7	L	-98.0	-0.00033	134.9	3.5
RX_J0048.3+3941	1526.47	ISMLG	Si II	1526.7	L	-46.0	-0.00015	224.5	1.6
RX_J0048.3+3941	1526.73	ISMLG	Si II	1526.7	L	5.0	0.00000	239.5	3.0
RX_J0048.3+3941	1529.25	IGMABS	Si IV	1393.7	H	29143.0	0.09723	14.8	6.0
RX_J0048.3+3941	1539.14	IGMABS	Si IV	1402.7	H	29143.0	0.09723	18.3	5.7
RX_J0048.3+3941	1545.94	ISMLG	C IV	1548.2	L	-439.0	-0.00145	20.0	4.9
RX_J0048.3+3941	1546.22	ISMLG	C IV	1548.2	L	-384.0	-0.00126	54.5	5.4
RX_J0048.3+3941	1546.74	ISMLG	C IV	1548.2	L	-283.0	-0.00095	46.7	4.3
RX_J0048.3+3941	1546.98	ISMLG	C IV	1548.2	L	-237.0	-0.00080	190.3	3.2
RX_J0048.3+3941	1547.25	ISMLG	C IV	1548.2	L	-184.0	-0.00060	115.2	4.1
RX_J0048.3+3941	1547.66	ISMLG	C IV	1548.2	L	-105.0	-0.00033	38.8	6.1
RX_J0048.3+3941	1547.96	ISMLG	C IV	1548.2	L	-47.0	-0.00015	71.7	3.9
RX_J0048.3+3941	1548.24	ISMLG	C IV	1548.2	L	7.0	0.00000	92.9	4.8
RX_J0048.3+3941	1548.80	ISMLG	C IV	1550.7	L	-383.0	-0.00126	21.0	4.1
RX_J0048.3+3941	1549.28	ISMLG	C IV	1550.7	L	-291.0	-0.00095	25.6	4.2
RX_J0048.3+3941	1549.56	ISMLG	C IV	1550.7	L	-236.0	-0.00080	149.4	4.2
RX_J0048.3+3941	1549.83	ISMLG	C IV	1550.7	L	-184.0	-0.00060	64.9	4.1
RX_J0048.3+3941	1550.51	ISMLG	C IV	1550.7	L	-52.0	-0.00015	36.1	4.5
RX_J0048.3+3941	1550.75	ISMLG	C IV	1550.7	L	-5.0	0.00000	63.3	5.1
RX_J0048.3+3941	1607.46	ISMLG	Fe II	1608.4	L	-185.0	-0.00060	29.1	7.3
RX_J0048.3+3941	1607.96	ISMLG	Fe II	1608.4	L	-91.0	-0.00033	50.3	5.5
RX_J0048.3+3941	1608.17	ISMLG	Fe II	1608.4	L	-53.0	-0.00015	217.6	4.8
RX_J0048.3+3941	1608.49	ISMLG	Fe II	1608.4	L	7.0	0.00000	177.9	6.4
RX_J0048.3+3941	1611.18	ISMLG	Fe II	1611.2	L	-3.0	0.00000	28.0	7.3
RX_J0048.3+3941	1656.69	ISMLG	C I	1656.9	L	-43.0	-0.00015	37.0	6.5
RX_J0048.3+3941	1656.94	ISMLG	C I	1656.9	L	3.0	0.00000	31.2	6.2
RX_J0048.3+3941	1668.69	ISMLG	Al II	1670.7	L	-376.0	-0.00126	34.7	8.0
RX_J0048.3+3941	1669.41	ISMLG	Al II	1670.7	L	-247.0	-0.00080	20.8	6.6
RX_J0048.3+3941	1669.80	ISMLG	Al II	1670.7	L	-177.0	-0.00060	93.8	8.0
RX_J0048.3+3941	1670.24	ISMLG	Al II	1670.7	L	-98.0	-0.00033	193.6	6.4
RX_J0048.3+3941	1670.53	ISMLG	Al II	1670.7	L	-47.0	-0.00015	220.3	2.9
RX_J0048.3+3941	1670.84	ISMLG	Al II	1670.7	L	9.0	0.00000	238.9	6.4
RX_J0048.3+3941	1686.46	OTHER	FPN	0.0	H	0.0	-1.00000	24.6	8.6
RX_J0048.3+3941	1698.74	IGMABS	C IV	1548.2	H	29150.0	0.09723	35.8	7.2
RX_J0048.3+3941	1699.16	IGMABS	C IV	1548.2	H	29230.0	0.09753	76.2	8.1
RX_J0048.3+3941	1701.55	IGMABS	C IV	1550.7	H	29146.0	0.09723	47.0	9.0
RX_J0048.3+3941	1702.04	IGMABS	C IV	1550.7	H	29241.0	0.09753	30.6	7.9
RX_J0048.3+3941	1709.36	ISMLG	Ni II	1709.6	L	-42.0	-0.00015	28.6	5.4
RX_J0048.3+3941	1709.61	ISMLG	Ni II	1709.6	L	2.0	0.00000	44.3	7.1
RX_J0048.3+3941	1741.31	ISMLG	Ni II	1741.5	L	-43.0	-0.00015	39.8	5.1
RX_J0048.3+3941	1741.51	ISMLG	Ni II	1741.5	L	-7.0	0.00000	54.8	4.6
RX_J0048.3+3941	1751.62	ISMLG	Ni II	1751.9	L	-50.0	-0.00015	22.2	5.5
RX_J0048.3+3941	1751.90	ISMLG	Ni II	1751.9	L	-4.0	0.00000	34.6	5.7
RX_J0048.3+3941	1757.53	INTRINSIC	C IV	1548.2	H	40533.0	0.13519	357.9	7.6
RX_J0048.3+3941	1760.45	PROXIMATE	H I	1550.7	H	40532.0	0.13519	268.4	8.3
RX_J0050.8+3536	1134.09	ISMLG	N I	1134.1	L	-20.0	-0.00010	289.9	36.4
RX_J0050.8+3536	1134.30	ISMLG	N I	1134.4	L	-31.0	-0.00010	177.1	37.6
RX_J0050.8+3536	1134.86	ISMLG	N I	1134.9	L	-30.0	-0.00010	248.6	35.7
RX_J0050.8+3536	1142.26	ISMLG	Fe II	1142.3	L	-29.0	-0.00010	85.2	18.2

Table A1 *continued*

Table A1 (*continued*)

Target	λ_{obs}	Type	Ion	λ_{rest}	Frame	cz	z	W_{λ}	$\sigma_{W_{\lambda}}$
	(Å)			(Å)		(km s ⁻¹)		(mÅ)	(mÅ)
RX_J0050.8+3536	1143.13	ISMLG	Fe II	1143.2	L	-26.0	-0.00010	188.4	17.0
RX_J0050.8+3536	1144.87	ISMLG	Fe II	1144.9	L	-19.0	-0.00010	322.0	13.6
RX_J0050.8+3536	1152.74	ISMLG	P II	1152.8	L	-20.0	-0.00010	117.3	14.0
RX_J0050.8+3536	1189.89	ISMLG	Si II	1190.4	L	-134.0	-0.00045	93.1	8.4
RX_J0050.8+3536	1190.29	ISMLG	Si II	1190.4	L	-32.0	-0.00010	408.3	6.9
RX_J0050.8+3536	1192.33	OTHER	FPN	0.0	H	0.0	-1.00000	30.4	6.6
RX_J0050.8+3536	1192.79	ISMLG	Si II	1193.2	L	-127.0	-0.00045	93.3	8.3
RX_J0050.8+3536	1193.19	ISMLG	Si II	1193.2	L	-26.0	-0.00010	399.7	6.8
RX_J0050.8+3536	1199.49	ISMLG	N I	1199.5	L	-16.0	-0.00010	325.0	9.9
RX_J0050.8+3536	1200.16	ISMLG	N I	1200.2	L	-16.0	-0.00010	275.1	11.7
RX_J0050.8+3536	1200.64	ISMLG	N I	1200.7	L	-17.0	-0.00010	286.8	11.2
RX_J0050.8+3536	1205.50	ISMLG	Si III	1206.5	L	-248.0	-0.00081	98.6	8.1
RX_J0050.8+3536	1205.95	ISMLG	Si III	1206.5	L	-136.0	-0.00045	204.6	7.4
RX_J0050.8+3536	1206.37	ISMLG	Si III	1206.5	L	-33.0	-0.00010	473.1	8.4
RX_J0050.8+3536	1222.62	IGMABS	H I	1215.6	H	1713.0	0.00571	72.3	15.2
RX_J0050.8+3536	1223.34	IGMABS	H I	1215.6	H	1890.0	0.00631	56.2	8.9
RX_J0050.8+3536	1243.44	IGMABS	H I	1215.6	H	6849.0	0.02285	126.8	9.1
RX_J0050.8+3536	1250.50	ISMLG	S II	1250.5	L	-19.0	-0.00010	184.3	7.6
RX_J0050.8+3536	1253.72	ISMLG	S II	1253.8	L	-20.0	-0.00010	245.6	9.0
RX_J0050.8+3536	1259.42	ISMLG	S II	1259.5	L	-23.0	-0.00010	268.0	6.5
RX_J0050.8+3536	1259.88	ISMLG	Si II	1260.4	L	-129.0	-0.00045	196.6	5.3
RX_J0050.8+3536	1260.27	ISMLG	Si II	1260.4	L	-35.0	-0.00010	465.6	3.8
RX_J0050.8+3536	1260.65	ISMLG	C I	1260.7	L	-20.0	-0.00010	51.0	4.3
RX_J0050.8+3536	1260.91	IGMABS	H I	1215.6	H	11157.0	0.03722	97.4	4.9
RX_J0050.8+3536	1276.51	INTRINSIC	Si III	1206.5	H	17395.0	0.05806	55.2	6.6
RX_J0050.8+3536	1276.70	INTRINSIC	Si III	1206.5	H	17444.0	0.05820	38.2	4.3
RX_J0050.8+3536	1277.09	INTRINSIC	Si III	1206.5	H	17540.0	0.05849	168.8	4.0
RX_J0050.8+3536	1277.29	INTRINSIC	Si III	1206.5	H	17590.0	0.05868	89.1	3.3
RX_J0050.8+3536	1280.05	ISMLG	C I	1280.1	L	-21.0	-0.00010	13.3	5.7
RX_J0050.8+3536	1283.78	PROXIMATE	H I	1215.6	H	16797.0	0.05603	112.8	3.8
RX_J0050.8+3536	1284.21	INTRINSIC	H I	1215.6	H	16903.0	0.05638	325.9	2.4
RX_J0050.8+3536	1284.48	INTRINSIC	H I	1215.6	H	16970.0	0.05660	548.3	3.8
RX_J0050.8+3536	1286.25	INTRINSIC	H I	1215.6	H	17406.0	0.05806	653.2	2.2
RX_J0050.8+3536	1286.42	INTRINSIC	H I	1215.6	H	17447.0	0.05820	419.8	0.7
RX_J0050.8+3536	1286.78	INTRINSIC	H I	1215.6	H	17536.0	0.05849	285.6	0.6
RX_J0050.8+3536	1287.01	INTRINSIC	H I	1215.6	H	17593.0	0.05868	413.2	2.4
RX_J0050.8+3536	1301.56	ISMLG	O I	1302.1	L	-140.0	-0.00045	59.2	6.5
RX_J0050.8+3536	1302.02	ISMLG	O I	1302.1	L	-34.0	-0.00010	391.2	7.0
RX_J0050.8+3536	1303.75	ISMLG	Si II	1304.3	L	-143.0	-0.00045	76.8	8.9
RX_J0050.8+3536	1304.25	ISMLG	Si II	1304.3	L	-27.0	-0.00010	372.2	6.1
RX_J0050.8+3536	1308.67	INTRINSIC	N v	1238.8	H	16903.0	0.05638	52.8	5.7
RX_J0050.8+3536	1310.74	INTRINSIC	N v	1238.8	H	17404.0	0.05806	120.6	3.8
RX_J0050.8+3536	1310.86	INTRINSIC	N v	1238.8	H	17434.0	0.05820	145.0	3.6
RX_J0050.8+3536	1311.24	INTRINSIC	N v	1238.8	H	17525.0	0.05849	56.8	3.9
RX_J0050.8+3536	1311.53	INTRINSIC	N v	1238.8	H	17595.0	0.05868	45.2	5.6
RX_J0050.8+3536	1312.86	INTRINSIC	N v	1242.8	H	16898.0	0.05638	36.3	5.6
RX_J0050.8+3536	1314.92	INTRINSIC	N v	1242.8	H	17397.0	0.05806	89.5	5.9
RX_J0050.8+3536	1315.11	INTRINSIC	N v	1242.8	H	17443.0	0.05820	69.9	3.6
RX_J0050.8+3536	1315.45	INTRINSIC	N v	1242.8	H	17525.0	0.05849	43.4	6.3
RX_J0050.8+3536	1315.73	INTRINSIC	N v	1242.8	H	17592.0	0.05868	35.0	6.4
RX_J0050.8+3536	1317.14	ISMLG	Ni II	1317.2	L	-18.0	-0.00010	92.9	9.7
RX_J0050.8+3536	1328.73	ISMLG	C I	1328.8	L	-24.0	-0.00010	31.6	9.8
RX_J0050.8+3536	1333.44	ISMLG	C II	1334.5	L	-245.0	-0.00081	39.8	7.7

Table A1 continued

Table A1 (*continued*)

Target	λ_{obs}	Type	Ion	λ_{rest}	Frame	cz	z	W_{λ}	$\sigma_{W_{\lambda}}$
	(Å)			(Å)		(km s ⁻¹)		(mÅ)	(mÅ)
RX_J0050.8+3536	1333.93	ISMLG	C II	1334.5	L	-136.0	-0.00045	243.6	5.9
RX_J0050.8+3536	1334.41	ISMLG	C II	1334.5	L	-27.0	-0.00010	532.5	6.2
RX_J0050.8+3536	1335.61	ISMLG	C II*	1335.7	L	-22.0	-0.00010	226.9	8.5
RX_J0050.8+3536	1369.98	ISMLG	Ni II	1370.1	L	-33.0	-0.00010	75.8	10.2
RX_J0050.8+3536	1393.60	ISMLG	Si IV	1393.7	L	-35.0	-0.00010	157.5	12.0
RX_J0050.8+3536	1402.61	ISMLG	Si IV	1402.7	L	-34.0	-0.00010	80.0	11.7
RX_J0050.8+3536	1454.74	ISMLG	Ni II	1454.8	L	-21.0	-0.00010	47.2	9.5
RX_J0050.8+3536	1474.62	INTRINSIC	Si IV	1393.7	H	17393.0	0.05806	23.2	7.1
RX_J0050.8+3536	1474.87	INTRINSIC	Si IV	1393.7	H	17446.0	0.05820	103.1	11.3
RX_J0050.8+3536	1475.31	INTRINSIC	Si IV	1393.7	H	17541.0	0.05849	156.5	7.5
RX_J0050.8+3536	1475.53	INTRINSIC	Si IV	1393.7	H	17589.0	0.05868	103.5	6.4
RX_J0050.8+3536	1484.43	INTRINSIC	Si IV	1402.7	H	17451.0	0.05820	42.6	9.4
RX_J0050.8+3536	1484.82	INTRINSIC	Si IV	1402.7	H	17535.0	0.05849	79.8	8.5
RX_J0050.8+3536	1485.10	INTRINSIC	Si IV	1402.7	H	17594.0	0.05868	65.9	6.9
RX_J0050.8+3536	1525.98	ISMLG	Si II	1526.7	L	-143.0	-0.00045	87.1	13.1
RX_J0050.8+3536	1526.56	ISMLG	Si II	1526.7	L	-30.0	-0.00010	460.5	9.5
RX_J0050.8+3536	1546.94	ISMLG	C IV	1548.2	L	-245.0	-0.00081	92.2	14.1
RX_J0050.8+3536	1547.46	ISMLG	C IV	1548.2	L	-143.0	-0.00045	60.9	13.5
RX_J0050.8+3536	1548.04	ISMLG	C IV	1548.2	L	-32.0	-0.00010	241.3	14.5
RX_J0050.8+3536	1549.59	ISMLG	C IV	1550.7	L	-230.0	-0.00081	53.0	11.6
RX_J0050.8+3536	1550.62	ISMLG	C IV	1550.7	L	-32.0	-0.00010	117.8	13.1
RX_J0050.8+3536	1560.19	ISMLG	C I	1560.3	L	-23.0	-0.00010	70.0	16.4
RX_J0050.8+3536	1608.35	ISMLG	Fe II	1608.4	L	-19.0	-0.00010	381.3	22.3
RX_J0050.8+3536	1638.11	INTRINSIC	C IV	1548.2	H	17409.0	0.05806	228.7	5.1
RX_J0050.8+3536	1638.29	INTRINSIC	C IV	1548.2	H	17444.0	0.05820	538.3	7.1
RX_J0050.8+3536	1638.79	INTRINSIC	C IV	1548.2	H	17540.0	0.05849	698.2	5.4
RX_J0050.8+3536	1639.05	INTRINSIC	C IV	1548.2	H	17592.0	0.05868	203.6	4.4
RX_J0050.8+3536	1640.83	INTRINSIC	C IV	1550.7	H	17408.0	0.05806	187.6	4.7
RX_J0050.8+3536	1640.99	INTRINSIC	C IV	1550.7	H	17439.0	0.05820	433.7	6.9
RX_J0050.8+3536	1641.50	INTRINSIC	C IV	1550.7	H	17537.0	0.05849	655.0	8.2
RX_J0050.8+3536	1641.75	INTRINSIC	C IV	1550.7	H	17586.0	0.05868	192.0	5.5
RX_J0050.8+3536	1656.84	ISMLG	C I	1656.9	L	-16.0	-0.00010	82.0	16.8
RX_J0050.8+3536	1670.08	ISMLG	Al II	1670.7	L	-128.0	-0.00045	81.3	17.5
RX_J0050.8+3536	1670.65	ISMLG	Al II	1670.7	L	-25.0	-0.00010	478.8	15.3
RX_J0050.8+3536	1709.48	ISMLG	Ni II	1709.6	L	-22.0	-0.00010	84.4	23.4
RX_J0050.8+3536	1741.36	ISMLG	Ni II	1741.5	L	-33.0	-0.00010	85.2	21.4
RX_J0050.8+3536	1751.72	ISMLG	H I	1751.9	L	-33.0	-0.00010	60.5	26.9
RX_J0053.7+2232	1134.11	ISMLG	N I	1134.1	L	-14.0	-0.00007	178.0	57.5
RX_J0053.7+2232	1134.35	ISMLG	N I	1134.4	L	-18.0	-0.00007	95.6	53.3
RX_J0053.7+2232	1134.93	ISMLG	N I	1134.9	L	-14.0	-0.00007	158.0	41.1
RX_J0053.7+2232	1143.13	ISMLG	Fe II	1143.2	L	-26.0	-0.00007	120.0	23.7
RX_J0053.7+2232	1144.83	ISMLG	Fe II	1144.9	L	-28.0	-0.00007	260.1	24.7
RX_J0053.7+2232	1152.75	ISMLG	P II	1152.8	L	-17.0	-0.00007	92.1	28.5
RX_J0053.7+2232	1178.54	INTRINSIC	H I	1025.7	H	44664.0	0.14897	198.4	13.2
RX_J0053.7+2232	1185.28	INTRINSIC	O VI	1031.9	H	44552.0	0.14861	92.8	10.3
RX_J0053.7+2232	1185.66	INTRINSIC	O VI	1031.9	H	44664.0	0.14897	133.8	10.5
RX_J0053.7+2232	1190.32	ISMLG	Si II	1190.4	L	-24.0	-0.00007	402.7	8.9
RX_J0053.7+2232	1191.83	INTRINSIC	O VI	1037.6	H	44556.0	0.14861	85.5	9.4
RX_J0053.7+2232	1192.18	INTRINSIC	O VI	1037.6	H	44656.0	0.14897	63.7	8.4
RX_J0053.7+2232	1193.22	ISMLG	Si II	1193.2	L	-19.0	-0.00007	425.1	11.7
RX_J0053.7+2232	1199.46	ISMLG	N I	1199.5	L	-22.0	-0.00007	335.8	19.7
RX_J0053.7+2232	1200.15	ISMLG	N I	1200.2	L	-19.0	-0.00007	307.2	16.8
RX_J0053.7+2232	1200.61	ISMLG	N I	1200.7	L	-24.0	-0.00007	288.6	14.9

Table A1 continued

Table A1 (*continued*)

Target	λ_{obs}	Type	Ion	λ_{rest}	Frame	cz	z	W_{λ}	$\sigma_{W_{\lambda}}$
	(Å)			(Å)		(km s ⁻¹)		(mÅ)	(mÅ)
RX_J0053.7+2232	1205.18	ISMLG	Si III	1206.5	L	-328.0	-0.00110	118.9	8.3
RX_J0053.7+2232	1205.43	ISMLG	Si III	1206.5	L	-267.0	-0.00091	134.9	9.9
RX_J0053.7+2232	1205.94	ISMLG	Si III	1206.5	L	-139.0	-0.00045	81.1	10.6
RX_J0053.7+2232	1206.43	ISMLG	Si III	1206.5	L	-18.0	-0.00007	474.9	11.4
RX_J0053.7+2232	1222.53	IGMABS	H I	1215.6	H	1692.0	0.00564	88.4	18.6
RX_J0053.7+2232	1225.51	IGMABS	H I	1215.6	H	2426.0	0.00809	251.2	16.5
RX_J0053.7+2232	1226.74	IGMABS	H I	1215.6	H	2731.0	0.00911	78.3	18.2
RX_J0053.7+2232	1245.86	IGMABS	H I	1215.6	H	7446.0	0.02484	80.7	14.9
RX_J0053.7+2232	1250.50	ISMLG	S II	1250.5	L	-18.0	-0.00007	108.4	14.9
RX_J0053.7+2232	1253.70	ISMLG	S II	1253.8	L	-25.0	-0.00007	145.8	12.3
RX_J0053.7+2232	1259.01	ISMLG	Si II	1260.4	L	-335.0	-0.00110	54.2	13.4
RX_J0053.7+2232	1259.41	ISMLG	S II	1259.5	L	-25.0	-0.00007	208.0	13.5
RX_J0053.7+2232	1260.31	ISMLG	Si II	1260.4	L	-27.0	-0.00007	505.5	13.9
RX_J0053.7+2232	1296.84	IGMABS	H I	1215.6	H	20018.0	0.06677	114.3	17.6
RX_J0053.7+2232	1302.07	ISMLG	O I	1302.1	L	-23.0	-0.00007	359.7	25.3
RX_J0053.7+2232	1304.27	ISMLG	Si II	1304.3	L	-24.0	-0.00007	345.1	23.5
RX_J0053.7+2232	1313.44	IGMABS	H I	1215.6	H	24110.0	0.08042	140.8	23.0
RX_J0053.7+2232	1314.29	IGMABS	H I	1215.6	H	24321.0	0.08113	326.3	26.1
RX_J0053.7+2232	1317.14	ISMLG	Ni II	1317.2	L	-17.0	-0.00007	27.5	20.0
RX_J0053.7+2232	1333.08	ISMLG	C II	1334.5	L	-325.0	-0.00110	76.4	17.5
RX_J0053.7+2232	1334.45	ISMLG	C II	1334.5	L	-19.0	-0.00007	551.4	16.3
RX_J0053.7+2232	1335.65	ISMLG	C II*	1335.7	L	-13.0	-0.00007	144.5	16.1
RX_J0053.7+2232	1356.26	IGMABS	H I	1215.6	H	34669.0	0.11564	77.0	19.0
RX_J0053.7+2232	1360.43	IGMABS	H I	1215.6	H	35698.0	0.11907	150.0	19.1
RX_J0053.7+2232	1370.01	ISMLG	Ni II	1370.1	L	-27.0	-0.00007	70.2	15.5
RX_J0053.7+2232	1381.37	IGMABS	H I	1215.6	H	40862.0	0.13630	138.0	15.1
RX_J0053.7+2232	1386.25	INTRINSIC	Si III	1206.5	H	44665.0	0.14897	91.9	9.9
RX_J0053.7+2232	1392.17	ISMLG	Si IV	1393.7	L	-342.0	-0.00110	18.5	5.8
RX_J0053.7+2232	1393.67	ISMLG	Si IV	1393.7	L	-20.0	-0.00007	167.2	7.2
RX_J0053.7+2232	1394.56	INTRINSIC	H I	1215.6	H	44114.0	0.14715	18.1	6.6
RX_J0053.7+2232	1396.77	INTRINSIC	H I	1215.6	H	44660.0	0.14897	350.1	7.1
RX_J0053.7+2232	1402.68	ISMLG	Si IV	1402.7	L	-19.0	-0.00007	121.3	13.0
RX_J0053.7+2232	1526.57	ISMLG	Si II	1526.7	L	-26.0	-0.00007	428.1	17.9
RX_J0053.7+2232	1548.10	ISMLG	C IV	1548.2	L	-19.0	-0.00007	150.1	27.6
RX_J0053.7+2232	1550.65	ISMLG	C IV	1550.7	L	-26.0	-0.00007	80.2	27.1
RX_J0053.7+2232	1608.29	ISMLG	Fe II	1608.4	L	-29.0	-0.00007	376.5	33.9
RX_J0053.7+2232	1670.63	ISMLG	Al II	1670.7	L	-28.0	-0.00007	494.7	36.8
RX_J0053.7+2232	1778.82	INTRINSIC	C IV	1548.2	H	44656.0	0.14897	163.7	37.2
RX_J0053.7+2232	1781.77	PROXIMATE	H I	1550.7	H	44653.0	0.14897	147.4	37.6
SDSSJ011623.06+142940.6	1190.36	ISMLG	Si II	1190.4	L	-15.0	-0.00003	322.6	24.0
SDSSJ011623.06+142940.6	1193.24	ISMLG	Si II	1193.2	L	-11.0	-0.00003	417.5	27.9
SDSSJ011623.06+142940.6	1197.18	ISMLG	Mn II	1197.1	L	-1.0	-0.00003	77.0	27.4
SDSSJ011623.06+142940.6	1199.51	ISMLG	N I	1199.5	L	-10.0	-0.00003	251.8	45.1
SDSSJ011623.06+142940.6	1200.19	ISMLG	N I	1200.2	L	-7.0	-0.00003	252.9	36.8
SDSSJ011623.06+142940.6	1200.69	ISMLG	N I	1200.7	L	-4.0	-0.00003	229.4	45.1
SDSSJ011623.06+142940.6	1205.36	ISMLG	Si III	1206.5	L	-283.0	-0.00094	151.5	27.2
SDSSJ011623.06+142940.6	1205.95	ISMLG	Si III	1206.5	L	-137.0	-0.00044	130.6	21.2
SDSSJ011623.06+142940.6	1206.49	ISMLG	Si III	1206.5	L	-1.0	-0.00003	477.0	27.1
SDSSJ011623.06+142940.6	1210.97	IGMABS	H I	1025.7	H	54142.0	0.18059	213.7	43.2
SDSSJ011623.06+142940.6	1226.23	IGMABS	H I	919.3	H	100070.0	0.33379	53.8	25.2
SDSSJ011623.06+142940.6	1228.39	IGMABS	H I	920.9	H	100074.0	0.33379	128.6	30.6
SDSSJ011623.06+142940.6	1231.30	IGMABS	H I	923.1	H	100072.0	0.33379	112.6	24.2
SDSSJ011623.06+142940.6	1232.51	IGMABS	H I	1215.6	H	4152.0	0.01385	108.1	27.8

Table A1 continued

Table A1 (*continued*)

Target	λ_{obs}	Type	Ion	λ_{rest}	Frame	cz	z	W_{λ}	$\sigma_{W_{\lambda}}$
	(Å)			(Å)		(km s ⁻¹)		(mÅ)	(mÅ)
SDSSJ011623.06+142940.6	1235.40	IGMABS	H I	926.2	H	100070.0	0.33379	173.1	31.6
SDSSJ011623.06+142940.6	1241.42	IGMABS	H I	930.7	H	100066.0	0.33379	224.9	22.7
SDSSJ011623.06+142940.6	1242.75	IGMABS	H I	1215.6	H	6678.0	0.02227	69.5	22.3
SDSSJ011623.06+142940.6	1243.47	IGMABS	H I	1215.6	H	6856.0	0.02287	130.3	30.1
SDSSJ011623.06+142940.6	1250.58	ISMLG	S II	1250.5	L	0.0	-0.00003	156.8	17.5
SDSSJ011623.06+142940.6	1250.83	IGMABS	H I	937.8	H	100066.0	0.33379	239.3	13.8
SDSSJ011623.06+142940.6	1253.75	ISMLG	S II	1253.8	L	-13.0	-0.00003	179.4	22.4
SDSSJ011623.06+142940.6	1259.47	ISMLG	S II	1259.5	L	-12.0	-0.00003	255.5	23.7
SDSSJ011623.06+142940.6	1259.85	ISMLG	Si II	1260.4	L	-137.0	-0.00044	81.2	21.1
SDSSJ011623.06+142940.6	1260.36	ISMLG	Si II	1260.4	L	-15.0	-0.00003	475.2	21.4
SDSSJ011623.06+142940.6	1263.16	IGMABS	H I	1025.7	H	69397.0	0.23150	132.0	28.5
SDSSJ011623.06+142940.6	1266.76	IGMABS	H I	949.7	H	100068.0	0.33379	320.5	19.0
SDSSJ011623.06+142940.6	1267.12	IGMABS	H I	1215.6	H	12688.0	0.04232	194.3	19.3
SDSSJ011623.06+142940.6	1270.66	IGMABS	H I	1215.6	H	13561.0	0.04524	144.0	27.9
SDSSJ011623.06+142940.6	1280.12	ISMLG	C I	1280.1	L	-3.0	-0.00003	138.5	21.8
SDSSJ011623.06+142940.6	1288.29	IGMABS	H I	1215.6	H	17907.0	0.05973	276.4	19.1
SDSSJ011623.06+142940.6	1297.15	IGMABS	H I	972.5	H	100066.0	0.33379	310.7	39.0
SDSSJ011623.06+142940.6	1320.41	IGMABS	H I	1215.6	H	25829.0	0.08616	116.9	33.2
SDSSJ011623.06+142940.6	1333.97	ISMLG	C II	1334.5	L	-126.0	-0.00044	89.9	21.0
SDSSJ011623.06+142940.6	1334.49	ISMLG	C II	1334.5	L	-10.0	-0.00003	474.8	24.2
SDSSJ011623.06+142940.6	1335.67	ISMLG	C II*	1335.7	L	-9.0	-0.00003	163.1	29.5
SDSSJ011623.06+142940.6	1359.89	IGMABS	H I	1215.6	H	35566.0	0.11863	123.9	24.1
SDSSJ011623.06+142940.6	1364.58	IGMABS	H I	1215.6	H	36722.0	0.12249	253.2	20.2
SDSSJ011623.06+142940.6	1366.11	IGMABS	H I	1215.6	H	37100.0	0.12375	292.6	18.4
SDSSJ011623.06+142940.6	1368.09	IGMABS	H I	1025.7	H	100066.0	0.33379	666.7	27.0
SDSSJ011623.06+142940.6	1376.12	IGMABS	H I	1215.6	H	39569.0	0.13199	124.1	24.0
SDSSJ011623.06+142940.6	1376.40	IGMABS	O VI	1031.9	H	100077.0	0.33379	179.3	22.9
SDSSJ011623.06+142940.6	1383.95	IGMABS	O VI	1037.6	H	100063.0	0.33379	179.8	27.9
SDSSJ011623.06+142940.6	1393.75	ISMLG	Si IV	1393.7	L	-2.0	-0.00003	169.8	29.1
SDSSJ011623.06+142940.6	1402.73	ISMLG	Si IV	1402.7	L	-9.0	-0.00003	138.2	32.9
SDSSJ011623.06+142940.6	1403.12	IGMABS	H I	1025.7	H	110304.0	0.36792	124.2	19.2
SDSSJ011623.06+142940.6	1424.19	IGMABS	H I	1215.6	H	51424.0	0.17153	58.5	13.7
SDSSJ011623.06+142940.6	1435.20	IGMABS	H I	1215.6	H	54138.0	0.18059	562.3	16.3
SDSSJ011623.06+142940.6	1436.86	IGMABS	H I	1215.6	H	54546.0	0.18195	213.9	13.9
SDSSJ011623.06+142940.6	1444.87	IGMABS	H I	1215.6	H	56522.0	0.18854	84.8	16.5
SDSSJ011623.06+142940.6	1472.78	IGMABS	H I	1215.6	H	63406.0	0.21150	161.3	23.2
SDSSJ011623.06+142940.6	1497.10	IGMABS	H I	1215.6	H	69403.0	0.23150	416.5	22.5
SDSSJ011623.06+142940.6	1511.28	IGMABS	H I	1215.6	H	72900.0	0.24317	266.6	24.5
SDSSJ011623.06+142940.6	1517.74	IGMABS	H I	1215.6	H	74494.0	0.24848	106.9	19.4
SDSSJ011623.06+142940.6	1526.66	ISMLG	Si II	1526.7	L	-8.0	-0.00003	404.8	32.6
SDSSJ011623.06+142940.6	1547.49	ISMLG	C IV	1548.2	L	-139.0	-0.00044	125.5	23.5
SDSSJ011623.06+142940.6	1548.20	ISMLG	C IV	1548.2	L	0.0	-0.00003	216.4	27.3
SDSSJ011623.06+142940.6	1550.10	ISMLG	C IV	1550.7	L	-132.0	-0.00044	83.3	21.6
SDSSJ011623.06+142940.6	1550.79	ISMLG	C IV	1550.7	L	2.0	-0.00003	126.8	25.7
SDSSJ011623.06+142940.6	1600.87	IGMABS	H I	1215.6	H	94993.0	0.31686	100.4	37.1
SDSSJ011623.06+142940.6	1608.38	ISMLG	Fe II	1608.4	L	-13.0	-0.00003	264.8	40.9
SDSSJ011623.06+142940.6	1609.24	IGMABS	Si III	1206.5	H	100074.0	0.33379	280.0	44.5
SDSSJ011623.06+142940.6	1621.45	IGMABS	H I	1215.6	H	100067.0	0.33379	940.1	38.0
SDSSJ011623.06+142940.6	1650.85	IGMABS	H I	1215.6	H	107319.0	0.35798	228.1	41.0
SDSSJ011623.06+142940.6	1653.26	IGMABS	H I	1215.6	H	107913.0	0.35996	351.6	51.1
SDSSJ011623.06+142940.6	1662.94	IGMABS	H I	1215.6	H	110301.0	0.36792	267.5	30.6
SDSSJ011623.06+142940.6	1670.71	ISMLG	Al II	1670.7	L	-15.0	-0.00003	457.5	29.5
SDSSJ011623.06+142940.6	1691.50	PROXIMATE	H I	1215.6	H	117344.0	0.39142	50.2	16.5

Table A1 *continued*

Table A1 (*continued*)

Target	λ_{obs}	Type	Ion	λ_{rest}	Frame	cz	z	W_{λ}	$\sigma_{W_{\lambda}}$
	(Å)			(Å)		(km s ⁻¹)		(mÅ)	(mÅ)
SDSSJ014143.20+134032.0	1144.84	ISMLG	Fe II	1144.9	L	-26.0	-0.00002	248.5	95.9
SDSSJ014143.20+134032.0	1163.48	UNIDENTIFIED	UNIND	1000.0	H	0.0	-1.00000	368.2	93.5
SDSSJ014143.20+134032.0	1190.31	ISMLG	Si II	1190.4	L	-27.0	-0.00002	475.2	79.4
SDSSJ014143.20+134032.0	1193.20	ISMLG	Si II	1193.2	L	-23.0	-0.00002	566.4	72.3
SDSSJ014143.20+134032.0	1193.56	IGMABS	Si II	1190.4	H	792.0	0.00263	148.8	43.3
SDSSJ014143.20+134032.0	1196.45	IGMABS	Si II	1193.2	H	793.0	0.00263	917.7	120.1
SDSSJ014143.20+134032.0	1206.42	ISMLG	Si III	1206.5	L	-19.0	-0.00002	649.2	78.2
SDSSJ014143.20+134032.0	1209.05	IGMABS	Si III	1206.5	H	634.0	0.00213	270.9	47.4
SDSSJ014143.20+134032.0	1209.69	IGMABS	Si III	1206.5	H	794.0	0.00263	187.7	37.4
SDSSJ014143.20+134032.0	1218.27	IGMABS	H I	1215.6	H	640.0	0.00213	501.5	108.1
SDSSJ014143.20+134032.0	1218.87	IGMABS	H I	1215.6	H	789.0	0.00263	1070.4	140.9
SDSSJ014143.20+134032.0	1228.81	IGMABS	H I	1215.6	H	3240.0	0.01081	1327.5	143.1
SDSSJ014143.20+134032.0	1244.09	INTRINSIC	Si II	1190.4	H	13518.0	0.04508	283.0	41.5
SDSSJ014143.20+134032.0	1247.10	INTRINSIC	Si II	1193.2	H	13519.0	0.04508	286.3	49.1
SDSSJ014143.20+134032.0	1253.73	ISMLG	S II	1253.8	L	-19.0	-0.00002	292.0	53.3
SDSSJ014143.20+134032.0	1259.44	ISMLG	S II	1259.5	L	-18.0	-0.00002	210.0	45.2
SDSSJ014143.20+134032.0	1260.32	ISMLG	Si II	1260.4	L	-24.0	-0.00002	658.6	43.4
SDSSJ014143.20+134032.0	1263.75	IGMABS	Si II	1260.4	H	791.0	0.00263	292.0	38.3
SDSSJ014143.20+134032.0	1267.96	PROXIMATE	H I	1215.6	H	12896.0	0.04301	229.2	36.7
SDSSJ014143.20+134032.0	1269.17	INTRINSIC	H I	1215.6	H	13193.0	0.04401	497.5	23.1
SDSSJ014143.20+134032.0	1270.48	INTRINSIC	H I	1215.6	H	13516.0	0.04508	141.0	11.3
SDSSJ014143.20+134032.0	1317.29	INTRINSIC	Si II	1260.4	H	13527.0	0.04508	324.6	68.0
SDSSJ014143.20+134032.0	1334.45	ISMLG	C II	1334.5	L	-19.0	-0.00002	496.3	41.3
SDSSJ014143.20+134032.0	1335.61	ISMLG	C II*	1335.7	L	-22.0	-0.00002	132.1	41.4
SDSSJ014143.20+134032.0	1337.42	IGMABS	C II	1334.5	H	649.0	0.00213	162.4	38.6
SDSSJ014143.20+134032.0	1338.06	IGMABS	C II	1334.5	H	793.0	0.00263	327.3	47.9
SDSSJ014143.20+134032.0	1393.71	ISMLG	Si IV	1393.7	L	-12.0	-0.00002	211.1	40.0
SDSSJ014143.20+134032.0	1394.73	INTRINSIC	C II	1334.5	H	13522.0	0.04508	398.4	53.9
SDSSJ014143.20+134032.0	1397.42	IGMABS	Si IV	1393.7	H	788.0	0.00263	191.0	50.5
SDSSJ014143.20+134032.0	1406.51	IGMABS	H I	1402.7	H	798.0	0.00263	326.4	67.6
SDSSJ015952.95+134554.3	1152.83	ISMLG	P II	1152.8	L	3.0	-0.00001	91.7	32.9
SDSSJ015952.95+134554.3	1157.64	IGMABS	H I	972.5	H	57058.0	0.19029	144.6	29.4
SDSSJ015952.95+134554.3	1162.96	IGMABS	C III	977.0	H	57055.0	0.19029	66.3	23.3
SDSSJ015952.95+134554.3	1184.69	UNIDENTIFIED	UNIND	1000.0	H	0.0	-1.00000	102.5	20.2
SDSSJ015952.95+134554.3	1188.84	ISMLG	C I	1188.8	L	3.0	-0.00001	125.8	19.6
SDSSJ015952.95+134554.3	1190.02	ISMLG	Si II	1190.4	L	-101.0	-0.00034	108.9	14.2
SDSSJ015952.95+134554.3	1190.37	ISMLG	Si II	1190.4	L	-12.0	-0.00001	310.1	13.0
SDSSJ015952.95+134554.3	1192.88	ISMLG	Si II	1193.2	L	-104.0	-0.00034	116.3	12.4
SDSSJ015952.95+134554.3	1193.25	ISMLG	Si II	1193.2	L	-11.0	-0.00001	361.4	12.4
SDSSJ015952.95+134554.3	1197.17	ISMLG	Mn II	1197.1	L	-3.0	-0.00001	44.7	13.1
SDSSJ015952.95+134554.3	1199.53	ISMLG	N I	1199.5	L	-5.0	-0.00001	244.4	19.7
SDSSJ015952.95+134554.3	1200.22	ISMLG	N I	1200.2	L	0.0	-0.00001	190.2	19.3
SDSSJ015952.95+134554.3	1200.69	ISMLG	N I	1200.7	L	-5.0	-0.00001	177.8	21.4
SDSSJ015952.95+134554.3	1202.83	IGMABS	O III	832.9	H	133138.0	0.44412	132.3	17.1
SDSSJ015952.95+134554.3	1205.88	ISMLG	Si III	1206.5	L	-155.0	-0.00052	77.2	13.8
SDSSJ015952.95+134554.3	1206.11	ISMLG	Si III	1206.5	L	-97.0	-0.00034	145.0	11.9
SDSSJ015952.95+134554.3	1206.46	ISMLG	Si III	1206.5	L	-10.0	-0.00001	448.9	14.8
SDSSJ015952.95+134554.3	1220.91	IGMABS	H I	1025.7	H	57047.0	0.19029	425.3	34.2
SDSSJ015952.95+134554.3	1228.35	IGMABS	O VI	1031.9	H	57065.0	0.19029	86.7	16.8
SDSSJ015952.95+134554.3	1229.96	IGMABS	H I	1215.6	H	3524.0	0.01175	47.2	16.7
SDSSJ015952.95+134554.3	1234.75	IGMABS	H I	1215.6	H	4706.0	0.01570	238.0	19.4
SDSSJ015952.95+134554.3	1235.12	IGMABS	O VI	1037.6	H	57065.0	0.19029	49.6	18.8
SDSSJ015952.95+134554.3	1239.93	ISMLG	Mg II	1239.9	L	0.0	-0.00001	28.6	12.9

Table A1 continued

Table A1 (*continued*)

Target	λ_{obs}	Type	Ion	λ_{rest}	Frame	cz	z	W_{λ}	$\sigma_{W_{\lambda}}$
	(Å)			(Å)		(km s ⁻¹)		(mÅ)	(mÅ)
SDSSJ015952.95+134554.3	1242.95	IGMABS	Si II	1190.4	H	13230.0	0.04413	83.0	13.6
SDSSJ015952.95+134554.3	1245.95	IGMABS	Si II	1193.2	H	13231.0	0.04413	109.9	17.6
SDSSJ015952.95+134554.3	1250.58	ISMLG	S II	1250.5	L	1.0	-0.00001	80.2	14.9
SDSSJ015952.95+134554.3	1253.75	ISMLG	S II	1253.8	L	-13.0	-0.00001	110.3	13.5
SDSSJ015952.95+134554.3	1255.17	IGMABS	H I	1215.6	H	9741.0	0.03249	68.1	17.7
SDSSJ015952.95+134554.3	1259.49	ISMLG	S II	1259.5	L	-6.0	-0.00001	246.7	11.3
SDSSJ015952.95+134554.3	1259.75	IGMABS	Si III	1206.5	H	13232.0	0.04413	358.2	8.5
SDSSJ015952.95+134554.3	1259.97	ISMLG	Si II	1260.4	L	-107.0	-0.00034	194.4	8.1
SDSSJ015952.95+134554.3	1260.37	ISMLG	Si II	1260.4	L	-11.0	-0.00001	473.9	11.1
SDSSJ015952.95+134554.3	1260.74	ISMLG	C I	1260.7	L	1.0	-0.00001	126.2	9.5
SDSSJ015952.95+134554.3	1269.31	IGMABS	H I	1215.6	H	13229.0	0.04413	901.4	12.6
SDSSJ015952.95+134554.3	1270.36	IGMABS	H I	1215.6	H	13488.0	0.04499	457.4	11.4
SDSSJ015952.95+134554.3	1270.83	IGMABS	H I	1215.6	H	13603.0	0.04537	81.5	15.7
SDSSJ015952.95+134554.3	1276.10	IGMABS	H I	1215.6	H	14903.0	0.04971	30.7	14.1
SDSSJ015952.95+134554.3	1277.23	ISMLG	C I	1277.2	L	-3.0	-0.00001	74.4	13.3
SDSSJ015952.95+134554.3	1284.94	IGMABS	H I	1215.6	H	17084.0	0.05699	91.5	17.0
SDSSJ015952.95+134554.3	1301.71	ISMLG	O I	1302.1	L	-106.0	-0.00034	128.3	25.1
SDSSJ015952.95+134554.3	1302.12	ISMLG	O I	1302.1	L	-12.0	-0.00001	363.8	27.5
SDSSJ015952.95+134554.3	1303.90	ISMLG	Si II	1304.3	L	-107.0	-0.00034	102.7	20.4
SDSSJ015952.95+134554.3	1304.39	ISMLG	Si II	1304.3	L	5.0	-0.00001	417.1	26.8
SDSSJ015952.95+134554.3	1316.08	IGMABS	Si II	1260.4	H	13238.0	0.04413	184.7	35.3
SDSSJ015952.95+134554.3	1317.23	ISMLG	Ni II	1317.2	L	2.0	-0.00001	62.0	23.7
SDSSJ015952.95+134554.3	1328.82	ISMLG	C I	1328.8	L	-3.0	-0.00001	45.6	26.3
SDSSJ015952.95+134554.3	1334.11	ISMLG	C II	1334.5	L	-94.0	-0.00034	181.0	12.8
SDSSJ015952.95+134554.3	1334.48	ISMLG	C II	1334.5	L	-12.0	-0.00001	483.3	18.1
SDSSJ015952.95+134554.3	1335.72	ISMLG	C II*	1335.7	L	3.0	-0.00001	115.7	17.9
SDSSJ015952.95+134554.3	1347.26	ISMLG	Cl I	1347.2	L	5.0	-0.00001	42.9	17.6
SDSSJ015952.95+134554.3	1354.30	IGMABS	H I	937.8	H	133143.0	0.44412	92.2	21.7
SDSSJ015952.95+134554.3	1371.52	IGMABS	H I	949.7	H	133135.0	0.44412	187.2	28.3
SDSSJ015952.95+134554.3	1375.30	IGMABS	H I	1215.6	H	39365.0	0.13131	149.2	24.6
SDSSJ015952.95+134554.3	1376.42	IGMABS	H I	949.7	H	134683.0	0.44927	69.9	21.7
SDSSJ015952.95+134554.3	1378.28	IGMABS	H I	1215.6	H	40100.0	0.13376	70.1	21.5
SDSSJ015952.95+134554.3	1382.00	IGMABS	H I	972.5	H	126220.0	0.42105	46.2	12.6
SDSSJ015952.95+134554.3	1393.47	IGMABS	C II	1334.5	H	13241.0	0.04413	268.6	17.6
SDSSJ015952.95+134554.3	1393.74	ISMLG	Si IV	1393.7	L	-5.0	-0.00001	296.9	18.5
SDSSJ015952.95+134554.3	1394.57	IGMABS	C II	1334.5	H	13488.0	0.04499	54.2	21.0
SDSSJ015952.95+134554.3	1395.01	IGMABS	H I	1215.6	H	44225.0	0.14752	67.3	17.3
SDSSJ015952.95+134554.3	1402.02	IGMABS	H I	972.5	H	132392.0	0.44161	203.0	25.5
SDSSJ015952.95+134554.3	1402.72	ISMLG	Si IV	1402.7	L	-11.0	-0.00001	88.9	23.6
SDSSJ015952.95+134554.3	1404.46	IGMABS	H I	972.5	H	133143.0	0.44412	277.1	26.2
SDSSJ015952.95+134554.3	1408.47	IGMABS	C III	977.0	H	132389.0	0.44161	160.0	21.9
SDSSJ015952.95+134554.3	1409.46	IGMABS	H I	972.5	H	134687.0	0.44927	196.6	18.5
SDSSJ015952.95+134554.3	1410.94	IGMABS	C III	977.0	H	133147.0	0.44412	351.9	21.7
SDSSJ015952.95+134554.3	1415.92	IGMABS	C III	977.0	H	134675.0	0.44927	138.4	20.3
SDSSJ015952.95+134554.3	1417.06	IGMABS	H I	1215.6	H	49665.0	0.16567	80.4	20.9
SDSSJ015952.95+134554.3	1419.65	IGMABS	H I	1215.6	H	50304.0	0.16780	55.6	25.6
SDSSJ015952.95+134554.3	1422.04	IGMABS	H I	1215.6	H	50893.0	0.16976	116.4	27.1
SDSSJ015952.95+134554.3	1428.55	IGMABS	H I	1215.6	H	52497.0	0.17511	220.3	22.9
SDSSJ015952.95+134554.3	1430.05	IGMABS	H I	1215.6	H	52866.0	0.17634	162.7	30.4
SDSSJ015952.95+134554.3	1447.00	IGMABS	H I	1215.6	H	57049.0	0.19029	609.9	36.9
SDSSJ015952.95+134554.3	1455.14	IGMABS	H I	1215.6	H	59054.0	0.19698	222.0	45.0
SDSSJ015952.95+134554.3	1457.60	IGMABS	H I	1025.7	H	126227.0	0.42105	162.0	53.3
SDSSJ015952.95+134554.3	1460.08	PROXIMATE	H I	1215.6	H	60274.0	0.20105	124.8	39.1

Table A1 *continued*

Table A1 (*continued*)

Target	λ_{obs}	Type	Ion	λ_{rest}	Frame	cz	z	W_{λ}	$\sigma_{W_{\lambda}}$
	(Å)			(Å)		(km s ⁻¹)		(mÅ)	(mÅ)
SDSSJ021348.53+125951.4	1260.36	ISMLG	Si II	1260.4	L	-15.0	-0.00002	538.3	90.0
SDSSJ021348.53+125951.4	1290.14	IGMABS	H I	1215.6	H	18365.0	0.06126	415.0	187.6
SDSSJ021348.53+125951.4	1334.05	ISMLG	C II	1334.5	L	-108.0	-0.00036	190.5	45.7
SDSSJ021348.53+125951.4	1334.51	ISMLG	C II	1334.5	L	-5.0	-0.00002	467.4	70.1
SDSSJ021348.53+125951.4	1393.73	ISMLG	Si IV	1393.7	L	-7.0	-0.00002	271.1	107.4
SDSSJ021348.53+125951.4	1402.74	ISMLG	Si IV	1402.7	L	-6.0	-0.00002	331.9	81.7
SDSSJ021348.53+125951.4	1415.39	IGMABS	H I	1215.6	H	49252.0	0.16429	340.2	93.7
SDSSJ021348.53+125951.4	1432.58	IGMABS	H I	1215.6	H	53491.0	0.17843	2748.1	170.4
SDSSJ021348.53+125951.4	1481.51	INTRINSIC	H I	1215.6	H	65557.0	0.21867	403.4	32.0
SDSSJ021348.53+125951.4	1526.62	ISMLG	Si II	1526.7	L	-16.0	-0.00002	437.6	84.4
SDSSJ021348.53+125951.4	1548.18	ISMLG	C IV	1548.2	L	-4.0	-0.00002	254.4	89.8
SDSSJ021348.53+125951.4	1550.71	ISMLG	C IV	1550.7	L	-13.0	-0.00002	305.1	104.3
SDSSJ021348.53+125951.4	1608.42	ISMLG	Fe II	1608.4	L	-5.0	-0.00002	311.6	105.7
SDSSJ021348.53+125951.4	1614.34	UNIDENTIFIED	UNIND	1000.0	H	0.0	-1.00000	574.8	138.4
SDSSJ021348.53+125951.4	1620.47	UNIDENTIFIED	UNIND	1000.0	H	0.0	-1.00000	824.0	168.0
SDSSJ021348.53+125951.4	1627.50	UNIDENTIFIED	UNIND	1000.0	H	0.0	-1.00000	2078.4	251.0
SDSSJ021348.53+125951.4	1670.74	ISMLG	Al II	1670.7	L	-8.0	-0.00002	482.1	163.0
SDSSJ021348.53+125951.4	1687.83	PROXIMATE	H I	1000.0	H	0.0	-1.00000	1036.8	288.1
SDSSJ225738.20+134045.0	1140.13	IGMABS	H I	1025.7	H	33439.0	0.11154	148.0	44.6
SDSSJ225738.20+134045.0	1143.13	ISMLG	Fe II	1143.2	L	-24.0	-0.00003	132.8	58.9
SDSSJ225738.20+134045.0	1144.87	ISMLG	Fe II	1144.9	L	-19.0	-0.00003	373.5	63.1
SDSSJ225738.20+134045.0	1148.27	IGMABS	O III	832.9	H	113500.0	0.37861	127.1	41.1
SDSSJ225738.20+134045.0	1153.94	IGMABS	H I	1025.7	H	37474.0	0.12497	333.4	66.7
SDSSJ225738.20+134045.0	1180.74	IGMABS	O IV	787.7	H	149581.0	0.49895	283.2	30.3
SDSSJ225738.20+134045.0	1181.15	IGMABS	O IV	787.7	H	149738.0	0.49947	117.6	21.1
SDSSJ225738.20+134045.0	1189.00	ISMLG	Si II	1190.4	L	-357.0	-0.00116	199.7	29.5
SDSSJ225738.20+134045.0	1190.34	ISMLG	Si II	1190.4	L	-20.0	-0.00003	440.6	27.0
SDSSJ225738.20+134045.0	1191.94	ISMLG	Si II	1193.2	L	-340.0	-0.00116	170.7	26.0
SDSSJ225738.20+134045.0	1193.21	ISMLG	Si II	1193.2	L	-19.0	-0.00003	446.5	26.8
SDSSJ225738.20+134045.0	1193.99	ISMLG	C I	1193.9	L	-1.0	-0.00003	47.9	23.3
SDSSJ225738.20+134045.0	1194.85	IGMABS	H I	972.5	H	68531.0	0.22862	65.8	33.0
SDSSJ225738.20+134045.0	1199.50	ISMLG	N I	1199.5	L	-13.0	-0.00003	292.0	31.1
SDSSJ225738.20+134045.0	1200.18	ISMLG	N I	1200.2	L	-12.0	-0.00003	305.1	27.9
SDSSJ225738.20+134045.0	1200.65	ISMLG	N I	1200.7	L	-14.0	-0.00003	253.3	29.6
SDSSJ225738.20+134045.0	1204.77	ISMLG	Si III	1206.5	L	-431.0	-0.00145	114.2	18.1
SDSSJ225738.20+134045.0	1205.12	ISMLG	Si III	1206.5	L	-342.0	-0.00116	368.7	20.1
SDSSJ225738.20+134045.0	1206.50	ISMLG	Si III	1206.5	L	-1.0	-0.00003	636.7	29.7
SDSSJ225738.20+134045.0	1226.14	IGMABS	H I	1215.6	H	2582.0	0.00861	210.5	26.5
SDSSJ225738.20+134045.0	1231.79	IGMABS	H I	1025.7	H	60230.0	0.20090	48.2	21.2
SDSSJ225738.20+134045.0	1248.50	IGMABS	O III	832.9	H	149577.0	0.49895	149.3	24.4
SDSSJ225738.20+134045.0	1250.54	ISMLG	S II	1250.5	L	-9.0	-0.00003	178.6	19.5
SDSSJ225738.20+134045.0	1250.93	IGMABS	H I	1215.6	H	8695.0	0.02900	101.0	20.0
SDSSJ225738.20+134045.0	1251.64	IGMABS	H I	1215.6	H	8870.0	0.02959	516.8	26.2
SDSSJ225738.20+134045.0	1253.75	ISMLG	S II	1253.8	L	-13.0	-0.00003	202.8	18.8
SDSSJ225738.20+134045.0	1256.67	IGMABS	H I	1215.6	H	10110.0	0.03372	151.5	21.5
SDSSJ225738.20+134045.0	1258.61	ISMLG	Si II	1260.4	L	-430.0	-0.00145	67.0	14.4
SDSSJ225738.20+134045.0	1258.92	ISMLG	Si II	1260.4	L	-356.0	-0.00116	247.2	18.2
SDSSJ225738.20+134045.0	1259.45	ISMLG	S II	1259.5	L	-17.0	-0.00003	234.6	16.2
SDSSJ225738.20+134045.0	1260.22	IGMABS	H I	1025.7	H	68537.0	0.22862	294.6	17.0
SDSSJ225738.20+134045.0	1260.34	ISMLG	Si II	1260.4	L	-20.0	-0.00003	577.3	20.5
SDSSJ225738.20+134045.0	1260.72	ISMLG	C I	1260.7	L	-3.0	-0.00003	82.9	13.2
SDSSJ225738.20+134045.0	1261.37	IGMABS	H I	1215.6	H	11269.0	0.03759	148.3	23.2
SDSSJ225738.20+134045.0	1263.26	ISMLG	Si II*	1264.7	L	-350.0	-0.00116	37.2	27.0

Table A1 continued

Table A1 (*continued*)

Target	λ_{obs}	Type	Ion	λ_{rest}	Frame	cz	z	W_{λ}	$\sigma_{W_{\lambda}}$
	(Å)			(Å)		(km s ⁻¹)		(mÅ)	(mÅ)
SDSSJ225738.20+134045.0	1264.19	IGMABS	H I	1215.6	H	11965.0	0.03991	165.9	25.2
SDSSJ225738.20+134045.0	1277.23	ISMLG	C I	1277.2	L	-3.0	-0.00003	99.4	29.9
SDSSJ225738.20+134045.0	1280.17	ISMLG	C I	1280.1	L	8.0	-0.00003	119.8	46.5
SDSSJ225738.20+134045.0	1286.95	IGMABS	H I	1215.6	H	17579.0	0.05864	98.2	26.0
SDSSJ225738.20+134045.0	1290.33	IGMABS	H I	1215.6	H	18412.0	0.06142	148.8	44.7
SDSSJ225738.20+134045.0	1291.32	IGMABS	H I	937.8	H	113012.0	0.37695	86.1	14.5
SDSSJ225738.20+134045.0	1292.85	IGMABS	H I	937.8	H	113501.0	0.37861	81.2	34.4
SDSSJ225738.20+134045.0	1302.10	ISMLG	O I	1302.1	L	-15.0	-0.00003	439.2	36.5
SDSSJ225738.20+134045.0	1304.32	ISMLG	Si II	1304.3	L	-11.0	-0.00003	303.4	35.8
SDSSJ225738.20+134045.0	1307.73	IGMABS	H I	949.7	H	113001.0	0.37695	103.2	34.7
SDSSJ225738.20+134045.0	1307.93	IGMABS	H I	949.7	H	113063.0	0.37713	94.5	36.5
SDSSJ225738.20+134045.0	1309.33	IGMABS	H I	949.7	H	113507.0	0.37861	136.7	32.3
SDSSJ225738.20+134045.0	1310.95	IGMABS	H I	972.5	H	104320.0	0.34801	79.7	15.7
SDSSJ225738.20+134045.0	1317.03	IGMABS	C III	977.0	H	104330.0	0.34801	174.8	27.9
SDSSJ225738.20+134045.0	1318.20	IGMABS	H I	1215.6	H	25285.0	0.08434	90.9	24.6
SDSSJ225738.20+134045.0	1326.98	IGMABS	H I	1215.6	H	27450.0	0.09156	212.5	30.9
SDSSJ225738.20+134045.0	1328.80	ISMLG	C I	1328.8	L	-7.0	-0.00003	53.9	22.1
SDSSJ225738.20+134045.0	1332.66	ISMLG	C II	1334.5	L	-420.0	-0.00145	58.5	13.0
SDSSJ225738.20+134045.0	1332.96	ISMLG	C II	1334.5	L	-353.0	-0.00116	309.6	23.7
SDSSJ225738.20+134045.0	1334.53	ISMLG	C II	1334.5	L	-2.0	-0.00003	610.0	19.3
SDSSJ225738.20+134045.0	1335.67	ISMLG	C II*	1335.7	L	-9.0	-0.00003	208.8	25.2
SDSSJ225738.20+134045.0	1338.16	IGMABS	H I	1215.6	H	30207.0	0.10076	259.2	27.2
SDSSJ225738.20+134045.0	1339.12	IGMABS	H I	972.5	H	113004.0	0.37695	128.3	16.5
SDSSJ225738.20+134045.0	1339.31	IGMABS	H I	972.5	H	113060.0	0.37713	169.0	17.8
SDSSJ225738.20+134045.0	1340.76	IGMABS	H I	972.5	H	113508.0	0.37861	275.4	19.8
SDSSJ225738.20+134045.0	1341.15	IGMABS	H I	1215.6	H	30944.0	0.10322	112.9	20.1
SDSSJ225738.20+134045.0	1346.92	IGMABS	C III	977.0	H	113500.0	0.37861	404.1	31.0
SDSSJ225738.20+134045.0	1348.99	IGMABS	H I	1215.6	H	32877.0	0.10967	309.1	32.9
SDSSJ225738.20+134045.0	1350.39	IGMABS	H I	1215.6	H	33223.0	0.11082	85.7	22.1
SDSSJ225738.20+134045.0	1350.80	IGMABS	H I	1215.6	H	33324.0	0.11116	314.9	17.2
SDSSJ225738.20+134045.0	1351.27	IGMABS	H I	1215.6	H	33439.0	0.11154	321.0	11.6
SDSSJ225738.20+134045.0	1357.21	IGMABS	H I	1215.6	H	34906.0	0.11643	335.5	33.8
SDSSJ225738.20+134045.0	1367.60	IGMABS	H I	1215.6	H	37466.0	0.12497	555.4	30.7
SDSSJ225738.20+134045.0	1368.92	IGMABS	H I	1215.6	H	37791.0	0.12606	121.5	25.3
SDSSJ225738.20+134045.0	1370.07	ISMLG	Ni II	1370.1	L	-14.0	-0.00003	82.0	27.3
SDSSJ225738.20+134045.0	1374.79	IGMABS	H I	917.1	H	149574.0	0.49895	75.8	33.7
SDSSJ225738.20+134045.0	1376.22	IGMABS	H I	918.1	H	149579.0	0.49895	84.4	26.8
SDSSJ225738.20+134045.0	1377.14	IGMABS	H I	1215.6	H	39819.0	0.13282	122.6	27.6
SDSSJ225738.20+134045.0	1378.07	IGMABS	H I	919.3	H	149583.0	0.49895	84.9	29.0
SDSSJ225738.20+134045.0	1380.47	IGMABS	H I	920.9	H	149579.0	0.49895	83.5	31.1
SDSSJ225738.20+134045.0	1381.38	IGMABS	H I	1215.6	H	40864.0	0.13631	84.0	29.8
SDSSJ225738.20+134045.0	1382.29	IGMABS	H I	1025.7	H	104217.0	0.34763	102.6	16.4
SDSSJ225738.20+134045.0	1382.69	IGMABS	H I	1025.7	H	104333.0	0.34801	210.8	14.8
SDSSJ225738.20+134045.0	1383.75	IGMABS	H I	923.1	H	149579.0	0.49895	106.3	31.3
SDSSJ225738.20+134045.0	1388.35	IGMABS	H I	926.2	H	149575.0	0.49895	212.1	36.7
SDSSJ225738.20+134045.0	1391.03	IGMABS	O VI	1031.9	H	104327.0	0.34801	151.1	22.0
SDSSJ225738.20+134045.0	1392.12	ISMLG	Si IV	1393.7	L	-352.0	-0.00116	293.7	26.5
SDSSJ225738.20+134045.0	1393.72	ISMLG	Si IV	1393.7	L	-8.0	-0.00003	330.5	25.3
SDSSJ225738.20+134045.0	1395.14	IGMABS	H I	930.7	H	149579.0	0.49895	265.6	32.9
SDSSJ225738.20+134045.0	1398.74	IGMABS	O VI	1037.6	H	104336.0	0.34801	58.4	19.8
SDSSJ225738.20+134045.0	1401.21	ISMLG	Si IV	1402.7	L	-334.0	-0.00116	204.8	28.9
SDSSJ225738.20+134045.0	1402.78	ISMLG	Si IV	1402.7	L	0.0	-0.00003	148.3	35.5
SDSSJ225738.20+134045.0	1405.71	IGMABS	H I	937.8	H	149577.0	0.49895	462.3	31.8

Table A1 *continued*

Table A1 (*continued*)

Target	λ_{obs}	Type	Ion	λ_{rest}	Frame	cz	z	W_{λ}	$\sigma_{W_{\lambda}}$
	(Å)			(Å)		(km s ⁻¹)		(mÅ)	(mÅ)
SDSSJ225738.20+134045.0	1412.40	IGMABS	H I	1025.7	H	113015.0	0.37695	245.8	15.0
SDSSJ225738.20+134045.0	1412.55	IGMABS	H I	1025.7	H	113060.0	0.37713	210.0	13.7
SDSSJ225738.20+134045.0	1414.07	IGMABS	H I	1025.7	H	113504.0	0.37861	310.6	23.5
SDSSJ225738.20+134045.0	1422.62	IGMABS	O VI	1031.9	H	113503.0	0.37861	210.2	22.9
SDSSJ225738.20+134045.0	1423.61	IGMABS	H I	949.7	H	149579.0	0.49895	483.5	36.1
SDSSJ225738.20+134045.0	1430.47	IGMABS	O VI	1037.6	H	113505.0	0.37861	164.2	24.0
SDSSJ225738.20+134045.0	1436.67	IGMABS	H I	1215.6	H	54501.0	0.18180	101.0	31.4
SDSSJ225738.20+134045.0	1444.74	IGMABS	H I	972.5	H	145560.0	0.48549	115.1	29.0
SDSSJ225738.20+134045.0	1457.75	IGMABS	H I	972.5	H	149570.0	0.49895	400.4	14.0
SDSSJ225738.20+134045.0	1459.90	IGMABS	H I	1215.6	H	60229.0	0.20090	315.0	29.3
SDSSJ225738.20+134045.0	1464.52	IGMABS	C III	977.0	H	149585.0	0.49895	200.6	14.9
SDSSJ225738.20+134045.0	1479.16	IGMABS	H I	1215.6	H	64979.0	0.21675	214.9	38.1
SDSSJ225738.20+134045.0	1493.60	IGMABS	H I	1215.6	H	68538.0	0.22862	387.8	25.8
SDSSJ225738.20+134045.0	1499.59	IGMABS	H I	1215.6	H	70017.0	0.23355	147.7	31.4
SDSSJ225738.20+134045.0	1507.37	IGMABS	H I	1215.6	H	71934.0	0.23995	119.6	29.0
SDSSJ225738.20+134045.0	1523.70	IGMABS	H I	1025.7	H	145547.0	0.48549	219.4	35.8
SDSSJ225738.20+134045.0	1524.96	ISMLG	Si II	1526.7	L	-344.0	-0.00116	90.0	31.3
SDSSJ225738.20+134045.0	1526.61	ISMLG	Si II	1526.7	L	-18.0	-0.00003	401.1	27.3
SDSSJ225738.20+134045.0	1537.50	IGMABS	H I	1025.7	H	149581.0	0.49895	664.3	31.0
SDSSJ225738.20+134045.0	1545.95	ISMLG	C IV	1548.2	L	-437.0	-0.00145	100.1	20.7
SDSSJ225738.20+134045.0	1546.43	ISMLG	C IV	1548.2	L	-343.0	-0.00116	360.0	24.3
SDSSJ225738.20+134045.0	1546.79	IGMABS	O VI	1031.9	H	149576.0	0.49895	223.5	19.1
SDSSJ225738.20+134045.0	1547.33	IGMABS	O VI	1031.9	H	149733.0	0.49947	164.1	21.0
SDSSJ225738.20+134045.0	1548.24	ISMLG	C IV	1548.2	L	7.0	-0.00003	315.8	32.1
SDSSJ225738.20+134045.0	1548.95	ISMLG	C IV	1550.7	L	-354.0	-0.00116	180.1	25.2
SDSSJ225738.20+134045.0	1550.82	ISMLG	C IV	1550.7	L	7.0	-0.00003	256.6	36.0
SDSSJ225738.20+134045.0	1555.34	IGMABS	O VI	1037.6	H	149582.0	0.49895	86.6	14.5
SDSSJ225738.20+134045.0	1555.86	IGMABS	O VI	1037.6	H	149732.0	0.49947	123.7	18.0
SDSSJ225738.20+134045.0	1560.33	ISMLG	C I	1560.3	L	5.0	-0.00003	130.1	29.8
SDSSJ225738.20+134045.0	1573.70	IGMABS	H I	1215.6	H	88293.0	0.29451	167.2	34.2
SDSSJ225738.20+134045.0	1574.49	IGMABS	H I	1215.6	H	88487.0	0.29516	180.2	36.7
SDSSJ225738.20+134045.0	1593.07	IGMABS	C IV	1548.2	H	8687.0	0.02900	164.9	58.1
SDSSJ225738.20+134045.0	1608.42	ISMLG	Fe II	1608.4	L	-7.0	-0.00003	799.7	64.7
SDSSJ225738.20+134045.0	1634.35	IGMABS	H I	1215.6	H	103250.0	0.34440	227.2	35.0
SDSSJ225738.20+134045.0	1637.75	IGMABS	H I	1215.6	H	104087.0	0.34720	102.1	30.5
SDSSJ225738.20+134045.0	1638.27	IGMABS	H I	1215.6	H	104217.0	0.34763	319.0	18.2
SDSSJ225738.20+134045.0	1638.74	IGMABS	H I	1215.6	H	104331.0	0.34801	430.8	17.5
SDSSJ225738.20+134045.0	1656.82	ISMLG	C I	1656.9	L	-19.0	-0.00003	103.9	30.1
SDSSJ225738.20+134045.0	1660.65	IGMABS	H I	1215.6	H	109734.0	0.36603	220.1	39.6
SDSSJ225738.20+134045.0	1663.31	IGMABS	Si III	1206.5	H	113508.0	0.37861	92.9	27.9
SDSSJ225738.20+134045.0	1668.85	ISMLG	Al II	1670.7	L	-348.0	-0.00116	155.3	41.8
SDSSJ225738.20+134045.0	1670.68	ISMLG	Al II	1670.7	L	-20.0	-0.00003	579.8	48.3
SDSSJ225738.20+134045.0	1673.91	IGMABS	H I	1215.6	H	113006.0	0.37695	398.9	29.9
SDSSJ225738.20+134045.0	1674.13	IGMABS	H I	1215.6	H	113060.0	0.37713	400.5	26.9
SDSSJ225738.20+134045.0	1674.94	IGMABS	H I	1215.6	H	113260.0	0.37779	222.9	37.2
SDSSJ225738.20+134045.0	1675.94	IGMABS	H I	1215.6	H	113505.0	0.37861	618.8	44.7
SDSSJ225738.20+134045.0	1677.34	IGMABS	H I	1215.6	H	113851.0	0.37977	118.5	46.9
SDSSJ225738.20+134045.0	1679.69	IGMABS	H I	1215.6	H	114431.0	0.38170	193.0	60.6
SDSSJ225738.20+134045.0	1728.49	PROXIMATE	H I	1215.6	H	126464.0	0.42184	223.8	61.9
UGC12163	905.82	ISMLG	H ₂	905.8	L	-1.0	-0.00001	63.0	0.0
UGC12163	907.61	ISMLG	H ₂	907.6	L	-1.0	-0.00001	35.1	0.0
UGC12163	912.95	ISMLG	H ₂	912.9	L	-1.0	-0.00001	41.4	0.0
UGC12163	913.77	ISMLG	H ₂	913.7	L	-1.0	-0.00001	40.4	0.0

Table A1 continued

Table A1 (*continued*)

Target	λ_{obs}	Type	Ion	λ_{rest}	Frame	cz	z	W_{λ}	$\sigma_{W_{\lambda}}$
	(Å)			(Å)		(km s ⁻¹)		(mÅ)	(mÅ)
UGC12163	914.39	ISMLG	H ₂	914.3	L	-1.0	-0.00001	80.7	0.0
UGC12163	914.60	ISMLG	H ₂	914.6	L	-1.0	-0.00001	83.1	0.0
UGC12163	915.40	ISMLG	H ₂	915.4	L	-1.0	-0.00001	84.5	0.0
UGC12163	915.42	ISMLG	H ₂	915.4	L	-1.0	-0.00001	60.4	0.0
UGC12163	916.61	ISMLG	H ₂	916.6	L	-1.0	-0.00001	64.2	0.0
UGC12163	916.87	ISMLG	H ₂	916.8	L	-1.0	-0.00001	46.3	0.0
UGC12163	917.25	ISMLG	H ₂	917.2	L	-1.0	-0.00001	68.8	0.0
UGC12163	917.36	ISMLG	H ₂	917.3	L	-1.0	-0.00001	49.1	0.0
UGC12163	917.92	ISMLG	H ₂	917.9	L	-1.0	-0.00001	74.4	0.0
UGC12163	918.41	ISMLG	H ₂	918.4	L	-1.0	-0.00001	66.6	0.0
UGC12163	918.43	ISMLG	H ₂	918.4	L	-1.0	-0.00001	52.2	0.0
UGC12163	919.41	ISMLG	H ₂	919.4	L	-1.0	-0.00001	51.7	0.0
UGC12163	919.54	ISMLG	H ₂	919.5	L	-1.0	-0.00001	37.5	0.0
UGC12163	920.24	ISMLG	H ₂	920.2	L	-1.0	-0.00001	41.5	0.0
UGC12163	923.98	ISMLG	H ₂	923.9	L	-1.0	-0.00001	69.5	0.0
UGC12163	924.64	ISMLG	H ₂	924.6	L	-1.0	-0.00001	74.6	0.0
UGC12163	925.17	ISMLG	H ₂	925.1	L	-1.0	-0.00001	68.9	0.0
UGC12163	926.13	ISMLG	H ₂	926.1	L	-1.0	-0.00001	50.9	0.0
UGC12163	927.01	ISMLG	H ₂	927.0	L	-1.0	-0.00001	46.5	0.0
UGC12163	929.53	ISMLG	H ₂	929.5	L	-1.0	-0.00001	85.4	0.0
UGC12163	929.68	ISMLG	H ₂	929.6	L	-1.0	-0.00001	87.8	0.0
UGC12163	930.44	ISMLG	H ₂	930.4	L	-1.0	-0.00001	64.4	0.0
UGC12163	930.57	ISMLG	H ₂	930.5	L	-1.0	-0.00001	90.2	0.0
UGC12163	931.06	ISMLG	H ₂	931.0	L	-1.0	-0.00001	74.7	0.0
UGC12163	931.73	ISMLG	H ₂	931.7	L	-1.0	-0.00001	80.3	0.0
UGC12163	931.78	ISMLG	H ₂	931.7	L	-1.0	-0.00001	69.0	0.0
UGC12163	931.81	ISMLG	H ₂	931.8	L	-1.0	-0.00001	50.7	0.0
UGC12163	932.26	ISMLG	H ₂	932.2	L	-1.0	-0.00001	71.3	0.0
UGC12163	932.60	ISMLG	H ₂	932.6	L	-1.0	-0.00001	55.6	0.0
UGC12163	933.23	ISMLG	H ₂	933.2	L	-1.0	-0.00001	58.4	0.0
UGC12163	933.58	ISMLG	H ₂	933.5	L	-1.0	-0.00001	57.7	0.0
UGC12163	934.14	ISMLG	H ₂	934.1	L	-1.0	-0.00001	46.5	0.0
UGC12163	934.79	ISMLG	H ₂	934.7	L	-1.0	-0.00001	45.8	0.0
UGC12163	935.57	ISMLG	H ₂	935.5	L	-1.0	-0.00001	42.8	0.0
UGC12163	938.46	ISMLG	H ₂	938.4	L	-1.0	-0.00001	74.5	0.0
UGC12163	939.12	ISMLG	H ₂	939.1	L	-1.0	-0.00001	79.9	0.0
UGC12163	939.70	ISMLG	H ₂	939.7	L	-1.0	-0.00001	73.6	0.0
UGC12163	940.62	ISMLG	H ₂	940.6	L	-1.0	-0.00001	57.7	0.0
UGC12163	941.59	ISMLG	H ₂	941.5	L	-1.0	-0.00001	52.2	0.0
UGC12163	942.96	ISMLG	H ₂	942.9	L	-1.0	-0.00001	41.2	0.0
UGC12163	944.33	ISMLG	H ₂	944.3	L	-1.0	-0.00001	35.1	0.0
UGC12163	945.08	INTRINSIC	H I	923.1	H	7123.0	0.02374	343.2	57.1
UGC12163	945.33	INTRINSIC	H I	923.1	H	7202.0	0.02402	231.7	45.2
UGC12163	945.48	INTRINSIC	H I	923.1	H	7251.0	0.02418	283.4	36.8
UGC12163	945.95	INTRINSIC	H I	923.1	H	7405.0	0.02467	490.7	48.1
UGC12163	946.16	ISMLG	H ₂	946.1	L	-1.0	-0.00001	54.9	0.0
UGC12163	946.22	INTRINSIC	H I	923.1	H	7491.0	0.02498	198.4	53.7
UGC12163	946.38	ISMLG	H ₂	946.3	L	-1.0	-0.00001	87.8	0.0
UGC12163	946.42	ISMLG	H ₂	946.4	L	-1.0	-0.00001	91.4	0.0
UGC12163	946.97	ISMLG	H ₂	946.9	L	-1.0	-0.00001	70.4	0.0
UGC12163	947.11	ISMLG	H ₂	947.1	L	-1.0	-0.00001	66.9	0.0
UGC12163	947.42	ISMLG	H ₂	947.4	L	-1.0	-0.00001	96.1	0.0
UGC12163	947.51	ISMLG	H ₂	947.5	L	-1.0	-0.00001	75.9	0.0

Table A1 continued

Table A1 (*continued*)

Target	λ_{obs}	Type	Ion	λ_{rest}	Frame	cz	z	W_{λ}	$\sigma_{W_{\lambda}}$
	(Å)			(Å)		(km s ⁻¹)		(mÅ)	(mÅ)
UGC12163	948.21	INTRINSIC	H I	926.2	H	7116.0	0.02374	279.8	40.1
UGC12163	948.42	ISMLG	H ₂	948.4	L	-1.0	-0.00001	54.2	0.0
UGC12163	948.47	ISMLG	H ₂	948.4	L	-1.0	-0.00001	66.0	0.0
UGC12163	948.47	INTRINSIC	H I	926.2	H	7200.0	0.02402	341.7	45.6
UGC12163	948.61	ISMLG	H ₂	948.6	L	-1.0	-0.00001	73.5	0.0
UGC12163	948.63	INTRINSIC	H I	926.2	H	7252.0	0.02418	148.3	39.1
UGC12163	949.09	INTRINSIC	H I	926.2	H	7400.0	0.02467	371.9	58.3
UGC12163	949.35	ISMLG	H ₂	949.3	L	-1.0	-0.00001	63.3	0.0
UGC12163	949.35	INTRINSIC	H I	926.2	H	7486.0	0.02498	272.5	19.7
UGC12163	950.39	ISMLG	H ₂	950.3	L	-1.0	-0.00001	62.7	0.0
UGC12163	950.81	ISMLG	H ₂	950.8	L	-1.0	-0.00001	51.3	0.0
UGC12163	951.67	ISMLG	H ₂	951.6	L	-1.0	-0.00001	54.3	0.0
UGC12163	952.87	INTRINSIC	H I	930.7	H	7124.0	0.02374	313.2	37.8
UGC12163	953.11	INTRINSIC	H I	930.7	H	7203.0	0.02402	289.4	45.5
UGC12163	953.25	INTRINSIC	H I	930.7	H	7247.0	0.02418	345.0	48.4
UGC12163	953.73	INTRINSIC	H I	930.7	H	7401.0	0.02467	545.1	41.0
UGC12163	953.99	INTRINSIC	H I	930.7	H	7486.0	0.02498	246.1	18.3
UGC12163	953.99	ISMLG	N I	953.9	L	7.0	-0.00001	223.9	46.7
UGC12163	954.41	ISMLG	H ₂	954.4	L	-1.0	-0.00001	79.5	0.0
UGC12163	955.06	ISMLG	H ₂	955.0	L	-1.0	-0.00001	85.3	0.0
UGC12163	955.55	INTRINSIC	S VI	933.3	H	7122.0	0.02374	70.3	31.2
UGC12163	955.71	ISMLG	H ₂	955.7	L	-1.0	-0.00001	78.3	0.0
UGC12163	955.80	INTRINSIC	S VI	933.3	H	7200.0	0.02402	262.3	46.0
UGC12163	955.96	INTRINSIC	S VI	933.3	H	7252.0	0.02418	307.1	46.6
UGC12163	956.58	ISMLG	H ₂	956.5	L	-1.0	-0.00001	63.4	0.0
UGC12163	957.65	ISMLG	H ₂	957.6	L	-1.0	-0.00001	57.4	0.0
UGC12163	958.94	ISMLG	H ₂	958.9	L	-1.0	-0.00001	49.2	0.0
UGC12163	960.08	INTRINSIC	H I	937.8	H	7122.0	0.02374	415.0	55.6
UGC12163	960.33	INTRINSIC	H I	937.8	H	7201.0	0.02402	206.3	75.3
UGC12163	960.45	ISMLG	H ₂	960.4	L	-1.0	-0.00001	41.7	0.0
UGC12163	960.49	INTRINSIC	H I	937.8	H	7252.0	0.02418	226.5	62.1
UGC12163	960.95	INTRINSIC	H I	937.8	H	7400.0	0.02467	656.0	37.5
UGC12163	961.24	INTRINSIC	H I	937.8	H	7492.0	0.02498	265.9	44.0
UGC12163	962.97	ISMLG	H ₂	962.9	L	-1.0	-0.00001	79.8	0.0
UGC12163	963.60	ISMLG	H ₂	963.6	L	-1.0	-0.00001	83.3	0.0
UGC12163	964.31	ISMLG	H ₂	964.3	L	-1.0	-0.00001	80.6	0.0
UGC12163	964.98	ISMLG	H ₂	964.9	L	-1.0	-0.00001	97.0	0.0
UGC12163	965.04	ISMLG	H ₂	965.0	L	-1.0	-0.00001	42.3	0.0
UGC12163	965.06	ISMLG	H ₂	965.0	L	-1.0	-0.00001	101.7	0.0
UGC12163	965.79	ISMLG	H ₂	965.7	L	-1.0	-0.00001	76.6	0.0
UGC12163	966.09	ISMLG	H ₂	966.0	L	-1.0	-0.00001	101.7	0.0
UGC12163	966.27	ISMLG	H ₂	966.2	L	-1.0	-0.00001	61.2	0.0
UGC12163	966.78	ISMLG	H ₂	966.7	L	-1.0	-0.00001	49.3	0.0
UGC12163	966.96	INTRINSIC	S VI	944.5	H	7122.0	0.02374	83.7	39.7
UGC12163	967.20	INTRINSIC	S VI	944.5	H	7199.0	0.02402	162.0	37.5
UGC12163	967.28	ISMLG	H ₂	967.2	L	-1.0	-0.00001	77.4	0.0
UGC12163	967.39	INTRINSIC	S VI	944.5	H	7256.0	0.02418	92.3	38.2
UGC12163	967.67	ISMLG	H ₂	967.6	L	-1.0	-0.00001	61.3	0.0
UGC12163	968.29	ISMLG	H ₂	968.2	L	-1.0	-0.00001	62.4	0.0
UGC12163	969.04	ISMLG	H ₂	969.0	L	-1.0	-0.00001	66.4	0.0
UGC12163	969.09	ISMLG	H ₂	969.0	L	-1.0	-0.00001	49.7	0.0
UGC12163	970.56	ISMLG	H ₂	970.5	L	-1.0	-0.00001	52.1	0.0
UGC12163	971.98	ISMLG	H ₂	971.9	L	-1.0	-0.00001	84.5	0.0

Table A1 continued

Table A1 (*continued*)

Target	λ_{obs}	Type	Ion	λ_{rest}	Frame	cz	z	W_{λ}	$\sigma_{W_{\lambda}}$
	(Å)			(Å)		(km s ⁻¹)		(mÅ)	(mÅ)
UGC12163	972.63	ISMLG	H ₂	972.6	L	-1.0	-0.00001	90.9	0.0
UGC12163	973.34	ISMLG	H ₂	973.3	L	-1.0	-0.00001	82.9	0.0
UGC12163	974.15	ISMLG	H ₂	974.1	L	-1.0	-0.00001	68.4	0.0
UGC12163	975.34	ISMLG	H ₂	975.3	L	-1.0	-0.00001	62.1	0.0
UGC12163	975.63	ISMLG	C III	977.0	L	-426.0	-0.00141	222.6	35.5
UGC12163	975.88	ISMLG	C III	977.0	L	-350.0	-0.00117	157.3	29.6
UGC12163	976.55	ISMLG	H ₂	976.5	L	-1.0	-0.00001	55.5	0.0
UGC12163	978.21	ISMLG	H ₂	978.2	L	-1.0	-0.00001	47.6	0.0
UGC12163	981.43	ISMLG	H ₂	981.4	L	-1.0	-0.00001	85.8	0.0
UGC12163	982.07	ISMLG	H ₂	982.0	L	-1.0	-0.00001	91.7	0.0
UGC12163	982.83	ISMLG	H ₂	982.8	L	-1.0	-0.00001	85.2	0.0
UGC12163	983.59	ISMLG	H ₂	983.5	L	-1.0	-0.00001	68.1	0.0
UGC12163	984.86	ISMLG	H ₂	984.8	L	-1.0	-0.00001	65.0	0.0
UGC12163	985.63	ISMLG	H ₂	985.6	L	-1.0	-0.00001	99.8	0.0
UGC12163	985.64	ISMLG	H ₂	985.6	L	-1.0	-0.00001	103.9	0.0
UGC12163	985.96	ISMLG	H ₂	985.9	L	-1.0	-0.00001	50.4	0.0
UGC12163	986.24	ISMLG	H ₂	986.2	L	-1.0	-0.00001	76.7	0.0
UGC12163	986.79	ISMLG	H ₂	986.7	L	-1.0	-0.00001	105.2	0.0
UGC12163	987.44	ISMLG	H ₂	987.4	L	-1.0	-0.00001	65.2	0.0
UGC12163	987.76	ISMLG	H ₂	987.7	L	-1.0	-0.00001	52.2	0.0
UGC12163	987.97	ISMLG	H ₂	987.9	L	-1.0	-0.00001	79.6	0.0
UGC12163	989.08	ISMLG	H ₂	989.0	L	-1.0	-0.00001	65.3	0.0
UGC12163	989.72	ISMLG	H ₂	989.7	L	-1.0	-0.00001	68.4	0.0
UGC12163	991.37	ISMLG	H ₂	991.3	L	-1.0	-0.00001	89.2	0.0
UGC12163	991.38	ISMLG	H ₂	991.3	L	-1.0	-0.00001	55.9	0.0
UGC12163	992.01	ISMLG	H ₂	992.0	L	-1.0	-0.00001	96.1	0.0
UGC12163	992.80	ISMLG	H ₂	992.8	L	-1.0	-0.00001	87.4	0.0
UGC12163	993.54	ISMLG	H ₂	993.5	L	-1.0	-0.00001	72.8	0.0
UGC12163	994.87	ISMLG	H ₂	994.8	L	-1.0	-0.00001	66.3	0.0
UGC12163	995.64	INTRINSIC	H I	972.5	H	7121.0	0.02374	475.3	58.7
UGC12163	995.90	INTRINSIC	H I	972.5	H	7201.0	0.02402	313.5	44.3
UGC12163	995.97	ISMLG	H ₂	995.9	L	-1.0	-0.00001	60.2	0.0
UGC12163	996.05	INTRINSIC	H I	972.5	H	7249.0	0.02418	307.8	45.8
UGC12163	996.55	INTRINSIC	H I	972.5	H	7403.0	0.02467	732.5	47.7
UGC12163	996.84	INTRINSIC	H I	972.5	H	7492.0	0.02498	203.4	43.0
UGC12163	997.82	ISMLG	H ₂	997.8	L	-1.0	-0.00001	52.6	0.0
UGC12163	1000.23	INTRINSIC	C III	977.0	H	7123.0	0.02374	494.9	51.4
UGC12163	1000.49	INTRINSIC	C III	977.0	H	7201.0	0.02402	234.1	45.2
UGC12163	1000.66	INTRINSIC	C III	977.0	H	7253.0	0.02418	201.4	51.3
UGC12163	1001.15	INTRINSIC	C III	977.0	H	7403.0	0.02467	463.6	56.8
UGC12163	1001.82	ISMLG	H ₂	1001.8	L	-1.0	-0.00001	90.7	0.0
UGC12163	1002.45	ISMLG	H ₂	1002.4	L	-1.0	-0.00001	94.3	0.0
UGC12163	1003.29	ISMLG	H ₂	1003.2	L	-1.0	-0.00001	89.6	0.0
UGC12163	1003.98	ISMLG	H ₂	1003.9	L	-1.0	-0.00001	73.6	0.0
UGC12163	1005.39	ISMLG	H ₂	1005.3	L	-1.0	-0.00001	68.5	0.0
UGC12163	1006.41	ISMLG	H ₂	1006.4	L	-1.0	-0.00001	60.5	0.0
UGC12163	1008.38	ISMLG	H ₂	1008.3	L	-1.0	-0.00001	55.5	0.0
UGC12163	1008.49	ISMLG	H ₂	1008.4	L	-1.0	-0.00001	100.6	0.0
UGC12163	1008.55	ISMLG	H ₂	1008.5	L	-1.0	-0.00001	97.2	0.0
UGC12163	1009.03	ISMLG	H ₂	1009.0	L	-1.0	-0.00001	74.1	0.0
UGC12163	1009.77	ISMLG	H ₂	1009.7	L	-1.0	-0.00001	102.2	0.0
UGC12163	1010.13	ISMLG	H ₂	1010.1	L	-1.0	-0.00001	60.2	0.0
UGC12163	1010.93	ISMLG	H ₂	1010.9	L	-1.0	-0.00001	77.8	0.0

Table A1 continued

Table A1 (*continued*)

Target	λ_{obs}	Type	Ion	λ_{rest}	Frame	cz	z	W_{λ}	$\sigma_{W_{\lambda}}$
	(Å)			(Å)		(km s ⁻¹)		(mÅ)	(mÅ)
UGC12163	1011.81	ISMLG	H ₂	1011.8	L	-1.0	-0.00001	13.2	0.0
UGC12163	1012.17	ISMLG	H ₂	1012.1	L	-1.0	-0.00001	62.5	0.0
UGC12163	1012.51	ISMLG	S III	1012.4	L	5.0	-0.00001	162.5	24.3
UGC12163	1012.68	ISMLG	H ₂	1012.6	L	-1.0	-0.00001	66.0	0.0
UGC12163	1012.81	ISMLG	H ₂	1012.8	L	-1.0	-0.00001	93.1	0.0
UGC12163	1013.43	ISMLG	H ₂	1013.4	L	-1.0	-0.00001	100.8	0.0
UGC12163	1014.32	ISMLG	H ₂	1014.3	L	-1.0	-0.00001	91.5	0.0
UGC12163	1014.50	ISMLG	H ₂	1014.5	L	-1.0	-0.00001	52.3	0.0
UGC12163	1014.97	ISMLG	H ₂	1014.9	L	-1.0	-0.00001	75.9	0.0
UGC12163	1014.98	ISMLG	H ₂	1014.9	L	-1.0	-0.00001	19.2	0.0
UGC12163	1016.46	ISMLG	H ₂	1016.4	L	-1.0	-0.00001	69.8	0.0
UGC12163	1017.42	ISMLG	H ₂	1017.4	L	-1.0	-0.00001	63.3	0.0
UGC12163	1019.50	ISMLG	H ₂	1019.5	L	-1.0	-0.00001	56.3	0.0
UGC12163	1020.67	ISMLG	Si II	1020.6	L	-7.0	-0.00001	279.8	21.0
UGC12163	1020.76	ISMLG	H ₂	1020.7	L	-1.0	-0.00001	15.7	0.0
UGC12163	1024.37	ISMLG	H ₂	1024.3	L	-1.0	-0.00001	94.3	0.0
UGC12163	1024.98	ISMLG	H ₂	1024.9	L	-1.0	-0.00001	102.3	0.0
UGC12163	1025.93	ISMLG	H ₂	1025.9	L	-1.0	-0.00001	93.0	0.0
UGC12163	1026.52	ISMLG	H ₂	1026.5	L	-1.0	-0.00001	76.6	0.0
UGC12163	1028.10	ISMLG	H ₂	1028.1	L	-1.0	-0.00001	71.0	0.0
UGC12163	1028.98	ISMLG	H ₂	1028.9	L	-1.0	-0.00001	63.8	0.0
UGC12163	1030.99	ISMLG	O VI	1031.9	L	-271.0	-0.00091	121.3	16.1
UGC12163	1031.19	ISMLG	H ₂	1031.1	L	-1.0	-0.00001	57.9	0.0
UGC12163	1032.35	ISMLG	H ₂	1032.3	L	-1.0	-0.00001	15.5	0.0
UGC12163	1034.89	ISMLG	C II	1036.3	L	-418.0	-0.00141	108.0	15.2
UGC12163	1035.10	ISMLG	C II	1036.3	L	-357.0	-0.00117	79.1	15.5
UGC12163	1035.65	ISMLG	C II	1036.3	L	-198.0	-0.00067	85.8	20.7
UGC12163	1036.34	ISMLG	C II	1036.3	L	1.0	-0.00001	544.4	21.3
UGC12163	1036.54	ISMLG	H ₂	1036.5	L	-1.0	-0.00001	95.1	0.0
UGC12163	1036.66	ISMLG	O VI	1037.6	L	-277.0	-0.00091	80.5	16.7
UGC12163	1037.15	ISMLG	H ₂	1037.1	L	-1.0	-0.00001	103.1	0.0
UGC12163	1038.15	ISMLG	H ₂	1038.1	L	-1.0	-0.00001	93.9	0.0
UGC12163	1038.69	ISMLG	H ₂	1038.6	L	-1.0	-0.00001	77.0	0.0
UGC12163	1039.21	ISMLG	O I	1039.2	L	-5.0	-0.00001	352.0	23.1
UGC12163	1040.36	ISMLG	H ₂	1040.3	L	-1.0	-0.00001	71.6	0.0
UGC12163	1041.16	ISMLG	H ₂	1041.1	L	-1.0	-0.00001	63.8	0.0
UGC12163	1043.50	ISMLG	H ₂	1043.5	L	-1.0	-0.00001	58.2	0.0
UGC12163	1044.54	ISMLG	H ₂	1044.5	L	-1.0	-0.00001	14.9	0.0
UGC12163	1048.20	ISMLG	Ar I	1048.2	L	-6.0	-0.00001	113.0	14.0
UGC12163	1049.36	ISMLG	H ₂	1049.3	L	-1.0	-0.00001	95.1	0.0
UGC12163	1049.96	ISMLG	H ₂	1049.9	L	-1.0	-0.00001	103.1	0.0
UGC12163	1050.08	INTRINSIC	H I	1025.7	H	7120.0	0.02374	641.0	16.7
UGC12163	1050.36	INTRINSIC	H I	1025.7	H	7200.0	0.02402	263.6	16.0
UGC12163	1050.53	INTRINSIC	H I	1025.7	H	7251.0	0.02418	284.5	15.9
UGC12163	1051.02	INTRINSIC	H I	1025.7	H	7393.0	0.02467	884.2	14.6
UGC12163	1051.03	ISMLG	H ₂	1051.0	L	-1.0	-0.00001	94.0	0.0
UGC12163	1051.34	INTRINSIC	H I	1025.7	H	7488.0	0.02498	379.6	10.9
UGC12163	1051.49	ISMLG	H ₂	1051.4	L	-1.0	-0.00001	76.6	0.0
UGC12163	1053.28	ISMLG	H ₂	1053.2	L	-1.0	-0.00001	71.3	0.0
UGC12163	1053.97	ISMLG	H ₂	1053.9	L	-1.0	-0.00001	63.0	0.0
UGC12163	1055.28	ISMLG	Fe II	1055.2	L	5.0	-0.00001	88.9	9.3
UGC12163	1056.47	INTRINSIC	O VI	1031.9	H	7130.0	0.02374	572.9	9.0
UGC12163	1056.47	ISMLG	H ₂	1056.4	L	-1.0	-0.00001	57.4	0.0

Table A1 continued

Table A1 (*continued*)

Target	λ_{obs}	Type	Ion	λ_{rest}	Frame	cz	z	W_{λ}	$\sigma_{W_{\lambda}}$
	(Å)			(Å)		(km s ⁻¹)		(mÅ)	(mÅ)
UGC12163	1056.71	INTRINSIC	O VI	1031.9	H	7200.0	0.02402	199.2	12.0
UGC12163	1056.88	INTRINSIC	O VI	1031.9	H	7249.0	0.02418	216.0	10.2
UGC12163	1057.38	ISMLG	H ₂	1057.3	L	-1.0	-0.00001	13.5	0.0
UGC12163	1057.40	INTRINSIC	O VI	1031.9	H	7401.0	0.02467	882.2	11.3
UGC12163	1057.72	INTRINSIC	O VI	1031.9	H	7493.0	0.02498	247.0	10.7
UGC12163	1062.26	INTRINSIC	O VI	1037.6	H	7121.0	0.02374	575.2	11.8
UGC12163	1062.53	INTRINSIC	O VI	1037.6	H	7199.0	0.02402	204.1	15.6
UGC12163	1062.71	INTRINSIC	O VI	1037.6	H	7251.0	0.02418	238.5	16.5
UGC12163	1062.88	ISMLG	H ₂	1062.8	L	-1.0	-0.00001	93.9	0.0
UGC12163	1063.21	INTRINSIC	O VI	1037.6	H	7394.0	0.02467	901.0	13.4
UGC12163	1063.46	ISMLG	H ₂	1063.4	L	-1.0	-0.00001	102.4	0.0
UGC12163	1063.55	INTRINSIC	O VI	1037.6	H	7491.0	0.02498	233.4	12.5
UGC12163	1064.60	ISMLG	H ₂	1064.6	L	-1.0	-0.00001	92.8	0.0
UGC12163	1064.99	ISMLG	H ₂	1064.9	L	-1.0	-0.00001	75.0	0.0
UGC12163	1066.64	ISMLG	Ar I	1066.6	L	-6.0	-0.00001	110.4	13.9
UGC12163	1066.90	ISMLG	H ₂	1066.9	L	-1.0	-0.00001	69.6	0.0
UGC12163	1067.47	ISMLG	H ₂	1067.4	L	-1.0	-0.00001	60.6	0.0
UGC12163	1070.14	ISMLG	H ₂	1070.1	L	-1.0	-0.00001	54.8	0.0
UGC12163	1077.14	ISMLG	H ₂	1077.1	L	-1.0	-0.00001	90.8	0.0
UGC12163	1077.70	ISMLG	H ₂	1077.7	L	-1.0	-0.00001	98.1	0.0
UGC12163	1078.92	ISMLG	H ₂	1078.9	L	-1.0	-0.00001	89.9	0.0
UGC12163	1079.22	ISMLG	H ₂	1079.2	L	-1.0	-0.00001	71.4	0.0
UGC12163	1081.26	ISMLG	H ₂	1081.2	L	-1.0	-0.00001	65.7	0.0
UGC12163	1081.71	ISMLG	H ₂	1081.7	L	-1.0	-0.00001	55.4	0.0
UGC12163	1083.96	ISMLG	N II	1083.9	L	-9.0	-0.00001	516.7	107.5
UGC12163	1084.56	ISMLG	H ₂	1084.5	L	-1.0	-0.00001	48.8	0.0
UGC12163	1092.19	ISMLG	H ₂	1092.1	L	-1.0	-0.00001	84.9	0.0
UGC12163	1092.73	ISMLG	H ₂	1092.7	L	-1.0	-0.00001	91.9	0.0
UGC12163	1094.05	ISMLG	H ₂	1094.0	L	-1.0	-0.00001	83.9	0.0
UGC12163	1094.24	ISMLG	H ₂	1094.2	L	-1.0	-0.00001	64.0	0.0
UGC12163	1096.43	ISMLG	H ₂	1096.4	L	-1.0	-0.00001	57.3	0.0
UGC12163	1096.72	ISMLG	H ₂	1096.7	L	-1.0	-0.00001	43.9	0.0
UGC12163	1096.86	ISMLG	Fe II	1096.8	L	-6.0	-0.00001	222.9	14.8
UGC12163	1099.78	ISMLG	H ₂	1099.7	L	-1.0	-0.00001	36.2	0.0
UGC12163	1108.12	ISMLG	H ₂	1108.1	L	-1.0	-0.00001	72.3	0.0
UGC12163	1108.63	ISMLG	H ₂	1108.6	L	-1.0	-0.00001	79.7	0.0
UGC12163	1110.06	ISMLG	H ₂	1110.0	L	-1.0	-0.00001	71.3	0.0
UGC12163	1110.12	ISMLG	H ₂	1110.1	L	-1.0	-0.00001	44.8	0.0
UGC12163	1112.04	ISMLG	Fe II	1112.0	L	-2.0	-0.00001	59.0	14.6
UGC12163	1112.49	ISMLG	H ₂	1112.4	L	-1.0	-0.00001	35.1	0.0
UGC12163	1112.58	ISMLG	H ₂	1112.5	L	-1.0	-0.00001	20.7	0.0
UGC12163	1115.89	ISMLG	H ₂	1115.8	L	-1.0	-0.00001	15.4	0.0
UGC12163	1121.97	ISMLG	Fe II	1121.9	L	0.0	-0.00001	143.6	19.9
UGC12163	1122.53	ISMLG	Fe III	1122.5	L	1.0	-0.00001	98.8	21.9
UGC12163	1125.45	ISMLG	Fe II	1125.4	L	2.0	-0.00001	116.9	17.2
UGC12163	1133.69	ISMLG	Fe II	1133.6	L	6.0	-0.00001	52.7	16.6
UGC12163	1134.19	ISMLG	N I	1134.1	L	7.0	-0.00001	170.5	16.6
UGC12163	1134.42	ISMLG	N I	1134.4	L	1.0	-0.00001	166.4	17.2
UGC12163	1134.95	ISMLG	N I	1134.9	L	-8.0	-0.00001	229.5	22.8
UGC12163	1142.37	ISMLG	Fe II	1142.3	L	1.0	-0.00001	63.7	22.3
UGC12163	1143.20	ISMLG	Fe II	1143.2	L	-6.0	-0.00001	120.4	66.9
UGC12163	1144.91	ISMLG	Fe II	1144.9	L	-8.0	-0.00001	372.0	57.2
UGC12163	1152.80	ISMLG	P II	1152.8	L	-5.0	-0.00001	107.1	32.5

Table A1 continued

Table A1 (*continued*)

Target	λ_{obs}	Type	Ion	λ_{rest}	Frame	cz	z	W_{λ}	$\sigma_{W_{\lambda}}$
	(Å)			(Å)		(km s ⁻¹)		(mÅ)	(mÅ)
UGC12163	1189.61	ISMLG	Si II	1190.4	L	-202.0	-0.00067	50.3	17.1
UGC12163	1190.39	ISMLG	Si II	1190.4	L	-6.0	-0.00001	584.5	21.7
UGC12163	1190.72	ISMLG	Si II	1190.4	L	76.0	0.00025	74.6	12.8
UGC12163	1192.46	ISMLG	Si II	1193.2	L	-208.0	-0.00067	59.0	17.4
UGC12163	1193.27	ISMLG	Si II	1193.2	L	-6.0	-0.00001	583.4	20.5
UGC12163	1193.58	ISMLG	Si II	1193.2	L	74.0	0.00025	70.9	13.0
UGC12163	1197.18	ISMLG	Mn II	1197.1	L	-1.0	-0.00001	20.2	18.0
UGC12163	1199.52	ISMLG	N I	1199.5	L	-8.0	-0.00001	389.1	19.1
UGC12163	1200.19	ISMLG	N I	1200.2	L	-8.0	-0.00001	417.0	18.2
UGC12163	1200.69	ISMLG	N I	1200.7	L	-6.0	-0.00001	280.8	17.1
UGC12163	1201.08	ISMLG	Mn II	1201.1	L	-8.0	-0.00001	66.0	17.4
UGC12163	1204.79	ISMLG	Si III	1206.5	L	-426.0	-0.00141	224.5	14.2
UGC12163	1205.09	ISMLG	Si III	1206.5	L	-349.0	-0.00117	59.8	13.7
UGC12163	1206.48	ISMLG	Si III	1206.5	L	-4.0	-0.00001	696.5	17.2
UGC12163	1206.81	ISMLG	Si III	1206.5	L	76.0	0.00025	144.3	10.1
UGC12163	1235.44	INTRINSIC	Si III	1206.5	H	7192.0	0.02402	139.0	11.1
UGC12163	1235.68	INTRINSIC	Si III	1206.5	H	7250.0	0.02418	103.9	9.5
UGC12163	1238.85	ISMLG	N V	1238.8	L	6.0	-0.00001	40.7	12.5
UGC12163	1239.92	ISMLG	Mg II	1239.9	L	-1.0	-0.00001	42.4	8.9
UGC12163	1240.41	ISMLG	Mg II	1240.3	L	3.0	-0.00001	24.5	8.3
UGC12163	1244.54	INTRINSIC	H I	1215.6	H	7118.0	0.02374	717.6	3.7
UGC12163	1244.87	INTRINSIC	H I	1215.6	H	7201.0	0.02402	428.6	4.2
UGC12163	1245.06	INTRINSIC	H I	1215.6	H	7249.0	0.02418	288.6	3.4
UGC12163	1245.66	INTRINSIC	H I	1215.6	H	7396.0	0.02467	1318.6	2.6
UGC12163	1246.04	INTRINSIC	H I	1215.6	H	7489.0	0.02498	347.8	1.6
UGC12163	1250.57	ISMLG	S II	1250.5	L	-2.0	-0.00001	139.7	7.9
UGC12163	1253.81	ISMLG	S II	1253.8	L	0.0	-0.00001	158.6	10.2
UGC12163	1258.65	ISMLG	Si II	1260.4	L	-421.0	-0.00141	59.8	11.5
UGC12163	1259.50	ISMLG	S II	1259.5	L	-4.0	-0.00001	198.8	11.8
UGC12163	1260.40	ISMLG	Si II	1260.4	L	-5.0	-0.00001	675.3	12.6
UGC12163	1260.72	ISMLG	C I	1260.7	L	-4.0	-0.00001	93.0	8.3
UGC12163	1260.74	ISMLG	Si II	1260.4	L	75.0	0.00025	116.0	7.2
UGC12163	1268.27	INTRINSIC	N V	1238.8	H	7127.0	0.02374	561.7	6.4
UGC12163	1268.58	INTRINSIC	N V	1238.8	H	7201.0	0.02402	344.0	6.0
UGC12163	1268.78	INTRINSIC	N V	1238.8	H	7250.0	0.02418	291.2	10.8
UGC12163	1269.42	INTRINSIC	N V	1238.8	H	7405.0	0.02467	287.3	10.7
UGC12163	1269.74	INTRINSIC	N V	1238.8	H	7483.0	0.02498	51.5	7.5
UGC12163	1272.32	INTRINSIC	N V	1242.8	H	7120.0	0.02374	392.4	6.9
UGC12163	1272.66	INTRINSIC	N V	1242.8	H	7202.0	0.02402	310.9	6.4
UGC12163	1272.88	INTRINSIC	N V	1242.8	H	7255.0	0.02418	343.6	9.8
UGC12163	1273.51	INTRINSIC	N V	1242.8	H	7406.0	0.02467	186.1	10.6
UGC12163	1273.83	INTRINSIC	N V	1242.8	H	7484.0	0.02498	27.3	8.4
UGC12163	1277.28	ISMLG	C I	1277.2	L	7.0	-0.00001	43.1	13.1
UGC12163	1302.14	ISMLG	O I	1302.1	L	-7.0	-0.00001	600.6	28.7
UGC12163	1304.33	ISMLG	Si II	1304.3	L	-8.0	-0.00001	495.7	49.8
UGC12163	1317.20	ISMLG	Ni II	1317.2	L	-5.0	-0.00001	34.2	20.2
UGC12163	1328.82	ISMLG	C I	1328.8	L	-3.0	-0.00001	39.3	16.3
UGC12163	1332.64	ISMLG	C II	1334.5	L	-425.0	-0.00141	130.6	14.9
UGC12163	1332.99	ISMLG	C II	1334.5	L	-347.0	-0.00117	43.0	12.4
UGC12163	1333.65	ISMLG	C II	1334.5	L	-198.0	-0.00067	59.7	11.4
UGC12163	1334.54	ISMLG	C II	1334.5	L	2.0	-0.00001	781.4	11.9
UGC12163	1334.86	ISMLG	C II	1334.5	L	74.0	0.00025	159.0	6.5
UGC12163	1335.69	ISMLG	C II*	1335.7	L	-4.0	-0.00001	241.6	11.1

Table A1 continued

Table A1 (*continued*)

Target	λ_{obs}	Type	Ion	λ_{rest}	Frame	cz	z	W_{λ}	$\sigma_{W_{\lambda}}$
	(Å)			(Å)		(km s ⁻¹)		(mÅ)	(mÅ)
UGC12163	1370.11	ISMLG	Ni II	1370.1	L	-4.0	-0.00001	40.6	16.4
UGC12163	1391.77	ISMLG	Si IV	1393.7	L	-429.0	-0.00141	113.0	17.1
UGC12163	1392.11	ISMLG	Si IV	1393.7	L	-354.0	-0.00117	45.1	18.6
UGC12163	1393.79	ISMLG	Si IV	1393.7	L	7.0	-0.00001	316.3	18.0
UGC12163	1400.78	ISMLG	Si IV	1402.7	L	-425.0	-0.00141	81.9	20.0
UGC12163	1402.80	ISMLG	Si IV	1402.7	L	5.0	-0.00001	285.6	24.1
UGC12163	1426.87	INTRINSIC	Si IV	1393.7	H	7123.0	0.02374	79.9	12.5
UGC12163	1427.22	INTRINSIC	Si IV	1393.7	H	7196.0	0.02402	198.7	16.2
UGC12163	1427.46	INTRINSIC	Si IV	1393.7	H	7248.0	0.02418	109.5	18.1
UGC12163	1428.17	INTRINSIC	Si IV	1393.7	H	7401.0	0.02467	130.4	21.2
UGC12163	1428.53	INTRINSIC	Si IV	1393.7	H	7478.0	0.02498	50.3	15.6
UGC12163	1436.09	INTRINSIC	Si IV	1402.7	H	7120.0	0.02374	51.4	11.4
UGC12163	1436.47	INTRINSIC	Si IV	1402.7	H	7201.0	0.02402	216.2	17.0
UGC12163	1436.69	INTRINSIC	Si IV	1402.7	H	7249.0	0.02418	201.7	19.5
UGC12163	1437.42	INTRINSIC	Si IV	1402.7	H	7405.0	0.02467	115.5	20.8
UGC12163	1454.87	ISMLG	Ni II	1454.8	L	6.0	-0.00001	34.9	16.2
UGC12163	1526.67	ISMLG	Si II	1526.7	L	-8.0	-0.00001	612.1	21.1
UGC12163	1527.10	ISMLG	Si II	1526.7	L	77.0	0.00025	69.2	14.2
UGC12163	1546.02	ISMLG	C IV	1548.2	L	-423.0	-0.00141	117.4	22.1
UGC12163	1548.23	ISMLG	C IV	1548.2	L	6.0	-0.00001	459.5	25.2
UGC12163	1548.57	ISMLG	C IV	1548.2	L	71.0	0.00025	74.5	15.7
UGC12163	1550.80	ISMLG	C IV	1550.7	L	3.0	-0.00001	365.3	27.4
UGC12163	1551.18	ISMLG	C IV	1550.7	L	77.0	0.00025	60.0	17.4
UGC12163	1560.29	ISMLG	C I	1560.3	L	-4.0	-0.00001	50.3	20.7
UGC12163	1584.99	INTRINSIC	C IV	1548.2	H	7123.0	0.02374	557.1	17.6
UGC12163	1585.39	INTRINSIC	C IV	1548.2	H	7200.0	0.02402	280.0	25.6
UGC12163	1585.66	INTRINSIC	C IV	1548.2	H	7253.0	0.02418	252.2	26.1
UGC12163	1586.42	INTRINSIC	C IV	1548.2	H	7401.0	0.02467	361.9	16.4
UGC12163	1586.89	INTRINSIC	C IV	1548.2	H	7492.0	0.02498	218.9	17.8
UGC12163	1587.64	INTRINSIC	C IV	1550.7	H	7126.0	0.02374	345.1	16.5
UGC12163	1588.04	INTRINSIC	C IV	1550.7	H	7204.0	0.02402	356.2	17.5
UGC12163	1588.30	INTRINSIC	C IV	1550.7	H	7252.0	0.02418	375.4	24.9
UGC12163	1589.07	INTRINSIC	C IV	1550.7	H	7403.0	0.02467	338.4	13.7
UGC12163	1589.49	INTRINSIC	C IV	1550.7	H	7483.0	0.02498	288.7	14.3
UGC12163	1608.40	ISMLG	Fe II	1608.4	L	-10.0	-0.00001	435.0	47.8
UGC12163	1656.89	ISMLG	C I	1656.9	L	-8.0	-0.00001	77.0	31.1
UGC12163	1670.74	ISMLG	Al II	1670.7	L	-9.0	-0.00001	644.2	26.8
UGC12163	1709.56	ISMLG	Ni II	1709.6	L	-8.0	-0.00001	110.5	36.4
UGC12163	1741.56	ISMLG	Ni II	1741.5	L	1.0	-0.00001	84.9	42.1
UGC12163	1751.86	PROXIMATE	H I	1751.9	L	-9.0	-0.00001	76.0	39.6
UM228	1143.24	ISMLG	Fe II	1143.2	L	3.0	0.00001	83.2	36.5
UM228	1144.93	ISMLG	Fe II	1144.9	L	-3.0	0.00001	141.9	36.1
UM228	1166.90	INTRINSIC	S IV	1062.6	H	29405.0	0.09808	245.6	44.5
UM228	1171.28	UNIDENTIFIED	UNIND	1000.0	H	0.0	-1.00000	200.9	53.5
UM228	1190.19	ISMLG	Si II	1190.4	L	-56.0	-0.00022	95.0	27.1
UM228	1190.46	ISMLG	Si II	1190.4	L	10.0	0.00001	187.8	25.9
UM228	1193.03	ISMLG	Si II	1193.2	L	-66.0	-0.00022	122.2	31.7
UM228	1193.31	ISMLG	Si II	1193.2	L	6.0	0.00001	180.3	25.1
UM228	1199.54	ISMLG	N I	1199.5	L	-1.0	0.00001	101.0	42.9
UM228	1200.24	ISMLG	N I	1200.2	L	3.0	0.00001	204.1	51.3
UM228	1200.71	ISMLG	N I	1200.7	L	0.0	0.00001	238.1	47.8
UM228	1206.22	ISMLG	Si III	1206.5	L	-68.0	-0.00022	218.0	26.9
UM228	1206.52	ISMLG	Si III	1206.5	L	5.0	0.00001	272.9	31.8

Table A1 continued

Table A1 (*continued*)

Target	λ_{obs}	Type	Ion	λ_{rest}	Frame	cz	z	W_{λ}	$\sigma_{W_{\lambda}}$
	(Å)			(Å)		(km s ⁻¹)		(mÅ)	(mÅ)
UM228	1222.72	IGMABS	H I	1215.6	H	1738.0	0.00580	227.2	62.6
UM228	1227.60	IGMABS	H I	1215.6	H	2941.0	0.00981	116.2	43.9
UM228	1232.65	INTRINSIC	Fe III	1122.5	H	29412.0	0.09808	372.7	49.5
UM228	1237.94	IGMABS	H I	1215.6	H	5491.0	0.01832	265.1	33.9
UM228	1239.26	IGMABS	H I	1215.6	H	5816.0	0.01940	630.6	61.5
UM228	1250.57	ISMLG	S II	1250.5	L	-1.0	0.00001	104.9	25.8
UM228	1253.84	ISMLG	S II	1253.8	L	8.0	0.00001	105.7	28.1
UM228	1259.52	ISMLG	S II	1259.5	L	0.0	0.00001	69.7	22.3
UM228	1260.12	ISMLG	Si II	1260.4	L	-73.0	-0.00022	172.3	22.7
UM228	1260.45	ISMLG	Si II	1260.4	L	7.0	0.00001	205.2	20.4
UM228	1323.82	INTRINSIC	Si III	1206.5	H	29153.0	0.09723	617.4	57.3
UM228	1324.84	INTRINSIC	Si III	1206.5	H	29405.0	0.09808	786.1	53.4
UM228	1333.88	INTRINSIC	H I	1215.6	H	29150.0	0.09723	633.0	21.9
UM228	1334.90	INTRINSIC	H I	1215.6	H	29404.0	0.09808	688.0	24.4
UM228	1393.75	ISMLG	Si IV	1393.7	L	-2.0	0.00001	130.2	39.8
UM228	1464.33	INTRINSIC	C II	1334.5	H	29158.0	0.09723	217.9	34.8
UM228	1465.43	INTRINSIC	C II	1334.5	H	29404.0	0.09808	306.7	33.6
UM228	1526.39	ISMLG	Si II	1526.7	L	-62.0	-0.00022	121.8	32.0
UM228	1526.74	ISMLG	Si II	1526.7	L	7.0	0.00001	193.6	26.7
UM228	1529.25	INTRINSIC	Si IV	1393.7	H	29144.0	0.09723	633.9	55.0
UM228	1530.48	INTRINSIC	Si IV	1393.7	H	29408.0	0.09808	785.0	50.1
UM228	1539.17	INTRINSIC	Si IV	1402.7	H	29150.0	0.09723	541.4	50.9
UM228	1540.36	INTRINSIC	Si IV	1402.7	H	29403.0	0.09808	632.0	50.0
UM228	1547.86	ISMLG	C IV	1548.2	L	-67.0	-0.00022	91.1	32.6
UM228	1548.23	ISMLG	C IV	1548.2	L	5.0	0.00001	111.5	30.4
UM228	1550.83	ISMLG	C IV	1550.7	L	9.0	0.00001	122.6	41.5
UM228	1670.82	ISMLG	Al II	1670.7	L	6.0	0.00001	420.8	69.7
UM228	1698.77	INTRINSIC	C IV	1548.2	H	29155.0	0.09723	1298.7	198.6
UM228	1700.09	INTRINSIC	C IV	1548.2	H	29410.0	0.09808	819.8	145.9
UM228	1701.59	INTRINSIC	C IV	1550.7	H	29153.0	0.09723	713.3	165.4
UM228	1702.91	PROXIMATE	H I	1550.7	H	29409.0	0.09808	1309.6	112.4
Zw535.012	1134.74	ISMLG	N I	1134.9	L	-65.0	-0.00021	137.6	23.2
Zw535.012	1134.99	ISMLG	N I	1134.9	L	3.0	0.00000	198.8	28.8
Zw535.012	1143.24	ISMLG	Fe II	1143.2	L	3.0	0.00000	65.0	12.6
Zw535.012	1144.49	ISMLG	Fe II	1144.9	L	-117.0	-0.00037	46.3	11.8
Zw535.012	1144.68	ISMLG	Fe II	1144.9	L	-67.0	-0.00021	120.1	9.0
Zw535.012	1144.95	ISMLG	Fe II	1144.9	L	4.0	0.00000	167.2	13.1
Zw535.012	1152.56	ISMLG	P II	1152.8	L	-67.0	-0.00021	33.1	10.0
Zw535.012	1152.80	ISMLG	P II	1152.8	L	-5.0	0.00000	80.4	11.3
Zw535.012	1157.90	ISMLG	C I	1157.9	L	-2.0	0.00000	34.2	11.8
Zw535.012	1188.82	ISMLG	C I	1188.8	L	-4.0	0.00000	19.2	7.9
Zw535.012	1189.75	ISMLG	Si II	1190.4	L	-168.0	-0.00058	46.2	7.1
Zw535.012	1189.96	ISMLG	Si II	1190.4	L	-114.0	-0.00037	168.2	5.7
Zw535.012	1190.16	ISMLG	Si II	1190.4	L	-64.0	-0.00021	175.5	3.6
Zw535.012	1190.44	ISMLG	Si II	1190.4	L	7.0	0.00000	320.0	5.6
Zw535.012	1192.60	ISMLG	Si II	1193.2	L	-174.0	-0.00058	50.6	7.8
Zw535.012	1192.83	ISMLG	Si II	1193.2	L	-116.0	-0.00037	185.5	5.4
Zw535.012	1193.03	ISMLG	Si II	1193.2	L	-66.0	-0.00021	170.3	2.9
Zw535.012	1193.32	ISMLG	Si II	1193.2	L	8.0	0.00000	335.3	5.4
Zw535.012	1194.00	ISMLG	C I	1193.9	L	1.0	0.00000	19.7	8.2
Zw535.012	1197.19	ISMLG	Mn II	1197.1	L	1.0	0.00000	22.0	8.1
Zw535.012	1199.09	ISMLG	N I	1199.5	L	-115.0	-0.00037	78.4	12.0
Zw535.012	1199.29	ISMLG	N I	1199.5	L	-65.0	-0.00021	146.7	8.0

Table A1 continued

Table A1 (*continued*)

Target	λ_{obs}	Type	Ion	λ_{rest}	Frame	cz	z	W_{λ}	$\sigma_{W_{\lambda}}$
	(Å)			(Å)		(km s ⁻¹)		(mÅ)	(mÅ)
Zw535.012	1199.58	ISMLG	N I	1199.5	L	7.0	0.00000	288.4	8.9
Zw535.012	1199.97	ISMLG	N I	1200.2	L	-63.0	-0.00021	138.1	8.4
Zw535.012	1200.22	ISMLG	N I	1200.2	L	0.0	0.00000	264.4	8.2
Zw535.012	1200.46	ISMLG	N I	1200.7	L	-63.0	-0.00021	148.5	7.9
Zw535.012	1200.73	ISMLG	N I	1200.7	L	5.0	0.00000	228.7	10.5
Zw535.012	1201.13	ISMLG	Mn II	1201.1	L	2.0	0.00000	21.3	7.6
Zw535.012	1205.05	ISMLG	Si III	1206.5	L	-362.0	-0.00127	63.9	9.2
Zw535.012	1205.79	ISMLG	Si III	1206.5	L	-176.0	-0.00058	112.2	6.9
Zw535.012	1206.06	ISMLG	Si III	1206.5	L	-109.0	-0.00037	167.9	4.4
Zw535.012	1206.24	ISMLG	Si III	1206.5	L	-63.0	-0.00021	183.2	4.0
Zw535.012	1206.53	ISMLG	Si III	1206.5	L	8.0	0.00000	325.7	6.2
Zw535.012	1236.26	IGMABS	H I	1215.6	H	5078.0	0.01694	63.4	7.9
Zw535.012	1236.57	IGMABS	H I	1215.6	H	5155.0	0.01720	175.4	8.1
Zw535.012	1238.83	ISMLG	N V	1238.8	L	3.0	0.00000	47.3	8.0
Zw535.012	1239.92	ISMLG	Mg II	1239.9	L	-1.0	0.00000	15.5	5.6
Zw535.012	1250.32	ISMLG	S II	1250.5	L	-62.0	-0.00021	45.2	4.6
Zw535.012	1250.57	ISMLG	S II	1250.5	L	-3.0	0.00000	147.7	4.8
Zw535.012	1253.34	ISMLG	S II	1253.8	L	-110.0	-0.00037	20.7	5.2
Zw535.012	1253.55	ISMLG	S II	1253.8	L	-61.0	-0.00021	62.3	4.2
Zw535.012	1253.78	ISMLG	S II	1253.8	L	-5.0	0.00000	171.6	3.8
Zw535.012	1259.03	ISMLG	S II	1259.5	L	-117.0	-0.00037	31.1	4.2
Zw535.012	1259.26	ISMLG	S II	1259.5	L	-61.0	-0.00021	68.0	3.4
Zw535.012	1259.48	ISMLG	S II	1259.5	L	-8.0	0.00000	193.6	2.8
Zw535.012	1259.72	ISMLG	Si II	1260.4	L	-167.0	-0.00058	105.0	3.3
Zw535.012	1259.92	ISMLG	Si II	1260.4	L	-119.0	-0.00037	154.1	1.9
Zw535.012	1260.15	ISMLG	Si II	1260.4	L	-65.0	-0.00021	226.9	1.1
Zw535.012	1260.44	ISMLG	Si II	1260.4	L	4.0	0.00000	359.8	1.7
Zw535.012	1260.72	ISMLG	C I	1260.7	L	-4.0	0.00000	98.9	3.6
Zw535.012	1262.40	PROXIMATE	H I	1215.6	H	11523.0	0.03844	92.8	5.9
Zw535.012	1264.54	INTRINSIC	Si III	1206.5	H	14423.0	0.04812	25.5	4.2
Zw535.012	1272.82	INTRINSIC	H I	1215.6	H	14093.0	0.04701	61.6	3.4
Zw535.012	1273.41	INTRINSIC	H I	1215.6	H	14238.0	0.04749	49.3	2.1
Zw535.012	1273.78	INTRINSIC	H I	1215.6	H	14330.0	0.04780	130.2	2.4
Zw535.012	1274.16	INTRINSIC	H I	1215.6	H	14425.0	0.04812	156.8	2.4
Zw535.012	1276.69	PROXIMATE	H I	1215.6	H	15048.0	0.05019	9.9	3.3
Zw535.012	1277.24	ISMLG	C I	1277.2	L	-2.0	0.00000	57.8	3.3
Zw535.012	1280.10	ISMLG	C I	1280.1	L	-8.0	0.00000	16.9	4.1
Zw535.012	1298.45	INTRINSIC	N V	1238.8	H	14430.0	0.04812	90.6	9.7
Zw535.012	1301.71	ISMLG	O I	1302.1	L	-106.0	-0.00037	179.2	4.5
Zw535.012	1301.90	ISMLG	O I	1302.1	L	-62.0	-0.00021	235.3	2.8
Zw535.012	1302.19	ISMLG	O I	1302.1	L	5.0	0.00000	348.4	4.2
Zw535.012	1302.63	INTRINSIC	N V	1242.8	H	14430.0	0.04812	47.3	8.2
Zw535.012	1303.89	ISMLG	Si II	1304.3	L	-110.0	-0.00037	90.5	6.4
Zw535.012	1304.09	ISMLG	Si II	1304.3	L	-64.0	-0.00021	172.1	4.1
Zw535.012	1304.40	ISMLG	Si II	1304.3	L	6.0	0.00000	283.0	5.9
Zw535.012	1317.19	ISMLG	Ni II	1317.2	L	-7.0	0.00000	43.2	11.0
Zw535.012	1328.84	ISMLG	C I	1328.8	L	2.0	0.00000	35.7	9.1
Zw535.012	1333.75	ISMLG	C II	1334.5	L	-175.0	-0.00058	71.5	7.3
Zw535.012	1334.01	ISMLG	C II	1334.5	L	-118.0	-0.00037	198.0	3.6
Zw535.012	1334.24	ISMLG	C II	1334.5	L	-65.0	-0.00021	242.2	2.6
Zw535.012	1334.56	ISMLG	C II	1334.5	L	6.0	0.00000	429.4	4.1
Zw535.012	1335.42	ISMLG	C II*	1335.7	L	-66.0	-0.00021	61.4	6.8
Zw535.012	1335.71	ISMLG	C II*	1335.7	L	1.0	0.00000	164.6	8.2

Table A1 continued

Table A1 (*continued*)

Target	λ_{obs}	Type	Ion	λ_{rest}	Frame	cz	z	W_{λ}	$\sigma_{W_{\lambda}}$
	(Å)			(Å)		(km s ⁻¹)		(mÅ)	(mÅ)
Zw535.012	1347.23	ISMLG	Cl I	1347.2	L	-1.0	0.00000	35.4	8.2
Zw535.012	1370.12	ISMLG	Ni II	1370.1	L	-3.0	0.00000	49.2	8.0
Zw535.012	1393.28	ISMLG	Si IV	1393.7	L	-104.0	-0.00037	49.0	8.7
Zw535.012	1393.73	ISMLG	Si IV	1393.7	L	-7.0	0.00000	79.9	10.3
Zw535.012	1402.28	ISMLG	Si IV	1402.7	L	-105.0	-0.00037	21.4	8.3
Zw535.012	1402.76	ISMLG	Si IV	1402.7	L	-4.0	0.00000	48.7	11.5
Zw535.012	1454.87	ISMLG	Ni II	1454.8	L	5.0	0.00000	42.8	10.9
Zw535.012	1526.16	ISMLG	Si II	1526.7	L	-107.0	-0.00037	156.2	13.9
Zw535.012	1526.38	ISMLG	Si II	1526.7	L	-64.0	-0.00021	176.3	9.3
Zw535.012	1526.73	ISMLG	Si II	1526.7	L	5.0	0.00000	381.0	11.0
Zw535.012	1547.30	ISMLG	C IV	1548.2	L	-175.0	-0.00058	82.7	16.5
Zw535.012	1547.59	ISMLG	C IV	1548.2	L	-118.0	-0.00037	66.1	14.2
Zw535.012	1547.87	ISMLG	C IV	1548.2	L	-65.0	-0.00021	55.0	14.3
Zw535.012	1548.17	ISMLG	C IV	1548.2	L	-6.0	0.00000	103.5	17.5
Zw535.012	1550.81	ISMLG	C IV	1550.7	L	6.0	0.00000	49.3	17.9
Zw535.012	1560.34	ISMLG	C I	1560.3	L	6.0	0.00000	48.3	18.9
Zw535.012	1607.82	ISMLG	Fe II	1608.4	L	-117.0	-0.00037	94.2	14.8
Zw535.012	1608.12	ISMLG	Fe II	1608.4	L	-62.0	-0.00021	156.4	12.0
Zw535.012	1608.47	ISMLG	Fe II	1608.4	L	4.0	0.00000	279.0	15.8
Zw535.012	1622.73	INTRINSIC	C IV	1548.2	H	14430.0	0.04812	218.1	9.5
Zw535.012	1625.43	INTRINSIC	C IV	1550.7	H	14431.0	0.04812	160.9	7.4
Zw535.012	1656.94	ISMLG	C I	1656.9	L	2.0	0.00000	141.0	19.8
Zw535.012	1670.16	ISMLG	Al II	1670.7	L	-113.0	-0.00037	121.6	19.8
Zw535.012	1670.43	ISMLG	Al II	1670.7	L	-65.0	-0.00021	187.5	17.4
Zw535.012	1670.84	ISMLG	Al II	1670.7	L	10.0	0.00000	391.6	21.8
Zw535.012	1709.61	ISMLG	Ni II	1709.6	L	2.0	0.00000	37.8	22.4
Zw535.012	1741.51	ISMLG	H I	1741.5	L	-7.0	0.00000	51.6	24.8

NOTE—Definition of the identified types of absorption features: ISMLG: ISM/CGM/IGM absorption from the Local group environment (mostly the MW and M31); IGMABS: intervening IGM/CGM absorber at $\Delta v > 3000$ km s⁻¹ from the QSO redshift; PROXIMATE: proximate/associated absorber at $500 < \Delta v < 3000$ km s⁻¹ from the QSO redshift; INTRINSIC: intrinsic absorber at $\Delta v < 500$ km s⁻¹ from the QSO redshift; UNIDENTIFIED: unknown origin of the absorption; OTHER: FPN: fixed-pattern noise feature; OTHER: EDGE: special case of fixed-pattern noise feature occurring near the edge of the COS detector; OTHER: FLAW: refers to the 1043 Å detector flaw in the *FUSE* data that causes a fake line. In the frame column, “L” stands for LSR frame (any absorption at $|v_{\text{LSR}}| \leq 500$), “H” for heliocentric frame (any absorption at $|v_{\text{LSR}}| > 500$). Note that the equivalent widths (W_{λ}) and errors are provided for guidelines and should not be used for quantitative scientific purposes. The H₂ lines are not individually measured, but are based on a model of the H₂ absorption, which is the reason for not providing an error on W_{λ} (i.e., in the table it is set to “0.0”).

Table A2. Comparison between COS and STIS

Ion/Instrument	$[v_1, v_2]$	v	$\log N$
	(km s ⁻¹)	(km s ⁻¹)	[cm ⁻²]
MRK335			
C II $\lambda 1334$ COS	-450, -372	-406.9 ± 3.7	13.22 ± 0.08
C II $\lambda 1334$ STIS	-450, -372	-403.2 ± 4.7	13.34 ± 0.11
C II $\lambda 1334$ COS	-372, -310	-334.6 ± 2.1	13.34 ± 0.06
C II $\lambda 1334$ STIS	-372, -310	-338.8 ± 2.0	13.52 ± 0.06
Si III $\lambda 1206$ COS	-450, -372	-409.7 ± 1.8	12.49 ± 0.04
Si III $\lambda 1206$ STIS	-450, -372	-406.5 ± 5.3	12.51 ± 0.13
Si III $\lambda 1206$ COS	-372, -310	-339.9 ± 0.8	12.75 ± 0.02
Si III $\lambda 1206$ STIS	-372, -310	-337.8 ± 2.2	12.82 ± 0.07
Si III $\lambda 1206$ COS	-310, -273	-296.6 ± 0.8	12.40 ± 0.04
Si III $\lambda 1206$ STIS	-310, -273	-301.8 ± 2.2	12.64 ± 0.17
Si III $\lambda 1206$ COS	-273, -190	-246.9 ± 3.7	12.28 ± 0.06
Si III $\lambda 1206$ STIS	-273, -190	...	< 12.2
UGC12163			
C II $\lambda 1334$ COS	-475, -375	-423.3 ± 3.6	> 13.94
C II $\lambda 1334$ STIS	-475, -375	-425.2 ± 5.0	14.05 ± 0.13
C II $\lambda 1334$ COS	-375, -310	-353.0 ± 7.3	13.35 ± 0.20
C II $\lambda 1334$ STIS	-375, -310	...	< 13.28
C II $\lambda 1334$ COS	-220, -180	-196.6 ± 3.1	13.26 ± 0.18
C II $\lambda 1334$ STIS	-220, -180	-200.8 ± 3.6	$13.37^{+0.16}_{-0.26}$
Si III $\lambda 1206$ COS	-475, -375	-426.0 ± 2.3	> 13.30
Si III $\lambda 1206$ STIS	-475, -375	-425.5 ± 21.4	> 13.45
Si III $\lambda 1206$ COS	-375, -310	-349.8 ± 6.2	12.43 ± 0.18
Si III $\lambda 1206$ STIS	-375, -310	...	< 12.57
NGC7469			
C II $\lambda 1334$ COS	-400, -268	-335.3 ± 0.7	> 14.27
C II $\lambda 1334$ STIS	-400, -268	-337.6 ± 0.8	> 14.44
C II $\lambda 1334$ COS	-268, -210	-251.4 ± 3.8	13.06 ± 0.09
C II $\lambda 1334$ STIS	-268, -210	-251.1 ± 3.3	13.10 ± 0.08
C II $\lambda 1334$ COS	-202, -150	-176.2 ± 3.4	12.94 ± 0.11
C II $\lambda 1334$ STIS	-202, -150	-184.9 ± 6.8	$12.66^{+0.14}_{-0.20}$
Si III $\lambda 1206$ COS	-400, -268	-325.2 ± 0.5	> 13.57
Si III $\lambda 1206$ STIS	-400, -268	-332.7 ± 5.9	> 13.76
Si III $\lambda 1206$ COS	-268, -210	-246.9 ± 0.9	12.63 ± 0.02
Si III $\lambda 1206$ STIS	-268, -210	-250.1 ± 1.7	12.76 ± 0.16
Si III $\lambda 1206$ COS	-202, -150	-178.8 ± 1.3	12.32 ± 0.04
Si III $\lambda 1206$ STIS	-202, -150	-174.8 ± 1.2	12.58 ± 0.04

NOTE—COS stands here for COS G130M and STIS for STIS E140M.
The SNRs (per resolution element) near C II and Si III are, respectively: MRK335: 36.6, 32.2 (COS), 9.5, 4.8 (STIS); UGC12163: 10.7, 10.8 (COS), 5.1, 2.3 (STIS); NGC7469: 37.5, 35.4 (COS), 16.5, 9.0 (STIS).

Table A3. Summary of the Profile Fit Results

Target	Ion	Comp.	v (km s ⁻¹)	σ_v (km s ⁻¹)	b (km s ⁻¹)	σ_b (km s ⁻¹)	$\log N$ [cm ⁻²]	$\sigma_{\log N}$
RX_J0048.3+3941	C II	1	-471.4	4.3	13.8	7.7	12.90	0.13
RX_J0048.3+3941	C II	2	-418.9	4.5	17.5	7.6	13.21	0.13
RX_J0048.3+3941	C II	3	-373.8	0.9	17.3	1.7	14.07	0.02
RX_J0048.3+3941	C II	4	-329.1	3.2	14.6	5.1	13.21	0.10
RX_J0048.3+3941	C II	5	-244.3	0.8	17.3	1.3	13.85	0.02
RX_J0048.3+3941	C II	6	-177.3	1.0	20.0	1.3	14.25	0.03
RX_J0048.3+3941	C IV	1	-386.7	4.2	39.2	6.3	13.25	0.05
RX_J0048.3+3941	C IV	2	-239.0	0.6	21.7	0.9	14.07	0.01
RX_J0048.3+3941	C IV	3	-183.6	0.8	11.7	1.3	13.59	0.02
RX_J0048.3+3941	C IV	4	-30.5	4.6	40.0	3.7	13.62	0.07
RX_J0048.3+3941	C IV	5	-8.8	2.6	11.7	6.0	13.09	0.20
RX_J0048.3+3941	Si II	1	-374.7	1.3	15.4	2.0	12.83	0.04
RX_J0048.3+3941	Si II	2	-323.1	5.2	28.5	10.3	12.49	0.10
RX_J0048.3+3941	Si II	3	-251.8	1.8	13.1	3.2	12.79	0.04
RX_J0048.3+3941	Si II	4	-179.3	0.5	16.2	0.8	13.52	0.02
RX_J0048.3+3941	Si III	1	-374.6	0.9	10.2	2.4	12.97	0.08
RX_J0048.3+3941	Si III	2	-366.3	6.0	61.4	13.0	12.86	0.05
RX_J0048.3+3941	Si III	3	-278.2	1.8	1.6	21.4	12.89	24.70
RX_J0048.3+3941	Si III	4	-239.8	0.7	13.8	1.5	13.23	0.05
RX_J0048.3+3941	Si III	5	-180.6	0.6	16.9	1.1	13.28	0.04
RX_J0048.3+3941	Si IV	1	-386.6	3.8	24.2	6.1	12.44	0.07
RX_J0048.3+3941	Si IV	2	-238.0	0.6	16.9	0.9	13.21	0.01
RX_J0048.3+3941	Si IV	3	-177.1	0.7	13.4	1.2	12.97	0.02
RX_J0048.3+3941	Si IV	4	-49.8	6.2	64.4	6.6	13.08	0.05
RX_J0048.3+3941	Si IV	5	-8.1	0.7	12.0	1.5	13.02	0.04
RX_J0048.3+3941	O VI	1	-388.2	6.3	44.0	8.8	13.84	0.10
RX_J0048.3+3941	O VI	2	-227.6	2.4	21.4	4.5	13.94	0.12
RX_J0048.3+3941	O VI	3	-224.7	7.1	99.0	16.6	14.40	0.04
RX_J0048.3+3941	O VI	4	-184.6	1.3	4.8	3.4	13.57	0.14
RX_J0048.3+3941	O VI	5	-5.2	2.7	39.4	3.7	14.08	0.04
MRK352	C II	1	-303.9	9.3	32.0	16.5	13.73	0.13
MRK352	C II	2	-192.4	4.8	28.5	8.0	14.05	0.08
MRK352	C IV	1	-278.4	2.8	17.6	4.8	13.68	0.06
MRK352	C IV	2	-220.9	1.8	19.7	2.9	14.01	0.04
MRK352	C IV	3	-31.2	1.9	22.0	3.0	13.87	0.04
MRK352	C IV	4	54.4	6.3	23.8	11.0	13.34	0.11
MRK352	Si II	1	-206.4	2.0	5.9	2.4	13.67	0.35
MRK352	Si III	1	-300.0	4.7	20.2	7.8	12.89	0.09
MRK352	Si III	2	-242.0	3.3	9.7	12.3	12.96	0.30
MRK352	Si III	3	-199.0	2.8	10.0	6.4	13.53	0.77
MRK352	Si IV	1	-302.2	23.7	34.7	71.6	12.75	0.34
MRK352	Si IV	2	-199.8	8.8	47.9	14.4	13.38	0.10
MRK352	Si IV	3	-21.7	3.9	38.4	5.6	13.61	0.05
RBS2055	C II	1	-407.1	3.2	15.6	5.5	13.51	0.07
RBS2055	C II	2	-328.5	1.2	15.3	2.1	14.20	0.06
RBS2055	C II	3	-266.2	11.4	23.8	27.6	13.14	0.22
RBS2055	C IV	1	-443.9	14.4	28.1	36.4	13.32	0.25
RBS2055	C IV	2	-322.1	3.6	49.9	5.4	13.90	0.04
RBS2055	C IV	3	-0.6	1.4	31.4	2.2	14.19	0.02
RBS2055	Si II	1	-406.3	1.0	9.3	2.2	12.39	0.03

Table A3 continued

Table A3 (*continued*)

Target	Ion	Comp.	v	σ_v	b	σ_b	$\log N$	$\sigma_{\log N}$
			(km s ⁻¹)	(km s ⁻¹)	(km s ⁻¹)	(km s ⁻¹)	[cm ⁻²]	
RBS2055	Si II	2	-330.3	1.3	13.3	2.2	13.28	0.04
RBS2055	Si III	1	-421.2	1.4	27.3	2.3	13.22	0.03
RBS2055	Si III	2	-326.0	1.1	28.5	1.9	13.47	0.03
RBS2055	Si IV	1	-439.3	7.6	43.5	13.3	12.93	0.09
RBS2055	Si IV	2	-322.7	3.0	32.1	4.6	13.21	0.04
RBS2055	Si IV	3	-7.6	1.0	29.3	1.6	13.78	0.02
MRK335	C II	1	-410.4	2.5	13.7	4.4	13.28	0.07
MRK335	C II	2	-330.9	2.1	14.8	3.5	13.40	0.05
MRK335	C IV	1	-334.2	7.0	15.1	14.4	12.89	0.20
MRK335	C IV	2	-294.9	2.6	14.2	5.4	13.29	0.09
MRK335	C IV	3	-246.4	2.7	15.2	5.7	13.22	0.08
MRK335	C IV	4	-206.6	2.5	6.7	6.7	12.98	0.09
MRK335	C IV	5	8.2	1.1	35.3	1.5	14.05	0.01
MRK335	Si II	1	-414.8	2.0	17.4	3.4	12.31	0.04
MRK335	Si II	2	-334.8	1.9	19.4	3.1	12.42	0.04
MRK335	Si III	1	-412.6	1.7	15.0	2.9	12.52	0.04
MRK335	Si III	2	-340.3	1.6	18.0	2.7	12.79	0.03
MRK335	Si III	3	-298.1	1.8	9.9	3.8	12.49	0.06
MRK335	Si III	4	-250.3	2.1	10.4	4.2	12.29	0.06
MRK335	Si IV	1	-318.5	17.9	47.5	48.3	12.60	0.31
MRK335	Si IV	2	-252.7	3.2	9.9	6.7	12.50	0.17
MRK335	Si IV	3	-35.0	10.0	68.5	7.2	13.31	0.08
MRK335	Si IV	4	5.3	1.5	23.8	3.1	13.35	0.07
PG0003+158	C II	1	-399.9	1.7	23.1	2.7	13.83	0.03
PG0003+158	C II	2	-325.8	1.0	18.7	1.8	14.10	0.03
PG0003+158	C II	3	-279.6	9.7	11.4	999.0	12.90	0.53
PG0003+158	C II	4	-240.0	3.9	19.9	8.2	13.50	0.11
PG0003+158	C II	5	-176.9	0.9	20.3	1.5	14.26	0.03
PG0003+158	C IV	1	-396.7	20.1	44.2	21.2	13.59	0.22
PG0003+158	C IV	2	-355.7	2.9	14.8	6.7	13.49	0.24
PG0003+158	C IV	3	-307.2	14.2	36.6	20.5	13.30	0.21
PG0003+158	C IV	4	-227.8	1.4	8.2	2.8	13.30	0.06
PG0003+158	C IV	5	-3.5	3.4	32.4	4.2	13.82	0.05
PG0003+158	C IV	6	57.2	4.2	24.2	5.4	13.52	0.09
PG0003+158	Si II	1	-387.6	1.8	10.8	3.5	12.45	0.05
PG0003+158	Si II	2	-323.7	0.6	13.6	1.0	13.20	0.03
PG0003+158	Si III	1	-406.0	2.8	29.7	4.5	12.91	0.04
PG0003+158	Si III	2	-335.6	1.5	22.0	2.5	13.16	0.03
PG0003+158	Si III	3	-249.3	4.9	35.8	8.3	12.62	0.06
PG0003+158	Si IV	1	-431.5	9.3	16.9	26.4	12.32	0.27
PG0003+158	Si IV	2	-358.2	6.1	38.0	9.6	12.94	0.08
PG0003+158	Si IV	3	-232.1	2.5	3.6	6.4	12.50	0.18
PG0003+158	Si IV	4	-4.5	1.6	26.1	2.4	13.39	0.03
PG0003+158	Si IV	5	57.2	2.0	14.4	3.3	12.97	0.05
PG2349-014	C II	1	-328.2	5.5	23.3	8.9	13.91	0.24
PG2349-014	C II	2	-294.3	1.9	8.8	16.5	14.45	0.64
PG2349-014	C II	3	-259.6	3.2	15.9	7.3	13.75	0.25
PG2349-014	C II	4	-204.0	7.4	11.3	999.0	13.10	0.48
PG2349-014	C II	5	-172.1	2.4	5.8	8.7	13.40	0.13
PG2349-014	Si II	1	-327.3	6.4	25.2	9.4	13.06	0.11
PG2349-014	Si II	2	-289.0	1.2	7.9	2.2	13.56	0.12
PG2349-014	Si II	3	-259.0	2.6	3.0	4.1	12.81	0.32
PG2349-014	Si III	1	-336.6	4.0	15.4	5.8	13.05	0.18

Table A3 continued

Table A3 (*continued*)

Target	Ion	Comp.	v	σ_v	b	σ_b	$\log N$	$\sigma_{\log N}$
			(km s^{-1})	(km s^{-1})	(km s^{-1})	(km s^{-1})	[cm^{-2}]	
PG2349–014	Si III	2	–301.0	3.9	6.5	2.9	14.70	1.44
PG2349–014	Si III	3	–267.0	10.9	51.2	8.6	13.63	0.12
PG2349–014	Si III	4	–166.5	1.7	7.9	4.0	12.52	0.08
PG2349–014	Si IV	1	–349.9	1.8	9.4	4.0	12.82	0.10
PG2349–014	Si IV	2	–296.9	1.8	18.0	6.2	13.23	0.28
PG2349–014	Si IV	3	–256.7	35.8	48.5	33.4	13.15	0.37
PG2349–014	Si IV	4	–8.6	5.6	26.3	10.3	13.04	0.52
PG2349–014	Si IV	5	26.6	36.2	46.1	22.4	13.12	0.43

NOTE—Error v , b , and N are 1σ errors.